



QST-P-3

Proceeding of the 13th International Workshop
on Beryllium Technology (BeWS-13)

National Institutes for Quantum and
Radiological Science and Technology

**Proceeding of the 13th International Workshop on
Beryllium Technology (BeWS-13)**

Date of Publishing : February 2018

Editing and Publication :

Breeding Functional Materials Development Group,
Dept. of Blanket Systems Research, Rokkasho Fusion Institute,
National Institutes for Quantum and Radiological Science
and Technology

2-166 Omotedate, Obuchi, Rokkasho, Aomori, 039-3212 JAPAN.

Tel : +81-175-71-6537 Fax : +81-175-71-6602

E-mail : kim.jaehwan@qst.go.jp

URL : <http://www.qst.go.jp>

©2018 National Institutes for Quantum and Radiological Science
and Technology All Rights Reserved

Printed in Japan

QST-P-3

ISBN 978-4-907894-09-2



QST-P-3

第 13 回ベリリウム技術に関する国際会議 (BeWS-13) 論文集

国立研究開発法人 量子科学技術研究開発機構

第13回ベリリウム技術に関する国際会議 (BeWS-13) 論文集

発行年月 2018年2月

編集発行 国立研究開発法人 量子科学技術研究開発機構

連絡先 〒039-3212

青森県上北郡六ヶ所村大字尾駁字表館2番166

六ヶ所研究所 ブランケット研究開発部
増殖機能材料開発グループ

TEL : 0175-71-6537 Fax : 0175-71-6602

Email : kim.jaehwan@qst.go.jp

URL : <http://www.qst.go.jp/>

©2018 国立研究開発法人 量子科学技術研究開発機構

Printed in Japan
QST-P-3
ISBN 978-4-907894-09-2

QST-P-3

Proceedings of the 13th International Workshop on Beryllium Technology (BeWS-13)

(Eds.) Jae-Hwan KIM, Masaru NAKAMICHI

Fusion Energy Research and Development Directorate, Rokkasho Fusion Institute,

Rokkasho-mura, Kamikita-gun, Aomori-ken

(Received Jan. 17, 2018)

The 13th International Workshop on Beryllium Technology (BeWS-13) was held on 21-22 September 2017, at the Hilton Tokyo Narita Airport Hotel, Chiba, Japan. This workshop has been holding every 2 years from 1993. The objective of this workshop is to disseminate results of research and technology development in areas relevant to beryllium utilization in fusion nuclear power systems. In this workshop, a lot of researchers and technicians engaged in R&D on beryllium related materials and fusion engineering attended and discussed. This report has been compiled the manuscripts and the presentation files in the BeWS-13.

Keywords : Beryllium, Fusion engineering, Irradiation effect, Health and safety, Beryllide application

QST-P-3

第 13 回ベリリウム技術に関する国際会議 (BeWS-13) 論文集

量子科学技術研究開発機構 核融合エネルギー研究開発部門

(編) 金 幸煥、中道 勝

(2018 年 1 月 17 日受理)

第 13 回ベリリウム技術に関する国際会議 (The 13th International Workshop on Beryllium Technology (BeWS-13)) は、平成 29 年 9 月 21 日 (木) 及び 22 日 (金) の 2 日間に渡り、日本千葉県のヒルトン東京成田空港ホテルにて開催された。本国際会議は、1993 年から 2 年毎に開催されており、今回で 13 回目となる。本国際会議では、世界におけるベリリウム関連材料 (ベリリウム金属及びその合金、金属間化合物など) と核融合炉工学研究開発に携わる研究者及び技術者が一同に会し、最新研究成果報告、討論及び情報交換を行うものであり、本テーマにおける研究活動の一層の活性化を図ることを目的としている。本報告書は、当該会議における論文及び発表資料を取りまとめたものである。

Content

1. Introduction.....	1
2. Manuscripts and presentation files	
2.1 Agenda of BeWS-13.....	3
2.2 Keynote Session	
2.2.1 Overview of fusion R&D in QST	7
S. Ohira (QST)	
2.3 Plenary Session	
2.3.1 Broader Approach(BA) R&D research status of the JET-ILW divertor tile and dust in Rokkasho: Be deposition study.....	28
N. Asakura (QST) <i>et al.</i>	
2.3.2 Beryllium materials for Fusion reactor wall applications...43	
C.K.Dorn (Be4Fusion) <i>et al.</i>	
2.3.3 Post-irradiation examination of beryllium pebbles from HIDOBE-02 experiment.....	64
V. Chakin (KIT) <i>et al.</i>	
2.3.4 Status of material development for HCCR TBM in Korea...78	
Y.-H.Park (NFRI) <i>et al.</i>	
2.3.5 Preparation for manufacturing of the Beryllium armor of the ITER First Wall in the Russian Federation.....	94
R. Giniyatulin (JSC, NII-EFA) <i>et al.</i>	
2.4 Technical Session1: Fabrication process	
2.4.1 Overview of R&D on beryllide as advanced neutron multipliers in Japan.....	104
M. Nakamichi (QST) <i>et al.</i>	
2.4.2 Distribution of beryllium pebble size by rotating electrode process.....	115
R.Fukatsu (NGK) <i>et al.</i>	
2.4.3 Trial fabrication and characterization of Be12V pebbles.....	121
P. Kurinskiy (QST) <i>et al.</i>	
2.5 Technical Session 2: Characterizations	

2.5.1 Experimental study on oxidation of beryllium pebbles in air and steam.....	128
R.Rolli (KIT) <i>et al.</i>	
2.5.2 Beryllium oxide on dust particles produced by ITER like wall materials in JET.....	143
N. Ashikawa (NIFS) <i>et al.</i>	
2.5.3 Ternary beryllide pebbles as advanced neutron multipliers.....	153
J.-H.Kim (QST) <i>et al.</i>	
2.5.4 A study on heat shock resistance of beryllium.....	160
K. Yonehara (KAKEN) <i>et al.</i>	
2.5.5 New method for beryllide production using arc plasma.....	170
N. Ikemoto (KAKEN) <i>et al.</i>	
2.5.6 Thermal conductivity of compressed binary beryllium pebble beds.....	178
J.Reimann (KIT) <i>et al.</i>	
2.5.7 Thermal creep of compressed binary beryllium pebble beds	193
J.Reimann (KIT) <i>et al.</i>	
2.6 Technical Session 3: Industry and safety issues	
2.6.1 United States beryllium industry update.....	206
K. Smith (Materion) <i>et al.</i>	
2.6.2 Overview of the current beryllium environmental, health and safety regulatory activities	228
D. Vidal (Materion) <i>et al.</i>	
2.6.3 Beryllium business of NGK insulators and topics of beryllium safety issue.....	241
K.Nojiri (NGK) <i>et al.</i>	
2.6.4 Recent achievements and related safety issues concerning beryllide applications	250
A.Goraieb (KBHF GmbH) <i>et al.</i>	
2.6.5 Facility introduction and safety issues in Rokkasho fusion institute, QST.....	258
M.Nakamichi (QST) <i>et al.</i>	

2.7 Technical Session 4: Modelling	
2.7.1 Modelling study of thermal excursion of chemical reactions of beryllium/beryllide pebbles with steam and its implication to fusion DEMO safety.....	271
M.Nakamura (QST) <i>et al.</i>	
2.7.2 Beryllium and titanium beryllide Be ₁₂ Ti as candidates for fusion applications.....	279
D.Bachurin (KIT) <i>et al.</i>	
2.8 Technical Session 5: Irradiation properties	
2.8.1 Ion and neutron irradiation tests on beryllium specimens.....	287
S.-H.Kang (KAERI) <i>et al.</i>	
2.8.2 Effects of argon ion irradiation on microstructure of beryllium...300	
P.Liu (USTB) <i>et al.</i>	
2.8.3 Present status of He ion irradiation hardening of Japanese beryllide pebbles by REM.....	311
T.Shibayama (Hokkaido Univ.) <i>et al.</i>	
2.8.4 Deuterium and Helium properties in beryllium irradiated with low energy ions.....	320
Y.Sugimoto (Shimane Univ.) <i>et al.</i>	
2.8.5 Surface property of tungsten exposed to beryllium containing high density plasma in PISCES.....	333
M.Miyamoto (Shimane Univ.) <i>et al.</i>	
2.8.6 Beryllium as plasma facing material: Erosion and surface damage behavior under intense transient plasma heat loads.....	344
I. Kupriyanov (A.A.Bochvar) <i>et al.</i>	
Appendix group photos	354

目次

1. はじめに.....	1
2. 原稿（発表資料）	
2.1 アジェンダ.....	3
2.2 キーノートセッション	
2.2.1 QSTにおける核融合 R&D の概要.....	7
S. Ohira (QST)	
2.3 プレナリーセッション	
2.3.1 JET-ILW ダイバータタイル及びダストに関する BA 研究活動の現状：Be 積層の研究	28
N. Asakura (QST) <i>et al.</i>	
2.3.2 核融合炉壁応用のためのベリリウム材料.....	43
C.K.Dorn (Be4Fusion) <i>et al.</i>	
2.3.3 HIDOBE-02 実験からのベリリウム微小球の照射後試験.....	64
V. Chakin (KIT) <i>et al.</i>	
2.3.4 韓国における HCCR TBM のための材料開発の現状.....	78
Y.-H.Park (NFRI) <i>et al.</i>	
2.3.5 ロシアにおける ITER 第一壁のベリリウムアーマー材の製造準備状況.....	94
R. Giniyatulin (JSC, NIIEFA) <i>et al.</i>	
2.4 テクニカルセッション 1：製造工程	
2.4.1 日本における先進的中性子増倍材としてのベリライドの R&D 概要.....	104
M. Nakamichi (QST) <i>et al.</i>	
2.4.2 回転電極法によるベリリウム微小球のサイズ分布	115
R.Fukatsu (NGK) <i>et al.</i>	
2.4.3 Be12V 微小球の予備的な製造及び特性評価.....	121
P. Kurinskiy (QST) <i>et al.</i>	
2.5 テクニカルセッション 2：特性評価	
2.5.1 空気と水蒸気雰囲気下でのベリリウム微小球の酸化試験.....	128
R.Rolli (KIT) <i>et al.</i>	
2.5.2 JET-ILW 材料から形成されるベリリウムダスト粒子の酸化.....	143

N. Ashikawa (NIFS) <i>et al.</i>	
2.5.3 先進的中性子増倍材としての 3 元系ベリライド微小球の研究開発.....	153
J.-H.Kim (QST) <i>et al.</i>	
2.5.4 ベリリウムの熱衝撃抵抗に関する研究.....	160
K. Yonehara (KAKEN) <i>et al.</i>	
2.5.5 アークプラズマを用いた新しいベリライドの製造技術.....	170
N. Ikemoto (KAKEN) <i>et al.</i>	
2.5.6 2 次球充填したベリリウム微小球充填体の熱伝導率.....	178
J.Reimann (KIT) <i>et al.</i>	
2.5.7 2 次球充填したベリリウム微小球充填体の熱クリップ特性.....	193
J.Reimann (KIT) <i>et al.</i>	
2.6 テクニカルセッション 3: 産業、安全問題	
2.6.1 アメリカにおけるベリリウム産業の進捗情報.....	206
K. Smith (Materion) <i>et al.</i>	
2.6.2 現在のベリリウム環境、健康そして安全規定活動の概要.....	228
D. Vidal (Materion) <i>et al.</i>	
2.6.3 NGK 社のベリリウム事業とベリリウム安全問題.....	241
K.Nojiri (NGK) <i>et al.</i>	
2.6.4 最新成果とベリライド応用に関する安全問題.....	250
A.Goraieb (KBHF GmbH) <i>et al.</i>	
2.6.5 六ヶ所研究所の設備紹介と安全管理.....	258
M.Nakamichi (QST) <i>et al.</i>	
2.7 テクニカルセッション 4: モデリング	
2.7.1 ベリリウム/ベリライド微小球の水化学反応における熱暴走のモデリング研究と DEMO 炉安全に及ぼす影響.....	271
M.Nakamura (QST) <i>et al.</i>	
2.7.2 核融合応用のための候補材としてのベリリウムとチタン系ベリライド (Be_{12}Ti)	279
D.Bachurin (KIT) <i>et al.</i>	
2.8 テクニカルセッション 5: 照射特性	

2.8.1	ベリリウム材料のイオン及び中性子照射試験.....	287
	S.-H.Kang (KAERI) <i>et al.</i>	
2.8.2	ベリリウムの微細組織に与えるアルゴンイオン照射効果.....	300
	P.Liu (USTB) <i>et al.</i>	
2.8.3	回転電極製のベリライド微小球の He イオン照射硬化研究の現状...	311
	T.Shibayama (Hokkaido Univ.) <i>et al.</i>	
2.8.4	低エネルギーイオン照射されたベリリウムにおける重水素と He 放出特性.....	320
	Y.Sugimoto (Shimane Univ.) <i>et al.</i>	
2.8.5	PISCES の高密度プラズマ照射によるベリリウムに露出されたタングステンの表面特性.....	333
	M.Miyamoto (Shimane Univ.) <i>et al.</i>	
2.8.6	プラズマに接する材料としてのベリリウム：強力且つ瞬間的なプラズマ熱負荷下での腐食と表面損傷挙動.....	344
	I. Kupriyanov (A.A.Bochvar) <i>et al.</i>	
付録	集合写真.....	354

1. Introduction

The 13th International Workshop on Beryllium Technology (BeWS-13) was held on 21-22 September at the Hilton Tokyo Narita Airport Hotel, Chiba, Japan. This workshop has been holding every 2 years from 1993. The objective of this workshop is to disseminate results of research and technology development in areas relevant to beryllium utilization in fusion nuclear power systems. In this workshop, a lot of researchers and technicians engaged in R&D on beryllium related materials and fusion engineering attended and discussed. This QST-P-3 has been compiled the manuscripts and the presentation files in the BeWS-13.

The BeWS-13 was divided into one keynote, one plenary and five technical sessions. As to the keynote, overview of fusion R&D in QST, Japan was presented by a vice-president (Dr. S. Ohira) of Rokkasho Institute, QST, demonstrating the overview and current status of Fusion R&D activities in QST.

In the plenary session, 5 presentations were delivered covering JET-ILW divertor tile and dust topics, reactor wall application, TBM/DEMO breeding blankets, development of TBMs and preparing their procurement in EU, JA KO, and Russia.

23 presentations were given as technical sessions as follows,

- 1) Fabrication process
- 2) Characterizations
- 3) Industry and safety issues
- 4) Modelling
- 5) Irradiation properties

In this workshop, there were 29 oral presentations with 35 attendees of 10 persons from EU, 17 persons from Japan, 2 persons from Korea, 2 persons from Russia, 3 persons from US and 1 person from China.

Prof. Mario Dalle Donne Memorial Award (MDDMA) has been established at previous BeWS-11 held in Barcelona for encouraging someone with outstanding achievements concerning beryllium-related research. It had been awarded to Dr. Joerg Reimann who engaged in KIT and have a lot of outstanding scientific achievement in the beryllium-related fields.

1.はじめに

第 13 回ベリリウム技術に関する国際会議(The 13th International Workshop on Beryllium Technology(BeWS-13))は、平成 29 年 9 月 21 日(木)及び 22 日(金)の 2 日間に渡り、日本千葉県のホテル東京成田空港ホテルにて開催された。本国際会議は、IEA 国際協力における核融合炉材料のフレームワークにおける活動で、1993 年から 2 年毎に開催されており、今回は 13 回目となる。本国際会議は、世界におけるベリリウム関連材料(ベリリウム金属及びその合金、金属間化合物など)と核融合炉工学研究開発に携わる研究者及び技術者が一同に会し、最新研究成果報告、討論及び情報交換を行うものであり、本テーマにおける研究活動の一層の活性化を図ることを目的としている。本報告書は、当該会議における論文及び発表資料を取りまとめたものである。

今回の BeWS-13 では、キーノートセッションとプレナリーセッションそして、5つの技術セッションに分かれて発表が行われた。

キーノートセッションは、QST 六ヶ所研究所の S.Ohira 副所長からの核融合 R&D 活動に関する最新成果及び概要の発表が行われた。プレナリーセッションとしては、5つの発表が行われ、JET-ILW ダイバータタイルやダストの最新成果、TBM/DEMO 増殖ブランケット研究、TBM 関連材料開発の最新成果、各国の材料準備状況等について議論が行われた。

5つの技術セッションは、以下の通りである。

- 1) 製造工程
- 2) 特性評価
- 3) 産業と安全問題
- 4) モデリング
- 5) 照射特性

本国際会議では、口頭発表件数が 29 件、参加者数は 35 名であり、その内訳は、欧州 10 名、日本 17 名、アメリカ 3 名、韓国 2 名、ロシア 2 名、中国 1 名であった。

ベリリウム微小球の充填体特性評価に関わる優れた研究功績が認められた KIT の Reimann 氏が、MDDMA 賞(Prof. Mario Dalle Donne Memorial Award (MDDMA))の受賞者として選出された。

2.1 Agenda of BeWS-13

BeWS-13 final program (21-22 September 2015)

Thursday, September 21

08:00 - 09:30 Registration open

08:00 - 09:00 Coffee break

Keynote Presentation

Chair : M. Nakamichi

Opening speech 09:00 09:10

S. Ohira QST, Japan 09:10 09:40 Overview of fusion R&D in QST

Plenary Session 1: Overview of Beryllium R&D

Chair : C.K. Dorn

N. Asakura QST, Japan 09:40 10:10 Broader Approach (BA) R&D research status of the JET-ILW divertor tile and dust in Rokkasho: Be deposition study

C.K. Dorn Be4FUSION, USA 10:10 10:40 Beryllium Materials for Fusion Reactor Wall Applications

10:40 - 11:00 Coffee break

V. Chakin KIT, Germany 11:00 - 11:30 Post-irradiation examination of beryllium pebbles from HIDOBE-02 experiment

Y.H.Park NFRI, South Korea 11:30 - 12:00 Status of Material development for HCCR TBM in Korea

R. Giniyatulin JSC "NIIIEFA", Saint Petersburg, Russia 12:00 - 12:30 Preparation for manufacturing of the beryllium armor of the ITER first wall in the Russian Federation

12:30 - 14:00 Lunch break

Technical Session 1 : Fabrication Process

Chair : J. Reimann

M. Nakamichi	QST, Japan	14:00	14:20	Overview of R&D on beryllide as advanced neutron multipliers in Japan
R. Fukatsu	NGK, Japan	14:20	14:40	Distribution of Beryllium Pebble Size by Rotation Electrode Process
P. Kurinskiy	QST, Japan	14:40	15:00	Trial fabrication and characterization of Be12V pebbles

15:00 15:30 Coffee break

Technical Session 2 : Characterizations

Chair : V. Chakin

R. Rolli	KIT, Germany	15:30	15:50	Experimental Study of Oxidation of Beryllium Pebbles in Air and Steam
N. Ashikawa	National Institute for Fusion Science, Japan	15:50	16:10	Beryllium oxide on dust particles produced by ITER like wall materials in JET
J.-H. Kim	QST, Japan	16:10	16:30	Ternary beryllide pebbles as advanced neutron multipliers
K. Yonehara	Kaken, Japan	16:30	16:50	A Study on Heat Shock Resistance of Beryllium
N. Ikemoto	Kaken, Japan	16:50	17:10	New method for beryllide production using arc plasma
J. Reimann	KIT, Germany	17:10	17:30	Thermal Conductivity of Compressed Binary Beryllium Pebble Beds
J. Reimann	KIT, Germany	17:30	17:50	Thermal Creep of compressed Binary beryllium pebble Beds

Workshop Banquet 19:00 Restaurant

Friday, September 22

Technical Session 3 : Industry and safety issues

Chair : C.K. Dorn

K. Smith	Materion Brush, USA	09:30	09:50	United States Beryllium Industry Update
E. Vidal	Materion Brush, USA	09:50	10:10	Overview of the current beryllium environmental, health and safety regulatory activities
K. Nojiri	NGK, Japan	10:10	10:30	Beryllium business of NGK Insulators and topics of beryllium safety issue
A. Goraieb	KBHF GmbH, Germany	10:30	10:50	Recent achievements and related safety issues concerning Beryllide applications
M. Nakamichi	QST, Japan	10:50	11:10	Facility introduction and safety issues in Rokkasho Institute, QST.

11:10 - 11:30 Coffee break

Technical Session 4 : Modelling

Chair : V. Kuksenko

M. Nakamura	QST, JAPAN	11:30	11:50	Modelling study of thermal excursion of chemical reactions of beryllium/beryllide pebbles with steam and its implication to fusion DEMO safety
D.V. Bachurin	KIT, Germany	11:50	12:10	Beryllium and titanium beryllide Be ₁₂ Ti as candidates for fusion applications

12:10 - 14:00 Lunch break

Technical Session 5 : Irradiation properties

Chair : D.V. Bachurin

S.H. Kang	KAERI, Korea	14:00	14:20	Ion and neutron irradiation tests on beryllium specimens
P. Liu	USTB, China	14:20	14:40	Effects of argon ion irradiation on microstructure of beryllium
T. Shibayama	Hokkaido University, Japan	14:40	15:00	Present status of He ion irradiation hardening of Japanese beryllide pebbles by REM
		15:00	15:40	Coffee break
Y. Sugimoto	Shimane University, Japan	15:40	16:00	Deuterium and helium properties in beryllium irradiated with low energy ions
M. Miyamoto	Shimane University, Japan	16:00	16:20	Surface property of tungsten exposed to beryllium containing high density plasma in PISCES
I. Kupriyanov	A.A. Bochvar High Technology Research Institute of Inorganic Materials, Russia	16:20	16:40	Beryllium as plasma facing material: Erosion and surface damage behavior under intense transient plasma heat loads

Adjourn

Sponsored by



2.2 Keynote session

2.2.1 Overview of fusion R&D in QST

S. Ohira

Rokkasho Fusion Institute

Fusion Energy Research and Development Directorate

National Institutes for Quantum and Radiological Science and Technology (QST)

E-mail: ohira.shigeru@qst.go.jp

National Institutes for Quantum and Radiological Science and Technology (QST) has a variety of rolls on fusion R&D in Japan, now mainly ITER and Broader Approach Activities as the Japanese Domestic/Implementation Agency for the both big international projects. For ITER, JADA(QST) procures many key components, such as Toroidal Field Coil, Center Solenoid Coil, Electron Cyclotron/Neutral Beam Heating systems, Divertor, Remote Handling System, Detritiation System, etc. JADA has signed 12 PAs, corresponding to about 90% in credit value out of total Japanese contribution to the ITER in-kind procurement. For Broader Approach Activities, started in 2007 in the framework of collaboration between Japan and EURATOM, aim at complementing the ITER project and at an acceleration of realization of fusion energy. Three research projects are to be undertaken: (1) International Fusion Energy Research Centre (IFERC), (2) Engineering Validation and Engineering Design Activities for the International Fusion Materials Irradiation Facility (IFMIF/EVEDA), and (3) Satellite Tokamak Programme. In IFERC project, the DEMO Design activity implements work on DEMO pre-conceptual design, and DEMO R&D activity addressed five tasks, focused on the materials and components for breeding blankets and on the technology of tritium production and extraction and also Computational Simulation Center for simulation studies for DEMO Design including that for safety, material design/analysis, etc. In the IFMIF/EVEDA project, its engineering validation is still on going for the IFMIF Prototype Accelerator (LIPAc) expected to produce D⁺ beam with 125 mA, 9 MeV is being carried out at the IFERC site in Rokkasho by 2020. While the Satellite Tokamak Programme (JT-60SA) is to be conducted at the site of the former JT-60 tokamak in Naka. JT-60SA has about half-size plasma of ITER for exploring and optimizing operation scenarios of ITER and DEMO with flexible plasma shaping capability. One of the main mission is to conduct long-pulse high performance operation up to 100s under the powerful auxiliary heating of 41 MW at the final stage. The first plasma is planned in 2020.

In parallel with these BA Activities, the Japanese Test Blanket Module (TBM) program is ongoing. The TBM program is a unique project to compete the test module of each ITER joint party in ITER. The Japanese TBM is featured by water-cooled ceramic breeder to easily conduct the power generation technology in future. The coolant conditions is 15.5 MPa of pressure and about 300°C of temperature. Several safety demonstration tests are planned on the real scale module. The conceptual design of Japanese TBM was accepted in 2016 by

ITER Organization and the final design will be completed after the safety demonstration tests in 2022 utilizing a new facility planned in Rokkasho.

Overview of fusion R&D in QST



Shigeru O'hira

National Institutes for Quantum and Radiological Science and Technology (QST)
Directorate of Fusion Energy Research & Development
Rokkasho Fusion Institute

1



Fusion R&D in QST



QST has made comprehensive progress in research and development on ITER, BA, fusion plasma and technologies.

- **Activities related to the ITER Project**
- **Activities related to the three projects of the BA Activities**
- **Other Fusion Research and Development**
 - International collaboration (US, KO, CN, IAEA, IAE, etc.).
 - Test Blanket Program
 - Domestic R&D program

2

Activities for Fusion R&D in Japan by QST and ...

From April 2016

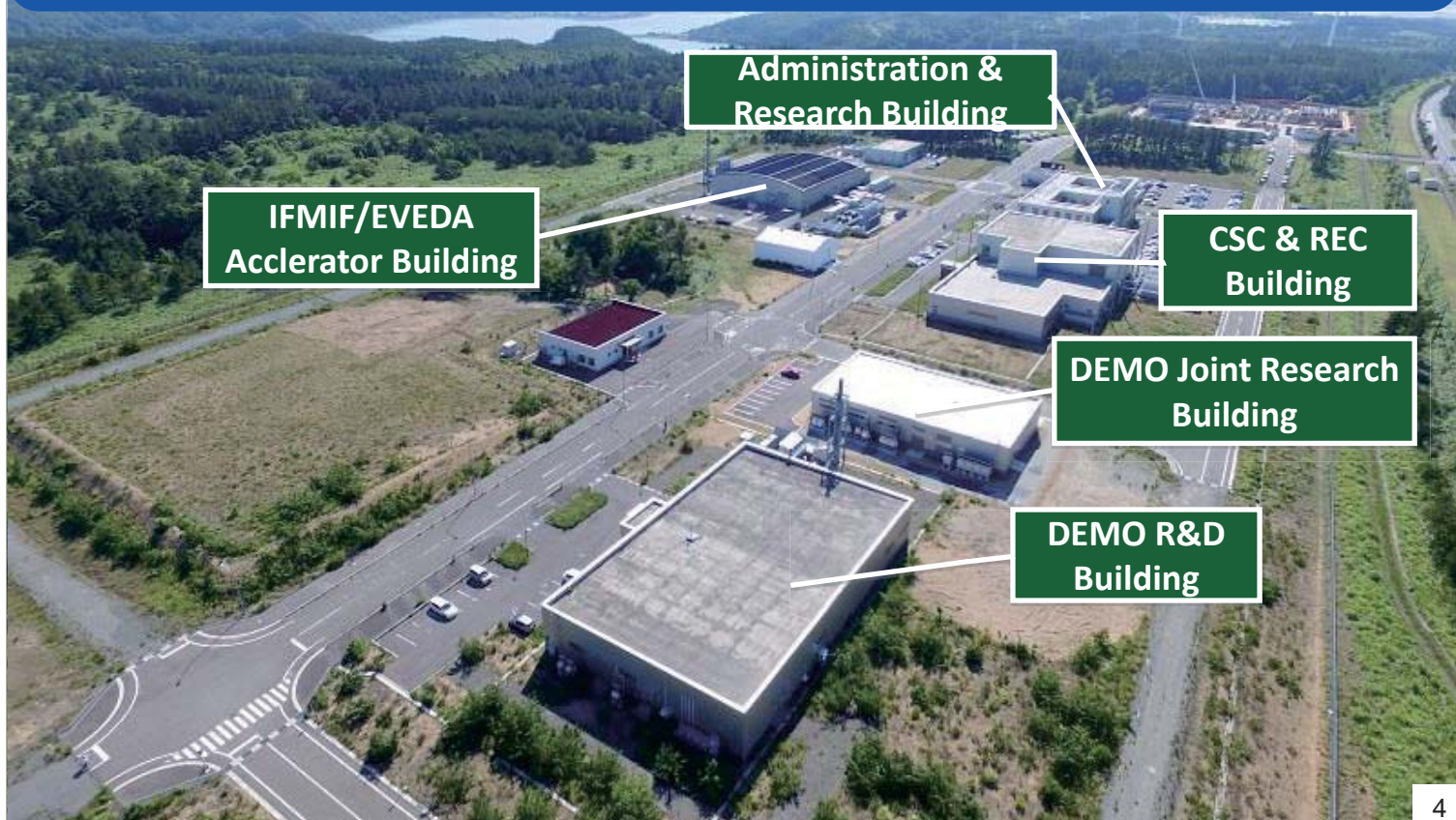
Directorates of Quantum Beam Science and Fusion R&D were separated from  and merged to National Institute of Radiological Sciences, and then  was established.



QST: National Institutes for Quantum and Radiological Science and Technology

3

Rokkasho Fusion Institute International Fusion Energy Research Centre



4

Naka Fusion Institute

Purchasing new power supply devices is minimized by the maximum reuse of existing thyristor converters and others.

RF heating system
Three type of heating systems (IC: 120MHz, LH: 2GHz, EC: 110GHz) produces over 10 MW, which is one of the largest RF systems in worldwide

Ion source of N-NBI heating system
Plasma input power of 40 MW by P-NBI is the largest record in the world, the beam energy of 500 keV in N-NBI is the highest as used in experiments

Secondary Water Cooling Tower
Central Power Sub-Station
Motor-Generator Building
Rectifier Building
JT-60 Tokamak Building
High Pressure Machinery Building
Primary Water Cooling Tower
Power Supply for Heating Systems
Central Control Room

One of the largest tokamak deives in the world which can produce 3 MA plasmas with the magnetic field of 4 T.

Transformer Yard
The electric devices which handles the maximum power of ~1.3 GW in nominal operation.

Motor-Generatos
The total capacity is ~1.1GW, which is the world record class as flywheel generators.

Electricity Receiving Transformer at 275 kV Power Grid

New Tokamak Machine with renewal of main components such as Magnets, Vacuum vessel

15 m
14 m

JT-60U Storage Building

Central Power Sub-station

Electricity Receiving Transformer at 275 kV Power Grid



Roadmap to Fusion Energy

3rd phase of the fusion R&D plan by the Atomic Energy Commission, June 1992

Plasma Experiment Phase

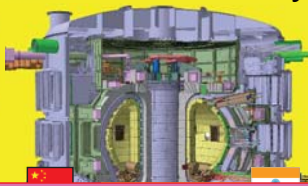
Scientific feasibility

Experimental Reactor Phase

Scientific/Technical Feasibility

ITER

•500 MW Fusion power



Electricity Production

Fusion DEMO



Power of ~1GW

ITER is the core machine in 3rd phase of the fusion R&D plan, and it is an "experimental reactor of Japan" being constructed in France under international collaboration

Support ITER

Broader Approach

For early realization of DEMO

Rokkasho, Aomori

R&D for Producing Fusion Electricity
IFERC, IFMIF/EVEDA

Naka, Ibaraki

Satellite Tokamak
JT-60SA

In Japan

JA-EU
Collaboration



Establish Engineering Basis for DEMO



1985~

2007~

Middle of 21st century

QST Key R&D for Fusion DEMO Reactor

Fusion Plasma

ITER



Saint-Paul-les-Durance, France

BA activities

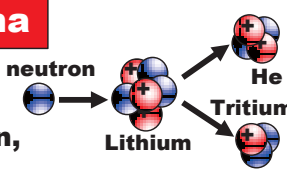
JT-60SA



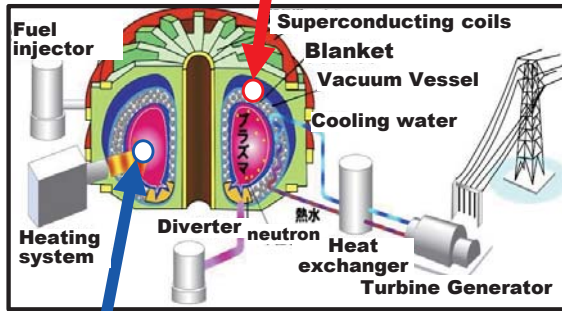
Naka, Ibaraki Japan

Outside of plasma

Robust Material against high heat flux and neutron irradiation, Production of Tritium

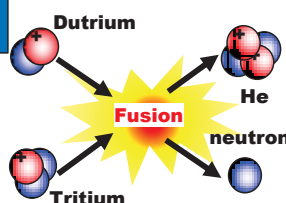


neutron → Lithium → He, Tritium



Inside of Plasma

Control of burning plasma, High performance of plasma operation

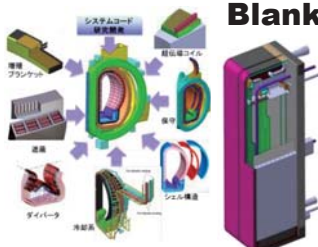


Deuterium + Tritium → Fusion → He, neutron

Fusion Engineering


BA activities

IFERC: Reactor design/R&D



Blanket

IFMIF/EVEDA: Accelerator type Neutron source (for Material R&D)




Rokkasho, Aomori



QST Japanese In-Kind Procurement for ITER

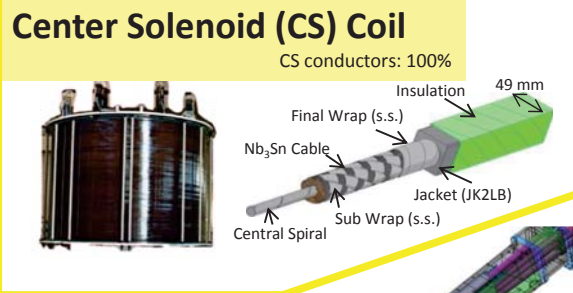
Toroidal Field (TF) Coil

TF Conductors: 25%
TF winding, assembly: 47%
TF Structures: 100%



Center Solenoid (CS) Coil

CS conductors: 100%



Diagnostics

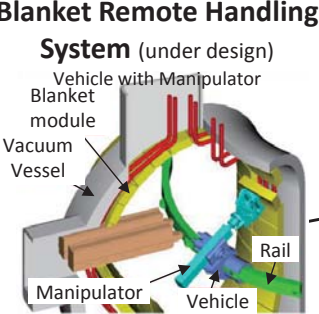
(under design)

- Micro Fission Chamber
- Poloidal Polarimeter
- Edge Thomson Scattering
- Divertor Impurity Monitor
- IR Thermography
- Thermocouples
- Upper Port Integration
- Lower Port Integration

Blanket Remote Handling System

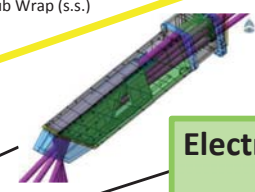
(under design)

- Vehicle with Manipulator
- Blanket module
- Vacuum Vessel
- Rail
- Manipulator
- Vehicle




Electron Cyclotron H&CD

Equatorial Launcher
Gyrotron



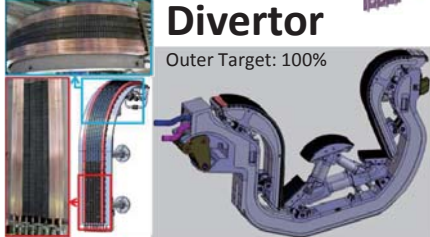
Neutral Beam H&CD

HV Bushing: 100%
1 MV Power Supply HV part: 100%
1 MeV Accelerator: 33%




Divertor

Outer Target: 100%

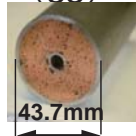



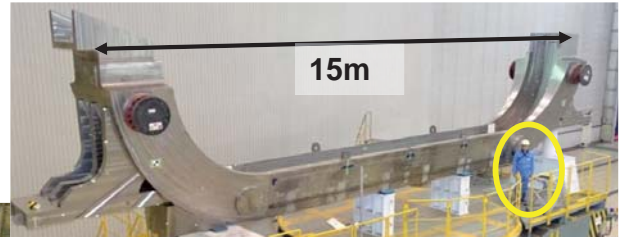




Detritiation System (ADS, under design)

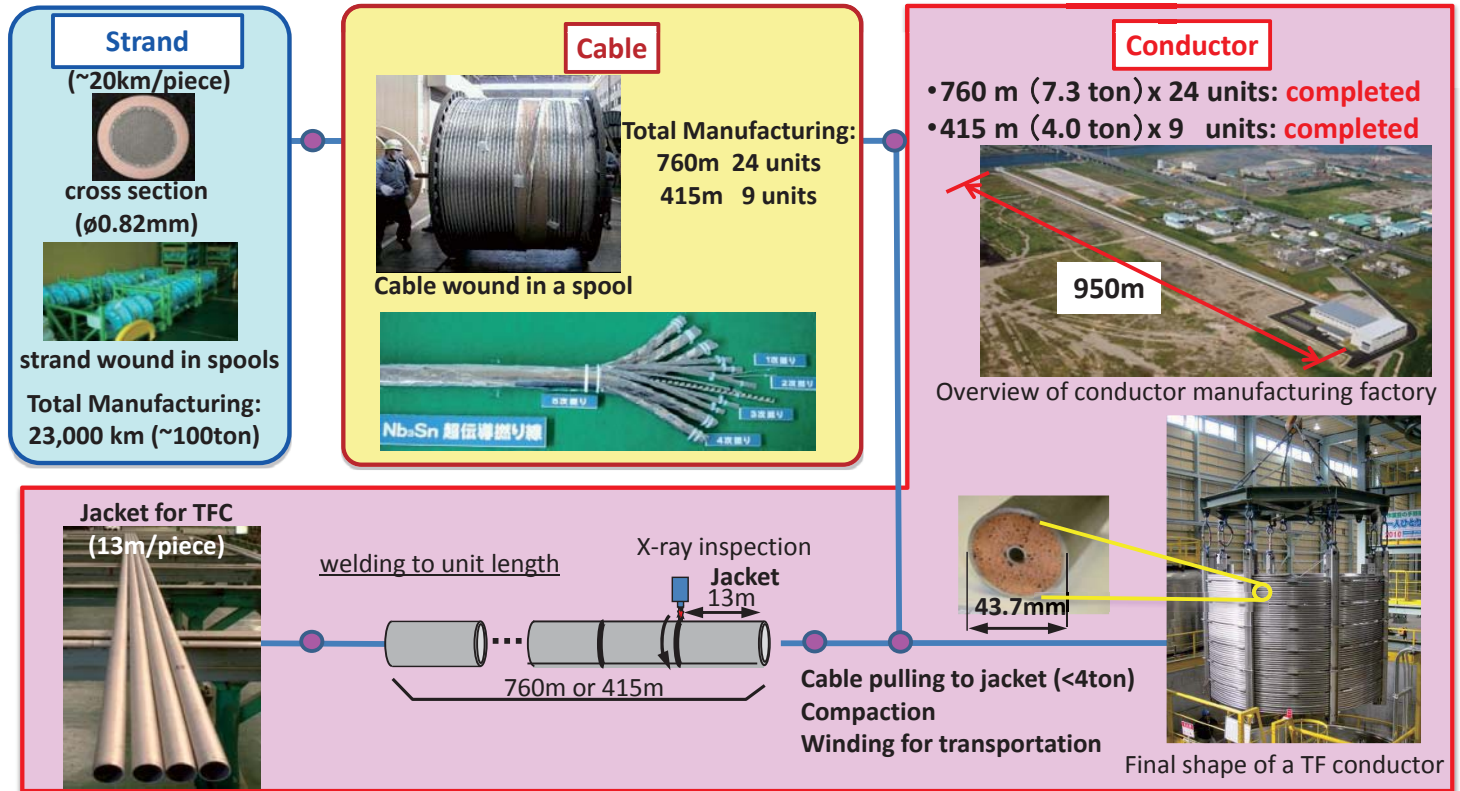


QST ITER TF Coils: Fabrication flow of the TF coil

JA-DA (QST) has procured TF coil itself and its structural parts. Winding for the first TF coil and Inboard Sub-assembly consisting of 3 basic segments were completed

TF conductor (33)	Winding (for 9 TF coils)	(Structure (19))	Full assembly (for 9TFcoils)
 43.7mm			 15m
<p>Completion of all conductors by JA-DA (Dec. 2014)</p>			<p>2 Inboard Sub-assemblies have been shipped.</p>  15m
	<p>Insulation wrapping of first 7 DPs stacked for TF#1 was completed in Jan. 2017</p> 		<p>Outboard Sub-assembly : Final machining for the first assembly was completed</p> 
	<p>Insulation wrapping for TF#2 was completed in August</p>		

TF and CS conductors



JA-DA has successfully completed procurement of all TF conductors. 84% CS conductors has completed, and 69% already shipped to US.

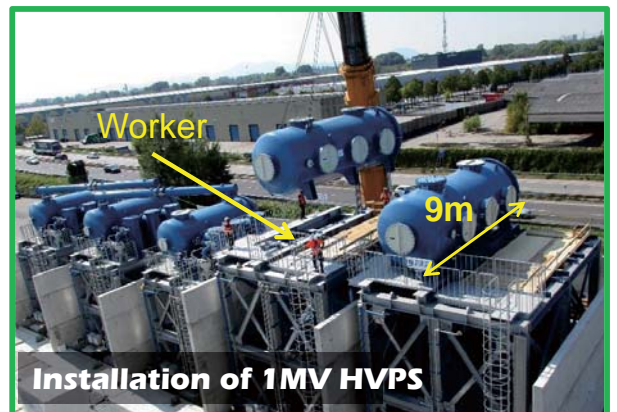
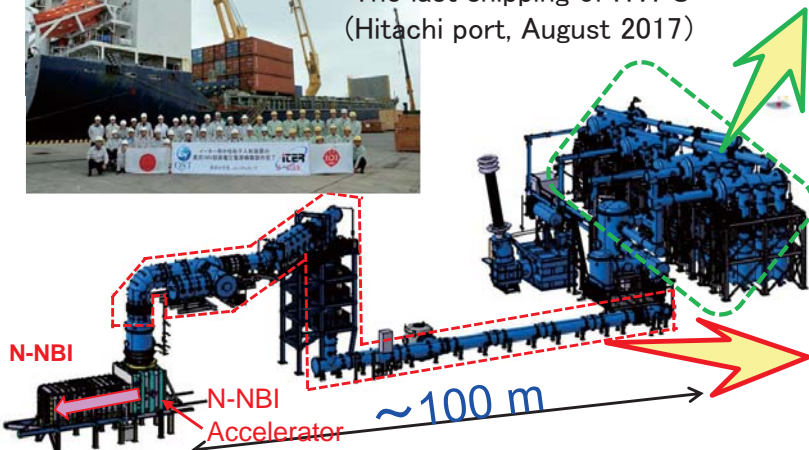
Neutral Beam Test Facility

Development and production of DC ultra-high voltage power supply equipment generating hydrogen negative ion beam with energy 1 MeV and current 40 A for neutral particles (Performance required for High Voltage Power Supply (HVPS))
Voltage: 1 MV, Current 60A, Pulse length : 3600 sec.

- All HVPS(14) have been manufactured.
- Shipping to Padova Italy has been completed in Sep. 2017. Installation to NBTf is undergoing.
- In 2018, the integration test with European equipment will be carried out.



The last shipping of HVPS (Hitachi port, August 2017)

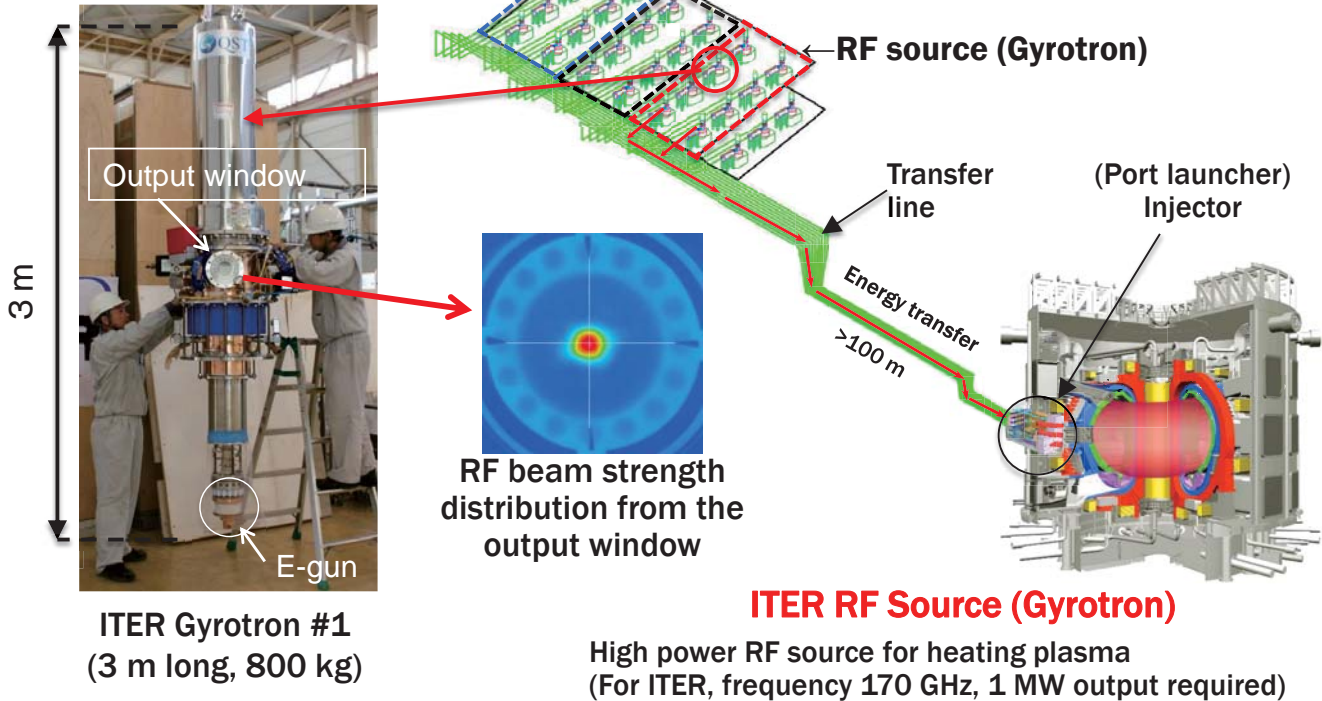


Transmission line assembly: Multiple high-voltage conductors are mounted in the pressure vessel



- ITER RF source (Gyrotron) #1 and #2 were completed in February 2017.
- 170 GHz, 1 MW output (short pulse) was confirmed in July 2017.

RF Heating System Overview

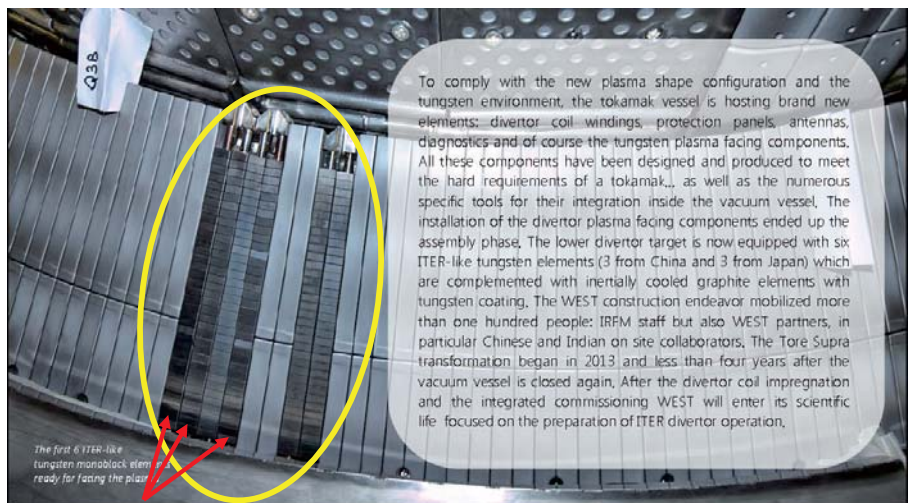


QST Full Tungsten Divertor Outer Vertical Target (OVT):

QST has completed manufacturing of plasma facing units (PFUs) for the CEA WEST-project to support QST's ITER divertor OVT procurement. Three PFUs, which simulate the ITER divertor OVT, have been installed in Tore Supra tokamak in CEA, and the first plasma was achieved in Dec. 2016. The plasma irradiation experiment is scheduled in 2017. The manufacturing of ITER full-W divertor OVT prototype will start in late 2017.



Witnessing of CEA's acceptance test by QST member.



QST's PFUs

ITER divertor-like PFUs have successfully been installed in Tore Supra. (<http://west.cea.fr/Images/astImg/53/Newsletter-WEST15.pdf>)

QST Detritiation System : Qualification Activity

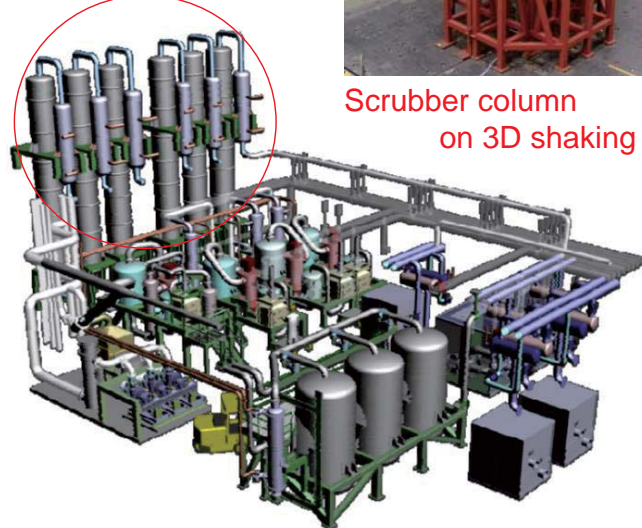
Joint procurement of detritiation system has been progressed between IO and JADA .

PA on Detritiation System Qualification activity (DSQ) was signed (2015.9) and DSQ activity has been conducted in Japan. The main progress of the last fiscal year was the shaking table test of a scrubber column in order to qualify the negligible earthquake vibration impact on detritiation performance (2017.3).

Scrubber (SC) columns



Scrubber column on 3D shaking table



Bird view image of ITER Detritiation System for Tokamak Building



Pilot scale experimental apparatus for qualification of detritiation performance of scrubber column

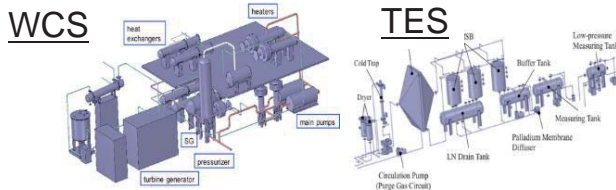
15



ITER-TBM activity

Water Cooling Ceramic Breeder (WCCB)-TBS

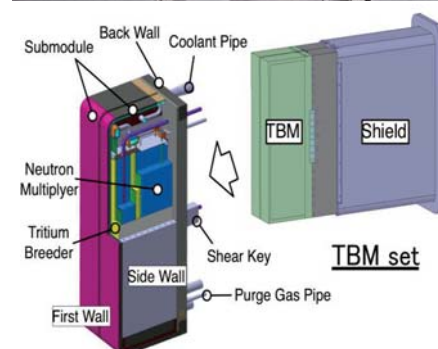
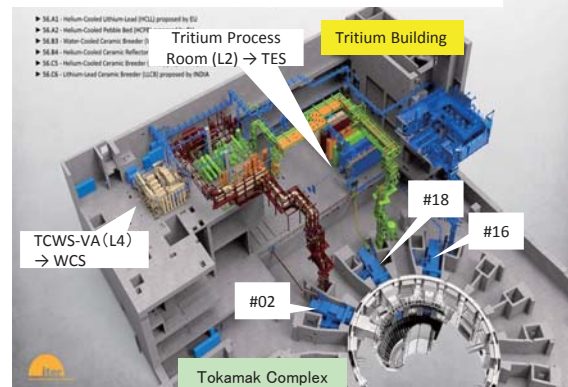
A water cooled ceramic breeder test blanket system (WCCB-TBS) is proposed by Japan as primary option for the Test Blanket Module (TBM) program of ITER.



WCCB-TBS consists of

- TBM set (TBM + Shield)
- Water Cooling System (WCS)
- Tritium Extraction System (TES)
- Neutron Analysis System (NAS)
- Tritium Analysis System (TAS)

Structural Material	F82H
Size	H1.67m x W0.462m x T0.6m
Surface Heat Flux	0.3 MW/m ²
Neutron Wall Load	0.78 MW/m ²
Breeder	Li ₂ TiO ₃ 37 kg
Multiplier	Be 200 kg
Coolant	Water 15.5 MPa, 280-325 °C
	Flow Rate 3.59 kg/s



16

Kick-off meeting for Preliminary Design Phase was held at QST(Naka)

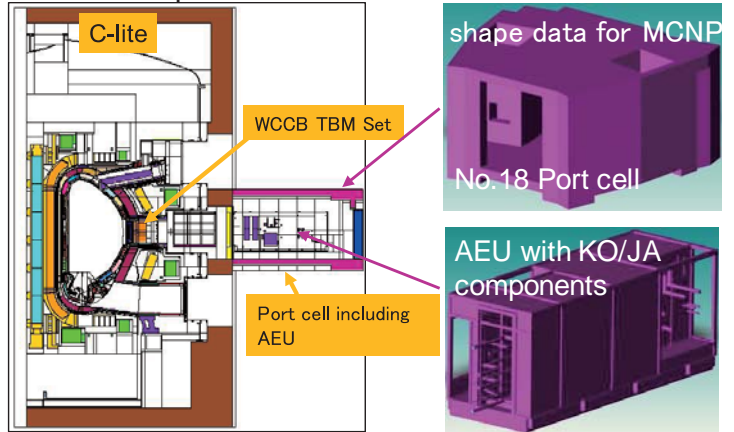
- Conceptual design of WCCB-TBS was approved in November 2016.
- Kick-off Meeting for Preliminary Design of WCCB TBS was held on 4-6th April 2017.



Kick-off Meeting for PD of WCCB-TBS

JA/KO joint activity on Nuclear analysis for TBM Program Safety Demonstration

- JA and KO have joint activity for TBM Program Safety Demonstration (TPSD).
- JA Team developed MCNP models for Port cell and AEU with KO/JA components.



Embedding shape data of Port Cell including AEU to C-lite

- JA will assess Shut Down Dose Rate in Port cell area by use of C-lite.



Activities related to the three projects of the BA Activities

3rd phase of the fusion R&D plan by the Atomic Energy Commission, June 1992

Plasma Experiment Phase

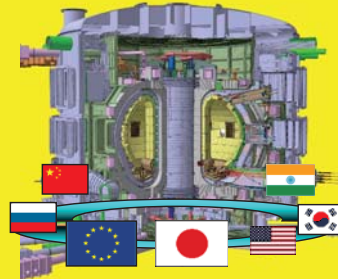
Scientific feasibility

Experimental Reactor Phase

Scientific/Technical Feasibility

ITER

- 500 MW Fusion power
- Continuous fusion burning



Support ITER

Electricity Production

Fusion DEMO



Electric Power of 0.3~1GW

Establish Engineering Basis for DEMO

Broader Approach In Japan

For early realization of DEMO

Rokkasho, Aomori

R&D for Producing Fusion Electricity
IFERC, IFMIF/EVEDA

Naka, Ibaraki
Satellite Tokamak
JT-60SA

JA-EU
Collaboration



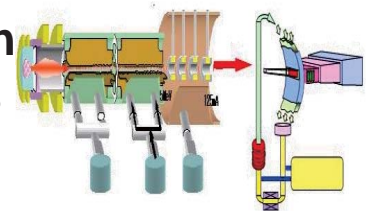
JT-60

1985~

2007~

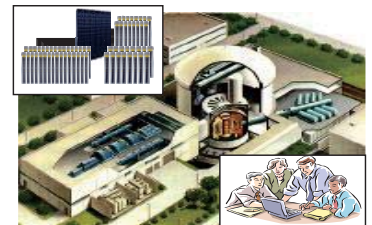
Middle of 21st century

1) **Engineering Validation and Engineering Design Activities for the International Fusion Materials Irradiation Facility (IFMIF/EVEDA:2007-2020)**



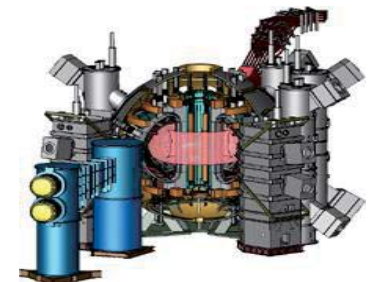
2) **International Fusion Energy Research Centre (IFERC:2007-2020),**

- DEMO Design and R&D coordination Centre
- Computational Simulation Centre
- ITER Remote Experimentation Centre



3) **Satellite Tokamak Programme (2007-2020)**

Participation to upgrade of JT-60 Tokamak to JT-60SA and its exploitation.



IFERC Activity

(International Fusion Energy Research Center)

DEMO Design



- Gap study between ITER and DEMO
- Analysis on critical design issues
- System design and design integration toward DEMO conceptual designs

DEMO R&D

Tritium Breeder

neutron multiplier

neutron

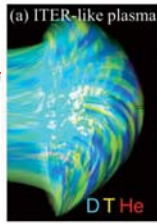
Tritium Collecting gas

Cooling water

- Advanced neutron multiplier
- Tritium Breeder
- Reduce Activation Ferritic Steel
- SiC/SiC
- Tritium Diagnostics and Control

Blanket

Computer Simulation



- 1.23 Pflops (mission complete) + 0.2 Pflops (cont.)
- About 5 years, ~600 papers with ~600 EU-JA users
- Utilization rate: more than 90%
- Activity was successfully completed by Dec. 2018.

ITER Remote Experimentation



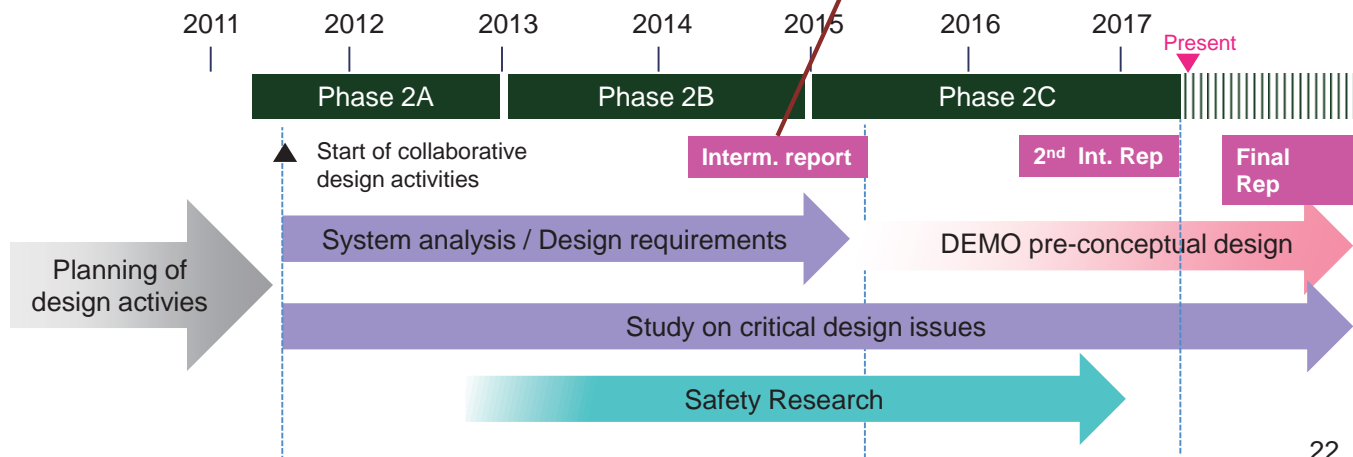
- Technical infrastructure for Remote Experimentation
- Succeed High Speed Data Transportation from ITER to Rokkasho in Aug. 2016: ~8Gbps

Outline of DEMO Design Activities

- Pre-conceptual design of possible DEMO options will be fulfilled addressing critical DEMO design issues.
- The Second Intermediate Report is completed, which describes possible solutions and unsolved issues on DEMO.



Discussion to make the Intermediate report (Nov. 2014)



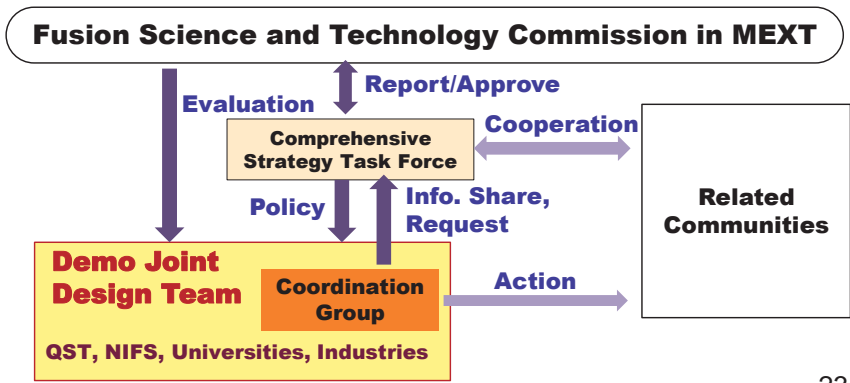
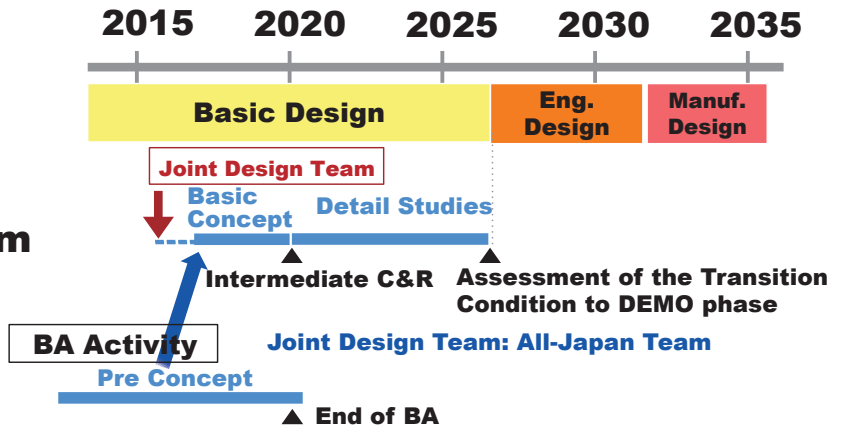
From 1st June 2015, the DEMO Joint Design Team made a start in Rokkasho Fusion Institute.

Joint Design Team: 81 staffs including Part time staffs from Universities and Industries

Intermediate C&R : ~2020

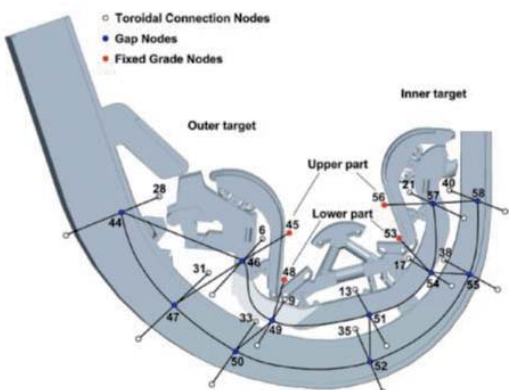
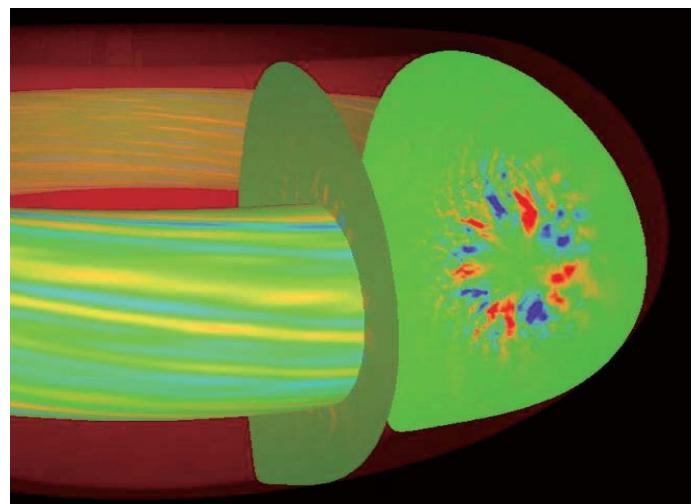


First Meeting at 18th June, 2015



Fast particle Physics

MHD instabilities driven by energetic alpha particles and beam deuterium particles were investigated for ITER operation scenarios using a hybrid simulation MEGA code for energetic particles interacting with an MHD fluid. For the ITER steady-state scenario with 9MA plasma current, β -induced Alfvén eigenmodes (BAE modes) with low toroidal mode number ($n = 3, 5$) were found to become dominant in the nonlinear phase although many TAE with $n \sim 15$ are most unstable in the linear phase. (Y. Todo)



Reactor Technology

An integrated software tool for modelling and simulation of complex gas distribution systems operating under any vacuum conditions was developed and validated. Detailed calculations were performed of the flow patterns and paths in the ITER cassettes, in the gaps between the cassettes and along the divertor ring, as well as of the total throughput for various pumping scenarios and dome pressures (Vasileiadis et al.)

Fusion Computational Simulation Centre

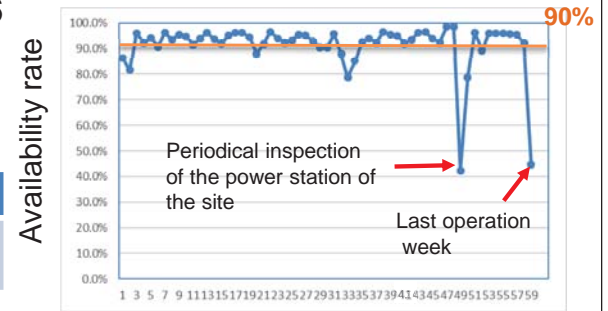


- ◆ As scheduled in the BA agreement, CSC was started from Jan. 2012 and was closed at the end of Dec. 2016 after 5 years operation.
- ◆ CSC HPS, Helios, had been used very heavily by EU and JA users.

cycle	1 st	2 nd	3 rd	4 th	5 th
Weekly average availability rate*	65.6%	85.9%	89.7%	91.4%	91.3%

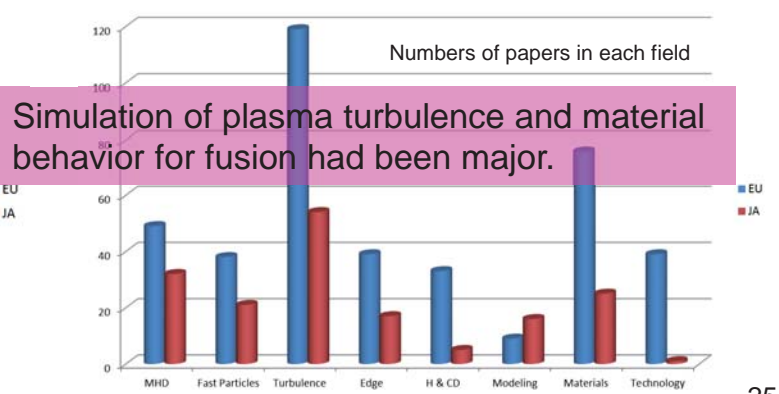
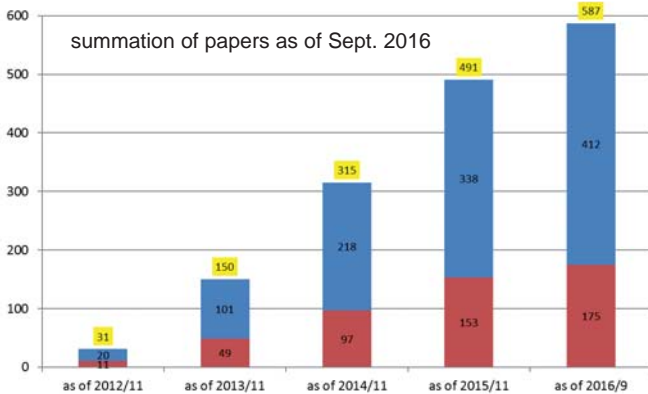
*: except for maintenance week

Weekly average availability rate (the 5th cycle)



Min 16.4% (the 1st week in the 1st cycle) → Max 98.6% (the 47th week in the 5th cycle)

◆ 587 papers with peer review have been by JA and EU users, by the end of Sept. 2016.

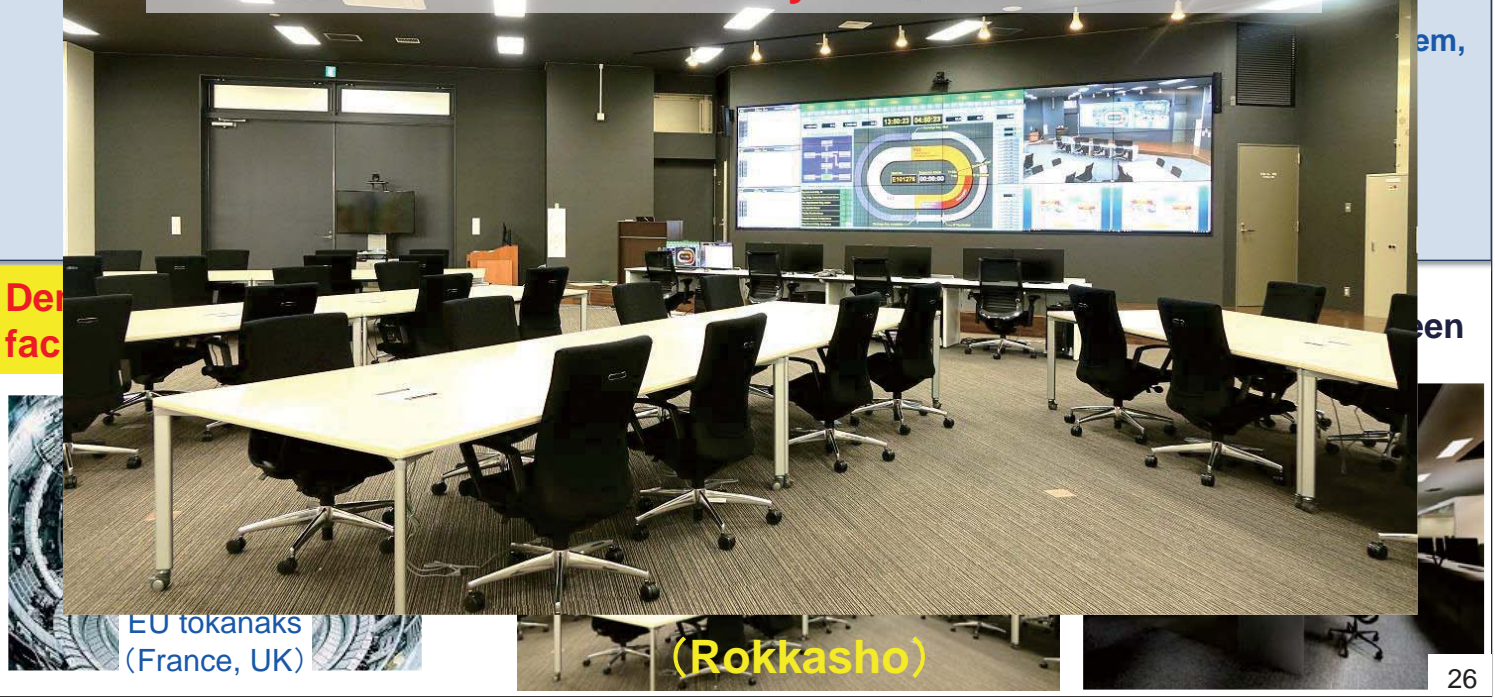


ITER Remote Experimentation Centre (REC)



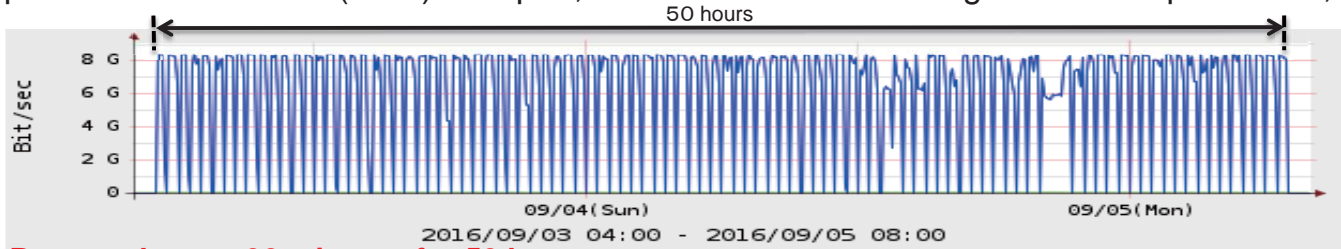
The facility and equipment for the ITER Remote Experimentation Centre (REC) is being prepared in the IFERC site.

Now the real ITER Remote Experimentation Centre is ready!



ITER Remote Experimentation Centre (REC) IFERC

Repeated transfer of 1 Tera Byte (TB) data within 30 minutes, which are the conditions assumed in the initial experiments of ITER, from ITER in France to ITER Remote Experimentation Centre (REC) in Japan, was demonstrated in August 30 to September 5, 2016.



Repeated every 30 minutes for 50 hours

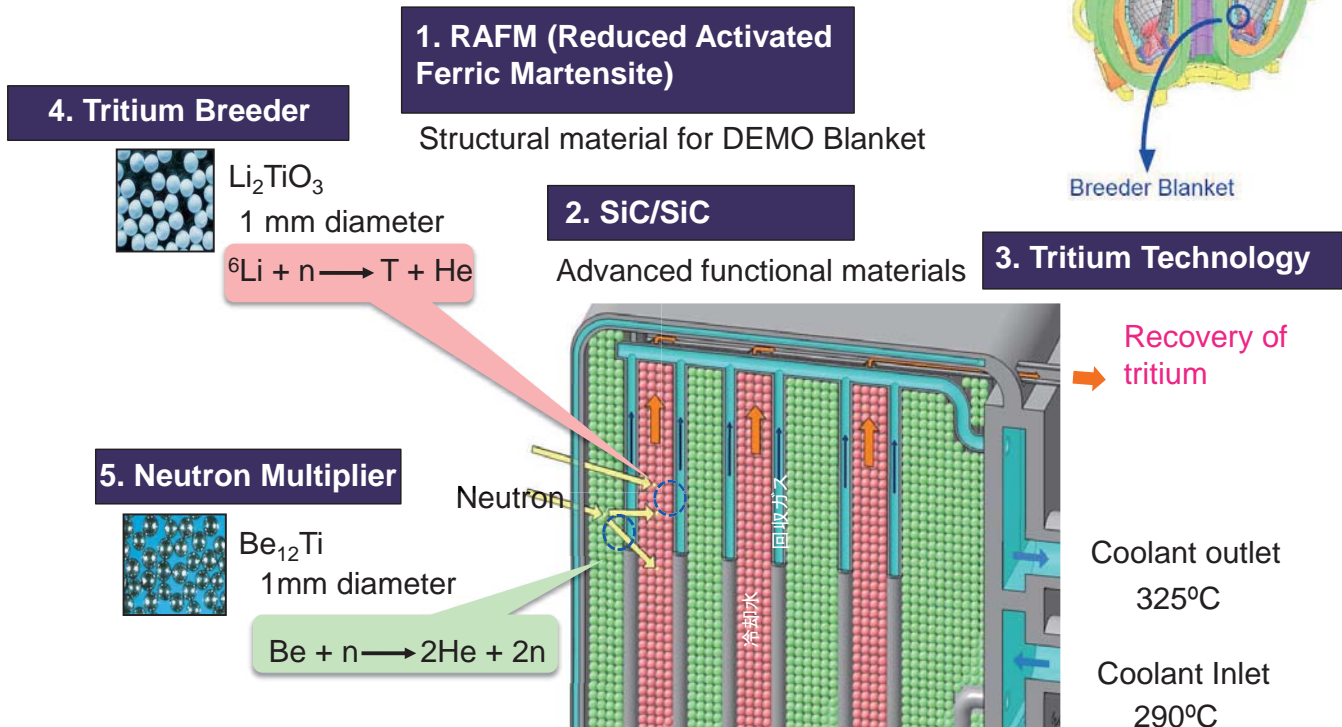
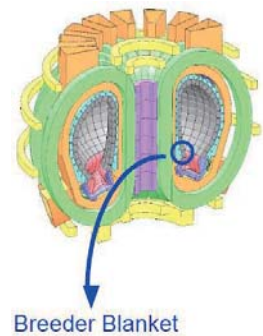


Reported in ITER Newline (10 Oct. 2016)
<http://www.iter.org/newsline/-/2547>

BA-R&D on Nuclear Technology for DEMO Reactor

BA Activities

Five R&D subjects for DEMO Blanket from 2007 to 2017 (extension to end of March 2020)



R&D on RAFM

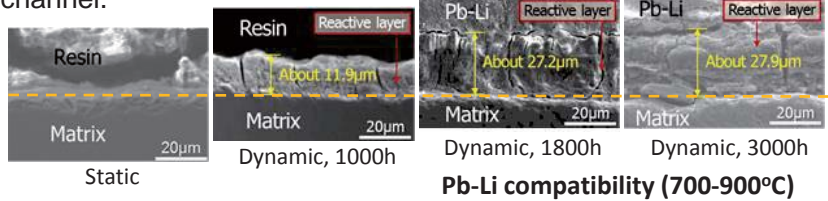
In order to simulate fusion-neutron irradiation effects with ion beam irradiation experiments, micro-specimen for tensile test has been developed. A successful result was obtained.



R&D on SiC

Functional structure applications in the advanced blanket system, e.g., flow channel.

Pb-Li compatibility of CVD SiC and CVI SiC/SiC composite was measured, demonstrating no accelerating corrosion by liquid Pb-Li flow at 700-1000°C up to 3000h.

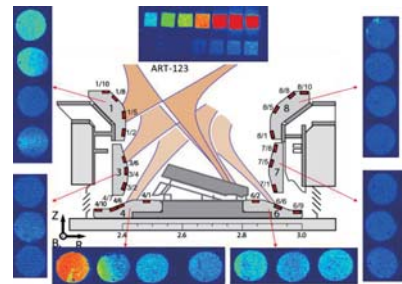


R&D on Tritium Technology

Basic Tritium data in several key materials -RAFM, W.

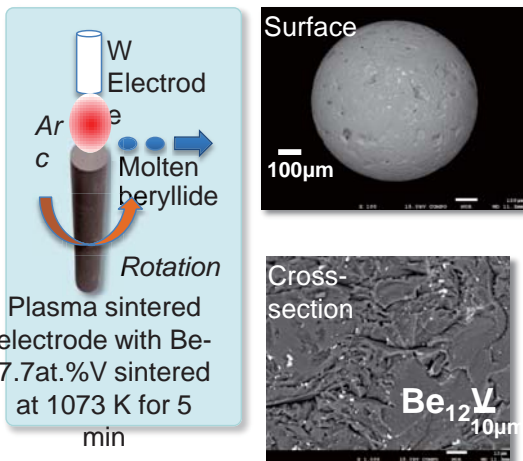
Tritium Durability Test –organic compounds, stainless steel.

Analysis of JET tiles (Evaluation of amount of tritium in tiles and dust etc.)



R&D on Neutron Multiplier

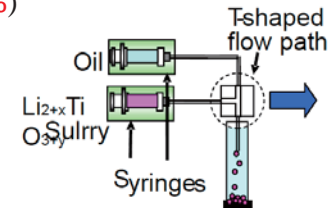
A new beryllide granulation process that combined processes with a plasma sintering method and REM (Rotating Electrode Method) was developed. Be₁₂V pebbles were successfully made.



- Be₁₂V single phase pebbles demonstrated a lower reactivity than Be pebbles.
- H₂ generation ratio of Be₁₂V is two orders of magnitude less than that of Be.

R&D on Tritium Breeder

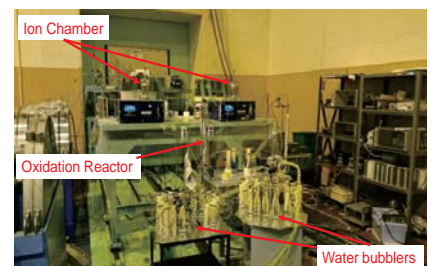
R&D on fabrication and characterization of advanced tritium breeders (The addition of Li into Li₂TiO₃ 10%)



This granulator consisted of two syringes, a T-shaped flow path and an oil-filled container. The size of the gel particles could be controlled by the flow speeds of oil and slurry.

R&D on Tritium release properties

The released amount of HT gas was greater than the released amount of HTO water vapor.



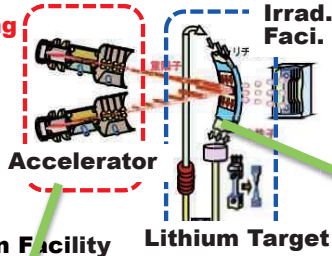
International Fusion Material Irradiation Facility (IFMIF)

Confirm soundness of fusion materials under strong neutron irradiation from Fusion Demo Plasma

Engineering Design and Engineering Validation Activities (EVEDA)

Engineering Design and Validation of Key Components in IFMIF

Prototype Accelerator, Lithium Target, Irradiation Facility



Engineering Design: Completed in 2013

Lithium Target Validation

The validation test using the test loop was successfully completed in 2014.



Lithium Flow (20 m/s)

IFMIF/EVEDA Prototype Accelerator (9MeV, 125mA, D+ beam)

World longest RFQ (~10m): transported from INFN @Legnaro Italy, ready for operation at Rokkasho (0.1 MeV > 5MeV, 125mA)

In construction at CEA France (5 MeV > 9MeV, 0.125mA)

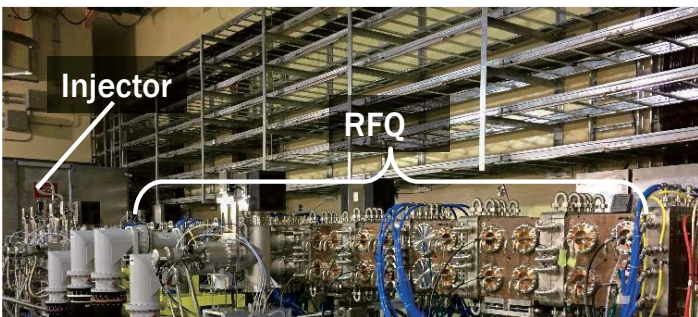
Validation was completed in Mar. 2016 (0.1MeV, 125mA)

In construction at CEA France (5 MeV > 9MeV, 0.125mA)

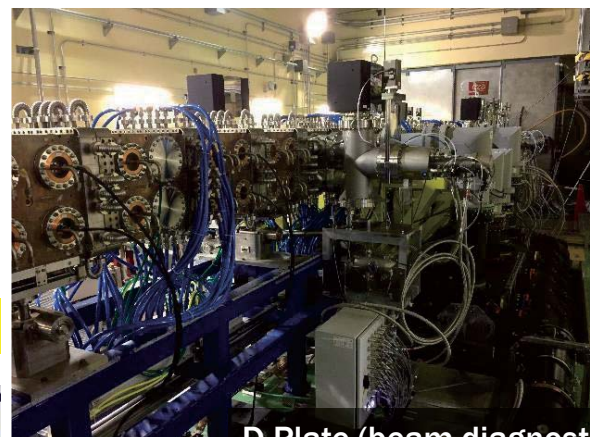
Status of LIPAc

BA Activities

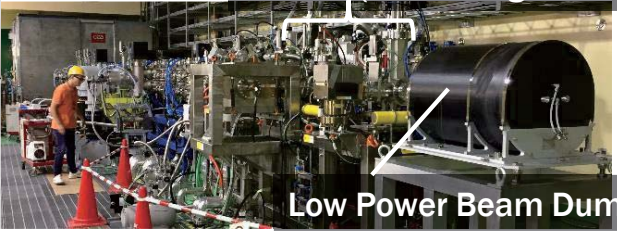
Installation of beam line including components, RFQ, MEBT, D-Plate and LPBD has been completed. Check-out and pre-commissioning has been started in June 2017. Conditioning and test operation of RFQ will start from Oct. 2017.



First RF introduction from 8 RF modules!



D-Plate (beam diagnostics)



Low Power Beam Dump

The JT-60SA Project(Naka city, Ibaraki prefecture)

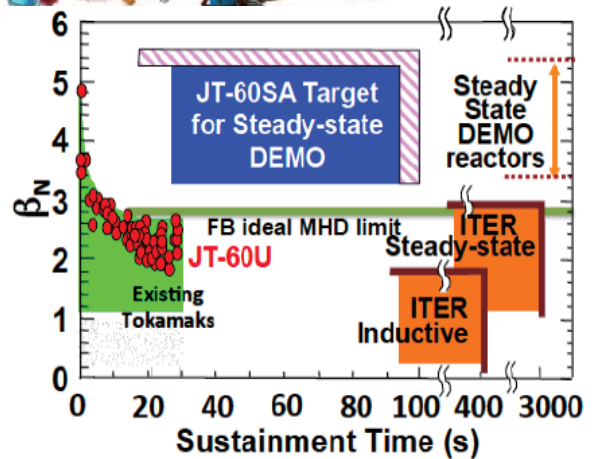
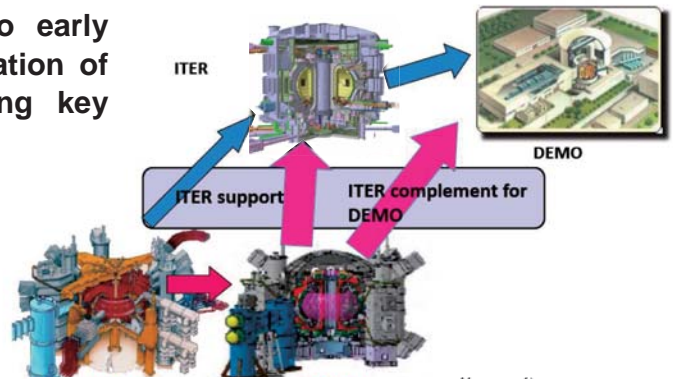
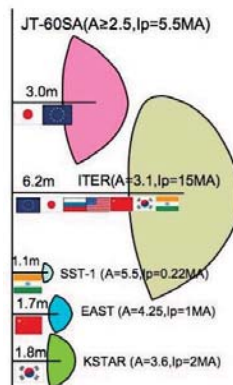
BA Activities

The JT-60SA project mission is to contribute to early realization of fusion energy by supporting exploitation of ITER and by complementing ITER with resolving key physics and engineering issues for DEMO reactors.

JT-60SA is a fully superconducting, highly shaped large tokamak capable of confining break-even equivalent class deuterium plasmas (I_p -max=5.5 MA) lasting for a duration (typically 100s) longer than the timescales characterizing the key plasma processes, such as current diffusion and particle recycling with high heating power (41MW).

JT-60SA should pursue full non-inductive steady-state operations with high β_N (> no-wall ideal MHD stability limits).

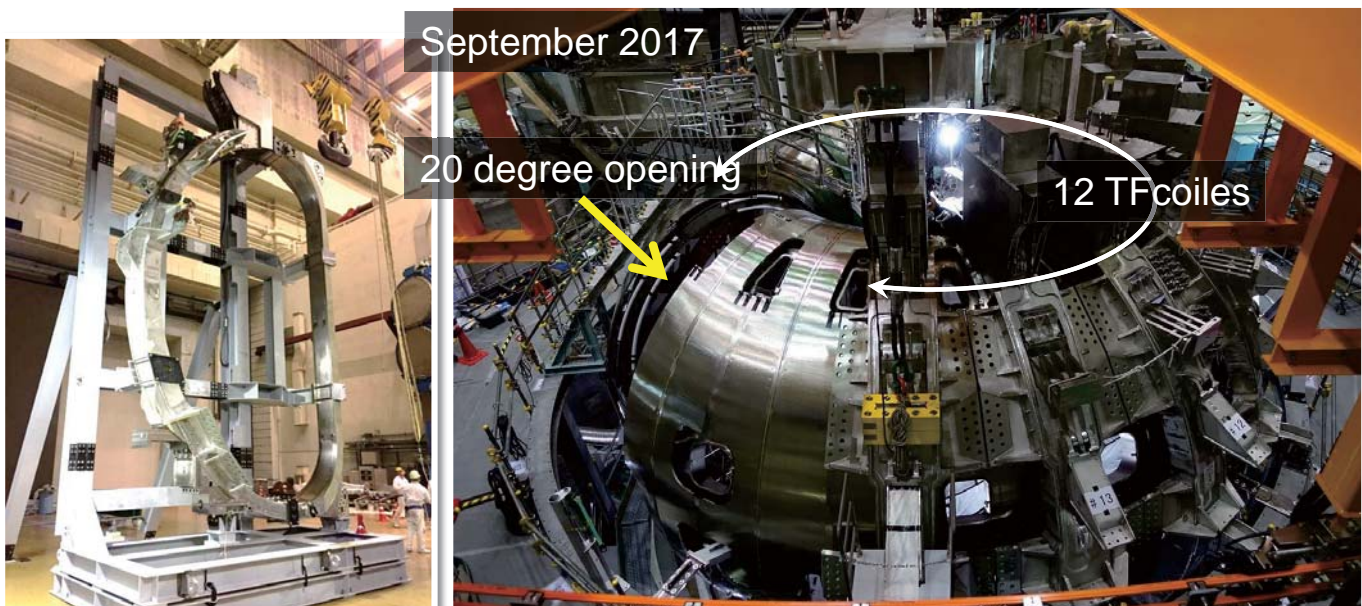
N-NB 500keV 10MW (Co)
P-NB 85keV 24MW (Co, Ctr, Bal)
ECH 110 GHz 7MW



33

The JT-60SA Project(Naka city, Ibaraki prefecture)

BA Activities

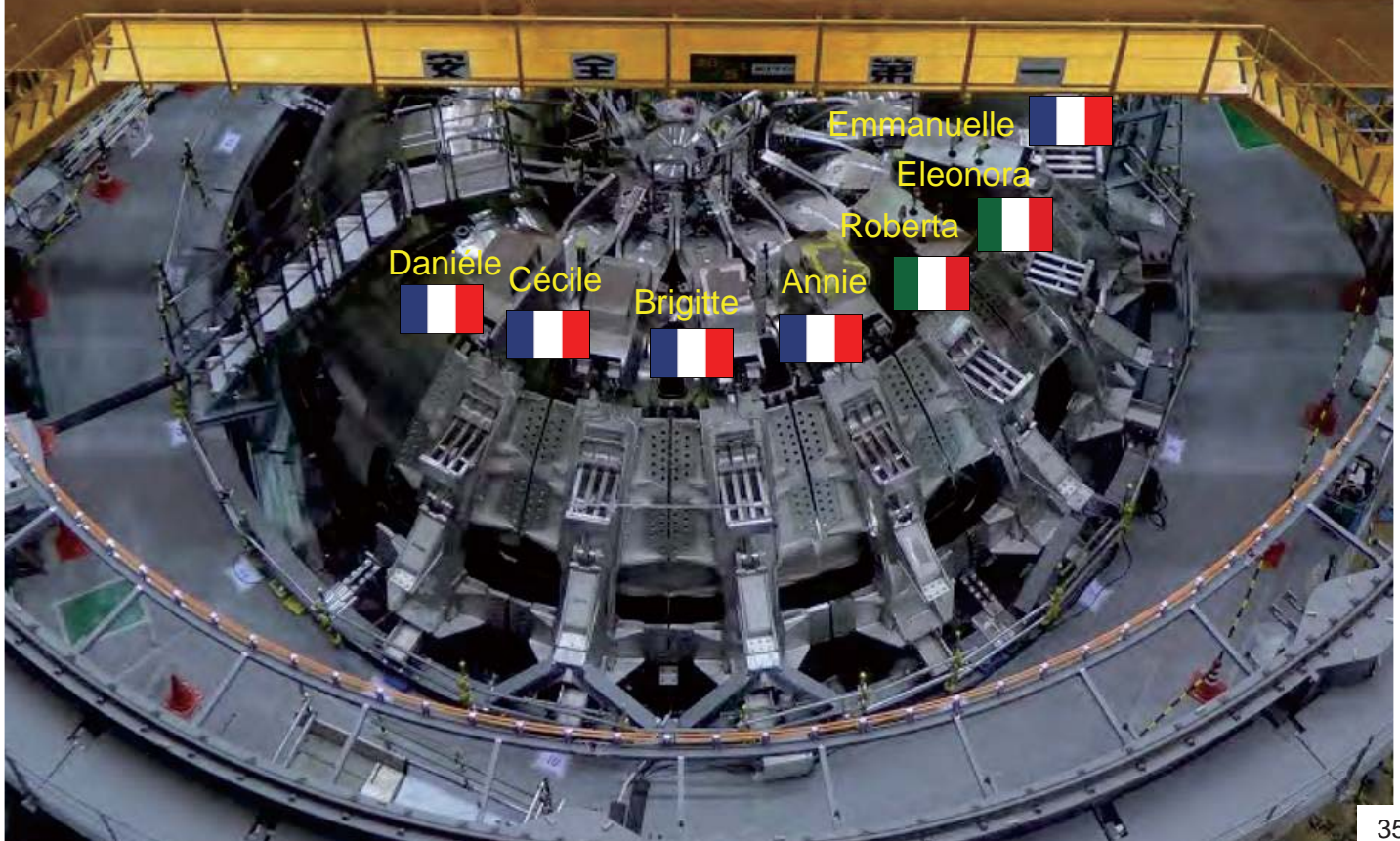





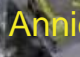



D type TFC (7.5 m in height, 4.6 m in width, 22 ton) fixed to the standing jig

Superconducting Toroidal Magnetic Field Coil made in Europe is being installed. Up to 12 of 18 TFCs have been installed.

Construction is progressing with the aim of first plasma in 2020.

34

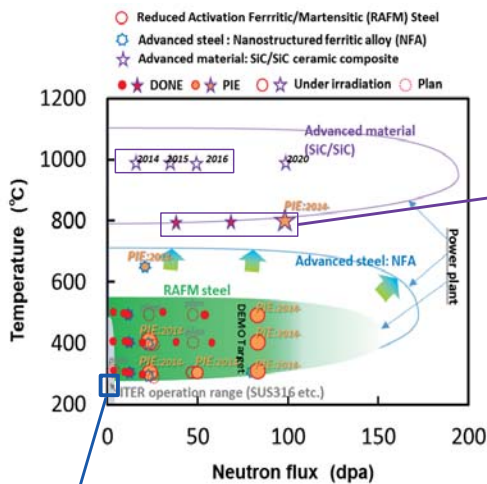


Emmanuelle 
 Eleonora 
 Roberta 
 Annie 
 Brigitte 
 Cécile 
 Danièle 

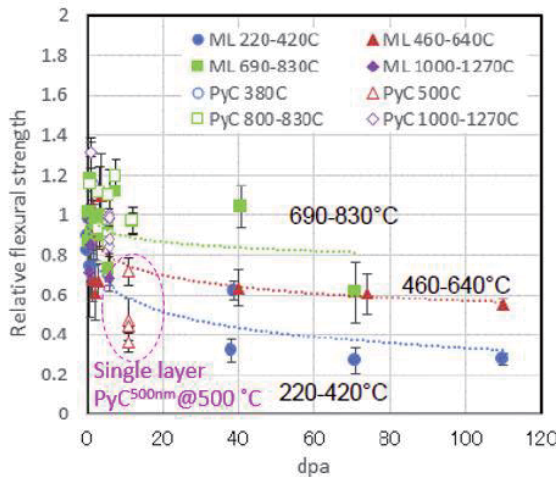
QST/DOE HFIR Collaboration (1984-): Fusion Materials

Fusion Research & Development

Target design window and HFIR irradiation conditions

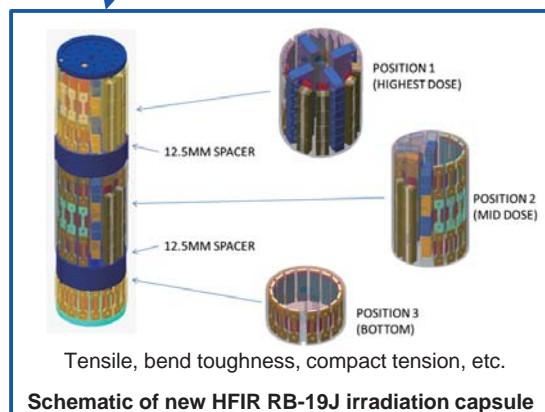


Key findings from HFIR irradiation

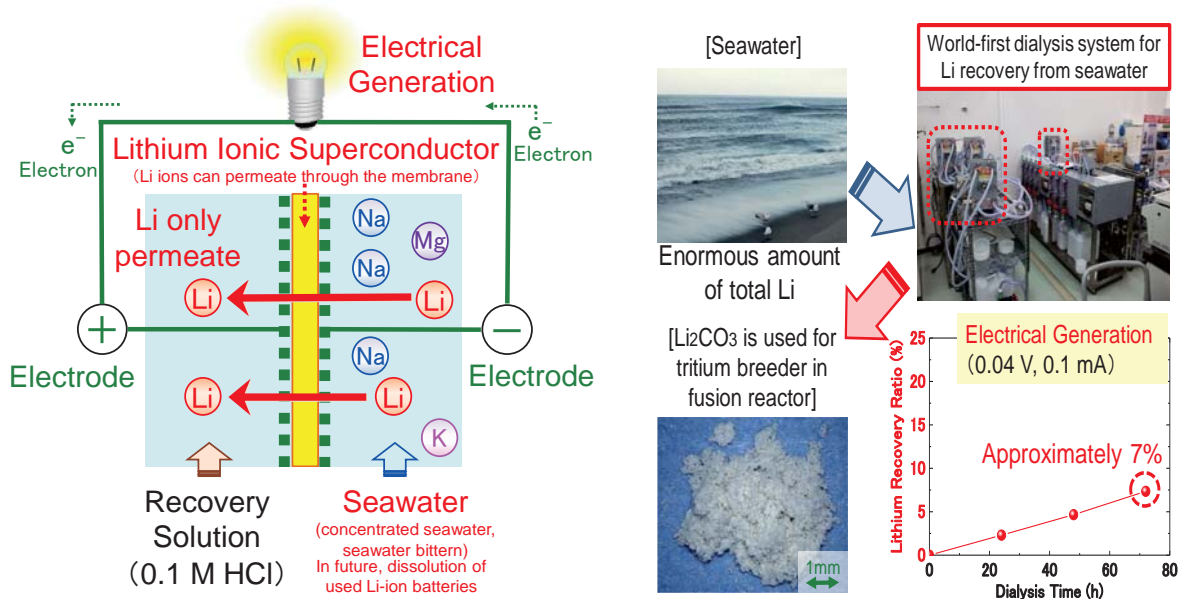


- ✓ Fracture strength of 1st generation nuclear grade SiC composites show high irradiation resistance at higher temperature.
- ✓ Pyrolytic C-SiC multi-layer interphase is turned out to be essential for good irradiation resistance, by comparing to that of single-layer

- Post irradiation examination (PIE) of RAFM steel irradiated in HFIR to 20dpa/80dpa was continued.
- Continued irradiation of RAFM in 50dpa rabbit and SiC/SiC composites in high dose rabbits
- HFIR RB-19J (~250°C/3dpa) irradiation was completed by December 2016.
- The JWG meeting on the continuing activity of Annex I will be held March 6th and 7th, 2017. Discussion on new irradiation program concerning divertor materials is started.



Other R&D activities - Basic R&D on Li recovery from sea water



1) Li only permeates from the negative electrode side to the positive electrode side through a Li ionic superconductor. Li becomes selectively concentrated in a Li recovery solution. Furthermore, electrical power is generated.

2) Then, Li₂CO₃ powder, as a raw tritium breeder for fusion reactors, was fabricated by the chemical reaction by adding CO₂.

37

Conclusions

• Activities related to the ITER Project

– Design, qualification, fabrication are in progress for TFC structures, TFC winding, CS conductor, Blanket remote handling system, HV power supply and HV bushing for NB test facility, Diagnostics, Gyrotrons for EC system and Detritiation System.

• Activities related to the three projects of the BA Activities

– In order to reinforce DEMO design and R&D activities that have been mainly carried out under the Broader Approach, an all-Japan team named “Special Design Team for Fusion DEMO” was organized in June 2015 with the participation of industry.

– JT-60SA: 28 Procurement Arrangements have been concluded: (JA: 91%, EU:100%). JT-60SA tokamak assembly is proceeding on schedule. The JT-60SA Research Plan Ver.3.3 was completed in Mar. 2016 by 378 EU&JA researchers.

• Major Progress in Fusion Research and Development in QST

– JT-60 data analyses, collaboration with US/EU/KO tokamaks, integrated modeling and computer simulations contribute to ITER physics and the advanced tokamak physics for JT-60SA and DEMO.

– ECRF and NBI systems for heating and current drive technologies in JT-60SA and ITER have shown good progress. Design study and R&Ds for TBM system has also been developed.

– US-Japan Collaboration for irradiation/PIE of fusion materials in HIFR is undergoing.

– Domestic R&D program for recovery of Li from sea water is undergoing.

38

2.3 Plenary session

2.3.1 Broader Approach (BA) R&D research status of the JET-ILW divertor tile and dust in Rokkasho:

Be deposition study

N. Asakura¹, S. Masuzaki², M. Tokitani², N. Ashikawa², T. Otsuka³, Y. Oya⁴, Y. Hatano⁵, M. Miyamoto⁶, R. Sakamoto², S. Sakurada⁴, Y. Uemura⁴, K. Azuma⁴, K. Yumizuru⁵, K. Isobe¹, M. Oyaizu¹, T. Suzuki¹, H. Kurotaki¹, D. Hamaguchi¹, H. Nakamura¹, A. Widdowson⁷, K. Heinola⁸, S. Jachmich⁹, M. Rubel¹⁰

¹National Institutes for Quantum and Radiological Science and Technology (QST), Rokkasho Aomori 039-3212, Japan

²National Institute for Fusion Science, Oroshi 322-6, Toki 509-5292, Japan

³Kindai University, 3-4-1 Kowakae, Higashiosaka, Osaka 577-8502, Japan

⁴Shizuoka University, Shizuoka, 422-8529, Japan

⁵University of Toyama, Gofuku 3190, Toyama 930-8555, Japan

⁶Shimane University, Matsue, Shimane 690-8504, Japan

⁷Culham Centre for Fusion Energy, Culham Science Centre, Abingdon, OX 14 3DB, UK

⁸University of Helsinki, Box 43, FIN-00014 Helsinki, Finland

⁹Association Euratom-Etat Belge, ERM-KMS, Brussels Belgium

¹⁰Royal Institute of Technology (KTH), 100 44 Stockholm, Sweden

E-mail: asakura.nobuyuki@qst.go.jp

Comprehensive analysis of the divertor tile surface and dust produced by the 1st campaign (2011-2012) of the JET ITER-Like-Wall (ILW) experiment has been performed in QST Rokkasho as a part of the Broader Approach (BA) DEMO R&D activity. The R&D facility is a unique facility where tritium, beryllium and activation materials can be handled. Plasma-Wall-Interaction analyses on these samples were carried out by NIFS, universities and QST collaboration with strong support by JET and EU. Microstructure, atomic composition and chemical states of the surfaces on the tiles and dust have been analysed. The divertor target in JET-ILW is made partly of tungsten (W) bulk lamellar plates and mainly of W-coating on the carbon fiber composite (CFC) bulk tiles by Vacuum Plasma Spray (VPS) process. In this analysis, W-coating tile samples (diameter of 17mm) were used, retracted from the inboard and outboard vertical targets and at the divertor floor. Two bottles of dust samples were collected by a vacuum cleaner on the inner and outer divertor surfaces. In JET-ILW, most of the first wall surface is covered by Be, and Be impurity is transported with the plasma from the first wall to the divertor with repeating the deposition and erosion processes.

Recently, some unique analysis results were obtained, in addition to standard surface analysis. Microstructure analysis of tile and dust cross-sections as well as their surfaces have been performed, using a transmission electron microscope (TEM) after the focused ion beam (FIB) fabrication. In particular, in the thick Be-deposition layers on the inner W-target, nano-size bubbles-like structure was generated, and the deposition layers were composed by mixture of W, Be, C, Ni and O, evaluated by using X-ray photoelectron spectroscopy (XPS) and Electron Probe Micro Analyzer (EPMA). These deposition layers might be affected by various plasma operations in the experiment campaign. Local pattern of the Be-deposition on a rough VPS-W surface against the plasma incident angle was investigated. The microstructure analysis of dust particles showed that bubble-like structure was also generated inside a Be dominant dust (large 100 µm size dusts were so far analyzed), and chemical components

and state analysis showed that BeO in a Be dominant dusts and some W and/or C dusts were determined. The analysis method of the tile and dust samples were established. Evaluations of hydrogen isotope retention and Tritium-specific activity (Bq/g) in JET-ILW tile surface and dust particles will be also presented.

Broader Approach (BA) R&D research status of the JET-ILW divertor tile and dust in Rokkasho: Be deposition study

**N. Asakura¹, S. Masuzaki², M. Tokitani², N. Ashikawa², T. Otsuka³, Y. Oya⁴, Y. Hatano⁵,
 M. Miyamoto⁶, R. Sakamoto², S. Sakurada⁴, Y. Uemura⁴, K. Azuma⁴, K. Yumizuru⁵,
 K. Isobe¹, M. Oyaizu¹, T. Suzuki¹, H. Kurotaki¹, D. Hamaguchi¹, T. Hayashi¹
 A. Widdowson⁷, M. Rubel⁸, K. Heinola⁹, S. Jachmich¹⁰, J. Likonen¹¹, J. Grzonka¹²**

**13th International Workshop on Beryllium Technology,
 21-22 September 2017, Hilton Tokyo Narita Airport Hotel**

¹National Institutes for Quantum and Radiological Science and Technology (QST), Rokkasho, Aomori, Japan

²National Institute for Fusion Science, Toki, Gifu, Japan

³Kindai University, Higashiosaka, Osaka, Japan

⁴Shizuoka University, Shizuoka, Japan

⁵University of Toyama, Toyama, Japan

⁶Shimane University, Matsue, Shimane, Japan

⁷Culham Centre for Fusion Energy, Culham Science Centre, Abingdon, UK

⁸Royal Institute of Technology (KTH), 100 44 Stockholm, Sweden

⁹University of Helsinki, Helsinki, Finland

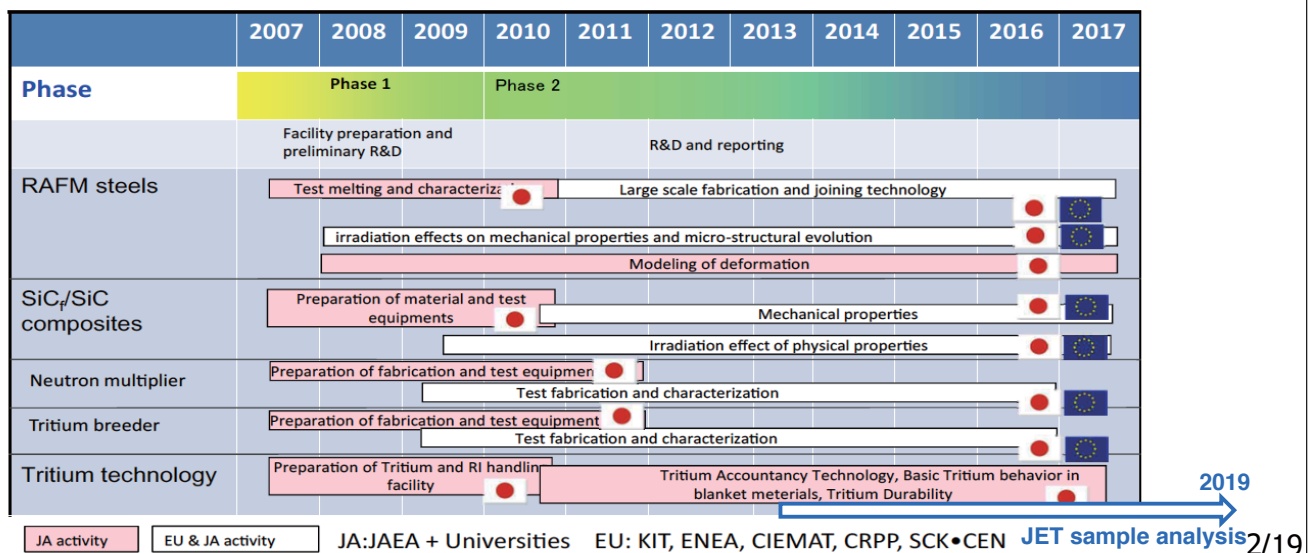
¹⁰Association Euratom-Etat Belge, Brussels Belgium

¹¹VTT Technical Research Centre, Espoo, Finland

¹²Warsaw University of Technology, Poland

1. Introduction: JET-ILW PWI analysis in BA, IFERC

- **Broader Approach:** Integrated approach to support the ongoing fusion programme: JT-60SA, ITER and preparation for the engineering design of DEMO.
- **International Fusion Energy Research Center (IFERC):** one of 3 main projects (IFMIF/EVEDA and JT-60SA) of the “Broader Approach”, which started from 2007:
- **DEMO R&D for Tritium tech., T-breeder/n-multiplier and structural materials:** one of 4 activities (Demo design, Computer simulation, ITER remote exp.) in IFERC.

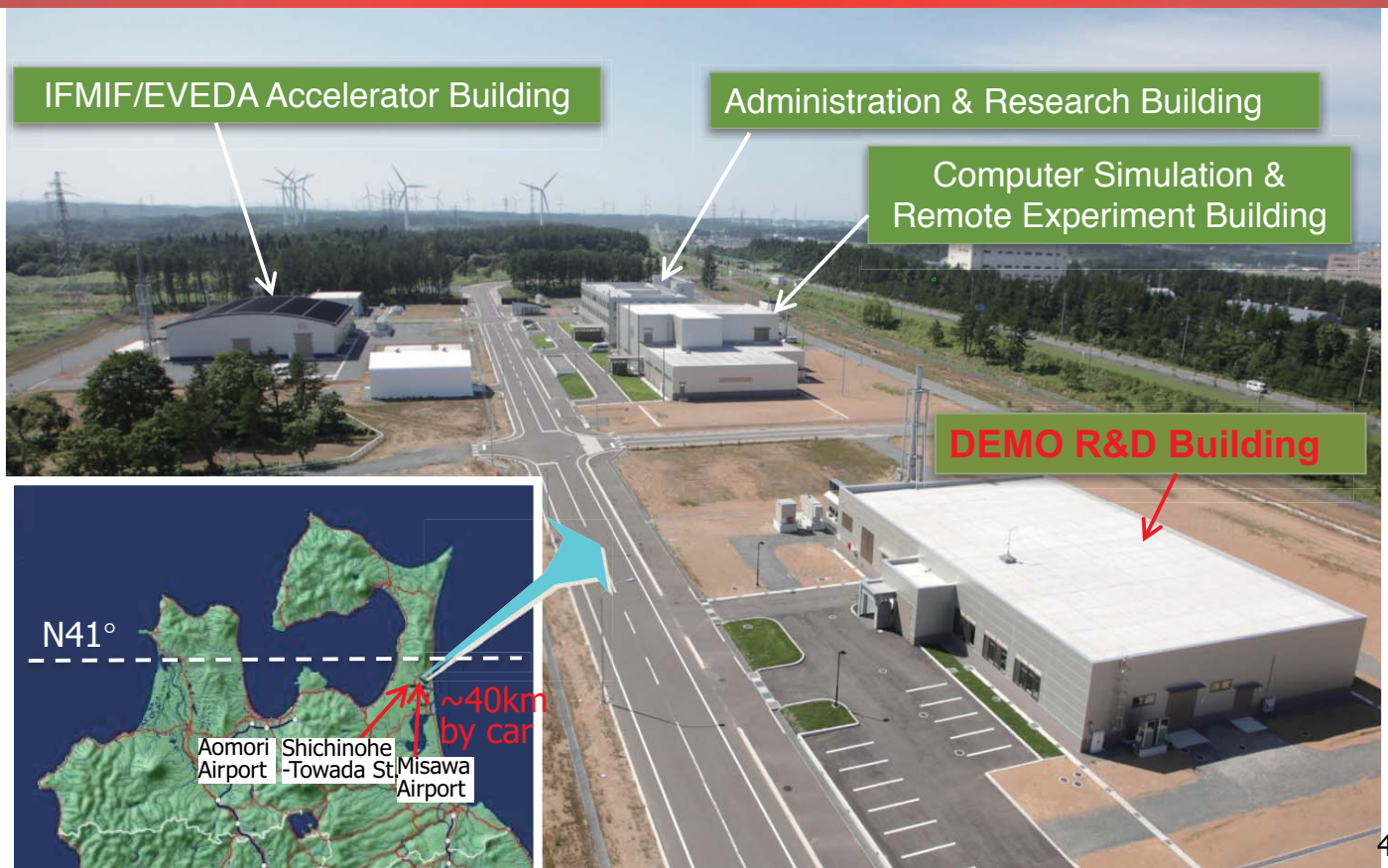


Contents

1. Introduction: JET-ILW PWI analysis in BA, IFERC
2. Analysis of divertor tile samples
3. Dust sample analysis
4. Analysis summary in IFERC, Rokkasho

/19

International Fusion Energy Research Center (IFERC): QST, Rokkasho Fusion Institute



4/19

Radiation control area in IFERC DEMO R&D building

DEMO R&D facility is unique facility where **tritium**, **beryllium** and **activation materials** can be handled in the world: Important analytical equipment, such as Focused ion beam (FIB), Transmission electron microscope (TEM), Electron Probe Micro Analyzer (EPMA), X-ray photoelectron spectroscopy (XPS), X-ray diffraction (XRD) and thermal desorption spectroscopy (TDS), are installed in the facility.

Radiation control area

Laboratories for testing and characterization of irradiated materials and tritium.

Material Analysis Room

- Chemical analyses, structural identification by X-ray

RA-1	ICP	Perkin Elmer Optima7000DV
RA-2	ICP mass spectrometry	Perkin Elmer CLAVIO ICP-MS
RA-3	Microprobe sample preparation system	Perkin Elmer Multiwave3000
RA-4	Oscillator	ULVAC LUK
RA-5	XRD	Reaktor D5000V (18kW)

XRD

ICP

ICP-Mass

Material Test Room

- Mechanical test and fracture surface observation using irradiated materials
- Sample prep. (polish and cut) for RI samples

RA-1	Scanning electron microscope SEM	Kentech VE-8000
RA-2	Fatigue test machine	Instron ElectroPulsE3000
RA-3	Vickers microhardness	HiVision VH-1000
RA-4	Vickers hardness tester	Mitsubishi AVU-500
RA-5	Universal test machine	Shimadzu AG-10M40E
RA-6	Digital 3D-scan system	Coordinate Solutions VC-30
RA-7	Servo microscope system	Lamont MS, Gensler Optics
RA-8	Electrolytic thinning apparatus	Struers TenUp-5
RA-9	Low speed rotation saw	QUENCHER 1000
RA-10	Constant potential electrolytic etching system	Polymer Scientific Corporation, Good analysis DLS-30

RI Experimental Room

- 370 GBq/hood for development of tritium accountability technology, basic tritium safety research and tritium durability test

RI-1	TG/DTA-Mass	Physis ThermoMass Probo
RI-2	Tritium storage bed	Zirconium-Cobalt bed
RI-3	Tritium removal system	Catalytic oxidation - chemisorption activation removal

Tritium removal system

Microstructure Analysis Room

- High-precision specimen prep. for micro/nano structural observations
- High-resolution micro/nano-structural observations
- Nano-scale surface analyses
- Nano-scale mechanical test

RA-1	Field emission transmission electron microscope FE-TEM	JEOL JEM-2100F
RA-2	Transmission electron microscope TEM	TEM
RA-3	Phase-contrast beam FIB system	Hitachi FB-2100
RA-4	Field emission scanning electron microscope FE-SEM	Carl Zeiss ULTRA30
RA-5	Phase imager	JEOL JEM-9500P
RA-6	Atomic force microscope AFM	DIPIPER INF-1100
RA-7	Atomic force microscope AFM	Agilent 5500; 8010
RA-8	Low energy e-beam FIB	Hitachi SU8000; JEM-FLY-514
RA-9	Carbon replica	JEOL JEC-5015
RA-10	Plasma cleaner	MCPANAFOS Co. Ltd. PC2000 E
RA-11	Serbo-robotic removal system	JEOL JCS-250P
RA-12	Thermal desorption spectrometry	DETAOS-MINCO VARD
RA-13	Thermal desorption spectrometry (TDS)	TSD
RA-14	Laser microscope	Leica DM1000

SEM

Fatigue test machine

Hardness tester

Universal test machine

Low-speed precision saw

Electrolytic thinning apparatus

Iron shield w/ MSM

FIB

FE-TEM

FE-EPMA

FE-SEM

Nano-indentor

LEG

Plasma cleaner

AFM

Laser microscope

RI Experimental Room

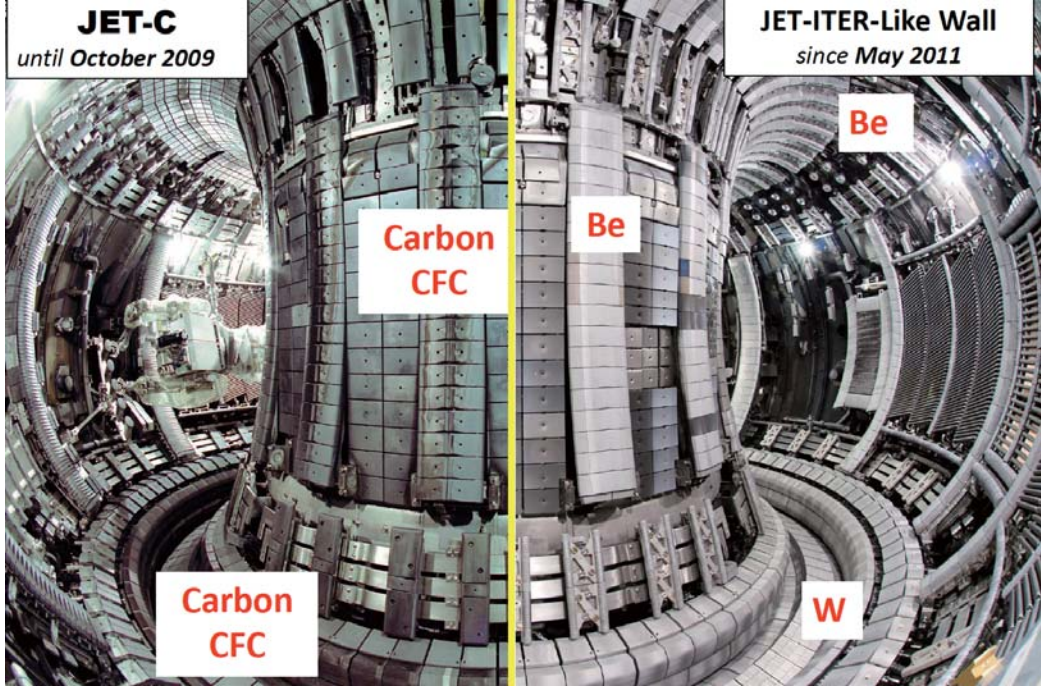
Material Analysis Room

Material Test Room

Microstructure Analysis Room

JET Plasma Facing Components changed from 2011

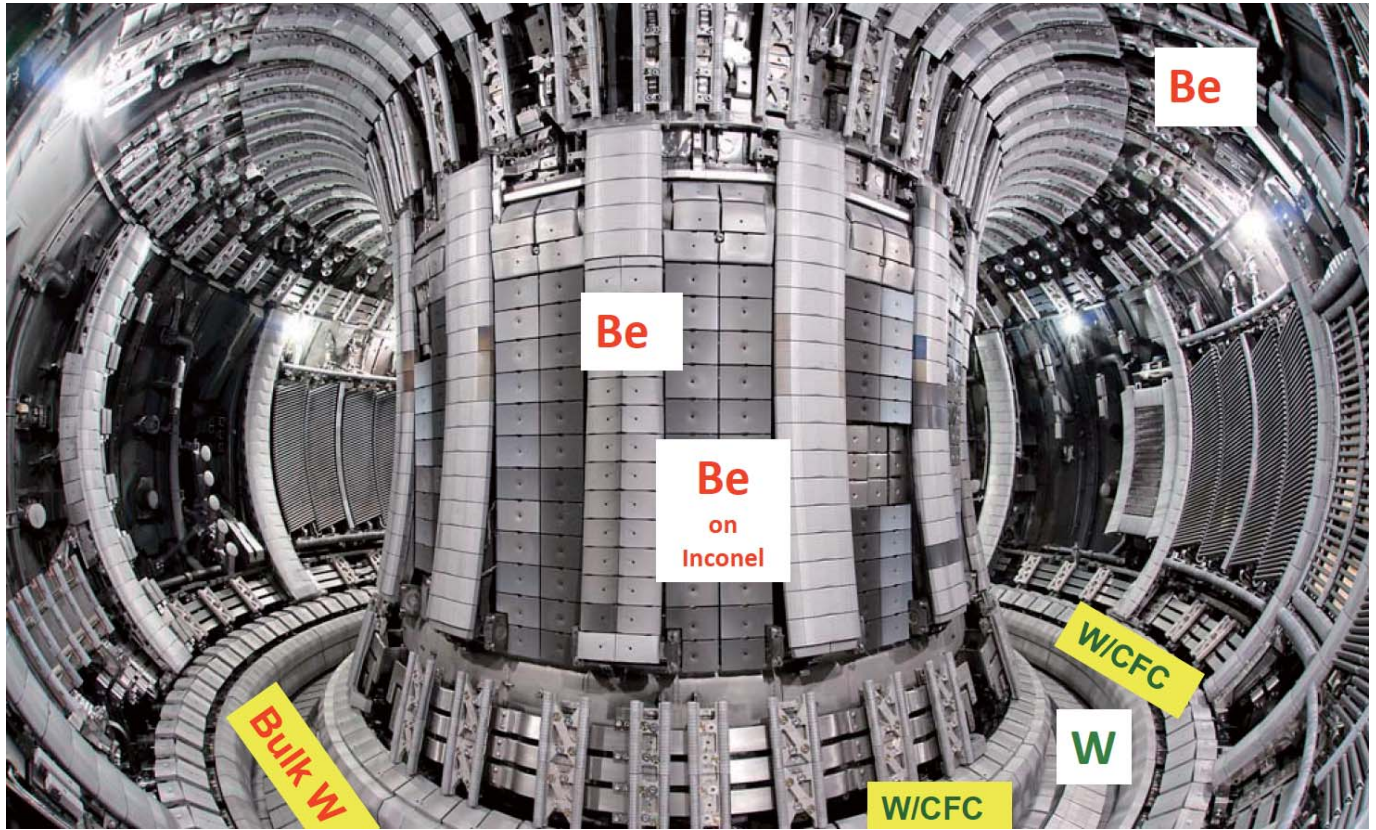
- Joint European Tours (JET) implemented W-coated CFC and bulk-W tiles in the divertor, and carried out the plasma experiments of ITER Like Wall (ILW).
- JA & EU decided in 2013 to carry out analysis of tile surface and dust produced in the 1st campaign of the ILW experiment as part of DEMO R&D of BA activity.**



Note:
 3 campaigns were conducted up to now.
 1st campaign 2011-2012
 2nd campaign 2013-2014
 3rd campaign 2015-2016

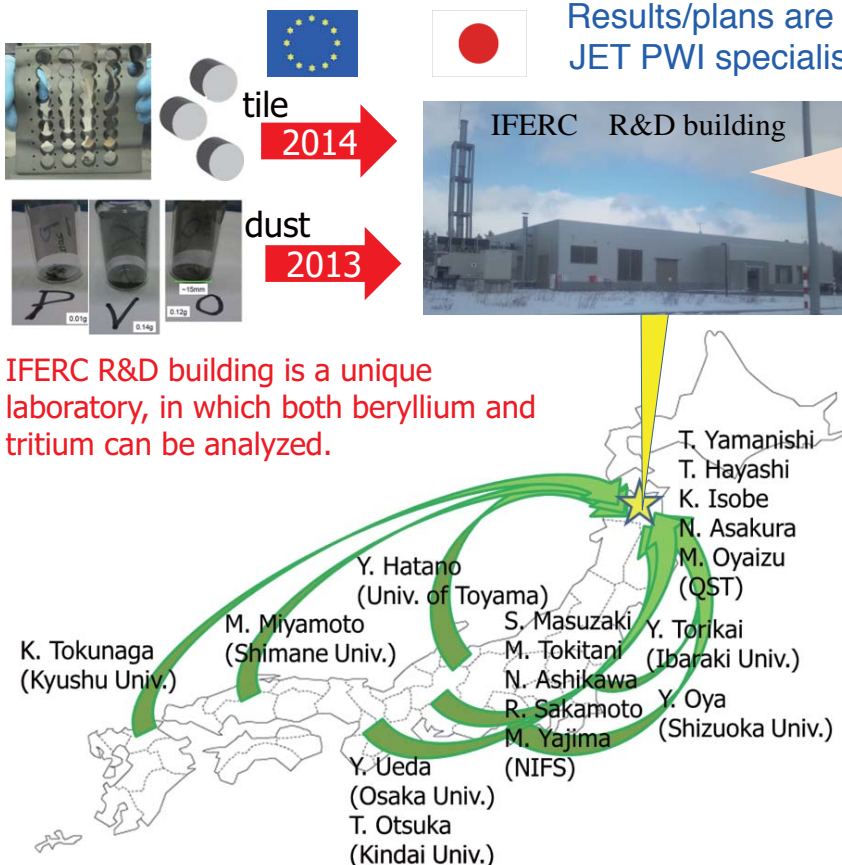
Plasma Facing Components: **Beryllium** and **Tungsten**:

Be is used for ITER, and will NOT deteriorate the plasma performance.



7/19

Collaborative studies have been carried out by a joint team of 8 universities from 2013: NIFS, U.Toyama, Shizuoka U., Osaka U., Shimane U., Ibaraki U., Kindai U., Kyushu U.



Results/plans are discussed monthly in TV meetings with JET PWI specialists, and they visited to join the analysis.

Devices for analyses of;

Microstructure

- Transmission electron microscope
- Scanning electron microscope
- Focused ion beam

Composition and Chemical State

- Energy dispersive X-ray analysis
- Electron probe X-ray microanalysis
- X-ray photoelectron spectroscopy
- X-ray diffraction

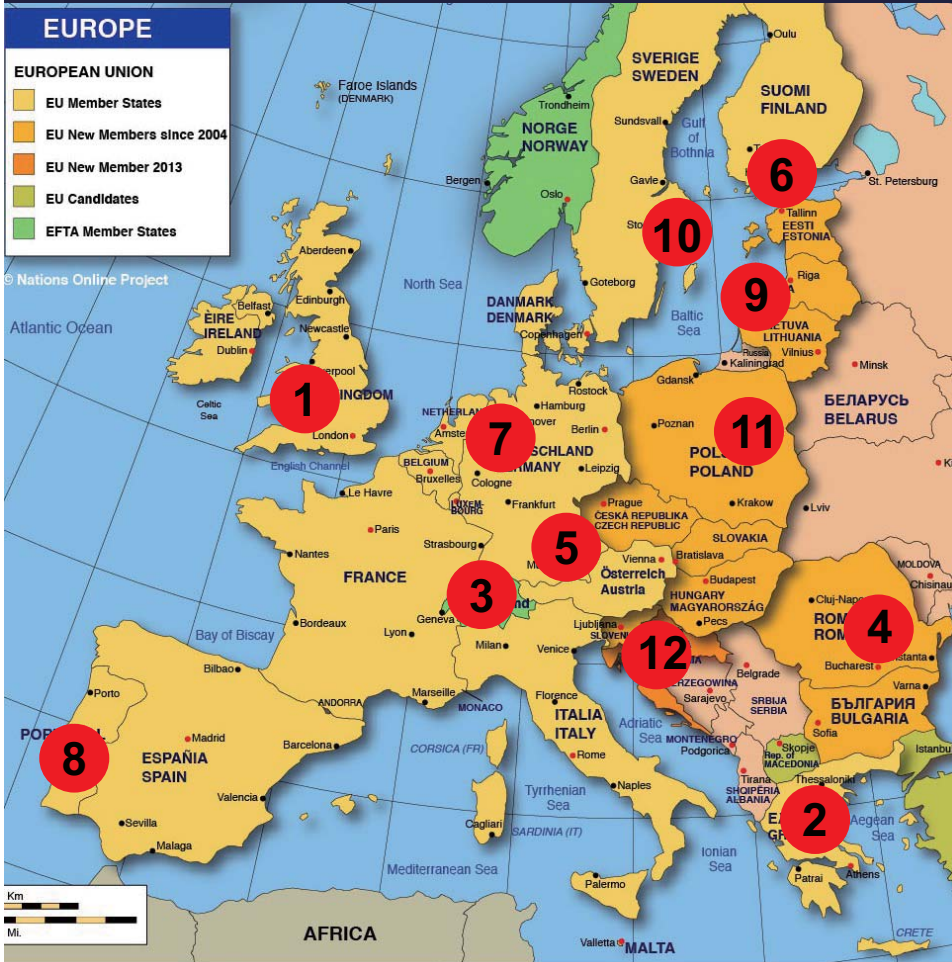
Hydrogen isotopes retention (D/T)

- Thermal desorption spectroscopy
- Imaging plate technique
- β -ray induced X-ray spectroscopy
- Liquid scintillation

IFERC R&D building is a unique laboratory, in which both beryllium and tritium can be analyzed.

8/19

Network of laboratories for JET materials in EU



1. Culham – JET: *UK*
2. Athens: *Greece*
3. Basel: *Switzerland*
4. Bucharest: *Romania*
5. Garching: *Germany*
6. Helsinki: *Finland*
7. Jülich: *Germany*
8. Lisbon: *Portugal*
9. Riga: *Latvia*
10. Stockholm: *Sweden*
11. Warsaw: *Poland*
12. Zagreb: *Croatia*

9/19

Analysis of JET-ILW PFCs: **Beryllium** and **Tungsten**

Analysis results will provide physics/chemical information of the ITER like Plasma Facing Materials (metal wall device), and impact on the plasma performance (impurity, radiation and operation such as conditioning and long-pulse).

JA group has focused on analysis of material surface and dust properties, including hydrogen isotope retention:

- **Microstructure of W-tile surface and the deposition layers:** Be and chemical compounds may change the surface characteristics of conductance, erosion and retention, etc.
- **Atomic compositions and hydrogen isotope retentions of dust particles in JET-C and JET-ILW:** Tritiated-Be/W dust impacts on radioactive safety in remote maintenance and severe accidents.
- **Analysis method and procedure,** at the same time, are developed in order to handle small amount of activated samples.

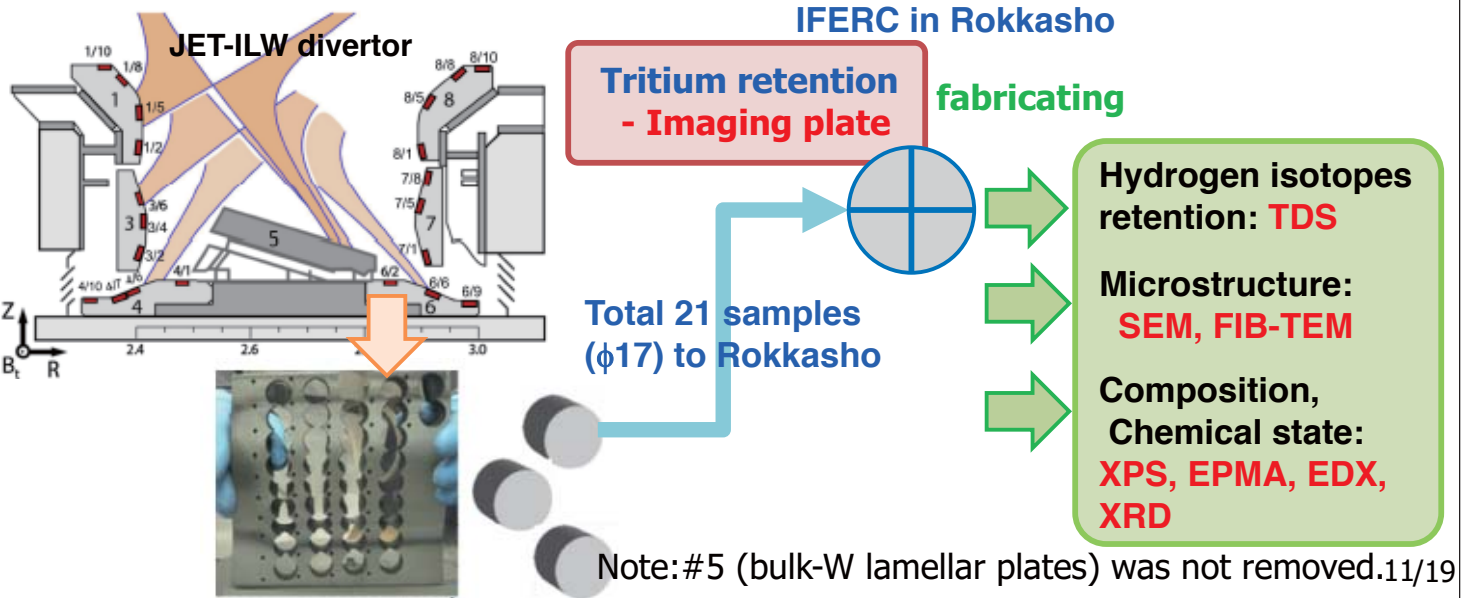


Prediction of the plasma performance, PWI in ITER and DEMO

10/19

2. Tile analysis: divertor tile samples were extracted from the inner and outer targets (#1, 3, 4, 6, 7 and 8) after the 1st campaign

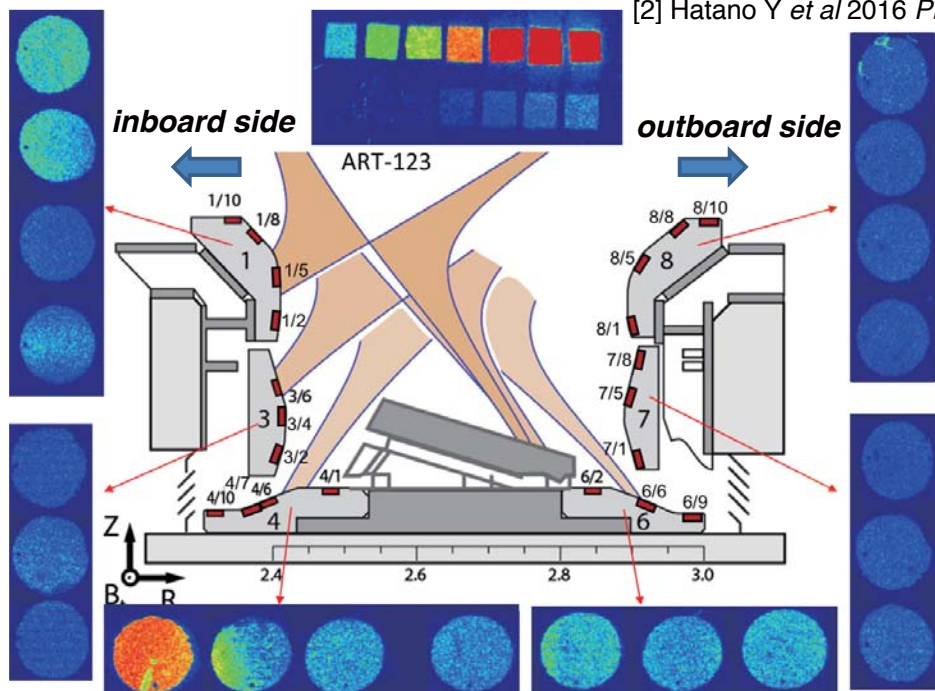
- 21 core samples ($\phi 17\text{mm}$, $t 5\text{mm}$) of inner and outer target tiles ($10\mu\text{m}$ W-coating CFC by combined magnetron sputtering and ion implantation technique) were transported.
- Tritium retention analysis (IP) was performed before fabrication, then the surface microstructure (SEM, FIB&TEM), H-isotope retention (TDS), composition (XPS, EPMA, EDX, XRD) were analyzed.



Tritium amount near the surface was evaluated by using Tritium Imaging Plate (T-IP)

- T-IP is sensitive to β -ray from tritium: detectable depth is restricted within escapable depth of β -ray ($< 1\mu\text{m}$) \Rightarrow **Large T-retention is seen on the inner and outer floor tiles (#4, #6) and inboard upper tile (#1)** [1,2].

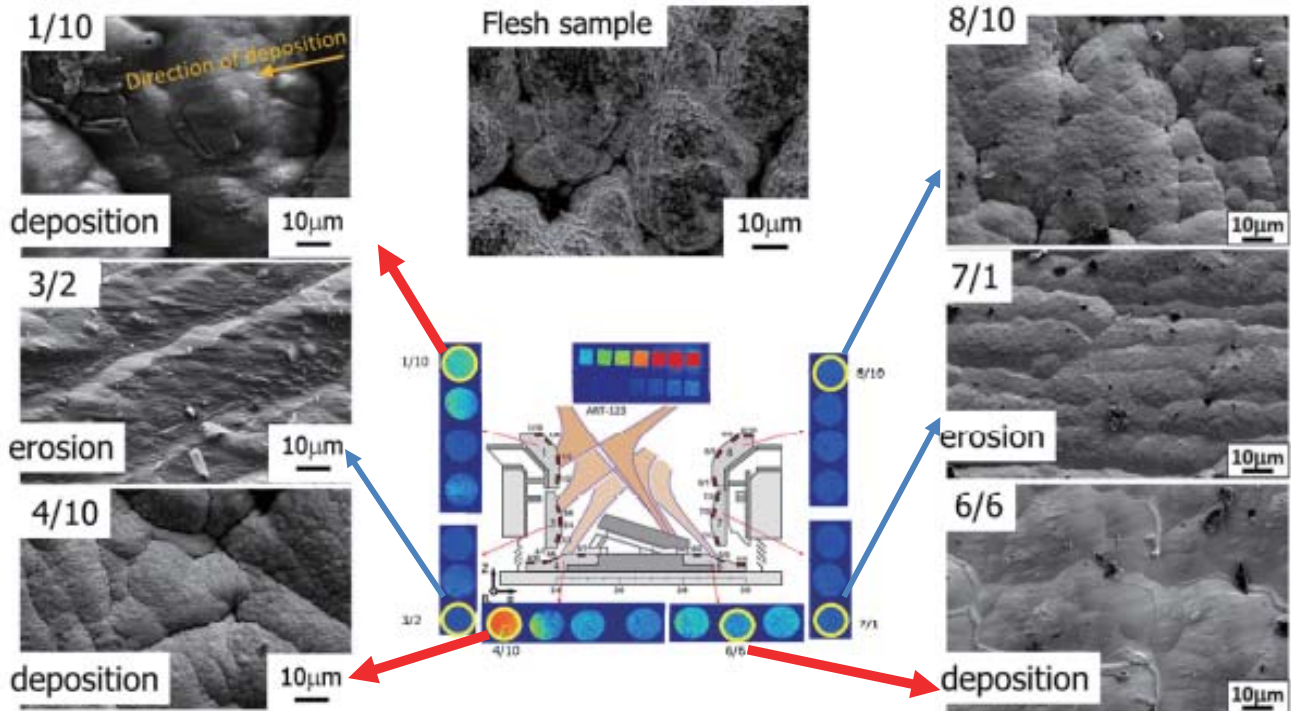
[1] Hatano Y *et al* 2015 *J. Nucl. Mater.* **463** 966
 [2] Hatano Y *et al* 2016 *Phys. Scr.* **T167** 014009



Surface morphology of coating-W observed with SEM

T (H-isotope)-retention was increased with Be and/or C-deposition.

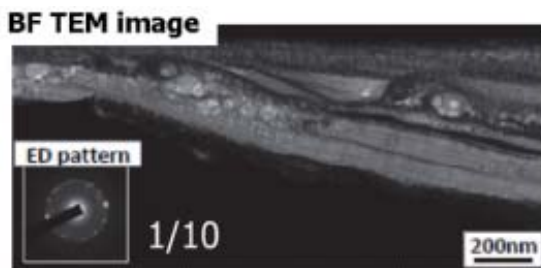
⇒ microstructure on the surface has been analyzed by SEM.



Results of the inboard side tiles are from M. Tokitani et al Fusion Eng. Des. 116 (2017) 1-4.

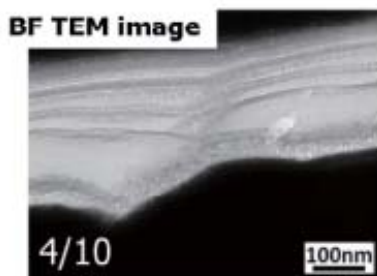
13/19

Microstructure in deposition layers observed by FIB/TEM

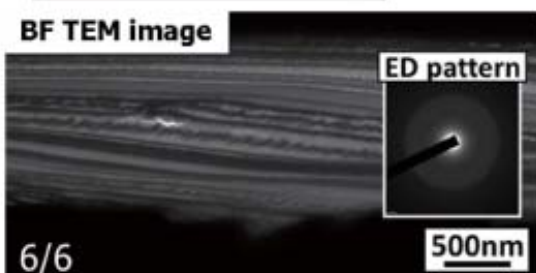


• Cross-sectional view was observed by TEM, using the focused ion beam (FIB).

⇒ Thick deposition layers were observed on 1/10, 4/10 and 6/6. These deposition layers have stratified structures with amorphous features.



• **1/10: nano-size bubble-like structures were seen.** Deposition layer was composed by mixture of W, C, O, Ni and Be (EPMA).
Note[4]: large Be-dominant dust (100 μ m-size) was found: many bubble-like structures on the surface.



• **4/10: grain size of the deposits varied from an initial growth phase to a latter phase.** No bubble-like structure was observed. The layer was composed by C, Be, W, and O.

• **6/6: No bubble-like structure was observed.** The layer was composed by Ni, Be, C, O and W.

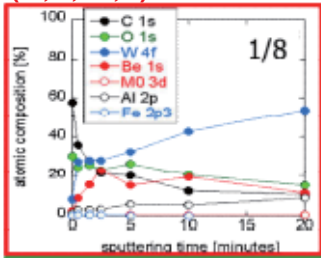
[3] M. Tokitani et al Fusion Eng. Des. 116 (2017) 1-4. [4] N. Ashikawa, et al., IAEA-FEC 2016.

14/19

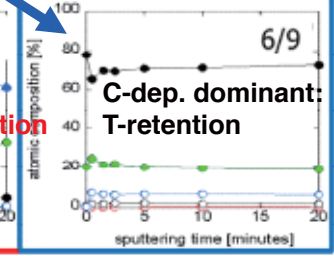
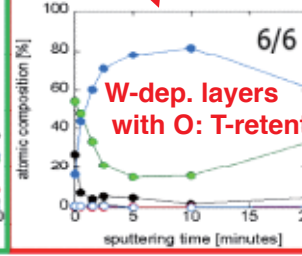
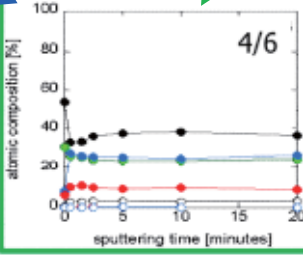
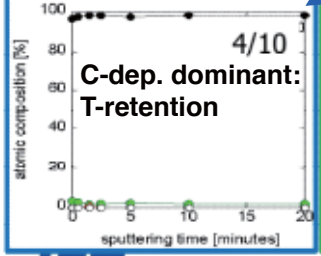
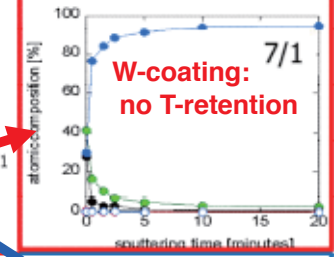
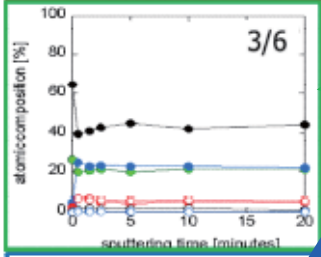
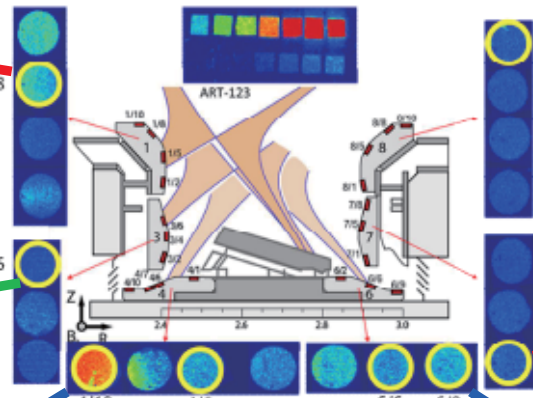
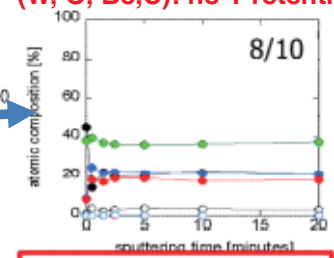
Composition of surfaces and deposition layers with XPS

- Thick mixed-Be-deposition was seen at top of inner divertor (apron): from the first wall.
- (remaining) C-deposition was seen at the inner and outer remote regions.

Thick mixed-dep. layers
(W,O,Be,C): T-retention



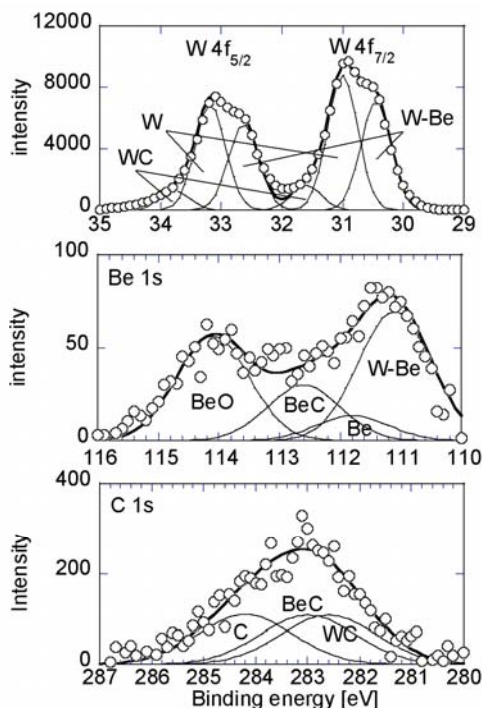
Thin mixed-dep. layer
(W, O, Be,C): no T-retention



15/19

Chemical states analysis by XPS shows W-Be alloy may be formed

- In the W4f spectra, shoulder structures appear at lower binding energy sides: these shoulders are considered to be the sign of W-Be compounds formation. [5]



W 4f (top), Be 1s (middle), and C 1s (bottom) XPS spectra of 1/8 tile after 10 minutes sputtering with Ar ion beam.

Gaussian fitting was applied with fixed binding energies for metallic W 4f_{7/2} (31 eV) and 4f_{5/2} (33.28 eV), metallic Be (111.8 eV) and BeO (114.1 eV). For W-Be compounds, binding energies of 30.45 eV and 32.63 eV for W 4f, and 111.1 eV for Be were assumed.

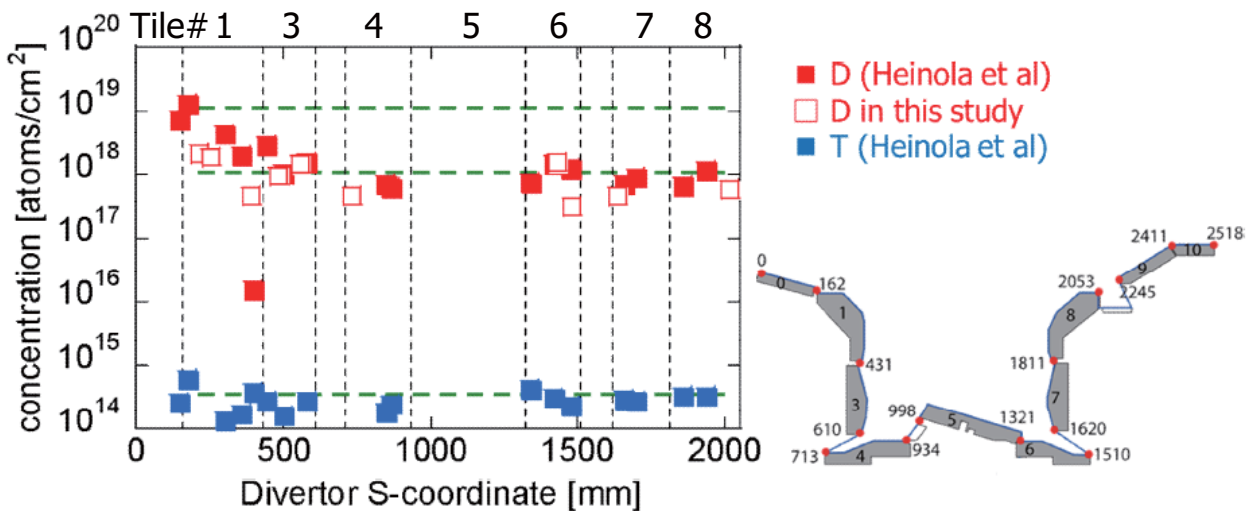
For C 1s case, binding energies of graphite (284.2 eV), WC (282.6 eV), and BeC (283 eV) were assumed.

[5] S. Masuzaki, et al, PFMC 2017.

16/19

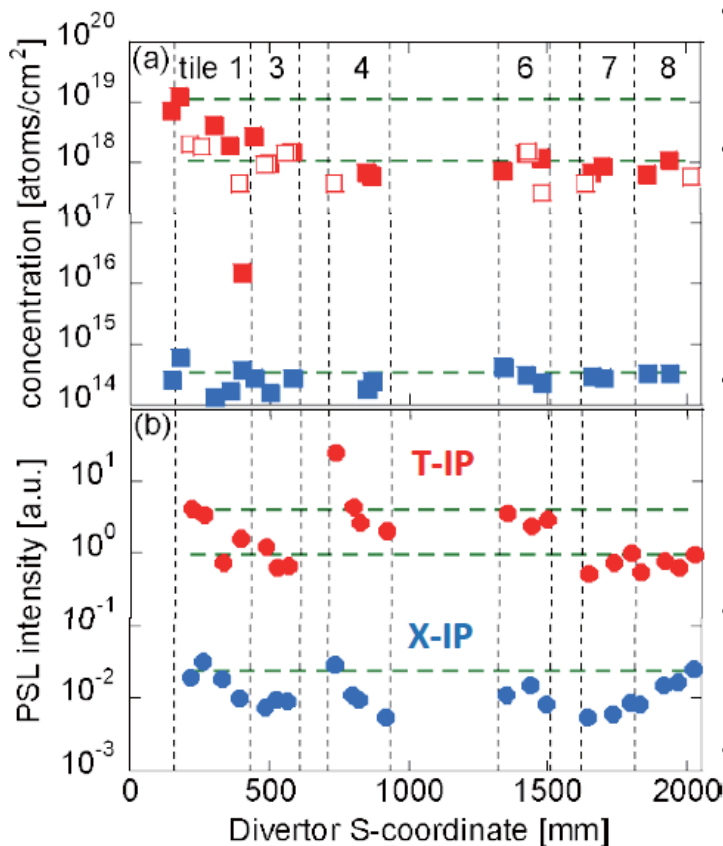
Evaluation of Hydrogen retention on tile surface by TDS

- Deuterium concentration at inboard side is larger than that at outboard side, while Tritium concentration looks more uniform.
 - Deuterium concentrations obtained in this study is consistent with that in previous study except tile#1.
 - At tile#1, D concentrations in this study is smaller than that in previous study: this is attributed to the much thinner deposition layer on the samples ($\sim 1.5\mu\text{m}$) in this study than that in previous study ($10\text{-}20\mu\text{m}$).
- ⇒ That is considered to be caused by the toroidal inhomogeneity of deposition.



17/19

Evaluation of T-retention by two types of Imaging Plates



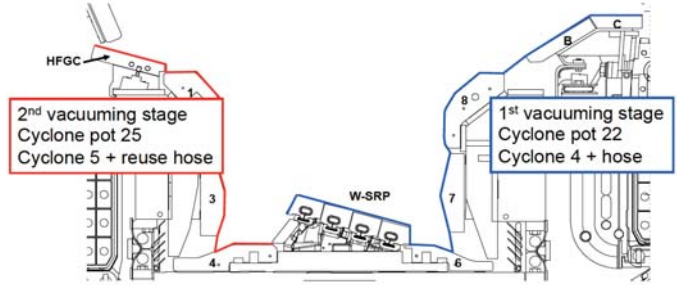
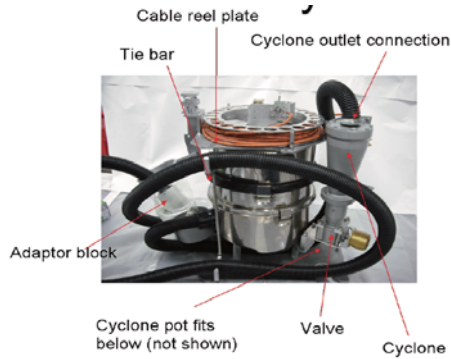
- Tritium-IP (T-IP) is sensitive to β -ray from T: detectable depth of β -ray ($< \sim 1\text{mm}$).
- X-ray-IP (X-IP) detect β -ray induced X-ray: much deeper detectable depth ($< \sim 100\ \mu\text{m}$), X-IP does not detect β -ray by attenuation in the cover sheet on the IP surface.
- PSL intensities of T-IP at the outboard tiles are smaller than that at the inboard tiles: the profile is similar to the profile of retained deuterium amount--- Thermalized triton
- In-out asymmetry of X-IP PSL profile is NOT significant --- High energy triton
- Both IPs shows large PSL at inner remote area on tile#4, similar in C wall campaign.

[6] Hatano Y et al 2016 Phys. Scr. T167 014009)

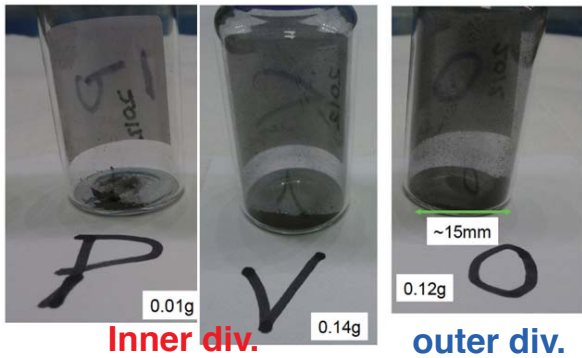
18/19

3. Dusts analysis: samples collected both in JET-ILW and JET-C

- Dust particles were collected by using vacuum cleaner after the 1st campaign (2 yrs): Total weight collected at the inner and outer divertor were 0.7 and 0.3 g, respectively. Note: this amount was significantly smaller than JET-C campaign such as 188g. ⇒ Three pots (P: 0.01g, V: 0.14g, O: 0.12g) were transported to Rokkasho.



2 vacuuming stages: Red = inner divertor, Blue = outer divertor
360° around divertor, excluding Module 2 and Module 14 where tiles for analysis are located (i.e. only 22/24th of divertor vacuumed)



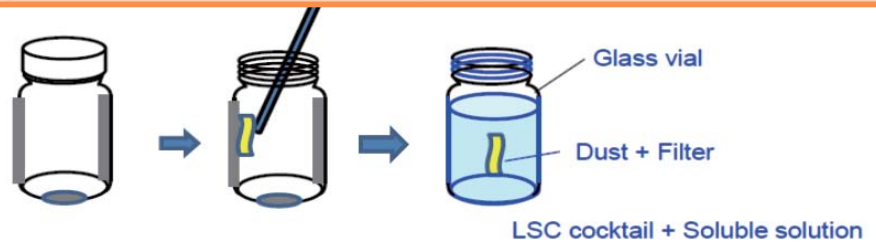
➔ **Rokkasho**

Note: Dust samples collected after the last JET-Carbon PFC campaign was also transported.

19/19

Analyses of dust: surface structure, composition, T-retention

➔ Tritium retention: T-retention on dust surface and volume
IP
Dust combustion and T-trap
Liquid Scintillation Counting



➔ Hydrogen isotopes retention
TDS

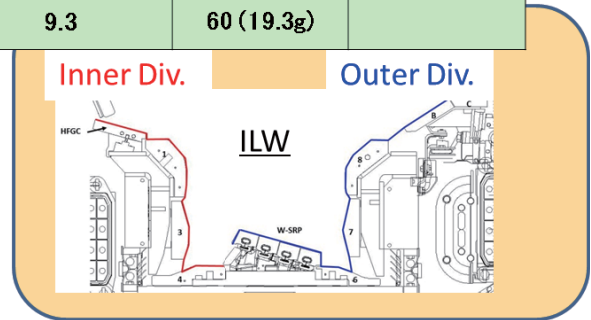
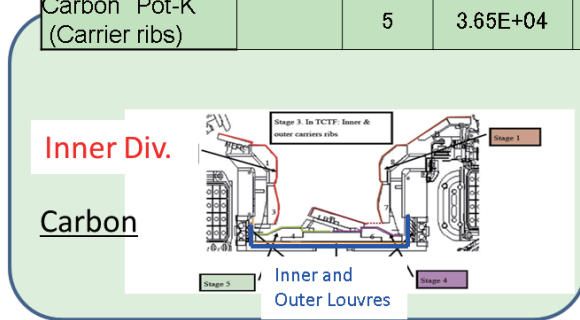
➔ Microstructure on surface
SEM, FIB-TEM

➔ Composition, Chemical state
EDX, EPMA
XPS

20/19

Specific activity of ILW dusts were comparable to that of Carbon wall dusts

LSC : Liquid Scintillation Counting	LSC Bottle no.	weight (mg)	Activity by LSC (Bq)	Specific activity (MBq/g) LSC	Activity (MBq)	Total activity (MBq)
ILW, Pot-P (outer div)	14	0.66	2.72E+03	4.1	1.11 (0.27 g)	94.3
ILW, Pot-V (inner div)	19	2.3	2.79E+05	121	93.2 (0.77g)	
Carbon Pot-B (inner div)	25	6.8	7.57E+03	11	1211 (110.1g)	$5.88 \times 10^3 + \alpha$
Carbon Pot-T (In/Out Louvres)	31	18.8	8.79E+05	47	4672 (99.4 g)	
Carbon Pot-M (Outer div)		3	8.88E+03	3	500 (51.4g)	
Carbon Pot-K (Carrier ribs)		5	3.65E+04	9.3	60 (19.3g)	

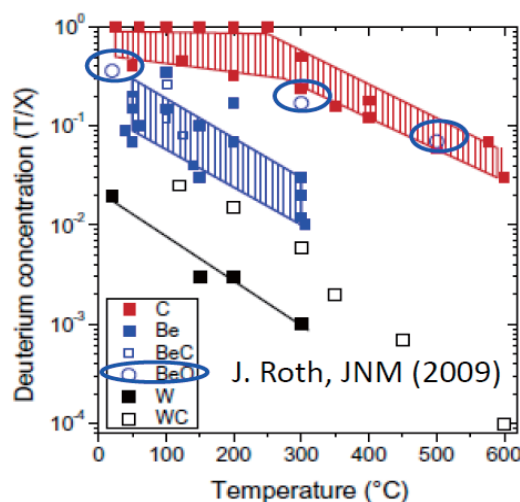


- Specific activities of dust particles : ILW ~ Carbon wall
- Total amount of retained tritium : Carbon wall >> ILW

21/19

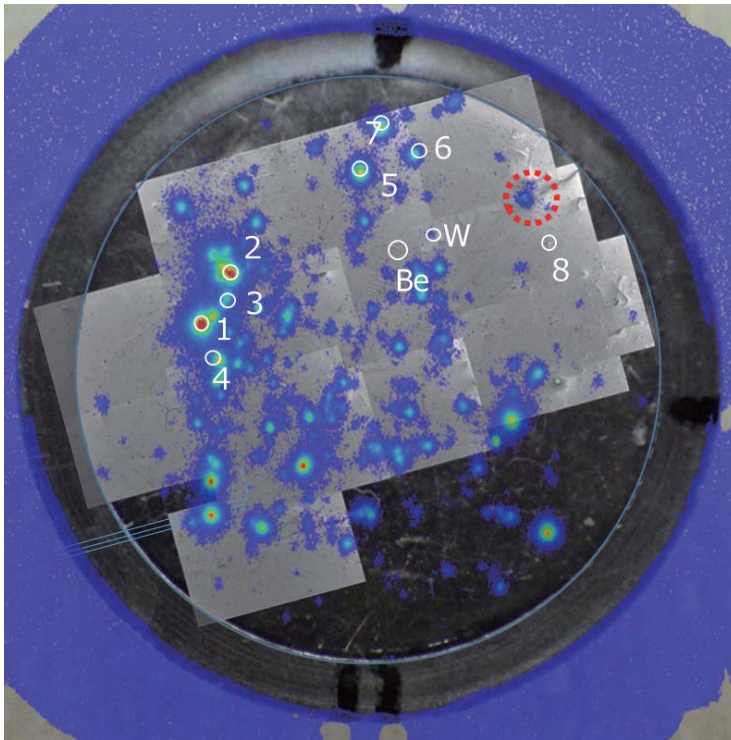
Candidates of large specific activity in ILW dust

- Remained Carbon dust after the C-wall campaign was collected with ILW dusts ⇒ T-retention in C-dust is dominant.
- Be-oxide was produced on the ILW dust surface, which may retain large amount of hydrogen isotopes like C.



22/19

Tritium-retention amount in each dust particle was evaluated by IP technique, and composition analysis was conducted.



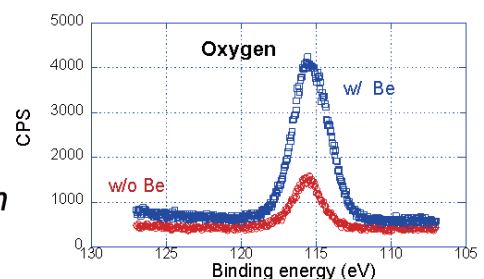
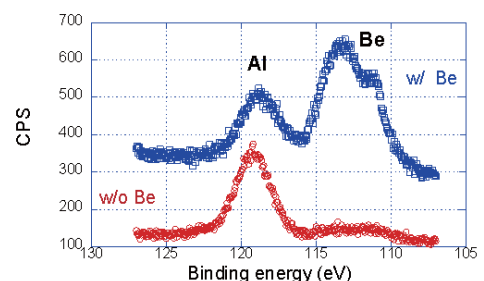
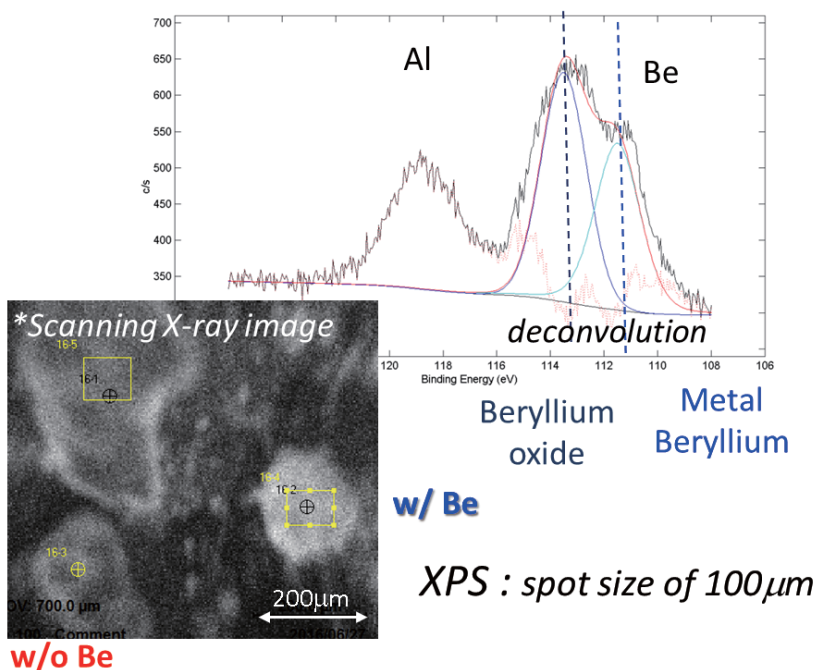
- Dust particles from the inner divertor were mounted on an indium disk.
- IP analysis: T-retention is different in each dust particle.
- SEM observation and EDX analysis of composition were conducted: C, Be, W, O, Fe, Al were determined: Dominant component of dust#1-8 was C, which retain relatively large T-amount.

Superimposed photo (IP, SEM, usual photo)

23/19

Be dust tends to Oxide (XPS)

- Chemical bindings of Be were measured by XPS after argon(Ar) ion etching. Beryllium oxide on the ILW dust was observed.
- Oxygen (O) concentration on Be dominant is higher than that the dust without Be.



24/19

4. Analysis summary in IFERC, Rokkasho

- Divertor tiles and dust of JET ILW 1st campaign have been analyzed in IFERC, Rokkasho, which has been carried out by JA/QST collaboration with strong support by JET/EU members.
- Some unique results were presented recently, which will impact on ITER divertor operation, and DEMO design and R&D: erosion, material transport, change in surface characteristics, T-retention, dust generation and deposition:
 - Tritium retention analysis using IP technique, liquid scintillator counting, TDS
 - T-retention near and inside the tile surface is caused by thermalized and fast triton.
 - T-retention on dust surface (IP), and the total retention (TDS, LSC, Comb.) were evaluated.
 - T-specific activity (Bq/g) in JET-ILW dust is comparable to that in the dust in JET-C.
 - Microstructure analysis of cross-section as well as surface using TEM and FIB fabrication:
 - Bubbles-like structure was generated in Be-deposition layers on the inner W-target.
 - Be-deposition pattern on a rough W-surface vs the plasma incident is investigated.
 - Bubbles-like structure was generated inside a Be dominant dust.
 - Chemical components and state analysis on surface and cross-section using XPS, EPMA
 - Dep. pattern of Be, W, C, O, Mo was determined on the inner targets and remote regions.
 - Be-oxide in Be dominant dusts, and some W and/or C dusts were determined.
- Analysis study will be extended until the end of extended BA (2019).
- Transport of new samples (tile cores and dust in the 3rd campaign of JET-ILW) including bulk-W lamellar plate and Be wall sample, are planned in 2017.

25/19

Presentations in major international meetings/conferences

2014: 1 report in ITPA meeting

- **Studies of Dust from JET-ILW:** M. Rubel, et al, 20th ITPA SOL and Div. Physics TG meeting, Prague (2014)

2015: 1 report in ITPA meeting

- **Tritium Distributions on Tungsten and Carbon Tiles Used in JET Divertor:**

Y. Hatano, et al, 21st ITPA SOL and Div. Physics TG meeting, Princeton (2015)

2016: 3 presentations to Int. Conferences, 3 reports in ITPA meetings

- **Comprehensive Analysis of Metal Dust Particles in JET-ILW, and Impact on Fusion Reactor:**

N. Ashikawa, et al, 26th IAEA-FEC, Kyoto (2016)

- **Comprehensive Characterisation of Dust Particles from JET-ILW:** N. Ashikawa, et al, 22nd PSI, Roma (2016)

- **Micro/nano characterization of the surface structures in the divertor tile in JET ITER-like wall:**

M. Tokitani, et al, 29th SOFT 2016, Prague (2016)

- **Characterization of dust particles removed from the JET-ILW divertor by vacuum cleaning after the 2011-2012 campaign:** N. Ashikawa, et al, 22nd ITPA SOL and Div. Physics TG meeting, Frascati (2016)

- **Update on post-mortem analysis of divertor tiles from JET-ILW:**

M. Tokitani, et al, 23rd ITPA SOL and Div. Physics TG meeting, Naka (2016)

- **New results of JET dust analysis “Progress of analytical results for Be and T on ILW dust particles” :**

N. Ashikawa, et al, 23rd ITPA SOL and Div. Physics TG meeting, Naka (2016)

2017: 4 submissions to Int. Conferences, 2 reports in ITPA meeting

- **Analyses of Structure, Composition and Retention of Hydrogen Isotopes in the JET-ILW Divertor Tiles:**

S. Masuzaki, et al, 16th PFMC, Neuss/Düsseldorf (2017) -- invited

- **Tritium Analysis of Divertor Tiles Used in JET ITER-like Wall Campaigns by Means of β -ray Induced X-ray Spectrometry:** Y. Hatano, et al, 16th PFMC, Neuss/Düsseldorf (2017)

- **Plasma-Wall Interaction on the Divertor Tiles of JET ITER-Like Wall from the Viewpoint of Micro/Nanoscale Observations:** M. Tokitani, et al, 13th ISFNT, Kyoto (2017)

- **Dust Generation in Tokamaks: Overview of Beryllium and Tungsten Dust Studies in JET with the ITER-Like Wall:** M. Rubel, et al, 13th ISFNT, Kyoto (2017)

- 2? presentations to ITPA SOL and Div. Physics TG meeting, York, May (2017)

26/19

2.3.2 Beryllium Materials for Fusion Reactor Wall Applications

C.K. Dorn¹, E.E. Vidal², and S.H. Goods³

¹ *Be4FUSION LLC, Prescott Valley, Arizona, U.S.A.*

² *Materion Beryllium & Composites, Elmore, Ohio, U.S.A.*

³ *S.H. Goods Consulting, Livermore, California, U.S.A.*

E-mail: chris.dorn@be4fusion.com

Beryllium metal and other beryllium-containing materials are known for their unusual combination of properties, which accounts for the long-standing interest in these materials since the 1930s. Important fields of application for beryllium metal, beryllium composites, and beryllium compounds include acoustics, aerospace structures, x-ray transmission, motion control, nuclear test reactors, laser-based optical systems, high-energy particle physics research, high-performance automotive applications, and thermal management. Beryllium-containing alloys (which typically contain less than 2% Be) are used extensively in commercial electronics, telecommunications infrastructure, automotive electronics, oil and gas equipment, tooling for plastic molding, and medical equipment applications. Generally speaking, the utilization of beryllium and Be-containing materials has mainly been limited by its high cost and the need for special handling during fabrication.

Beryllium Materials for Fusion Reactor Wall Applications

Christopher K. Dorn¹, Edgar E. Vidal², and Steven H. Goods³

1 Be4FUSION LLC, Upland, California, U.S.A.

2 Materion Beryllium & Composites, Elmore, Ohio, U.S.A.

3 S.H. Goods Consulting, Livermore, California, U.S.A.

Abstract

Beryllium metal and other beryllium-containing materials are known for their unusual combination of properties, which accounts for the long-standing interest in these materials since the 1930s. Important fields of application for beryllium metal, beryllium composites, and beryllium compounds include acoustics, aerospace structures, x-ray transmission, motion control, nuclear test reactors, laser-based optical systems, high-energy particle physics research, high-performance automotive applications, and thermal management. Beryllium-containing alloys (which typically contain less than 2% Be) are used extensively in commercial electronics, telecommunications infrastructure, automotive electronics, oil and gas equipment, tooling for plastic molding, and medical equipment applications. Generally speaking, the utilization of beryllium and Be-containing materials has mainly been limited by its high cost and the need for special handling during fabrication.

1. Introduction

Notwithstanding the wide range of technological applications, the intent in this paper is to focus on the use of beryllium materials in fusion wall applications. The use of metallic beryllium in fusion research has its origin in the 1980s, when it was first used in the UNITOR and ISX-B tokamaks [1]. The first major use of beryllium was in the Joint European Torus (JET), which began operation in 1983 [2]. JET used beryllium in specific areas inside the torus, in the form of tiles to act as the plasma-facing armor and as a coating for the carbon walls of the reactor.

The use of beryllium took a major step forward when, in November 1985, General Secretary of the Communist Party of the Soviet Union, Mikhail Gorbachev and U.S. President, Ronald Reagan agreed that the two nations should find a way to work together on a peaceful use for fusion energy [3]. This historic agreement led to the project that is now known as ITER (originally an acronym for “International Thermonuclear Experimental Reactor”). Beryllium was selected as the plasma-facing material for its First Wall. Today, ITER remains under development and is now being built in Cadarache, France.

2. Candidate Materials for Fusion Wall Applications

The aforementioned historical use of beryllium in JET provided the data and provenance for selecting beryllium for use in ITER. There are, however, some differences in how the beryllium has been processed for use in JET and how it will be processed for use in ITER.

2.1 How Beryllium is Made

Before delving into details regarding candidate beryllium grades for use in First Wall applications, a few basics on how it is made should be covered. Beryllium is a naturally occurring element, with atomic number 4. Due to its high reactivity, however, it is virtually never found in elemental form. After initial refining from ore, beryllium is often vacuum-cast for further purification [4]. Be exhibits a hexagonal close-pack crystal (HCP) structure, which is highly anisotropic in nature, and is characterized by preferential cleavage along the basal plane of the crystal. The vacuum-cast material has a very large grain size, which exacerbates the intrinsically poor properties of the HCP material. As a result, vacuum-cast Be is not considered useful for most applications.

Due to these inherent problems with vacuum-cast material, powder metallurgy is used to make fine-grained, mechanically isotropic beryllium for almost all applications of interest, which certainly includes fusion First Wall components. Purity, mechanical properties, and isotropy of powder-derived beryllium are most heavily influenced by both the powder-making technique and by the consolidation method chosen for producing any given grade of material.

Historically, beryllium powders have been produced on an industrial scale by the following methods: attrition milling, impact grinding, rotating electrode process, and inert gas atomization. The first two methods are mechanical means of creating powders, and the latter two are metallurgical methods. With respect to mechanical methods, impact grinding is generally favored over attrition milling, as it yields a more equi-axed particle. This, in turn, gives better packing densities during processing, and results in a more mechanically isotropic material after consolidation compared to attrition milling. In regards to metallurgical methods, inert gas atomization is generally favored over a rotating electrode process due to its better economies of scale.

Several consolidation methods have also been used when producing powder-derived beryllium on an industrial scale. These include vacuum hot-pressing (VHP), axial cold-pressing and free sintering, cold isostatic pressing (CIP) and free sintering, and hot isostatic pressing (HIP). As previously stated, different combinations of powder-making method and consolidation techniques will influence the properties of the resulting beryllium material, which will be illustrated in greater detail in the next sections.

2.2 Historical Use of Beryllium in JET

When JET began operation in 1983, the plasma-facing material was carbon. Unable to control the density and purity of the plasma due to contamination from carbon sputtering, by 1989, a number of beryllium components were installed in the vessel. These included the belt limiter and RF (radio frequency) antenna tiles (see Figure 1). The oxygen-gettering quality of beryllium dramatically reduced impurities in the plasma. The change resulted in making beryllium the main impurity in the plasma, but due to its low atomic number, the effective Z (Z_{eff}) of the plasma was not significantly impacted, and the introduction of the material achieved its desired effect [1].

The belt limiter and RF antenna tiles were made by Materion Brush Inc. in Ohio, U.S.A. (then known as Brush Wellman Inc.) from near-net-shaped, axially cold-pressed and sintered S-65 beryllium. S-65

is a powder-derived, structural grade beryllium that was chosen by JET over other available structural grades (such as S-200E or S-200F) due to its combination of higher purity and higher ductility, as shown in Table 1.

Table 1. Comparison of impurity levels and ductility for several commercially available industrial-scale grades of beryllium in the 1980s [5].

Be Grade	Be Assay (% min.)	BeO (% max.)	Fe (% max.)	C (% max.)	Elongation (% min.)
I-70	99.0	0.7	0.10	0.70	2.0
I-220	98.0	2.2	0.15	0.15	2.0
I-400	94.0	4.2*	0.25	0.25	N/A
S-65	99.0	1.0	0.08	0.10	3.0
S-200E	98.0	2.0	0.18	0.15	1.0
S-200F	98.5	1.5	0.13	0.15	2.0

*BeO content for I-400 was % minimum rather than maximum. All other grades were specified as % maximum.

Axial cold-pressing and free sintering was chosen as the production method over standard VHP purely as a cost-saving measure. Since part volumes were high (several hundreds to more than one thousand pieces), it was possible to justify the up-front expense of a custom die for cold-pressing the impact-ground beryllium powder. The cold-pressed parts were then free-sintered in a vacuum furnace to full density and machined to final size. A smaller quantity of divertor target tiles was also made for JET using standard S-65 Be VHP [6].

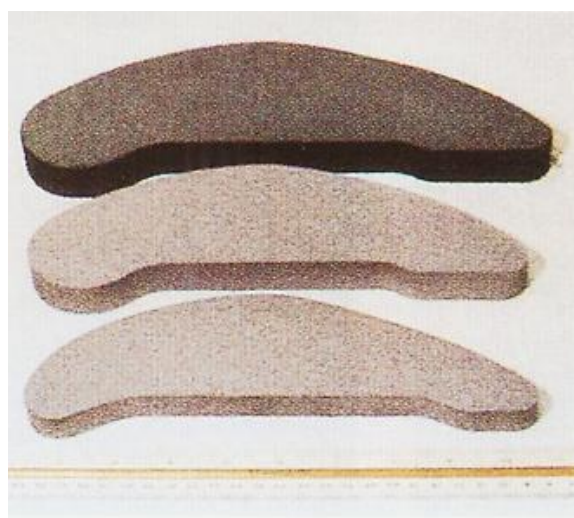


Fig. 0. From top to bottom: as-axially cold-pressed “sub-dense” RF antenna tile blank, as-sintered full-density tile blank, and finish-machined tile [7].

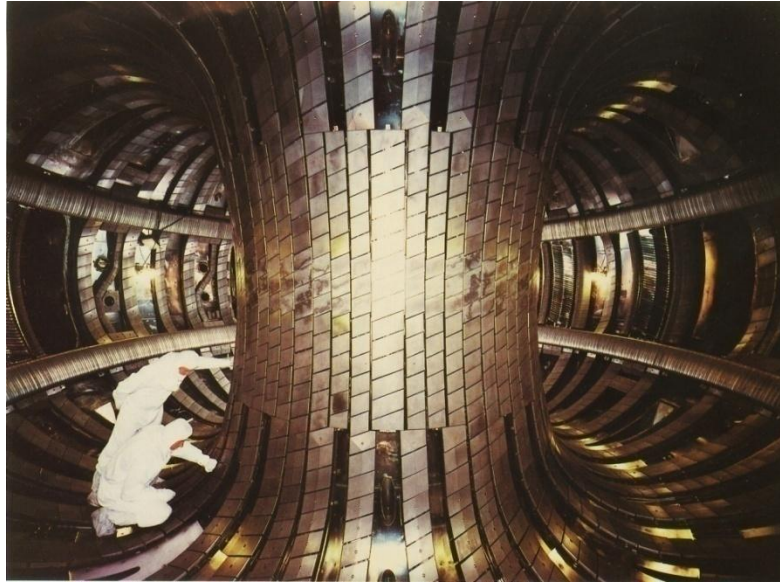


Fig. 2. JET vessel interior after the installation of the beryllium in the 1980s. The two horizontal bands just above the technicians are the beryllium tiles. The rest of the tiles are carbon fiber composite [7].

2.3 Current Use of Beryllium in JET

By the mid-2000s, as operations were beginning to wind down, it was suggested that the JET team could perform some important research in their reactor which would greatly benefit the ITER program. From this idea was born the ITER-Like Wall Project. In brief, the concept was to retrofit the JET tokamak with beryllium plasma-facing tiles and tungsten divertor tiles similar to what is planned for ITER [8].

Economics of the project were a critical issue, but JET was able to meet both their technical and construction cost goals by recycling used S-65 tiles into new Be raw material. The project posed some challenges due to the fact that the old tiles contained small amounts of tritium. A safe-handling plan was devised; the old tiles were re-melted and made into new S-65 HIPed beryllium. The new beryllium was then machined into complex, castellated tiles at specialist machining houses in the U.S. and Europe [9].

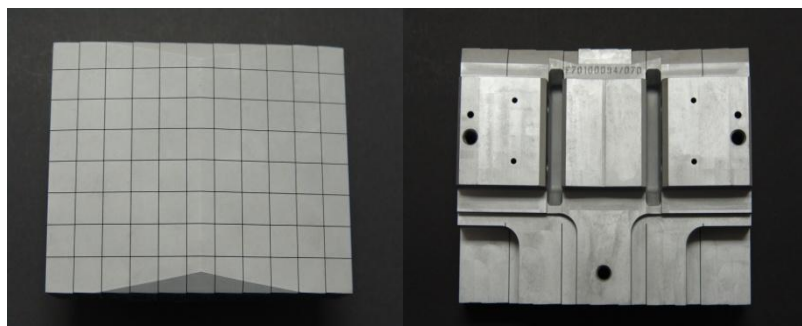


Fig. 3. These photos depict the front (left) and back (right) of a finish-machined, castellated beryllium tile for the ITER-Like Wall Project at JET [10].

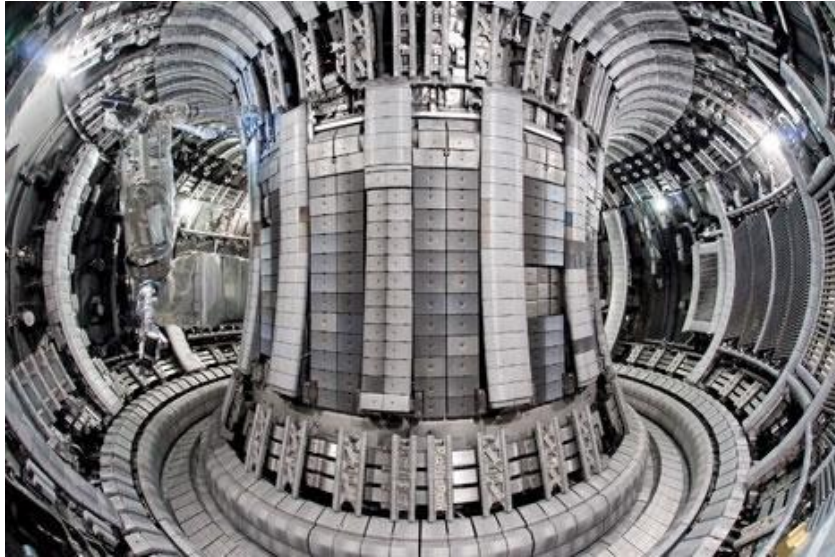


Fig. 4. JET vessel interior after the installation of the ITER-Like Wall in 2009. Apart from the tungsten divertor, all of the tiles are now beryllium [11].

2.4 Specifications for Beryllium in ITER

Beryllium was chosen over carbon, tungsten, or other candidate materials for the ITER First Wall, covering about 80% of the inside of the vessel, because:

- It will have a minimal effect on plasma contamination, since it does not chemically sputter as carbon does.
- It will give low radiative power losses.
- It is a good oxygen getter.
- It will retain a low bulk tritium inventory.
- It offers the possibility of in-situ or hot-cell tile repair [12].

Table 2 summarizes the grades and sources of Be available to the ITER program in the timeframe of the mid-to-late 1990s.

Table 2. Candidate beryllium material grades evaluated by ITER in the 1990s [13].

Grade	S-65	S-65	S-65	S-200F	S-200F	SR-200	I-400
Mfg. Method	VHP	HIP	CIP	VHP	HIP	VHP & Rolled	VHP
Source	MBI	MBI	MBI	MBI	MBI	MBI	MBI
Grade	DShG-200	TShG-56	TR-30	DIP-30	TShGT	TGP-56	TShG-200
Source	RF	RF	RF	RF	RF	RF	RF

Notes: MBI = Materion Brush Inc., U.S.A.

S-65 Be made by VHP was designated by ITER as the reference grade, due to its thermal fatigue resistance. Other factors that influenced this selection were its commercial availability, technical database, and its successful use in JET. At the same time, DShG-200 was selected as a back-up grade [13].

Since then, other grades of Be have been qualified, and these are designated as TGP-56FW [14] and CN-G01 [15]. During this same period, Materion Brush Inc. has also upgraded some of the

specification limits on S-65 VHP, and the specification has gone from Rev. C to Rev. E [16]. It should be noted that ITER documents still refer to this material as S-65C, with the “C” intended to signify Rev. C of the specification. The supplier generally does not use a revision designator in this manner, lest it be confused with S-65-C, which would be the specification title for S-65 made by CIP.

Table 3. Specification and typical (typ) values for selected impurities in the three ITER First Wall Be grades (wt %) [13-16, 74].

Grade	Be		BeO		Al		C		Fe	
	min	typ	max	typ	max	typ	max	typ	max	typ
S-65	99.2	99.4	0.9	0.66	0.05	0.036	0.09	0.02	0.08	0.078
TGP-56FW	99.0	99.02	1.0	0.95	0.04	0.018	0.1	0.05	0.12	N/R
CN-G01	99.0	N/R	1.0	N/R	0.06	N/R	0.1	N/R	0.08	N/R

TGP-56FW typical values are actuals from one lot with Fe content of 0.16 [14]; impurity spec max levels changed a few years later, but no new actuals or typicals were cited [74].

ITER’s official position is that the three different grades of beryllium are expected to perform similarly, and the data generated to date seem to support that conclusion. The important difference at this writing is that S-65 has been in production since 1975 [18], and more than 200 tons of material have been manufactured in over 40+ years. TGP-56FW and CN-G01 are just recently developed, and have only been produced in small quantities to date. The challenge going forward for these materials will be ramping up production to meet the ITER technical and schedule requirements without sacrificing quality and performance.

3. Basic Material Properties

3.1 Physical Properties

Over the years (1955-2009), there have been several summaries of the general physical properties of beryllium [19-22], with slightly varying value ranges on some properties, but all generally quite similar. The ITER Material Properties Handbook also has a summary [1].

Table 0.4. Below is a summary of some selected physical properties of beryllium as published in *Beryllium Chemistry and Processing* in 2009, with aluminum and iron shown for purposes of comparison [22]. Specific heat in SI units was found from another source [23].

Property	Al	Fe	Be
Atomic Number	13	26	4
Atomic Weight	26.98	55.85	9.0122
Density (g/cm ³)	2.70	7.87	1.85
Melting Point (°C)	660	1537	1285
Boiling Point (°C)	2494	2750	2770
Latent Heat of Fusion (kJ/mol)	10.79	13.80	12.2
Electrical Conductivity at 20°C [$\mu\Omega\text{-cm}$] ⁻¹	0.372	0.103	0.25
Thermal Conductivity (W/m-°K)	247	80.2	210
Specific Heat (kJ/kg-°K)	0.91	0.45	1.83
Elastic Modulus (GPa)	9.9	28.5	303
Coefficient of Thermal Expansion (ppm/°C)	23.2	11.9	11.5

ITER International, the organization established to run the ITER program, reports that physical properties of all three ITER First Wall beryllium grades have now been measured and compared for: density, thermal conductivity, coefficient of thermal expansion (CTE), elastic modulus, Poisson's Ratio, and specific heat [17]. Figures 5 and 6 present the temperature-dependent CTE and thermal conductivity for all three grades.

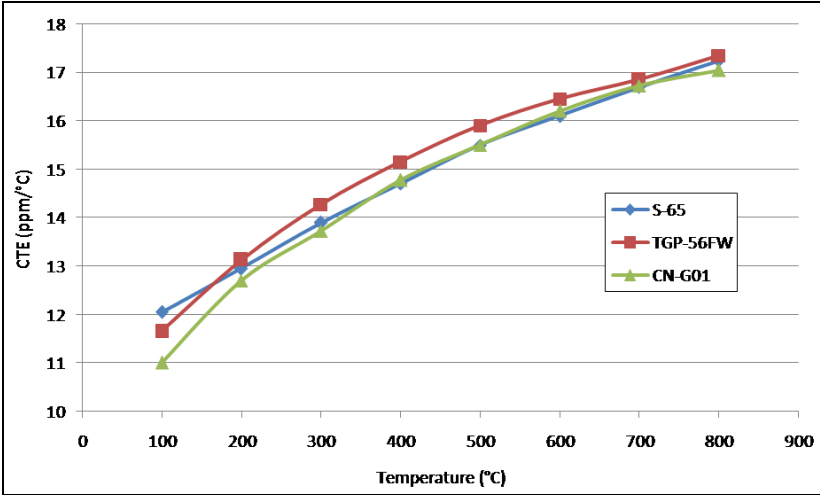


Fig. 5. Temperature dependence of the averaged coefficient of thermal expansion for S-65, TGP-56FW, and CN-G01 beryllium [17].

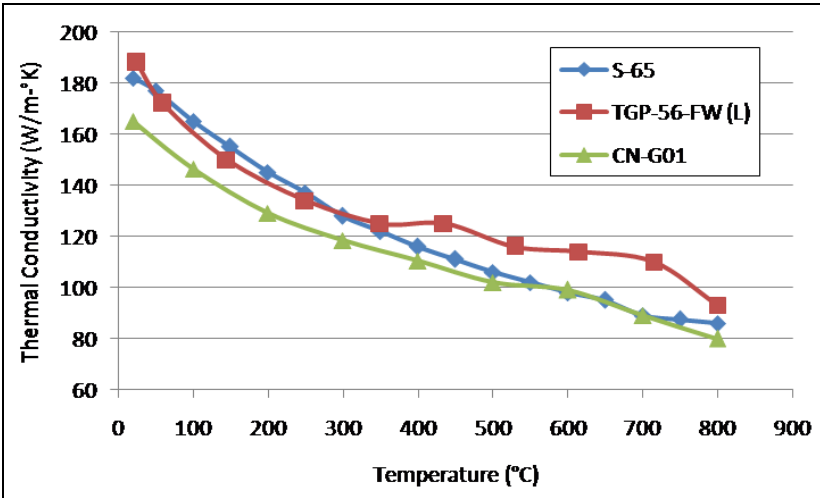


Fig. 6. Temperature dependence of the thermal conductivity for S-65, TGP-56FW, and CN-G01 beryllium [17].

To simplify the comparison of the three grades, the longitudinal and transverse values for CTE for TGP-56FW and CN-G01 were averaged. CN-G01 thermal conductivity is also presented this way. The longitudinal and transverse thermal conductivity for TGP-56FW were not available over the same temperatures ranges. Therefore, only the longitudinal data for TGP-56FW are presented in the comparison, as this set was more complete than that in the transverse direction. ITER International's conclusion is that there is generally good agreement between the physical property data for S-65, TGP-56FW, and CN-G01, and that all three grades are acceptable for the ITER First Wall [17].

3.2 Mechanical Properties

3.2.1 General Considerations

Beryllium is an inherently low ductility material at room temperature. When first made widely available, from the 1940s through 1960s, the state-of-the-art grades offered only 1-2% tensile ductility. Through process refinements in the 1970s, it became possible to offer material with greater than 3% elongation and improved isotropy [18]. Wrought material, either in the form of rolled sheet or extruded rod/tube has always offered the possibility of much higher mechanical strength and elongation in the direction(s) of work, but unfortunately at the expense of those same properties in the transverse direction [24]. The specification for hot-rolled sheet, for example, offers minimum values for yield (YS) and ultimate tensile (UTS) strengths at roughly 50% greater than for VHP block, and minimum elongation of 10% in the plane of the sheet [25]. Through the thickness of the sheet, however, the elongation becomes much less than 1%, a value that is not even routinely measured or defined in the specification.

3.2.2 Considerations Specific to Fusion Wall Applications

The higher tensile elongation of S-65 compared to other grades of beryllium block helped lead to its original selection by JET, and also to its selection for the ITER First Wall. TGP-56FW and CN-G01 have had to meet similar properties in order to become qualified for use in the ITER First Wall as well. It should also be noted that ITER specifically chose VHP-consolidated beryllium for the First Wall as opposed to HIPed material because of the slight anisotropy in mechanical properties between the longitudinal and transverse directions. The longitudinal direction has slightly lower tensile strength and elongation [26]. By defining a specific orientation of the First Wall tiles with respect to the pressing direction of the VHP beryllium, ITER can ensure that if a tile cracks, it will do so through the thickness of the tile thereby creating what is effectively a new castellation, rather than causing layers of a tile to spall off in the reactor. Sufficient data now exist to allow for a meaningful comparison of the mechanical properties of all three ITER First Wall beryllium grades as shown in Table 5 [14-17].

Table 5. Comparison of specification and typical values for mechanical properties at room temperature for ITER First Wall Be grades [14-17].

Grade	YS		UTS		Elongation		Grain Size	
	min	typ	min	typ	min	typ	max	typ
	(MPa)		(MPa)		(%)		(μm)	
S-65	206	230	289	386	3.0	5.2	20	10
TGP-56FW	250	N/R	350	N/R	2.0	N/R	20	13-14
CN-G01	210	N/R	340	N/R	3.0	N/R	20	N/R

Notes: N/R = not reported.

Data illustrating the uniaxial tensile behavior of all three grades as a function of temperature is also now available, and the results for UTS and elongation are presented in Figures 7 and 8 [17].

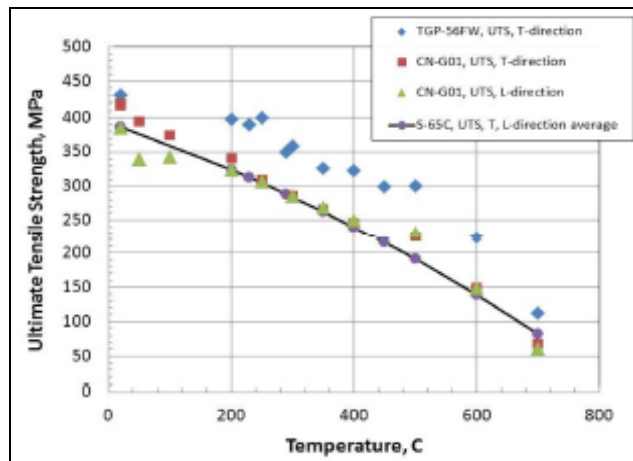


Fig. 7. Temperature dependence of the UTS for all three principal candidate beryllium materials [17].

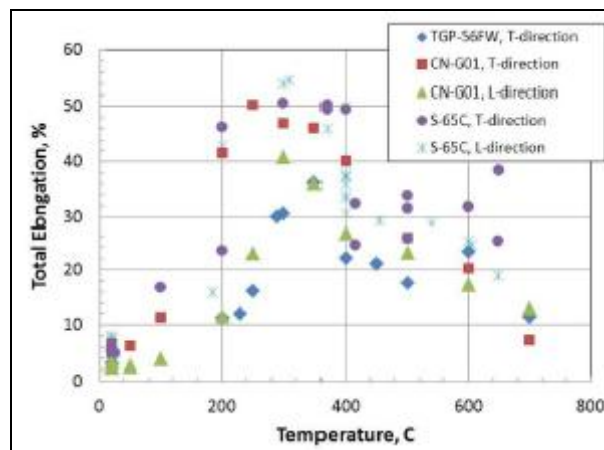


Fig. 8. Temperature dependence of the total elongation for all three principal candidate beryllium materials [17].

TGP-56FW shows consistently higher strength than the other grades, as shown in Figure 7, but also lower elongation (see Table 5). This is likely a result of its higher BeO content (see Figure 8 and Table 3). In powder-derived beryllium grades, higher BeO content results in higher strength, but lower ductility.

While there is significant scatter in the ductility data, all three materials show the same general trend: increasing ductility with increasing temperature, peaking at 350°C and then trending lower as the test temperature increases. As with the physical properties, it is once again ITER International's conclusion that there is generally good agreement between the mechanical property data for S-65, TGP-56FW, and CN-G01, and that all three grades are acceptable for the ITER First Wall [17].

4. Fabrication and Joining Technology

4.1 General Considerations

Due to its use in a wide range of applications as mentioned in the introduction to this paper, it has been essential to develop a variety of methods for fabricating beryllium into its desired form as a finished

part, as well as to be able to join it to itself and other materials so that it may function as part of an assembly.

Beryllium is intrinsically a metal, and as such, it may be fabricated by the same methods as other metals are. It can be machined (conventionally or by electro-discharge methods), ground, polished, chemically etched, rolled, extruded, forged, etc. Beryllium can be joined to itself and other materials by mechanical fastening and adhesive bonding, as well as a variety of metallurgical methods which include atmosphere brazing (done in air, using flux to inhibit oxidation), vacuum brazing, indirect diffusion bonding (using a braze alloy), electron beam welding, laser welding, and HIP bonding.

In solid form, handling of beryllium poses no special risks. One key difference, however, in fabricating with beryllium compared to many other materials is the need for special handling due to environmental, health, and safety (EH&S) concerns. There are many detailed treatises on the ever-evolving world of beryllium EH&S, but suffice it to say that any operation which generates airborne beryllium particulate, dust, or fumes will need engineering controls and possibly respiratory protection for workers. Manufacturing and fabrication operations which always require special controls include melting, casting, powder-making, powder-consolidation, machining, chemical etching, grinding, extruding, forging, hot-forming, rolling, welding, brazing, etc. [27].

Any organization or individual considering establishing beryllium manufacturing or fabrication capabilities should consult the current local, federal, and international regulations for safe handling of beryllium before undertaking any actual processing of the material [28-29].

4.2 Considerations Specific to Beryllium

Beryllium is located in the galvanic series in between magnesium and aluminum [30]. It is, therefore, a highly reactive metal and is prone to form brittle intermetallic compounds with a wide variety of elements. For this reason, the use of low-melting-point braze alloys (Ag-based alloys for example) can be particularly problematic where residual mechanical properties are important. This problem has been overcome in industry by using a closely monitored liquidus-brazing process wherein the work pieces spend only short times at high temperature, suppressing the formation of the deleterious intermetallics [31].

In the case of solid-state diffusion bonding, which is performed in a vacuum furnace with special tooling, the formation of intermetallics is effectively suppressed by using a combination of lower temperature (below the melting point of the braze alloy) and pressure to create the joint. These two processes have been used effectively since the 1970s for making beryllium x-ray transmission window assemblies for a variety of end-uses, for example, and they are still used today [31].

Joining beryllium via traditional welding processes can be problematic. Powder-derived beryllium is generally not tungsten-inert-gas (TIG) welded due to the fact that it recrystallizes in the weld zone, resulting in highly directional and dramatically reduced mechanical properties. It can, however, be electron-beam (EB) welded to itself by using an aluminum interlayer. Beryllium-aluminum composites with at least 38% Al content were developed to be TIG and EB-weldable without

interlayer materials [32]. Beryllium has been successfully EB-welded directly to aluminum and to stainless steel by using an aluminum-stainless transition material [31].

Due to beryllium's inherently brittle nature, machining processes must be carefully controlled in order to avoid surface micro-cracking and twinning. It is common to acid etch machined parts to remove residual surface damage [33]. For ITER, it appears that First Wall components will be manufactured via wire electro-discharge machining (EDM), where tiles will be cut out of bulk material, or for creating castellations in larger pieces of beryllium [34].

4.3 Considerations Specific to Fusion Wall Applications

In order to use beryllium as a plasma-facing material, it must be joined to other materials as needed to perform its particular functions. For the ITER-Like Wall program at JET, the beryllium tiles were mechanically installed in the torus. The attachment points for those tiles are the holes and slots machined into the back of the tile, which is shown in the photo on the right in Figure 3.

Mechanical attachment of the beryllium tiles has been acceptable for JET since the beryllium could adequately handle the thermal loads characteristic of JET operation. For ITER and its follow-on (DEMO), mechanical attachment will not be acceptable due to the significantly higher thermal loads [6]. The ITER First Wall assembly is a complex structure consisting of the plasma-facing Be tiles joined to a copper alloy heatsink, which in turn, is joined to a stainless steel support. The size, shape, and thickness of these Be tiles has evolved over the design cycle. The tiles are now expected to be on the order of 5-6mm in thickness with planar dimensions that vary by the location within the torus [35].

As currently designed, ITER incorporates two different heat-flux sectors, with loads of $2\text{MW}/\text{m}^2$ (low-heat flux) and $4.7\text{MW}/\text{m}^2$ (high-heat flux) [36]. These two sectors will feature First Wall assemblies of entirely different designs and construction details to deal with these loads. From a joining point of view, however, the issue is the same, which is that beryllium needs to be joined to a copper-chromium-zirconium (CuCrZr) alloy by a method which will handle the thermal loads and not be compromised by the radiation environment. As described earlier, conventional metallurgical joining of beryllium to copper alloys is typically done by vacuum brazing or indirect diffusion bonding. Either of these processes typically relies on silver-based braze alloys. Silver, however, will activate in ITER's radiation environment to form low melting point constituents that will compromise bond integrity.

Prior to mid-2010, six ITER domestic agencies (DAs) were to participate in the construction of the First Wall beryllium tile assemblies: China, Europe, Japan, Korea, Russia, and the U.S. Five DAs worked to develop a HIP bonding process for joining Be to CuCrZr, while ITER Russia went in a different direction entirely, developing a "fast brazing" process that avoids the issues associated with using Ag-based braze alloys as described earlier [37-38]. As a result, most of the R&D work which has been done is in the area of HIP bonding. Federici et al. [1] has already written an in-depth summary of the development and results for the manufacturing of the Be-to-CuCrZr-to-RAFM steel from all six ITER DAs who were originally involved with the project. The results are well documented in technical papers from China, Europe, Japan, Korea, Russia, and the U.S. [39-50].

There has been some debate in the ITER community whether the better way to make First Wall panels will be to join large pieces of beryllium to the CuCrZr first, and then finish machine, or to make finished, individual tiles first and join those to the heatsink material. ITER Russia, which has become the first DA to begin manufacturing the actual First Wall (not simply prototypes or test assemblies), favors the wire EDMing of discrete tiles and then fast brazing to the CuCrZr [35].

4.4 Other ITER-Related Fabrication and Joining Results

Be-to-CuCrZr has been the primary focus of joining R&D, but there has also been some investigation of Be to Reduced Activation Ferritic-Martensitic (RAFM) steel for armor applications in the ITER Test Blanket Modules (TBMs) [51]. This latter R&D work has become, at least for the moment, less important, as ITER design changes have now recessed the TBMs further from the plasma, potentially eliminating the need for Be armor on the RAFM steel plasma-facing surfaces [52]. The Be-to-RAFM steel joining has been studied in both Korea [53-55] and the U.S., with the most extensive work done by Hunt at UCLA [51, 56].

5. Irradiation Effects

Materials in proximity of the plasma must have very well defined properties and must not affect the plasma's stability or its characteristics. The plasma-facing blanket material plays several important roles. It must protect the vacuum vessel and ancillary components from the intense radiation environment. It does this by moderating the neutron energy, converting that kinetic energy to sensible thermal energy, which in turn, is extracted by the reactor cooling system.

While doing this, the First Wall material should not contaminate the plasma via erosion or sputtering. If erosion or sputtering does occur, there should be minimal impact on the plasma characteristics. Furthermore, the ideal First Wall material should be a good oxygen getter, have low radiative power losses, and exhibit low tritium retention. Within the ITER operating parameters, beryllium meets these requirements [1].

Unfortunately, there is not a great deal of irradiation data available on the three ITER First Wall beryllium grades, especially TGP56-FW and CN-G01. Data for S-65 Be is presented when possible, but data for other U.S. and Russian beryllium grades is used in many instances. No irradiation data on any Chinese beryllium grades could be found.

It should also be noted that while beryllium metal is not likely to be used as a plasma-facing material in fusion reactors after ITER, such as DEMO, it has been suggested that beryllide intermetallic compounds such as TiBe_{12} may be suitable. Beryllides have much higher melting points than beryllium metal, better oxidation resistance, and have a much lower Z_{eff} than other candidate materials such as tungsten [57].

5.1 Physical Properties

5.1.1 Micro- and Macrostructure

It is long-established that beryllium swells under neutron irradiation. The swelling is caused by the formation of helium atoms, which are produced from the fission of the beryllium with low energy neutrons as:



Helium produced in this way can migrate to trapping sites, such as point defects, grain boundaries, etc., to form bubbles that can also arrest the motion of dislocations, pin grain boundaries, and serve as stress concentrators and crack-initiation sites [58]. Tritium is produced at higher neutron energies as:



Tritium effects on the properties of beryllium will be discussed in Section 6. In this section, the effects of entrapped helium and point-defect generation are briefly reviewed.

At this writing, comparison data for swelling in irradiated S-65, TGP-56FW, and CN-G01 are not yet available. In 2000, Barabash et al. [59] published a review of S-65 compared to Russian grades, including THP-56P, a predecessor to TGP-56FW. The data were taken from multiple sources [60-62] to make the comparison shown in Figure 9.

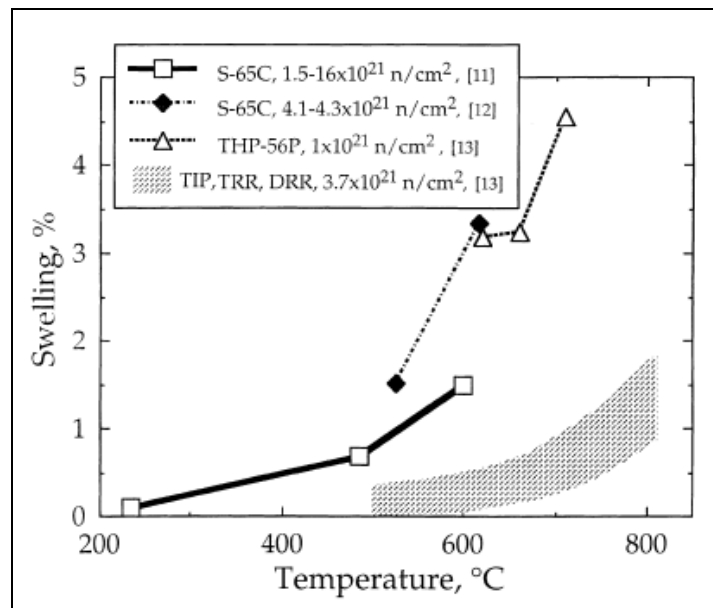


Fig. 9. Swelling of S-65 VHP Be compared to selected Russian beryllium grades as a function of temperature at different neutron fluences [59].

Barabash et al. conclude from their compiled data that S-65 and Russian grades of beryllium all exhibit moderate swelling ($\sim <1\%$) for irradiation temperatures $<500^\circ\text{C}$, but higher rates ($\sim 2\text{-}4\%$) above 500°C , which is generally consistent with historical data on other beryllium grades [59]. They also note that above 500°C , S-65 had a slightly higher swelling rate when compared to S-200F, another beryllium grade from the same producer (Materion Brush Inc.) which has higher BeO content and higher mechanical strength than S-65.

From the data on the Russian grades, Barabash et al. conclude that beryllium grades with the smallest grain size and highest BeO content (TRR, DRR, TIP, and DIP) exhibit the least amount of high-temperature swelling due to the presence of many small BeO particles which prevent the migration of helium and formation of the bubbles which cause the swelling. A computer code called ANFIBE, the acronym for which is derived from the name “Analysis of Fusion Irradiated Beryllium”, was developed around 1998 to predict the amount of swelling in irradiated beryllium, but as Barabash et al. point out, there is still the need to verify the code with additional data on the beryllium grades of interest [59].

5.1.2 Thermal Properties

Snead irradiated S-65 beryllium in a temperature range of 100-300°C with a fast neutron fluence ($E > 0.1\text{MeV}$) of $0.05\text{-}1.0 \times 10^{21} \text{ n/cm}^2$. He found that the thermal conductivity (TC) was similar to that of unirradiated beryllium, within 4% experimental error [63].

The Russian beryllium grade TE-56, when irradiated between $1 \text{ and } 6 \times 10^{22} \text{ n/cm}^2$ at 70°C, showed a substantial decrease in TC as shown in Figure 10. For a neutron fluence of $2.4 \times 10^{22} \text{ n/cm}^2$ at 70°C, TC fell to about $50\text{W/m}\cdot\text{K}$ from an initial value of $\sim 225\text{W/m}\cdot\text{K}$. After annealing at 500°C for one hour, TC recovered to $\sim 150\text{W/m}\cdot\text{K}$. The significant reduction in the thermal conductivity after irradiation and the subsequent recovery after annealing could only be explained by the radiation-induced generation of point defects. At higher irradiation temperatures (400°C) the reduction in thermal conductivity was only 15% after $1.6 \times 10^{22} \text{ n/cm}^2$ compared to the unirradiated material [64].

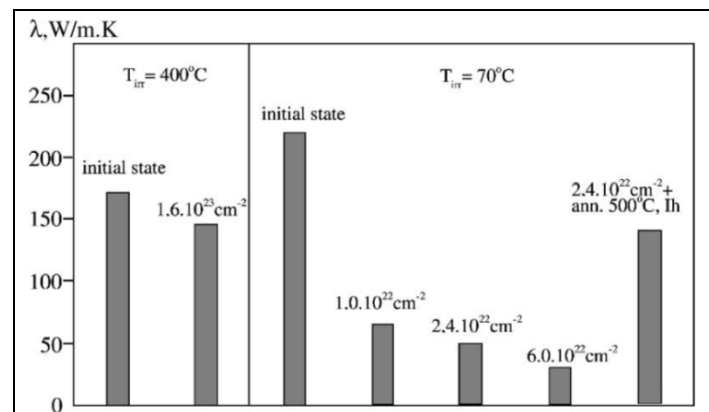


Fig. 10. Thermal conductivity of irradiated beryllium at room temperature [64].

5.2 Mechanical Properties

Studies have shown that irradiated beryllium exhibits hardening due to pinning of dislocations and separation at grain boundary interfaces due to the presence of the aforementioned helium bubbles [1]. Gelles et al. have published a comprehensive literature review on the effects of neutron irradiation on beryllium [65], and they have summarized the general, qualitative effects as follows:

- At low-to-moderate irradiation temperatures (20-500°C), strength typically increases, but ductility decreases, in some cases to zero.

- At high irradiation temperatures (>600°C), ductility decreases, but without the accompanying increase in strength as shown in the low-to-moderate temperature range (20-500°C).
- Increasing the fluence (dose) leads to saturation of the changes in strength and ductility [1, 59, 65].

Snead notes, as also cited by Federici et al. [1], that the principal result of low-temperature (<~200°C) irradiation on the mechanical properties is embrittlement of the beryllium due to the accumulation of radiation defects in the form of dislocation loops. At high temperatures (>~400°C), the embrittlement is due to the formation of helium bubbles at the grain boundaries [63]. It was further noted that more recent mechanical property studies on beryllium conducted at ITER-relevant temperatures show that no major embrittlement occurred [1, 59].

Barabash et al. [59] have graphically summarized neutron-irradiation effects on key mechanical properties of S-65 beryllium based on the data from Snead and Chaouadi et al. as shown in Figure 11 [63, 66].

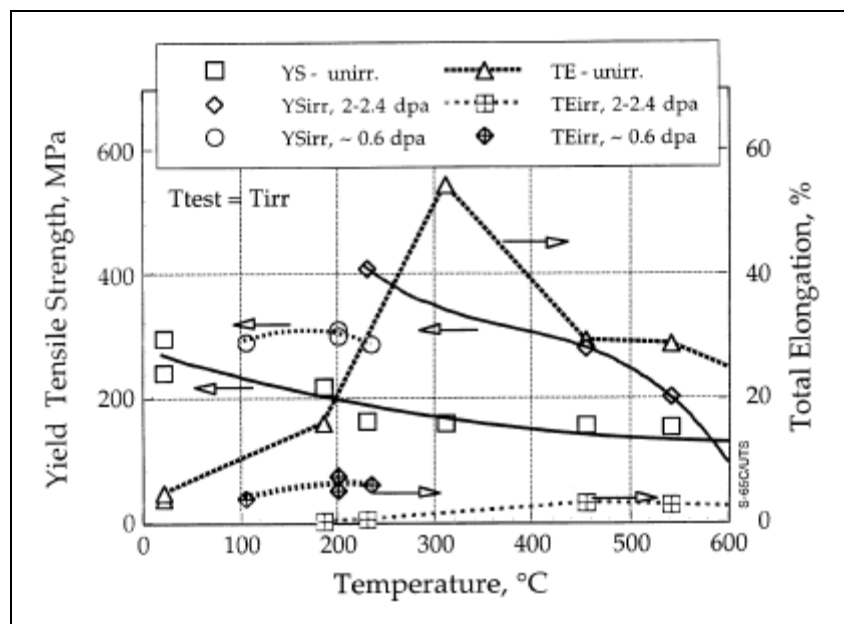


Fig. 11. Temperature dependence of the yield strength (YS) and total elongation (TE) of S-65 beryllium after neutron irradiation [59, 63, 66].

Kupriyanov et al. studied the effects of high-temperature irradiation (700-750°C) on the mechanical properties of various Russian beryllium grades prior to the completion of the development of TGP-56FW [67]. Typical ductility losses were reported. For grades with higher resistance to swelling, due to finer grain size and higher BeO content, some ductility remained (<~5%), but brittle failures resulted for grades with larger grain size and lower BeO content. As previously mentioned in the last paragraph of Section 5.1.1, this resistance to swelling is explained by the reduced migration of helium in these beryllium grades [59].

A few mechanical-property studies have also examined irradiation effects on beryllium's fracture toughness. A comparison between irradiated HIPed beryllium (S-65-H, S-200F-H) and VHP beryllium (S-65, S-200F) was performed. Irradiation was performed under neutron fluences of 2.1×10^{21} n/cm² at 200, 400, and 600°C. The results showed that all beryllium grades had very similar

fracture toughness (K_{Ic}), which increases as the irradiation temperature increases. Typical K_{Ic} values varied from 6.8-15.9MPa \sqrt{m} [68]. In a previous study using the same four beryllium grades, the same author demonstrated that at 1.5×10^{21} n/cm², both S-65 and S-200F-H had slightly higher elongation and strength after irradiation [69].

More mechanical-property studies still need to be carried out on all three ITER beryllium grades at ITER-relevant conditions, and this will certainly be the focus of ongoing work in this area leading up to ITER's scheduled first plasma with the First Wall installed.

6. Tritium Retention and Erosion

Due to the production of high energy neutrons in a fusion reaction, the ${}^9\text{Be} + n \rightarrow {}^7\text{Li} + {}^3\text{H}$ reaction dominates, and tritium generation in the plasma-facing beryllium was originally a major concern. So, in the late 1990s, Kwast et al. and Wu et al. investigated bulk tritium retention in various grades of beryllium (but not S-65, which was the only ITER-approved grade at that time), and they found that tritium retention can increase with neutron fluence by a factor of 3 to 10 [1, 70-71].

Tritium implantation experiments in beryllium conducted at low energies, high fluxes, and high particle fluences showed that after reaching fluences of $\sim 1 \times 10^{22}$ n/cm², further implantation resulted in a negligible increase in tritium inventory. It was theorized that this observation may be explained by the creation of surface-connected porosity that provides the tritium a quick path back to the plasma. The overall impact of these results is that tritium retention in beryllium is expected to be less serious than originally expected [1, 59].

That being said, further experiments have been conducted since those results were published, notably by Chakin et al. and Kurinskiy et al., which indicate that tritium retention in beryllium, including S-65 grade, decreases as the grain size decreases [72-73]. This effect may ultimately become important for potential beryllium use as a neutron multiplier material in a large-scale fusion machine such as DEMO.

Federici et al. have published an excellent, comprehensive study of the erosion characteristics of beryllium as a plasma-facing material [1]. The authors' extensive exploration of this subject covers in detail the fact that beryllium is subject to virtually all possible forms of erosion (with the exception of chemical sputtering), including physical sputtering, mixed material erosion, chemically assisted sputtering, and enhanced erosion at elevated temperatures. Readers seeking in-depth coverage of beryllium erosion characteristics are directed to this source.

7. Summary and Conclusion

Beryllium has been used successfully for plasma-facing components in the JET fusion reactor since the 1980s and for the ITER-Like Wall at JET in the 2000s. Beryllium will be used again for the ITER First Wall in the 2020s. Due to its low atomic number (Z) and high melting point for a light metal, beryllium has been an effective choice as a plasma-facing material. It offers low plasma contamination due to its lack of chemical sputtering; it gives low radiative power losses; it is a good oxygen getter; it will retain a low bulk tritium inventory; and it offers the possibility of in-situ repair [12].

Despite these advantages for JET and ITER, pure beryllium is unlikely to be used as a plasma-facing material in follow-on fusion reactors, such as DEMO, although it has been suggested that beryllide intermetallic compounds such as TiBe_{12} may be suitable [57]. Beryllides have much higher melting points than beryllium metal; they offer better oxidation resistance; and they also offer much lower Z_{eff} than other candidate materials such as tungsten. The combination of actual results from the ITER-Like Wall at JET and the performance of the ITER First Wall, together with the achievements of ongoing research and development efforts, will determine the future of beryllium and whatever form it may take in future fusion wall applications.

References

- [1] Federici, G., Doerner, R., Lorenzetto, P., and Barabash, V. *Comprehensive Nuclear Materials*, Vol. 4, "Beryllium as a Plasma-Facing Material for Near-Term Fusion Devices," pp. 621–666 (2012).
- [2] European Fusion Development Agreement (EFDA) and Joint European Torus (JET). <http://www.efda.org/jet/> (2013).
- [3] ITER International Organization. (2013) *International Collaboration for a New Source of Energy*, article on <http://www.iter.org/proj/iterhistory>.
- [4] Krenzer, R.W. (1979) *Beryllium Science and Technology*, Vol. 2, eds. Floyd, D.R. and Lowe, J.N., Ch. 3 "Casting," (Plenum Press, New York) pp. 31-56.
- [5] Brush Wellman Inc. (circa 1985) *Designing With Beryllium*, Section 3 "Properties of Mill Products," (Brush Wellman Inc., Cleveland) pp. 9-13.
- [6] ITER International Organization. (1998) *Materials Assessment Report G A1 DDD 1 98-05-28 W 0.3*, Chapter 2.1 "Beryllium," pp. 2.1-1 through 2.1-44.
- [7] Brush Wellman Inc. (1999) *Designing With Beryllium*, Section 3 "Properties of Mill Products," (Brush Wellman Inc., Cleveland) pp. 9-14.
- [8] Eur. Fusion Dev. Agreement (EFDA) and Joint Eur. Torus (JET). (2013) *ITER-Like Wall Project*, <http://www.efda.org/jet/jet-iter/iter-like-wall-project/>.
- [9] Dorn, C., Hattan, L., Acreman, M., and Gossett, D. (2009). Manufacturing of Beryllium Tiles for the JET ITER-Like Wall Project, *9th IEA International Workshop on Beryllium Technology*, Almaty, Kazakhstan.
- [10] Dorn, C., Hattan, L., Acreman, M., and Gossett, D. (2009) MS PowerPoint presentation of "Manufacturing of Beryllium Tiles for the JET ITER-Like Wall Project," *9th IEA Int'l Workshop on Beryllium Tech.*, Almaty, Kazakhstan.
- [11] European Fusion Development Agreement (EFDA) and Joint European Torus (JET). (2009) *ITER-Like Wall Project*, photo <http://www.efda.org/jet/>.
- [12] ITER International Organization. (2001) *Plant Description Document G A0 FDR 1 01-07-13 RI.0*, Ch. 2.13 "Materials Assessment," pp. 1-28.
- [13] ITER International Organization. (1998) *Materials Assessment Report G A1 DDD 1 98-05-28 W 0.3*, Ch. 2.1 "Beryllium," pp. 2.1-1 through 2.1-44.
- [14] Kupriyanov, I.B., Basaleev, E.V., Nikolaev, G.N., and Kurbatova, L.A. (2012) Experimental Simulation of Beryllium Damage Under Intense Transient Plasma Loads, presented at *10th IEA Int'l Workshop on Beryllium Tech.* held in Karlsruhe, Germany.
- [15] Liu, X., Chen, J.M., Wu, J.H., Wang, Z.H., Wang, L., Zhong, J.M., Zhang, N.M., Wang, Q.M., Duan, X.R., Liu, Y., Rödig, M., and Linke, J. (2010) Characterization of Chinese Beryllium as the Candidate Armour Material for ITER First Wall (ITR/P1-46), *Proc. 23rd IAEA Fus. Energy Conf.*, IAEA, pp. 1-7.

- [16] Materion Brush Inc. (2012) *Spec Sheet S-65 Beryllium Grade, Rev. E*, (Materion Brush Inc., Elmore, Ohio, U.S.A.) pp. 1-6.
- [17] Barabash, V., Eaton, R., Hirai, T., Kupriyanov, I., Nikolaev, G., Wang, Z., Liu, X., Roedig, M., and Linke, J. (2011) MS PowerPoint presentation of "Beryllium Qualification Activities for ITER First Wall Applications," given at *13th Plasma-Facing Mat'ls & Components Workshop*, held in Rosenheim, Germany.
- [18] Stonehouse, A.J. (1991) *The Heat Treatment of Beryllium*, (Brush Wellman Inc., Elmore, Ohio, U.S.A.) pp. 1-24.
- [19] Lillie, D.W. (1955) *The Metal Beryllium*, eds. White, Jr., D.W. and Burke, J.E., Ch. VI-A "Properties; The Physical & Mechanical Properties of Beryllium Metal" (American Society for Metals, Cleveland, Ohio, U.S.A.) pp. 304-327.
- [20] Stonehouse, A.J., Carrabine, J.A., and Beaver, W.W. (1965) *Beryllium, Its Metallurgy and Properties*, ed. Hausner, H.H., Ch. 6 "Physical Properties," (University of California Press, Berkeley & Los Angeles, U.S.A.) pp. 191-205.
- [21] Pinto, N.P. (1979) *Beryllium Science and Technology, Vol. 2*, eds. Floyd, D.R. and Lowe, J.N., Chapter 16 "Properties," Section 3 "Physical Properties," (Plenum Press, New York, New York, U.S.A.) pp. 341-346.
- [22] Walsh, K.A. (2009) *Beryllium Chemistry and Processing*, eds. Vidal, E.E., Goldberg, A., Dalder, E.N.C., Olson, D.L., and Mishra, B., Ch. 1 "Introduction," (ASM Int'l, Materials Park, Ohio, U.S.A.) pp. 1-5.
- [23] The Engineering ToolBox (website). (2013) *Metals – Specific Heats*, http://www.engineeringtoolbox.com/specific-heat-metals-d_152.html.
- [24] Leslie, W.W. (1979) *Beryllium Science and Technology, Vol. 2*, eds. Floyd, D.R. and Lowe, J.N., Chapter 4 "Metalworking I: Rolling" (Plenum Press, New York, New York, U.S.A.) pp. 57-66.
- [25] Materion Brush Inc. (2011) *Hot-Rolled Beryllium Sheet Specification SR-200*, (Materion Brush Inc., Elmore, Ohio, U.S.A.) pp. 1-3.
- [26] Goods, S.H. & Dombrowski, D.E. (1997) Mechanical Properties of S-65C Grade Beryllium at Elevated Temperatures, *JAERI Proc. of 3rd International Workshop on Beryllium Technology for Fusion*, pp.39-52.
- [27] Materion Brush Inc. (2011) *Material Safety Data Sheet – No. M10 (Beryllium Solid)*, (Materion Brush Inc., Elmore, Ohio, U.S.A.) pp. 1-11.
- [28] Materion Brush Inc. (2011) *Interactive Guide to Working Safely with Be and Be-Containing Materials*, posted on <http://www.berylliumsafety.com/>.
- [29] International Programme on Chemical Safety (IPCS). (1990) *Beryllium Health and Safety Guide (HSG 44)*, (World Health Organization, Geneva).
- [30] Erb, L. (1998) *Corrosion Control – Galvanic Table*, based on Army Missile Command Report No. RS-TR-67-11 first pub. 1967, (Exp. Aircraft Ass'n).
- [31] Grant, L.A. (1979) *Beryllium Science and Technology, Vol. 2*, eds. Floyd, D.R. and Lowe, J.N., Ch. 13 "Joining II – Brazing and Soldering" (Plenum Press, New York) pp. 249-273.
- [32] London, G.J. (1979) *Beryllium Science and Technology, Vol. 2*, eds. Floyd, D.R. and Lowe, J.N., Chapter 15 "Alloys and Composites" (Plenum Press, New York, New York, U.S.A.) pp. 297-318.
- [33] Beitscher, S. (1979) *Beryllium Science and Technology, Vol. 2*, eds. Floyd, D.R. and Lowe, J.N., Chapter 11 "Machining-Induced Surface Damage" (Plenum Press, New York, New York, U.S.A.) pp. 197-230.
- [34] Uchida, M. (2006) Business meeting between NGK Insulators Ltd. and Brush Wellman Inc. to discuss ITER Japan FW Panel fabrication plan.
- [35] Mazul, I.V., Belyakov, V.A., Filatov, O.G., Giniyatulin, R.N., Gervash, A.A., Kuznetsov, V.Y., Makhankov, A.N., and Sizenev, V. (2011) Preparation to Manufacturing of ITER Plasma Facing Components in Russia, *Fusion Eng. Des.* 86, (Elsevier Ltd., Amsterdam, Netherlands).

- [36] Griffith, S. (2013) *ITER Newslines: Green light for ITER's blanket design*, <http://www.iter.org/newsline/264/1556/>. (ITER Int'l Org., Cadarache).
- [37] Khomutov, A.M., Gervash, A., Kolbasov, B.N., Kupriyanov, I.B., and Markushkin, Y.E. (2003) Status of Beryllium Study for Fusion in RF, pres. at *6th IEA Int'l Workshop on Beryllium Technology*, Miyazaki, Japan.
- [38] Gervash, A., Giniyatulin, R., Komarov, V., Mazul, I., Litunovsky, N., Ganenko, A., Vainerman, A., Fedotov, V., Davydov, D., and Zalavutdinov, R. (1998) *Fusion Eng. Des.* 39-40, (Elsevier Ltd., Amsterdam) pp. 543–549.
- [39] Liu, X. (2008) High heat flux tests of small-scale Be/Cu mock-ups for ITER, *22nd Int'l Conf. on Fusion Energy*, Geneva, Switz. (IAEA, Vienna) IT/pp. 2-6.
- [40] Chen, J. (2008) ITER First Wall fabrication technology in China, *22nd Int'l Conf. on Fusion Energy*, Geneva, Switzerland (IAEA, Vienna) IT/pp. 7-10.
- [41] Lorenzetto, P. et al. (2006) *Fusion Eng. Design*, 81, pp. 355-360.
- [42] Sherlock, P., Lorenzetto, P., Walton, N. and Keil, S. (2009) *Fusion Eng. Design*, 84, pp. 1759-1762.
- [43] Boudot, C., Boireau, B., Lorenzetto, P., and Macelc, D. (2007) *Fusion Eng. Design*, 82, pp. 1639-1644.
- [44] Nishi, H. et al. (2008) Study on characterization of dissimilar material joints for ITER First Wall, *22nd Int'l Conf. on Fusion Energy*, Geneva, Switzerland (IAEA, Vienna) IT/pp. 7-11.
- [45] Park, J.Y., Choi, B.K., Kim, H.G., Kim, J.H., Lee, M.H., Park, S.Y., Hong, B.G., and Jeong, Y.H. (2006) Optimization of Joining Condition for ITER First Wall Fabrication, *J. Korean Phys. Soc.*, 49, pp. S442-S446.
- [46] Park, J.Y., Choi, B.K., Lee, J.S., Lee, D.W., Hong, B.G., and Jeong, Y.H. (2009) Fabrication of Be/CuCrZr/SS mock-ups for ITER First Wall, *Fusion Eng. Design*, 84, pp. 1468-1471.
- [47] Jung, Y.I., Lee, J.S., Park, J.Y., Choi, B.K., Jeong, Y.H., and Hong, B.G. (2010) Ion-beam assisted deposition of coating interlayers for the joining of Be/CuCrZr, *Fusion Eng. Design*, 85, pp. 1689-1692.
- [48] Kalin, B., Fedotov, V., Sevryukov, O., Plyushev, A., Mazul, I., Gervash, A., and Giniyatulin, R. (1999) Be-Cu joints based on amorphous alloy brazing for divertor and First Wall, *J. Nuclear Materials*, 271-272, pp. 410-414.
- [49] Puskar, J.D., Goods, S.H., and Cadden, C.H. (2009) High Strength Diffusion Bonding of Beryllium to CuCrZr for ITER Applications, *Proc. 8th Int'l Conf. ASM International*, pp. 604-609.
- [50] Goods, S.H., Puskar, J.D., Watson, R.M., and Ulrickson, M.A. (2009) Development of Joining Processes and Fabrication of U.S. First Wall Qualification Mock-Ups for ITER, *Proc. 23rd IEEE/NPSS SOFE*, pp. 194-198.
- [51] Hunt, R.M., Goods, S.H., Ying, A., Dorn, C.K., and Abdou, M. (2012) Diffusion bonding beryllium to Reduced Activation Ferritic-Martensitic steel: Development of processes and techniques, *Fusion Eng. Des.* 87, (Elsevier Ltd., Amsterdam) pp. 1550-1557.
- [52] Ahn, M.Y. (2012) E-mail correspondence with NFRI about ITER Korea beryllium needs for ITER Test Blanket Module program.
- [53] Lee, J.S., Park, J.Y., Choi, B.K., Lee, D.W., Hong, B.G., and Jeong, Y.H. (2009) Beryllium/ferritic martensitic steel joining for the fabrication of the ITER test blanket module first wall, *Fusion Eng. Des.* 84, (Elsevier Ltd., Amsterdam) pp. 1170-1173.
- [54] Jung, Y.I., Park, J.Y., Choi, B.K., Jeong, Y.H., Lee, D.W., and Cho, S.Y. (2011) Joining methods of Be/FMS and W/FMS for the ITER TBM first wall, *Fusion Eng. Des.* 86, (Elsevier Ltd., Amsterdam) pp. 2390-2393.
- [55] Park, J.Y., Jung, Y.I., Choi, B.K., Jeong, Y.H., Kim, S.K., Lee, D.W., and Cho, S.Y. (2011) Joining of Be to Ferritic-Martensitic Steels with diffusion Barrier Interlayer, *Fusion Sci. Tech.* 60, (American Nuclear Society) pp. 422-425.

- [56] Hunt, R.M. (2011) Diffusion Bonding Beryllium to Reduced Activation Ferritic Martensitic Steel: Development of Processes and Techniques (ProQuest, UMI Dissertation Publishing).
- [57] Reimann, J., Kurinskiy, P., Lindau, R., Moeslang, A., Rohde, M., Dorn, C., Haws, W., Goraieb, A., Harsch, H., and Linsmeier, C. (2009) Beryllides for Fusion Reactors, *Fusion Eng., SOFE, 23rd IEEE/NPSS Symposium*, pp. 1-4.
- [58] Longhurst, G.R., Tsuchiya, K., Dorn, C.K., Folkman, S.L., Fronk, T.H., Ishihara, M., Kawamura, H., Tranter, T.N., Rohe, R., Uchida, M., and Vidal, E. (2011) Managing Beryllium in Nuclear Facility Applications, *Nuclear Tech. 176*, (American Nuclear Society) pp. 430-441.
- [59] Barabash, V., Federici, G., Rödig, M., Snead, L.L., and Wu, C.H. (2000) Neutron irradiation effects on plasma facing materials, *Journal of Nuclear Materials 283-287*, (Elsevier Ltd., Amsterdam) pp. 138-146.
- [60] Moons, F. et al. (1996) Neutron irradiated beryllium: tensile strength and swelling. *Journal of Nuclear Materials, 233-237*, pp. 823-827.
- [61] Ishitsuka, E., Kawamura, H., Terai, T., and Tanaka, S. (1997) Microstructure and mechanical properties of neutron irradiated beryllium, *Proc. 3rd IEA Int'l Workshop on Beryllium Tech. for Fusion*, Mito, Japan, p. 261.
- [62] Kupriyanov, I.B., Gorokhov, V.A., Nikolaev, G.N., and Burmistrov, V.N. (1995) Development of radiation resistant grades of beryllium for nuclear and fusion facilities, *Proc. 2nd IEA Int'l Workshop on Beryllium Tech. for Fusion*, Jackson Lake Lodge, Wyoming, U.S.A., p. 249.
- [63] Snead, L. (2004) Low-temperature low-dose neutron irradiation effects on beryllium. *Journal of Nuclear Materials, 326*, pp. 114-124.
- [64] Khomutov, A. et al. (2002) Beryllium for fusion application - recent results. *Journal of Nuclear Materials, 307-311*, pp. 630-637.
- [65] Gelles, D.S. et al. (1994) Radiation effects in beryllium used for plasma production, *Journal of Nuclear Materials, 212-215*, pp. 29-38.
- [66] Chaouadi, R., Moons, F., and Puzzolante, J.L. (1997) Tensile fracture toughness test results of neutron irradiated beryllium, *Proc. 3rd IEA Int'l Workshop on Beryllium Tech. for Fusion*, Mito, Japan, p. 251.
- [67] Kupriyanov, I.B. et al. (1998) Investigation of ITER candidate beryllium grades irradiated at high temperature. *Journal of Nuclear Materials, 258-263*, pp. 808-813.
- [68] Moons, F. (1998) Fracture behavior of neutron irradiated beryllium. *Fusion Eng. Des., 41*, (Elsevier Ltd., Amsterdam) pp. 187-193.
- [69] Moons, F. et al. (1996) Neutron irradiated beryllium: tensile strength and swelling. *Journal of Nuclear Materials, 233-237*, pp. 823-827.
- [70] Kwast, K., Werle, H., and Wu, C.H. (1996) *Physica Scripta*, T64.
- [71] Wu, C.H., Bonal, J.P., Kwast, H., Moons, F., Pott, G., Werle, H., and Vieider, G. (1998) *Fus. Eng. Des. 39-40*, (Elsevier Ltd., Amsterdam) p. 263.
- [72] Chakin, V., Rolli, R., Vladimirov, P., Kurinskiy, P., Klimenkov, M., Moeslang, A., Ryczek, L., Dorn, C., & Markovsky, A. (2009) Temperature-programmed desorption of tritium loaded into beryllium, *Physica Scripta T138*.
- [73] Kurinskiy, P., Cardella, A., Klimiankou, M., Möslang, A., and Goraieb, A.A. (2005) Production and thermal stability of beryllium with fine grain structure to improve tritium release during neutron irradiation, *Fus. Eng. Des. 75-79*, (Elsevier Ltd., Amsterdam) pp. 709-713.
- [74] Kupriyanov, I.B., Nikolaev, G.N., and Gorayev, G. (2017) Progress in Development and Qualification of Beryllium for ITER Blanket First Wall Application in Russian Federation, *Fusion Engineering and Design*, <https://doi.org/10.1016/j.fusengdes.2017.05.071>

2.3.3 Post-irradiation examination of beryllium pebbles from HIDOBE-02 experiment

V. Chakin¹, R. Rolli², P. Vladimirov¹, and M. Zmitko³

¹*Institute for Applied Materials - Applied Materials Physics, Karlsruhe Institute of Technology, Hermann-von-Helmholtz-Platz 1, 76344 Eggenstein-Leopoldshafen, Germany*

²*Institute for Applied Materials - Materials and Biomechanics, Karlsruhe Institute of Technology, Hermann-von-Helmholtz-Platz 1, 76344 Eggenstein-Leopoldshafen, Germany*

³*The European Joint Undertaking for ITER and the Development of Fusion Energy, c/ Josep Pla, n° 2, Torres Diagonal Litoral, Edificio B3, 08019 Barcelona, Spain*

E-mail: vladimir.chakin@kit.edu

In the European Helium-Cooled Pebble Bed (HCPB) blanket of a DEMO fusion power reactor, beryllium pebbles are planned to be used as neutron multiplier. Neutron irradiation causes formation of helium and tritium in beryllium which contribute to degradation of beryllium pebble properties. Beryllium pebbles with a diameter of 1 mm produced by the rotating electrode method (REM) by NGK Insulators Ltd., Japan have been irradiated in the HIDOBE-02 experiment in the HFR, Petten, the Netherlands, at temperatures of 370-650 °C up to damage doses of 19-38 dpa, corresponding to helium and tritium productions of 3630-6000 and 370-650 appm, accordingly. The beryllium pebbles were irradiated either as unconstrained pebble stacks or as constrained pebble beds.

The results of post-irradiation examination (PIE) of beryllium pebbles irradiated in the HIDOBE-02 include optical metallography and scanning electron microscopy (SEM) studies, micro-hardness measurements, creep and thermal desorption tests.

Optical images show that microstructure of irradiated beryllium pebbles contains pores, which average size strongly increases with irradiation temperature. Small bubbles arrange grain boundaries lining in chains. Pebbles in the pebble beds have more damaged structure near contact zones that might be caused by higher internal stresses in the beds compared to the free pebbles. However, open channels along grain boundaries, which are more effectively formed in the constrained pebbles, facilitate tritium release already during irradiation. SEM images of the pebble surface show formation of oxidized layers. The oxidation occurs with comparatively higher rates at higher irradiation temperatures of 600-650 °C. According to micro-hardness measurements, radiation hardening occurs in the irradiated beryllium pebbles. The hardening decreases with increase of irradiation temperature. The creep tests on individual pebbles were performed at temperatures at which they were irradiated. Three different loadings per each temperature were used. For two lowest test temperatures of 370 and 450 °C, practically no creep was observed. At these temperatures, radiation hardening takes place what manifests itself in reduction of deformation of the pebbles under loading. At higher test temperatures of 560 and 650 °C, the creep rates are significant. The creep rates strongly depend on testing temperatures and loadings. At high irradiation temperatures, internal stresses due to swelling of constrained pebbles can be relaxed easily by creep.

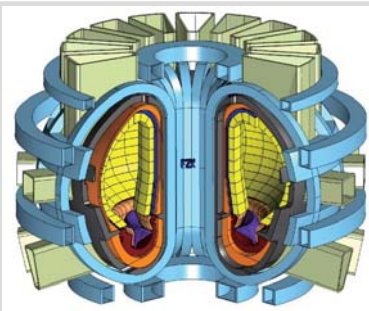
The HIDOBE-02 PIE being an essential input to the basement of the HCPB blanket provide the designers by new information for solving of issues and challengers of this blanket concept.

Post-irradiation examination of beryllium pebbles from HIDOBE-02 experiment

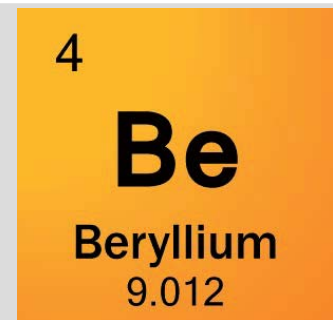
V. Chakin¹, R. Rolli¹, P. Vladimirov¹, M. Zmitko²

¹Institute for Applied Materials, Karlsruhe Institute of Technology, Hermann-von-Helmholtz-Platz 1, 76344 Eggenstein-Leopoldshafen, Germany

²The European Joint Undertaking for ITER and the Development of Fusion Energy, c/ Josep Pla, n° 2, Torres Diagonal Litoral, Edificio B3, 08019 Barcelona, Spain



KIT – University of the State of Baden-Wuerttemberg and National Research Center of the Helmholtz Association

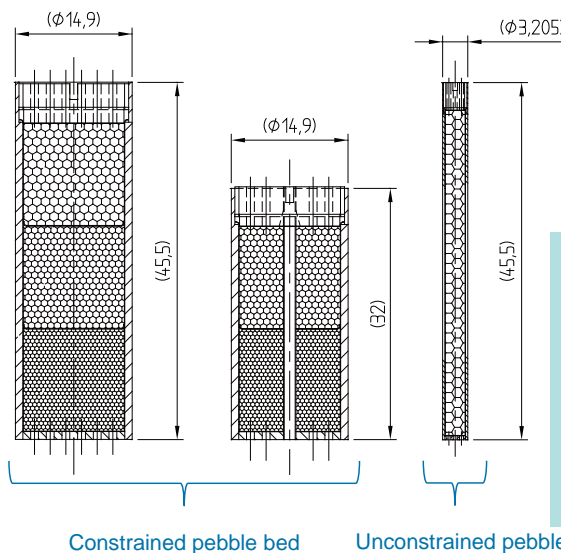
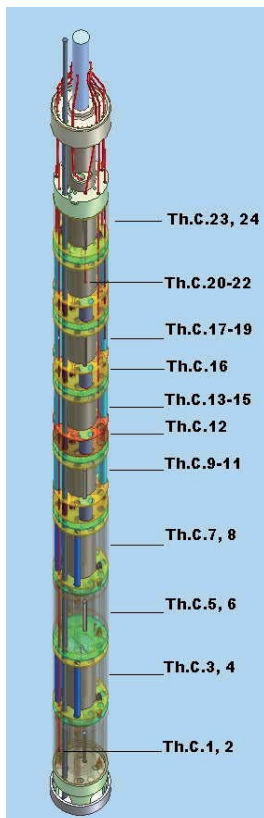


www.kit.edu

HIDOBE-02 experiment at HFR, Petten

European programme (EFDA) and F4E in collaboration JP:

- Irradiation behaviour of beryllium under DEMO blanket relevant helium/tritium productions and temperatures
- Study microstructure evolution and tritium release/retention
- Study thermo-mechanical behaviour under irradiation
- **Achieve 30% of DEMO End-Of-Life Helium production**



Deformation parameters for pebble beds

Type	Diameter of pebble, mm	Height of PB, mm	Decrease of PB height, %
PB	0.5	~13	1.24
	0.5		1.03
	1		0.41
	1		0.97

Pre-deformation allows to simulate the behavior of pebbles at high doses, when large swelling will be achieved. The pebble swelling will be limited by the walls of the pebble bed. The response of the walls from the pebble swelling at high doses will deform the structure. This is the situation of constrained Be pebble bed before irradiation.

Irradiation parameters for HIDOBE-02

Sample	Diameter, mm	Code	Target T _{irr} , °C	Maximum T _{irr} , °C	Average T _{irr} , °C	D, dpa	He, appm	T, appm
Unconstrained Be pebbles	0.5	41sPC	375	410	370	21	3632	367
		40sPC	470	477	440	29	4751	502
		4sPC	590	600	560	34	5524	596
		3sPC	675	682	650	37	5925	644
	1, 2001	49sPC	375	410	370	21	3632	367
		48sPC	470	477	440	29	4751	502
		12sPC	590	600	560	34	5524	596
		11sPC	675	682	650	37	5925	644
	1, 2003	45sPC	375	410	370	21	3632	367
		44sPC	470	477	440	29	4751	502
		8sPC	590	600	560	34	5524	596
		7sPC	675	682	650	37	5925	644
2	53sPC	375	410	370	21	3632	367	
	16sPC	590	600	560	34	5524	596	

The irradiation parameters are very high for neutron irradiation test with beryllium:

- Duration 2005-2011 (48 reactor cycles, 1247 Full Power Days)
- Average temperature 370-650 °C
- Damage dose 21-37 dpa
- Helium accumulation 3632-5925 appm
- Tritium accumulation 367-644 appm

Sample	Diameter, mm	Code	Target T _{irr} , °C	Maximum T _{irr} , °C	Average T _{irr} , °C	D, dpa	He, appm	T, appm
Constrained Be pebble beds	1, 2001	5mPC2	405	425	387	21	3632	367
	1, 2003	5mPC1	405	425	387	21	3632	367
	1, 2001	6mPC2	500	523	480	29	4751	502
	1, 2003	6mPC1	500	523	480	29	4751	502
	0.5	6bPC3	620	645	600	34	5524	596
	1, 2003	6bPC2	620	645	600	34	5524	596
	2	6bPC1	620	645	600	34	5524	596

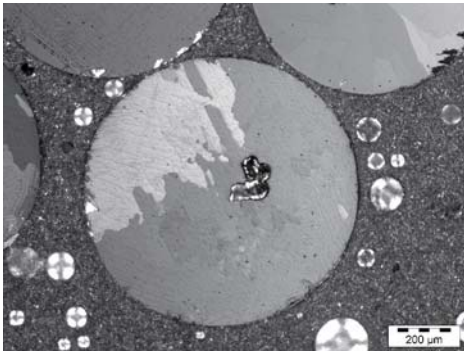
Samples and investigation methods at HIDOBE-02 PIE

Be pebbles produced in NGK by Rotating Electrode Method (REM) with diameters of 0.5, 1, and 2 mm

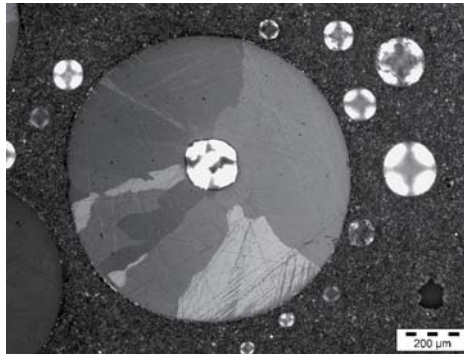
- ✓ Optical microscopy
- ✓ Scanning electron microscopy
- ✓ Vickers hardness
- ✓ Creep tests of individual pebbles
- ✓ Thermal Programmed Desorption tests

Evolution of Be microstructure after irradiation: Unconstrained REM pebbles Ø 1 mm, 2003

$T_{irr} = 370\text{ }^{\circ}\text{C}$, 3632 appm He



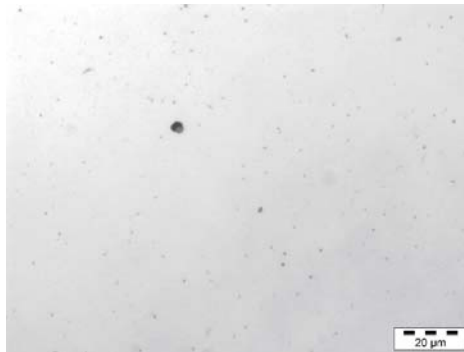
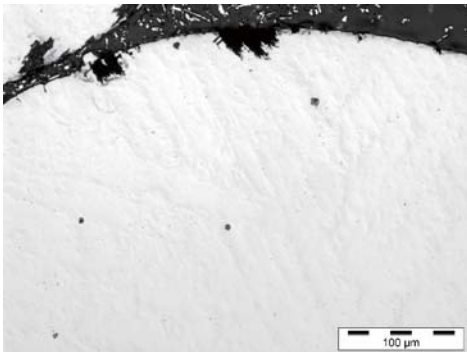
$T_{irr} = 440\text{ }^{\circ}\text{C}$, 4751 appm He



For two lowest irradiation temperatures:

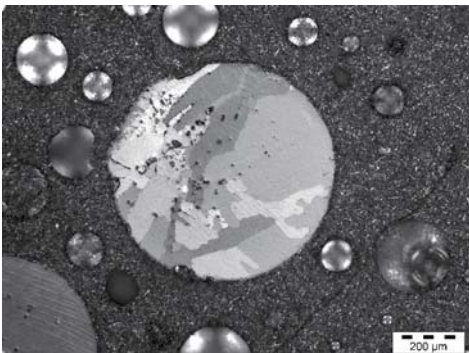
- Not so developed radiation-induced porosity.
- Formation sub-grain structure even in unconstrained pebbles.
- Sub-grain boundaries can play a role of open channels for tritium release from the pebbles.

$T_{irr} = 440\text{ }^{\circ}\text{C}$, 4751 appm He

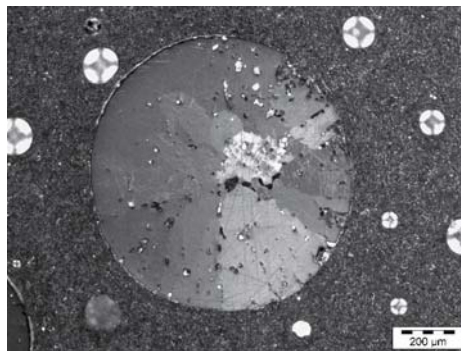


Unconstrained REM pebbles Ø 1 mm, 2003

$T_{irr} = 560\text{ }^{\circ}\text{C}$, 5524 appm He

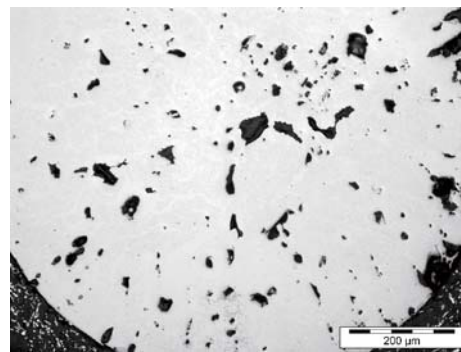
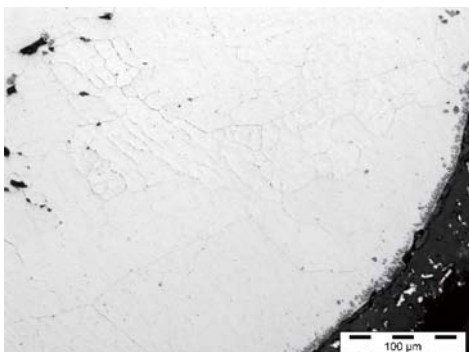


$T_{irr} = 650\text{ }^{\circ}\text{C}$, 5925 appm He



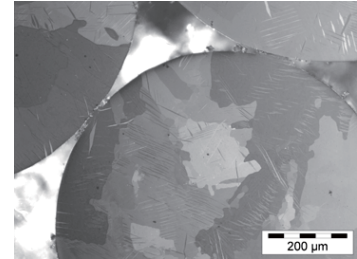
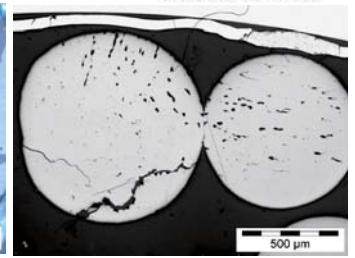
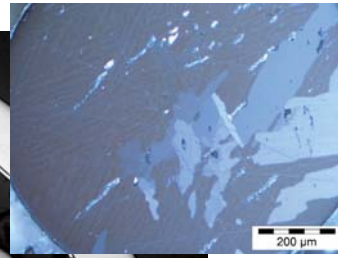
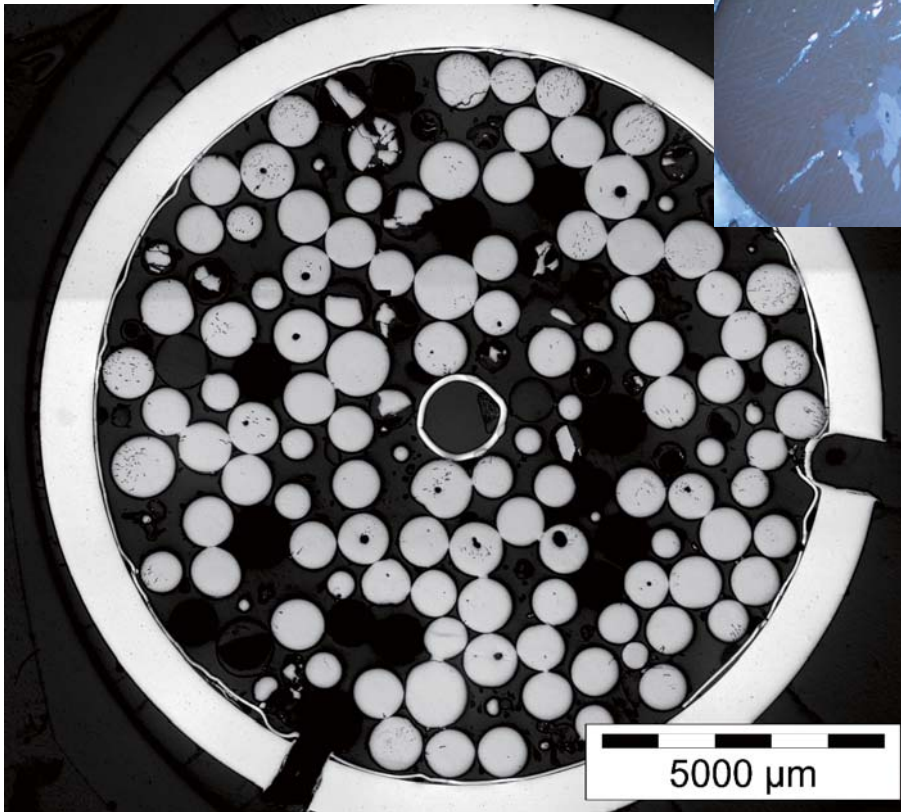
For two highest irradiation temperatures:

- High developed porosity, big pores.
- Formation of open channels which can facilitate the tritium release from the pebbles.



Constrained REM pebble bed Ø 1 mm, 2003

$T_{irr} = 387\text{ }^{\circ}\text{C}$, 3632 appm He



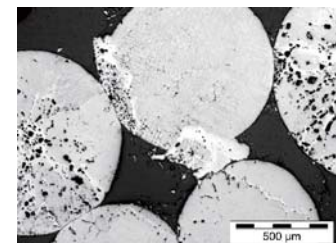
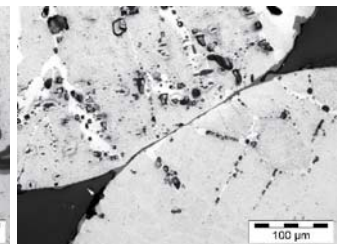
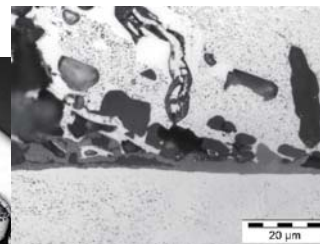
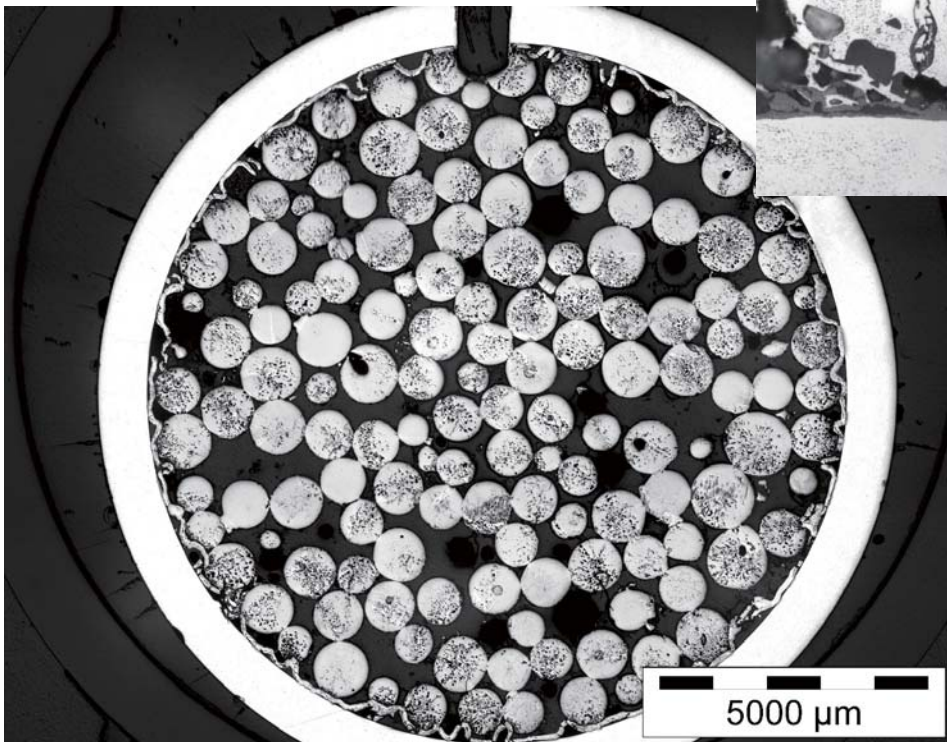
Main features:

- Low porosity
- Damage of Be pebbles in contact with Pt foil
- Sintering of pebbles in contact zones
- Defragmentation of pebbles
- Deformation of pebbles by twinning
- Oxidation of pebbles
- Formation of sub-grains structure

6

Constrained REM pebble bed Ø 1 mm, 2003

$T_{irr} = 600\text{ }^{\circ}\text{C}$, 5524 appm He



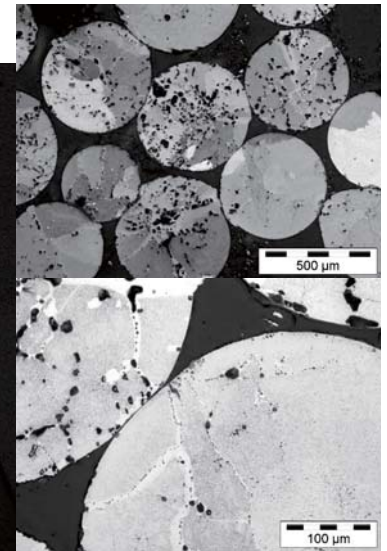
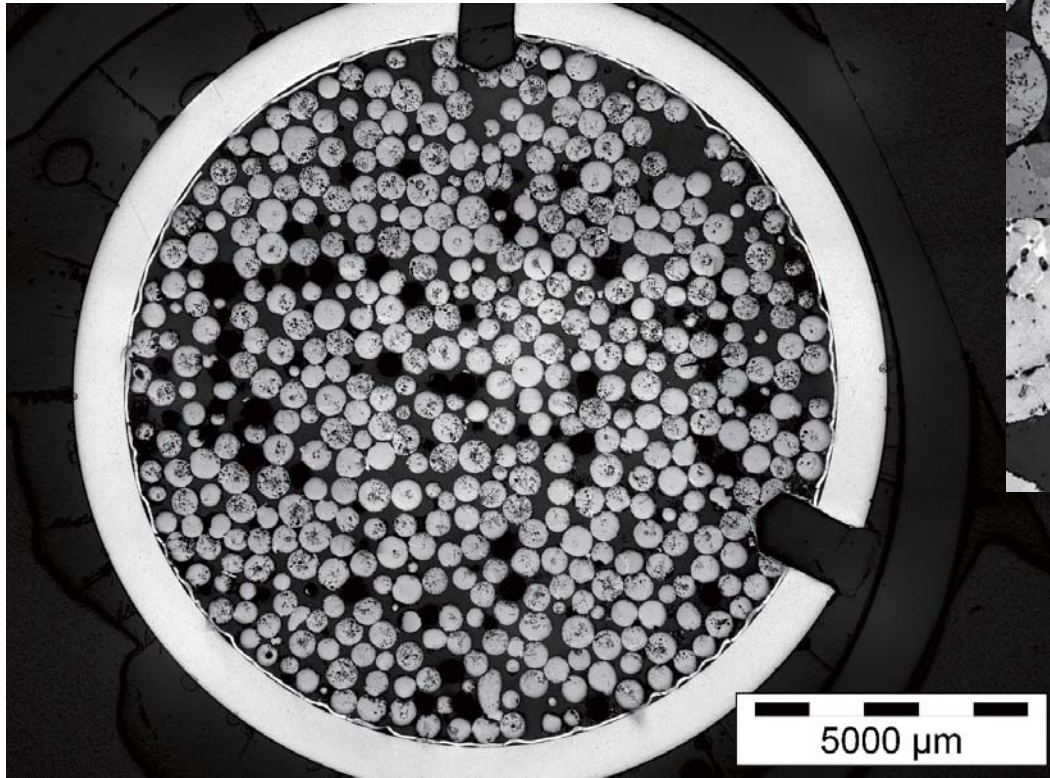
Main features:

- Much high porosity
- Higher damage of Be pebbles in contact with Pt foil
- Higher sintering of pebbles in contact zones
- Not visible defragmentation of pebbles
- Higher oxidation of pebbles
- Formation of open channel network

7

Constrained REM pebble bed Ø 0.5 mm

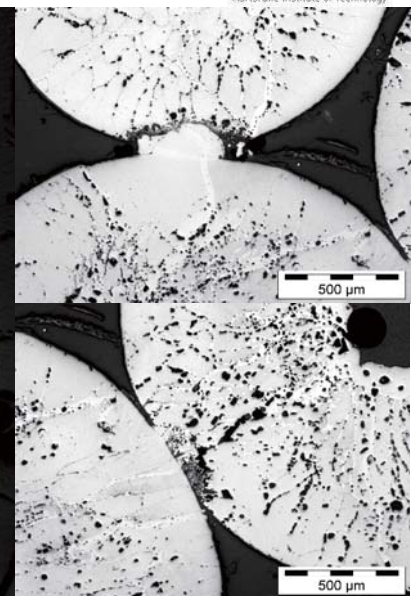
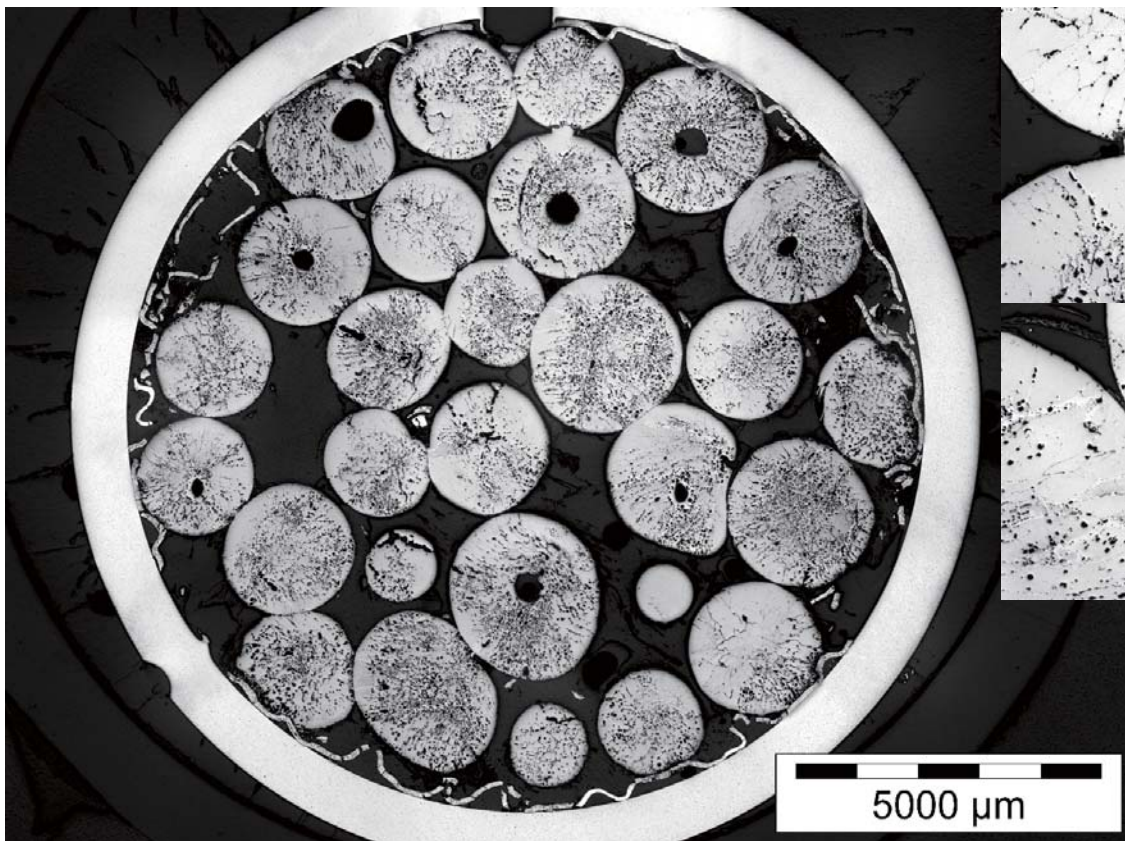
$T_{irr} = 600\text{ °C}$, 5524 appm He



Main features:

Similar effects to 1 mm pebbles (high porosity, open channels, damage of Be pebbles in contact with Pt foil, high sintering of pebbles, no defragmentation, high oxidation)

OM: Constrained REM pebble bed Ø 2 mm



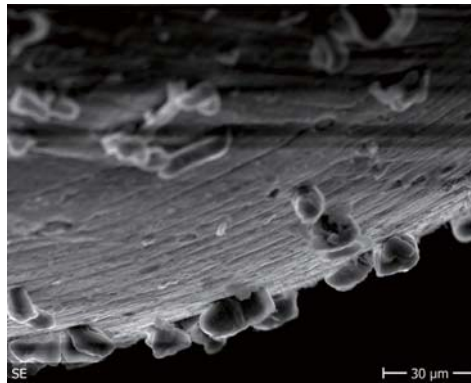
Main features:

Similar effects to 1 mm pebbles (high porosity, open channels, etc.)

Not so dense packing of 2 mm pebbles compared to 1 mm

SEM: Constrained REM pebble bed Ø 1 mm, 2003

$T_{\text{irr}} = 370\text{ }^{\circ}\text{C}$, 3632 appm He



$T_{\text{irr}} = 440\text{ }^{\circ}\text{C}$, 4751 appm He



Main features:

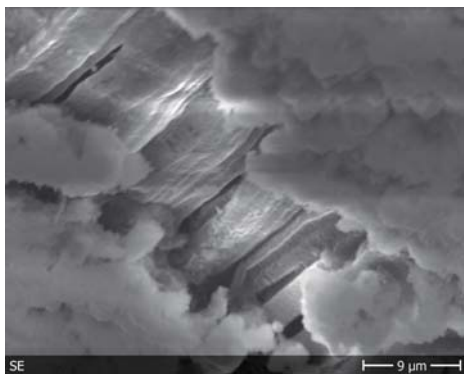
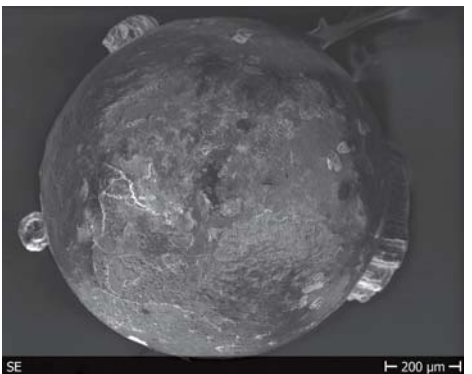
- Numerous objects with roughly cylindrical form cover the surface after irradiation at two lowest irradiation temperatures. The objects are early nuclei of beryllium oxide "islands".
- Increase of irradiation temperature up to from 370 °C to 450 °C did not lead to the principle changes of the surface state. Maybe, the sizes of the objects became more than they were at 370 °C.

10

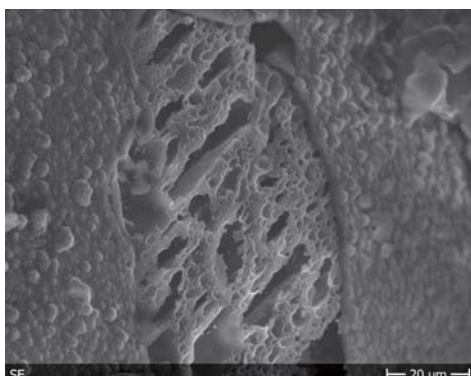
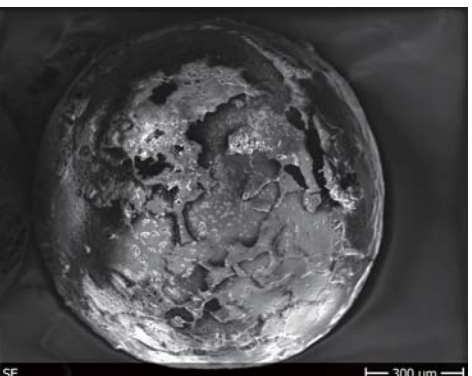
Institute for Applied Materials – Applied Materials Physics

SEM: Constrained REM pebble bed Ø 1 mm, 2003

$T_{\text{irr}} = 560\text{ }^{\circ}\text{C}$, 5524 appm He



$T_{\text{irr}} = 650\text{ }^{\circ}\text{C}$, 5925 appm He



Main features:

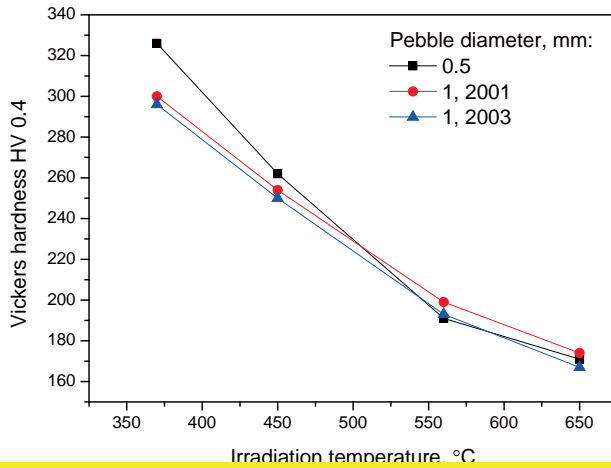
- Oxide layer covers practically all pebble surface. Sometimes, big hills are on the surface. Formation of these hills can be explained by uneven oxidation process of the pebble surface.
- The destruction and the detachment of the oxide layer can be observed on separate places of the pebble surface. This can be explained by high brittleness of beryllium oxide.
- On these areas where oxide layer was detached, we observe non-oxidized Be surface with open channel coming to the surface.

11

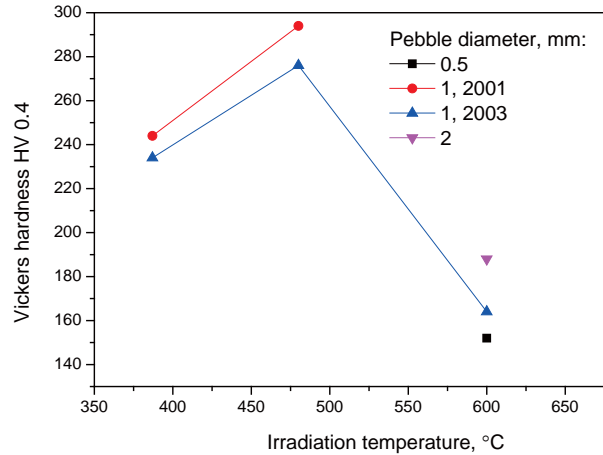
Institute for Applied Materials – Applied Materials Physics

Vickers hardness measurements of Be pebbles from HIDOBE-02

Unconstrained

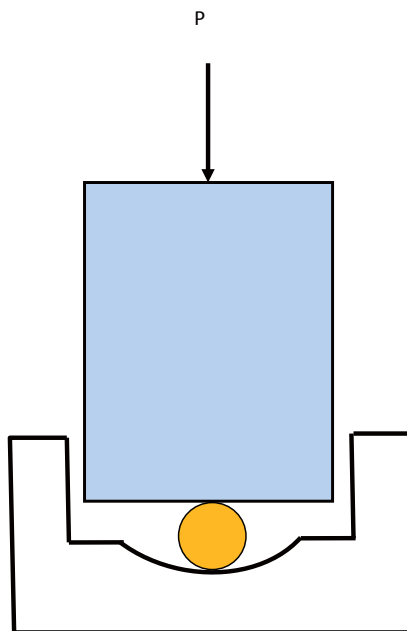


Constrained



- There is strong dependence of Vickers hardness values on irradiation temperatures regardless of the pebble diameters. Increasing irradiation temperature leads to decrease of hardness values of irradiated Be pebbles.
- At two highest irradiation temperatures recovery of hardness values to the non-irradiated state (HV 0.4 = 190) occurs.
- The results on constrained pebbles correlate with data obtained on unconstrained pebbles but there is a difference concerning of two lowest irradiation temperature. In particular, increase of the hardness occurs on increasing of temperature from 387 to 480°C. This difference can be explained of higher radiation hardening at higher irradiation temperature because more thermal stresses in the bed can be at higher temperature.

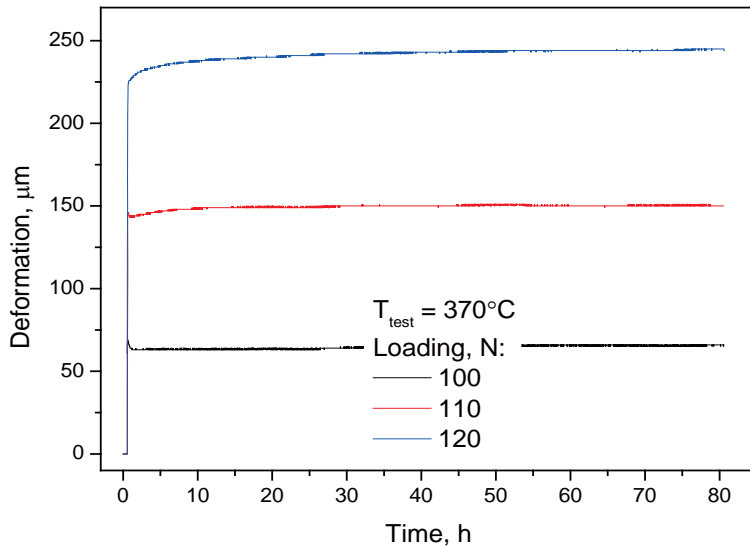
Scheme of the creep test of individual Be pebbles from HIDOBE-02



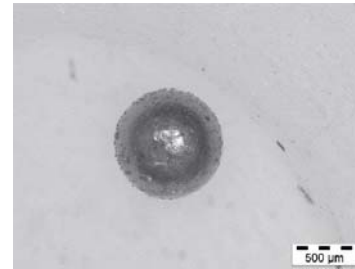
Parameters of creep tests:

- Location:** glove box with pure N₂
- Loading:** up to 1000 N
Three loadings were used for each testing temperature
- Temperature:** up to 1000 °C
 $T_{\text{test}} = T_{\text{irr}}$ to prevent annealing of radiation defects
- Duration:** 80 h

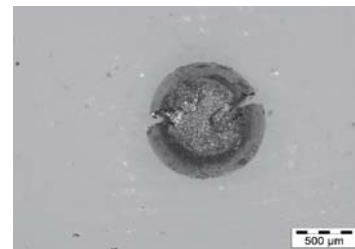
Creep tests of individual unconstrained Be pebbles \varnothing 1 mm, 2003 from HIDOBE-02: $T_{\text{test}} = T_{\text{irr}} = 370 \text{ }^{\circ}\text{C}$



Before test

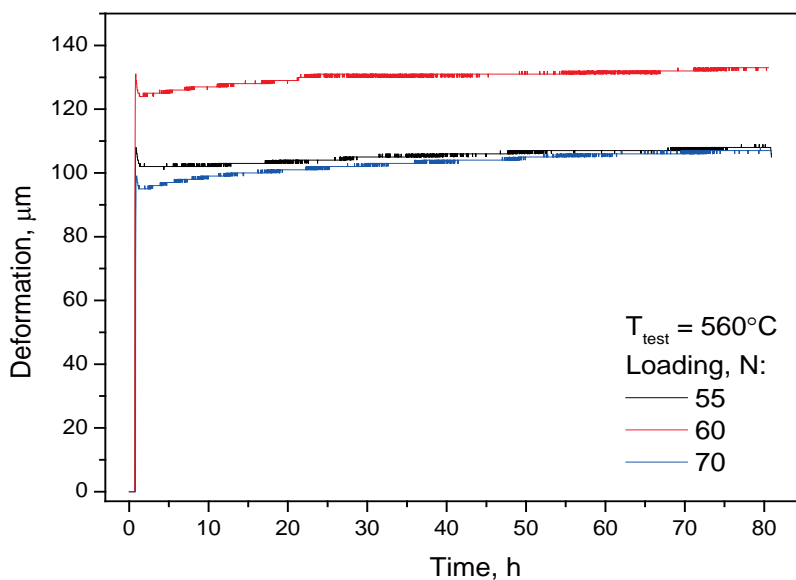


After test

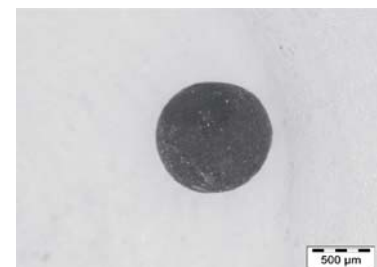


- In the beginning of a creep test, considerable deformations in a contact zone between the pebble and the piston occur. An imprint (plastic deformation zone) is formed on the pebble.
- Then, first stage of creep takes place during which deformation is slowing down with time. Finally, second stage of deformation occurs when the pebble is deformed with the steady-state creep rate.
- At low temperatures cracks often form which makes interpretation of the results difficult due to combination of crack propagation and creep processes.

Creep tests of individual unconstrained Be pebbles \varnothing 1 mm, 2003 from HIDOBE-02: $T_{\text{test}} = T_{\text{irr}} = 560 \text{ }^{\circ}\text{C}$



Before test



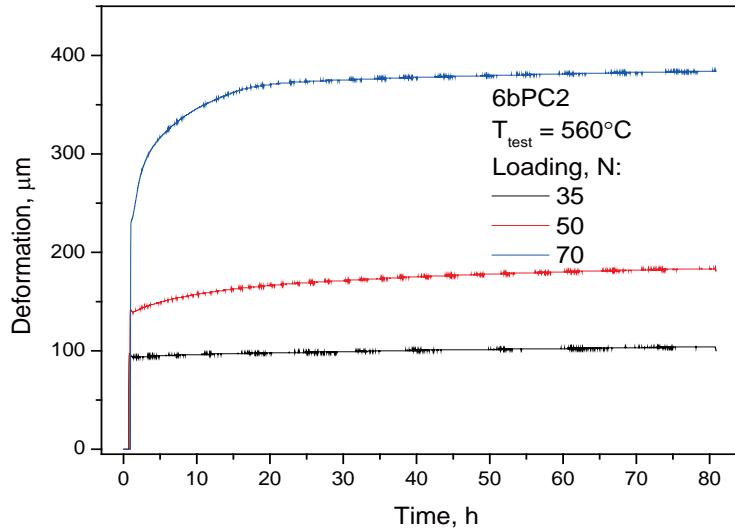
After test



- The low temperature tests at 370 and 450 °C do not show high creep rates despite of comparatively higher loadings. Under high loadings, the pebbles are deformed with crack formation. At lower loadings, there is no deformation.
- At higher temperatures of 560 and 650 °C, the pebbles reveal higher strain rates with lower loadings without crack formation.

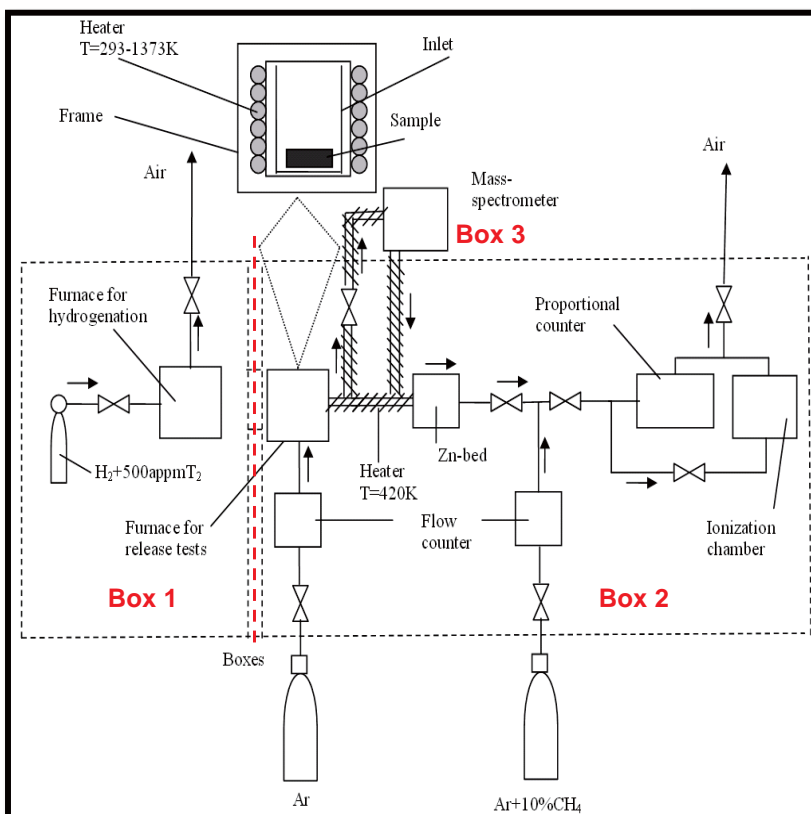
Creep tests of individual constrained Be pebbles

Ø 1 mm, 2003 from HIDOBE-02: $T_{\text{test}} = T_{\text{irr}} = 560 \text{ }^\circ\text{C}$



Comparison of creep rates at corresponding testing temperatures and loadings of unconstrained and constrained Be pebbles demonstrates an easier ability to deformation of constrained pebbles. At higher temperatures of 560 and 650 °C, the pebbles reveal higher strain rates with lower loadings without crack formation. This can be explained by easier formation of sub-grain structure contributing to the higher creep rate.

Set-up for TPD tests



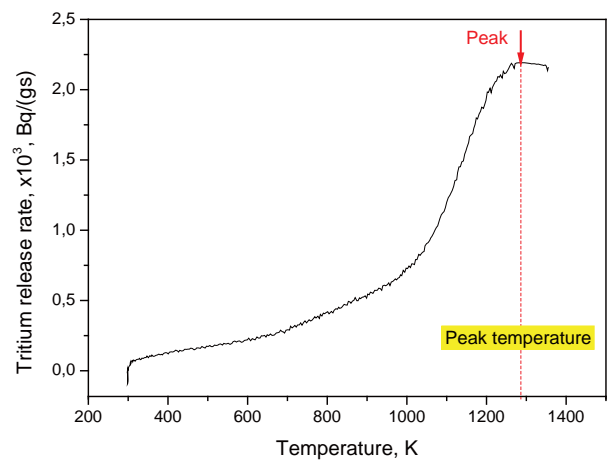
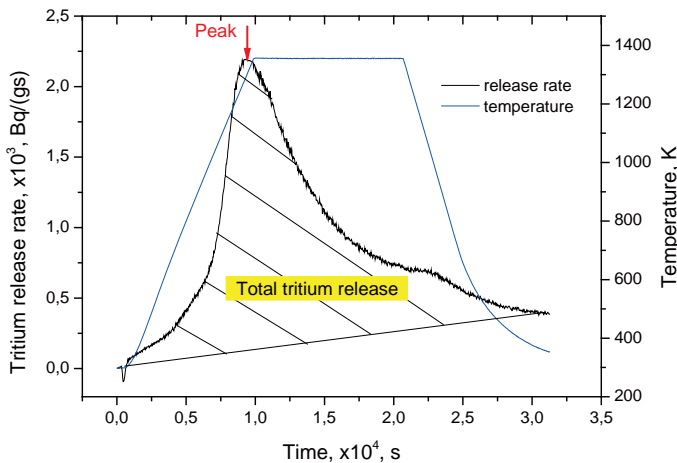
Three glove boxes filled by pure N_2

Box 1: loading system (furnace with crucible for sample, gas balloon with $\text{H}_2+500\text{ppm T}_2$)

Box 2: TPD facility (furnace with crucible for sample, pipelines, Zn-bed, proportional and ionization chambers)

Box 3: quadrupole mass-spectrometer (QMS)

Comparison of TPD tests

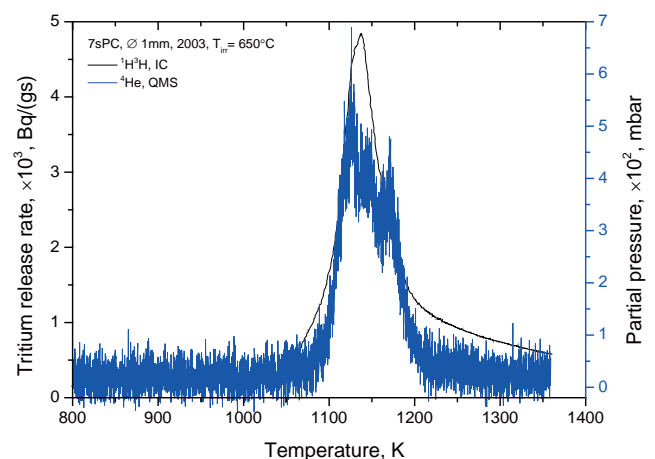
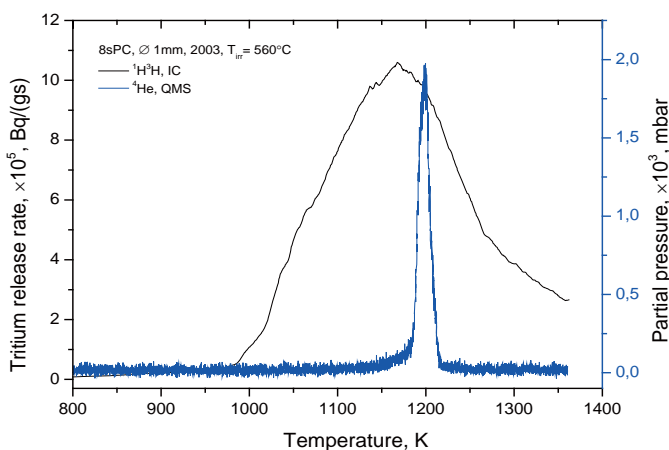


1. Temperature of tritium release peak in K.
2. Total tritium release in Bq/g.

18

Institute for Applied Materials – Applied Materials Physics

TPD tests of unconstrained Be pebbles $\varnothing 1$ mm, 2003 from HIDOBE-02: $T_{irr} = 560$ °C and 650 °C

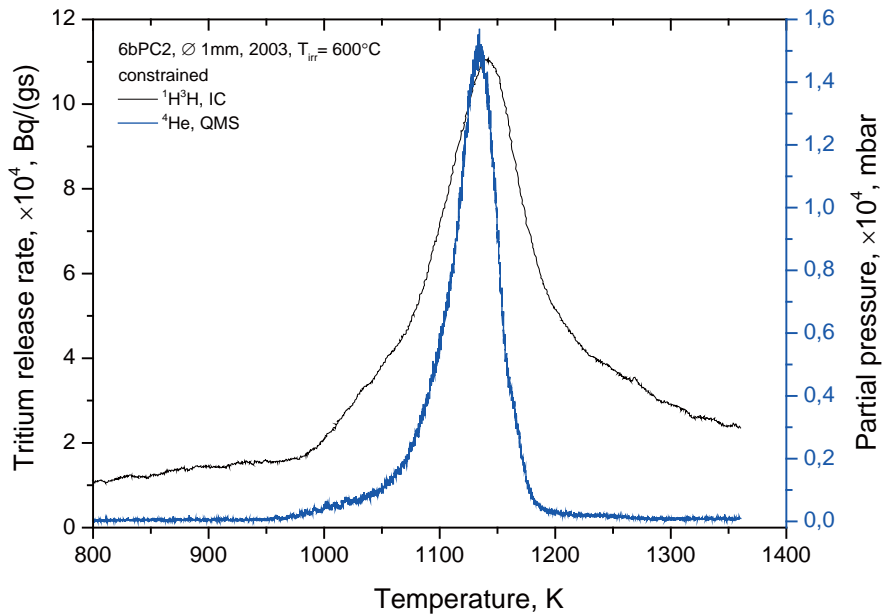


- Only one wide tritium release peak was always observed in the performed TPD tests
- Helium release from Be pebbles occurs also by means of a single peak but sometimes there are several sharp peaks. It can be tentatively explained by existence of various helium bubbles with various trapping energies
- The broad tritium release peak starts at much lower temperatures (950-1000 K) than helium release (1100-1200 K) regardless of irradiation temperature meaning that tritium can leave gas bubbles before formation of open channels necessary for the release of helium atoms
- At highest irradiation temperature of 650°C the release of tritium and helium occurs within the same narrow temperature range, namely at 1100-1200 K.

19

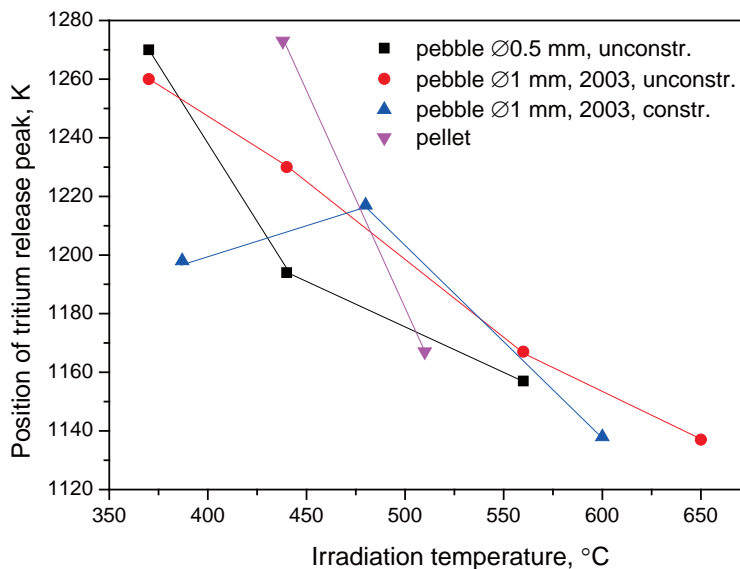
Institute for Applied Materials – Applied Materials Physics

TPD tests of constrained Be pebbles Ø1 mm , 2003 from HIDOBE-02: $T_{irr} = 600\text{ °C}$



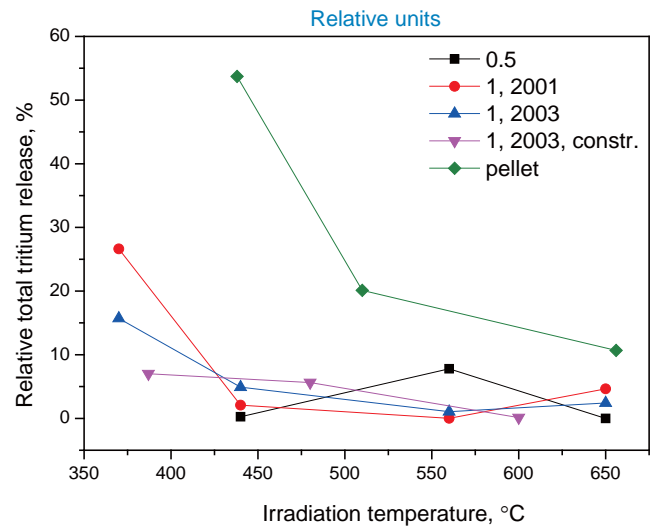
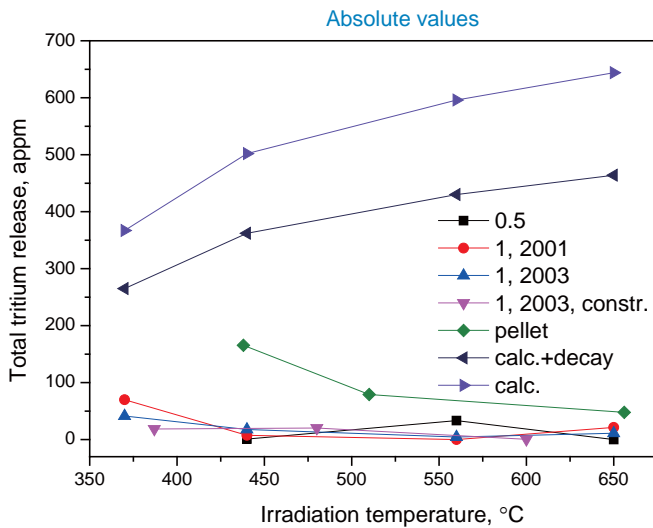
There are no principle differences in tritium and helium release behaviour of constrained pebbles to unconstrained one. Mutual location of tritium and helium release peaks is similar to that for unconstrained pebbles.

Positions of tritium release peaks for Be samples for various irradiation temperatures



Tritium release peaks shift systematically to lower temperature with increase of irradiation temperature. One exception can be found for constrained pebble bed for which the peak temperature increases by 10 K when irradiation temperature increases from 387 to 480°C.

Total tritium release from Be samples versus irradiation temperature



- Comparison of experimental results with theoretically calculated values of tritium production after the end of irradiation and taking into account radioactive decay of tritium to the time of the TPD tests shows significant decrease of the total tritium released even at two lowest irradiation temperatures
- The highest retention occurs in Be pellets, the lowest one – in constrained pebbles that correlates with microstructure evolution because formation of sub-grain structure which should contribute to the enhanced tritium release occurs in the microstructure of both unconstrained and constrained beryllium pebbles at all irradiation temperatures even at the lowest one
- Retention data should be additionally specified because there is a difference to the data obtained in NRG.

Conclusions

In this study, performed within the HIDOBE-02 PIE by KIT, four kinds of unconstrained Be pebbles have been investigated, differing in pebble size such as 0.5, 1, and 2 mm. The unconstrained Be pebbles were irradiated at four temperatures of 370, 440, 560, 650°C up to helium productions of 3632-5925 appm. Constrained Be pebble beds with pebbles 0.5, 1, and 2 mm diameters irradiated at 387, 480, 600°C up to helium productions of 3632-5524 appm. Outcomes are as follows:

1. Microstructure of irradiated unconstrained and constrained Be pebbles strongly depend on irradiation temperature regardless of the pebble diameter. No significant pore or bubble formations occur at two lowest temperatures but formation of a developed sub-grain structure takes place. Big pores and open porosity network are the main features of the microstructure of the pebbles irradiated at two highest irradiation temperatures.
2. External surface of Be pebbles irradiated at two lowest temperatures has numerous objects with cylindrical form. The objects were identified as first "islands" of beryllium oxide BeO which start to grow. Increasing irradiation temperature will lead to completed surface coverage by oxide layer.
3. Increasing irradiation temperature leads to decrease of hardness values of irradiated Be pebbles to the non-irradiated state.
4. The low temperature tests do not show high creep rates despite of considerably high loads. Under high loads, the pebbles are deformed with crack formation. At higher temperatures, the pebbles show higher strain rates with lower loadings without crack formation. Comparison of creep rates at corresponding testing temperatures and loads of unconstrained and constrained Be pebbles demonstrates an easier deformation of constrained pebbles.
5. Increasing irradiation temperature leads to significant decrease of tritium retention in the pebbles.

Thanks so much for your attention!



2.3.4 Status of Material Development for HCCR TBM in Korea

Yi-Hyun Park¹, Seungyon Cho¹, Mu-Young Ahn¹, Youngmin Lee¹ and Young-Bun Chun²

¹*National Fusion Research Institute, Daejeon, Republic of Korea*

²*Korea Atomic Energy Research Institute, Daejeon, Republic of Korea*

E-mail: yhpark@nfri.re.kr

Korea has developed a Helium Cooled Ceramic Reflector (HCCR) TBM in order to acquire experimental results and verify a breeding blanket concept for demonstration power reactor (DEMO) under the ITER TBM Program. The HCCR TBM is adopting a four sub-module concept considering the manufacturability and the post irradiation examination including the transfer of irradiated TBM. The HCCR TBM structure is made from the reduced activation ferritic/martensitic (RAFM) steel. The breeding zone of each sub-module consists of seven layers which are three neutron multiplier layers, three tritium breeder layers, and one neutron reflector layer. Beryllium and lithium ceramic pebbles are used as neutron multiplier and tritium breeder materials, respectively. The HCCR TBM has a unique concept among the ITER TBMs that graphite is employed as neutron reflector in order to reduce the beryllium amount.

The Advanced Reduced Activation Alloy (ARAA) is being developed as a structural material of the HCCR TBM. The total number of 91 model alloys were designed, fabricated, and evaluated. The commercial scale ARAA, which was 18 ton scale, was successfully fabricated by industrial company in Korea. The material properties database for unirradiated ARAA has been constructed. The neutron irradiation test up to 3 dpa has been planned using HANARO research reactor in KAERI. Lithium metatitanate (Li_2TiO_3) is candidate material for tritium breeder of HCCR TBM. The slurry droplet wetting method was developed to fabricate the pebble shape with 1 mm diameter by NFRI. The automatic slurry dispensing system was manufactured for mass-production of breeder pebbles. To improve the tritium release performance of breeder pebbles, the Li_2TiO_3 nano-powder, which was synthesized by solid-state reaction method, was adopted as law material for breeder pebbles. The beryllium pebbles and nuclear grade graphites will be purchased from industrial company for neutron multiplier and reflector in the HCCR TBM, respectively. Especially, in accordance with the radioprotection requirement limit of ITER and the activation product inventory in the irradiated TBM, the uranium content in beryllium pebble has to be strictly controlled.

References

- [1] Yi-Hyun Park, et al., Fusion Engineering and Design **109-111**, 443-447 (2016)
- [2] Young-Bum Chun, et al., Fusion Engineering and Design **109-111**, 629-633 (2016)

**13th International Workshop on Beryllium Technology
(BeWS-13)**

Narita, 21-22 September, 2017

Status of Material Development for HCCR TBM in Korea

Yi-Hyun Park, Seungyon Cho, Mu-Young Ahn,
Youngmin Lee, Young-Bum Chun
on behalf of KO TBM Team



Ministry of Science and ICT



NFRI
National Fusion Research Institute



KOREA DOMESTIC AGENCY



KAERI



Outline



Introduction



Status of Structural Material Development



Status of Functional Material Development



HCCR-TBS Development Schedule



Summary



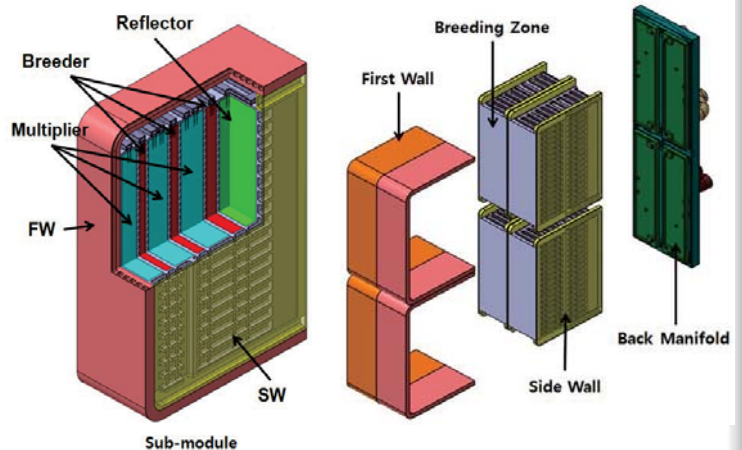
KAERI

HCCR TBM

◆ Helium Cooled Ceramic Reflector (HCCR) TBM (DEMO-relevant Breeding Blanket Concept)

(Main Design Parameters and Materials)

Parameter	Values
FW heat flux	0.3 MW/m ²
Neutron wall load	0.78 MW/m ²
Thermal Power	0.98 MW
Structural material	KO-RAFM (ARAA) (< 550 °C) 1.163 ton
Breeder	Li ₂ TiO ₃ (< 920 °C), 73.7 kg Li-6 Enrichment Ratio : 70 %
Multiplier	Be (< 650 °C), 102.3 kg
Reflector	Graphite (<1200 °C), 40.1 kg
Size	1670(P) x 462(T) x 535(R) (mm)
Coolant	8 MPa He
	1.14 kg/s (Nominal)
	300 °C inlet 500 °C outlet
Purge gas	He with 0.1 % H ₂



- Four Sub-module Concept
 - Manufacturability, PIE & Transportation of Irradiated TBM
 - EM Force Reduction, Endurance of Internal Over-Pressure
- Graphite as Neutron Reflector
 - Reduce the Amount of Be Multiplier
 - Comparable Nuclear Performance for tritium breeding and shielding
 - Decrease of Cost



BeWS-13, Narita, 21-22 Sep., 2017

2

Materials for HCCR TBM

◆ Materials Procurement Strategy for HCCR TBM

■ Structural Material

- To develop KO own RAFM steel
- To establish material property database up to 3 dpa
- To follow ITER Material Qualification Process (Particular Material Appraisal)

■ Breeder Material

- To develop KO own Li₂TiO₃ pebbles
- To establish material property database for pebble and pebble bed
- To compare with other fusion breeder materials (No-qualification)

■ Multiplier Material

- To purchase pure beryllium pebbles developed by companies
- To utilize the available material property database

■ Reflector Material

- To purchase commercially available nuclear grade graphite block from companies
- To utilize the available material property database established by companies



BeWS-13, Narita, 21-22 Sep., 2017

3

- I Introduction
- II Status of Structural Material Development**
- III Status of Functional Material Development
- IV HCCR-TBS Development Schedule
- V Summary

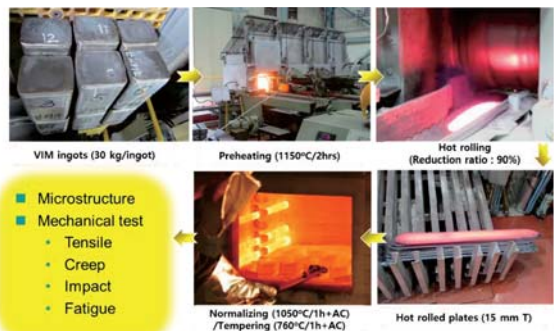
ARAA (Advanced Reduced Activation Alloy)

◆ Advanced Korean RAFM steel development with:

- Improved creep and impact resistances
- Good irradiation resistance under neutron



Advanced Reduced Activation Alloy



- NFRI and KAERI started R&D program on structural material for HCCR TBM application **in 2012**.

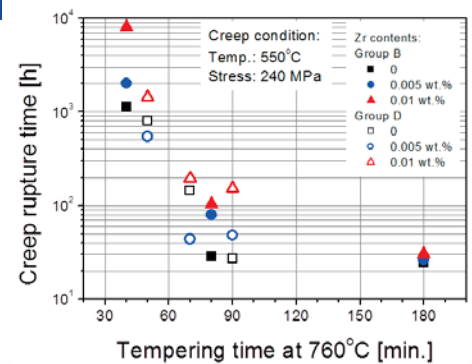
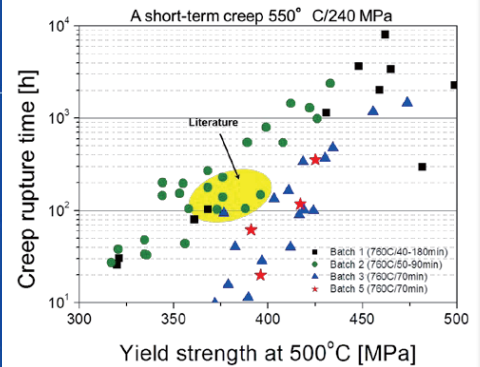
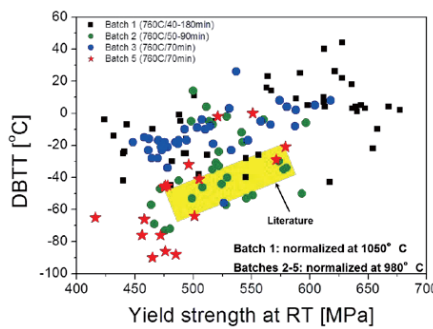
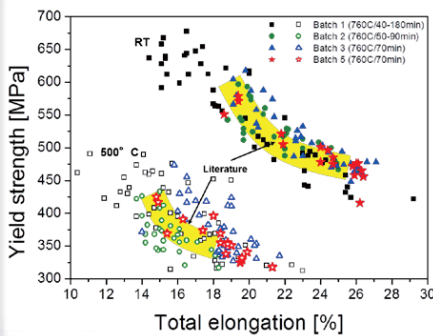
◆ Alloy Design : Strategy

- Basic guidelines
 - 8~9 Cr – 1~2 W base (good resistance to irradiation embrittlement)
 - Minimized induced-activity: (Nb, Mo, Ni, Co, Cu, Al)-free
 - Full-martensitic structure (delta-ferrite free)
- Approaches
 - Optimal combination of the amounts of alloying elements commonly used in the RAFM steels : Cr, W, Ta, V, Ti, ...
 - Addition of new alloying elements : Zr or Sc, or both

Model Alloys for ARAA Development

- ◆ Total of 90 alloys were designed, fabricated and evaluated

Group	C	Si	Mn	Cr	W	V	Ta	N	B	Ti	Zr	Sc
Batch 1 Group A (10 alloys)	0.07	0.10	0.40	9.0	1.0 - 2.0	0.2 - 0.3	0.04 - 0.12	0.03	-	-	-	-
Group B (12 alloys)	0.07	0.10	0.40	9.0	1.0	0.2 - 0.6	0.02 - 0.10	0.03	0.005	0.01	0.01	-
Batch 2 Group C (8 alloys)	0.07	0.05	0.4	8.0 - 9.0	1.0 - 1.5	0.2	0.05	0.03	-	0.01	-	-
Group D (7 alloys)	0.1	0.05	0.45	9.0	1.2	0.2	0.03	0.01	-	0.02	0.01	-
Batch 3 Group E (21 alloys)	0.07	0.05	0.4	8.0 - 10.0	0.8 - 1.6	0.2	0.07	0.04	-	0.01 - 0.02	0.01 - 0.04	0.01 - 0.05
Group F (15 alloys)	0.07	0.05	0.5	8.5	1.4	0.15 - 0.35	0.03 - 0.1	0.05	-	0.01 - 0.02	0.01 - 0.04	0.01 - 0.05
Batch 5 Group G (17 alloys)	0.1	0.1	0.45	9	1.2	0.2	0.07	-	-	0.01	0.01 - 0.05	0.01 - 0.05



BeWS-13, Narita, 21-22 Sep., 2017

6

Optimization for ARAA

- ◆ Optimized Chemical Composition of ARAA

Country	Name	C	Si	Mn	Cr	W	V	Ta	N	Ti	Zr
Japan	F82H	0.1	0.1	0.2	8	2	0.15	0.02	0.04	-	-
Japan	JLF-1	0.1	0.05	0.5	9	2	0.2	0.07	0.05	0.001	-
EU	Eurofer97	0.11	0.05	0.4	9	1.1	0.2	0.07	0.05	0.01	-
US	9Cr-2WVTa	0.1	0.25	0.4	9	2	0.25	0.07	0.003	0.01	-
Russia	Rusfer EK181	0.15	0.4	0.7	11	1.2	0.6	0.2	0.1	-	-
India	Indian-RAFM	0.1	0.09	0.5	9	1	0.2	0.07	0.02	0.005	-
China	CLAM	0.1	0.01	0.45	9	1.5	0.2	0.15	0.02	-	-
China	CLF-1	0.11	0.05	0.5	8.5	1.5	0.5	0.1	0.02	0.01	-
Korea	ARAA	0.1	0.1	0.45	9	1.2	0.2	0.07	0.01	0.01	0.01

- ◆ Characteristics of ARAA

- Cr (9 wt.%) : For Good Corrosion Resistance
Minimum DBTT before & after Irradiation
- W (1.2 wt.%) : Decrease in the Possibility of Laves Phase Precipitation
Balance between High-temp. Strength and Impact Properties
- Zr (0.01 wt.%) : Improvement of Creep and Impact Resistance

- ◆ Optimized Heat Treatments Condition of ARAA

- Normalizing : 1000 °C / 40 min. / AC, Tempering : 750 °C / 70 min. / AC



BeWS-13, Narita, 21-22 Sep., 2017

7

Large Scale Production of ARAA (2014)

◆ Large Scale Production

■ 5 ton-scale ARAA by POSCO Specialty Steel (ARAA-1)

- Produced by **VIM + ESR** Processes
- Utilized for Mock-up Fabrication & Material DB Development



ESR ingots



Forged bars



Hot-rolled plates

wt.%	C	Si	Mn	Cr	W	V	Ta	N	Ti	Zr
Target	0.10	0.10	0.45	9.0	1.2	0.20	0.07	0.01	0.01	0.01
Allowance	0.08~ 0.12	0.05~ 0.15	0.30~ 0.60	8.70~ 9.30	1.00~ 1.40	0.10~ 0.30	0.05~ 0.09	0.005~ 0.015	0.005~ 0.020	0.005~ 0.020
Analysis	0.09	0.078	0.40	8.88	1.20	0.18	0.053	0.006	0.008	0.006

Large Scale Production of ARAA (2015)

◆ Large Scale Production

■ 6 ton-scale ARAA by KPCM (ARAA-2)

- Produced by **VIM + VAR** Processes
- Utilized for Mock-up Fabrication & Material DB Development



Compounded
VIM ingots



VAR ingot

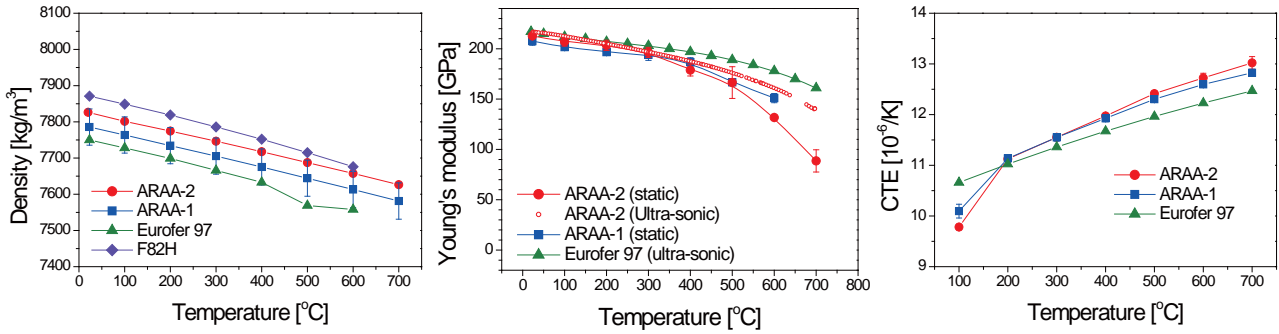


Tempered plates

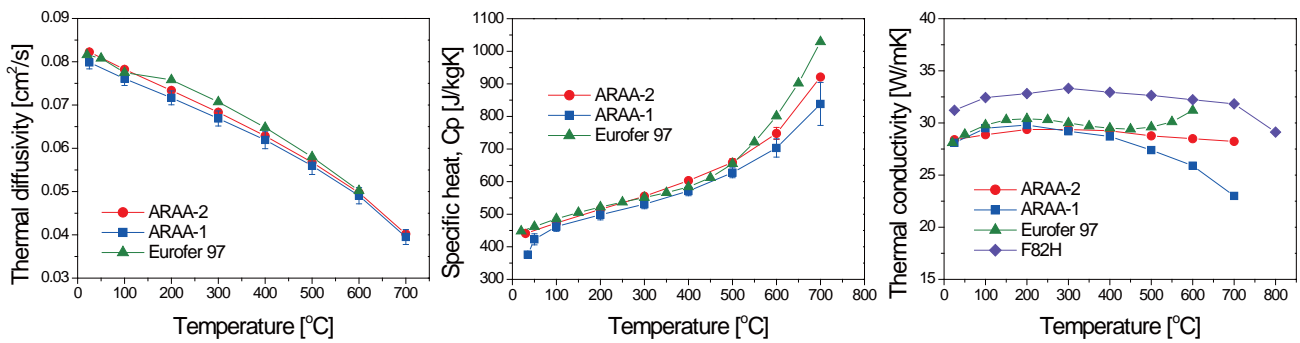
wt.%	C	Si	Mn	Cr	W	V	Ta	N	Ti	Zr
Target	0.10	0.10	0.45	9.0	1.2	0.20	0.07	0.01	0.01	0.01
Allowance	0.08~ 0.12	0.05~ 0.15	0.30~ 0.60	8.70~ 9.30	1.00~ 1.40	0.10~ 0.30	0.05~ 0.09	0.005~ 0.015	0.005~ 0.020	0.005~ 0.020
Analysis	0.10	0.11	0.26	9.04	1.25	0.20	0.06	0.0043	0.0061	0.011

Physical and Thermal Properties of ARAA

Physical Properties



Thermal Properties



* Eurofer 97 data from: F. Tavassoli, DISDC - Appendix A Material Design Limit Data, 2004.

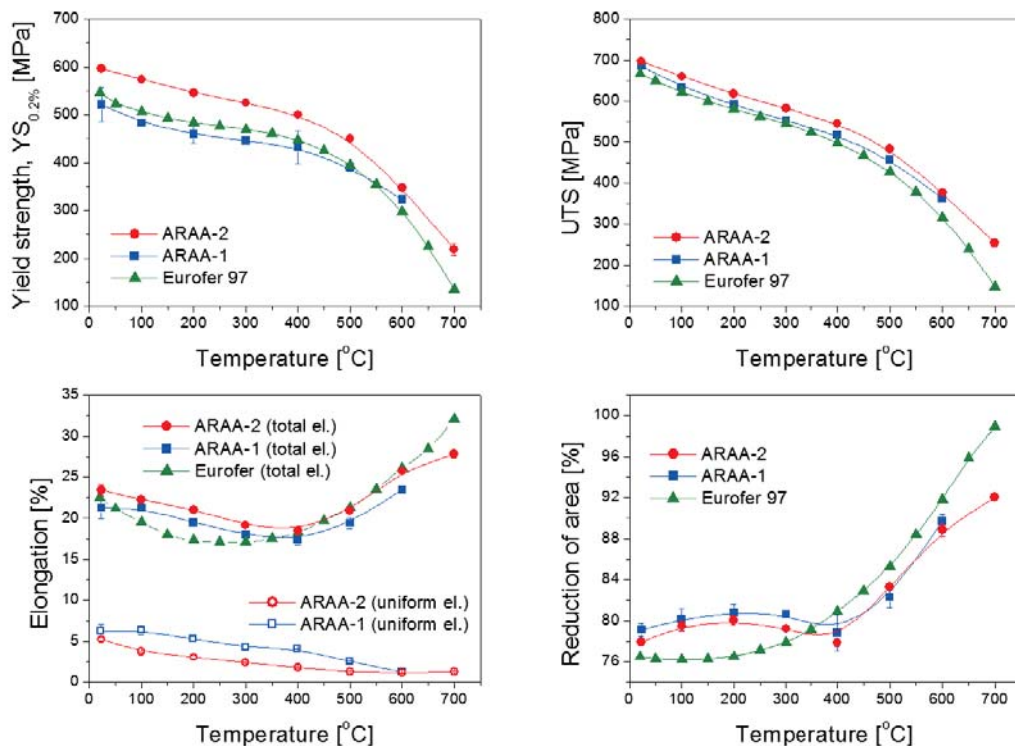


BeWS-13, Narita, 21-22 Sep., 2017

10

Tensile Properties of ARAA

Tensile Properties



* Eurofer 97 data from: F. Tavassoli, DISDC - Appendix A Material Design Limit Data, 2004.

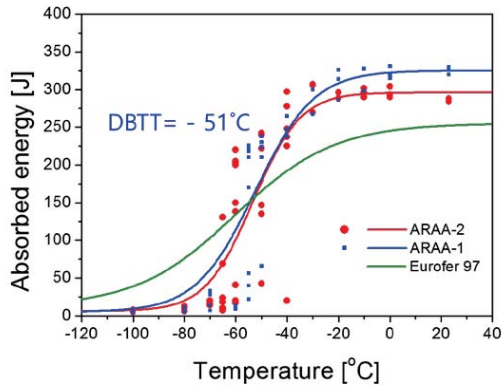


BeWS-13, Narita, 21-22 Sep., 2017

11

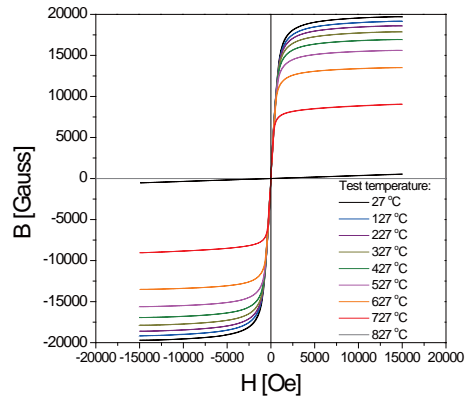
Impact, Magnetic, LCF, Creep-Fatigue Properties

Impact Properties



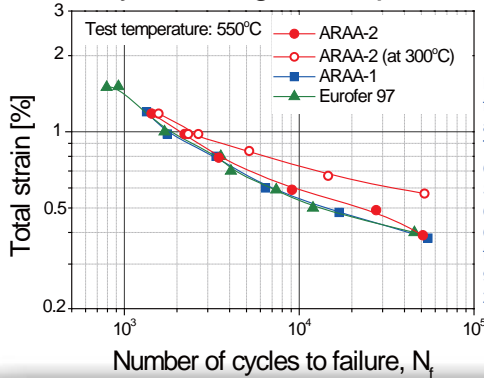
Eurofer 97 data from: F. Tavassoli, DISDC - Appendix A Material Design Limit Data, 2004.

Magnetic Properties



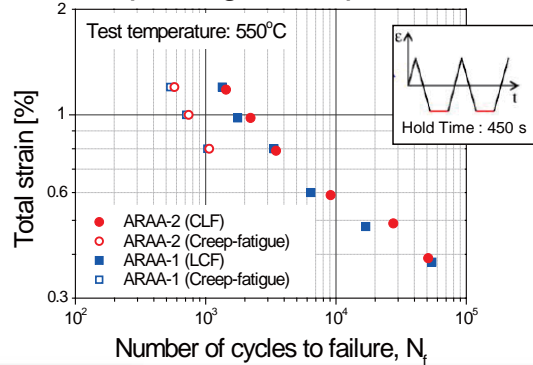
B-H curves measured by Prof. A. Żywczak in AGH Univ. in Poland

Low Cycle Fatigue Properties



Eurofer 97 data from: J. Aktaa et al., High Temperature Creep-Fatigue Structural Design Criteria for Fusion Components Built from EUROFER 97, FZKA 7309, 2007.

Creep-Fatigue Properties

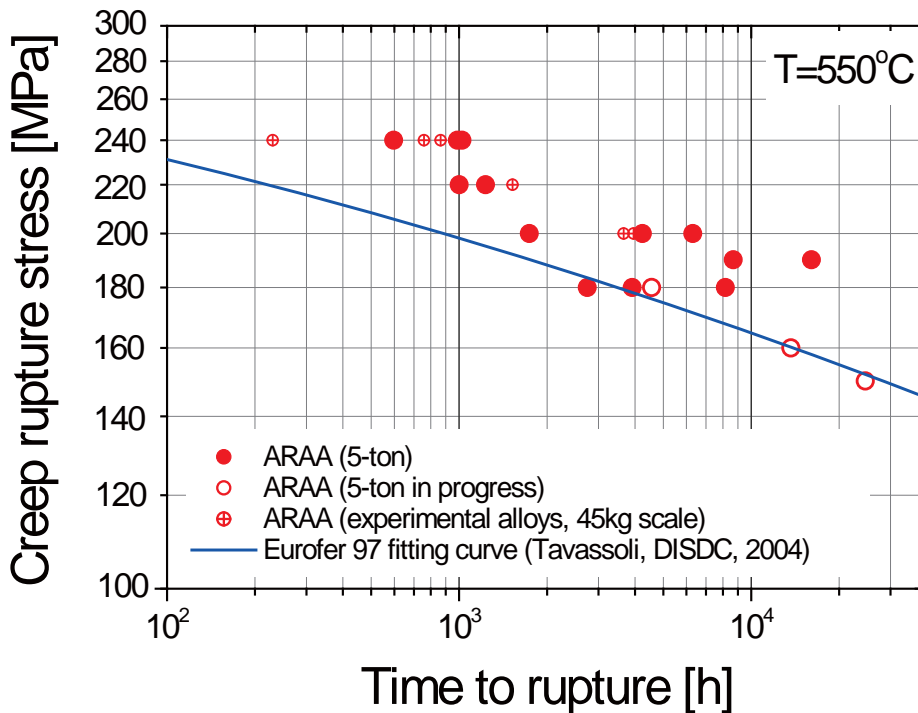


BeWS-13, Narita, 21-22 Sep., 2017

12

Creep Properties of ARAA

Creep Properties



* Eurofer 97 data from: F. Tavassoli, DISDC - Appendix A Material Design Limit Data, 2004.



BeWS-13, Narita, 21-22 Sep., 2017

13

Large Scale Production of ARAA (2017)

◆ Large Scale Production

■ 18 ton-scale (6 ton X 3ea) ARAA by KPCM (ARAA-3)

- Produced by **VIM + VAR** Processes
- Utilized for One Sub-module Mock-up Fabrication & Material DB Development



wt.%	C	Si	Mn	Cr	W	V	Ta	N	Ti	Zr
Target	0.10	0.10	0.45	9.0	1.2	0.20	0.07	0.01	0.01	0.01
Allowance	0.08~ 0.12	0.05~ 0.15	0.30~ 0.60	8.70~ 9.30	1.00~ 1.40	0.10~ 0.30	0.05~ 0.09	0.005~ 0.015	0.005~ 0.020	0.005~ 0.020
Analysis	0.10	0.10	0.37	9.04	1.17	0.21	0.08	-	0.008	0.005

Outline



Introduction



Status of Structural Material Development



Status of Functional Material Development
(Tritium Breeder Material, Li_2TiO_3)



HCCR-TBS Development Schedule



Summary

Development of Synthesis Process for Li₂TiO₃ Nano-powder

◆ Synthesis Process for Li₂TiO₃ Nano-powder by Solid-state Reaction Method

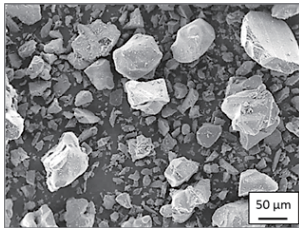


- Raw Material : Li₂O, TiO₂
- Molar Ratio : 1.00 : 0.89 ~ 1.00
- Solvent : Iso-propyl Alcohol

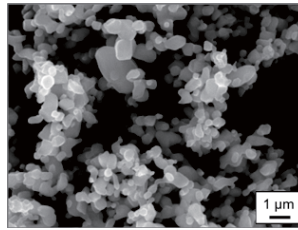
- Drying Temp. : 60 °C
- Drying Atmosphere : Vac.
- Drying Time : 6 h

- Temp. : 500 ~ 800 °C
- Atmosphere : Air
- Time : 2 ~ 24 h

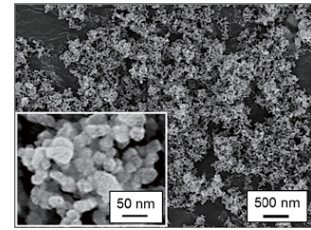
■ Starting Materials



- Li₂O (Lithium Oxide)
 - Purity : > 99 %



- TiO₂ (Titanium Dioxide)
 - Rutile
 - Purity : 99.99 %



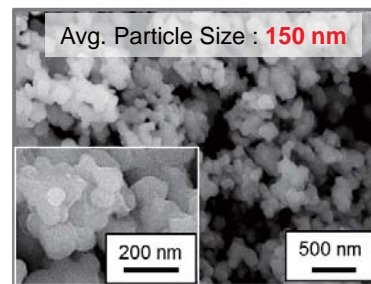
- TiO₂ (Titanium Dioxide)
 - Anatase
 - Purity : 99.99 %

Synthesized Li₂TiO₃ Nano-powder

◆ Morphology of Synthesized Li₂TiO₃ Nano-powder



(TiO₂ Form : Rutile)



(TiO₂ Form : Anatase)

◆ Impurities of Synthesized Li₂TiO₃ Nano-powder

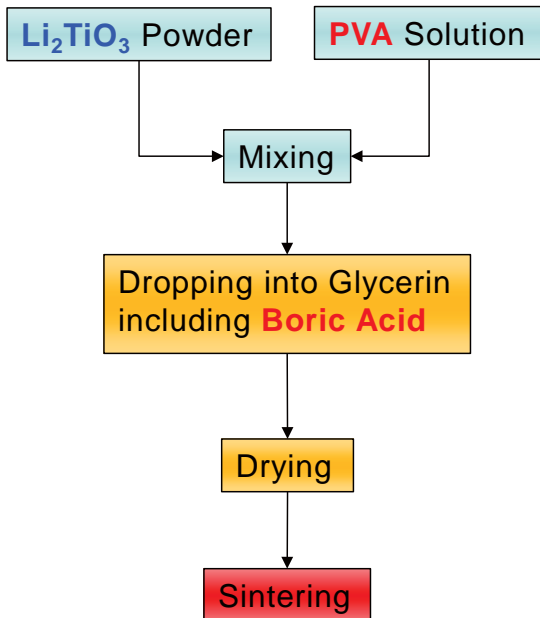
Element	Starting Materials			Li ₂ TiO ₃ Powder		
	Li ₂ O	TiO ₂ Rutile	TiO ₂ Anatase	Commercial	Synthesized by Rutile	Synthesized by Anatase
Al	49.5	13.8	N.D.	5.45	30.9	33.2
B	N.D.	N.D.	N.D.	N.D.	5.7	N.D.
Ca	39.1	N.D.	25.3	70.1	82.2	47.1
Co	N.D.	N.D.	N.D.	629.1	N.D.	N.D.
K	33.6	43.0	56.7	-	64.7	51.7
Na	33.4	47.5	57.0	144.4	77.7	61.0
Zr	N.D.	N.D.	7.6	-	3139.0	339.6

Pebble Fabrication Process

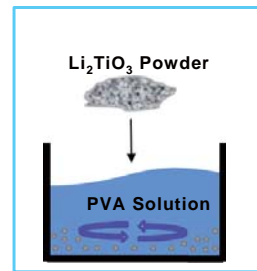
◆ Fabrication Process of Li_2TiO_3 Pebble

- Slurry Droplet Wetting Method based on the Cross-linking Reaction between PVA and Boric-acid

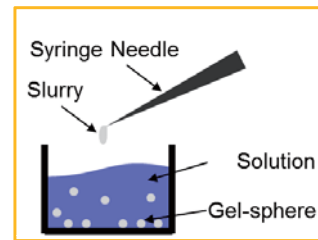
Fabrication Process



Mixing



Shaping



Sintering



BeWS-13, Narita, 21-22 Sep., 2017

18

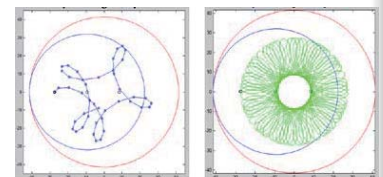
Automatic Slurry Dispensing System for Li_2TiO_3 Pebble

◆ Development of Automatic Slurry Dispensing System



Dispensing Unit

; for instillation of Li_2TiO_3 slurry

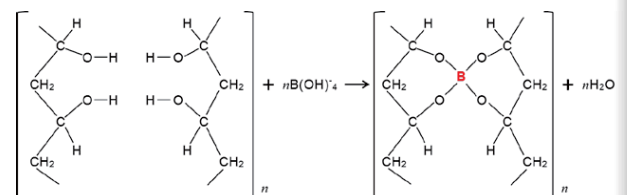


Trace of Drop Point through the Moving Needle



Glycerin Bath

; for hardening of droplets



Automatic maintaining Unit

; for constant distance between syringe needle and glycerin surface

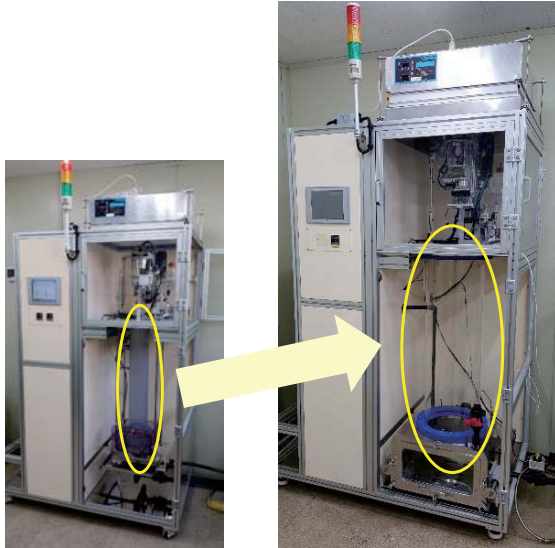


BeWS-13, Narita, 21-22 Sep., 2017

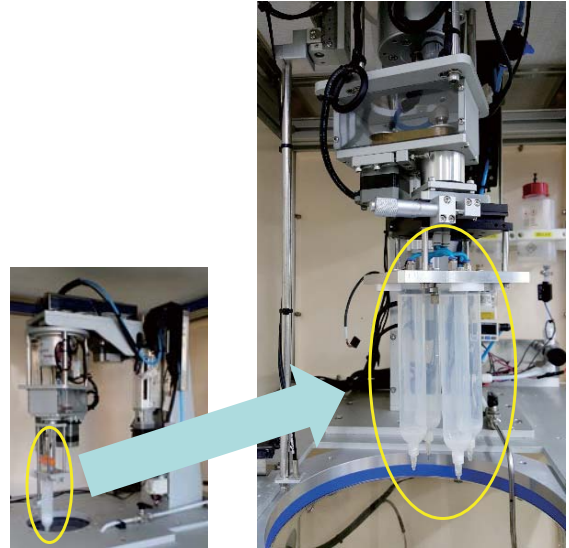
19

Improvement of Dispensing System

- ◆ Slurry dispensing system has been upgraded to improve pebbles uniformity and production rate.
 - Large glycerin bath was adapted to reduce the wall effect during droplets sinking.
 - Dispensing unit was upgraded to 4-needle system for high production rate.



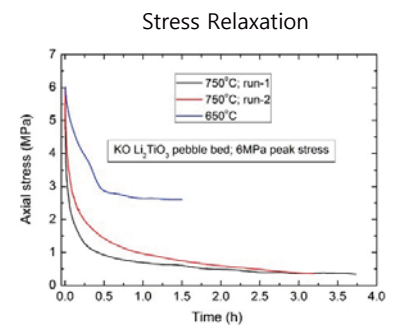
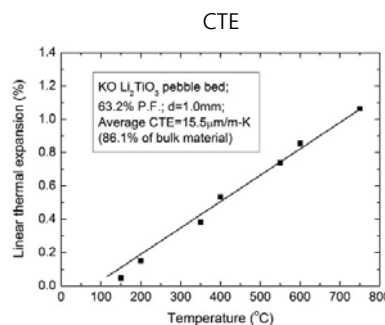
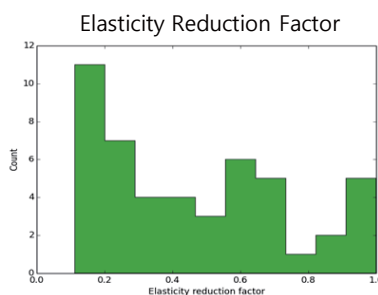
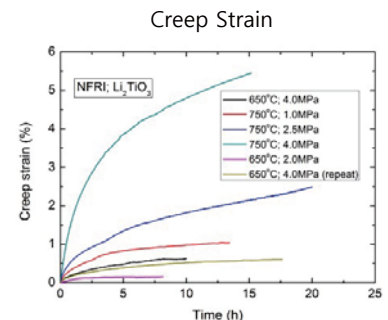
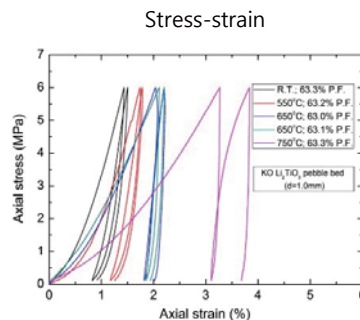
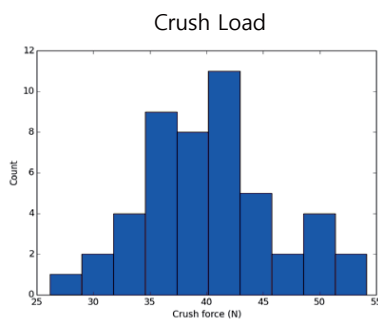
(Large Glycerin Bath for Pebbles Uniformity)



(4-needle System for High Production Rate)

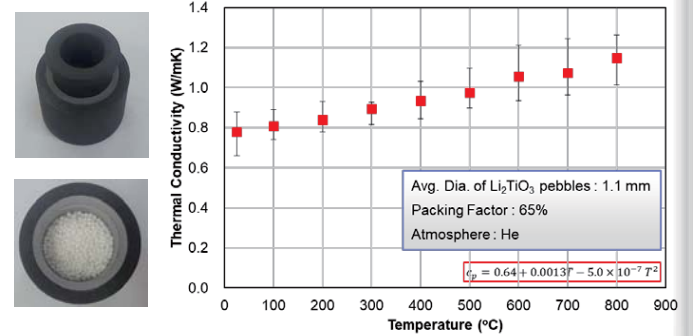
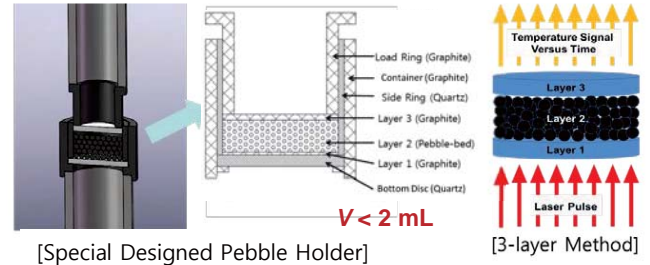
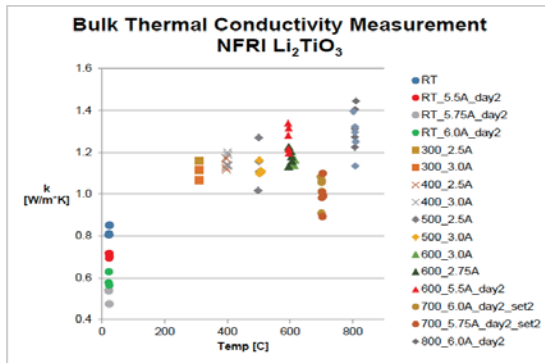
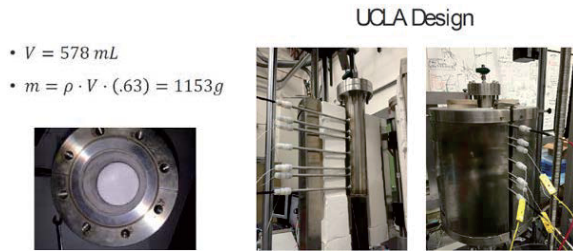
Establishment of Database for Li_2TiO_3 Pebble Bed

- ◆ Thermo-mechanical properties of breeder pebble and pebble bed have been established by UCLA colleagues under KO-US TBM collaboration program.



Establishment of Database for Li₂TiO₃ Pebble Bed

- ◆ Thermo-mechanical properties of breeder pebble and pebble bed have been established by UCLA colleagues under KO-US TBM collaboration program.
- ◆ Effective thermal conductivity of Li₂TiO₃ pebble bed was measured by transient hot wire method at UCLA and laser flash method at NFRI.

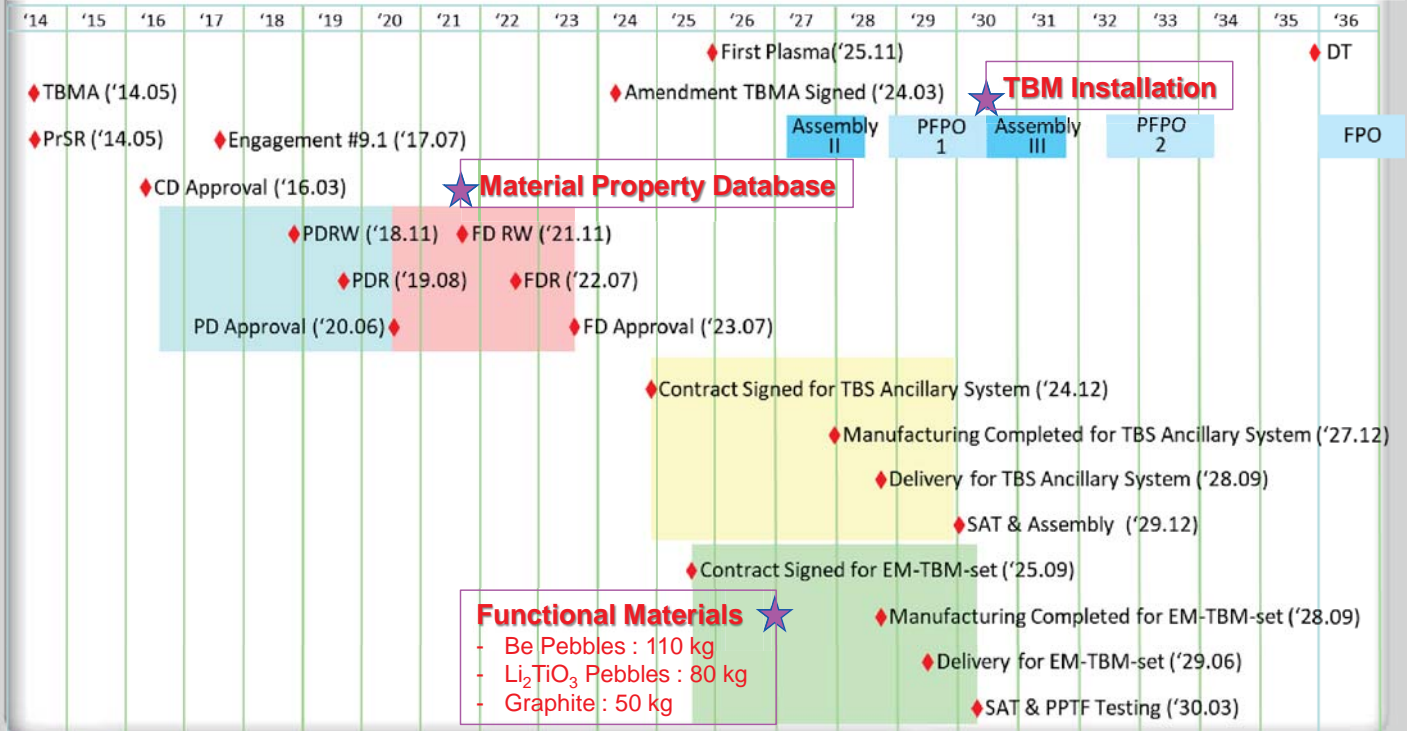


Outline

- I Introduction
- II Status of Structural Material Development
- III Status of Functional Material Development
- IV HCCR-TBS Development Schedule
- V Summary

HCCR-TBS Development Schedule

- ◆ Overall schedule is proposed based on that HCCR-TBS will be installed during Assembly phase III.
 - All materials database have to be prepared before FDRW (2021) or FDR (2022).
 - Functional materials have to be delivered by the end of 2026.



Outline

- I Introduction
- II Status of Structural Material Development
- III Status of Functional Material Development
- IV HCCR-TBS Development Schedule
- V Summary

Summary

- ◆ Advanced Reduced Activation Alloy (ARAA) was developed as structural material for HCCR TBM by NFRI and KAERI.
- ◆ Fabrication process for large scale production of ARAA was verified through three times experiences.
 - ARAA-1 : 5 ton-scale, POSCO Specialty Steel, VIM + ESR, 2014
 - ARAA-2 : 6 ton-scale, KPCM, VIM + VAR, 2015
 - ARAA-3 : 18 ton-scale (6 ton X 3 ea), KPCM, VIM + VAR, 2017
- ◆ Large scale ARAA is utilized to establish material property database and mock-up fabrication for HCCR TBM.
- ◆ Li_2TiO_3 pebbles were fabricated by slurry droplet wetting method for tritium breeder material of HCCR TBM.
- ◆ Mass-production system for Li_2TiO_3 pebbles is upgrading to improve uniformity and production rate.
- ◆ Material property database of Li_2TiO_3 pebble and pebble bed is being established not only by KO TBM Team but also by international collaborators.
- ◆ Regarding Be pebbles as neutron multiplier of HCCR TBM,
 - material database has to be prepared by the end of 2021.
 - pebbles have to be delivered by the end of 2026.

13th International Workshop on Beryllium Technology (BeWS-13)

Narita, 21-22 September, 2017

Thank you for your attention!!!

Yi-Hyun Park

yhpark@nfri.re.kr



2.3.5 Preparation for manufacturing of the beryllium armor of the ITER first wall in the Russian Federation

R. Giniyatulin¹, I. Mazul¹, A. Gervash¹, I Kupriyanov², V. Sizenev³, A. Milkov³, G. Garyaev⁴

¹ JSC "NIEFA", Saint Petersburg, RF

² JSC "A.A. Bochvar Institute", Moscow, RF

³ JSC "Kompozit", Korolev, Moscow Region, RF

⁴ FSUE "Bazalt", Saratov, RF

E-mail: giniirn@sintez.niefa.spb.su

The RF DA should deliver to the ITER site under the Procurement Arrangement 40% of enhanced heat-flux first-wall panels armored with beryllium tiles. In this delivery the beryllium armor is 260 m² in area, about 4 tons in weight and 8 mm in design thickness. With tiles 50x16x8 mm in size selected, as of now, for armor application, there will be the need in 300000 tiles. The report concerns the status of preparation for manufacturing of the beryllium armor. Two beryllium grades are proposed for armor application, namely, ТПН-56ПЦ beryllium grade specially developed in Russia and approved by ITER IO and S-65 American beryllium grade selected as the reference one for the ITER project. The report describes the main technological operations for manufacturing of the armor at enterprises participating in the program, as well as the characteristics of pilot lots of manufactured tiles of both grades. The report presents the technological approaches to cleaning of beryllium tiles required to ensure the safe operation conditions during assembly of first-wall panel elements. The report presents the last R&D results on elaboration of the technology for brazing of the beryllium armor to the bronze heat sink, as well as the results of life-time high heat flux tests of large-scale mock-ups of the first wall panels.



Preparation for manufacturing of the Beryllium armor of the ITER First Wall in the Russian Federation

Presented by Radmir Giniyatulin

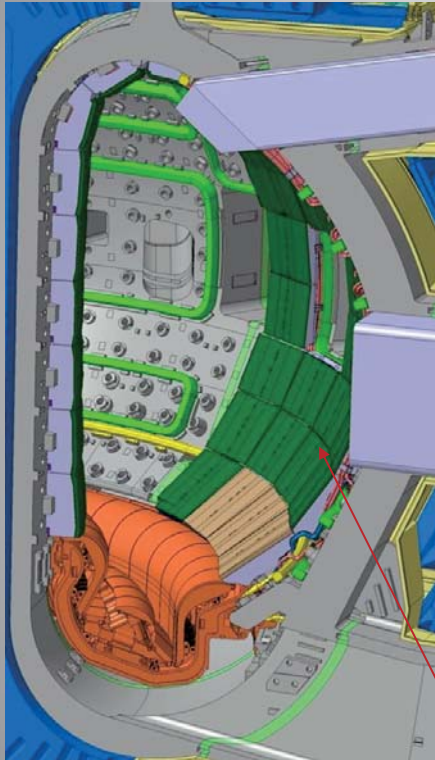
13th International Workshop on Beryllium Technology (BeWS-13)
September 21, 2017,
Narita, CHIBA, Japan



Content

- Current obligations to supply First Wall (FW) Panels
- The composition of FW Panel and key technologies
- Technological steps sharing in Be-related works
- Be-tiles for Enhanced Heat Flux First Wall Panels - dimensions
- Be-tiles manufacturing
- Be-armored PFU brazing
- FW mockups manufacturing and testing
- NDT methods of FW panel components
- FW Plasma Facing Units High Heat Flux tests
- Summary

Current obligations to supply First Wall Panels

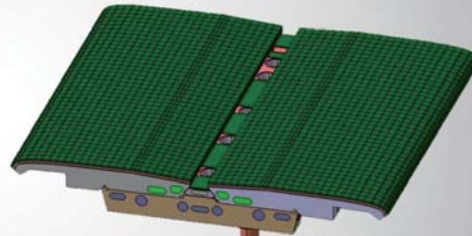


FW panels

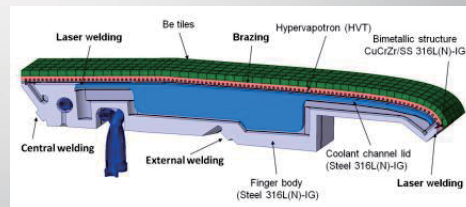
~ 700 m² of Be-armoured FW panels, ~ 10 tons of Be-tiles

Enhanced Heat Flux First Wall (FW) Panel:

- Manufacture and supply of 179 Enhanced First Wall Panels
- Panel weights ~1 t and has dimensions (1,5x1x0,3) m
- Panel consists of a massive steel support structure and 40 PFE armored with beryllium
- RF contribution – 40%



FW panel (1,5x1x0,3) m, N=179

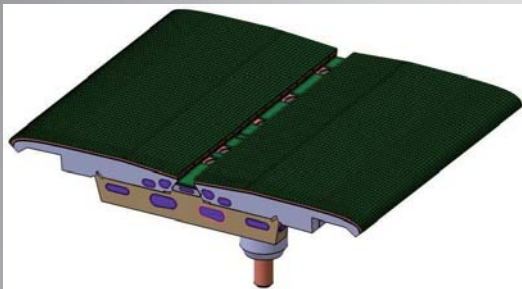


FW finger, N~6200

matulin

3

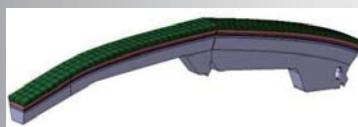
The composition of FW Panel and key technologies



- Manufacturing program :**
- 179 FW panels (32 modifications)
- The composition:**
- Plasma Facing Unit (Finger) – 6626 pc. (372 modifications)
 - Central slot insert – 179 pc.
 - Tubes – 358 pc.
 - Beryllium tile – 278882 pc.
 - Support structure (beam) – 179 pc.

- Key technologies:**
- Precise mechanical machining
 - EDM machining of beryllium
 - Explosion bonding
 - Hot isostatic pressuring
 - Laser welding
 - TIG orbital welding
 - Brazing
 - Nondestructive tests
 - HHF tests
 - Hydraulic and vacuum leak tests
 - Geometrical measuring
 - Cleaning
 - Vacuum annealing

Main FW Panel parts



Plasma Facing Unit



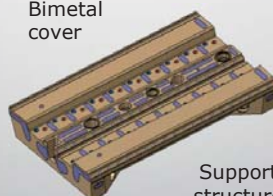
Bimetal cover



Central slot insert



Tubes



Support structure

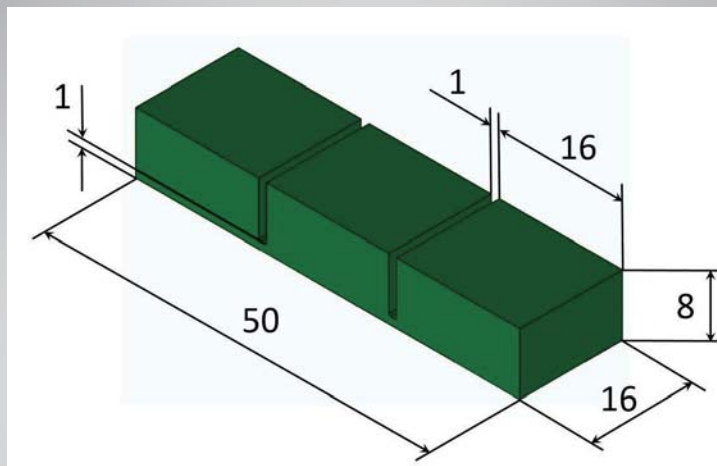


Beryllium tile

matulin

4

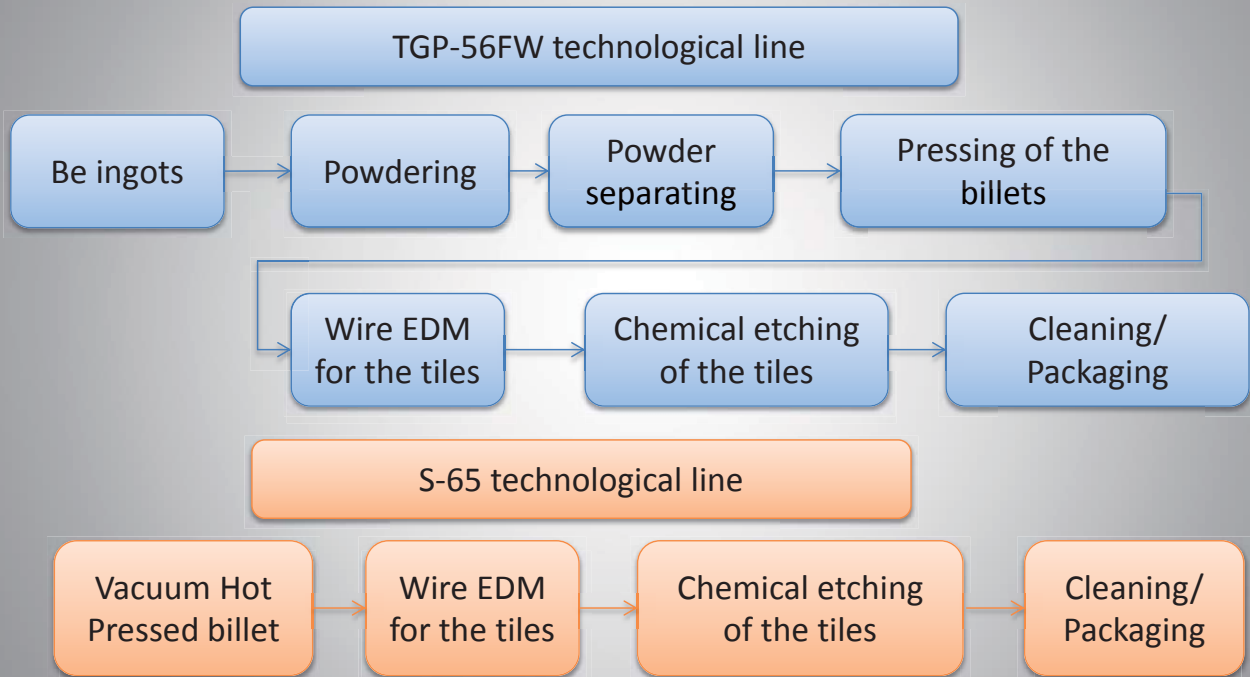
JSC Efremov Institute	JSC Bochvar Institute	FSUE Bazalt	JSC Kompozit
<ul style="list-style-type: none"> ▪ Brazing of Be-tiles with heat sink structure ▪ HHF tests by e-beam ▪ Vacuum and hydraulic tests ▪ Assembling of FW panels ▪ Cleaning of fingers and panels ▪ 3-D measuring ▪ Packaging ▪ Storing 	<ul style="list-style-type: none"> ▪ Technological works with powder and pressed billets ▪ Chemical analysis and mechanical tests of the samples from billets ▪ Machining of Be ▪ Tests of mockups at plasma accelerator facility ▪ Packaging ▪ Storing 	<ul style="list-style-type: none"> ▪ Technological and manufacturing works with powder and pressed billets ▪ Chemical analysis and mechanical tests of the samples from billets ▪ Machining of Be, tiles manufacturing ▪ Cleaning of the tiles ▪ Packaging ▪ Storing 	<ul style="list-style-type: none"> ▪ Machining of Be, tiles manufacturing ▪ Cleaning of the tiles ▪ Packaging ▪ Storing



Be-tiles manufacturing (1/2)

Two beryllium grades are using in RF for the tiles manufacturing:

- TGP-56FW: initial material – vacuum melted beryllium ingots from Ulba plant
- S-65 tiles: initial materials - VHP blocks from Materion



Amiatulin

7

Be-tiles manufacturing (2/2)

TGP-56FW (JSC Bazalt)



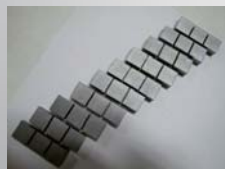
Beryllium ingots



VHP billets 220x220x60 mm



VHP billet ϕ 300, H120 mm



Tiles 16x50x8 mm castellated

S-65 (JSC Kompozit)



VHP billet ϕ 520, H 230 mm



Tiles 16x50x8 mm castellated

8



Wire-EDM machining of cylindrical S-65 beryllium block



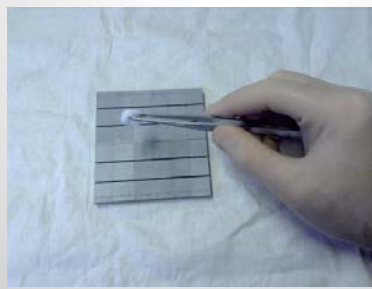
Chemical etching of the tiles



Laser marking of the tiles



Ultrasonic cleaning of the tiles:
Bath №1 – Ultrasonic bath
Bath №2 – Rinsing in distilled water with stirring
Bath №3 – Hot-air drying



Smearing is taken from 1 dm² of the surface of the tiles

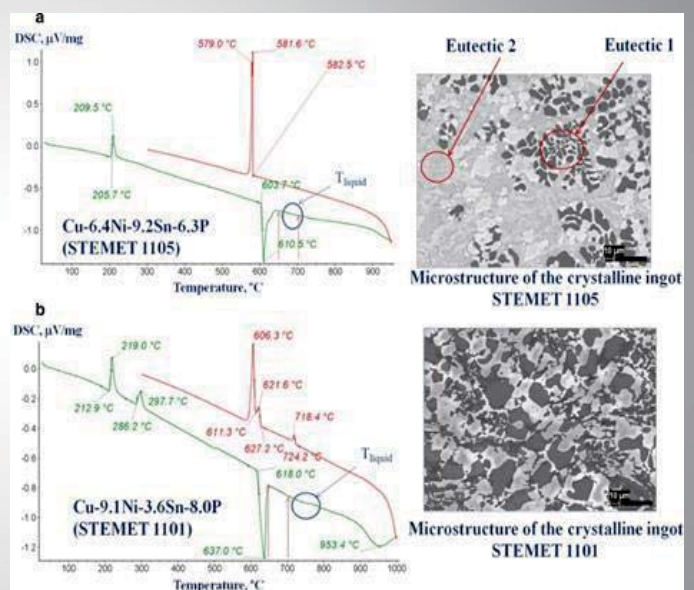


Packaging



The technological brazing process was modified:

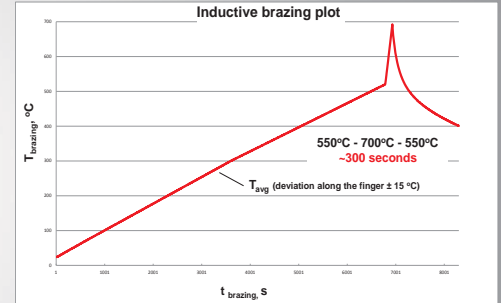
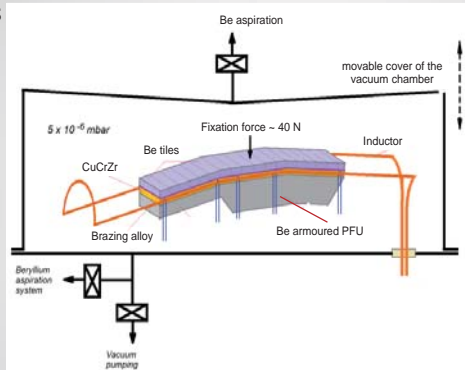
- Decrease in the brazing temperature to 650°C (the chemical composition of the STEMET brazing alloy was optimized and dispersed eutectics was obtained)
- Results: minimization of thickness of the brittle intermetallic layer in Be/CuCrZr zone; preservation the strength properties of bronze



- Previous method of heating by the electron beam led to a significant overheating of the Be tiles and fixation tools
- Alternative heating by inductor allows
 - ✓ directly heating beryllium/bronze joint zone, reduce the operation temperature of the clamping tools
 - ✓ significantly reduce the weight of clamping tools and provide their multiple use
 - ✓ simplify safety issues



Inductive brazing facility

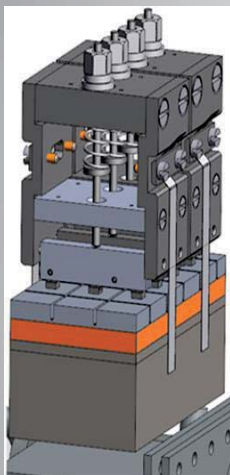


Inductive heating of the mockup with clamping tools



The mockup with modified clamping tools (in brazing chamber)

New design of elastic clamps for Beryllium tiles fixation

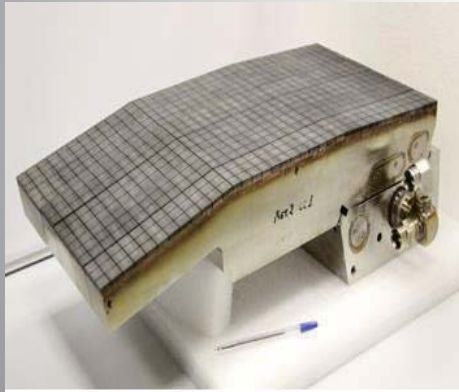


Main features:

- light-weight
- uniform distribution of pressure over the surface of the tile
- reduced operating temperature
- the possibility of repeated use



Single PFE with Be-tiles
(0.75x0.05x0.3 m³)

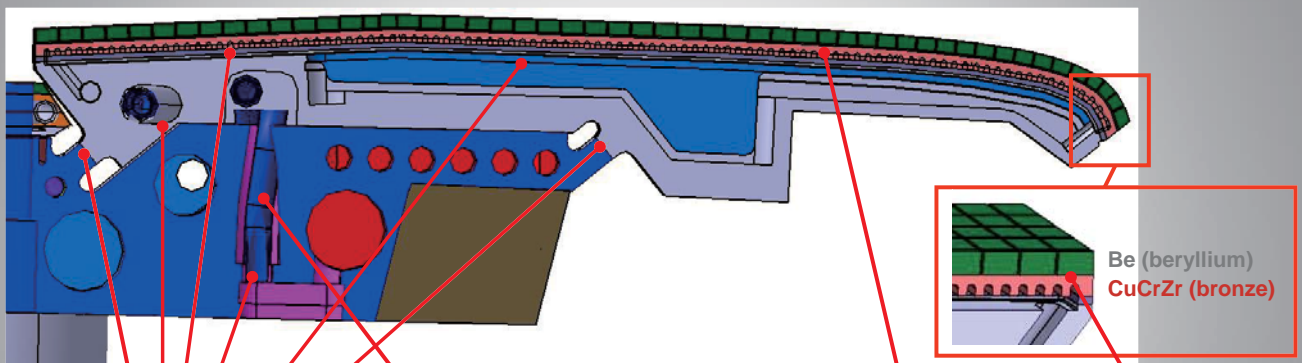


Be-armored FW semi-
prototype (0.75x0.3x0.3 m)



Two pair of PFU's installed in HHF testing facility

13



Laser welding –
VT, PT, RT, UT

Orbital TIG welding –
VT, PT, RT

Explosion welding / HIP –
UT

Brazing –
UT

Visual testing (VT)

Penetrant testing (PT)

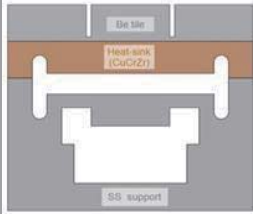
Radiographic testing (RT)

Ultrasonic testing (UT)

FW PFU's HHF tests

The thermal lifetime testing of the manufactured first wall proves the workability of both the structure and selected technologies (brazing, welding):

- The lifetime of the most critical joints was assessed under the cyclic thermal stresses (Be/CuCrZr brazing, CuCrZr/SS- and SS/SS-welding);
- The total number of heat pulses applied to all areas of each tested HHF unit amounted to 24000;
- All tested HHF units withstood the heat loads and retained completely the brazed beryllium armor;
- No zones of local overheating and no increase in the surface temperature by more than 20% were observed on all tested units.



Cross-section scheme of FW finger



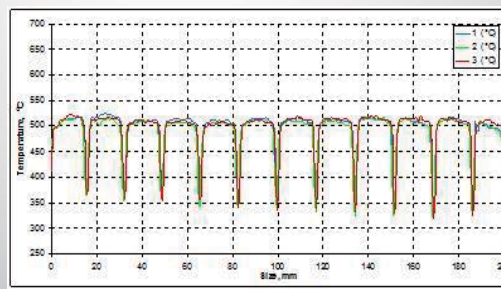
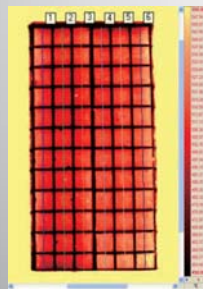
FW semi-prototype PFU's



FW PFU's in testing facility



FW PFU's with masks



IR-image and surface temperature distribution during HHF test

Summary

- About 300 000 Be-tiles will be manufactured in RF in the frame of ITER program
- Four RF companies (Efremov Institute, Bochvar Institute, JSC Bazalt, JSC Kompozit)
- Two beryllium grades (TGP-56FW and S-65) will be used for the program
- All participating companies are equipped for the tiles manufacturing
- The serial production of the tiles will start in 2019

Thank you for your attention!

2.4 Technical session 1: Fabrication process

2.4.1 Overview of beryllide R&D as advanced neutron multiplier in Japan

M. Nakamichi, J-H. Kim, P. Kurinskiy

¹*Fusion Energy Research and Development Directorat, National Institutes for Quantum and Radiological Science and Technology (QST)
2-166, Omotedate, Obuchi, Rokkasho, Kamikita, Aomori, 039-3212, Japan*

E-mail: nakamichi.masaru@qst.go.jp

DEMO reactors require advanced neutron multipliers that have higher stability at high temperature. Beryllium intermetallic compounds (beryllides) are the most promising advanced neutron multipliers. Development of the advanced neutron multipliers has been started between Japan and the EU in the DEMO R&D of the International Fusion Energy Research Centre (IFERC) project as a part of the Broader Approach activities. In Japan, beryllides fabrication R&D has been carried out in the DEMO R&D building at IFERC, Rokkasho. The Beryllium (Be) Handling Room has been installed in the DEMO R&D building. In this facility, synthesis, treatment, machining and characterizations of beryllides and its pebbles are being performed.

Because Beryllides are too brittle to allow production of the pebbles, establishing fabrication techniques for beryllides is a key issue for development of the advanced neutron multipliers. Conventional syntheses of the beryllides involve a powder metallurgy process involving a hot isostatic pressing method, a casting method, and an arc-melting method. However, beryllides synthesized conventionally are so brittle that it was not easy to fabricate the block or rod type by these methods.

On the other hand, a plasma sintering method has been proposed as a new technique for beryllides synthesis and joining because this method results in powder surface activation that enhances powder particle sinterability and reduces high temperature exposure. From the results of beryllide synthesis experiments, it was clarified that the not only disk type but rod type of beryllide has been successfully fabricated by the plasma sintering method.

To fabricate the prototypic beryllide pebbles using the plasma-sintered beryllide rod, the rotating electrode method (REM) was selected because the experience base for its use is broad for not only Be pebbles but also metallic pebbles in industry in general. The result of beryllide granulation revealed that the prototypic beryllide pebbles with 1 mm in average diameter were successfully fabricated. In this study, the recent progress on R&D of beryllides as the advanced neutron multipliers in Japan will be presented.

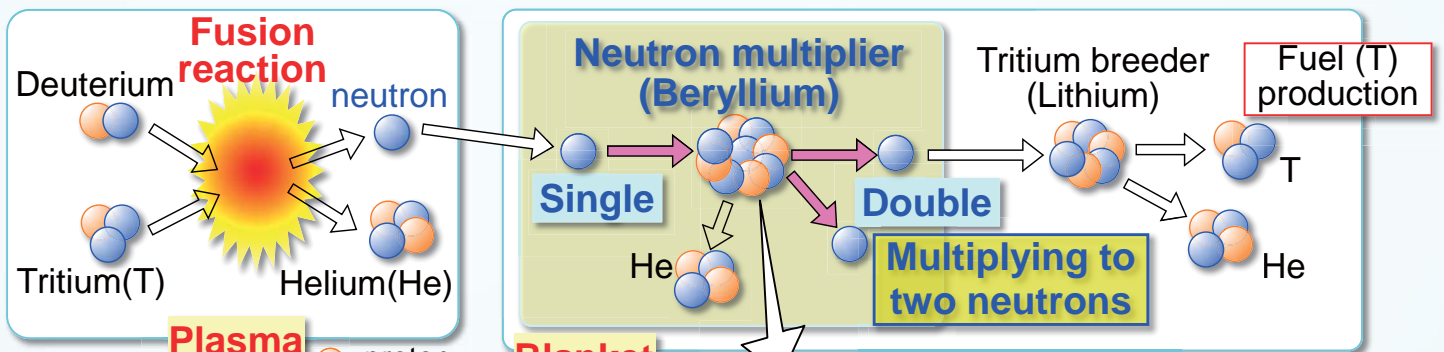
Overview of R&D on Beryllide as advanced neutron multipliers in Japan

Masaru NAKAMICHI,
 Jae-Hwan KIM, Petr KURINSKIY

National Institutes for Quantum and Radiological Science and Technology, QST



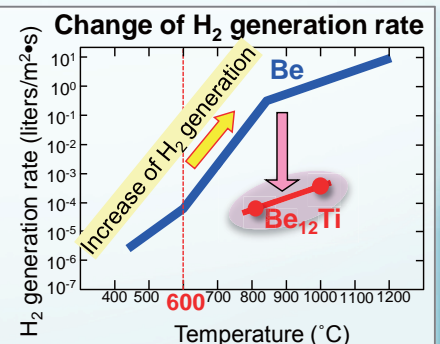
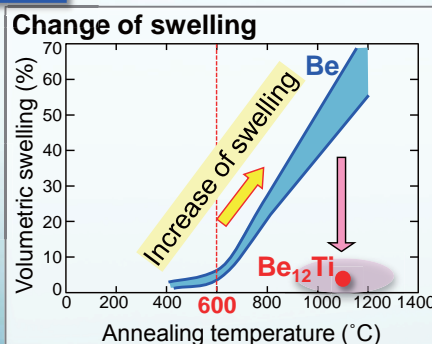
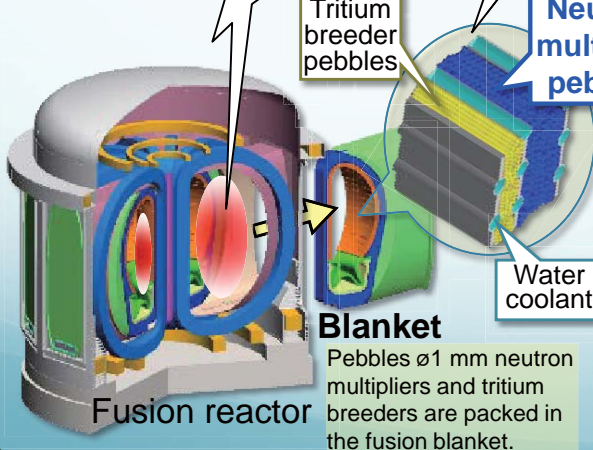
Necessity of Advanced Neutron Multiplier



Beryllium metal (Be) is candidate material.

There are some issues under high neutron fluence at high temperatures.

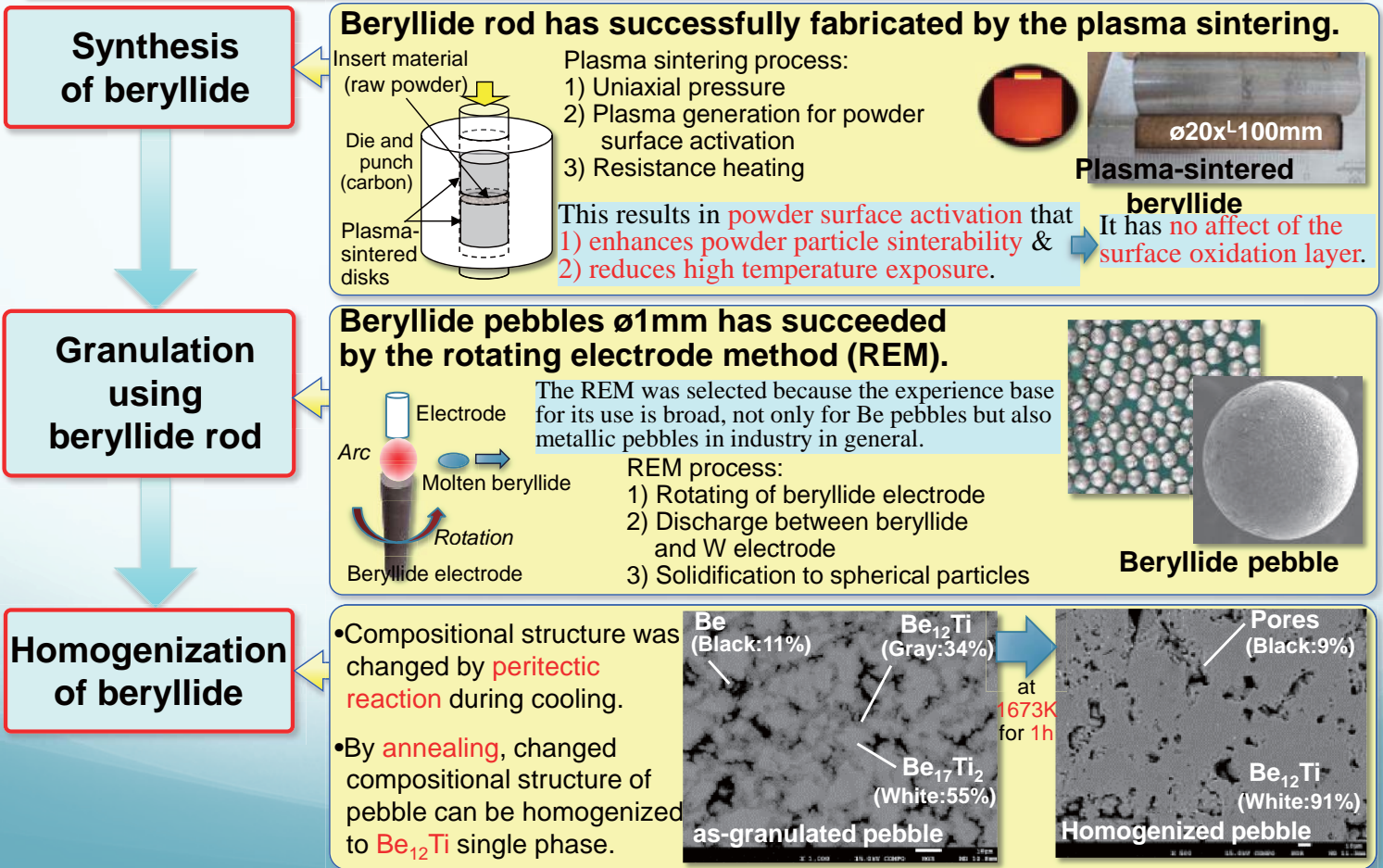
- Swelling and
- Hydrogen generation with vapor



Beryllide has a good potential for high temperature use.

Synthesis and Granulation of Beryllides

Novel granulation flow scheme of Be₁₂Ti beryllide



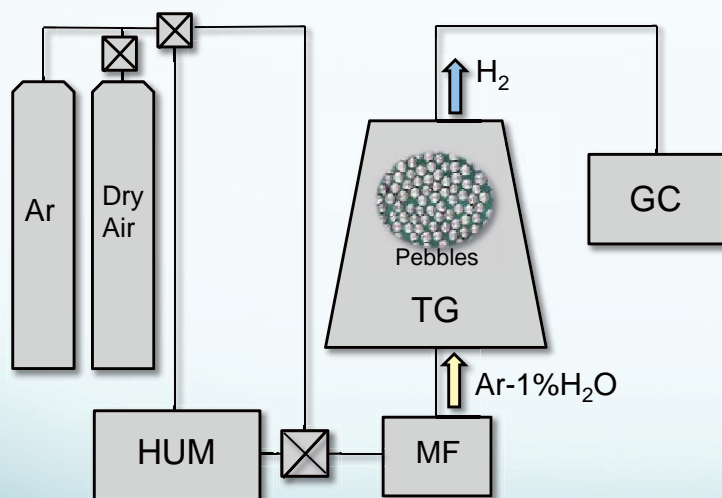
Characterization of Be-Ti Beryllides

- H₂ generation reaction with water vapor -

Reactivity experiment with water vapor

Reactivities of beryllides pebbles with 1% H₂O was examined using a thermo-gravimetric apparatus connected with a gas chromatography.

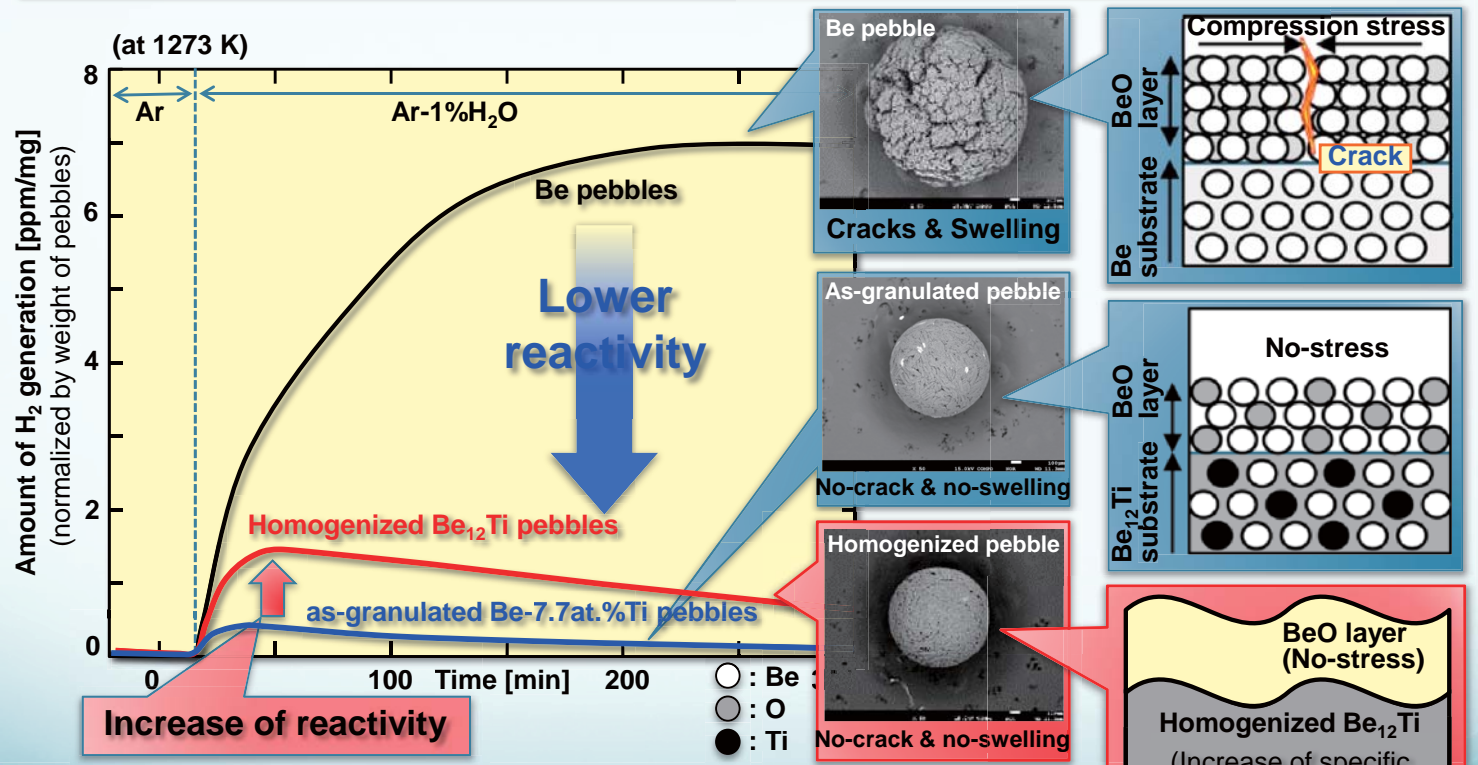
Schematic flow diagram of test apparatus



TG : Thermal-Gravimetric equipment
 GC : Gas Chromatographic equipment
 HUM: Water vapor generation equipment
 MF : Mass flow controller

Conditions

- Apparatus :
 - TG : TG-8110, Rigaku, Japan.
 - GC : CP-4900, Agilent, USA.
 - HUM : HUM-1E, Rigaku, Japan.
- Heating rate : 10 K/min
- Atmosphere : Ar with 10,000ppm H₂O
- Temperature: 1273 K
 (Ar gas flow during temperature ramping)



- Beryllides pebbles indicated the lower reactivity than Be pebbles.
- Be swelled up and exhibited many cracks, because compressive stress induces cracks.
- BeO was deposited to the beryllide surface with no crack and no swelling, because stress-free BeO can be formed.
- Homogenized Be₁₂Ti pebbles demonstrated increased reactivity relative to as-granulated pebbles.
- It was clarified that increased reactivity was caused by increased specific surface area of homogenized Be₁₂Ti pebbles.

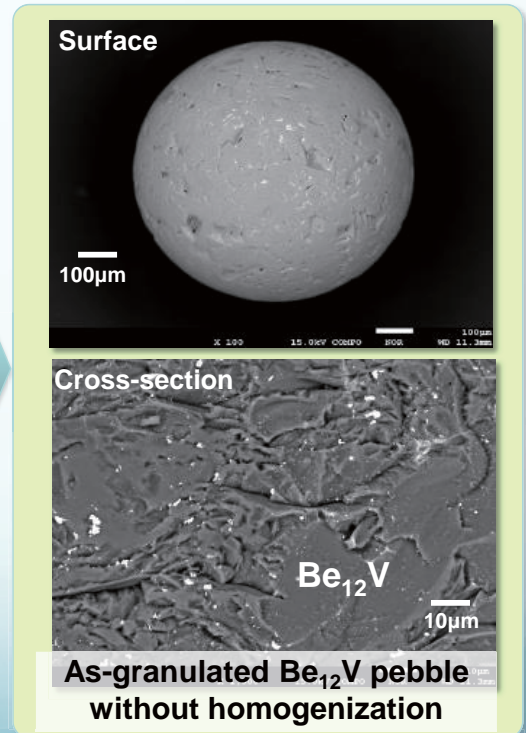
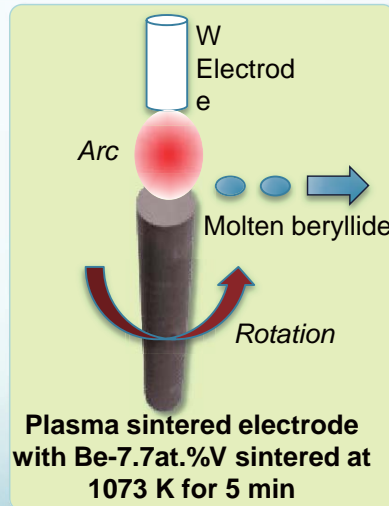
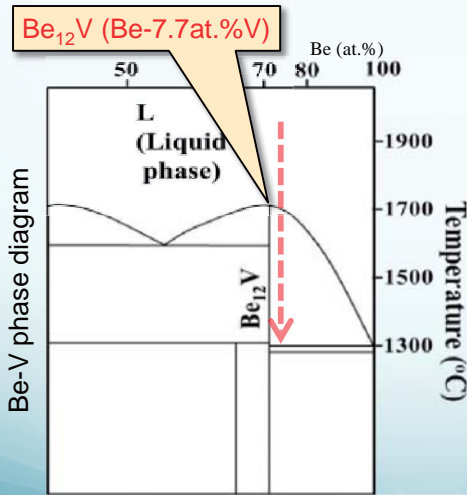
Other Beryllides Granulation without homogenization treatment

New granulation of single phase pebble without homogenization ⁹

- Be_{12}Ti pebble has a porous body by the homogenization treatment.
- To prevent increase of H_2 generation associated with increase of the specific surface area, other compositions of beryllides have been surveyed.

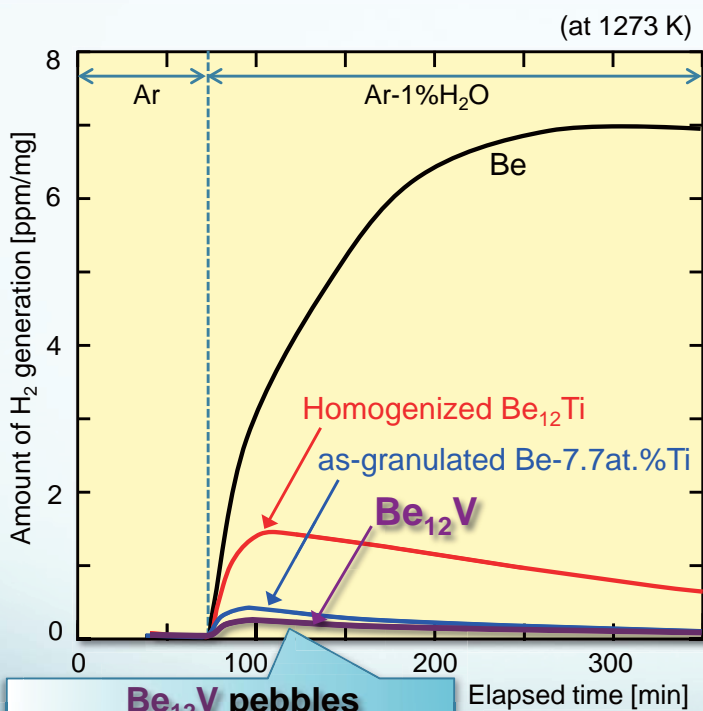
Be_{12}V composition was selected,

- No peritectic reaction,
- similar nuclear property to Be-Ti beryllide

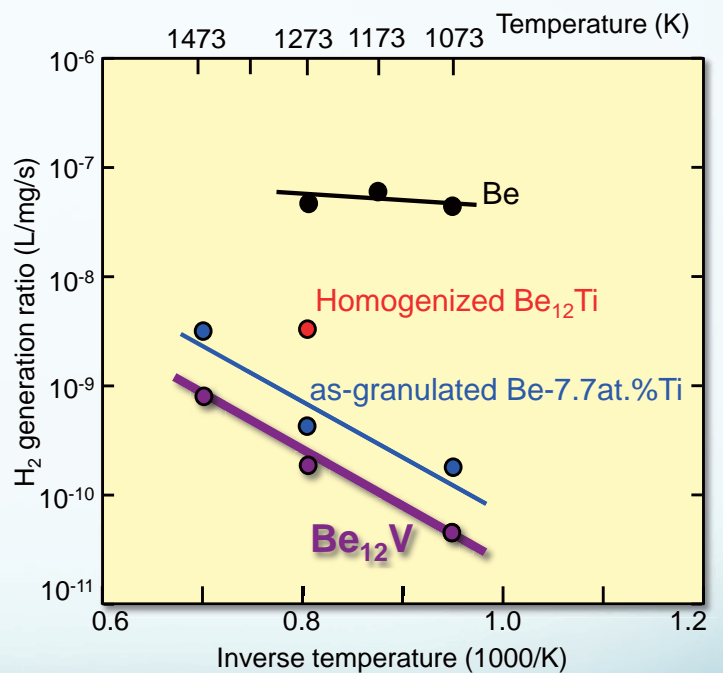


Be_{12}V single phase pebbles were successfully fabricated directly by the REM.

Reactivity with water vapor of Be_{12}V pebbles ¹⁰



Be_{12}V pebbles
Good results of reactivity



- Be_{12}V single phase pebbles demonstrated a lower reactivity than Be pebbles.
- H_2 generation ratio of Be_{12}V is two orders of magnitude less than that of Be.

Characterization of Beryllides

- Deuterium retention property -

Experimental procedure

Thermal desorption spectroscopy (TDS) in Shimane University was applied to understand fundamental aspects of the behavior of hydrogen isotopes in Beryllides.



◆ Sample from QST

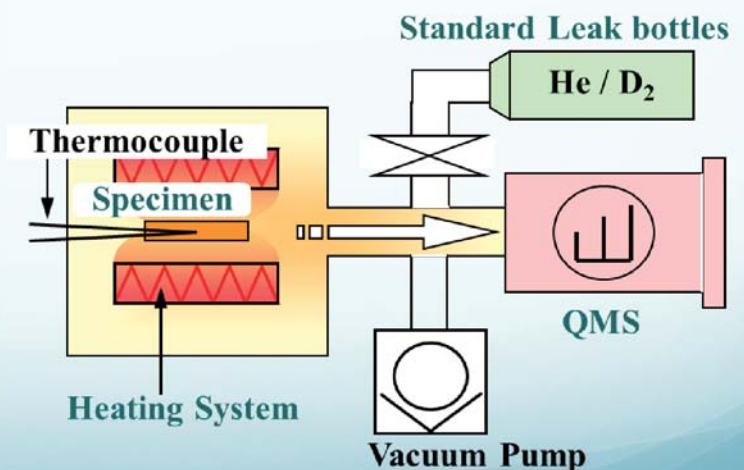
- Be pebbles
- Homogenized Be_{12}Ti pebbles
- As-granulated Be_{12}V pebbles

◆ Ion Irradiation

- Ion : 3 keV- D_2^+
- Irra. Temp. : R.T.
- Flux : $\sim 2 \times 10^{18}$ ions/ m^2/s
- Fluence : $\sim 1 \times 10^{20-23}$ ions/ m^2

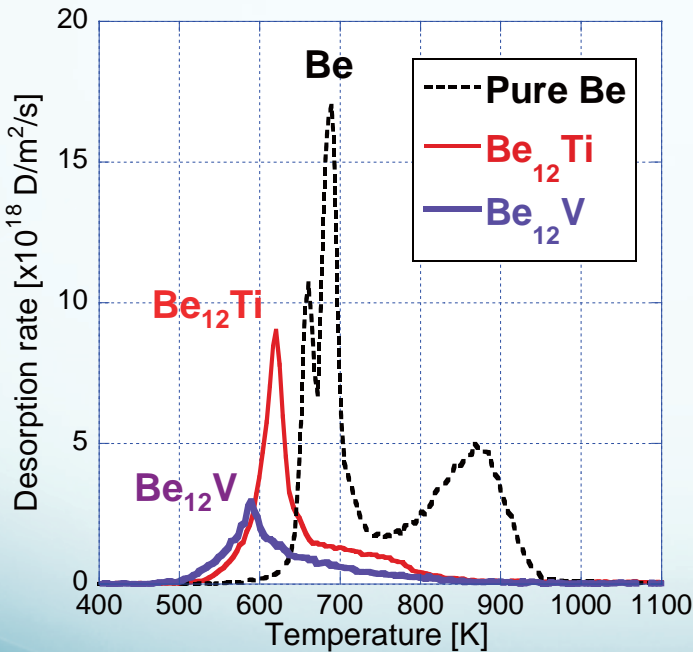
◆ TDS

- Temp. : R.T.~1273 K
- Rate : 1 K/s
- Mea.Mass : D_2 (m/e=4), DH (m/e=3)



Deuterium desorption spectra

● 3keV-D₂⁺, 1x10²² D/m², R.T.



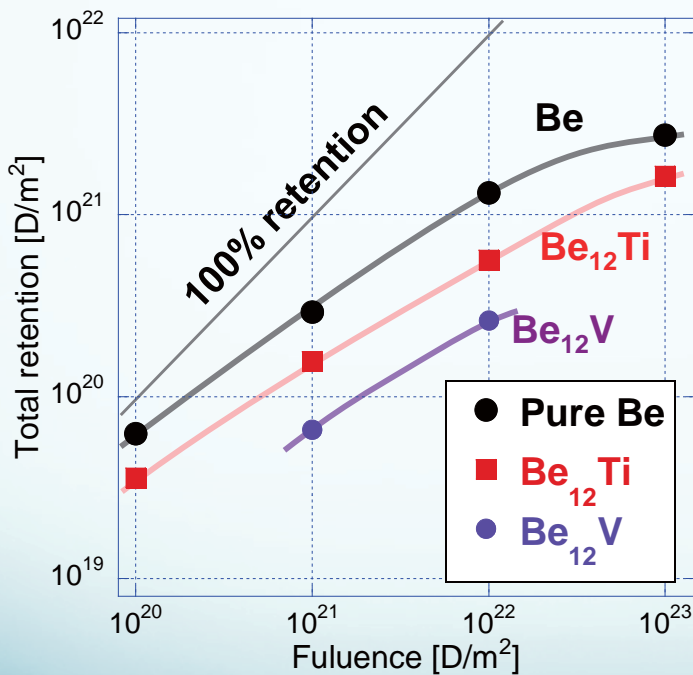
- While clear multiple desorption peaks occurred at high temperatures region above 650 K for pure Be, it was found for the Be₁₂Ti and Be₁₂V samples that **only a smaller peak at lower temperature** appeared with a tail extended to higher temperatures.
- As-granulated Be₁₂V pebbles shows a smaller single desorption peak at much lower temperature less than 600 K.



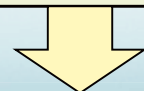
These indicate that beryllides have **rather less deuterium trapping efficiency.**

Total deuterium retention

● 3keV-D₂⁺, R.T.



- A difference in deuterium retention was observed between the pure Be pebble, the homogenized Be₁₂Ti pebbles and the as-granulated Be₁₂V pebbles.
- Beryllides such as Be₁₂Ti and Be₁₂V demonstrated a lower deuterium retention than pure Be pebbles.
- The as-granulated Be₁₂V pebbles has the least deuterium trapping efficiency in those pebbles.



Due to the small desorption from beryllides, the total deuterium retentions in beryllides were evaluated to be **~50% in Be₁₂Ti** and **~20% in Be₁₂V** of that in pure Be.

Be₁₃Zr R&D

- for increase of TBR -

Applicability of other beryllides except Be-Ti & -V beryllides

- Beryllide disturbs the tritium breeding by the metal in Be.
- From the viewpoint of the nuclear characteristics, other candidate beryllides prioritized except Ti&V.

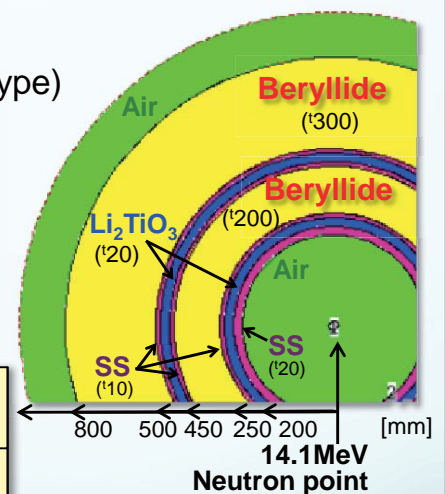
Tritium production rate (TPR) calculation

Geometry : Very simple shell model (stainless steel covered type)
 Code : Monte-calro simulation (MCNP-5)
 Nuclear data : FENDL-2.1 and JENDL-Dos. 99
 Calculation : Tritium production rate (TPR)
 [Dimension: Tritium/atom/source neutron (x10⁻²⁴)]

TPR reduction ratio compared with Be

	Be	Be ₁₃ Zr	Be ₁₂ Cr	Be ₁₂ V	Be ₁₂ Ti	Be ₁₂ Nb	Be ₂₂ Mo	Be ₂₂ W
Ratio*	1.0	0.86	0.73	0.68	0.65	0.65	0.64	0.22

*) Ratio = TPR(Beryllides) / TPR(Be)



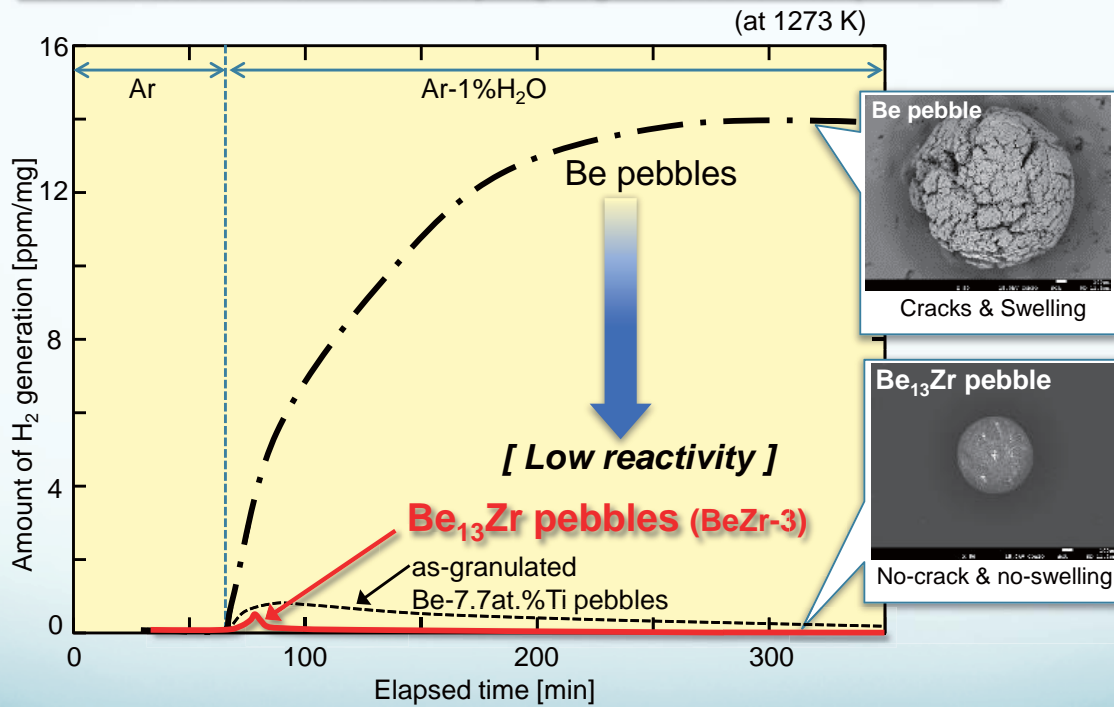
- Zr in Be is not so effective to the TPR reduction.
- Be₁₃Zr was selected because Be₁₃Zr not only has low neutron absorption property, but also has no peritectic reaction during granulation.

Granulation of Be-Zr pebble has been successfully fabricated.

Reactivity with water vapor of Be₁₃Zr pebbles

17

Be₁₃Zr pebbles with gray surface using BeZr-3 electrode were selected, and were used for evaluation of hydrogen generation reactivity.



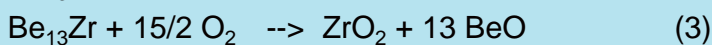
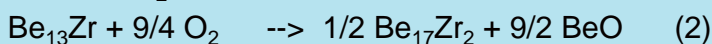
- Be₁₃Zr pebbles have oxidation property not only better than Be but also similar to the as-granulated Be-7.7 at.% Ti.
- BeO was deposited over the entire surface of the Be₁₃Zr pebble, and no cracking and no swelling was observed.
- Stable BeO layer covered on the surface of Be₁₃Zr pebble acts to improve the oxidation reactivity.

Mechanism of “Pest” phenomenon and action on issue

18

It is supposed that the “pest” reaction occurs in Be₁₃Zr by volumetric expansion caused by the formation of oxides, particularly BeO.

Oxidation reactions of BeO are shown as follows.

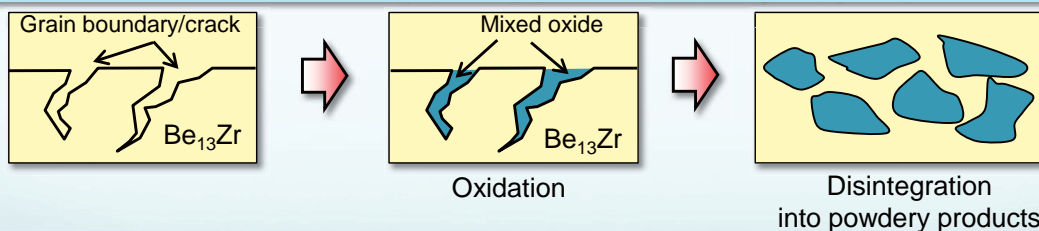


The oxidation as reaction formula of (1) has relatively less impact on the pest phenomenon, because it occurs on the surface of sample.

The oxidation reaction of Be₁₃Zr to form Be₁₇Zr₂ and BeO occurs as early reaction.

Then, the oxidation reaction of Be₁₃Zr to form ZrO₂ and BeO occurs after sufficient oxidation.

It is assumed that oxidation reactions as (2) and (3) influence mainly the pest phenomenon.



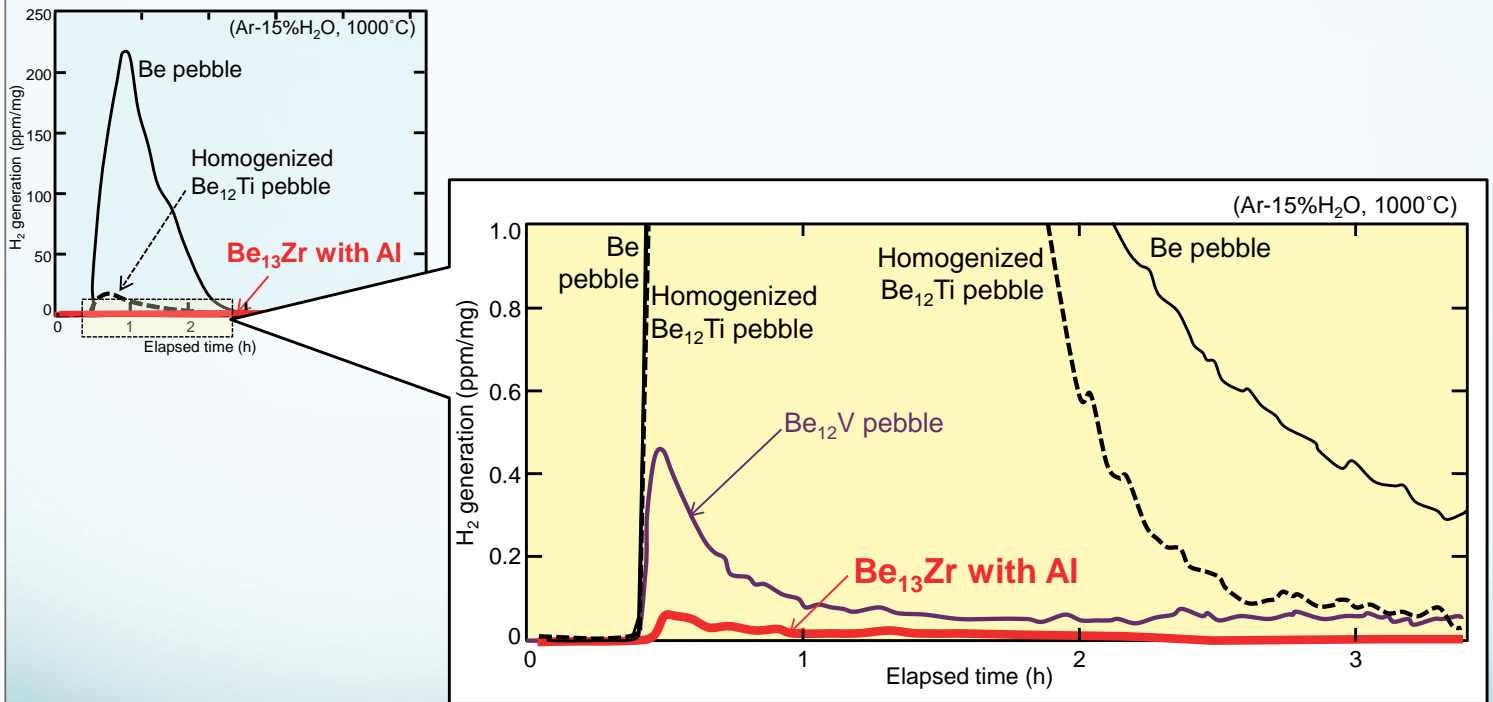
Action on Pest issue

Action #1: Pre-oxidation on the surface of Be₁₃Zr for forming protection layer by the annealing at 1000°C for 5h under He-100ppmO₂



- Pest reaction occurred in the case of surface modified Be₁₃Zr by the oxidation treatment.
- Surface oxidation layer is insufficient for prevention of pest reaction.

H₂ generation reaction with water vapor of Ar-15%H₂O at 1000 °C ¹⁹



Be₁₃Zr with Al showed the best performance of oxidization resistant with water vapor of Ar-15%H₂O at 1000 °C compared of other beryllides.

20

Summary

- Prototypic pebbles of beryllides were successfully fabricated by the rotating electrode granulation method using the plasma-sintered electrodes.
- Beryllide of **Be₁₃Zr** composition has good potential as advanced neutron multiplier, but it is one of intermetallic with “**Pest**” phenomenon that is disintegration of polycrystalline sample caused by oxidation.
- From the result of optimization study, **Be₁₃Zr without pest reaction** was successful in developing by **addition of Al**.
- The pest reaction was prevented by reduction of stress of oxidation reaction caused by dispersion of Al in grain boundary of Be₁₃Zr.
- Be₁₃Zr with Al showed the best performance of oxidization resistance with water vapor of Ar-15%H₂O at 1000 °C compared of other beryllides.

2.4.2 Distribution of Beryllium Pebble Size by Rotation Electrode Process

R. FUKATSU and K. NOJIRI

*NGK Insulators Ltd, 1 Maegata-cho, Handa, Aichi, 475-0825, Japan
E-mail: rfukatsu@ngk.co.jp*

Beryllium metal is used in various industrial and R&D scenes due to its unique and extremely excellent properties. One of these properties is a nuclear property. When a neutron collide the beryllium, ($n, 2n$) neutron reaction is caused. Therefore beryllium releases more neutrons than it absorbs.

Beryllium is candidate as neutron multiplier in ITER. Beryllium neutron multiplier will be used in form of pebble, small sphere of high quality. “BP-1” beryllium pebble is the reference material for the multiplier in ITER project (Fig. 1). The specification of “BP-1” shall contain a minimum beryllium content of 99.0 %. And it should be a sphere made by Rotation Electrode Process (REP) with diameter of 0.8–1.2 mm. REP is a method to produce metal sphere. High voltage electric power is charged between a rotating beryllium electrode and a tungsten electrode. The rotating beryllium electrode ejects beryllium droplets by centrifugal force. The beryllium melt drops form sphere shape before solidification. The schematic is shown in Fig.2.

Previously, the fundamental test to produce the beryllium pebble and to collect the several process data is carried out. As the 1st plasma in ITER is close, it's now to start considering the mass production. To determine the mass production conditions further investigation was carried out.

Specifically, the relationships between the process condition (e.g. the rotation speed of beryllium rods or electrode current between rods) and the size distribution of beryllium pebble have been investigated by using the apparatus which can keep the distance between the electrodes constant (KREP-1500). That detail will be presented in this workshop.

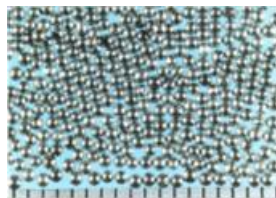


Figure 1 : BP-1 Pebble

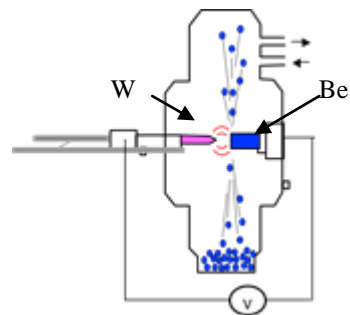


Figure 2 : Schematic of REP

21 September 2017, Narita, Japan

Distribution of Beryllium Pebble Size by Rotation Electrode Process

Ryohei Fukatsu, Keigo Nojiri

NGK Insulators, Ltd
Aichi Japan

Outline

1. Introduction
2. NGK's Product BP-1
3. Rotation Electrode Process
4. Previous Research
5. Experiments & Results
6. Future Plan

Beryllium has Favorable Properties!

- Low Density & High Young's Modulus
- Unique Nuclear Properties

X-ray window **Mirror** **Reflector** **Be 1st wall**

Speaker **Multiplier**

(n, 2n) neutron reaction

$$n + {}^9\text{Be} \rightarrow 2n + 2\text{}^4\text{He}$$

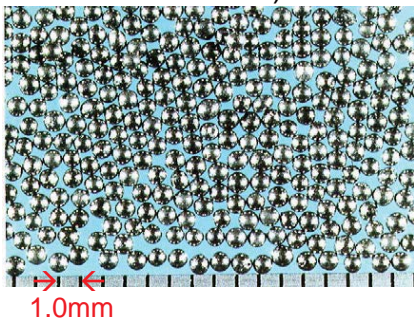
Nuclear Fusion Test Reactor (ITER)

NGK's Product BP-1

Fundamental Test Started to review manufacturing conditions.

NGK's Neutron Multiplier

(Product Name : BP-1)

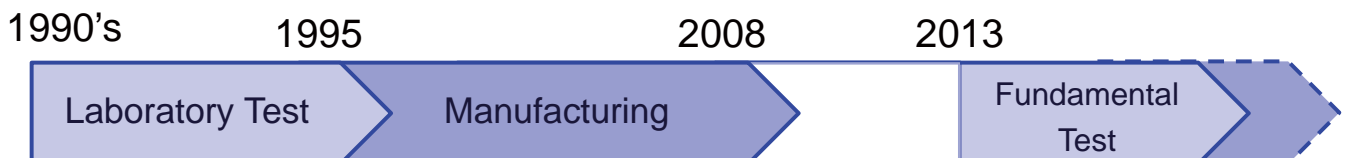


Specification

Form : Spherical balls, ϕ 0.8-1.2 mm

Method : Rotation Electrode Process \Rightarrow P 5

History of Research & Production



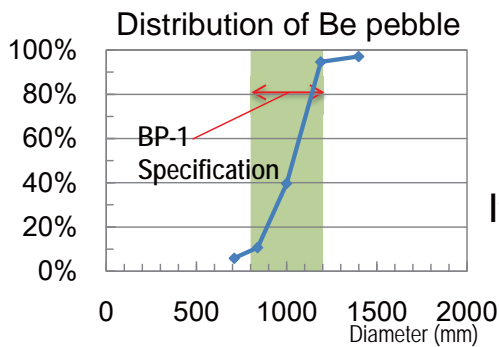
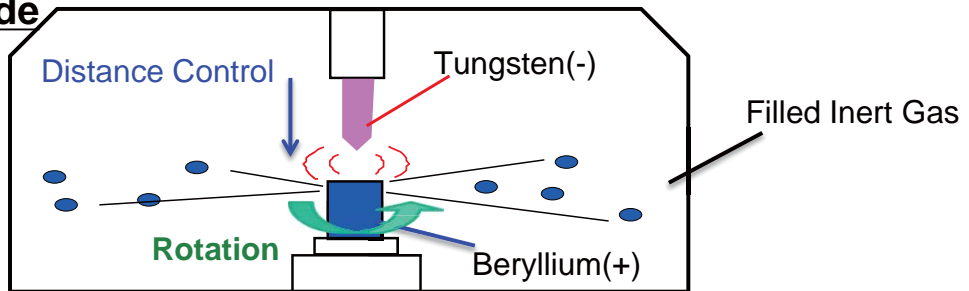
Rotation Electrode Process



It must be Possible to raise the yield rate more than before.

Rotation Electrode Process (REP)

[Schematic]



Out of Specification 16%!

It should be able to produce more efficiently.

Previous Research



Out of Specification : 8%.

The Best Result was Obtained Only Once.

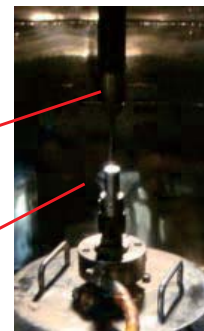
Experiments

Automatic Control of Distance between Tungsten and Beryllium

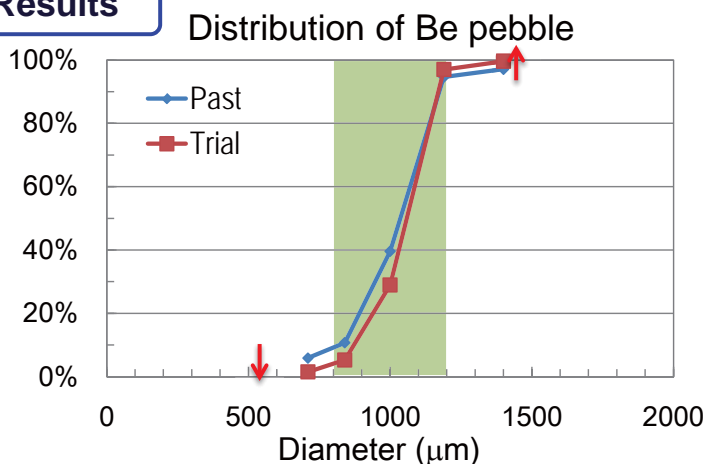
[Fig. in Chamber]

Tungsten(-)

Beryllium(+)
φ 15



Results



Pebble Size	Past	Trial
- 800 μm	10.7 %	5.3 %
800 - 1000 μm	28.9 %	23.6 %
1000 - 1200 μm	55.0 %	68.1 %
1200 μm -	5.4 %	2.6 %

Other Factors beside v & A are Important.

Experiments

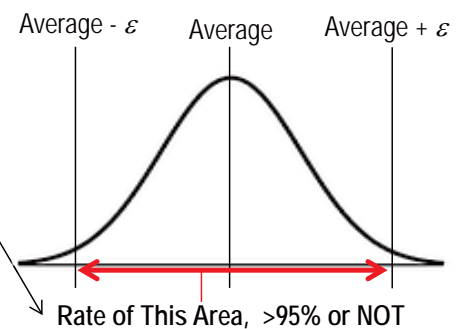
- Change the Experiment Conditions
(the Experiment Conditions = the Rotation Speed of Beryllium (v), and the Electrodes Current (A))
- Investigate the Relationship by the Experimental Design Method
(the Relationship = Distribution of Beryllium Pebble Size vs. v & A)

Result

Variance Analysis Table

Confidence Coefficient = 95%

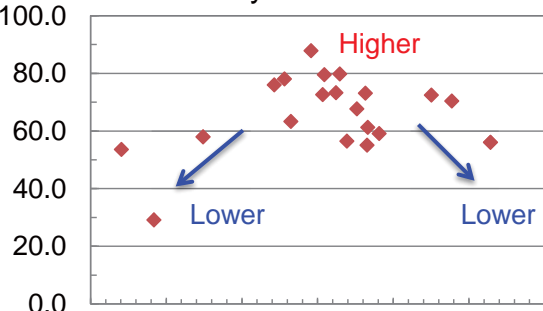
	n	Variance	F_0		F	Significant
v	4	377.00	3.43	<	4.1	NOT
A	2	80.55	0.73	<	5.3	NOT
$v \times A$	4	138.19	1.25	<	4.1	NOT
Error	8	109.74				
SUM	16					



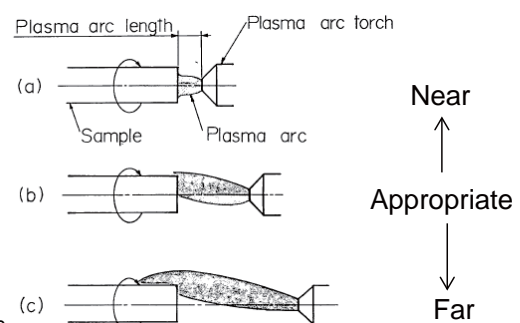
Electrode Distance is One of the Important Factors. Because Electrode Distance influences the State of arc.

Electrode Distance was particularly related to the Pass ratio.

(%) Pass Ratio of Beryllium Pebble's Diameter



Near ← Electrode Distance → Far



Conclusion

Appropriate the Electrode Distance increases Pass Ratio.

- Arc is Stabilized
- Beryllium rod melts uniformly

1) Isonoshi, K. 1990. Iron and Steel. Japan

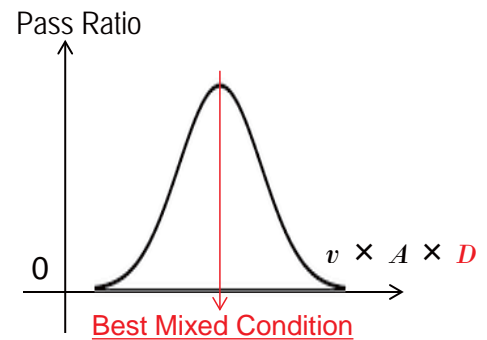
The Best Mixed Condition will be searched out.

Next Step

Considering Factors

- the Rotation Speed of Beryllium rod (v)
- the Electrodes Current (A)
- Electrode Distance (D)

Target : the Stable Pass Ratio over 90%



Future Step

The way of High Productivity

- the Diameter of Beryllium Rod : $\phi 15\text{mm}$ \rightarrow More Over
- the Continuous Manufacturing

Thank you for your attention

2.4.3 Trial fabrication and characterization of Be₁₂V pebbles

P. Kurinskiy^{*}, J.-H. Kim^{*}, M. Nakamichi

^{} National Institutes for Quantum and Radiological Science and Technology, Aomori, Japan*

Vanadium beryllide Be₁₂V belongs to one of the attractive materials from the point of view of its potential use as a neutron multiplier [1,2].

Several charges of vanadium beryllide pebbles were fabricated using rotating electrode method (REM) at QST, Japan. Be-V rods produced by combination of methods of plasma sintering and uniaxial hot pressing were used as targets to be melted by tungsten electrode in the chamber of REM apparatus under inert gas atmosphere.

In the present work, fabrication-related issues (e.g., yield) as well as microstructural characteristics of both, Be-V rods and pebbles, were investigated. It was shown that produced Be₁₂V pebbles have dense structure without big internal porosity and regular spherical shapes.

References

- [1] M. Nakamichi, J.-H. Kim, Development of beryllide pebbles with low-hydrogen generation as advanced neutron multipliers, Fusion Engineering and Design, In Press
- [2] M. Nakamichi, J.-H. Kim, Prevention of hydrogen generation reaction with water vapor by surface modification of beryllides as advanced neutron multipliers, Fusion Engineering and Design, In Press

Trial fabrication and characterization of Be₁₂V pebbles

Petr Kurinskiy^{1*}, Jae-Hwan Kim¹, Masaru Nakamichi¹

¹ QST, Fusion Energy Research & Development Directorate, Rokkasho Fusion Institute

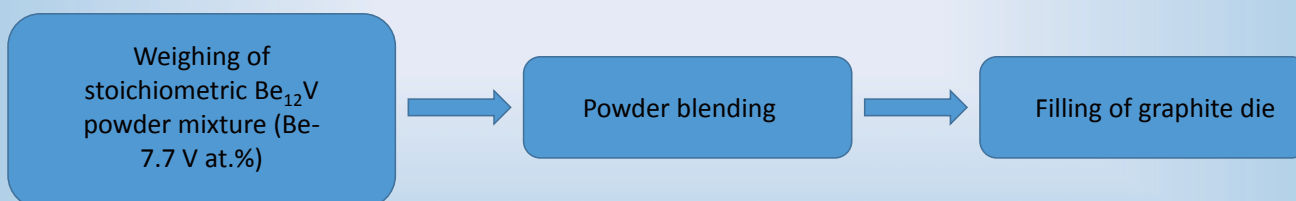
Introduction

- Vanadium beryllide Be₁₂V is one of the most promising materials to be used as neutron multiplier in breeder blankets
 - Good resistance to corrosion
 - Relatively high melting point
 - Smaller rates of hydrogen generation after chemical reaction with water vapour
- Rotating electrode method (REM) was used to fabricate single-phase Be₁₂V pebbles

Fabrication of Be-V rods

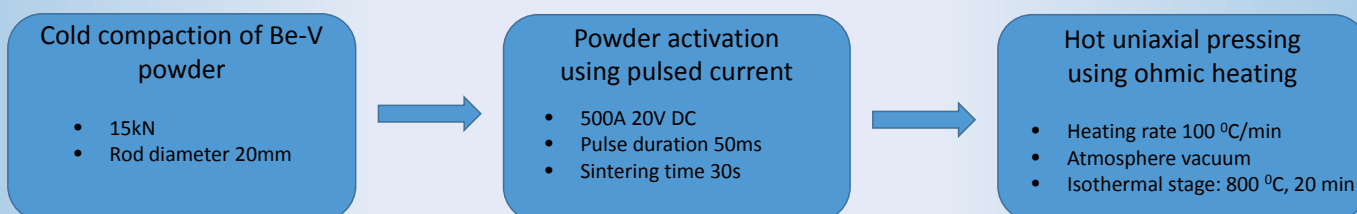
- Raw materials
 - <45 μm Be powder
 - <45 μm V powder

- Preparation



Fabrication of Be-V rods

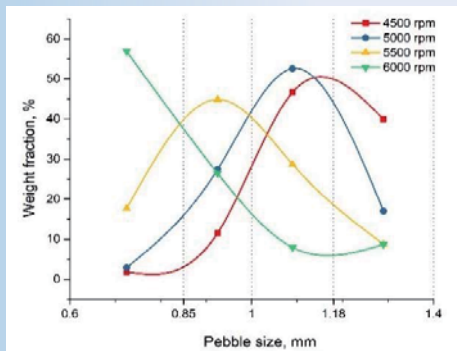
- Hot uniaxial pressing with preliminary SPS operation



Characterisation of Be-V pebbles

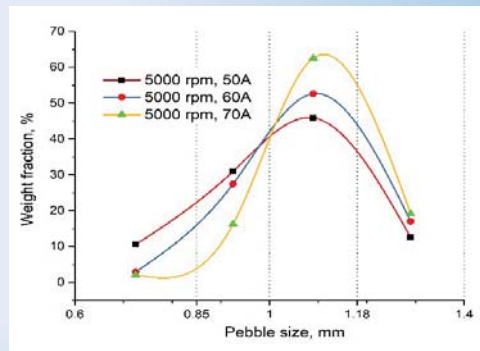
➤ Yield properties

Granulation using 60 A current



Granulation condition	4500 rpm	5000 rpm	5500 rpm	6000 rpm
Fraction weight, %	58.25	80.08	73.59	34.4

Granulation using 5000 rpm by rotation of Be-V rod



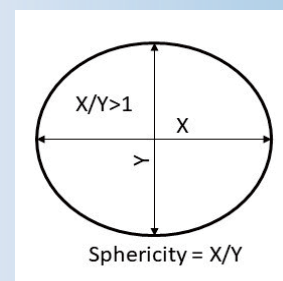
Granulation condition	50 A	60 A	70 A
Fraction weight, %	76.89	80.08	78.76

Characterisation of Be-V pebbles

➤ Sphericity

Granulation conditions	4500rpm 60A				5000rpm 60A				5500rpm 60A			
	0.6-0.85	0.85-1.0	1.0-1.18	1.18-1.40	0.6-0.85	0.85-1.0	1.0-1.18	1.18-1.40	0.6-0.85	0.85-1.0	1.0-1.18	1.18-1.40
Sphericity of pebbles	1.065	1.071	1.067	1.060	1.050	1.057	1.069	1.113	1.095	1.070	1.080	1.223

Granulation conditions	6000rpm 60A				5000rpm 50A				5000rpm 70A			
	0.6-0.85	0.85-1.0	1.0-1.18	1.18-1.40	0.6-0.85	0.85-1.0	1.0-1.18	1.18-1.40	0.6-0.85	0.85-1.0	1.0-1.18	1.18-1.40
Sphericity of pebbles	1.069	1.388	1.097	1.364	1.115	1.071	1.066	1.260	1.055	1.051	1.059	1.161



Summary

- ❖ It was demonstrated that Be_{12}V pebbles can be produced out of Be-V melt using Rotating Electrode Method
- ❖ Due to an absence of peritectic reactions, single-phase dense Be_{12}V pebbles rapidly solidify from multiphase Be-V electrode with chemical composition of Be-7.7 at.% avoiding precipitation of other intermetallic phases
- ❖ Excepting granulation conditions corresponding to 60 A, 4500 rpm and 60 A, 6000 rpm the yield of 0.85-1.18 mm size fraction exceeds 70% of the pebbles' total weight
- ❖ It was shown that beryllium vanadium Be_{12}V pebbles sizing 0.85-1.18 mm fabricated using different granulation parameters have very closed values of sphericity

2.5 Technical session 2: Characterizations

2.5.1 Experimental Study of Oxidation of Beryllium Pebbles in Air and Steam

R. Rolli¹, V. Chakin², P. Vladimirov², and P. Kurinskiy³

¹*Institute for Applied Materials - Materials and Biomechanics, Karlsruhe Institute of Technology, Hermann-von-Helmholtz-Platz 1, 76344 Eggenstein-Leopoldshafen, Germany*

²*Institute for Applied Materials - Applied Materials Physics, Karlsruhe Institute of Technology, Hermann-von-Helmholtz-Platz 1, 76344 Eggenstein-Leopoldshafen, Germany*

³*Fusion Energy Research & Development Directorate, Rokkasho Fusion Institute, Department of Blanket Systems Research, Breeding Functional Materials Development Group, National Institutes for Quantum and Radiological Science and Technology, QST, 2-166 Omotedate, Obuchi, Rokkasho, Aomori, 039-3212 JAPAN.*
E-mail: rolf.rolli@kit.edu

Chemical reactivity in air and steam remains a major safety concern associated with the use of beryllium pebbles as neutron multiplier in the European Helium-Cooled Pebble Bed (HCPB) blanket of fusion reactors. Different possible accidental scenarios involve the exothermal reactions between beryllium and air or steam at elevated temperatures. The purpose of this study is to provide additional data for the 1 mm beryllium pebbles produced by rotating electrode method (REM) which are the current reference material for the ITER Testing Blanket Module (TBM).

Two kinds (Lots) of 1 mm beryllium pebbles were used in the study differing by porosity values. In particular, Lot 1843 has a higher porosity than Lot 1473. Thermal analyzer Netzsch STA 449 F3 Jupiter supplied with the water vapor generator and appropriate oven (operating range: RT...1250 °C) was used for the experimental study of reactivity of 1 mm beryllium pebbles in water steam and a separate oven system (operating range: RT...1600°C) for the measurements in synthetic air. The mass increase of the pebbles was a parameter measured.

Isothermal heat treatment in air with the duration of 6 h was used in the temperature range of 700-1100 °C for Lot 1473 and 700-1050 °C for Lot 1843. Using a fitting, the constants of oxidation were calculated, resulting that the oxide layer remains playing a protective role for all testing temperatures for Lot 1473. For Lot 1843, having more developed porosity compared to Lot 1473, the oxide layer stops to be protective since the temperature of 1000 °C. Isothermal heat treatment in steam with the duration of 6 h was used in the temperature range 600-800 °C for both Lots of beryllium pebbles. The beryllium pebbles from Lot 1843 were characterized by higher mass increase (compared to Lot 1473) at all temperatures investigated. The more developed open porosity (or, accordingly, a more specific surface value) in the pebbles of Lot 1843 can be the main reason for the comparatively higher oxidation rate in steam.

Experimental Study on Oxidation of Beryllium Pebbles in Air and Steam

R. Rolli¹, V. Chakin², P. Vladimirov², H.-C. Schneider¹ and P. Kurinskiy³

¹*Institute for Applied Materials - Materials and Biomechanics, Karlsruhe Institute of Technology, Hermann-von-Helmholtz-Platz 1, 76344 Eggenstein-Leopoldshafen, Germany*

²*Institute for Applied Materials - Applied Materials Physics, Karlsruhe Institute of Technology, Hermann-von-Helmholtz-Platz 1, 76344 Eggenstein-Leopoldshafen, Germany*

³*Fusion Energy Research & Development Directorate, Rokkasho Fusion Institute, Department of Blanket Systems Research, Breeding Functional Materials Development Group, National Institutes for Quantum and Radiological Science and Technology, QST, 2-166 Omotedate, Obuchi, Rokkasho, Aomori,*

Abstract

Chemical reactivity in air and steam remains a major safety concern associated with the use of beryllium pebbles as neutron multiplier in the European Helium-Cooled Pebble Bed (HCPB) blanket of fusion reactors. This study provides additional data for the 1 mm beryllium pebbles produced by rotating electrode method (REM) which are the current reference material for the ITER Testing Blanket Module (TBM). The values of the experiments by air oxidation demonstrate that the oxide layers play a protective role dependent on temperature and open pores. The oxidation tests with steam shows a rapidly increasing of the reaction dependent on temperature and comes to a destruction of the pebble structure by increasing of temperature.

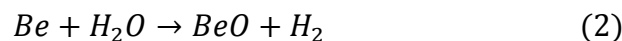
1. Introduction

Different possible accidental scenarios (LOVA loss of vacuum accidental, LOCA loss of cooling accidental, LOFA loss of fuel accidental) involve the exothermal reactions between beryllium and air or steam at elevated temperatures. Thermogravimetric (TG) analysis was used to study mass change of beryllium samples by isothermal high-temperature treatment in gas and water steam atmosphere.

The reaction of beryllium with air is described by the following equation



Pure beryllium reacts with water steam exothermally:



These reactions are accompanied by a mass increase due to a growth of beryllium oxide films.

2. Experimental

Two kinds (lots) of 1 mm beryllium pebbles were used in the study differing by porosity values. In particular, Lot 1843 has a higher porosity than Lot 1473. Thermal analyzer Netzsch STA 449 F3 Jupiter supplied with a water vapor generator and appropriate oven (operating range: RT...1250 °C) was used for the experimental study of reactivity of 1 mm beryllium

pebbles in water steam. A separate oven system (operating range: RT ... 1600 °C) served for the measurements in synthetic air.

Heating and cooling rates used during TG analysis were equal to 10 and 25 °C/min, accordingly. Argon with the flow rate of 25 (air) / 20(vapor) ml/min was utilized as protective gas in order to prevent interaction of high-sensitive balance with the corrosive atmosphere.

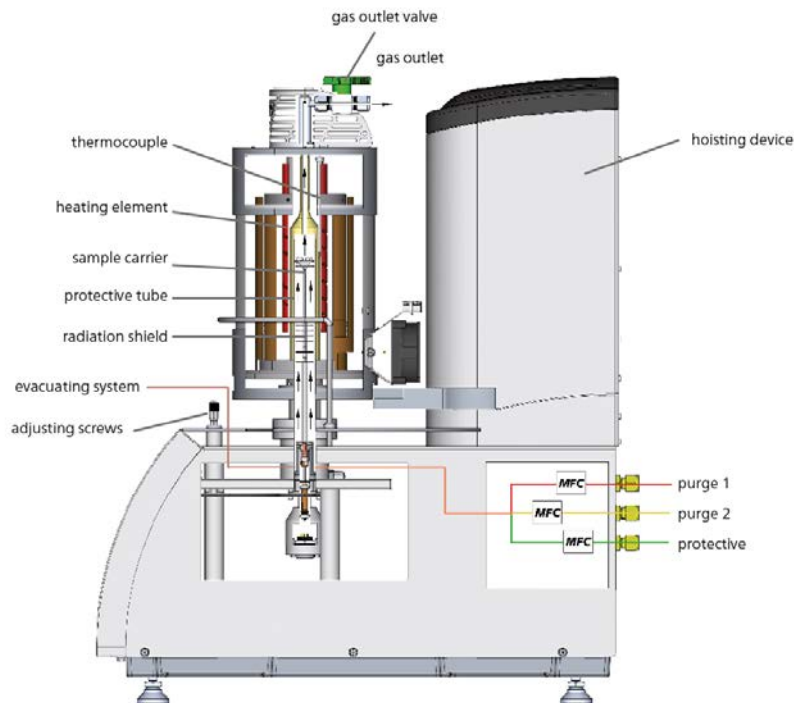


Fig. 1.1: Schematic view of the SiC furnace supplied with the high-precision balance [manufacturer]

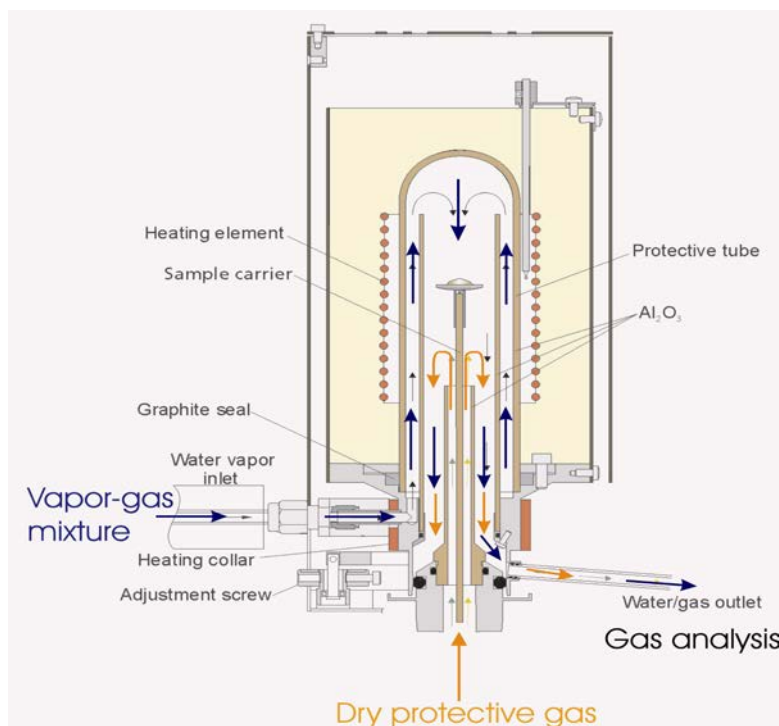


Fig. 1.2: Schematic view of the water vapor furnace [manufacturer]

Isothermal heat treatment with the duration of 6 h was used in the temperature range of 700 – 1100 °C for Lot 1473 and 700 – 1050 °C for Lot 1843 of 1 mm beryllium pebbles. Table 1.1

shows temperatures used for these oxidation tests in air, table 1.2 for the oxidation tests in steam.

It should be emphasized that the flow of protective gas was opened during the whole experiment, including the phases of heating and cooling, while the flow of reactive gas (synthetic air or nitrogen vapor mixture) was opened after achieving testing temperature and closed right after finishing of the isothermal phase of each experiment.

Table 1.1: Thermal conditions of TG analysis of beryllium pebbles in air

Lot	Testing temperature, °C
1473	700, 800, 930, 950, 1000, 1050, 1100
1843	700, 800, 900, 930, 950, 1000, 1050

Table 1.2: Thermal conditions of TG analysis of beryllium pebbles in steam

Lot	Testing temperature, °C
1473	600, 620, 650, 680, 700, 720, 750
1843	600, 620, 680, 700, 720, 750, 800

Synthetic air was used as reactive corrosive gas while performing the experimental measurements with air. The flow rate of synthetic air during the experiment was 100 ml/min. Mixture of water steam with nitrogen was used as reactive corrosive gas while performing the experiments in steam. In this case, nitrogen played a role of a carrier gas that assisted the introduction of water vapor into reactive chamber at 1.5 bar pressure (flow rate 10 ml/min). The water vapor flow rates used in the experimental campaign were 48 ml/min of water steam, corresponding to 1.5 g/h of steam generated at 150 °C.

Beryllium pebbles of 150 up to 179 mg of mass were used for the tests. During the thermogravimetric measurements, the pebbles were kept in a shallow crucible made of alumina Al_2O_3 with a coating of Y_2O_3 .

3. Experimental results

Fig. 3.1 shows one result on TG analysis for beryllium pebbles from Lot 1473 as an example for fitted using equation 3 [1]:

$$\Delta m = At^B \quad (3),$$

where Δm is the mass increase, t is the duration of the test, A , B – constants.

Table 3.1 shows the constants A and B obtained after fitting all curves. In the case of Lot 1473 tested at 1100 °C, a linear dependency of the mass increase versus time occurs.

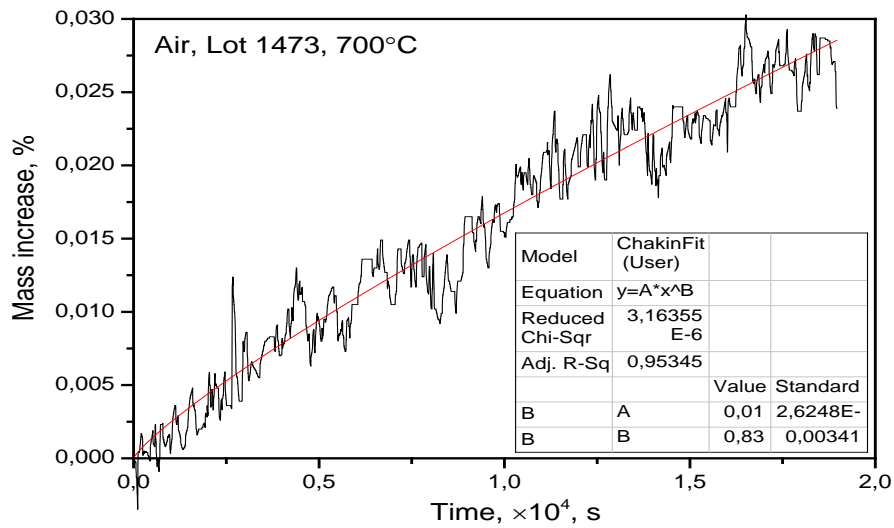


Fig. 3.1: TG curve with fitted curve from LOT 1473, 700 °C in air

Table 3.1: Constants *A* and *B* after fitting of the TG curves (in air) according to the equation (3)

Lot	Constants <i>A</i> / <i>B</i>							
	Testing temperature [°C]							
	700	800	900	930	950	1000	1050	1100
1473	0.01676/ 0.83201	0.02586/ 0.8058	-	0.10465/ 0.64982	0.06439/ 0.65106	0.15787/ 0.74323	0.25857/ 0.63836	0.134/ 1
1843	0.01256/ 1.22204	0.03446/ 0.83948	0.08419/ 0.72959	0.08098/ 0.80584	0.13277/ 0.65683	0.29536/ 2.25547	1.70993/ 1.03747	-

Table 3.2: Constants *A* and *B* after fitting of the TG curves (in steam) according to the equation (3)

Lot	Constants <i>A</i> / <i>B</i>							
	Testing temperature [°C]							
	600	620	650	680	700	720	750	800
1473	0.00612/ 6.23947	0.01936/ 0.83546	0.12386/ 0.78802	0.6216/ 1.11171	0.32725/ 1.32862	1.87763/ 1.43082	6.51227/ 1.88015	-
1843	0.00872/ 3.49319	0.47296/ 0.31974	-	0.82772/ 1.05644	2.74114/ 1.5247	2.99701/ 1.40475	6.82202/ 1.88758	43.01076/ 2.16217

It is known [1] that the beryllium oxidation kinetics can be expressed in general view by the equation:

$$\Delta m^b = kt \quad (4),$$

where Δm is the mass increase, t is the duration of the test, b , k – constants.

The oxidation surface layer is protective if $b > 1$ because the reaction rate decreases with time, and non-protective if $b < 1$. Obviously, the constant B from (3) connects with the constant b from (4) by the relation:

$$b = 1/B, \quad (5).$$

Table 3.3 shows the constants b (in air) calculated from constants B which demonstrate that the oxide layers play a protective role for all testing temperatures for Lot 1473 because $b > 1$. For Lot 1843, having more developed porosity compared to Lot 1473, the oxide layers stop to be protective since the temperature of 1000 °C when $b < 1$. The oxide layer seems to be non-protective for Lot 1843 at 700 °C as well. However, the high scattering of measured values and the low oxidation rate could affect the results of fitting.

Table 3.3: Constants b (Eq.(4)) calculated from constants B (Eq.(3)) in air

Lot	Constant b							
	Testing temperature [°C]							
	700	800	900	930	950	1000	1050	1100
1473	1.2019	1.241	-	1.5389	1.536	1.3455	1.5665	1
1843	0.8183	1.1912	1.3706	1.2409	1.5225	0.4434	0.9639	-

Table 3.4 shows the constants b calculated from constants B according to (5). There is no principle difference between two Lots investigated concerning resistance to interaction with steam. Both Lots have $b > 1$ up to 650°C (but the test for Lot 1843 at 650°C was not performed). For both Lots, $b < 1$ at 600°C, however in this case the curves have the high scattering therefore fitting might be affected.

Table 3.4: Constants b (4) calculated from constants B (3) in steam

Lot	Constant b							
	Testing temperature [°C]							
	600	620	650	680	700	720	750	800
1473	0.1603	1.1969	1.269	0.8995	0.7527	0.6989	0.5319	-
1843	0.2863	3.1275	-	0.9466	0.6559	0.7119	0.5298	0.4625

The temperature dependency of constant A from Eq.(3) is described by an Arrhenius equation [1]:

$$A = C \cdot \exp(-E_a/kT), \quad (6),$$

where E_a is the activation energy of oxidation[eV], C is the frequency factor, $k = 8.61733 \cdot 10^5$ eV/K – Boltzmann constant, T – the absolute temperature [K].

Taking natural logarithm of both parts of Eq. (6) we obtain

$$\ln A = \ln C - E_a/k \cdot 1/T, \quad (7).$$

Figs. 3.2 and 3.3 for air experiments and Figs. 3.4 and 3.5 for steam experiments show the dependency of $\ln A$ from the reverse temperature $1/T$ for both Lots, using Eq.(7). This dependency allows estimating E_a on the slope of the lines. Tables 3.5 and 3.6 include the values of E_a , calculated using this method.

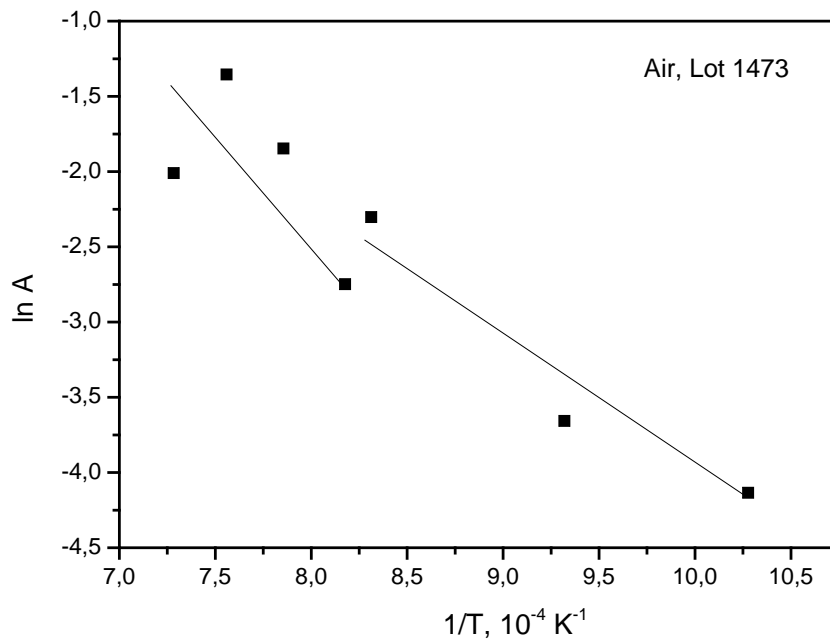


Fig. 3.2: Dependency of $\ln A$ on reverse temperature $1/T$ for oxidation tests in air of 1 mm beryllium pebbles, Lot 1473

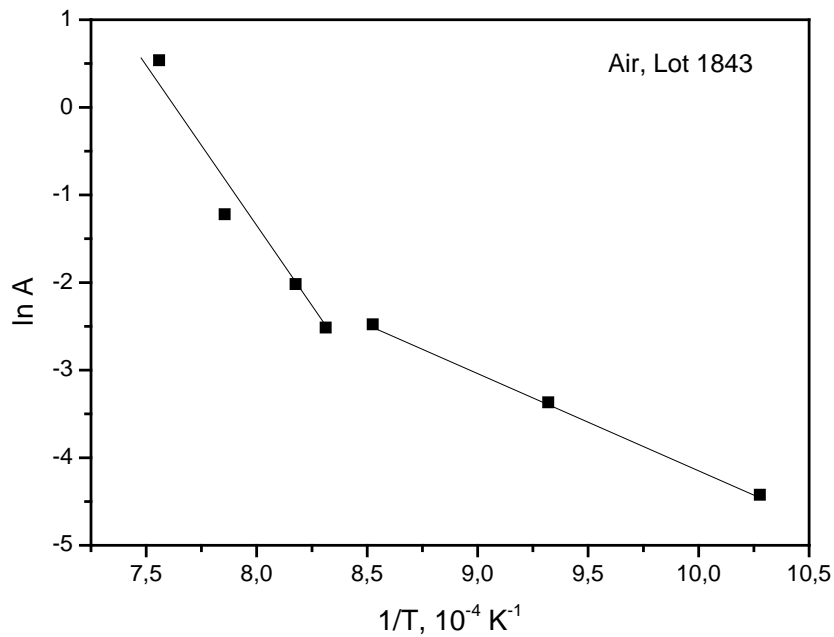


Fig. 3.3: Dependency of $\ln A$ on reverse temperature $1/T$ for oxidation tests in air of 1 mm beryllium pebbles, Lot 1843

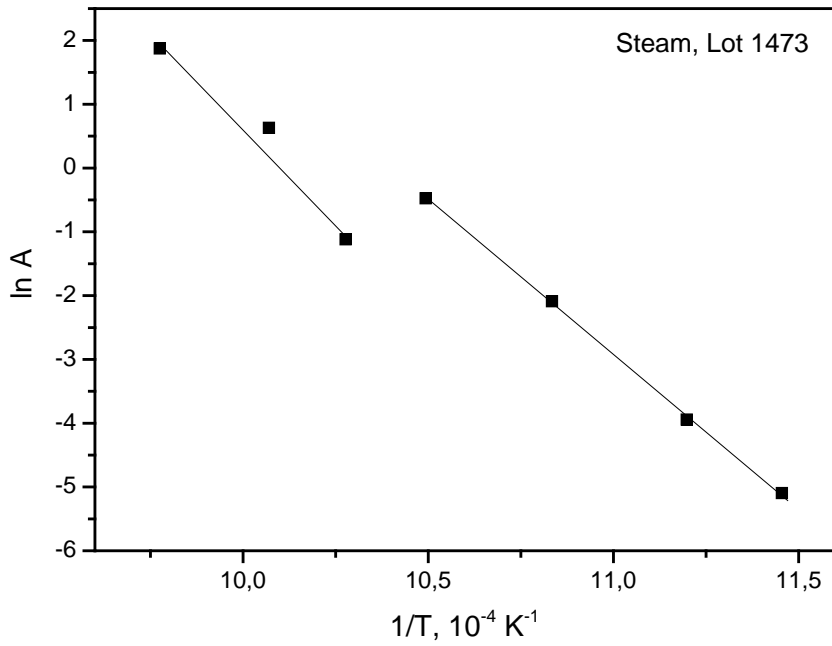


Fig. 3.4: Dependency of $\ln A$ on reverse temperature $1/T$ for oxidation tests in steam of 1 mm beryllium pebbles, Lot 1473

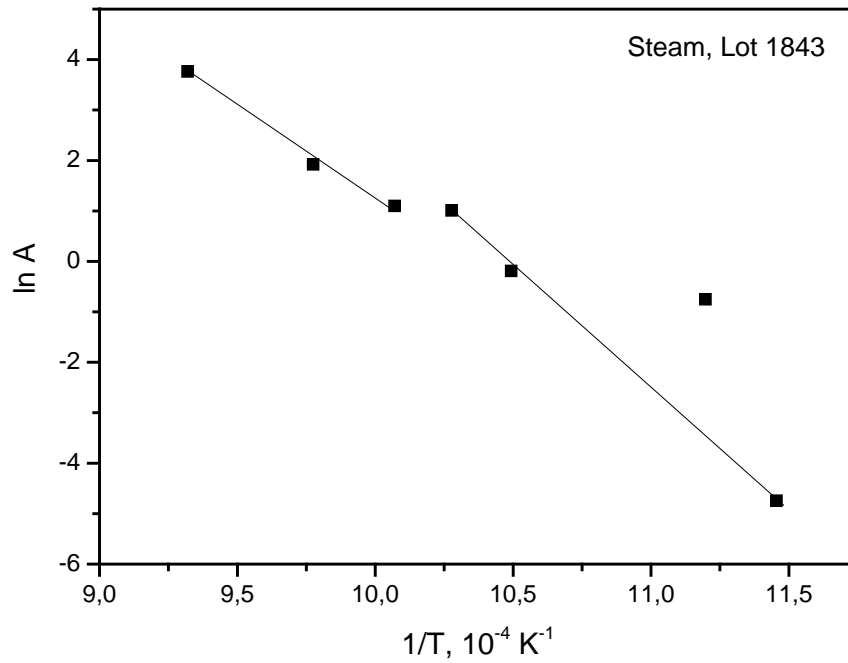


Fig. 3.5: Dependency of $\ln A$ on reverse temperature $1/T$ for oxidation tests in steam of 1 mm beryllium pebbles, Lot 1843

Table 3.5: Activation energy of oxidation in air of beryllium pebbles of Lots 1473 and 1843

Medium	Activation energy of oxidation E_a [eV]			
	Lot 1473		Lot 1843	
	$T = 700-950^\circ\text{C}$	$T = 1000-1100^\circ\text{C}$	$T = 700-930^\circ\text{C}$	$T = 950-1050^\circ\text{C}$
Synthetic air	0.83	1.26	0.97	3.13

The activation energies significantly differ for the temperature regions 700 - 950 (700 - 930) °C and 1000 - 1100 (950 - 1050) °C. Accordingly, there is a sharp change in the slope of the counter lines on the border between these temperature regions.

Table 3.6 Activation energy of oxidation in steam of beryllium pebbles of Lots 1473 and 1843

Medium	Activation energy of oxidation E_a , [eV]			
	Lot 1473		Lot 1843	
	$T = 600-680^\circ\text{C}$	$T = 700-750^\circ\text{C}$	$T = 600-700^\circ\text{C}$	$T = 720-800^\circ\text{C}$
Steam	4.16	5.14	4.17	3.31

Discontinuity of the curves accompanied by a slight change of the line's slope takes place between 680 and 720 °C. However, the activation energies do not differ significantly for both lots in the corresponding regions having a value from 3.3 to 5.1 eV.

3.1 Surface investigation of oxidized beryllium pebbles

Scanning electron microscopy (SEM) was applied for the investigation of surfaces' microstructure of 1 mm beryllium pebbles oxidized in synthetic air at temperatures 500 – 1000 °C. SEM micrographs reveal the complex character of surface oxidation changing with increasing oxidation temperature.

At low temperatures (see Figs. 3.7 a-b), a thin homogeneous oxide layer covers the pebble surface. At higher magnification, one can see that small dimples at the surface are in fact small beryllium grains (dropped down together with covering pieces of beryllium oxide layer). At intermediate temperatures, darker spots with higher number density are clearly seen on the general view (Fig. 3.7 c). Magnification demonstrates that these spots are larger beryllium grains (~20 μm) dropped down. Smaller grains dropped down at earlier oxidation stages are already partially healed and can be seen as white craters (Fig. 3.7 d).

At high temperatures (930 – 980 °C) the surface looks icy with some domains of parallel strips (Fig. 3.7 e). Higher magnification displays nearly complete healing of the dropped

grains with oxide layer which obeys moss-like structure (Fig. 3.7 f).

Based on the observations above, the following mechanism of dimple formation is proposed (Fig. 3.6): Oxygen diffusion along grain boundaries is accelerated with respect to that in the beryllium bulk. Faster growing oxide layer along grain boundaries creates high internal stresses due to large lattice constant mismatch

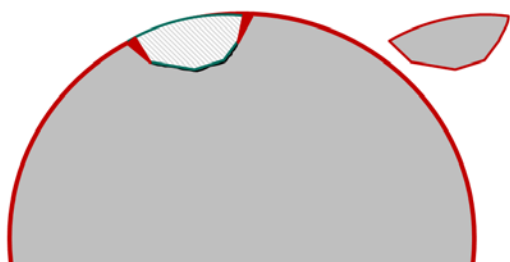


Fig. 3.6: Schematic view of the proposed mechanism of dimple formation under oxidation. Oxide layer (red) is acting as a wedge pressing small near-surface grains out of the pebble

between Be and BeO. These stresses increase in the course of oxidation, thus provoking brittle crack formation along grain boundaries. As a result, grain is detached from its surrounding and can be easily removed (drop down) from the pebble, forming pits clearly visible on the SEM pictures.

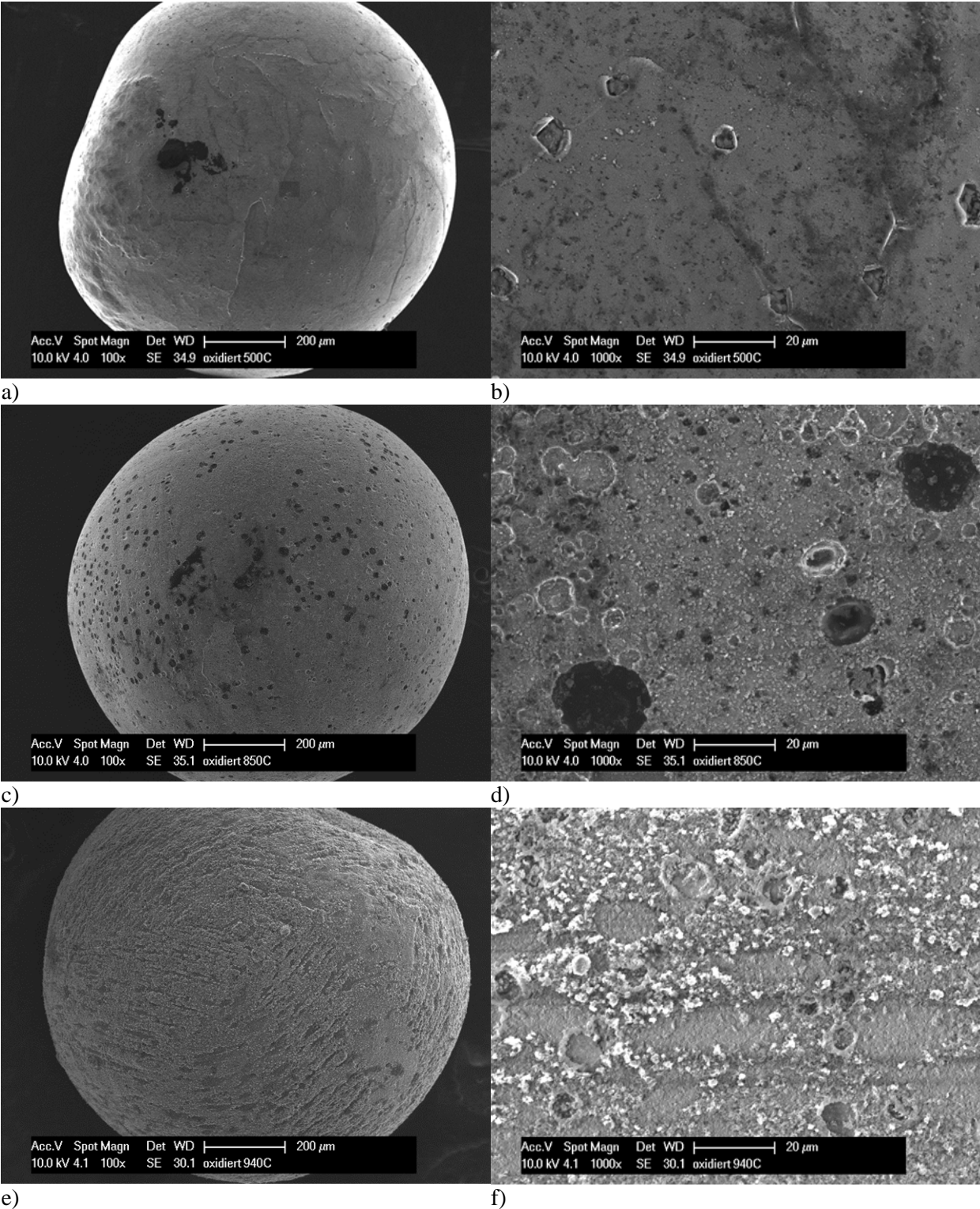


Fig. 3.7: Surface of 1 mm beryllium pebble oxidized in synthetic air at various temperatures: general view (left) and magnification (right). a - b) 500 °C, c - d) 850 °C, e - f) 940 °C.

Images taken by photo camera after TG experiments at 600, 700 and 750 °C performed on both kinds of beryllium specimens in atmosphere containing water vapor are shown in Fig. 3.8 a - f. No visible changes could be observed after testing at 600 °C (Fig. 3.8 a, b). The pebble color change starts from 700 °C (Fig. 3.8 c, d). Higher reactivity of the pebbles from Lot 1843 is reflected by more intensive change of their color and by larger size of the pebble remnants after testing at highest temperature (Fig. 3.8 e, f).

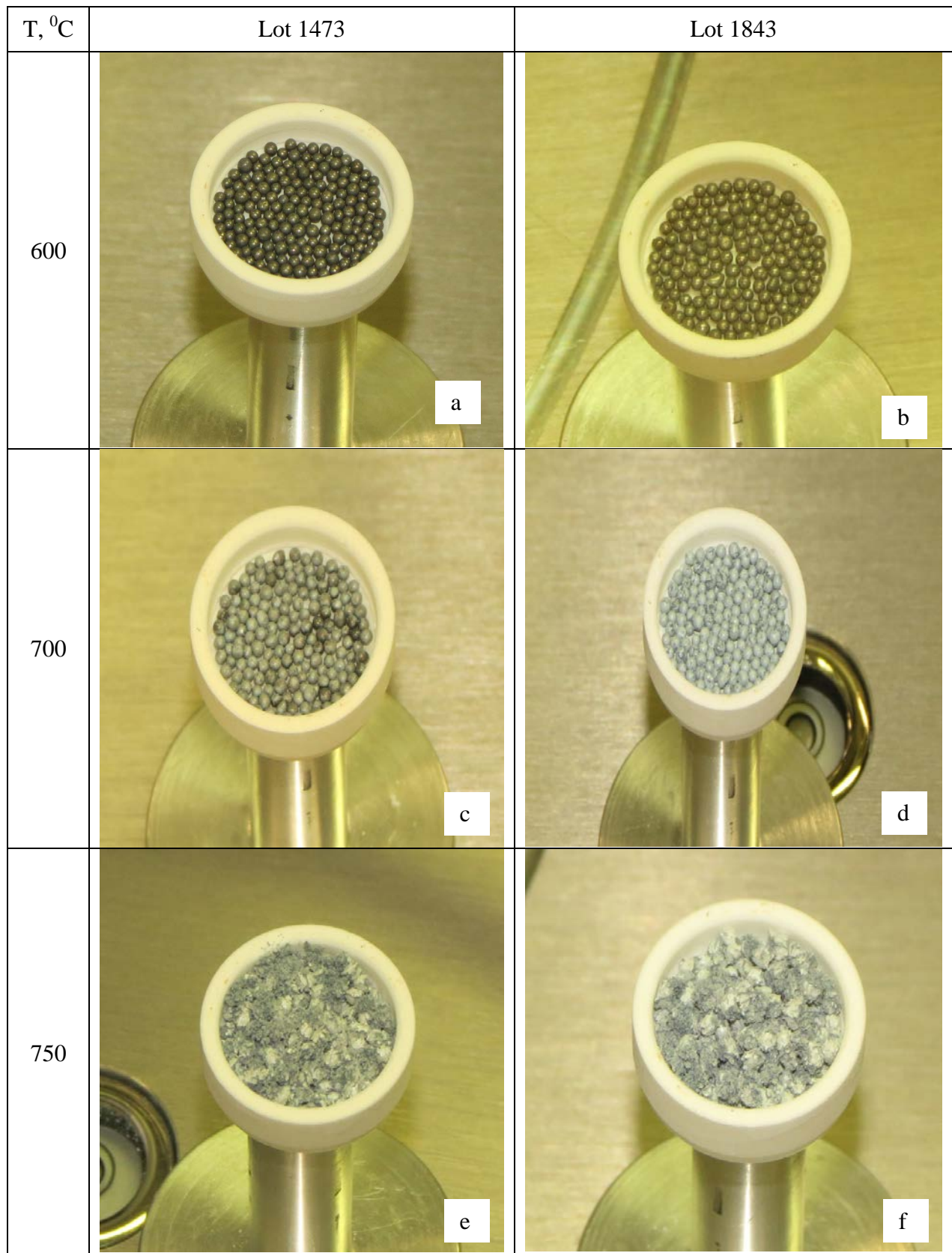


Fig. 3.8: Optical images of both kinds of beryllium specimens (Lots 1473 and 1843) after finishing of TG tests at 600 (a, b), 700 (c, d) and 750 °C (e, f)

TG analysis of beryllium pebbles from Lot 1843 at maximum temperature of 800 °C resulted in very intensive interaction with water vapor. One can see in Fig. 3.9 that dimensions of the

pebbles increased in such a great extent that they dropped out of the standard alumina crucible having the depth of 3 mm. Therefore, the upper testing temperature was limited to 750 °C.



Fig. 3.9: Standard alumina crucible filled with beryllium pebbles (Lot 1843) after testing at 800 °C

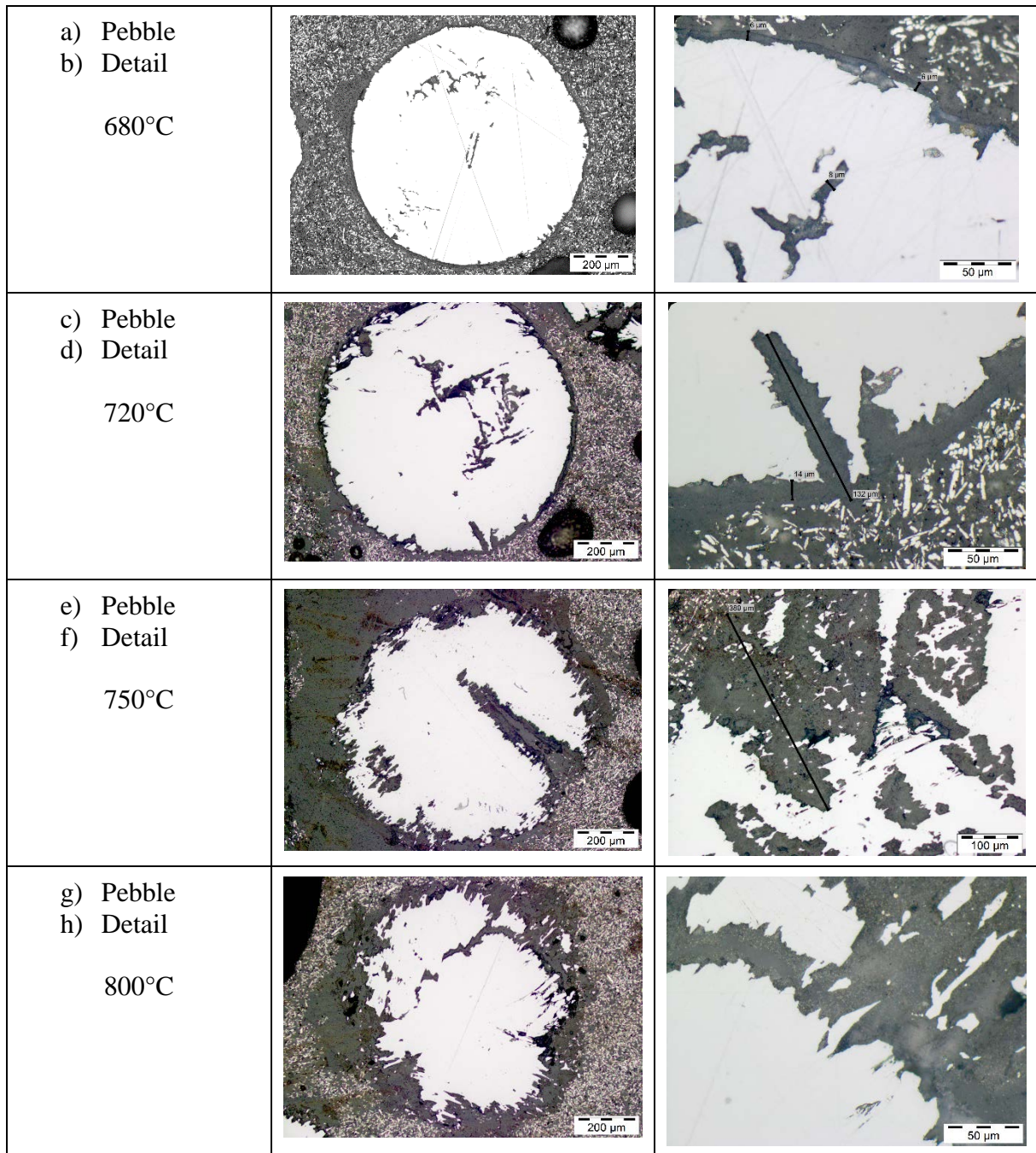


Fig. 3.10: Overview of micro sections Be pebbles and detail views, temp. range 680 °C (a, b), 720 °C (c, d), 750 °C (e, f) and 800 °C (g, h)

Fig. 3.10 shows the surface investigation by oxidation in steam. Oxidation rates increase rapidly over 680 °C, 700 °C. This is also given in Fig. 3.11, where the layer thicknesses for both lots are shown as a function of the temperature. The thickness increases from 5 µm (680 °C) up to 55 µm (750 °C). The oxide layer was observed to be spalling easily by temperatures above 700 °C. High oxidation rate > 700 °C, shows a destabilization of pebble structure, by removal of small parts from the surface by growing of the oxidation layers on the surface and in the open porosity (see Figs. 3.10 d, g, f). By a temperature about 800 °C ensued a destruction of the whole pebble (Fig. 3.10 g, h).

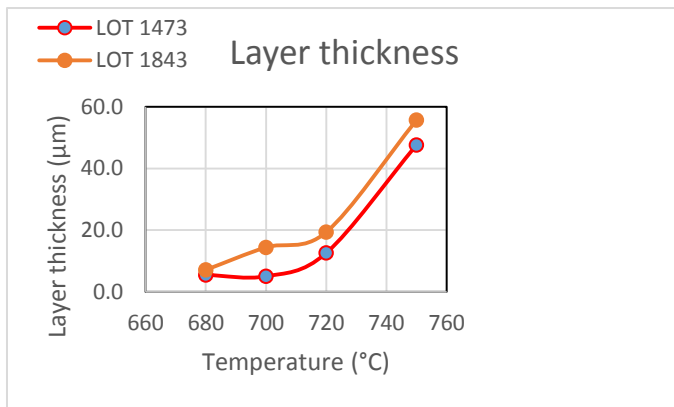


Fig. 3.11: Layer thickness in function of temperature by oxidation in steam

4. Conclusions

Extensive oxidation in synthetic air starts above 950 – 1050 °C depending on the batch of Be pebbles. The batch with higher porosity begins to react with air at lower temperatures. Based on the fitting results, it was established that the oxide layers play a protective role for all test temperatures for Lot 1473. For Lot 1843, having more developed porosity, the oxide layers appear to be non-protective above 1000 °C.

Although both Lots (1473 and 1843) demonstrate conservative interaction with steam up to 650 °C, the more porous Lot (1843) shows higher reactivity manifested in higher mass gain, more intensive surface coloring and large size of the pebble remnants after tests at 750 °C, higher thickness of the surface layer. Active interaction with steam occurs rapidly above 650 °C, while at 800 °C it results in formation of porous beryllium oxide and powder formation by destroying the pebble structure. Such extensive reaction with water vapor should be avoided in fusion reactor as it results in hydrogen production bearing a risk of hydrogen gas explosion.

Acknowledgment

The work leading to this publication has been funded by Fusion for Energy under the contracts F4E-GRT-030-A3 and F4E-FPA-380-SG01. This publication reflects the views only of the author, and Fusion for Energy cannot be held responsible for any use which may be made of the information contained therein.

References

- [1] F. Druyts, S. Smets, P. Van Iseghem, Report SCK·CEN-R-3750 for Contract EFDA TTBB-007 Subtask 3, KNT 90 99 1313, Mol, Belgium, 2003.
- [2] Kurinskiy, Petr (IAM, KIT), Rolli, Rolf (IAM, KIT), Klimenkov, Michael (IAM, KIT), Chakin, Vladimir (IAM, KIT), Reimann, Jörg (KBHF), Vladimirov, Pavel (IAM, KIT), Full Technical Report D4.1-full (Characterization of NGK Pebbles & Pebble Beds) F4E-FPA-380-A3: SG01

2.5.2 Beryllium oxide on dust particles produced by ITER like wall materials in JET

N. Ashikawa^{1,2}, N. Asakura³, M. Miyamoto⁴, M. Hara⁵, Y. Trikaï⁶, M. Oyaidzu³, M. Nakano³, J.H. Kim³, K. Isobe³, Y. Hatano⁵, T. Suzuki³, H. Kurotaki³, D. Hamaguchi³, M. Nakamichi³, H. Nakamura³, A. Widdowson⁷, K. Heinola⁸, M. Rubel⁹

¹National Institute for Fusion Science, Oroshi 322-6, Toki 509-529, Japan

²SOKENDAI, Oroshi 322-6, Toki 509-5292, Japan

³Japan National Institutes for Quantum and Radiological Science and Technology (QST), Rokkasho Aomori 039-3212, Japan

⁴Shimane University, Matsue, Shimane 690-8504, Japan

⁵University of Toyama, Gofuku 3190, Toyama 930-8555, Japan

⁶Ibaraki, University, 2-1-1, Bunkyo, Mito 310-8512, Japan

⁷Culham Centre for Fusion Energy, Culham Science Centre, Abingdon, OX 14 3DB, UK

⁸University of Helsinki, Box 43, FIN-00014 Helsinki, Finland

⁹Royal Institute of Technology (KTH), 100 44 Stockholm, Sweden

E-mail: ashikawa@LHD.nifs.ac.jp

Joint European Torus (JET) started operation with the ITER-like Wall (ILW) in 2011 using tungsten (W)-coated CFC/bulk-tungsten divertor tiles and beryllium first wall, respectively[1]. The main aims are: development of an integrated operation scenario for ITER, power handling and material behavior with metal walls, assessment of fuel inventory and development of ITER-oriented engineering solutions, e.g. remote handling.

The determination of dust characteristics, such as structures, material composition and hydrogen isotope retention are important issues. In particular, measurement of the total tritium amount and their relationship between amount and composition are required. Therefore, this study was focused on material composition and quantitative tritium amounts in JET-ILW dust particles.

In Ref.2, retained deuterium concentration in C, Be and W deposits under co-deposition was reported. Retention in beryllium oxide is one order of magnitude larger than metal beryllium. Hence, chemical bindings of beryllium in ILW materials are important for estimations of hydrogen isotope retention and tritium inventories.

Quantitative tritium measurements for ILW from the 2011 to 2012 campaign and carbon dust particles from 2007 to 2009 campaigns collected on the inner divertor targets were done using a liquid scintillation counting (LSC). Tritium specific activity of ILW dust particles of 120 MBq/g, is nearly the same as that of carbon wall dust particles of 10-60 MBq/g. Beryllium dominant dust particles show beryllium oxide on those surfaces measured by X-ray photoelectron spectroscopy (XPS) and one of these thicknesses is about two microns. This result was estimated that the reason of higher tritium inventory in ILW dust particles was related to thick beryllium oxide on those surfaces. It should be noted that produced conditions, such as after a vacuum vent or during plasma operations, of beryllium oxide is not clear due to the ex-situ measurements. However, the ratio of volume between beryllium oxide and metal beryllium into a dust particle is higher than that of beryllium tile specimens from JET, due to the estimated volume less than $5 \times 10^{-4} \text{ mm}^3$, in the case of 100 microns diameter. Therefore it is estimated that higher tritium specific activities on ILW dust particles, it is normalized amounts by weights, were observed.

Evaluations of tritium specific activity measured by a combustion method and beryllium observations measured by an electron probe micro analyzer (EPMA) in ILW dust particles will be also presented.

References

- [1] A. Widdowson, et al., Physica Scripta **T159**, 014010 (2014).
- [2] J. Roth, et al., Journal of Nuclear Materials **390**, 1 (2009).

Beryllium oxide on dust particles produced by ITER like wall materials in JET

N. Ashikawa^{1,2}, N. Asakura³, M. Miyamoto⁴, M. Hara⁵, Y. Torikai⁶, M. Oyaidzu³, K. Isobe³, A. Widdowson⁷, J. Grzonka^{8,9}, M. Rubel¹⁰, T. Otsuka¹¹, S. Nakano³, J.H. Kim³, D. Hamaguchi³, H. Kurotaki³, Y. Hatano⁵, K. Heinola¹², H. Tanigawa³, M. Nakamichi³, and JET Contributors **

NIFS¹, SOKENDAI², QST³, Shimane Univ.⁴, Toyama Univ.⁵, Ibaraki Univ.⁶, CCFE⁷, Warsaw University of Technology⁸, Institute of Electronic Materials Technology Warsaw⁹, KTH Royal Institute of Technology¹⁰, Kindai Univ.¹¹, Univ. of Helsinki¹²

BeWS-13, 2017 October, Narita, JAPAN

1

ITER Like Wall (ILW) Project in JET : Ex-situ analysis

- Dust collected in JET-ILW (after 2011-12 operation) was done and transported to Rokkasho, Japan, based on Broad approach(BA) work. An analysis was started from 2014.
- Motivation of analyses for JET ILW dust particles : ILW experiment is a real simulation of plasma facing materials toward ITER. Produced amounts, deposited areas, tritium amounts, irradiation level of dust particles are required.
 - In DEMO, it is important to estimate hydrogen isotope retention (fuel dilution) and consider a safety (the evaluation of floating irradiation waste).
 - **No data of tritium inventory from dust particles in metal devices.**
- The facility in the International Fusion Energy Research Center, Rokkasho, where **“tritium”, “beta and gamma RI species”, and “beryllium (Be) powders”** can simultaneously be used.



In this talk, a progress of analytical results, Be oxide and T amount, on ILW dust particles are shown.

2

JET-MKII-HD Total tritium amount is 79.3 GBq (79.3/37 = 2.1Ci)

JET-MKII-HD (C-dust) was reserved in cyclone pots after distribution to laboratories

Pot B (Inner vertical target) : Stage2 (110.1g) Vacuum cleaner

Pot K (Inner and Outer Carriers) : Stage3 (19.3g)

Pot M (Outer horizontal target) : Stage4 (51.4g)

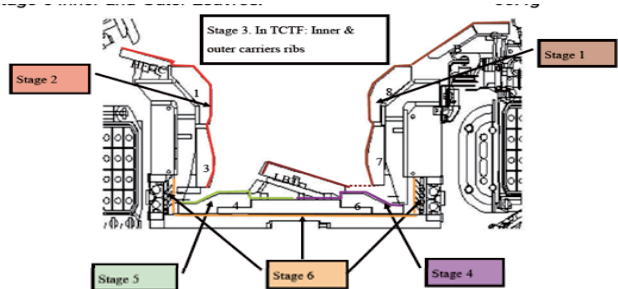
Pot T (Inner and outer louvres) : Stage6 (99.4g)

➡ All will be transported to Rokkasho

Carbon wall (2007-2009)



Four Carbon dust samples



Sample pots	Divertor Region	Offgas survey (Bq/d)	Specific Activity (GBq/g)	Dust (g)	Activity (GBq)	Comment
sample pot B	Inner divertor tiles: HFGC, 1, 3 360°	16001	0.031	6.36	0.2	Stage2 (110.1g)より選別?
sample pot K	Carrier ribs	16205	5.3	3	16.36	Stage3(19.3g)より選別?
sample pot M	Outer divertor base tiles: 6, base carrier 360°	16079	5	4.61	23.26	Stage4(51.4g)より選別?
sample pot T	Inner and outer louvres 360°	16038	6.5	6.03	39.38	Stage6(99.4g)より選別?

Total tritium amount is 1.42 GBq (1.42/37 = 0.038Ci)

Pot P (outer divertor) from Cyclone Pot22(0.27g)

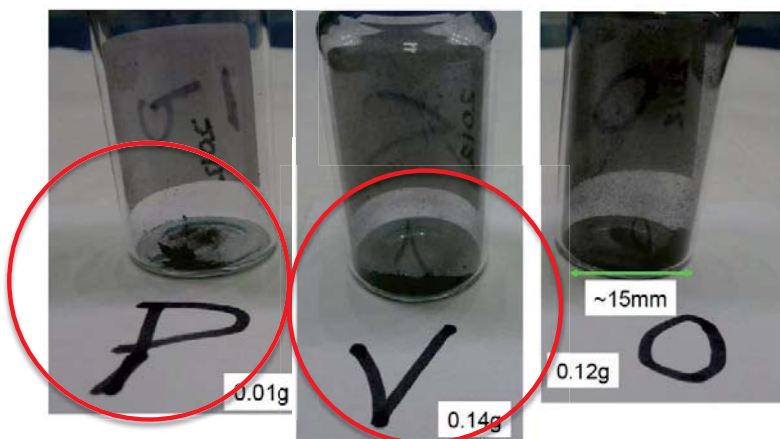
Pot O and Pot V (inner divertor) from Cyclone Pot25(0.77g)

➡ Pot P and Pot V will be transported to Rokkasho

1st-ILW (2011-2012)

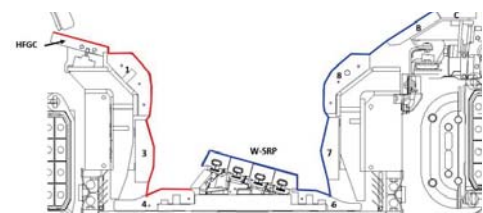
Three IWL dust samples

Sample pots	Divertor Region	Offgas survey (Bq/d)	Specific Activity (GBq/g)	Dust (g)	Activity (GBq)	Comment
sample pot P-2012	Outer divertor tiles: LBT, 6, 7, 8, B, C 360°	32856	1.4	0.01	0.014	Pot22より選別?
sample pot O-2012	Inner divertor tiles: HFGC, 1, 3, 4 360°	32888	5.4	0.12	0.65	Pot25より選別?
sample pot V2012	Inner divertor tiles: HFGC, 1, 3, 4 360°	32888	5.4	0.14	0.76	Pot25より選別?

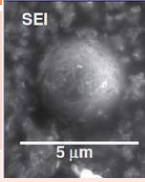
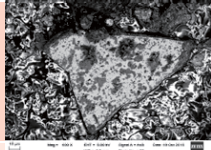
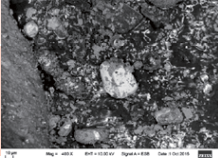
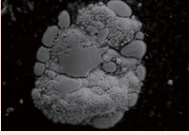
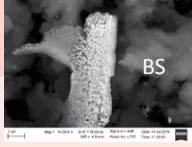
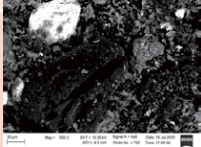
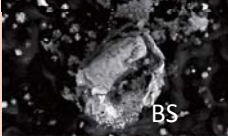
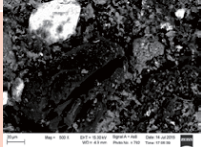


Inner Div.

Outer Div.



Surface morphology (ILW dust particles)


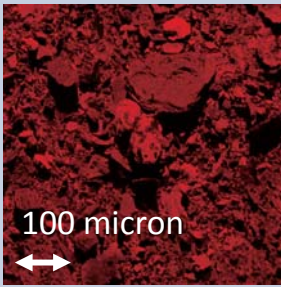
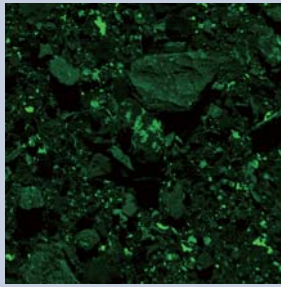

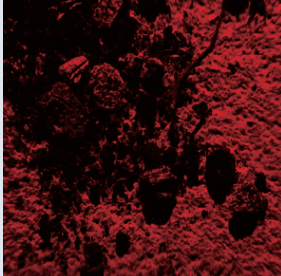
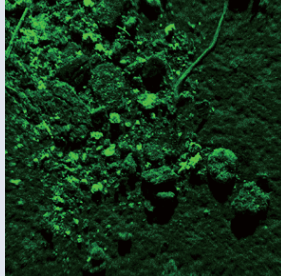
Types		Data		[1]This work, [2] A. Baron-Wiechec, NF (2015)
Be metal (flake/droplet)			[2] Droplet	 [1] FIB+TEM
Be amorphous			BS	 [1]
W metal (flake/droplet)			[2]	 [1]
W amorphous				 [1]
Other impurities	Mo, Ni, Carbon(C) Aluminum(Al)		[1]	 [1]

	Total amounts of collected dust	Materials
JET-Carbon wall	245g	C, Be, others
JET- ILW	1g	W, Be, others

Limited number of beryllium dust particles is observed.

5

SEM/EDX mapping (Carbon wall vs ILW)

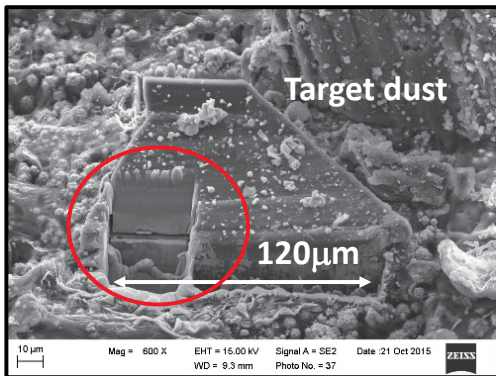
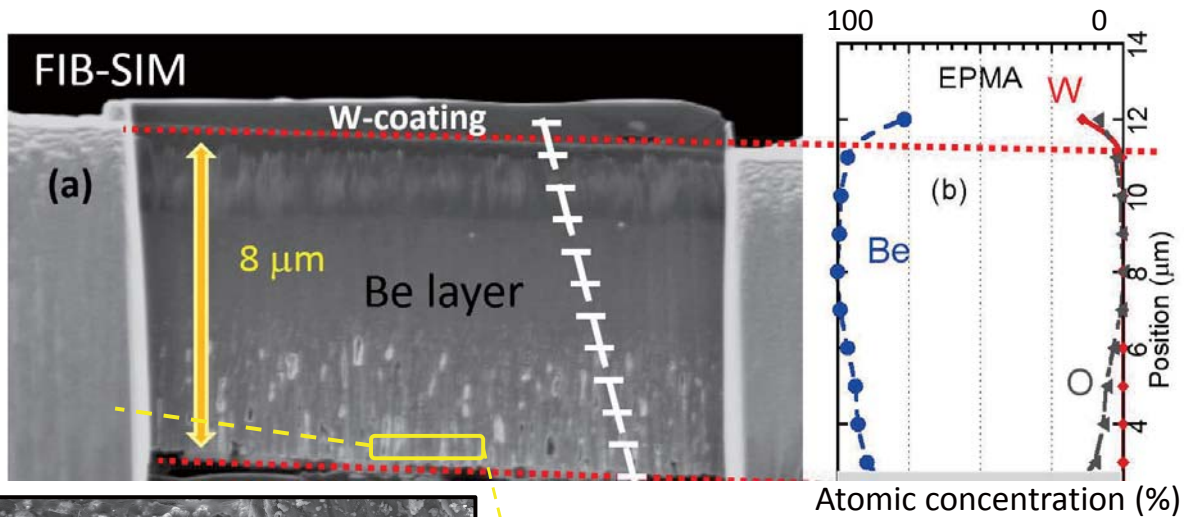
	Carbon	Oxygen	Tungsten
Carbon phase (Pot-T)			
ILW phase (Pot-V)			

Energy Dispersive X-ray spectrometry (EDX)

This EDX can not detect Be (element separation is available from boron)

- Oxygen (O) concentration on ILW dust particles with Be is higher than that without Be. The results are consistent with the XPS analyses (see next page).
- Areas with O counts in ILW are wider than carbon.

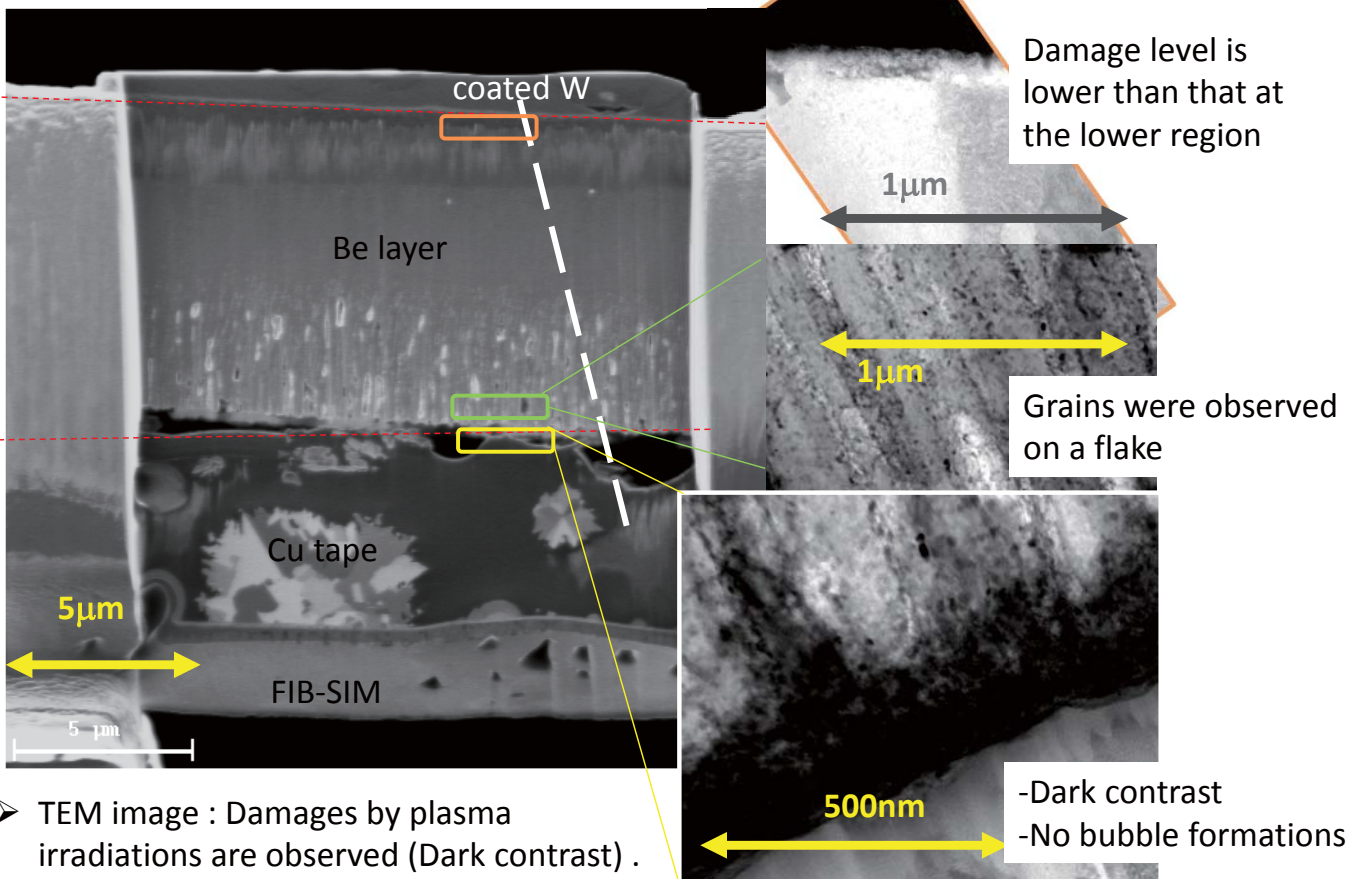
Be flake dust (Cross-section image)



- Using a focused ion beam (FIB) treatment, cross-section was made and that surface was measured by **Electron probe micro analyzer (EPMA)**.
- One side of Be layer, which thickness of 2 μm, shows high oxygen concentration.

7

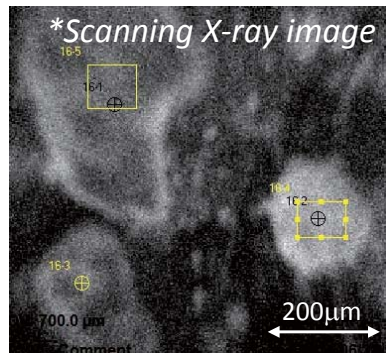
Cross-section images of Be flake(TEM)



- TEM image : Damages by plasma irradiations are observed (Dark contrast) . No bubble formations.

8

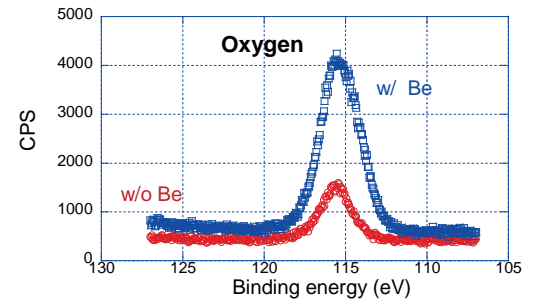
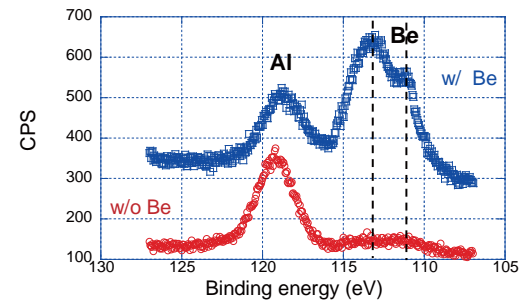
Be oxide on ILW dust particles : XPS



w/o Be

w/ Be

XPS : spot size of 100 μm

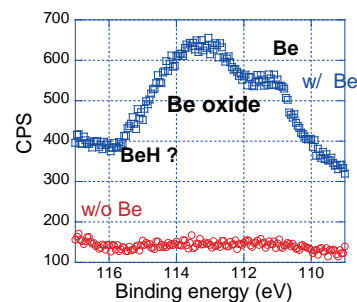
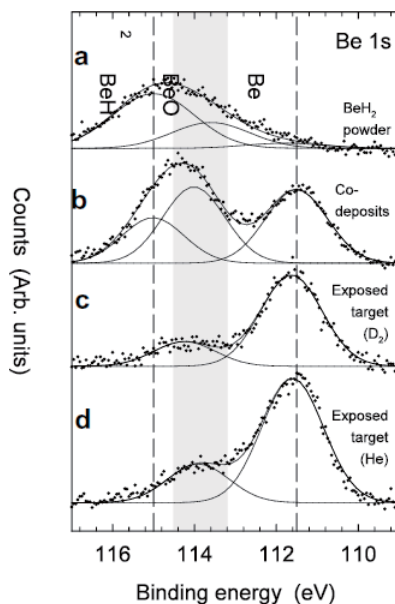


- Dust particles were set on a Cu tape, which was the same method for SEM/EDX.
- Al source is considered by a contamination during collection or transportation works.

- There were dust particles that detects Be (w/ Be) and not detecting Be (w/o Be)
- Chemical bindings of Be were measured by XPS after argon(Ar) ion etching. Beryllium oxide on the ILW dust particle was seen.
- Oxygen (O) concentration on ILW dust particles with Be is higher than that without Be. The results are consistent with the EDX analyses.

9

Be oxide on ILW dust particles : XPS



	Be Oxide	Metal Be
This work	113.3eV	111.3 eV
R. Doener [1]	~ 114 eV	111.5 eV
ILW tile (2011-12) [2]	114.1 eV	111.8 eV

Fig. 1. Deconvolution of XPS Be 1s spectra from BeH₂ powder (a), codeposited Be layer (b), Be target exposed to D plasma (c) and Be target exposed to He plasma (d). The spectra are fit with Be metallic (111.5 eV), Be oxide (~114 eV) and Be hydride (115.0 eV) Gaussian peaks.

[1] R.P. Doener, JNM 390-391 (2009) 681

[2] S. Masuzaki, Y. Oya, et al., PFMC (2017)

- In Be 1s peak, Be oxide is higher than that of metal Be at near the surface region (~100nm).

10

ILW 2011-2012 (EU) : Be measurement by EDX

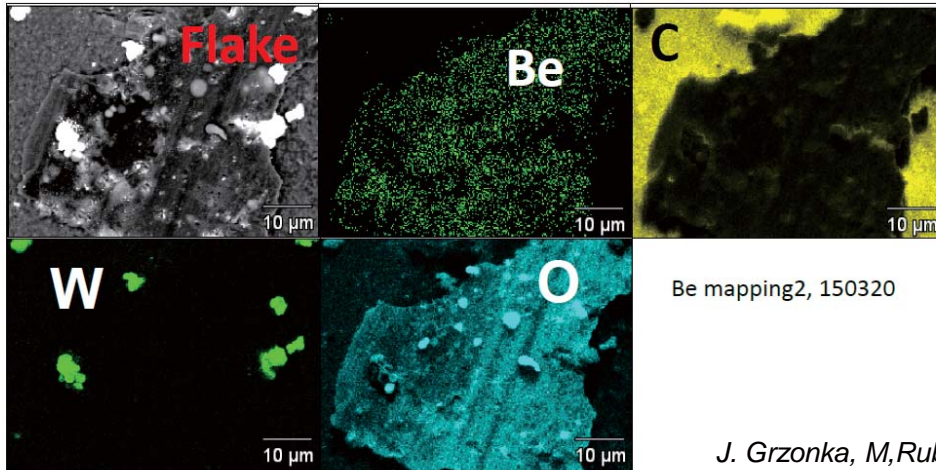
- Using special filter to expand to lower energy region, Be can be measured by EDX (Energy dispersive X-ray spectrometry).

Note: This EDX is used in EU.

-Ion micro-beam analysis is also available.

- Two mapping images of Be and O are similar, due to beryllium oxide.

ILW 2011-2012 Dust studies: Beryllium flake



J. Grzonka, M, Rubel, et al., PSI 2016

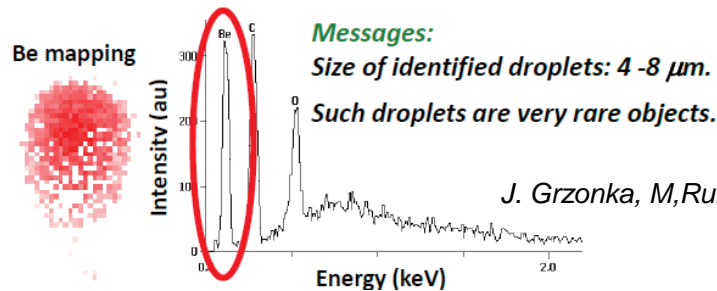
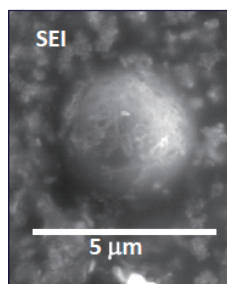
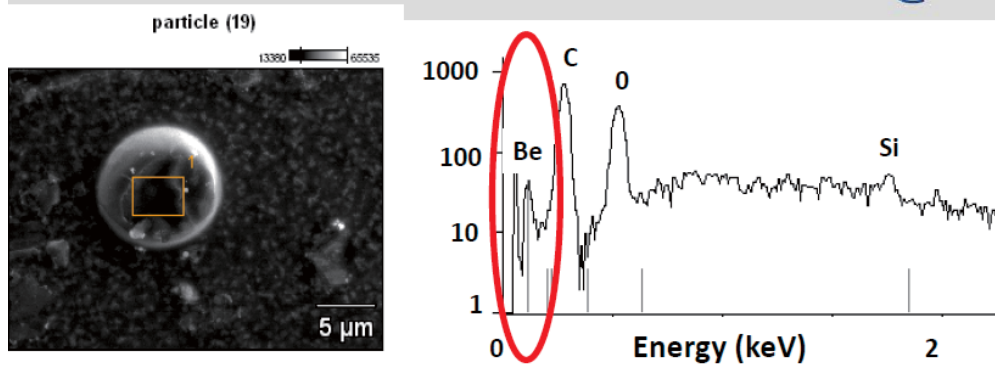
Challenge in Beryllium identification, quantitative analysis and mapping: low X-ray energy (108 eV)

11

ILW 2011-2012 (EU) : Be&C droplets

Using dust collection by a carbon tape, Be droplets were observed.

ILW 2011-2012 Dust studies: Droplet with Be & C



Messages:

Size of identified droplets: 4-8 µm.

Such droplets are very rare objects.

J. Grzonka, M, Rubel, et al., PSI 2016

12

Hydrogen isotope retention on beryllium oxide

Why **specific activities** of ILW dust particles so high?

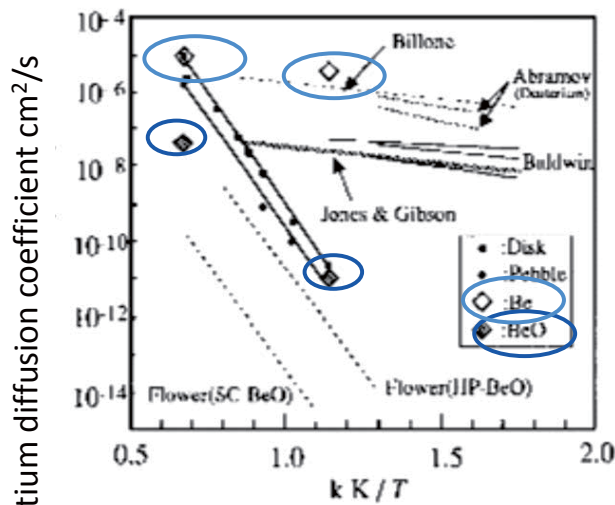
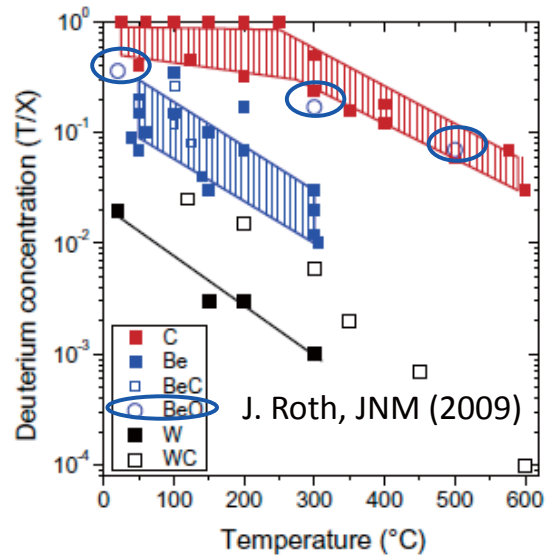


Fig. 4 Tritium diffusion coefficients for Be and BeO.

E.Ishitsuka (1994) SOFT-18



J. Roth, JNM (2009)

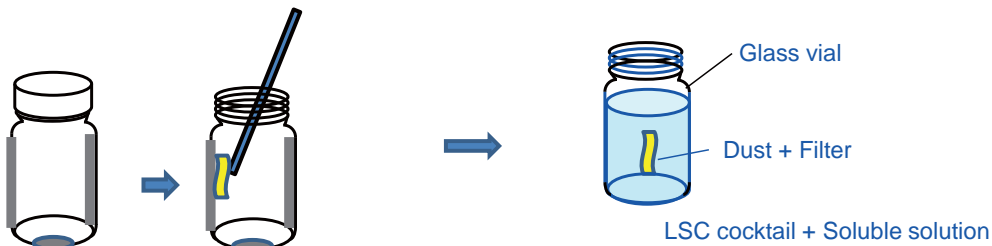
- Diffusion coefficient of **beryllium oxide** is lower than that of **metal beryllium**.
- Higher hydrogen isotope retention on beryllium oxide was reported.

13

Tritium : Liquid Scintillation Counting (LSC)

Quantitative tritium amount is required

Total amount of ILW dust particles is limited. Many particles are located on the inner wall of a vial by electrostatic force.



- To obtain high Counting efficiency for Quantitative analysis
- 4 π illuminations are required in LSC
- New combination between material of a filter and type of cocktail was used

<http://www.perkinelmer.co.jp>

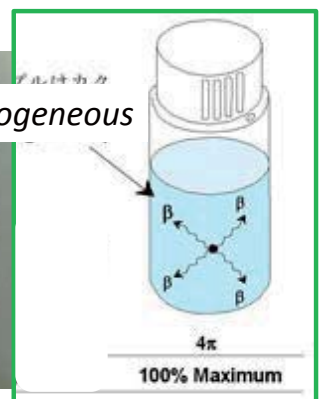
- Filter : polycarbonate membrane
- Cocktail : Hionic-Fluor
- Solution : Soluene-350 (Toluene base)

Amounts of dust particles in cocktails : 1-5 mg

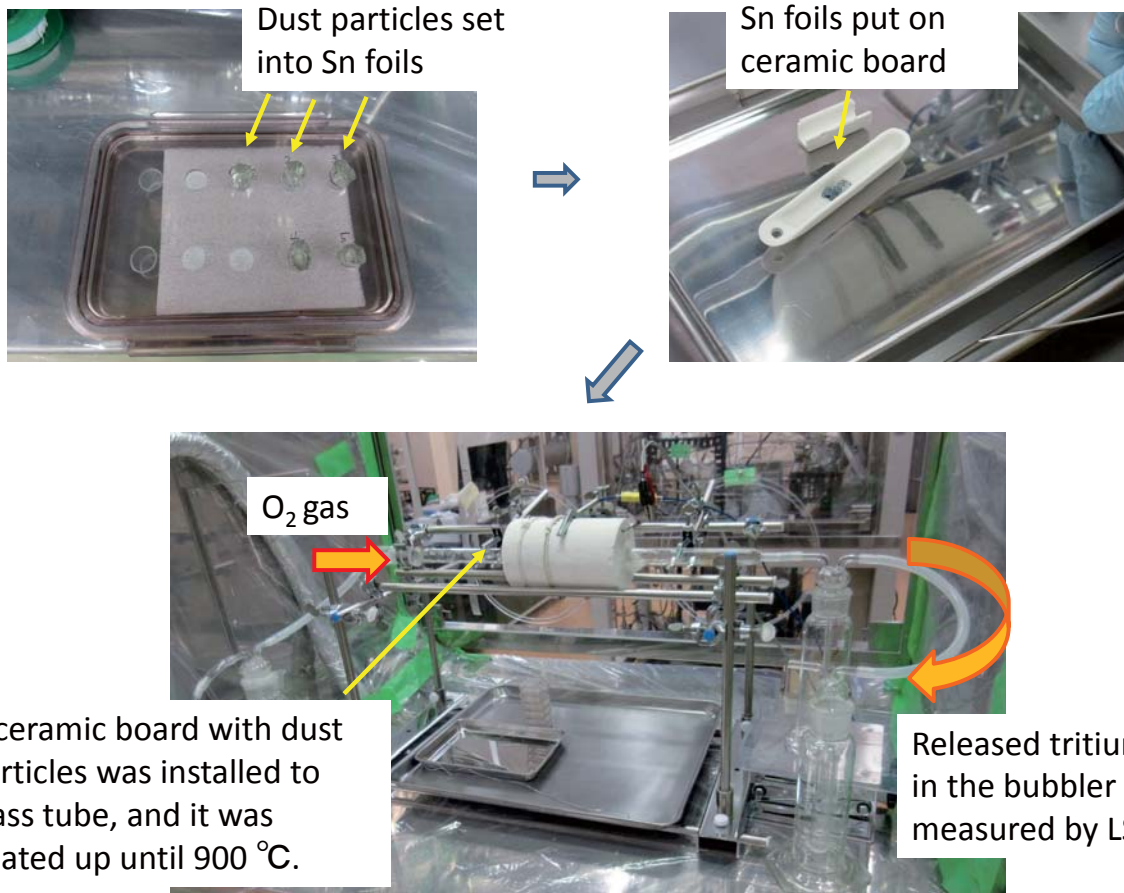
After mixing cocktails with ILW dust particles



Homogeneous



Tritium : Combustion Method



15

Tritium activity (Carbon wall vs ILW)

	Collected amounts (g)	Specific activity (MBq/g) LSC	Activity (MBq)	Specific activity (MBq/g) Combustion Method (CM)	Activity (MBq)	Total activity (MBq) LSC CM
ILW, Pot-P (outer div)	0.27	4.1	1.11	—	—	94
ILW, Pot-V (inner div)	0.77	121	93.2	750	580	580
Carbon Pot-B (inner div)	110.1	11	1211	5.5	610	7.0 × 10 ³ 3.4 × 10 ⁵
Carbon Pot-T (In/Out Louvres)	99.4	47	4672	3300	330000	
Carbon Pot-M (Outer div)	51.4	3	500	100	5100	
Carbon Pot-K (Carrier ribs)	19.3	9.3	60	—	—	

- Target amounts of dust particles for two analytical methods are from 1mg to 15 mg.
- LSC : quick measurement is available, but retained tritium into particles could not be observed.
- Combustion method : Tritium released from burned dust particles. Retained tritium in dust particles after burning is less than 2 Bq/mg. >> Total amounts of retained tritium in dust particles can be measured by the combustion method.
- Specific activities of dust particles : ILW ~ Carbon wall
**Beryllium oxide is related to these higher tritium amounts in ILW dust particles*
- **Total amount of retained tritium : Carbon wall >>> ILW**

16

Summary

A progress of analytical results, beryllium and tritium on ILW dust particles are presented.

1. **Beryllium oxide on ILW dust particles are measured by XPS.** Using a deconvolution was done for the beryllium peak and beryllium oxide is dominant intensity to compare with metal beryllium near the surface region.
 2. **Retained tritium of ILW and carbon wall dust particles are measured by LSC and the combustion method.**
 - Specific activities of dust particles show similar results between ILW and Carbon wall
 - Total amount of retained tritium in the vacuum vessel : Carbon wall >> ILW
 - Total amounts of retained tritium in dust particles can be measured by the combustion method.
- High level specific activities of ILW dust particles might be related to low diffusion coefficient on beryllium oxide of ILW dust particles.

2.5.3 Ternary beryllide pebbles as advance neutron multipliers

J.-H Kim and M. Nakamichi

*Fusion Energy Research and Development Directorate,
National Institutes for Quantum and Radiological Science and Technology, QST,
2-166 Obuchi, Omotedate, Rokkasho, Aomori 039-3212, Japan*

**Corresponding author : kim.jaehwan@qst.go.jp*

Beryllium intermetallic compounds (beryllides) such as Be_{12}Ti and Be_{12}V are the most promising advanced neutron multipliers in demonstration fusion power reactors. Advanced neutron multipliers are being developed by Japan and the EU as part of their Broader Approach activities. It has been previously shown, however, that beryllides are too brittle to fabricate into pebble- or rod-like shapes using conventional methods such as arc melting and hot isostatic pressing. To overcome this issue, we developed a new combined plasma sintering and rotating electrode method for the fabrication of beryllide rods and pebbles. By using these methods, preliminary synthesis of the ternary beryllide pebbles with different chemical compositions, $\text{Be}_{12}\text{Ti}_{1-x}\text{V}_x$ ($x=0.0\sim 1.0$) was successful. In addition to this composition, preliminary synthesis of the ternary beryllide pebbles with different chemical compositions, $\text{Be}_{13}\text{Zr}_{1-x}\text{Ti}_x$ ($x=0.1$ to 0.9), has been carried out.

In the present study, phase variation and reactivity with water vapor of the ternary pebbles will be reported.

Ternary beryllide pebbles as advanced neutron multipliers

Jae-Hwan Kim,

Petr Kurinskiy and Masaru Nakamichi



National Institutes for
Quantum and Radiological Science
and Technology

21st Sept. 2017, KIT, Germany



Jae-Hwan Kim | Hilton hotel, Japan | 21th Sept. 2017 | page (1/12)



Outline of my talk

1. Background
2. Beryllide pebbles (REM)
3. Ternary beryllide (1) Be-Ti-V
4. Ternary beryllide (2) Be-Zr-Ti
5. Ternary beryllide (3) Be-Zr-Ti
6. Conclusion

Jae-Hwan Kim | Hilton hotel, Japan | 21th Sept. 2017 | page (2/12)

1. Background

Fusion reaction

Deuterium + Tritium(T) → Helium(He) + neutron

Plasma

Neutron multiplier (Beryllium)

Single He → Double He

Multiplying to two neutrons

Tritium breeder (Lithium)

Fuel (T) production

Beryllium metal (Be) is candidate material. There are some issues under high neutron fluence at high temperatures.

Pebbles ϕ 1 mm neutron multipliers and tritium breeders are packed in the fusion blanket.

Change of swelling

Change of H₂ generation rate

Beryllium intermetallic compounds (**Beryllides**) have a good potential for high temperature use

Novel granulation method of Be₁₂Ti beryllide

Synthesis of beryllide

Granulation using beryllide rod

Homogenization of beryllide

Beryllide rod has successfully fabricated by the plasma sintering.

This results in **powder surface activation** that 1) enhances powder sinterability & 2) reduces high temperature exposure.

It has **no effect of the surface oxidation layer.**

Plasma sintering process:

- 1) Uniaxial pressure
- 2) Plasma generation for powder surface activation
- 3) Resistance heating

Beryllide block
 ϕ 20xL100mm

Plasma-sintered beryllide

Beryllide pebbles ϕ 1mm has succeeded by the rotating electrode method (REM).

The REM was selected because the experience base for its use is broad, not only for Be pebbles but also metallic pebbles in industry in general.

REM process:

- 1) Rotating of beryllide electrode
- 2) Discharge between beryllide and W electrode
- 3) Solidification to spherical particles

Beryllide pebble

• **Compositional structure** was changed by **peritectic reaction** during cooling.

• By **annealing**, beryllide pebble was becoming single phase of **Be₁₂Ti**.

as-granulated pebble: Be (Black:11%), Be₁₂Ti (Gray:34%), Be₁₇Ti₂ (White:55%)

Homogenized pebble: Pores (Black:9%), Be₁₂Ti (White:91%)

at 1673K for 1h

2. Beryllide pebbles

Binary beryllide

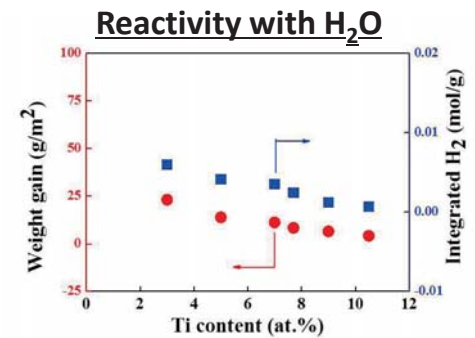
Be-3%Ti pebble
 Be-4%Ti pebble
 Be-5%Ti pebble
Be-7%Ti pebble
Be-7.3%Ti pebble
Be-7.7%Ti pebble (stoichiometric value of Be₁₂Ti) → **Single phase Be₁₂Ti pebble**
 Be-9%Ti pebble
 Be-10.5%Ti pebble (stoichiometric value of Be₁₇Ti₂) → Single phase Be₁₇Ti₂ pebble

Be-7.7%V pebble (stoichiometric value of Be₁₂V, single phase, need optimization)
 Be-7.14%Zr pebble (stoichiometric value of Be₁₃Zr, single phase, need optimization)

Rotating motor
annealing

[M. Nakamichi, JNM 440 (2013) 530], [Jae-Hwan Kim, JACOM 546 (2013) 171], [Jae-Hwan Kim, JACOM 556 (2013) 292], [M. Nakamichi, ISFNT12, FED, accepted (2015)]

	Be-3at.%Ti	Be-5at.%Ti	Be-7at.%Ti	Be-7.7at.%Ti	Be-9.0at.%Ti	Be-10.5at.%Ti
Surface BSE (×100)						
Cross section BSE (×100)						
Cross section BSE (×500)						

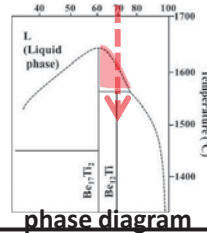
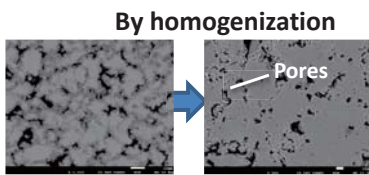


Jae-Hwan Kim | Hilton hotel, Japan | 21th Sept. 2017 | page (5/12)

Advantage and disadvantage

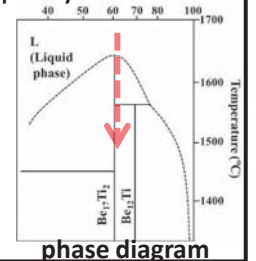
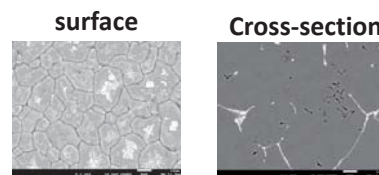
Be₁₂Ti (Be-7.7%Ti)

1. Homogenization treatment is necessary due to peritectic reaction (increase in cost)
2. Pore formation during the treatment
3. Needs to clarify the pore effect



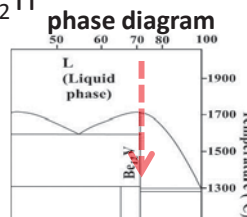
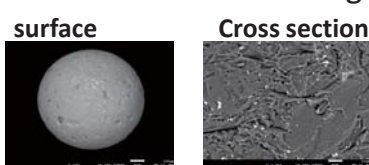
Be₁₇Ti₂ (Be-10.5%Ti)

1. No peritectic reaction/no homogenization (decrease in cost)
2. Relatively low nuclear property (neutronics)



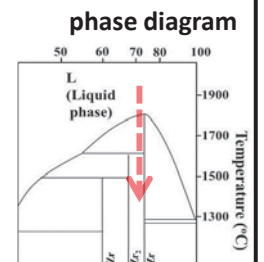
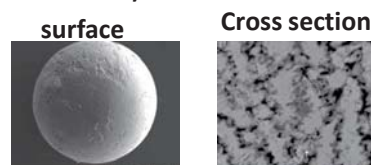
Be₁₂V (Be-7.7%V)

1. No peritectic reaction/no homogenization (decrease in cost)
2. Similar neutronics to Be₁₂Ti
3. Expensiveness
4. Low mechanical strength



Be₁₃Zr (Be-7.14%Zr)

1. No peritectic reaction/no homogenization (decrease in cost)
2. The highest neutronics
3. Less data
4. Difficulty to handle

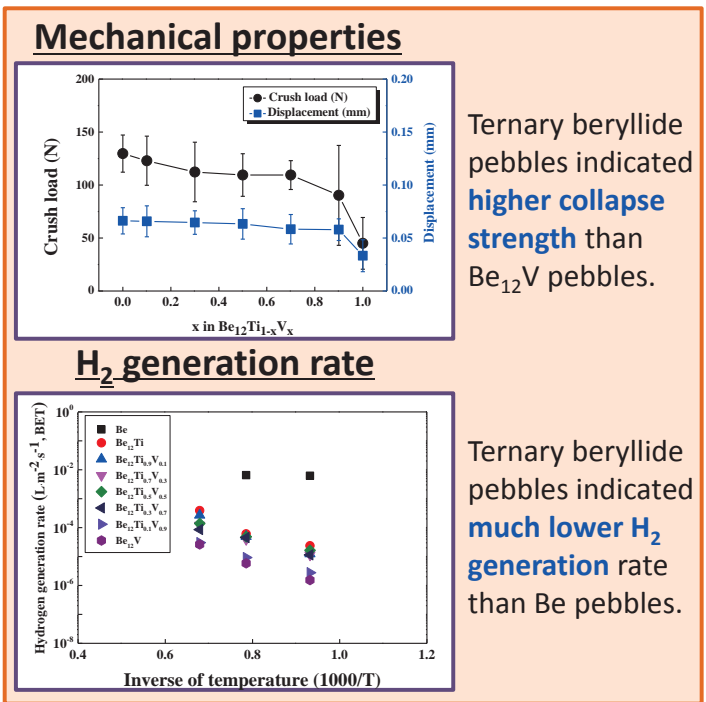
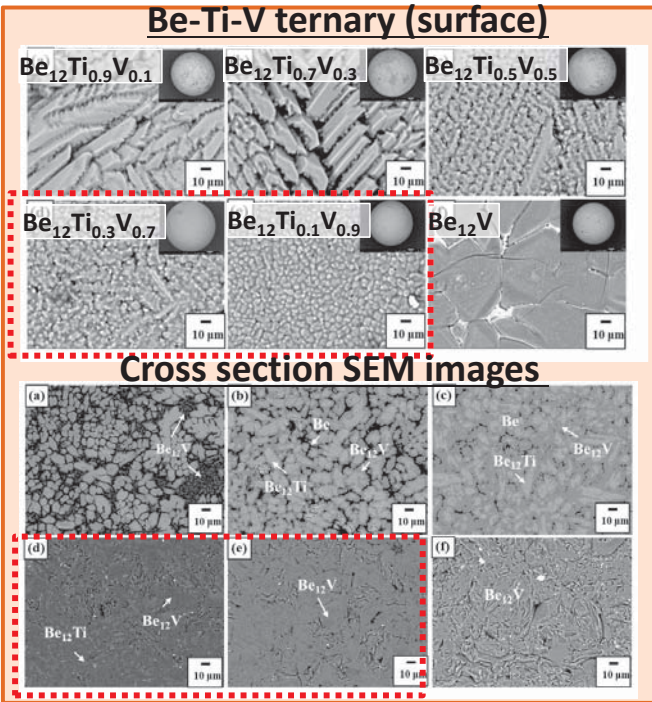


In order to solve some issues of binary beryllide pebble, R&D on ternary pebbles began

Jae-Hwan Kim | Hilton hotel, Japan | 21th Sept. 2017 | page (6/12)

3. Ternary beryllide pebble (1)

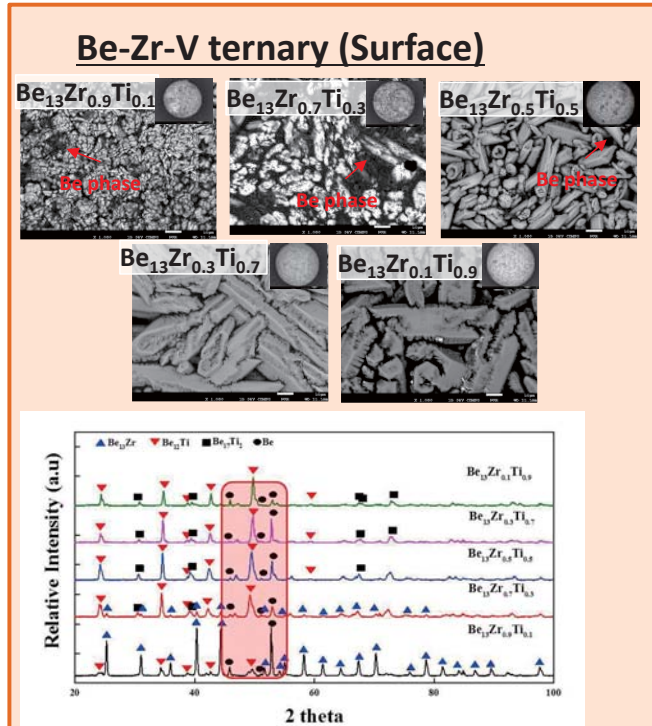
Ternary beryllide	(a) $\text{Be}_{12}\text{Ti}_{0.9}\text{V}_{0.1}$ pebble	(a) $\text{Be}_{13}\text{Zr}_{0.9}\text{Ti}_{0.1}$ pebble	Mixed $\text{Be}_{13}\text{Zr}+\text{Be}_{12}\text{Ti}$ pebble with ratio of 0.1:1, 0.2:1, 0.4:1, 0.6:1, 1:1 [Jae-Hwan Kim, M. Nakamichi, ISFNT13, Kyoto, Japan, 2017]
	(b) $\text{Be}_{12}\text{Ti}_{0.7}\text{V}_{0.3}$ pebble	(b) $\text{Be}_{13}\text{Zr}_{0.7}\text{Ti}_{0.3}$ pebble	
	(c) $\text{Be}_{12}\text{Ti}_{0.5}\text{V}_{0.5}$ pebble	(c) $\text{Be}_{13}\text{Zr}_{0.5}\text{Ti}_{0.5}$ pebble	
	(d) $\text{Be}_{12}\text{Ti}_{0.3}\text{V}_{0.7}$ pebble	(d) $\text{Be}_{13}\text{Zr}_{0.3}\text{Ti}_{0.7}$ pebble	
	(e) $\text{Be}_{12}\text{Ti}_{0.1}\text{V}_{0.9}$ pebble	(e) $\text{Be}_{13}\text{Zr}_{0.1}\text{Ti}_{0.9}$ pebble	



[Jae-Hwan Kim et al, FED, 109-111 (2016) 1764-1768] Jae-Hwan Kim | Hilton hotel, Japan | 21th Sept. 2017 | page (7/12)

4. Ternary beryllide pebble (2)

Ternary beryllide	(a) $\text{Be}_{12}\text{Ti}_{0.9}\text{V}_{0.1}$ pebble	(a) $\text{Be}_{13}\text{Zr}_{0.9}\text{Ti}_{0.1}$ pebble	Mixed $\text{Be}_{13}\text{Zr}+\text{Be}_{12}\text{Ti}$ pebble with ratio of 0.1:1, 0.2:1, 0.4:1, 0.6:1, 1:1 [Jae-Hwan Kim, M. Nakamichi, ISFNT13, Kyoto, Japan, 2017]
	(b) $\text{Be}_{12}\text{Ti}_{0.7}\text{V}_{0.3}$ pebble	(b) $\text{Be}_{13}\text{Zr}_{0.7}\text{Ti}_{0.3}$ pebble	
	(c) $\text{Be}_{12}\text{Ti}_{0.5}\text{V}_{0.5}$ pebble	(c) $\text{Be}_{13}\text{Zr}_{0.5}\text{Ti}_{0.5}$ pebble	
	(d) $\text{Be}_{12}\text{Ti}_{0.3}\text{V}_{0.7}$ pebble	(d) $\text{Be}_{13}\text{Zr}_{0.3}\text{Ti}_{0.7}$ pebble	
	(e) $\text{Be}_{12}\text{Ti}_{0.1}\text{V}_{0.9}$ pebble	(e) $\text{Be}_{13}\text{Zr}_{0.1}\text{Ti}_{0.9}$ pebble	



Preliminary Be-Zr-Ti ternary beryllides pebbles were successfully fabricated by plasma sintering method and rotating electrode method. But, unfortunately, all Be-Zr-Ti ternary beryllide pebbles contained Be phase inside the pebbles, corresponding to higher reactivity

[Jae-Hwan Kim et al, FED, 109-111 (2016) 1764-1768] Jae-Hwan Kim | Hilton hotel, Japan | 21th Sept. 2017 | page (8/12)

5. Ternary beryllide pebble (3)

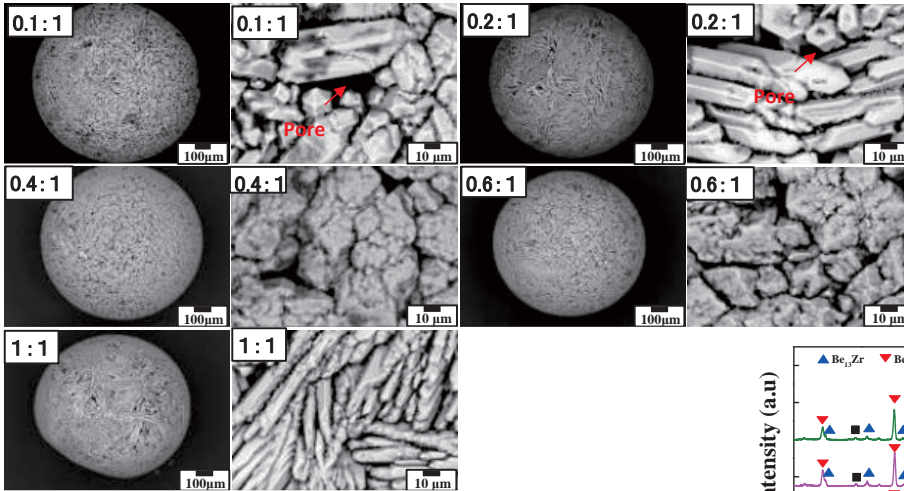
Ternary beryllide

- | | |
|--|---|
| (a) $\text{Be}_{12}\text{Ti}_{0.9}\text{V}_{0.1}$ pebble | (a) $\text{Be}_{13}\text{Zr}_{0.9}\text{Ti}_{0.1}$ pebble |
| (b) $\text{Be}_{12}\text{Ti}_{0.7}\text{V}_{0.3}$ pebble | (b) $\text{Be}_{13}\text{Zr}_{0.7}\text{Ti}_{0.3}$ pebble |
| (c) $\text{Be}_{12}\text{Ti}_{0.5}\text{V}_{0.5}$ pebble | (c) $\text{Be}_{13}\text{Zr}_{0.5}\text{Ti}_{0.5}$ pebble |
| (d) $\text{Be}_{12}\text{Ti}_{0.3}\text{V}_{0.7}$ pebble | (d) $\text{Be}_{13}\text{Zr}_{0.3}\text{Ti}_{0.7}$ pebble |
| (e) $\text{Be}_{12}\text{Ti}_{0.1}\text{V}_{0.9}$ pebble | (e) $\text{Be}_{13}\text{Zr}_{0.1}\text{Ti}_{0.9}$ pebble |

Mixed $\text{Be}_{13}\text{Zr}+\text{Be}_{12}\text{Ti}$ pebble with ratio of 0.1:1, 0.2:1, 0.4:1, 0.6:1, 1:1

[Jae-Hwan Kim, M. Nakamichi, ISFNT13, Kyoto, Japan, 2017]

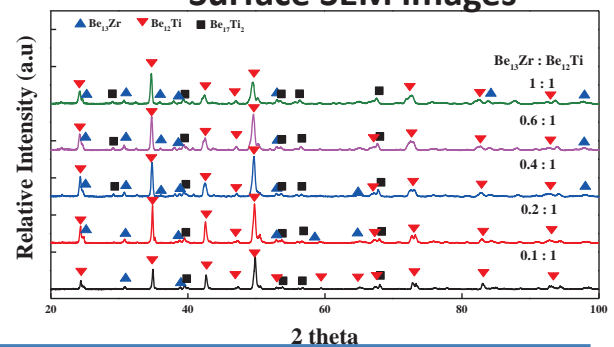
$\text{Be}_{13}\text{Zr} : \text{Be}_{12}\text{Ti}$ Surface SEM images



Unlike to $\text{Be}_{13}\text{Zr}_{1-x}\text{Ti}_x$ composition, no Be phase identified on the surface from not only SEM observation but XRD result.

Since no Be phase on the surface of pebble exists, these pebbles probably indicate better oxidation resistance as well as lower H_2 generation.

Surface SEM images



[Jae-Hwan Kim et al, FED, 109-111 (2016) 1764-1768] Jae-Hwan Kim | Hilton hotel, Japan | 21th Sept. 2017 | page (9/12)

6. Conclusion

Beryllides pebbles with different compositions have been successfully fabricated by combinational process, plasma sintering and rotating electrode method.

Using this process, we have come to try on many kinds of pebbles for searching the best pebble and are still undergoing looking for the best beryllide pebbles.

1. We successfully fabricated ternary beryllides pebbles.
2. Ternary beryllide pebbles indicated much lower H_2 generation.
3. Investigating the best beryllide pebble is continuing.
4. Collaborative studies (domestic/international) on the characterizations are always welcomed.

**Thank you for
your kind attention**

2.5.4 A Study on Heat Shock Resistance of Beryllium

K. Yonehara¹, F. Kano², M. Takiwaki², M. Nakamura¹, K. Tatenuma¹

¹ *KAKEN Co.,Ltd., 1044 Hori, Mito, Ibaraki 310-0903, Japan*

² *Toshiba Corporation, Power and Industrial Systems Research and Development Center,
8 Shinsugita-cho, Isogo-ku Yokohama 235-8523, Japan*

Abstract

For nuclear fusion reactor, it is necessary to load neutron multiplier in the blanket in order to increase tritium breeding ratio. Beryllium has been the first candidate for neutron multiplier because its melting point is particularly high among light metals and the effective cross section of (n, 2 n) reaction is large.

Beryllide(intermetallic compound of Beryllium and high melting point metal) has a small swelling by neutron irradiation and its generation ratio of hydrogen is small even when it comes into contact with high temperature water in a cooling pipe rupture accident. Neutron multiplier of Beryllium and beryllide are loaded into the blanket in the form of pebbles or blocks.

Beryllium has characteristic mechanical properties such as the brittle at room temperature but the ductility at high temperature about 500 ° C. It is important to investigate the phenomenon that occurs when it is directly reacted with water in a state of high temperature.

In this study, thermal shock damage of Beryllium is investigated for water at high temperature.

Beryllium block made by a plasma discharge sintering apparatus was cut to some thin test pieces and their surface were polished. The test piece was held at 500 ° C on a hot plate and pure water was sprayed. Evaluation of thermal shock resistance was performed by observation of cracks of specimen cooled rapidly. Several Beryllium test pieces of different sintering density block were tested.

As a result, cracks do not occur in all density test pieces, and it is founded that Beryllium is hard to crack even when quenched.

Study on Heat Shock Resistance of Beryllium

Outline

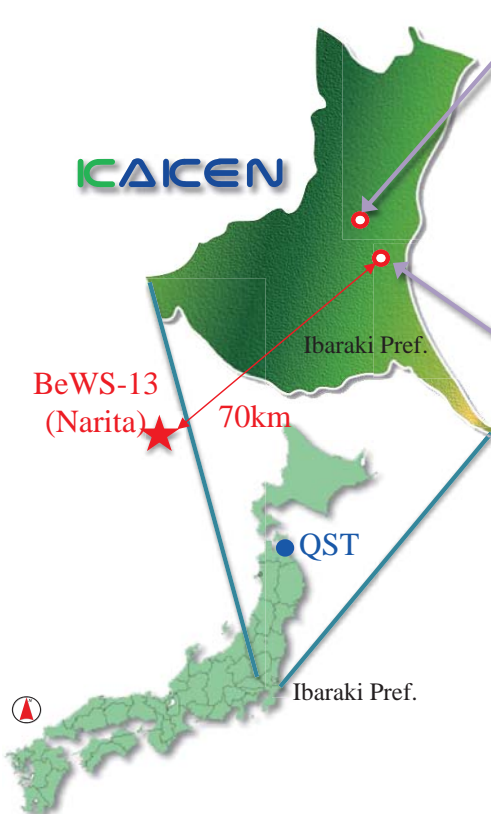
- KAKEN Co.,Ltd. profile
 - Beryllium heat shock resistance test
 - KAKEN Company products

K. Yonehara, M. Nakamura, K. Tatenuma
KAKEN Co., Ltd

1


What's KAKEN Co.,Ltd.?

KAKEN




Headquarter & Chemical Analysis Dept.: Mito Institute
[Environment, Energy, Nuclear, etc.]

- Headquarters office
- Chemical analysis department
 - Radioactivity measurement
 - Environmental pollutant analysis



R&D: **Hokota Functional-Materials Developmental Center**
[Fusion, System & equipment design, etc.]

- Design office
- Laboratory equipment R&D
- R&D of Highly Functional New Materials
- **Nuclear Fusion Materials R&D**
 - Hydrogen Isotopes(HDT) handling and separation
 - Advanced Tritium Breeder
 - **Advanced Neutron Multiplier(Beryllide)**



BeWS-13 (Narita) 70km

Ibaraki Pref.

QST

Ibaraki Pref.

2

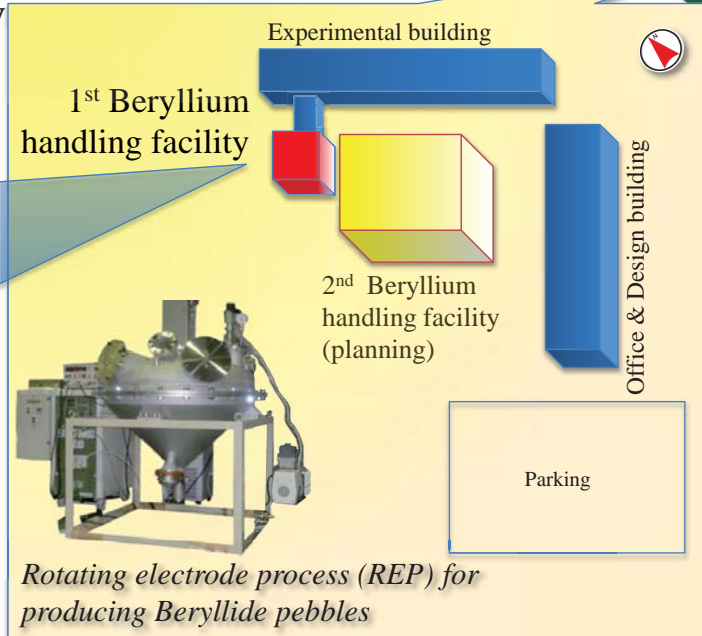
Beryllium handling facility(KAKEN)

Hokota Functional-Material Developmental Center, KAKEN



1st Beryllium handling facility for beryllides R&D

- Synthesis
 - Plasma sintering, etc.
- Treatment
 - Heating, Melting, etc.
- Machining
 - Cutting, Polishing, etc.
- Granulation
 - REM, etc.

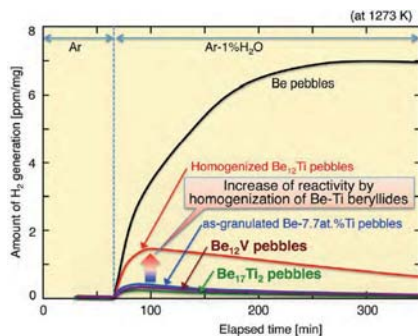


13th International Workshop on Beryllium Technology 21-22Sep., 2017 at Narita, JAPAN

Introduction of Beryllium heat shock resistance test

Concept of solid breeder Test Blanket module

Design	Neutron multiplier	breeder	coolant
JAPAN	Solid (Beryllium/Beryllide)	Solid (Li oxide type)	water
EU, China, Russia, India	Solid (Beryllium)	Solid (Li oxide type)	He
Korea	Solid (Beryllium reflector)	Solid (Li oxide type)	He



Hydrogen generation reaction of beryllides pebbles

Proceedings of the 12th International Workshop on Beryllium Technology (BeWS-12)
2.7.1 Masaru Nakamichi, Jae Hwan Kim

-Many studies have been made on the amount of hydrogen produced by the reaction of water vapor and beryllium or beryllide in high temperature at an accident.
-Beryllium heat shock resistance has not been studied so much when beryllium is rapidly cooled by water at an accident.

13th International Workshop on Beryllium Technology 21-22Sep., 2017 at Narita, JAPAN

Procedure for heat shock resistance test

Step1: Fabrication Beryllium test piece

Deferent density Beryllium blocks were fabricated by sintering, cutting, polishing



Step2: Beryllium heat shock resistance test

At Beryllium heat shock resistance test, purified water was dropped on the Beryllium test piece three times at high temperature



Step3: Observation of Beryllium test piece surface

Beryllium test piece surface were observed by Optical microscope and Secondary electron microscope(SEM)

Procedure for beryllium test piece fabrication

Step1: Sintering Beryllium blocks from Beryllium powder

Deferent density Beryllium blocks were sintered from S-65 Beryllium powder by Spark Plasma Sintering(SPS)



Step2: Cutting to Beryllium disk

Beryllium disk were cut form Beryllium blocks by Wire Electric Discharge Machine(WEDM)



Step3: Polishing of surface

Beryllium Sample surfaces were polished by Emery Abrasive Paper

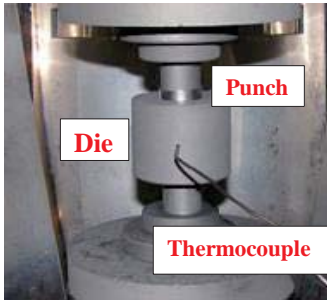


Step4: Cutting for circle test piece

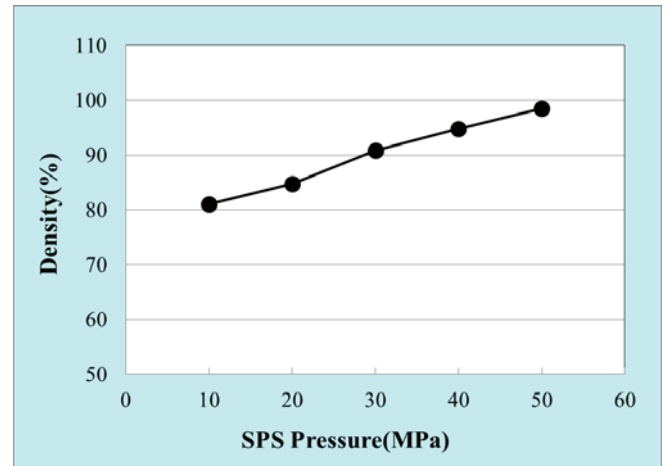
Beryllium disk were cut to ϕ 12mm diameter test piece by WEDM

Beryllium test piece fabrication

Step1: Sintering Beryllium blocks by Beryllium S-65 powder



Spark Plasma Sintering



Beryllium block density by SPS Pressure

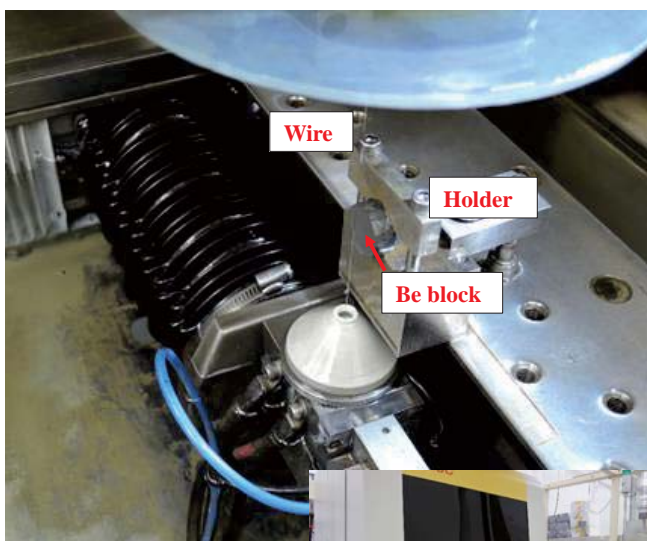
*The density was calculated from sample size and dry weight

Sintering Conditions

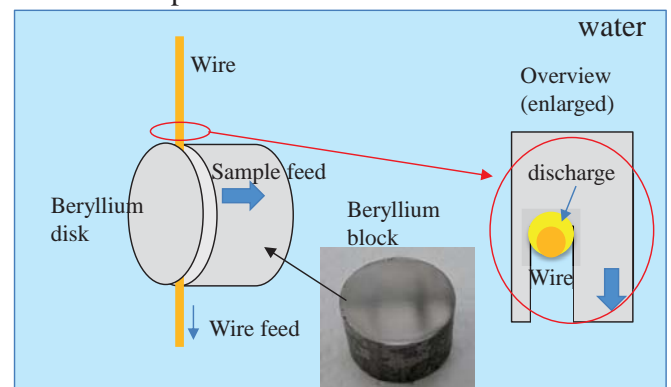
Item	Condition	
Powder	Be(99%up)	S-65 <325mesh 5.8g, Materion
Sintering Case	Die	Outer/Inner φ50/20.5mm,L40mm
	Punch	D20xL35mm
Sintering Condition	Max. Temp.	800°C
	Pressure	10-50MPa
	Max. Current	800A
	Sintering Time	20min
Beryllium Block	Size	D20xL10-12.5mm

Beryllium test piece fabrication

Step2: Cutting of Beryllium block



Principle of WEDM



WEDM
FANUC
ROBOCUT
α-0iD







- Electric discharge is generated between wire and block while feeding wire.
- Block part facing to wire is scraped by discharge.
- By moving block, Beryllium block is cut into 0.5mm thickness Beryllium disk.

Beryllium test piece fabrication

Step3: Polishing of Beryllium sample surface

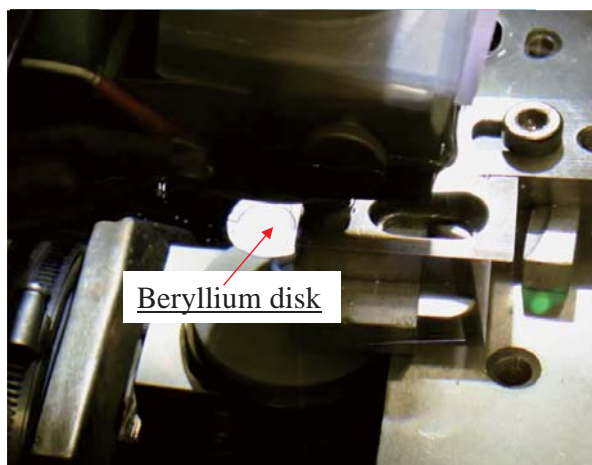
Surface oxide layers and large scratches that could affect heat shock resistance were removed with emery abrasive paper.

	Before	After
S-65 (VHP*) 5x20x1.0mm		
Beryllium disk (SPS) D20x0.5mm		

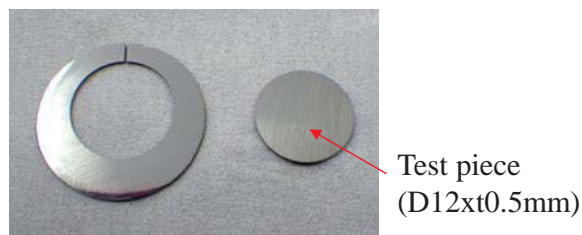
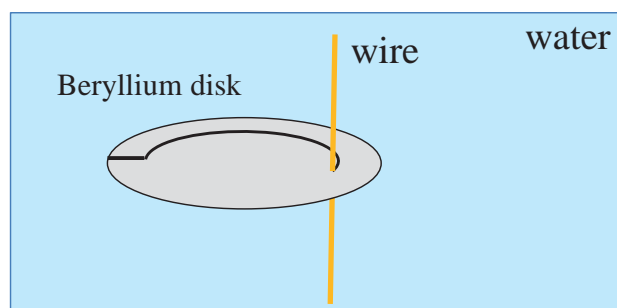
*VHP : Vacuum Hot Press

Beryllium test piece fabrication

Step4: Circle Cutting of Beryllium disk



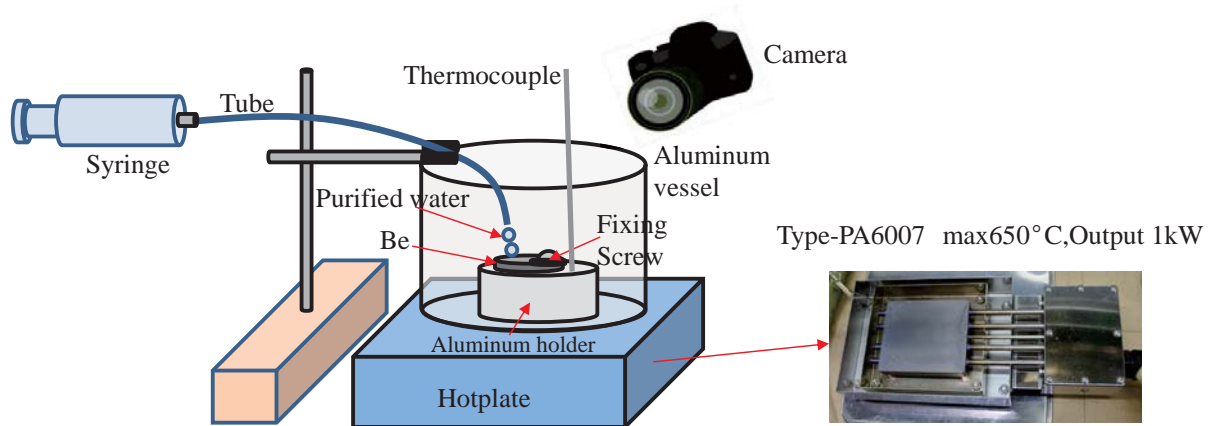
Circle cutting by WEDM



Schematic diagram of heat shock resistance test

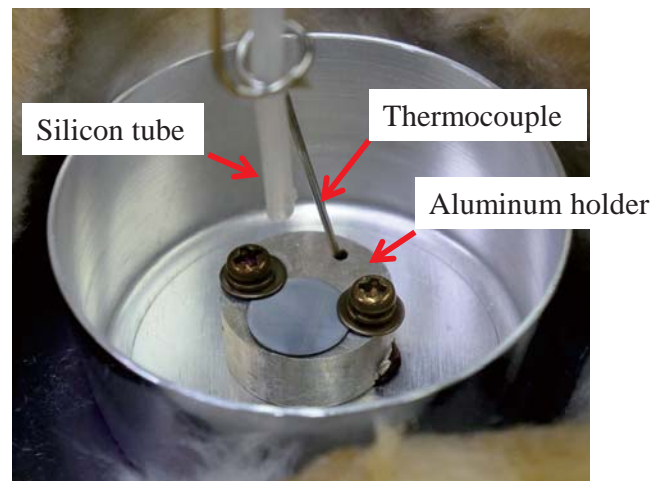
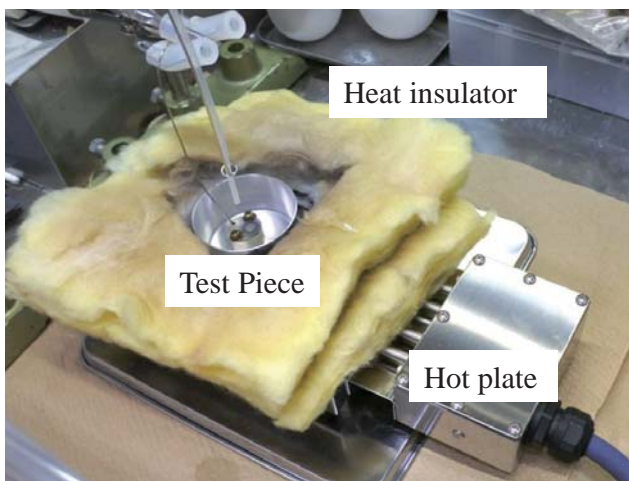
Conditions of Beryllium heat shock resistance

ITEM		Condition	
Test piece	shape	Beryllium disk	S-65 plate
	Density	85,95,99%	100%
	Size	D12x0.5mm	5x20x1mm
Temperature		500°C(Assumed operating temperature in blanket)	
Cooling Material		Purified Water 20°C	



Schematic diagram of Beryllium heat shock resistance

Actual heat shock resistance test

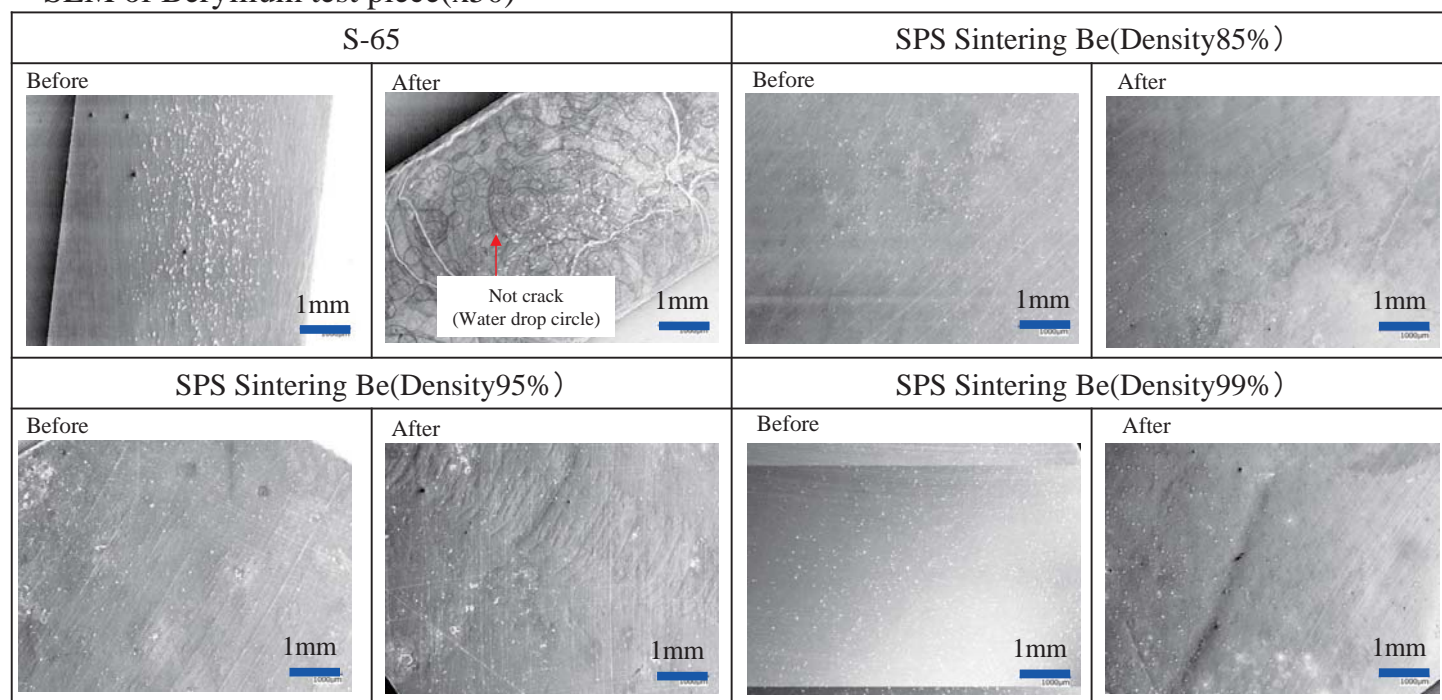


Video during heat shock test (x40speed)



Heat shock resistance test results

SEM of Beryllium test piece(x50)



- All test pieces were not cracked
- There was no difference by Beryllium test piece density

13th International Workshop on Beryllium Technology 21-22Sep., 2017 at Narita, JAPAN

13

Conclusion

1. Beryllium block density can be controlled by SPS pressure.
2. The Beryllium test pieces from 85 to 99% density are not cracked, Beryllium has high performance for heat shock resistance at 500°C.

Acknowledgments

We are grateful to Dr. F.Kano and K.Takiwaki of Toshiba Corporation for their helpful advises in summarizing this report.

Beryllium, Beryllides-related products

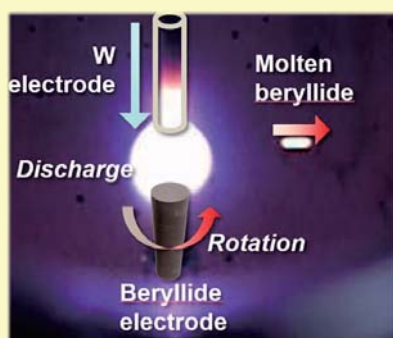
REM(Rotating Electrode Method) pebble fabrication apparatus



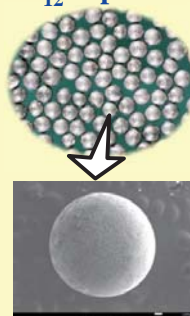
KREP-1000 D:1000mm



KREP-1500 D:1500mm



Be₁₂Ti pebble



Plasma sintering Beryllide rod fabrication apparatus



KE-Pas-III



During sintering



Be₁₂Ti rod

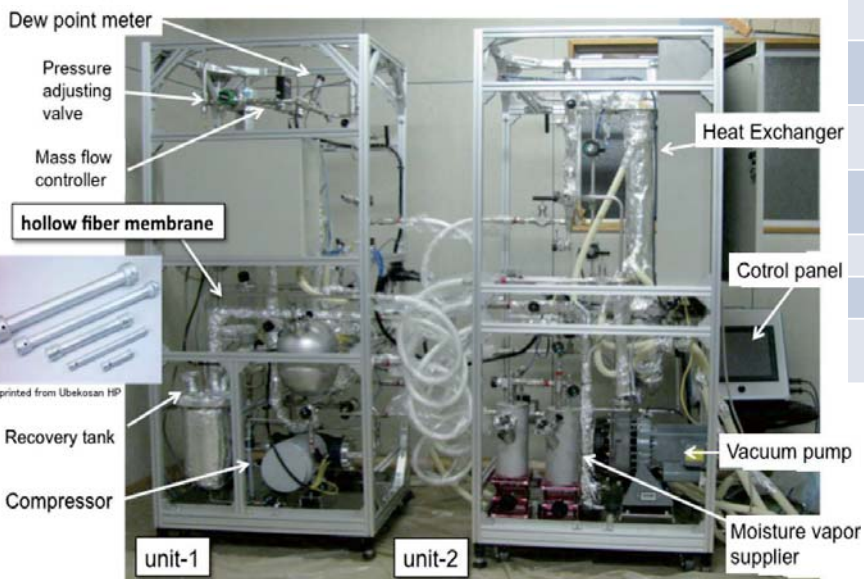
Beryllide synthesis powders at lower temperature without melting

Beryllide	Density [g/cm ³]	Be content [wt%]	Melting point [K]
Be ₁₂ Ti	2.26	69.30	1,823
Be ₁₃ Zr	2.72	56.22	2,200
Be ₁₂ V	2.37	67.98	1,973

Energy, Environment-related products

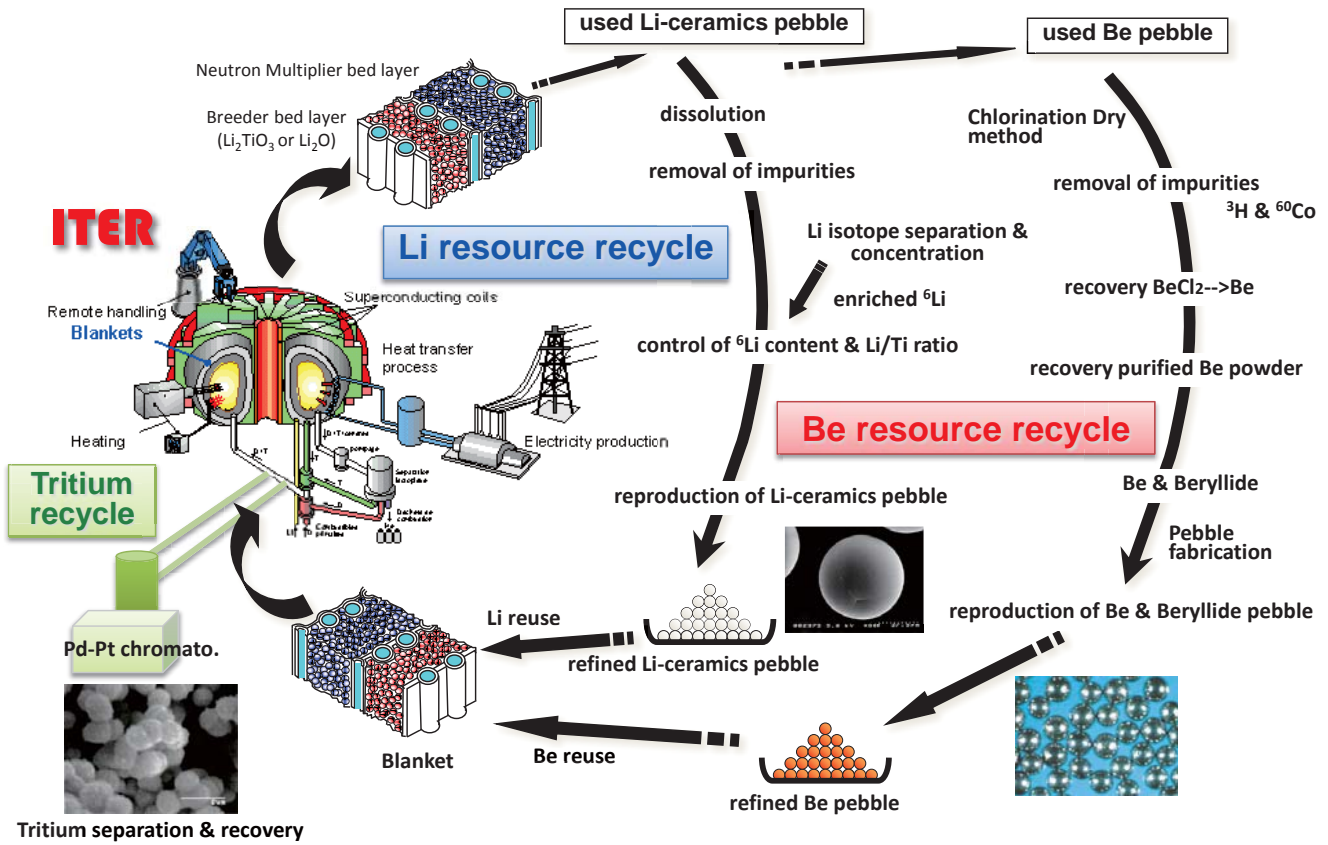
Tritium Removal equipment

Polyimide hollow fiber membrane method



Item	Spec.
Separation membrane	Polyimide hollow fiber membrane L1160 × D90
Compressed pump	Max. 140L/min. at 1atm, Discharge press 600kPa
Evacuation pump	Vacuum degree 5Pa, Exhaustion 250L/min.
Dew point / Coolant temp	Outlet -100~20° C, Inlet -40~60° C / Coolant 5° C
Gas flow rate	Processing gas 120L/min Purge gas 50L/min.
Tank vol.	Surge tank 5L Recovery tank 5L
Controller	PLC touch-panel
Size, Weight	Unit-1,2 W800 × D600 × H1800, total 300kg

Tritium(³H)/Li/Be Resource Recycle System



Thank you so much for your attention.

Kaken

2.5.5 A study on thermal process method of beryllide

N. Ikemoto, Y. Minagawa, K. Yonehara, M. Nakamura, K. Tatenuma

KAKEN Co.,Ltd., 1044 Hori, Mito, Ibaraki 310-0903, Japan

On fusion reactors, neutron multipliers multiplied neutron by DT reaction are needed to be filled in blankets to increase tritium breeding ratio. Due to beryllium has large effective cross section of (n, 2n) reaction and it has characteristically mechanical properties, it is chosen as the first candidate of neutron multipliers.

Beryllide (intermetallic compound of beryllium and high melting metals) is known as low swelling on neutron irradiation and low activity with high temperature water. For these reasons, beryllium and beryllide are important materials to achieve fusion power plants. However, their production and thermal process methods are an important issue because their shapes are assumed as microsphere.

In this study, experiments melted beryllium and beryllide are carried out using gas tungsten arc welding (GTAW). GTAW is one of a thermal process method of beryllium and beryllide, it is melted metals by occurring arc discharge between tungsten electrode and metals in high temperature plasma.

Beryllium-titanium alloy is utilized as beryllide. Beryllide powder are put into a titanium pipe, arc discharge is generated. By occurring arc discharge, powder are melted and beryllide bulk is generated.

Evaluation of shapes, compositions, and crystal structures of beryllium and beryllide bulk are reported in this workshop.

New method for beryllide production using arc plasma

N. Ikemoto, Y. Minagawa, K. Yonehara,
M. Nakamura, K. Tatenuma

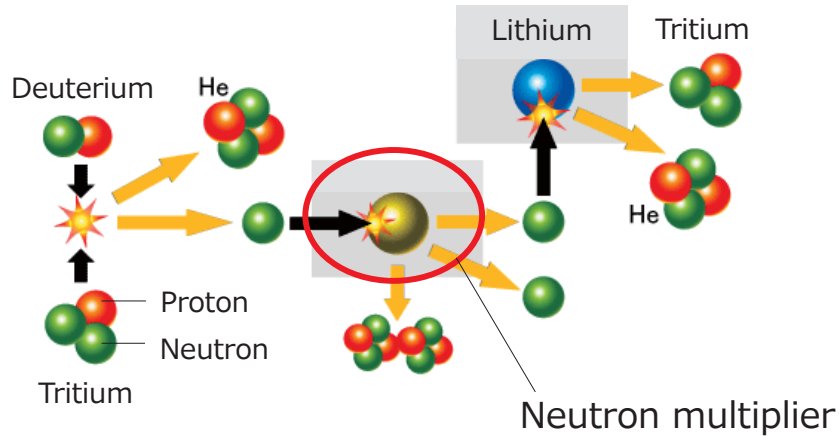
n.ikemoto@kakenlabo.co.jp
KAKEN Co.,Ltd., 1044 Hori, Mito, Ibaraki
310-0903, Japan

13th International Workshop on Beryllium Technology (BeWS-13), 21-22 September 2017 Narita, CHIBA, Japan

Contents

- Introduction
 - Background
 - Purpose
- Experiments
 - Apparatus
 - Sample
 - Condition
 - Procedure
- Results and discussion
 - Observation
 - Chemical composition
- Conclusion

13th International Workshop on Beryllium Technology (BeWS-13), 21-22 September 2017 Narita, CHIBA, Japan



Beryllium is chosen as the first candidate for neutron multiplier

- swelling on neutron irradiation
- easy to oxidize at high temperature
- chemical form → beryllide
- shapes → few mm pebbles

Need to produce beryllide pebble for fusion reactor

13th International Workshop on Beryllium Technology (BeWS-13), 21-22 September 2017 Narita, CHIBA, Japan

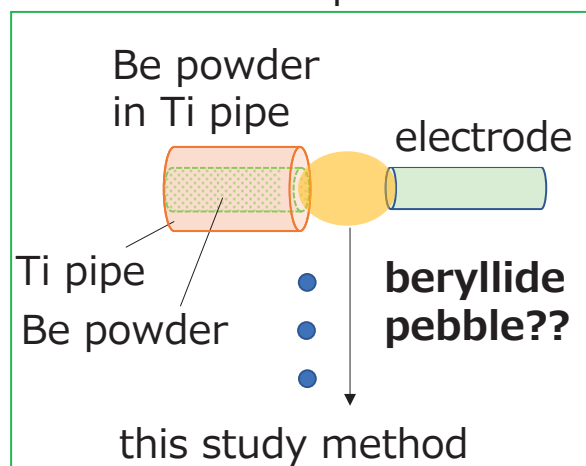
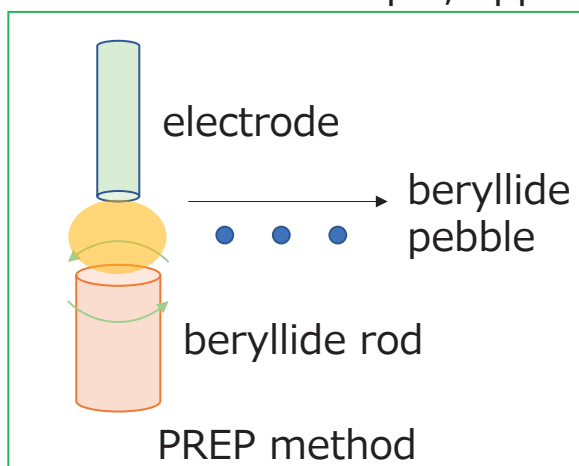
Purpose of this study

Produce beryllide pebble

We develop another method (right figure) with reference to plasma rotated electrode process (PREP, left figure).

Advantages of our method,

- due to easy to fabricate sample, need not to produce beryllide rod.
- not rotated sample, apparatus structure is simple.



13th International Workshop on Beryllium Technology (BeWS-13), 21-22 September 2017 Narita, CHIBA, Japan

Experiment apparatus

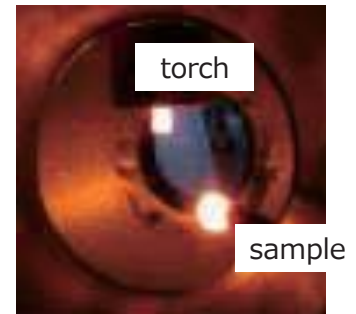
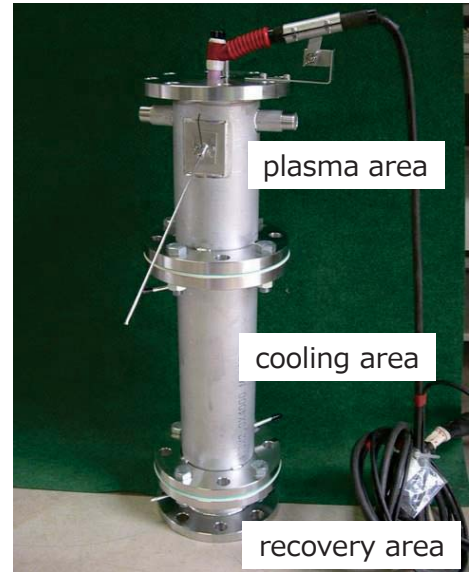
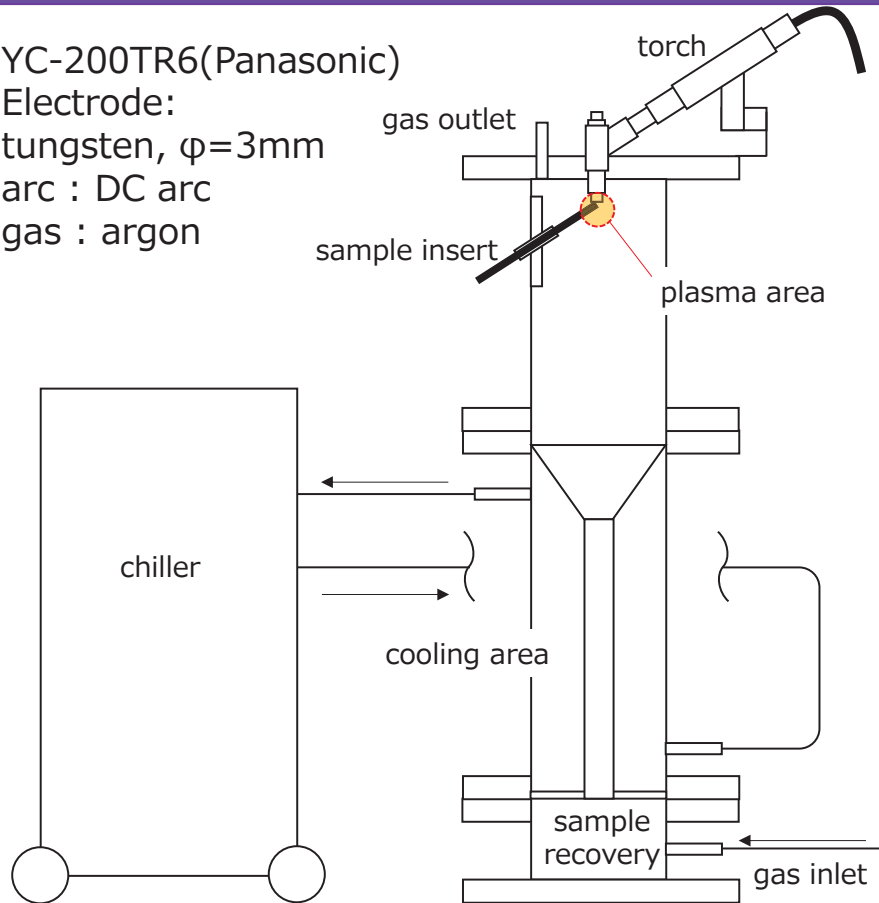
YC-200TR6(Panasonic)

Electrode:

tungsten, $\phi=3\text{mm}$

arc : DC arc

gas : argon



13th International Workshop on Beryllium Technology (BeWS-13), 21-22 September 2017 Narita, CHIBA, Japan

Sample preparation

$\phi=3.18\text{mm}$
SUS304 pipe

$\phi=1\text{mm}$
Al wire

Ti wire
 $\phi=1\text{mm}$

Strand
Al-Ti wire
Molar ratio of
Al:Ti \approx 1:1

Be powder
t=0.05mm
 $\phi=2\text{mm}$
L=200mm

Ti wire in
SUS304 pipe

Fill a Ti pipe
with 0.7g of
Be powder

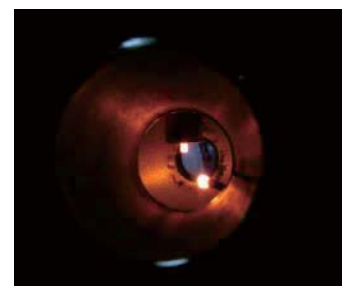
13th International Workshop on Beryllium Technology (BeWS-13), 21-22 September 2017 Narita, CHIBA, Japan

Experiments are carried out the following conditions.

	Number	Materials	Ar flow (L/min)	Current (A)
Mono metal	1	SUS304 pipe	15	100
	2	Aluminum wire		
2 types metal	3	Titanium wire/ SUS304 pipe	15	100
	4	Titanium wire/ Aluminum wire		
Beryllide	A	Beryllium powder/ titanium pipe	10	100
	B		15	100
	C		20	100
	D		15	150

13th International Workshop on Beryllium Technology (BeWS-13), 21-22 September 2017 Narita, CHIBA, Japan

Fabricate experimental sample



Molten sample by arc plasma

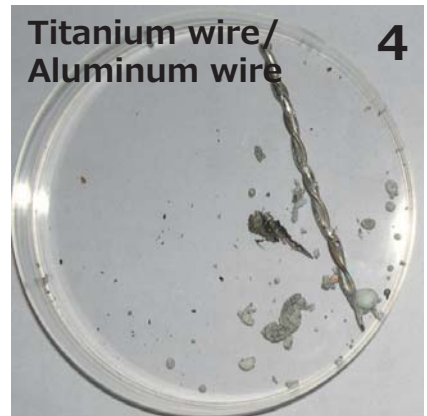
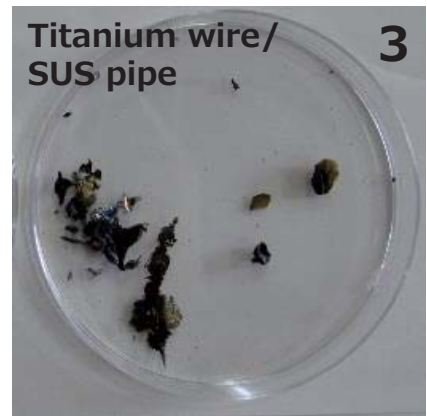
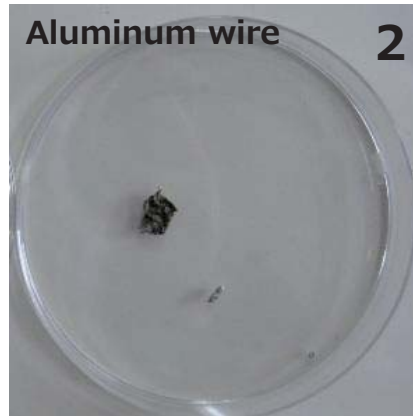
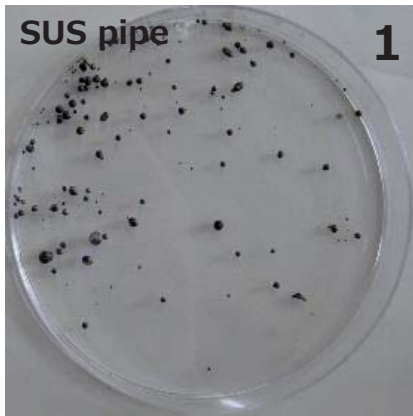
Recover cooled sample



Observe sample surface by X-ray diffraction

13th International Workshop on Beryllium Technology (BeWS-13), 21-22 September 2017 Narita, CHIBA, Japan

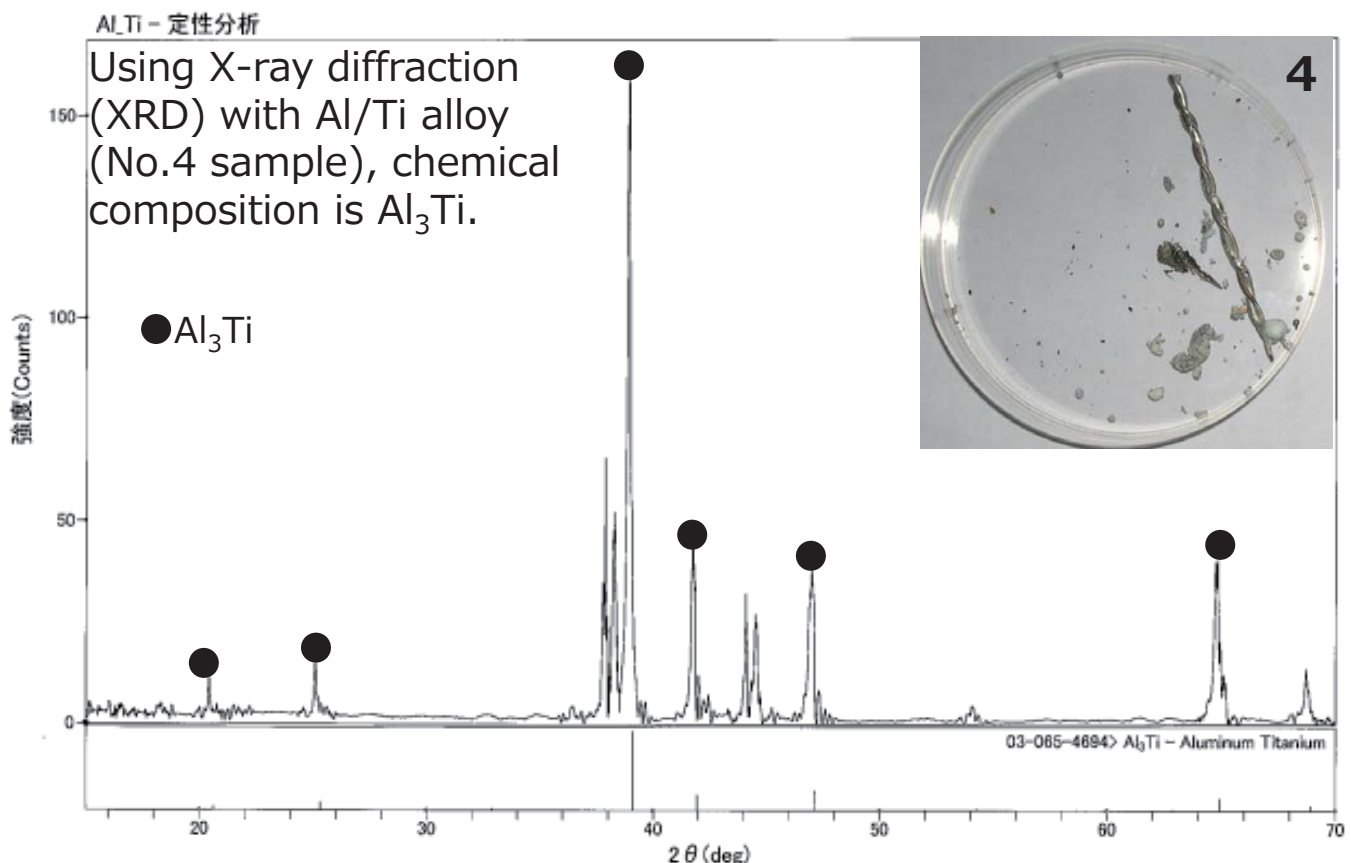
Results and discussion (pre-experiments)



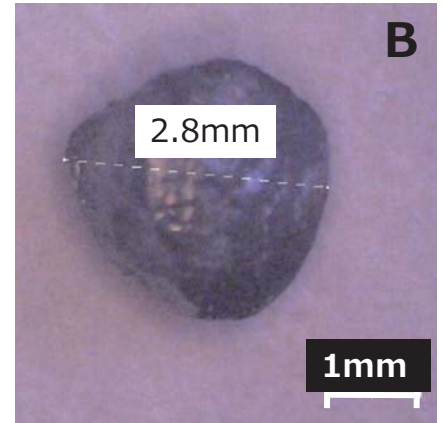
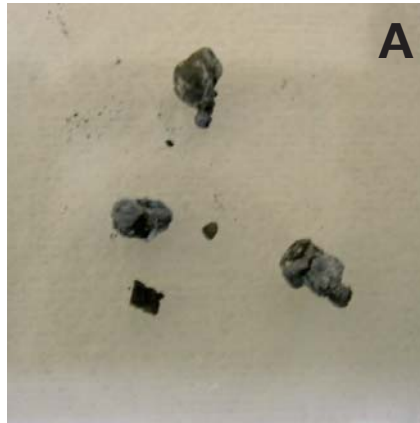
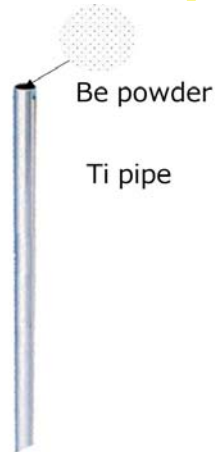
1. Some of $\phi 1 \sim 2$ mm pebbles are recovered.

2-4: Derived not spherical shapes.

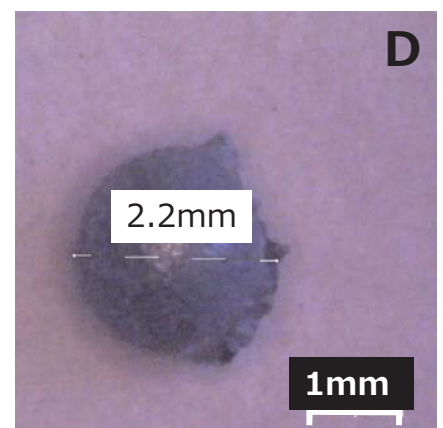
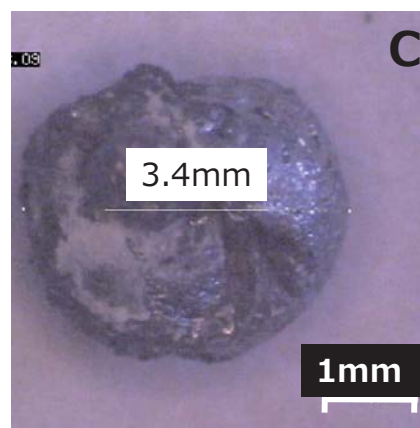
Results and discussion (pre-experiments)



Results and discussion (beryllide experiments)

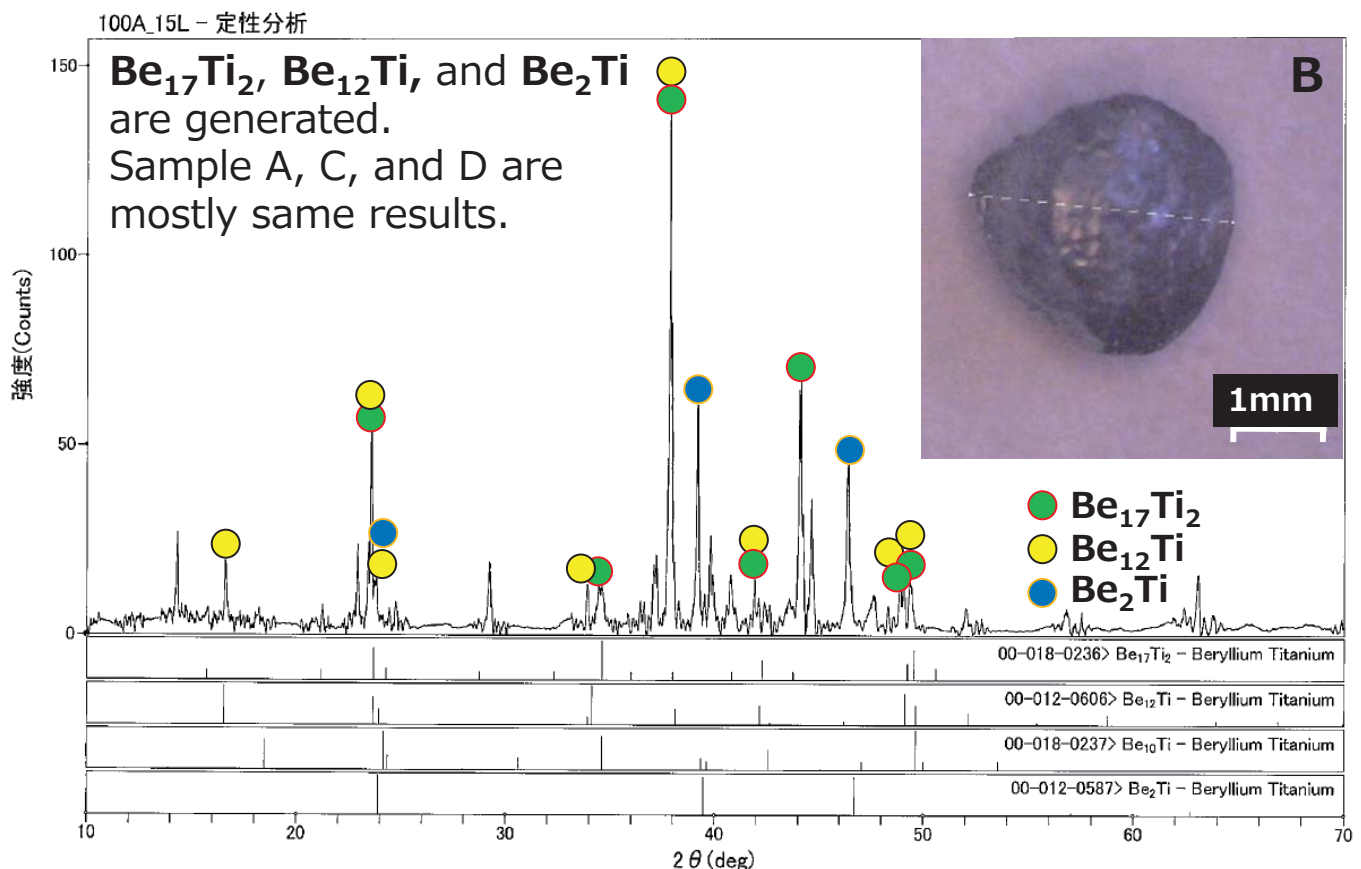


Number	Ar flow (L/min)	Current (A)
A	10	100
B	15	100
C	20	100
D	15	150



13th International Workshop on Beryllium Technology (BeWS-13), 21-22 September 2017 Narita, CHIBA, Japan

Results and discussion (beryllide experiments)



13th International Workshop on Beryllium Technology (BeWS-13), 21-22 September 2017 Narita, CHIBA, Japan

We try to produce beryllide (beryllium alloy with titanium) pebble in this study by arc welding.

- Pre-experiments especially a condition used only SUS pipe, we succeed to produce few mm pebbles.
- Beryllide experiments, we produce beryllide, but their shapes are not spherical.



Since uniform melting of samples are not possible due to difference of the heat capacity between beryllium and titanium, unstable shapes are derived.

Future works

- Modify length of cooling area will be longer than present apparatus.
- By melting samples, the distance between sample and tungsten electrode are far and far. Therefore, we will construct a mechanism to provide sample with distance between sample and electrode are constant.
- Since uniform melting is difficult with the shape of sample used in this study, we need to consider sample shapes to melt uniform.

13th International Workshop on Beryllium Technology (BeWS-13), 21-22 September 2017 Narita, CHIBA, Japan

Thank you for listening!

2.5.6 Thermal Conductivity of Compressed Binary Beryllium Pebble Beds

J. Reimann¹, A. Goraieb², H. Harsch³

¹ Karlsruhe Institute of Technology, Institute for Applied Materials- Applied Materials Physics (IAM-AWP), P.O. Box 3640, 76021 Karlsruhe, Germany

² Karlsruhe Beryllium Handling Facility (KBHF GmbH), Herrmann-von-Helmholtz-Platz 1, 76344 Eggenstein-Leopoldshafen, Germany

³ Bruker AG, Wikingenstr.13 76189 Karlsruhe, Germany
E-mail: joerg.reimann@partner.kit.edu

For advanced DEMO fusion reactors with ceramic breeder blankets, the use of binary pebble beds both for the ceramic breeder material and the beryllium material is attractive because of the higher pebble bed density (larger tritium breeding ratio) and the larger thermal conductivity (larger thermal blanket efficiency) compared to mono-sized pebble beds.

Measurements of the thermal conductivity k of binary beryllium pebble beds were performed using the HECOP facility at Forschungszentrum Karlsruhe. The pebbles have mean diameters of 2 and 0.15mm and were manufactured by Brush Wellman. The measurements of k were carried out as a function of pebble bed deformation (uniaxial strain ϵ) at temperatures of 280 and 550°C.

Similar to the results previously obtained for mono-sized pebble beds [1,2], a linear relationship between k and ϵ was obtained, $k = A\epsilon + k_0$, where k_0 is the conductivity for non-compressed beds. Compared to mono-sized beds, the slope A is about 2 times larger and k_0 is reasonably predicted by the SBZ model and the modified UCLA model. The temperature dependence of k is negligible within the investigated temperature range. The proposed correlation is

$$k(\text{W/mK}) = 3.5 + 17.6\epsilon(\%).$$

Although binary pebble beds have distinct advantages compared to mono-sized pebble beds, it must be proven that the thermal-mechanical behaviour for blanket relevant bed dimensions does not deteriorate during temperature cycling.

References

- [1] J. Reimann, G. Piazza, Z. Xu, A. Goraib, H. Harsch; FZKA 7096 (2005)
- [2] J. Reimann, G. Piazza, H. Harsch; Fusion Engineering and Design 81, p. 449 (2006)

Thermal Conductivity of Compressed Binary Beryllium Pebble Beds

J. Reimann¹, A. Goraieb², H. Harsch³

¹ Karlsruhe Institute of Technology, Institute for Applied Materials- Applied Materials Physics (IAM-AWP), P.O. Box 3640, 76021 Karlsruhe, Germany

² Karlsruhe Beryllium Handling Facility (KBHF GmbH), Hermann-von-Helmholtz-Platz 1, 76344 Eggenstein-Leopoldshafen, Germany

³ Bruker AG, Wikingenstr.13 76189 Karlsruhe, Germany

E-mail: joerg.reimann@partner.kit.edu

Abstract

For advanced DEMO fusion reactors with ceramic breeder blankets, the use of binary pebble beds both for the ceramic breeder material and the beryllium material is attractive compared to mono-sized pebble beds because of the higher pebble bed density and the larger thermal conductivity which both result in a larger tritium breeding ratio.

Measurements of the thermal conductivity k in the bulk of binary beryllium pebble beds are presented using the HECOP facility at the Karlsruhe Institute of Technology, KIT, the former Forschungszentrum Karlsruhe. The pebbles have mean diameters of 2 and 0.15mm and were manufactured by Materion, the former Brush Wellman company. The measurements of k were carried out as a function of pebble bed deformation (uniaxial strain ϵ) at temperatures of 280 and 550°C.

Similar to the results obtained previously for mono-sized pebble beds, a linear relationship between k and ϵ was obtained, $k = k_0 + A\epsilon$, where k_0 is the conductivity for non-compressed beds. Compared to mono-sized beds, the slope A is about 2 times larger and k_0 is reasonably predicted by the SBZ model and the modified UCLA model. The temperature dependence of k is negligible within the investigated temperature range. The proposed correlation is

$$k(\text{W/mK}) = 3.5 + 17.6\epsilon(\%).$$

Although binary pebble beds have distinct advantages compared to mono-sized pebble beds, it must be proven that the thermal-mechanical behaviour for blanket relevant bed dimensions does not deteriorate during temperature cycling.

1. Introduction

For advanced DEMO fusion reactors with ceramic breeder blankets the use of binary pebble beds (BPBs) is foreseen for both the ceramic breeder material and the beryllium material, required as a neutron multiplier [1]. BPBs consist of pebbles with two different mean diameters, d_1 , d_2 , with $d_1/d_2 \geq$

7. Compared to mono-sized pebble beds (MPBs), BPBs are characterised by a higher pebble bed density and a larger thermal conductivity which both result in a larger tritium breeding ratio.

Temperature differences and different thermal expansion coefficients between pebble beds and structural materials and swelling due to irradiation cause constrained strains, which result in elastic and plastic pebble deformations. These deformations influence significantly the thermal conductivity of beryllium pebble beds because of the large ratio of the beryllium conductivity to the helium gas conductivity. For ceramic breeder pebble beds, this ratio is much smaller and consequently the influence of deformation is small [2].

The modelling of the thermal-mechanical interaction between pebble beds and structural material requires as essential input data, among others, the dependence of the thermal conductivity of beryllium pebble beds on temperature and deformation state, see e.g. [3,4]. Although the deformations are caused by stresses imposed on the pebbles, the stress is not a primary quantity because there is no unique relationship between stress and strain. At elevated temperatures, thermal creep occurs and different deformation states can exist for the same stress value, for details, see [5]. As in previous work [6], the pebble bed strain ϵ is considered as the prime parameter and the dependence of the thermal conductivity k as a function of strain ϵ and temperature T is investigated.

For MPBs consisting of beryllium pebbles of fairly spherical shape with a narrow range of diameter variation, results from several investigations exist on the thermal conductivity for both non-compressed and compressed pebble beds; an overview was given by [6].

For beryllium BPBs, the data base is much smaller. The only existing data with non-compressed and slightly compressed BPBs were published by [7, 8] using an axis-symmetric test set-up with a radial heat flux from a centric heater rod through the annular pebble bed to the cooled cylindrical shell. Pebble bed compression is generated by temperature differences between the hot inner zone and the cooled outer structure. With this set-up, the achievable deformations are relatively small, deformations are not directly measured and cannot be controlled independently of temperature.

For the investigations reported in the present paper, the HECOP-facility was used as for the MPBs experiments using 1mm NGK beryllium pebbles [6, 9]. This facility is a combination of uniaxial compression test set-up and a heat transfer measurement system. The uniaxial set-up offers the possibility to vary and measure independently temperature, pebble bed pressure (uniaxial stress), and pebble bed deformation (uniaxial strain). An attractive feature of the HECOP-facility is that the thermal conductivity can be also measured during the thermal creep period. Further experimental details and results on thermal creep are presented by [5].

In the following, thermo-mechanical properties such as thermal conductivity, creep, etc are considered as bulk values, that is, the values are relevant for the pebble bed zone sufficiently far away from walls where no regular packing structures exist. For ideal mono-sized spheres these regular structures can persist in the total container space as determined recently by tomography experiments [10]. For MPBs consisting of NGK beryllium pebbles produced by the rotating electrode process with

diameter d between 0.8 and 1.2mm, this structured zone has a thickness of $<4d$ [11] as visualized best by measured void distributions, see Fig. 1.

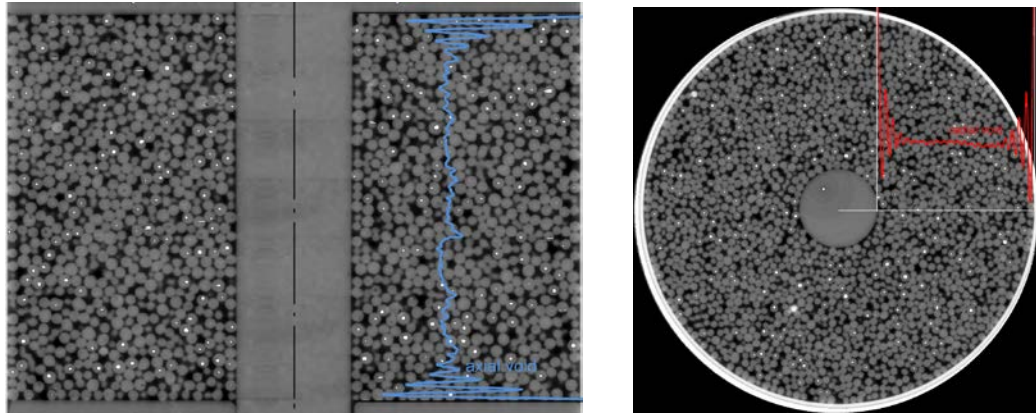


Fig. 1. Tomographic image with void distributions (Be pebble bed; annular container volume), from [11].

For BPBs, structured zones are even less developed because the small pebbles fill the voids generated by the large pebbles. This results in a large difference of the void distribution especially in the first wall layer zone of the large spheres [12].

It is general practice to extrapolate the bulk thermal conductivity to the wall and to take into account the different packing condition at the wall by the heat transfer coefficient h . Without going into detail, it can be stated that for beryllium BPB, especially in the compressed state, h is expected to be so large that temperature resistances can be neglected.

More recently, other beryllium materials than mentioned above became of interest: i) pebbles consisting of intermetallic beryllium alloys, beryllides, see e.g. [13], and ii) beryllium pebbles consisting of non-spherical shapes [11]. For beryllides, thermal conductivities were only measured for the solid materials [14,15], values for pebble bed conductivities were assessed by appropriate models, e.g. [16]. It showed that for all kinds of beryllides, the thermal conductivity is lower than for pure beryllium. In respect to i), screening tests of the pebble bed conductivity were performed using the hot wire technique [15]. Compared to the NGK pebble beds, the thermal conductivity is lower caused by i) the softer bed behavior (smaller stress σ for a given strain ε value), and, ii) the generation of smaller contact surfaces because of the non-regular shapes.

Thermomechanical properties depend on the container packing fraction γ which itself depends on filling and densification procedures and container dimensions. For fusion reactor blankets, large packing fractions are desired; filling and densification issues are discussed in detail by [5,11,17].

2. Experimental apparatus and procedure

Figure 2 shows a schematic drawing of the HECOP set-up. The pebble bed (diameter $D = 130\text{mm}$, height $H \approx 60\text{mm}$) is positioned between the pistons of a hydraulic press with a maximum pressure of 3.6MPa . Within the pebble bed, 4 capillaries (2mm outer diameter) are located at different bed heights; each of them contains 5 thermocouples at different radial positions.

For thermal control, a system of 7 heaters (H1...H7) is used. The desired temperature gradient in the pebble bed is imposed by the heaters H2 and H4 at the bottom and by the heaters H1 and H3 at the top.

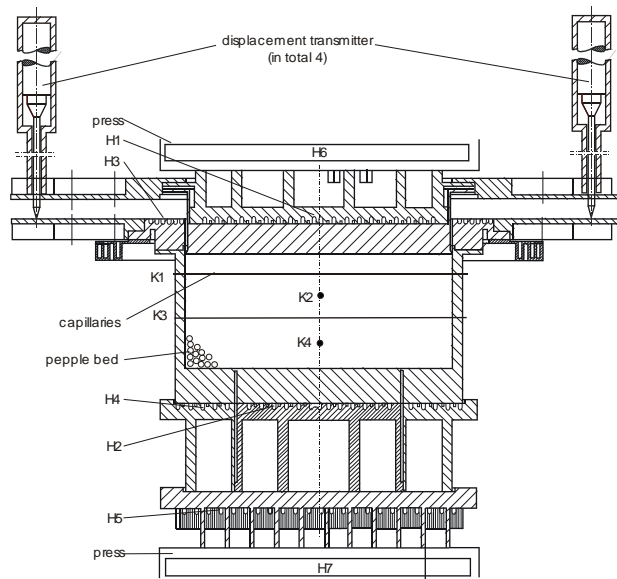


Fig. 2. Set-up of HECOP facility.

The heat flux Q [W/m^2] generated by H2 within a diameter of 80mm is used to determine the thermal bed conductivity k by

$$k(\text{W}/(\text{mK})) = (Q - Q_{\text{loss}}) \Delta x / \Delta T \quad (1),$$

where Δx (m) is the axial distance between bed thermocouples and ΔT (K) is the corresponding temperature difference. Q_{loss} is the residual heat loss.

H3 and H4 are used to minimise radial heat losses by controlling the heating power in such a way that the temperature difference between two neighbouring thermocouples becomes zero.

Heater H5 is used to minimise the axial heat flow from H2 to the press bottom plate, and is again controlled such that the temperature difference of a thermocouple pair in H2 and H5 becomes zero. The highest bed temperatures are reached by additionally using the heaters H6 and H7.

The set-up is thermally insulated by refractory ceramic fibre (Kerlane) and is operated in a glove box with a helium atmosphere of 0.1MPa .

Detailed temperature calculations show that residual radial and axial heat losses are unavoidable. These heat losses depend on both mean pebble bed temperature and pebble bed conductivity.

The investigated BPBs consisted of the same types of beryllium pebbles as used in previous experiments from [8]: large pebbles with diameters of 2mm +/- 0.3mm and small pebbles of 0.1-0.2mm in diameter, both produced by the company Brush Wellman, for details, see [5].

Special attention was paid on the filling procedure and the start-up phase of the experiments because the scatter of the thermal conductivity data found in literature depends sensitively on these features, especially for non-compressed beds.

The filling procedure is described in more detail in [5]. Table 1 shows the values of the achieved packing fractions γ , defined as ratio of pebbles volume to total volume.

Table 1

	large pebbles (l)	small pebbles (s)
diameter (mm)	2+/-0.3	0.15+/-0.05
density ρ (g/cm ³)	1.831	1.806
packing fraction γ (1)	0.635+/-0.005	0.183+/-0.005

In order to start the experiment, the upper piston was brought in contact with the pebble bed surface using a very small pressure of about 0.02MPa. Keeping this pressure constant, the system was heated up to the desired bed temperatures. The temperature differences between bottom and top plates were $\Delta T \approx 15$ or $\approx 30^\circ\text{C}$. Larger values were avoided because this could have resulted in non-uniform thermal creep behavior in the bed.

Test series were performed at mean bed temperatures of 280°C and 550°C. At the lower temperature level, thermal creep is negligible, different strain values were obtained by increasing stepwise the uniaxial stress. For each strain value, both a k measurement and an isothermal experiment ($\Delta T=0$) were performed. The latter were used in order to determine the heat losses Q_{loss} . At 550°C, isothermal measurements were taken when creep rates became negligible.

3. Results

3.1 Present experiments

Experiments at 280°C: Figure 3 shows a characteristic result of an UCT: the curves for uniaxial stress σ (piston pressure) increase and stress decrease differ characteristically. During stress increase, irreversible displacements of pebbles and elastic and plastic pebble deformation occur, resulting in

larger bed deformations (strain ϵ) compared to the stress decrease period, where the pebble bed expands only slightly due to elastic forces. The effect of temperature on the stress-strain dependence is discussed in [Rei17a].

At the positions of the small plateaus both Q_{loss} and k measurements were performed. The k values are listed besides the curve in Fig. 3. The strong increase of k with increasing stress is obvious. During stress decrease, k remains at quite high values; even at the very small stress value of ≈ 0.2 MPa, k is still ≈ 9 W/mK which is significantly larger than the corresponding value during the pressure increase period. This characteristic behaviour of was also observed for MPBs using 1mm beryllium pebbles [6].

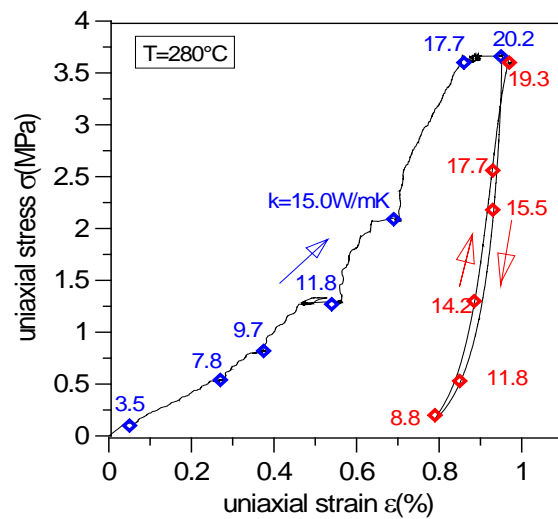


Fig. 3. Uniaxial compression test (UCT) with BPB at $T=280^{\circ}\text{C}$ and corresponding thermal conductivity data.

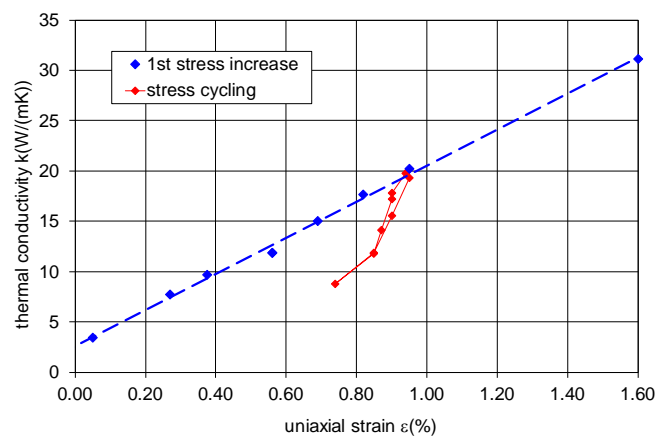


Fig. 4. Thermal conductivity k as a function of uniaxial strain ϵ for $T=280^{\circ}\text{C}$.

Figure 4 shows all results for $T=280^{\circ}\text{C}$ in a graph with k and ϵ as coordinates. As observed for MPBs, all data for the first pressure increase period are well fitted by a straight curve. The data point

at $\varepsilon \approx 1.6\%$ was obtained after the experiment at 550°C where larger ε values could be obtained because of thermal creep.

This figure shows also the results from Exp 5.1 for pressure cycling. There is no remarkable hysteresis for the pressure decrease and increase curves, compare also Fig. 3.

Experiment at 550°C : The time dependence of the experimental data is shown in Fig. 5. All data were taken every ten seconds. At a minimum pressure of 0.02MPa , Q_{loss} was first determined. Then, the temperature differences within the pebble bed were adjusted to measure k . After this, the pressure was increased with a ramp of $0.33\text{MPa}/\text{min}$ to 1.3MPa . This value was kept constant for about 5300min followed by a pressure increase to 3.6MPa . After further 1250min , the pressure was decreased with a small ramp of $0.1\text{MPa}/\text{min}$ to 0.2MPa and, after a period of about 200min , increased again to the maximum value. The continuous recording of the strain ε shows the expressed creep rates after each pressure increase. At the end of the periods with $p = \text{const}$, Q_{loss} measurements were performed. These data were used to evaluate k for a neighbouring point.

The continuous evaluation of k requires the knowledge of the actual heat loss. These values were interpolated from the individual Q_{loss} measurements. This procedure was already successfully applied recently [6]. For the present experiment at $T = 550^\circ\text{C}$, the heat losses could be well fitted by

$$Q_{\text{loss}} = 0.78Q \quad (2).$$

The evaluation of k by Eqs. (1) and (2) requires that the system is in thermal equilibrium. This requirement is the less fulfilled in periods following pressure increase steps (periods with exhibited strain gradients).

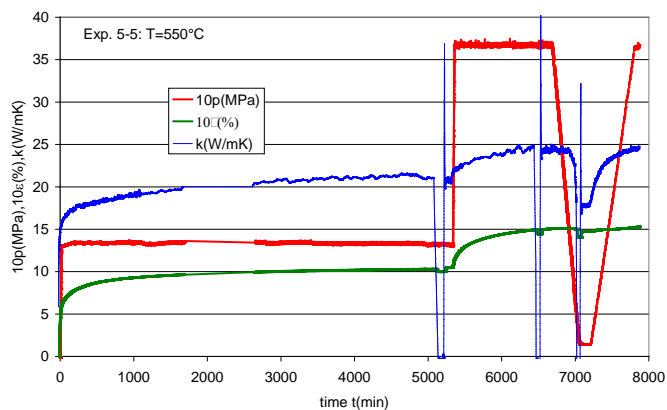


Fig. 5. Measured quantities as a function of time for experiment at $T=550^\circ\text{C}$.

Figure 5 contains also the continuous recording of k . The drops of the curve at large t results from the Q_{loss} experiments; the corresponding k values are physically not meaningful. Figure 6 shows the k values as a function of ε . Again, a fairly linear dependence of k on ε is observed.

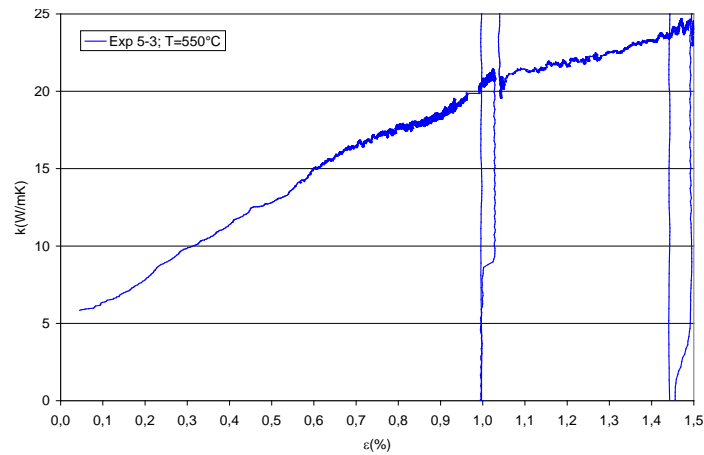


Fig. 6. $k = f(\epsilon)$ from transient evaluation ($T=550^{\circ}\text{C}$).

Some comments to thermal cycling in blanket relevant pebble beds. The results presented above for pressure cycling using a UCT facility is not generally relevant for temperature cycling in pebble beds blankets. In this case, the thickness of the beryllium pebble beds is about 30mm; the dimensions in the two other directions are much larger. Because of the varying inclination of these beds in the torus, there are always cases where one large dimension is close to the vertical direction. The temperatures are highest in the inner zone of the pebble bed and the largest irreversible deformations, enforced by thermal creep occur there. In addition, pebbles might agglomerate in this zone. Close to the wall, the pebble temperatures are the lowest. After blanket cool-down, small gaps might form between the pebble bed bulk and the wall and small pebbles might slip downwards and give rise to sedimentation (and a ratcheting process). The use of BPBs in blankets requires, therefore, further detailed experimental investigations with blanket relevant geometries.

3.2. Comparison with previous experimental data

Figure 7 shows a summary of the thermal conductivity results for the pressure increase phase for 280 and 550°C. For 550°C, only the measurements performed in thermal equilibrium are listed. The observed temperature influence is neglectable, therefore, the following correlation is proposed:

$$k(\text{W/mK}) = 3.5 + 17.6\epsilon(\%) \quad (3).$$

Compared to previous data for MPBs (1 or 2mm diameter beryllium pebbles) [6,9], it is obvious that the BPB data are much higher; the slope of the curve is larger by a fraction of 2.

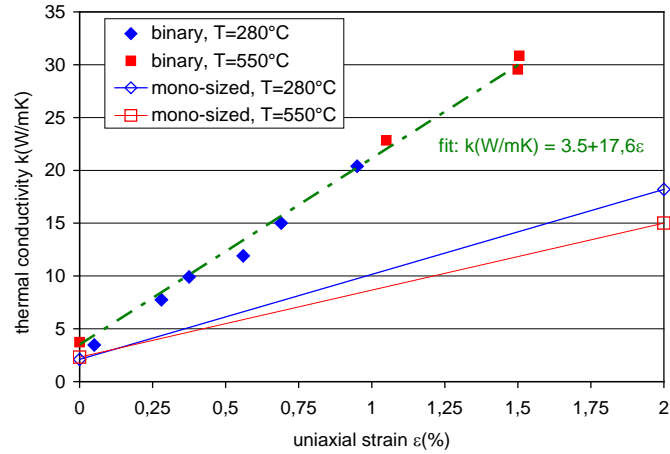


Fig. 7. Summary of experimental data for BPBs and comparison with MPBs.

Figure 8 shows results from [7] for non-compressed BPBs. The values from different experiments differ; an expressed temperature dependence is not observed.

Figure 9 shows corresponding results [Dal8] for compressed BPBs. Characteristic is that the curve starts from a high value; after the first internal pressure reduction (realised by temperature reduction), the value for non-compressed beds is considerably reduced. For the subsequent pressure increase, a distinct hysteresis is observed for case (a), but not for (b).

Comparing the present results with those from [Dal8] it is obvious that the latter ones are generally larger, especially at low deformations. This difference is attributed to the fact that in these experiments during both the filling period and measurement period a certain

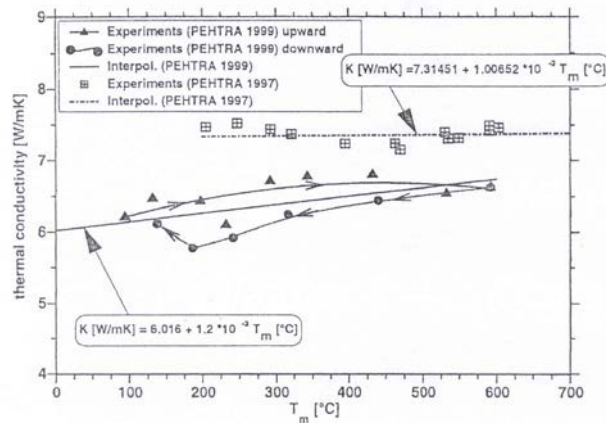
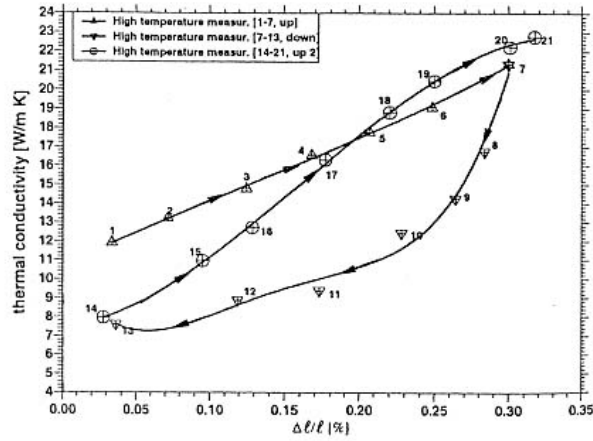
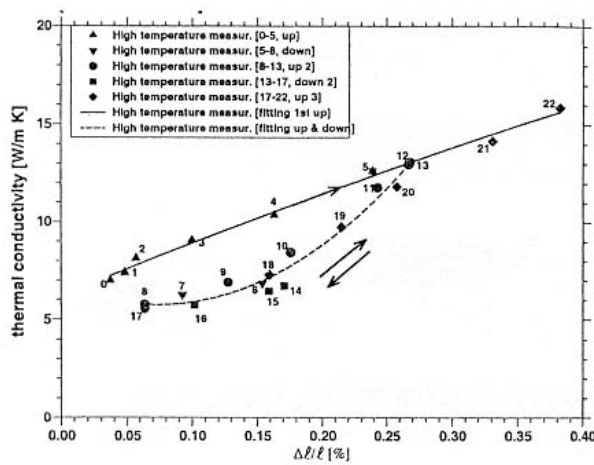


Fig. 8. Results from [7] for non-compressed binary beryllium pebble beds.



a)



b)

Fig. 9. Results from [8] for compressed BPBs.

degree of compression existed by using a piston at top of the vertical test section with a constant pressure of 0.2MPa.

In the present experiments, the pebble beds were prepared in such a way, that in the initial state the beds can be considered as being non-compressed. For non-compressed MPBs, there are several data sets from different experiments, compare [6,9]. A good agreement with these data was obtained using the present test facility and filling procedure. The observed differences for the BPBs are, therefore, referred mainly to non-defined initial conditions in the test facility used by [8].

3.3. Modelling of thermal conductivity of BPBs

Experimental data for non-deformed MPBs are well fitted by the SBZ model [16]. The dependence of k from strain ε was expressed by an empirical correlation [6].

For non-compressed BPBs, the SBZ model proposes to use a mean diameter and the actual packing fraction $\gamma_{total} = \gamma_1 + \gamma_s$. The UCLA model [18] has a different approach: the pebble bed

primarily consists of large spheres arranged in an orthorhombic way ($\gamma_1=0.635$). The interspaces between the large pebbles are filled with the small spheres being in the gas atmosphere; the thermal conductivity of this mixture is determined by calculations assuming again an orthorhombic sphere packing ($\gamma_s=0.635$). Close to the contacts between the large spheres the gaps are so small that the pebbles cannot penetrate. For this zone, the gas conductivity is relevant. Therefore, the conductivity in the interspaces is determined from these two contributions. Finally, the thermal conductivity of the pebble bed consisting of the large pebbles is calculated.

The basis of the UCLA model is used in the following, however, with the several modifications; the most important ones are:

- The experimentally determined packing fractions are used, see Table 1,
- The SBZ model is used both for the conductivity of the interspace and the large pebble bed.

The thermal conductivity of the interspace is given by

$$k_{\text{intersp}} = N_c (A_{\text{gap}}/A_{\text{sp}})k_g + (1 - N_c (A_{\text{gap}}/A_{\text{sp}}))k_{\text{SBZ}} \quad (4a).$$

k_{SBZ} is determined for the small pebbles with d_s and the effective packing fraction γ_{eff} :

$$\gamma_{\text{eff}} = \gamma_s (1 + V_{\text{eff}}/V_{\text{sp}}) / V_{\text{eff}}/V_{\text{sp}} \quad (4b),$$

with

$$V_{\text{eff}}/V_{\text{sp}} = (1 - \gamma_1)/\gamma_1 - N_c V_{\text{gap}}/V_{\text{sp}} \quad (4d).$$

N_c is the number of contacts of a spherical pebble with other pebbles; the gap volume where the small pebbles cannot penetrate, normalised with the volume of a large pebble is:

$$V_{\text{gap}}/V_{\text{sp}} = (3/2)d_s^2(d_1 - (2/3)d_s)/d_1^3 \quad (4e).$$

The ratio of large sphere surface to total sphere surface is given by:

$$A_{\text{gap}}/A_{\text{sp}} = d_s(d_1 - d_s/4)/d_1^2 \quad (4f).$$

Now the SBZ model is applied again with d_1 , γ_1 and using k_{intersp} instead of the usual gas conductivity.

With the values from Table 1 and $N_c=7$ [19], a packing fraction of $\gamma_s = 0.522$ is obtained. This value is considerably smaller than the value assumed in the original UCLA model. Furthermore, the surface fraction of the large pebbles in the narrow gaps (where no small pebbles exist) is 51.5% which is significantly larger than the original value.

Figure 10 shows a comparison between calculated values and present measurements. Both models predict a negligible T dependence. The present results are in between the predictions. It is interesting to note that experiments with binary aluminium pebble beds from [20] resulted also in smaller values than the predictions with the original UCLA model.

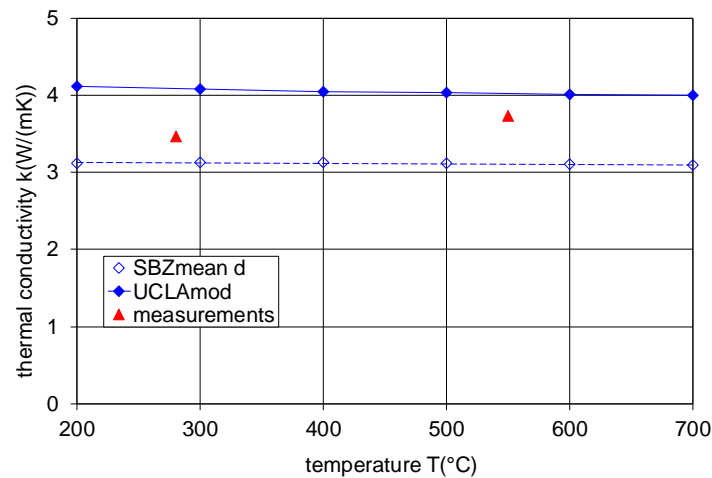


Fig. 10. Comparison between experimental results for non-compressed BPBs with model predictions.

4. Conclusions

Measurements of the thermal conductivity of binary beryllium beds were performed with independent variation of strain and temperature. Similar to previous results with mono-sized beds, a linear dependence between k and strain was obtained. Compared to mono-sized beds, the slope of the curve is larger by about a fraction of 2.

The conductivity of the non-compressed binary bed is between the predictions from the SBZ model using a mean diameter and the modified UCLA model. The measured values are significantly lower than previous measurements where probably a significant precompression during the filling procedure existed.

In respect to thermal conductivity (and beryllium density), binary beds appear to be superior to mono-sized pebble beds. Before using binary beds in blankets, it should be investigated if during thermal cycling the performance of binary beds with blanket relevant dimensions will change.

References

- [1] Y. Yanagi, S. Sato, M. Enoeda, T. Datano, S. Kikuchi, T. Kuroda, Y. Kosaku, Y. Ohara, Nuclear and thermal analyses of supercritical-ware-cooled solid breeder blanket for fusion DEMO reactor, *J Nuclear Sci. and Techn.*, Vol.38, No.11 (2001) 1014-1018.
- [2] J. Reimann, S. Hermsmeyer, Thermal conductivity of compressed ceramic breed pebble beds, *Fusion Eng. Des.* 61-62 (2002) 345-351.
- [3] Y. Gan, F. Hernandez, D. Hanaor, R. Annabattula, M. Kamlah, P. Pereslavtsev, A thermal discrete element analysis of EU solid breeder blanket subjected to neutron irradiation, *Fusion Science Techn.* 66 (2014) 83-80.
- [4] F. Cismondi et al., The fundamental role of fluid dynamic analyses in the design of the solid EU Test blanket module, *Fusion Eng. Des.* 87 (2012) 1123-1129.
- [5] J. Reimann, A. Goraieb, H. Harsch, Thermal creep behavior of compressed beryllium pebble beds, this conference.
- [6] J. Reimann, G. Piazza, Z. Xu, A. Goraib, H. Harsch; Measurements of the thermal conductivity of compressed beryllium pebble beds, *FZKA 7096*, (2005).
- [7] M. Dalle Donne, G. Piazza, A. Goraieb, G. Sordon, Measurement of the thermal conductivity and heat transfer coefficients of a binary bed of beryllium pebbles, in: 3rd International Workshop on Beryllium Technology for Fusion, Mito, Oct. 22–24, 1997, *JAERI-Conf.* 98-101.
- [8] M. Dalle Donne, A. Goraieb, G. Piazza, F. Scaffidi-Argentina, Measurements of the heat parameters in infiltrated binary beryllium beds: Comparison between the results with PEHTRA and Super-PEHTRA, *Fusion Technology*, Vol. 38, No. 3 (2000) 310-319.
- [9] J. Reimann, G. Piazza, H. Harsch; Thermal conductivity of compressed beryllium pebble beds, *Fusion Eng. Des.* 81 (2006) 449-454.
- [10] J. Reimann, J. Vicente, E. Brun, C. Ferrero, Y. Gan, A. Rack, X-ray tomography investigations of mono-sized sphere packing structures in cylindrical containers, *Powder Techn.* 318 (2017) 471-483.
- [11] J. Reimann, A. Abou-Sena, E. Brun, B. Fretz, Packing experiments of beryllium pebble beds for the fusion reactor HCPB blanket, *Proc. 11th Int. Workshop Beryllium Technol.*, P. Vladimirov & J. Reimann (Eds.), *KIT Scientific Reports 7686*, (2014).
- [12] F. Scaffidi-Argentina et al., Non-destructive three-dimensional analysis of the packing of a binary beryllium pebble bed, *Fusion Eng. Des.* 58–59 (2001) 707–712.
- [13] H. Kawamura et al., Application of beryllium intermetallic compounds to neutron multiplier of fusion blanket, *Fusion Eng. Des.* 61-62 (2002) 391-397.
- [14] M. Uchida, E. Ishitsuka, H. Kawamura, Thermal conductivity of neutron irradiated Be₁₂Ti, *Fusion Eng. Des.* 69 (2003) 499-503.
- [15] J. Reimann et al., Beryllides for Fusion Reactors, *SOFE-Conference*, San Diego, USA, June 1-5, (2009).

- [14] M. Uchida, E. Ishitsuka, H. Kawamura, Thermal conductivity of neutron irradiated Be₁₂Ti, *Fusion Eng. Des.* 69 (2003) 499-503.
- [16] E. Schlünder, Particle heat transfer, Proc 7th Int. Heat Transfer Conf., München, Germany, 1982, Vol1, RK10, (1982) 195-212.
- [17] J. Reimann, B. Fretz, S. Pupleschi, Thermo-mechanical screening tests to qualify beryllium pebble beds with non-spherical pebbles, *Fusion Eng. Des.* 98-99 (2015) 1851-1854.
- [18] A. Adnani, I. Catton A. R. Raffray, M. A. Abdou, Effective thermal conductivity of binary mixtures at high solid to gas conductivity ratios, *Chem. Eng. Comm.*, Vol. 120, (1993) 45-58.
- [19] J. Reimann; R. A. Pieritz; C. Ferrero; M. di Michiel, R. Rolli, X-ray tomography investigations on pebble bed structures, *Fusion Eng. Des.* 83 (2008) 1326-1330.
- [20] C.E.Tickle, Measurements of the thermal conductivity of metal-gas particle beds for solid breeder blankets, UCLA-FNT-34, University of California, Los Angeles, (1990).

2.5.7 Thermal Creep of Compressed Binary Beryllium Pebble Beds

J. Reimann¹, A. Goraieb², H. Harsch³

¹ Karlsruhe Institute of Technology, Institute for Applied Materials- Applied Materials Physics (IAM-AWP), P.O. Box 3640, 76021 Karlsruhe, Germany

² Karlsruhe Beryllium Handling Facility (KBHF GmbH), Herrmann-von-Helmholtz-Platz 1, 76344 Eggenstein-Leopoldshafen, Germany

³ Bruker AG, Wikingenstr.13 76189 Karlsruhe, Germany
E-mail: joerg.reimann@partner.kit.edu

For advanced fusion reactors with ceramic breeder blankets, the use of binary pebble beds (BPs) for both the ceramic breeder material and the beryllium material is attractive because of the larger tritium breeding ratio and the larger thermal conductivity, compared to mono-sized pebble beds (MPBs).

Expanding thermal creep experiments with beryllium MPBs [1], binary pebble beds have been performed consisting of Brush Wellman beryllium pebbles with mean diameters of 2 and 0.2mm in a temperature range between ambient temperature and 650C. Pressures were varied between 1.3 and 3.6MPa.

Results on the stress σ – strain ϵ dependence for the initial compression/pressure release period are presented and a correlation for the temperature dependent modulus of deformation was developed.

For thermal creep strain, the following correlation is proposed for blanket relevant creep time periods:

$$\epsilon_{cr}(\%) = 4.7 \exp(-3735/T(K)) \sigma(\text{MPa})^{0.62} t(\text{min})^{0.33}$$

Compared to MPBs consisting of 1mm beryllium pebbles, the present 2mm MPBs are softer. Adding the 0.2mm pebbles, the BPs become stiffer and thermal creep becomes smaller.

References

- [1] J. Reimann, H. Harsch, Fusion Engineering and Design, 75-79, p.1043 (2005)

Thermal Creep of Compressed Binary Beryllium Pebble Beds

J. Reimann¹, A. Goraieb², H. Harsch³

¹ Karlsruhe Institute of Technology, Institute for Applied Materials- Applied Materials Physics (IAM-AWP), P.O. Box 3640, 76021 Karlsruhe, Germany

² Karlsruhe Beryllium Handling Facility (KBHF GmbH), Hermann-von-Helmholtz-Platz 1, 76344 Eggenstein-Leopoldshafen, Germany

³ Bruker AG, Wikingenstr.13 76189 Karlsruhe, Germany

E-mail: joerg.reimann@partner.kit.edu

Abstract

For advanced DEMO fusion reactors with ceramic breeder blankets, the use of binary pebble beds for both the ceramic breeder material and the beryllium material is attractive because of the larger tritium breeding ratio compared to mono-sized pebble beds (MPBs).

Experiments with binary pebble beds (BPBs) have been performed consisting of Materion, formerly Brush Wellman, beryllium pebbles with mean diameters of 2 and 0.15mm in a temperature range between ambient temperature and 650C. Pressures were varied between 1.3 and 3.6MPa.

Results on the stress σ – strain ε dependence for the initial compression and pressure release period are presented and a correlation for the temperature dependent modulus of deformation is given.

For thermal creep strain, the following correlation is proposed for blanket relevant creep time periods:

$$\varepsilon_{cr}(\%) = 4.7 \exp(-3735/T(K)) \sigma(\text{MPa})^{0.62} t(\text{min})^{0.33}$$

Compared to 1mm beryllium MPBs, the present 2mm MPBs are softer. Adding the 0.2mm pebbles, the BPBs become stiffer and thermal creep becomes smaller.

1. Introduction

The thermo-mechanical behaviour of blanket components is described by computer codes using i) finite element models, FEM, based on continuum mechanics (pebble beds considered as pseudo-homogeneous materials), and, ii) discrete element models, DEM, which model the interaction between all individual pebbles, see e.g. [1].

For both types of codes, the knowledge of thermo-mechanical pebble bed properties is required. In FEM codes, these properties are directly used as input data; in DEM code development, these data serve as validation basis.

The dependence of thermo-mechanical pebble bed properties (most important: stress-strain relations for stress increase and decrease cycle, thermal creep and thermal conductivity) as a function of relevant parameters must be known both for the beginning of reactor operation, BOL, and, including the effect of irradiation, for the end of reactor operation, EOL.

At present, the data base of these pebble bed properties is quite sufficient for BOL and mono-sized pebble beds, MPBs, consisting of beryllium and ceramic breeder pebbles. For EOL, results from individual irradiated pebbles become presently available which will be used for the assessment of pebble bed data.

With FEM codes the thermo-mechanical behavior was described of a) blanket mock-ups, however without taking into account thermal creep [2], and b) small multiple-effect experiments, modelling also thermal creep [3]. At present, DEM codes are well suited to describe e.g. stress-strain behavior, pebble cracking [4] and wall heat transfer [5]. In the future, results from DEM might be useful to simplify FEM codes in order to reduce computing time.

For advanced DEMO ceramic breeder blankets, the use of binary pebble beds, BPBs is foreseen both for the ceramic breeder and the beryllium material, required as neutron multiplier [7]. BPBs consist of pebbles with two different mean diameters, d_1 and d_2 , where $d_1/d_2 \geq 7$. Compared to mono-sized pebble beds MPBs, BPBs are characterised by a higher pebble bed density and a larger thermal conductivity which both result in a larger tritium breeding ratio.

In contrast to MPBs, the pebble bed data base for BPBs is poor. Results on thermal conductivity of beryllium BPBs are presented in another paper [8]. For MPBs consisting of NGK beryllium pebbles of fairly spherical shape with diameters d between 0.8 and 1.2mm, thermal creep was investigated by [9] resulting in a correlation where thermal creep strain was expressed as a function of temperature, stress and time. Only screening data existed for beryllium BPBs [10].

For the investigations reported in this paper, the same uniaxial test set-up was used (HECOP-facility) as for the MPBs experiments [11]. A uniaxial set-up offers the possibility to independently vary and measure temperature, pebble bed pressure (uniaxial stress), and pebble bed deformation (uniaxial strain). An attractive feature of the HECOP-facility is that the thermal conductivity can be also measured during the thermal creep period [12].

2. Experimental

The BPBs consist of beryllium pebbles of two different sizes, fabricated by Materion, the former Brush Wellman company:

- Pebbles with diameters of 2 ± 0.3 mm, produced as intermediate product in the beryllium production with the method of Mg reduction of BeF_2 ,
- Pebbles with diameters between 0.1-0.2mm produced by melting and spraying in inert gas.

Due to different manufacturing processes, the impurity contents differ as well as the material densities, cf Table 1. Figure 1 shows a cut through a compressed pebble bed, from [10]: the large pebbles are of fairly spherical shape with indentations on the surface and a variety of coarse pores. The small pebbles are by far less regular than the large ones.

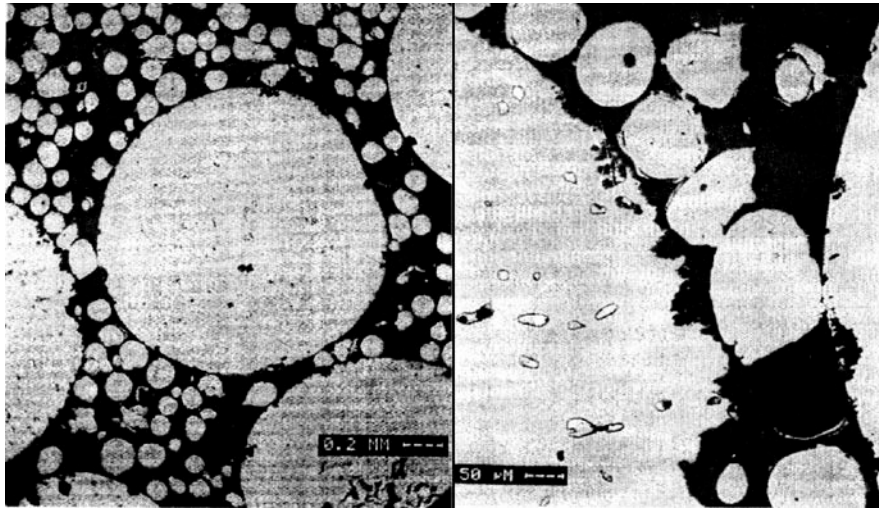


Fig. 1. Beryllium BPB (2mm and 0.15mm pebbles) after an UCT at T=470°C, from [10].

In the HECOP II facility the pebble bed (diameter $D = 130\text{mm}$, height $H \approx 60\text{mm}$) is positioned between the pistons of a hydraulic press with a maximum pressure of 3.6MPa.

Using binary beds, special attention must be paid on the filling procedure in order to avoid swimming-up of large pebbles (penetration of small pebbles into the gaps between large pebbles). For filling, the pebble bed container is moved horizontally by a special handling tool and deposited on a vibrating

Table 1: Pebble characteristics and packing factors

	large pebbles (l)	small pebbles (s)
diameter (mm)	2+/-0.3	0.15+/-0.05
density ρ (g/cm ³)	1.831	1.806
packing factor ϕ	0.635+/-0.005	0.183+/-0.005

Table 2: Experimental parameters

Exp No	T (°C)	σ_{max} (MPa)	t_{increase} (min)	σ_i rate (MPa/min)
5.1	25	3.40	11	0.032
5.2	280	3.40	*	*
5.3	550	1.34	18	0.074
5.4	450	3.35	68	0.047
5.5	550	2.7	40	0.067
5.6 MPB	550	2.7	40	0.067
5.7	650	0.7	20	0.035
5.8	650	2.04	21	0.097

* different values; thermal conductivity measurements

device. After filling the large pebbles into the cylindrical cavity, the pebble bed was vibrated with 50Hz with variable amplitudes. Then, a perforated sheet was mounted on the pebble surface in order to fix the positions of the pebbles when pouring in and vibrating the small pebbles. Finally, the sheet was removed and the pebble container was moved into the press of the HECOP facility. The values of the obtained packing factors are shown in Table 1.

The pebble beds were heated up to the desired temperature level T and then uniaxially compressed with a constant stress increase (σ_i) rate up to the maximum stress value σ_{max} , see Table 2. In contrast to previous experiments these ramps were much smaller and differed for different experiments.

3. Results

3.1. Stress-strain relations during pressure increase/decrease periods

Fig. 2 shows the UCT results at ambient temperature for different kinds of pebble beds. Common for all curves are the characteristic differences between the first uniaxial stress σ (piston pressure) increase period and the subsequent stress decrease period. During stress increase, irreversible displacements of pebbles and elastic and plastic pebble deformation occur, result in larger pebble bed deformations (strain ϵ) compared to the stress decrease period, where the pebble bed expands only slightly due to elastic deformations. The curves for additional stress cycles are similar to that of the first stress decrease branch; the hysteresis is small.

The stress-strain relationships obtained by UCTs are important for pebble bed models in order to describe the thermo-mechanical behaviour during the first thermal cycles of blanket operation.

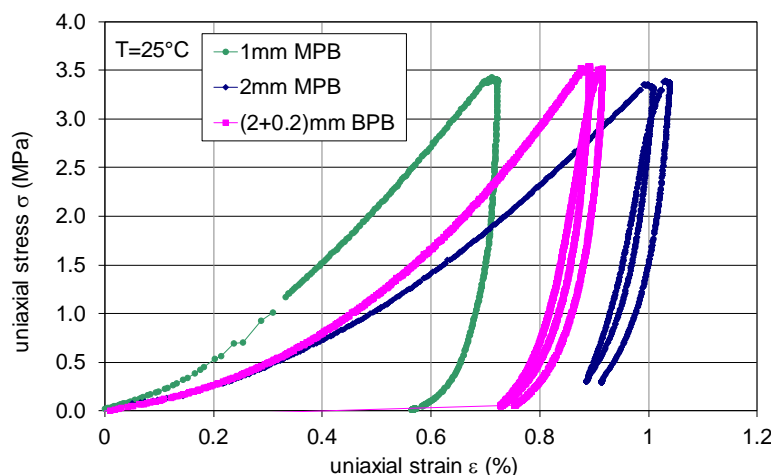


Fig. 2. Uniaxial stress for mono-sized and binary pebble beds at ambient temperature.

Pressure increase period: Compared to previously investigated MPBs with 1mm NGK beryllium pebbles [9], the 2mm MPBs are considerably softer, that is larger strains occur for the same stress

value. This fact is attributed to i) different pebble shapes, and ii) different inner properties (grain size, impurity levels). Of interest is the effect of small pebbles. Compared to the 2mm MPB, the BPB is stiffer because significantly more pebbles are now in mutual contact during compression. The increased number of contacts is also the reason for the much larger thermal conductivity of the BPBs, see [8].

With increasing temperature, the curves become softer, Fig. 3, because of

- the instantaneous plastic pebble deformation which increases with temperature because of the ultimate yield strength decrease, and
- the thermal creep strain ε_{cr0} which occurs during the stress increase period.

Again, the increase is smaller for the BPB (at 550°C the strain differences at $\sigma=2.7\text{MPa}$ is $\Delta\varepsilon=0.25\%$ for the BPB compared to 0.34% for the MPB).

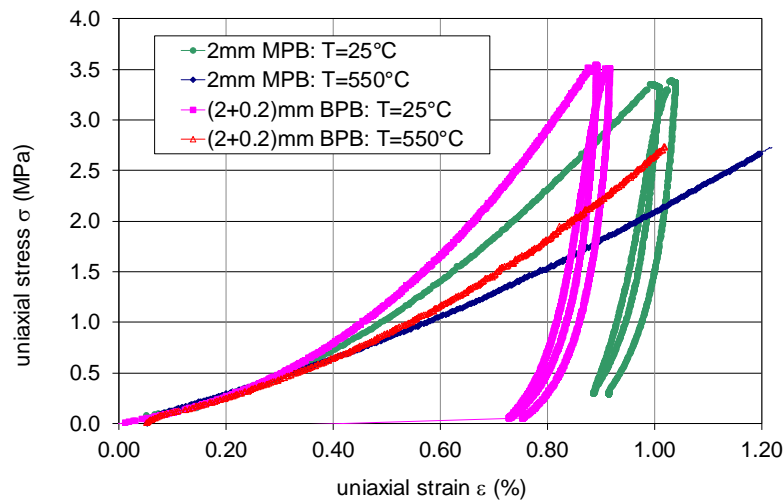


Fig. 3. Uniaxial stress increase for 2mm MPBs and (2mm+0.15mm) BPBs.

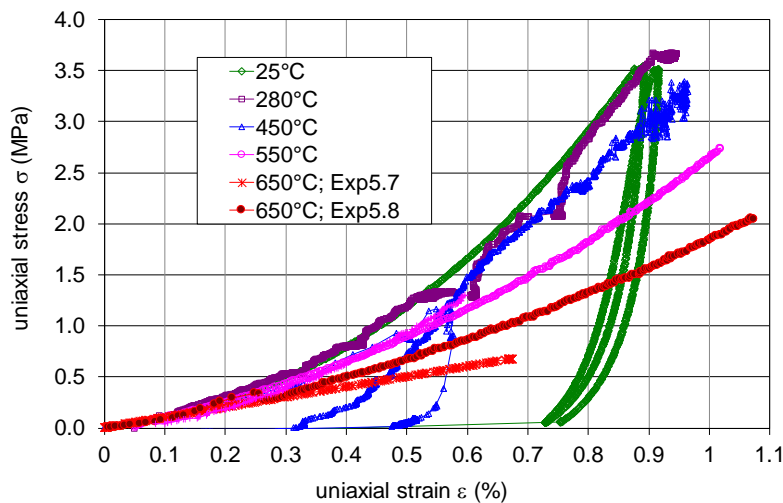


Fig. 4. Uniaxial stress increase for the BPB as a function of temperature.

Figure 4 shows a summary of the BPB results. For 280°C, the curve merely differs from that one for ambient temperature (the plateaus are caused by thermal conductivity measurements). A small influence is observed for T=450°C; for the larger temperatures, the softening becomes quite expressed. For 650°C, the curve for the smaller stress increase ramp is softer because of the larger time available for thermal creep.

For ambient temperature, the dependence between uniaxial stress σ and uniaxial strain ε can be approximated by:

$$\sigma(\text{MPa}) = 4.21\varepsilon(\%)^{1.78}. \quad (1)$$

The σ - ε dependence is used for the determination of the modulus of deformation $E_i(\text{MPa}) = \sigma(\text{MPa})/\varepsilon(1)$. From Eq.(1), it follows:

$$E_i = C\sigma^m \quad (2),$$

with $C=224.5$ and $m=0.439$. In Fig. 4, a significant increase of strain with increasing temperature is observed. The difficulty, however, is to differentiate between the effects of changing yield strength and occurring thermal creep strain ε_{cr0} . With the thermal creep correlation, presented in Section 3.2, the creep strain value ε_{cr0} during stress increase is determined. The remaining temperature dependence of C is shown in Fig. 5: C starts to decrease significantly with increasing T at temperatures above 450°C. The temperature dependence can be expressed by:

$$\begin{aligned} T \leq 400^\circ\text{C}: & \quad C=224.5 \\ T > 400^\circ\text{C}: & \quad C= 224.5 - 0.0012(T(^\circ\text{C}) - 400)^2 \end{aligned} \quad (2a).$$

Pressure decrease period: The residual strain value after the stress decrease to zero corresponds to the irreversible deformation of the pebble bed, ε_{irr} . This value is of importance in respect to the formation of gaps at the end of a thermal cycle. Assuming a σ - ε coordinate system starting at \square the modulus of deformation for the pressure decrease period is determined for ambient temperature as

$$E_d = 1010\sigma^{0.541} \quad (3).$$

At temperatures where thermal creep occurs, the curves during pressure decrease become steeper, that is, E_d becomes larger. For negligible elastic pebble bed strains, ε_{irr} approaches the strain value which occurs at σ_{max} .

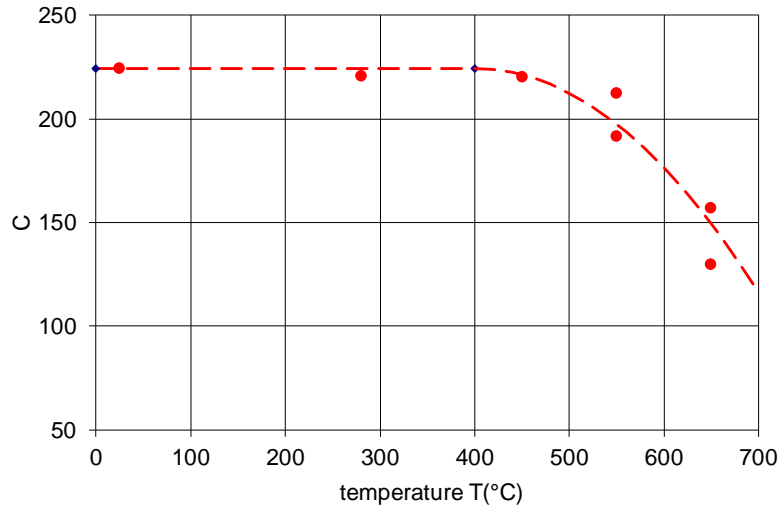


Fig. 5. Dependence of C on T.

3.2. Thermal creep strain for $\sigma = \text{const.}$

Thermal creep strain at $\sigma = \text{const.}$ is again expressed by a correlation of the type

$$\varepsilon_{cr}(\%) = A \exp(-B/T(K)) \sigma(\text{MPa})^p t_{cr}(\text{min})^n \quad (4),$$

where the constants A and B and the exponents p and n are determined by fitting the experimental data.

Creep strain ε_{cr} is conventionally determined as a function of creep time t^* , starting when σ_{\max} has been reached. In this way, the creep strain ε_{cr0} occurring during the stress increase period is not taken into account as well as the time period t_0 which would be required if this creep strain ε_{cr0} would be generated at $\sigma = \text{const.}$

For a constant stress increase rate during the stress increase period $t_{\sigma i}$, ε_{cr0} is determined by integration to

$$\varepsilon_{cr0}(\%) = n/(n+p) A \exp(-B/T(K)) \sigma(\text{MPa})^p t_{\sigma i}(\text{min})^n \quad (5).$$

Eq. (5) shows that ε_{cr0} is decreased by the factor of $n/(n+p)$ compared to the creep strain which would occur for $\sigma = \sigma_{\max}$ during the time period $t_{\sigma i}$. The value for t_0 is given by

$$t_0 = ((n+p)/n)^n t_{\sigma i} \quad (6).$$

For plotting the creep strain as a function of creep time, ε_{cr0} and t_0 are used to shift the coordinate system in the following way: $t_{cr} = t^* + t_0$, $\varepsilon_{cr} = \varepsilon_{cr^*} + \varepsilon_{cr0}$. Although in practice, the values ε_{cr0} and t_0 are quite small; the influence becomes quite pronounced if creep data are plotted in a log-log plot.

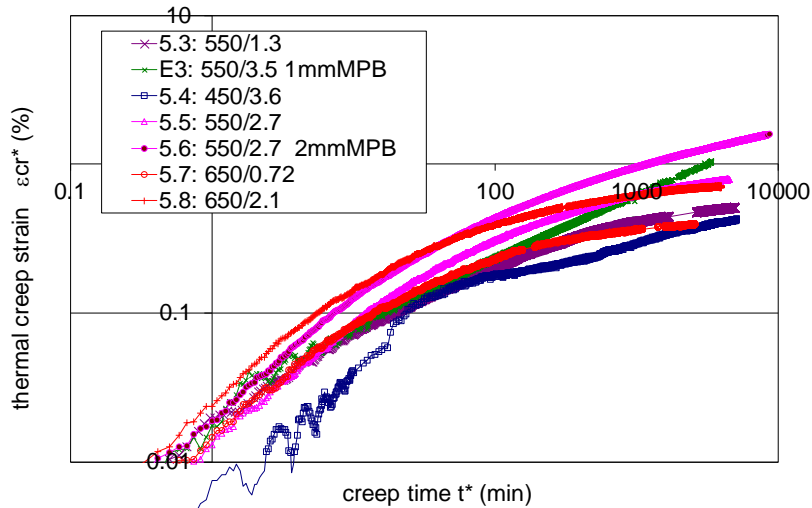


Fig. 6. Thermal creep strain ϵ_{cr}^* as a function of creep time t_{cr}^* .

Figure 6 shows thermal creep strain data in a plot with ϵ_{cr}^* and t^* as coordinates. The slopes of the curves are not constant which means that creep strain ϵ_{cr} cannot be described by a unique relationship of the type $\epsilon_{cr} \sim t^n$.

By taking into account the thermal creep strain occurring during the stress increase period, the slopes of the curves vary much less, see Fig. 7.

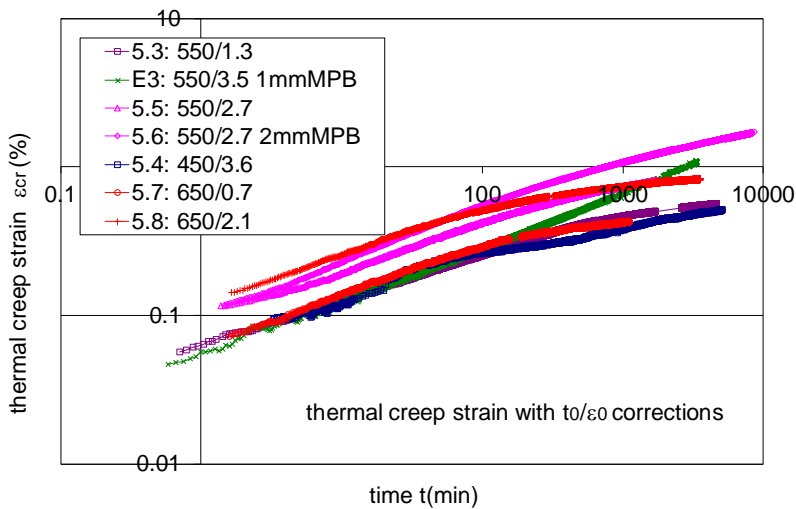


Fig. 7. Thermal creep strain ϵ_{cr} as a function of creep time t_{cr} .

For 1mm MPBs, the curve slopes became fairly constant over the total investigated creep time periods and the exponent $n=0.35$ fitted well all curves obtained at different temperatures.

For the 2mm MPBs, creep strain is larger compared to 1mm MPBs, however, the slopes are about the same.

For BPBs, the curve slopes are again fairly constant for the first creep period of about 100min. Then creep rates become smaller. This fact might be caused by complicated interactions between small and large pebbles. Compared to 2mm MPBs, creep strains are smaller.

For fusion blankets, creep periods of about 100min are of largest interest because stress relaxation effects are most pronounced in this period [12]. Therefore, the curves were fitted for this time period and an exponent $n=0.33$ yielded the best results for all data.

The temperature and stress dependence is obtained using an Arrhenius diagram shown in Fig. 8. The temperature dependence was determined by fitting the results by a straight curve, as expected for a thermally activated creep mechanism. The stress exponent m was varied such that the scatter from the straight curve becomes minimum.

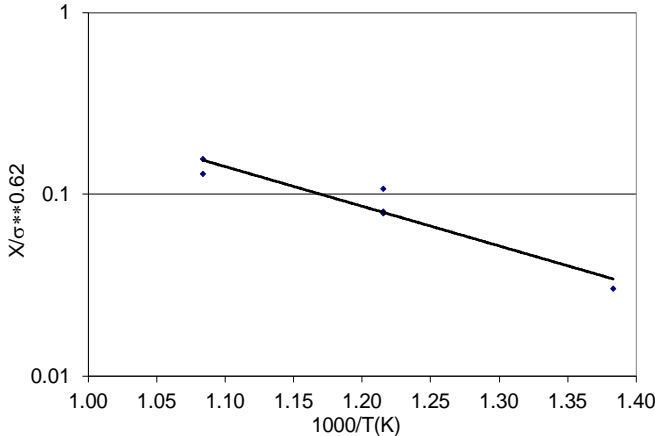


Fig. 8. Determination of temperature and stress dependence.

The final values of the correlation parameters are presented in Table 3, which also contains the corresponding values for the 1mm MPBs from [9].

Table 3: Proposed thermal creep correlation.

Granular material	$\epsilon_{cr}(\%) = A \exp(-B/T(K)) \sigma(\text{MPa})^p t(\text{min})^n$			
	A	B	p	n
(2+0.15)mm BPB	4.7	3735	0.62	0.33
1mm NGK pebbles	1614	9124	0.62	0.35

4. Conclusions

Binary beryllium pebble beds consisting of 2 and 0.15mm Brush Wellman pebbles have been characterized by uniaxial compression tests in respect to

- the stress-strain behaviour during stress increase, and,
- thermal creep strain.

Correlations have been proposed for the modulus of deformation E as a function of stress and temperature and thermal creep strain as a function of stress, time, and temperature.

Compared to mono-sized 2mm beryllium pebble beds, the binary beds behave stiffer (smaller strains during stress increase and smaller thermal creep). Compared to mono-sized 1mm NGK pebble beds, the 2mm pebble beds behave softer.

For advanced fusion blanket designs using binary pebble beds for both the breeder and multiplier material, corresponding experiments for the ceramic pebble beds are still missing. When these data are available, the thermo-mechanical interaction between these pebble beds and the structural material can be determined.

References

- [1] A. Ying et al., Status of ceramic breeder pebble bed thermo-mechanics R&D and impact on breeder material mechanical strength, *Fusion Eng. Des.* 87 (2012) 1130-37.
- [2] F. Cismondi et al., The fundamental role of fluid dynamic analyses in the design of the solid EU Test blanket module, *Fusion Eng. Des.* 87 (2012) 1123-1129.
- [3] Y. Gan, M. Kamlah Thermo-mechanical analyses of Helica and Hexcalibur mock-ups, *J. Nuclear Materials*, 386-388 (2009) 1060-1064.
- [4] R. Annabattula, S. Zhao, Y. Gan, M. Kamlah, Crushing analysis of pebbles in a pebble assembly using DEM, 16th Ceramic Breeder Blanket Interactions (CBBI-16), 8-10, Portland, USA, Sept. (2011).
- [5] Y. Gan, Thermo-mechanics of pebble bed in fusion blankets, *FZKA 7455*, Dec. (2008).
- [6] G. Delaney, T Di Matteo, T. Aste, Combining tomographic imaging and DEM simulations to investigate the structure of experimental sphere packings, *Soft Matter*, 6 (2010) 2992-3006.
- [7] Y. Yanagi, S. Sato, M. Enoeda, T. Datano, S. Kikuchi, T. Kuroda, Y. Kosaku, Y. Ohara, Nuclear and thermal analyses of supercritical-ware-cooled solid breeder blanket for fusion DEMO reactor, *J Nucl. Sci. Techn.*, Vol.38, No.11, p. 1014-1018 (Nov 2001).
- [8] J. Reimann, A. Goraib, H. Harsch, Thermal conductivity of compressed binary beryllium pebble beds, this conference.
- [9] J. Reimann, H. Harsch, Thermal creep of beryllium pebble beds, *Fusion Eng. Des.* 75-79 (2005) 1043-1047.

- [10] J. Reimann, M. Behnke, Mechanical behavior of monosized and binary beryllium pebble beds, Fusion Techn. Vol. 38, No. 3, (2000) 299-309.
- [11] J. Reimann, G. Piazza, H. Harsch, Thermal conductivity of compressed beryllium pebble beds, Fusion Eng. Des. 81 (2006) 449-454.
- [12] L. Bühler, J. Reimann, Thermal creep of granular breeder materials in fusion blankets, J. Nuclear. Mat. 307-31, (2002) 807-810.

2.6 Technical session 3: Industry and safety issues

2.6.1 United States Beryllium Industry Update

K. Smith¹ and E. Vidal PhD²

¹*Materion Brush, Inc. Elmore, OH USA*

²*Materion Brush, Inc. Elmore, OH USA*

E-mail: keith.smith@materion.com

Status of the beryllium industry in the US will be presented covering a wide variety of topics. Content will include an update of the US beryllium supply chain from mining operations through metal fabrication. A discussion of the status of the recently constructed Materion Primary Beryllium Production Facility (“Pebble Plant”), new commercial products, and recent beryllium corrosion issues identified during Electrical Discharge Machining (EDM). We will also provide an update on the US Occupational Safety and Health Administration (OSHA) new Occupational Exposure to Beryllium work standard and its implications to the Beryllium Industry.



MATERION

13th International Workshop
on Beryllium Technology
Narita, Japan

United States Beryllium Industry Update

Mr. Keith Smith
Dr. Edgar Vidal

Materion Beryllium & Composites
Elmore, Ohio, U.S.A.

BeWS-13 • 21 and 22 September 2017 • Narita, Chiba, Japan

Presentation Outline

- ▶ Materion Business Overview
 - ▶ New leader
 - ▶ New organization structure
 - ▶ Materion markets
- ▶ Beryllium Supply Update
- ▶ Beryllium Corrosion During EDM
- ▶ New Commercial Product



2400

Employees

50

Are serving customers in more than 50 countries

30

From more than 30 facilities

10

Located in 10 countries around the globe



MATERION

BeWS-13 • 21 and 22 September 2017 • Narita, Chiba, Japan

Materion Business Overview

- ▶ In 2017, Materion employees have a new leader
 - ▶ Materion CEO **Mr. Richard Hipple** will retire in 2017
 - ▶ New CEO – **Mr. Jugal Vijayvargiya** formerly from Delphi Corp



2017/07/11



BeWS-13 • 21 and 22 September 2017 • Narita, Chiba, Japan

Business Overview – Major Markets



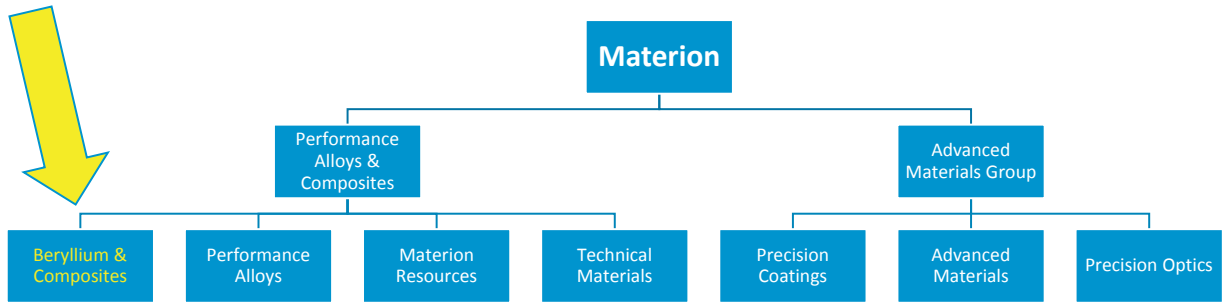
% of Value-added Sales 2016



BeWS-13 • 21 and 22 September 2017 • Narita, Chiba, Japan

Materion Business Overview

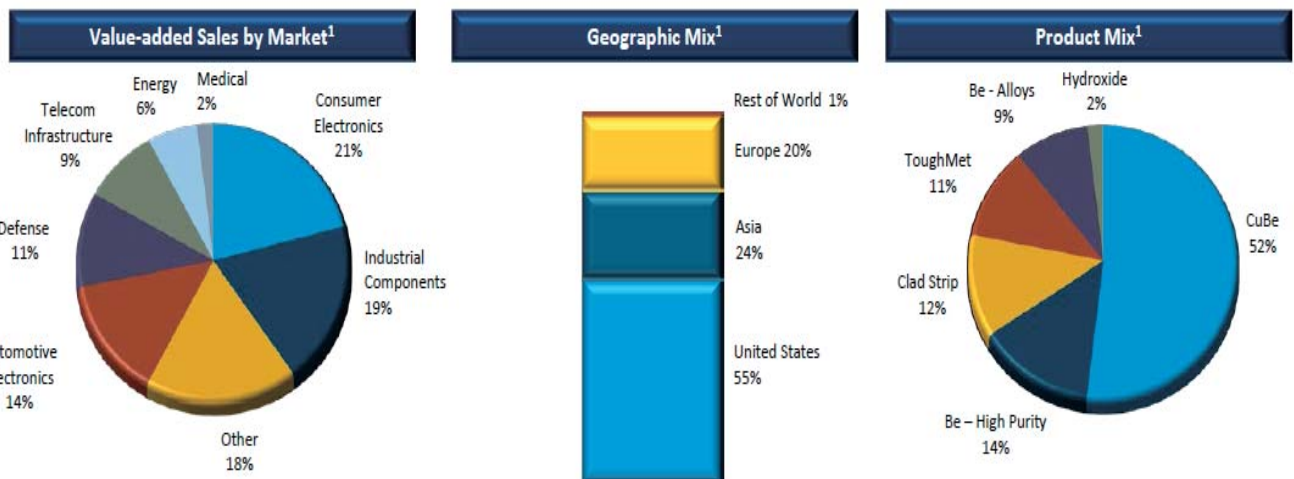
Materion Organizational Structure:



BeWS-13 • 21 and 22 September 2017 • Narita, Chiba, Japan

5

Performance Alloys & Composites



¹ Reflects 2016 mix by market, geography, and product

A.



BeWS-13 • 21 and 22 September 2017 • Narita, Chiba, Japan

6

Beryllium Supply Chain - US



BeWS-13 • 21 and 22 September 2017 • Narita, Chiba, Japan

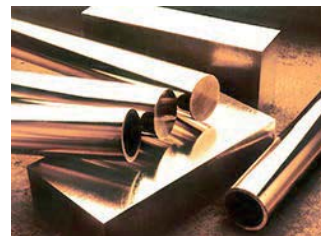
7

Beryllium Supply

- ▶ **Materion is the only fully integrated beryllium supplier in the world.**

- ▶ **Be production facilities in the US:**

- ▶ Delta, UT Mining
- ▶ Elmore, OH Extraction, casting, metal fabrication, machining
- ▶ Tucson, AZ BeO
- ▶ Fremont, CA Be foil and fabrication
- ▶ Lincoln, RI Clad products
- ▶ Reading, PA CuBe strip and wire
- ▶ Warren, MI CuBe
- ▶ Chicago, IL CuBe



BeWS-13 • 21 and 22 September 2017 • Narita, Chiba, Japan

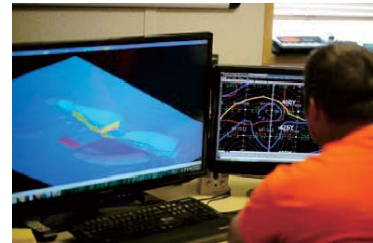
8

Materion Natural Resources – Mine Development

•The **Topaz-Spor Mountain** area in western Utah has been a commercial source of uranium and fluorspar. Beryllium was discovered in 1959

•The mineral is identified as **bertrandite**, a hydrous beryllium silicate ($\text{Be}_4\text{Si}_2\text{O}_7(\text{OH})_2$)

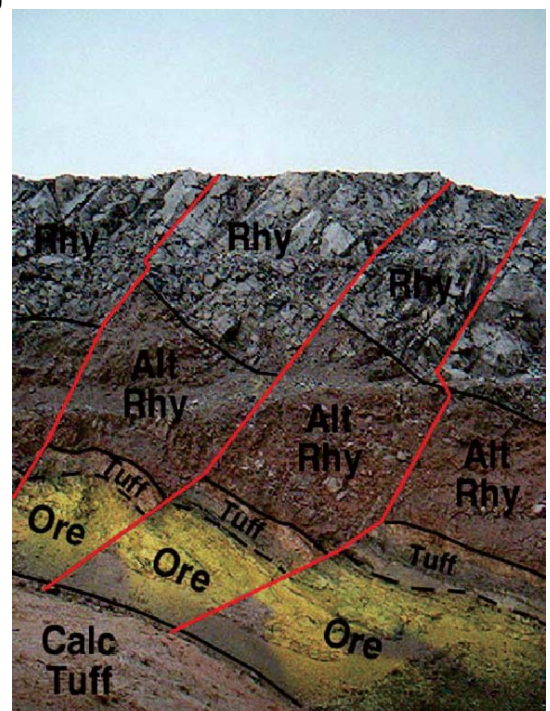
•**Materion holds estimated ore reserves for 70 years of production.**



BeWS-13 • 21 and 22 September 2017 • Narita, Chiba, Japan

Topaz Mine – Geology

- ▶ Beryllium mineralization from hydrothermal replacement
- ▶ Stratigraphic sequence is suited to seam modeling
 - Tilted Devonian limestone
 - Lower Miocene tuffs
 - Upper Miocene rhyolite flows
 - Quaternary sediments
- ▶ Area is extensively faulted



BeWS-13 • 21 and 22 September 2017 • Narita, Chiba, Japan

Be Production at Elmore, Ohio Plant



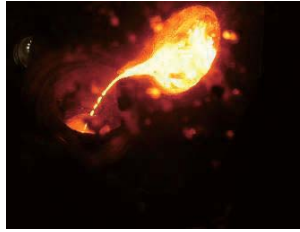
Beryllium Pebble Plant

- ▶ The Be Pebble Plant in Ohio is the world's most modern beryllium refining production facility.
- ▶ Cost: \$110,000,000
- ▶ First production: April 2011.
- ▶ Plant is fully operational.
- ▶ Design capacity of 70,000 kg/yr



Beryllium Manufacturing

- ▶ **Melting and Casting**



- ▶ **Powder Metallurgy**



- ▶ **Powder Consolidation**



- ▶ **Machining**



BeWS-13 • 21 and 22 September 2017 • Narita, Chiba, Japan

Beryllium Fabrication

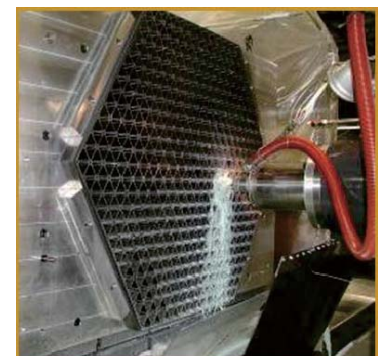
- ▶ **Materion Special Projects and Applications Development Engineering (SPADE):**

- ▶ Engineering services including:
- ▶ Project prime contracting
- ▶ Program management
- ▶ Engineering design



- ▶ **US Be Machining Contractors:**

- ▶ General Dynamics - GDMS
- ▶ LA Gauge
- ▶ Hardric Labs
- ▶ Skinner (EDM)
- ▶ REV Mfg
- ▶ WessDel
- ▶ Materion
- ▶ Others (5)

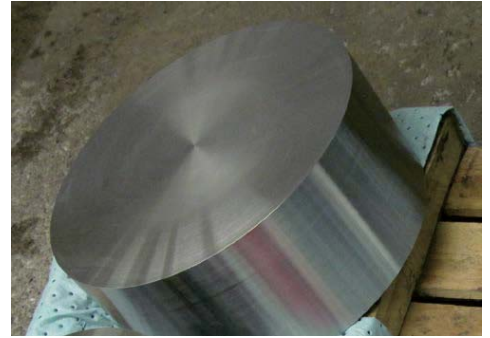


BeWS-13 • 21 and 22 September 2017 • Narita, Chiba, Japan

Beryllium Products

Beryllium:

- ▶ Seven commercial grades of Beryllium metal:
 - ▶ S-200-F, S-200-F-H, S-200-F-C, I-70, **S-65**, I-220, I-220-H
 - ▶ Block, Parts, Sheet, Extrusions
- ▶ Beryllium Foil – multiple grades (Materion Electrofusion)
- ▶ Ultra High-purity Beryllium
- ▶ Beryllium hydroxide
- ▶ Beryllium fluoride



Other Products

- ▶ AlBeMet – Be-38Al
- ▶ AlBeCast – Investment cast Al-Be
- ▶ Be/BeO Composites (E-Material)
- ▶ BeO ceramic components
- ▶ Bulk Metallic Glass – amorphous materials
- ▶ Cu-Be Alloys

Critical Processing Considerations for ITER First Wall Beryllium Tiles

Sayer, Qian, Smith – Materion
Dorn – Be4Fusion (formerly Materion)

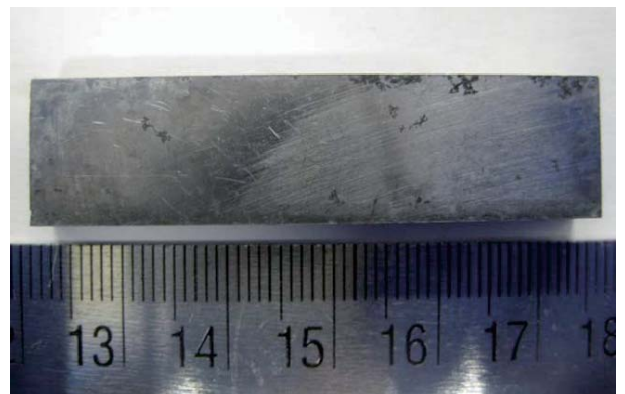
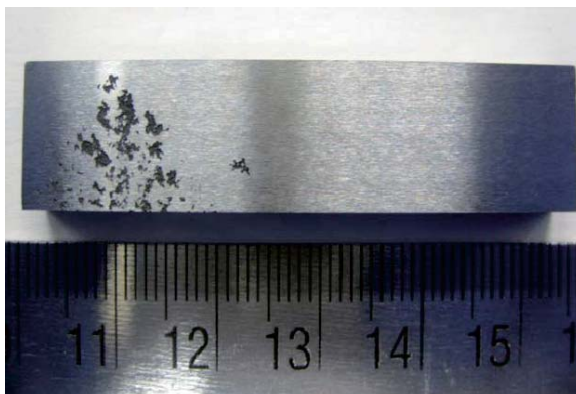


BeWS-13 • 21 and 22 September 2017 • Narita, Chiba, Japan

17

Critical Processing Considerations for ITER First Wall Beryllium Tiles – SOFT 2016 Poster Session

- ▶ In 2015 a Materion customer identified a surface anomaly on numerous beryllium bars following EDM processing.
 - ▶ Material: S-65-E bars purchased from Materion.
 - ▶ Parts were cut using a 0.12mm-diameter molybdenum wire EDM process.
 - ▶ After grinding to a tolerance of 0.002mm and polishing, the finished tiles were in two sizes: 6mm x 12mm x 51mm and 6mm x 12mm x 43mm.



BeWS-13 • 21 and 22 September 2017 • Narita, Chiba, Japan

18

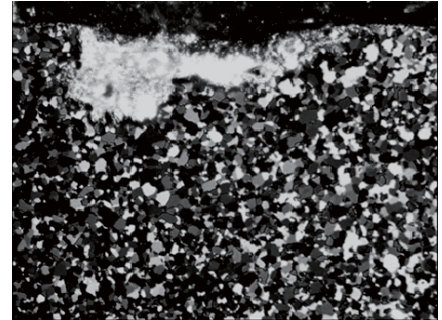
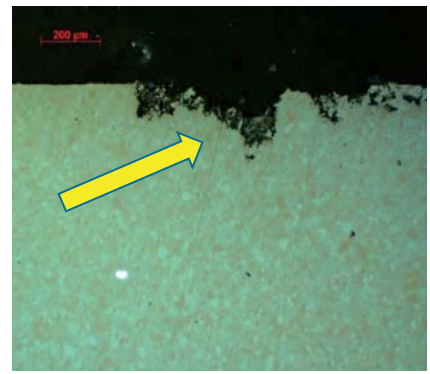
Investigation

▶ Metallography:

- ▶ Cross sectional analysis shows that the surface defects extend from the surface into the part.
- ▶ The base material did not exhibit and sub-surface porosity.
- ▶ No indication of incomplete consolidation.
- ▶ The appearance looks similar to common beryllium surface corrosion.

▶ Radiography:

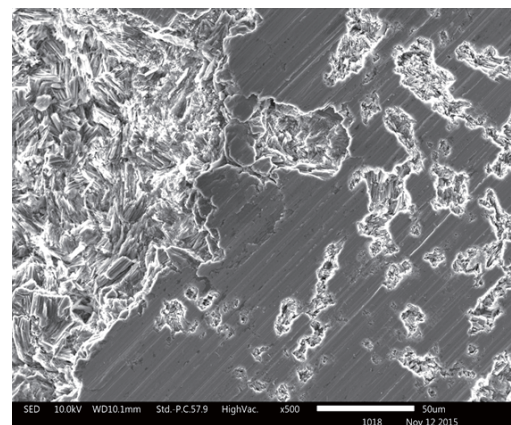
- ▶ X-Ray of material looks normal – no evidence of high or low density radiographic indications.



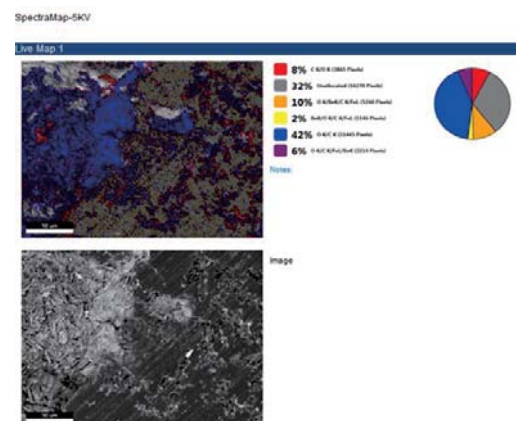
Investigation

▶ Surface evaluation:

- ▶ Evaluated utilizing SEM and EDS.
- ▶ Note lamellar structure within the “pitted area” indicating preferential attack based on crystallographic orientation within individual grains of this polycrystalline material.
- ▶ This topography is indicative of aqueous pitting corrosion. This phenomena has been studied in the past by Hill, Lillard, and others.
- ▶ EDS analysis indicate trace amounts of chlorine present within the pitted areas.
- ▶ Conclusion – The surface defects were the result of aqueous pitting corrosion.



Surface Image - SEM – 500x



SEM – EDS image

Investigation – Duplicate the Pitting

- ▶ To confirm the pitting theory, Materion EDM cut duplicate bars from remnant S-65-E beryllium from the same lot of material.
 - ▶ Two sample bars were cut on the EDM.
 - ▶ Both bars were immediately removed from the EDM solution.
 - ▶ One sample was immediately dried with a clean cloth.
 - ▶ The other sample was NOT dried.
 - ▶ Both samples were placed a clean paper and held at room temperature for 24 hours,

Investigation – Duplicate the Pitting

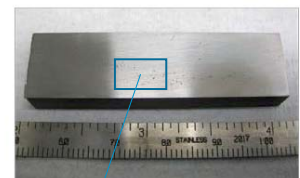
- ▶ Results:
 - ▶ The dried plate did not appear to have any pitting.
 - ▶ The part which remained wet had developed corrosion pits.



Sample 1 – Dry sample
(As cut above, surface
ground Below)



Sample 2 – Wet sample
(As cut above, surface
ground Below)



Conclusions and Recommendations

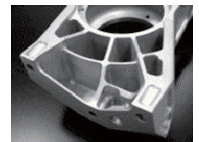
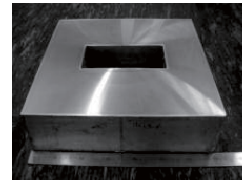
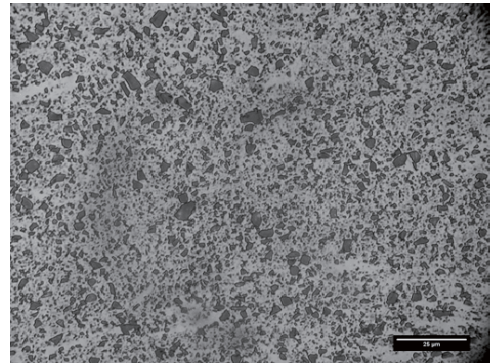
- ▶ The defects viewed on the surface of the plates received for evaluation are pits indicative of aqueous corrosion.
- ▶ Our experience with wire electrical discharge machining (EDM) of Beryllium is that the EDM process solutions or tap water can cause severe pitting to the cut surface if not removed immediately following processing.
 - ▶ Other causes of surface corrosion include:
 - ▶ Water with any halogens and air.
 - ▶ Swarf, machine chips or particulate sitting on top of a machined surface.
 - ▶ Galvanic coupling from steel clamps holding the material.
- ▶ Recommendations:
 - ▶ Keep beryllium surfaces clean and dry.
 - ▶ Clean with a dry cloth or with alcohol.
 - ▶ Store finished parts in a dry and clean environment.

New Al-B₄C Composite – Nuclear Shielding SupremEX Metal Matrix Composites

Dr Stuart Godfrey – Materion AMC

SupremEX Metal Matrix Composites (MMC's)

- ▶ SupremEX MMC's are aluminium alloys typically reinforced with ultra-fine SiC ceramic.
- ▶ Powder metallurgy route to produce an excellent distribution of ceramic within the metal.
- ▶ Improved stiffness, strength, fatigue, hardness etc. compared to aluminium alloys.
- ▶ Used in a range of performance applications including motorsport, space and defence and niche engineering.



BeWS-13 • 21 and 22 September 2017 • Narita, Chiba, Japan

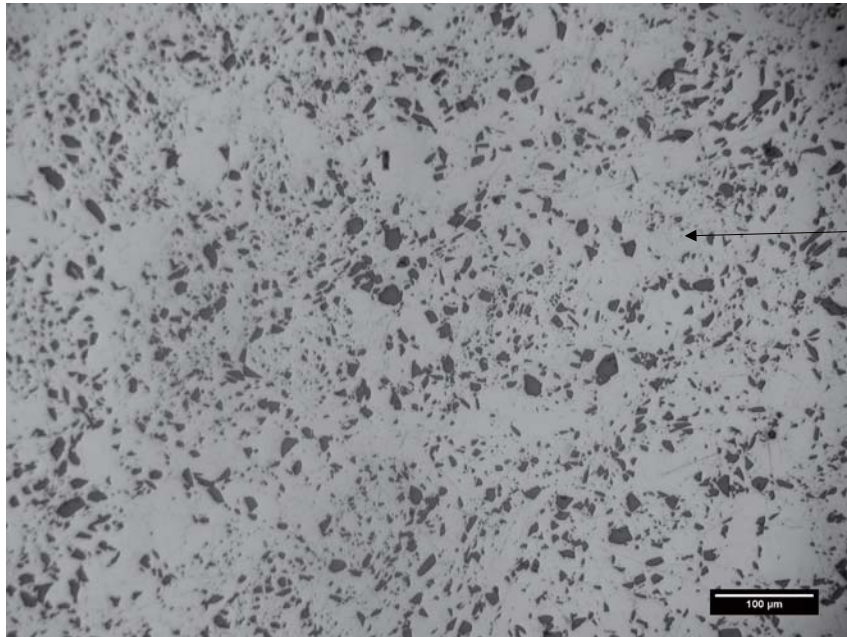
Boron Carbide (B₄C) MMC – Neutron Absorption

- ▶ **Boron is a natural absorber of neutrons**, specifically the B¹⁰ isotope that is present in naturally occurring boron is the important neutron absorbing element.
- ▶ In the nuclear industry (i.e. fuel rod storage casks) boron is used as an alloying element addition to sheet steel (~2% boron) or as B₄C ceramic addition to aluminium sheet.
- ▶ The Materion AMC manufacturing process used to produce MMC's can be applied to Al-B₄C composites.
- ▶ **Reinforcement levels of up to ~ 35% B₄C with excellent distribution of ceramic within the aluminium matrix.**
- ▶ Billets can be hot rolled into sheets that are ~5 m long x 1 m wide x 2 mm thick.



BeWS-13 • 21 and 22 September 2017 • Narita, Chiba, Japan

Boron Carbide (B_4C) MMC – Neutron Absorption



Micrograph showing excellent distribution of B_4C ceramic in an aluminium (6061) matrix



BeWS-13 • 21 and 22 September 2017 • Narita, Chiba, Japan



Aluminum beryllium casting, mag. 200x, viewed with Differential Interference Contrast.
– Daniel Slates; Materion Brush Performance Alloys; Elmore, Ohio USA



BeWS-13 • 21 and 22 September 2017 • Narita, Chiba, Japan

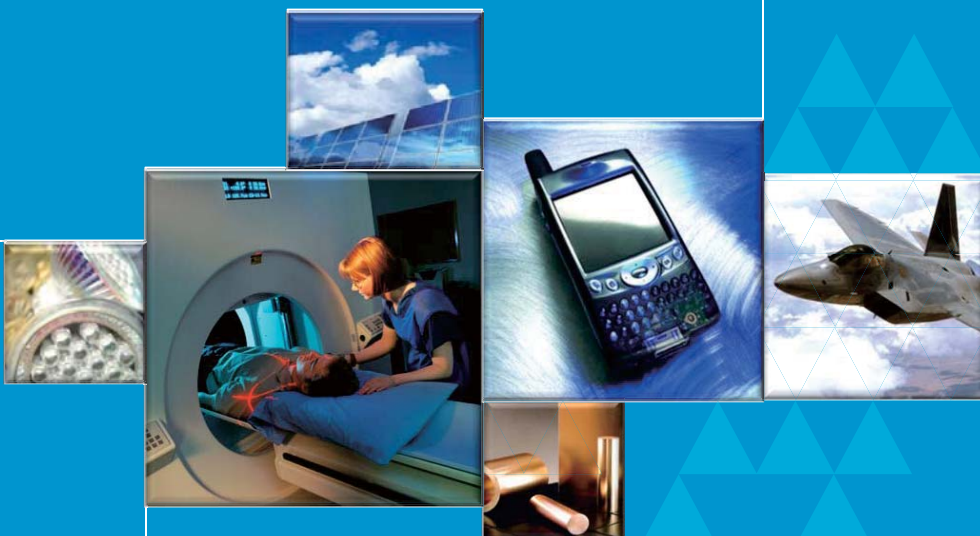
Additional Information



BeWS-13 • 21 and 22 September 2017 • Narita, Chiba, Japan



MATERION



October 25, 2011

Upgrading of S-65 Be Specification for ITER First Wall

Aaron B. Sayer, P.E.
Materion

- Grade Comparison
- Reasons for Improvement
- Production Flow Chart
- Micrographs
- Properties
- S-65 Specification Change – What’s New?

31

Comparison of Possible Beryllium Grades for ITER First Wall

Chemical element	3MC42Z				Published Results Chinese ****		Published Results Russian TGP-56FW*****		
	ITER I/O Spec	S-65 E (new)	S-65 C (old)	JET S-65 H	CN-G01	CN-G01m	Sample 1	Sample 2	Spec from BeWs 8, 2007
Beryllium Assay, % minimum *	99.0	99.2	99.0	99.0	>99	>99	99.02	98.84	98.8
Beryllium oxide, % maximum	1.0	0.9	1.0	1.0	0.9-1	0.7	0.95	1.35	1.3
Aluminium, % maximum	0.06	0.05	0.06	0.06	0.006	0.006	0.018	0.012	0.02
Carbon, % maximum	0.10	0.09	0.10	0.10	0.06	0.05	<0.05	0.05	0.1
Iron, % maximum	0.08	0.08	0.08	0.08	0.06	0.06	0.16	0.13	0.15
Magnesium, % maximum	0.06	0.01	0.06	0.06	0.005	0.005			
Silicon, % maximum	0.06	0.045	0.06	0.06	0.01	0.01	0.021	0.013	0.02
Uranium, % maximum **	0.0030	0.015 (will meet 0.0030 for ITER)	0.04	0.04			n/d	0.0005	0.002
Other metallic impurities, % maximum	0.04		0.04	0.04	<0.04	<0.04			
Physical Properties				Per paper*****			Actual Results		
UTS (MPa)	290	290	290	290	340		420		
TYS (MPa)	205	205	205	205	210		303		
Elongation (%)	3	3	3	3	>=3		3		

Items in red do not meet the ITER I/O specification

* Difference (i.e. 100% - other elements)

** Proven method of measurement of Uranium content shall be proposed by Manufacturer of material and agreed with DA and IO.

*** The content of other elements (e.g. Cr, Ni, Cu, Ti, Zr, Zn, Mn, Ag, Co, Pb, Ca, and Mo) shall be reported for information.

*****Recent Progress of Plasma Facing Material Research at SWIP", X. Liu, et al, Southwestern Institute of Physics, China

*****Progress in Production and Characterization of RF Beryllium for ITER First Wall, Presentation given at 8th IEA Be WS, Lisbon, Portugal, December 2007.

I. Kupriyanov, et al, Federal Agency of Atomic Energy, Russia

*****Characterization of Chinese Beryllium as the Candidate Armor Material of ITER First Wall, X. Liu et al, Southwestern Institute of Physics, China

Additional Elemental Reductions in S-65

Rev. E

Element	% Maximum
Cr	0.01
Ni	0.025
Cu	0.025
Ti	0.025
Zr	0.025
Zn	0.005
Mn	0.005
Ag	0.005
Co	0.005
Pb	0.005
Ca	0.005
Mo	0.005

Reasons for Improvement



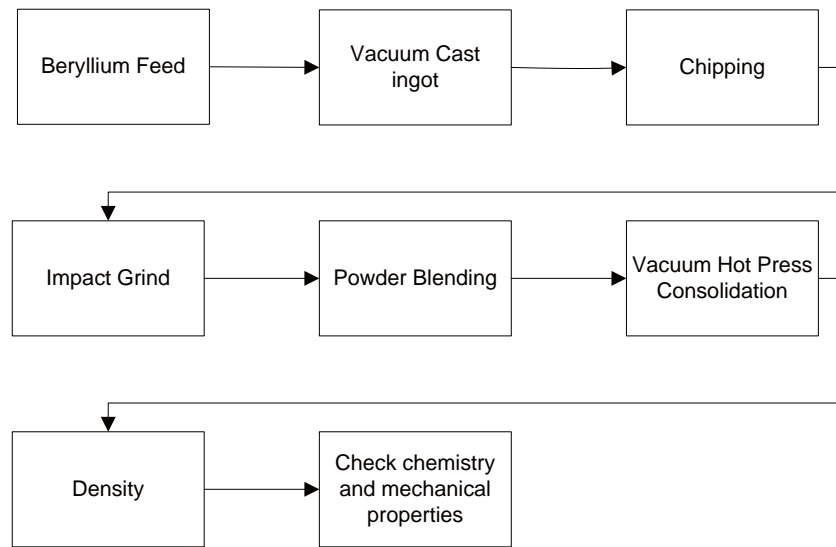
- 3MC42Z ITER I/O Beryllium Specification, “Material Specification for the supply of Beryllium blocks for the ITER First Wall application”
 - Uranium of 30 ppm
- Refinements and adjustments to the process for reduced Uranium led to reduction of other elements and an increase in %Be.
 - BeO, Al, C, Mg, Si, Cr, Ni, Cu, Ti, Zr, Zn, Mn, Ag, Co, Pb, Ca, Mo

- Discovered that steps can be taken to remove uranium from beryllium with the following results:
 - Product A: 3 – 6 ppm Uranium
 - Product B: 20 – 70 ppm Uranium
- In addition, Materion has a process to reduce Product A Uranium further:
 - Less than 5 ppm

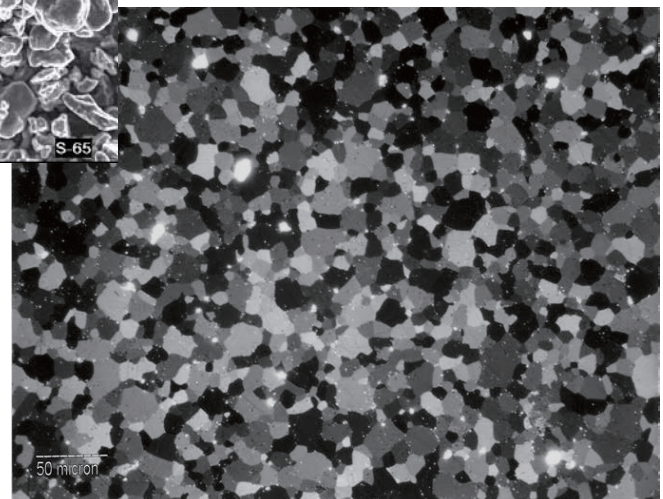
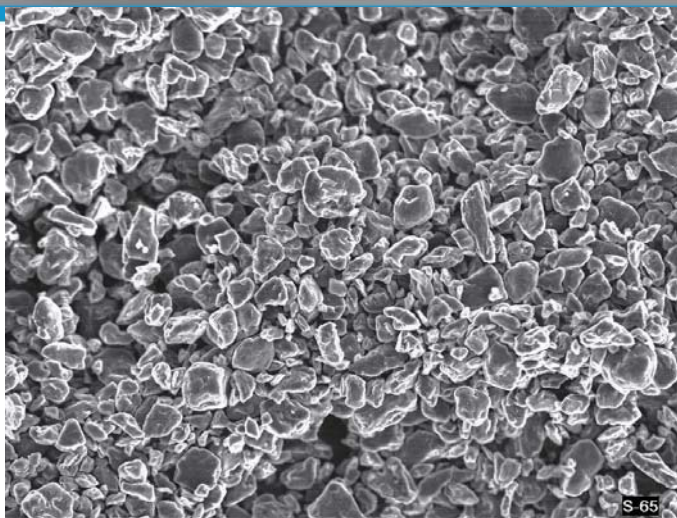
Lot	Fluorometric (ppm U)	Neutron Activation (ppm U)
Lot 1	2	
Lot 2	3	
Lot 3	1	1.0
Lot 4		2.9
Lot 5	1	1.0
Lot 6		1.2
Lot 7		1.9
Lot 8		0.8
Average	1.7	1.5

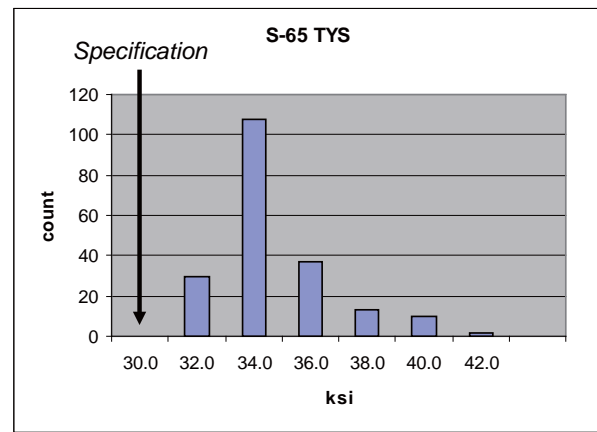
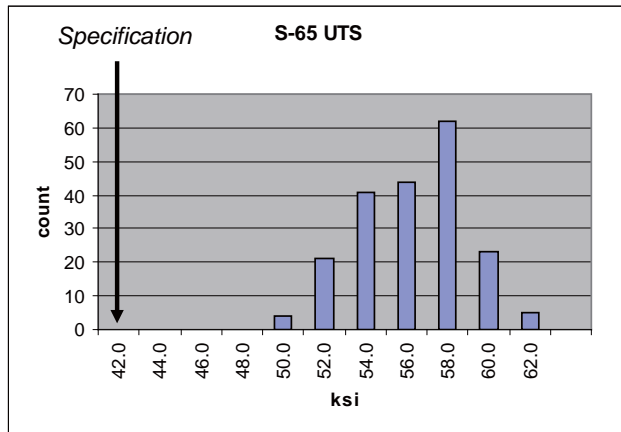
- First production S-65 lot shipped to ITER IO Specification 3MC42Z in 2011.
 - Not all Uranium reduction methods used
 - Uranium by GDMS: 7 ppm

S-65 Flow Chart



Impact Ground S-65 Powder





S-65 Specification Changes

	3MC42Z			
Chemical element	ITER I/O Spec	S-65 E (new)	S-65 C (old)	Typical
Beryllium Assay, % minimum *	99.0	99.2	99.0	99.4
Beryllium oxide, % maximum	1.0	0.9	1.0	0.66
Aluminium, % maximum	0.06	0.05	0.06	0.03
Carbon, % maximum	0.10	0.09	0.10	0.03
Iron, % maximum	0.08	0.08	0.08	0.075
Magnesium, % maximum	0.06	0.01	0.06	0.005
Silicon, % maximum	0.06	0.045	0.06	0.025
Uranium, % maximum **	0.0030	0.015 (will meet 0.0030 for ITER)	0.04	0.001
Other metallic impurities, % maximum	0.04		0.04	
Physical Properties				
UTS (MPa)	290	290	290	386
TYS (MPa)	205	205	205	234
Elongation (%)	3	3	3	4

SupremEX[®] Property Comparison



DATA SHEET

Test	Materion AMC Forged Plate Products						Aluminium Alloys		Titanium
	AMC217XE	AMC225XE	AMC640XA	AMC Xfine ₆₂₅	AMC Xfine ₂₁₇	AMC Xfine ₂₂₅	AA6061	AA7075	TI-6AL-4V
Heat Treatment	T4	T4	T6	T6	T4	T4	T6	T6	STA
UTS MPa (ksi)	580 (84)	610 (88)	570 (83)	500 (72)	630 (91)	680 (99)	310 (45)	572 (83)	1103 (160)
0.2% YS MPa (ksi)	420 (61)	440 (64)	480 (70)	425 (62)	450 (65)	550 (80)	275 (40)	503 (73)	945 (137)
Modulus GPa (msi)	100 (14.5)	115 (16.7)	140 (20)	110 (16.0)	100 (14.5)	115 (16.7)	70 (10.2)	72 (10.5)	114 (16.5)
Strain to Failure % (At)	6	4	2.5	6	5	3	12	11	>8
CTE @25°C ppm/°C (ppm/°F)	16.8 (9.3)	16.1 (8.9)	13.4 (7.4)	16.1 (8.9)	16.8 (9.3)	16.1 (8.9)	23.0 (12.7)	23.6 (13.1)	8.8 (4.9)
Thermal Conductivity @25°C W/m²K	155	150	130	150	155	150	156	130	22
Specific Heat @ 25°C J/kg°K	848	836	800	836	848	836	896	960	520
Density g/cm³ (lb/in³)	2.85 (0.103)	2.88 (0.104)	2.90 (0.105)	2.82 (0.102)	2.85 (0.103)	2.88 (0.104)	2.70 (0.097)	2.81 (0.102)	4.43 (0.160)
Poisson's Ratio	0.3	0.3	0.3	0.3	0.3	0.3	0.33	0.33	0.34
Fracture Toughness K _{IC} MPa·√m (ksi·√in)	23 (21)	19 (17)	14 (13)	23 (21)	23 (21)	19 (17)	35 (32)	28 (26)	>44 (>40)
RB Fatigue, Kt=1 (@ 1x10 ⁷) MPa (ksi)	292 (42)	310 (45)	271 (39)	240 (35)	331 (48)	353 (51)	110 (16)*	172 (25)*	414 (60)**
Specific Stiffness GPa/g/cm³ (msi/lb/in³)	35 (141)	40 (161)	48 (190)	39 (156)	35 (141)	40 (161)	26 (102)	26 (103)	26 (100)
Specific Strength MPa/g/cm³ (ksi/lb/in³)	204 (816)	212 (846)	197 (790)	177 (705)	221 (883)	244 (981)	115 (429)	204 (814)	250 (1000)
Stress Corrosion Crack (75% 0.2% YS)**	-	Class 1	Class 1	-	-	-	Class 1	Class 3	Class 1

Data is typical from forged plate at 10:1 forge ratio
*Axial fatigue, R=-1, Kt=1 (@ 1x10⁷)

Italicised values are predicted, based on existing AMC data
**Extruded bar, annealed **SCC testing carried out according to ECSS-Q-70-37A (ESA)

Aerospace Metal Composites Ltd.
1 RAE Road, Farnborough www.materion.com
Hampshire, England GU14 6XE
phone: +44(0)1252359712

MATERION CORPORATION

SUPREMEX



2.6.2 Overview of the Current Beryllium Environmental, Health and Safety Regulatory Activities

E. Vidal¹ and T. Knudson²

¹Materion Brush, Inc. Elmore, OH USA

²Materion Corporation, Mayfield Heights, OH USA

E-mail: Theodore.Knudson@materion.com

A brief overview of the current state of affairs related to exposure limits and standards in the USA will be presented. In particular, the status of standards in the EU and the OSHA standards will be addressed.



MATERION

13th International Workshop
on Beryllium Technology
Narita, Chiba, Japan

Overview of the Current Beryllium Environmental, Health and Safety Regulatory Activities

Dr. Edgar Vidal
Mr. Ted Knudson

Materion Beryllium & Composites
Mayfield Heights, Ohio
United States of America

BeWS-13 • 21 and 22 September 2017 • Narita, Chiba, Japan

► Presentation Outline

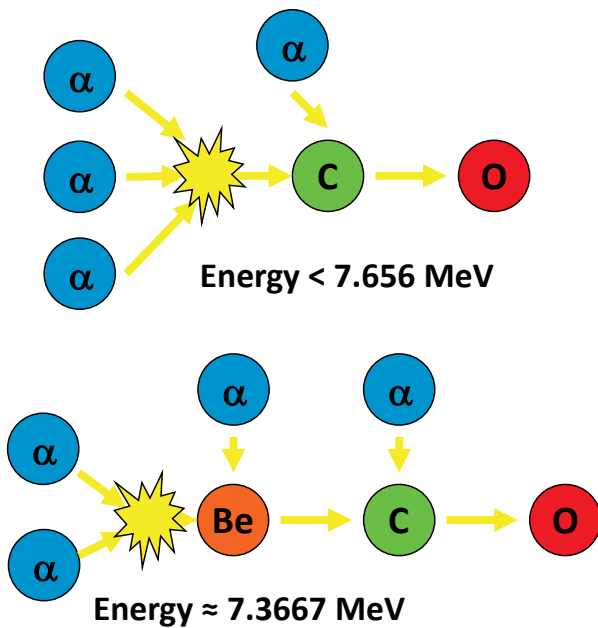
- ▶ Brief Background on Beryllium
 - ▶ Naturally Occurring Element
 - ▶ Where Commonly Found
 - ▶ Understanding CBD Basics
- ▶ Establishment of “BeST” Consortium
- ▶ Beryllium Occupational Exposure Limits
- ▶ Final U.S. OSHA Beryllium Standard
- ▶ Status of Standards within the EU
- ▶ Other Current Beryllium EH&S Issues
- ▶ ITER Workshop on Be Applications and EHS
- ▶ REACH Directive
- ▶ Summary & Conclusion



MATERION

BeWS-13 • 21 and 22 September 2017 • Narita, Chiba, Japan

Children of Beryllium?



- ▶ Carbon was and is still created in the stars
- ▶ It was initially thought that 3 alpha particles colliding would form the C (Triple α process) [Ed Salpeter, 1952]
- ▶ Fred Hoyle [1952], realized that C would only be stable if $E > 7.656$ MeV
- ▶ In conclusion, we are children of Be and grandchildren of He^{2+}

Source: John D. Barrow, "The Constants of Nature," Vintage Books New York, 2002.



BeWS-13 • 21 and 22 September 2017 • Narita, Chiba, Japan

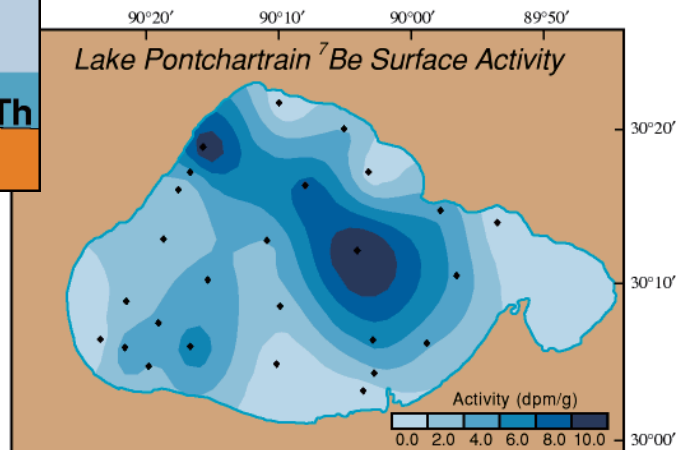
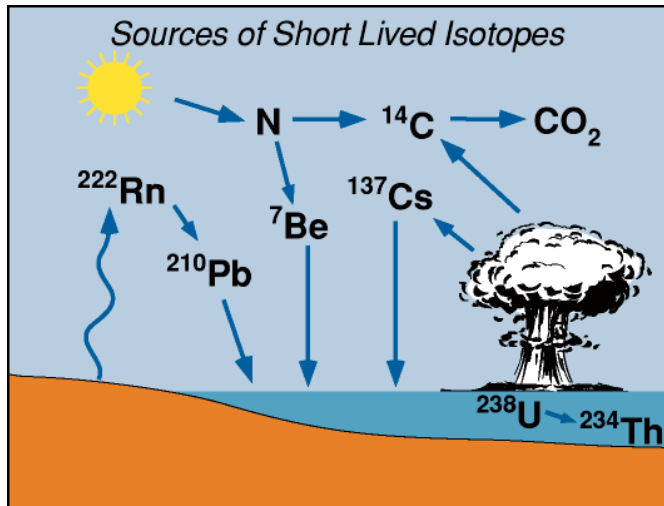
Be – Naturally occurring element

- ▶ Found at 0.5 to 2.5 ppm or higher in soils and rocks throughout the world
- ▶ Commonly found in coal, wood, and gemstones such as aquamarine and emerald
- ▶ Occurs naturally in ground and surface water
- ▶ Beryllium has been measured at ppb levels in most plants and vegetables, for example:
 - ▶ Rice: $72\mu\text{g}/\text{kg}$
 - ▶ Lettuce: $16\mu\text{g}/\text{kg}$
 - ▶ Peas: $109\mu\text{g}/\text{kg}$
 - ▶ Potatoes: $0.59\mu\text{g}/\text{kg}$
 - ▶ Kidney Beans: $2200\mu\text{g}/\text{kg}$
 - ▶ (Fresh Weight)



BeWS-13 • 21 and 22 September 2017 • Narita, Chiba, Japan

Be for Sedimentary Dynamics



"Short-Lived Isotopic Chronometers:
A Means of Measuring Decadal Sedimentary
Dynamics,"
USGS FS-073-98



BeWS-13 • 21 and 22 September 2017 • Narita, Chiba, Japan

Where is Be commonly found?

Beryllium is Found in Household & Construction Products

- ▶ Ceiling Tiles
- ▶ Fertilizers
- ▶ Detergents
- ▶ Charcoal
- ▶ Cat Litter
- ▶ Concrete Blocks
- ▶ Concrete Floors
- ▶ Metals
- ▶ Roofing Materials

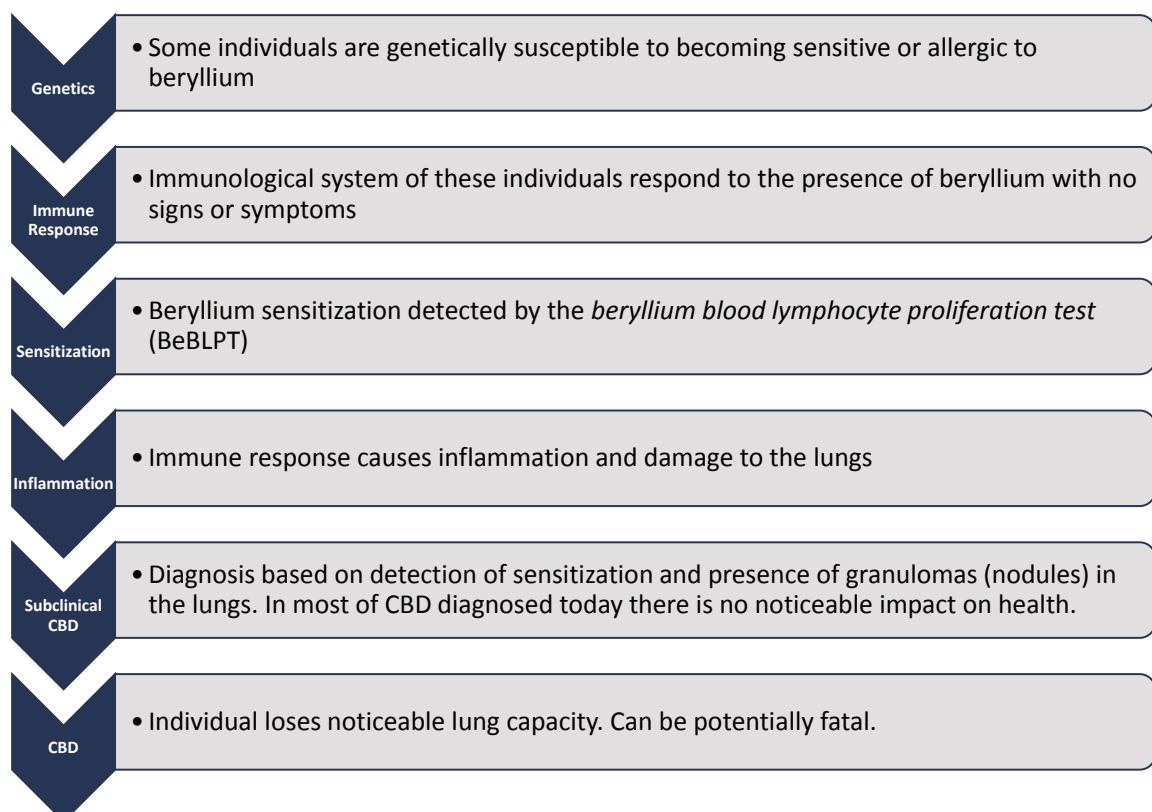


BeWS-13 • 21 and 22 September 2017 • Narita, Chiba, Japan

Understanding Chronic Beryllium Disease (CBD)

- ▶ Necessary conditions to contract CBD:
 - ▶ An individual must be allergic or sensitive to beryllium; AND,
 - ▶ Be exposed to sufficient respirable beryllium particulates in the form of a dust, fume, or mist, and less than 10µm in size.
- ▶ CBD is a disease which affects the lungs – it cannot be contracted by ingestion or skin contact:
 - ▶ Beryllium in solid form poses no special health risks
- ▶ Most end-users will never handle beryllium in ways which will generate respirable dust, fume or mist but some possible scenarios may need more review.

How does an individual contract CBD?



- ▶ Founded in September 2011
- ▶ Non-Profit Organization based in Brussels, Belgium
- ▶ Origin: REACH Beryllium Consortium
- ▶ Represents Manufacturers, Suppliers and Users of Beryllium
- ▶ Members:
 - ▶ Materion (U.S.A.)
 - ▶ NGK Berylco (France)
 - ▶ Schmelzmetall (Switzerland)
 - ▶ TROPAG Oscar H. Ritter Nachf. (Germany)
- ▶ See www.beryllium.eu

“To promote sound policies, regulations, science and actions related to the use of beryllium and to serve as an expert resource for the international community on the benefits and criticality of beryllium applications.”

Beryllium Occupational Exposure Limits

Exposure to Airborne Beryllium

- ▶ The Occupational Exposure Limit (OEL) for airborne beryllium varies in jurisdictions worldwide and ranges from 0.05 $\mu\text{g}/\text{m}^3$ to 5.0 $\mu\text{g}/\text{m}^3$ as an 8-hour, time-weighted average (TWA).
- ▶ Materion and BeST promote a Recommended Exposure Guideline (REG) of 0.2 $\mu\text{g}/\text{m}^3$ (Total) or 0.6 $\mu\text{g}/\text{m}^3$ (Inhalable) time-weighted average (TWA) which is based on decades of research with the National Institute for Occupational Safety & Health (NIOSH).
- ▶ REG already adopted by Spain, Ireland, and Poland.
- ▶ U.S. OSHA adopted an OEL of 0.2 $\mu\text{g}/\text{m}^3$ (Total) in January 2017.
- ▶ Germany adopted OEL of 0.14 $\mu\text{g}/\text{m}^3$ (Inhalable) and 0.06 $\mu\text{g}/\text{m}^3$ (Respirable) TWA (not yet published).
- ▶ EU wide OEL for beryllium under development.

Workshop on Beryllium Applications and Health & Safety Aspects for ITER

- ▶ Held 28 -30 June 2017 at ITER Organization (IO) Headquarters in Cadarache, France.
- ▶ The workshop was organized by the ITER Beryllium Management Committee (IBMC) and involved six sessions covering the following beryllium topics.
 - ▶ Session 1: Introduction to the ITER project
 - ▶ Session 2: Specifications and Design of Beryllium Facilities
 - ▶ Session 3: On-Site Operational Aspects
 - ▶ Session 4: Working with Beryllium (Monitoring, Occupational Hazard and Medical Follow-up, and Health & Safety)
 - ▶ Session 5: Beryllium Workers and Training
 - ▶ Session 6: Conclusion summary session

Workshop on Beryllium Applications and Health & Safety Aspects for ITER

- ▶ The objectives of the Workshop were to:
 - ▶ Promote a Beryllium safety culture and awareness within the ITER Project.
 - ▶ Clearly identify the IO internationally as a major user of Be products and a major Be actor in the coming decades.
 - ▶ Share the IO plan on dealing with Be issues to different international Beryllium stakeholders and obtain valuable feedback.
 - ▶ Learn from the plans, activities and experience of these other Beryllium stakeholders through specific invited presentations and discussion in sessions on dedicated Beryllium topics.
 - ▶ Provide transparency as to the ITER approach on Beryllium safety – sharing the knowledge internally and externally.
- ▶ Presentations as well as the Session Chair summaries can be found on the website for those registered for the workshop (<http://www.iter.org/beryllium-workshop>)

Beryllium OEL Regulatory Issue in EU

- ▶ European Commission (EC) initiated the development of an EU wide OEL for Beryllium.
- ▶ The Scientific Committee for Occupational Exposure Limits (SCOEL) issued a recommendation for an OEL which is unjustifiably low ($0.02 \mu\text{g}/\text{m}^3$ (Inhalable)).
- ▶ BeST provided information and data to the SCOEL regarding the identification of a scientifically supportable OEL and also provided comments during the public consultation.
- ▶ Following its issuance, the SCOEL recommendation was evaluated by the Advisory Committee on Safety and Health (ACSH).
- ▶ Following their review, the ACSH recommended that the OEL for beryllium be $0.6 \mu\text{g}/\text{m}^3$ (Inhalable) TWA for an initial 5 years and $0.2 \mu\text{g}/\text{m}^3$ (Inhalable) TWA thereafter.
- ▶ EC proposal for an OEL will be issued for consideration and adoption by European Parliament and Council in 2018.

Potential REACH Regulatory Issue in EU

- ▶ Bundesanstalt für Arbeitsschutz und Arbeitsmedizin (BAuA) is the REACH Authority that conducted the Risk Management Option Analysis (RMOA) for Beryllium
- ▶ BAuA published the results of RMOA in November 2016:
 - ▶ No recommendation to include beryllium on Candidate List or impose any restriction on use.
 - ▶ Require Beryllium Industry to develop and implement a Voluntary Product Stewardship Program (PSP) for EU processors.
 - ▶ Recommended development of a harmonized OEL in the EU.
- ▶ BeST developed and implemented “Be Responsible” PSP which is available at www.berylliumsafety.eu

Other Beryllium-Related Regulatory Issues

- ▶ REACH – Registration, Evaluation, Authorization, and Restriction of Chemicals
 - ▶ Most recent and relevant studies demonstrate that beryllium is not a carcinogen (cancer causing)
 - ▶ Current classification for beryllium needs revision
 - ▶ Beryllium does not meet REACH criteria
 - ▶ Studies show that recycling of electronics waste containing beryllium presents no health risk to workers



Summary & Conclusion

- ▶ Beryllium is Commonly Found in Nature & Everyday Materials
 - ▶ Solid Form Poses No Special Health Hazard
 - ▶ Uniquely Breathing Hazard from Airborne Particulate
- ▶ Occupational Exposure Limits for Beryllium are Changing
- ▶ Generally Positive as Old OEL was not Protective
- ▶ Potential Impact on ITER & Fusion of BAuA and EU Actions
- ▶ Beryllium Science & Technology Association (BeST)
- ▶ Working towards Scientific Evidence-Based Regulatory Decisions
- ▶ Please contact Ted Knudson for questions:
Theodore.Knudson@materion.com or +1.216.383.4040

Additional Information



BeWS-13 • 21 and 22 September 2017 • Narita, Chiba, Japan

Be – Typical Characteristics

Atomic number	4
Atomic radius	1.125 Å
Atomic volume	4.96 cm ³ /g-atom
Atomic weight	9.01218 g
Density	1.8477 g/cm ³ (Commercial grades in range of 1.82 to 1.85 g/cm ³)
Electronic structure	1s ² 2s ²
Crystal structure < 1250°C	Hexagonal close-packed (α -Be)
Crystal structure > 1250°C	Body-centered cubic (β -Be)
Lattice constants	a = 2.286 Å; c = 3.583 Å; c/a = 1.568; ideal = 1.633

- ▶ One of the lightest metals known to man
- ▶ One of the highest melting point for a light metal (1287°C)
- ▶ Elevated strength-to-weight and stiffness-to-weight ratio
- ▶ High corrosion resistance to acids
- ▶ High thermal conductivity and heat capacity



BeWS-13 • 21 and 22 September 2017 • Narita, Chiba, Japan

Be Artificial Isotopes

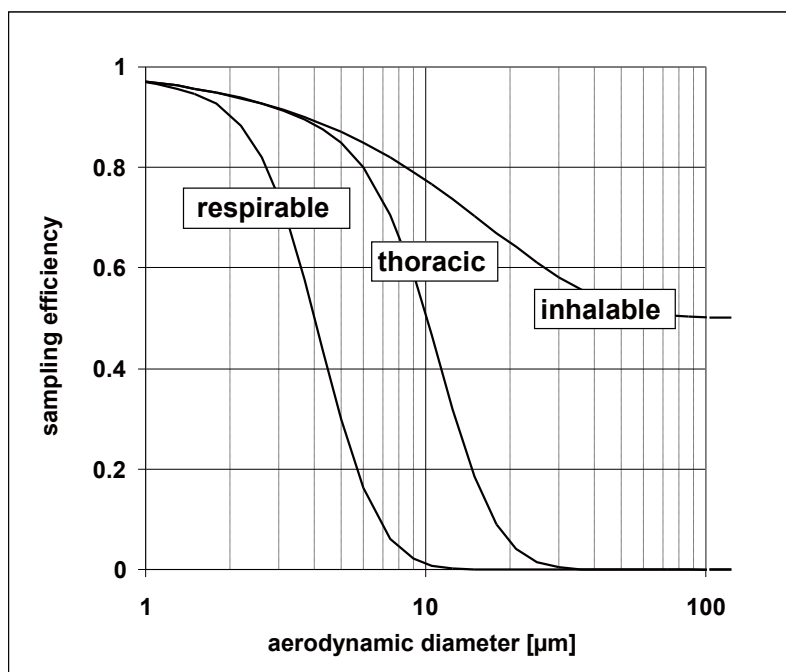
Isotope	Mass	Half-life	Mode of decay	Nuclear spin
${}^6\text{Be}$	6.01973	5.9×10^{-21} s	$2p$ to ${}^4\text{He}$	0
${}^7\text{Be}$	7.016929	53.28 d	EC to ${}^7\text{Li}$	$\frac{3}{2}$
${}^8\text{Be}$	8.0053051	about 7×10^{-17} s	2α to n	0
${}^{10}\text{Be}$	10.013534	1.52×10^6 y	β^- to ${}^{10}\text{B}$	0
${}^{11}\text{Be}$	11.02166	13.8 s	β^- to ${}^{11}\text{B}$; $\beta^- + \alpha$ to ${}^7\text{Li}$	$\frac{1}{2}$
${}^{12}\text{Be}$	12.02692	0.024 s	β^- to ${}^{12}\text{B}$; $\beta^- + n$ to ${}^{11}\text{B}$	0
${}^{13}\text{Be}$	13.0428	0.004 s	β^- to ${}^{13}\text{B}$; $\beta^- + n$ to ${}^{12}\text{B}$; $\beta^- + 2n$ to ${}^{11}\text{B}$	0

Environmental, Health & Safety (EH&S) Basics

- ▶ All Beryllium Materials Must Be Treated Alike
- ▶ Solid Forms Pose No Special Hazards
- ▶ Necessary Conditions
 - ▶ Allergic Reaction
 - ▶ Airborne & Ultra-Fine
- ▶ All Materials Recyclable
- ▶ Buy-Back Program



► Sampling Conventions



► Inhalable Samplers



GSP

IOM

Typical Inhalable Samplers
Used in Europe

- GSP (Gesamtstaubprobe) is a collection device with a cone-shaped inlet section (CIS)
- A filter capsule containing a 37 mm filter is placed inside the sampler for particulate sampling
- The GSP is operated at a flow rate of 3.5 liters/min

▶ Total Particulate Samplers

- ▶ The 37mm closed-face filter cassette is equipped with a 4mm inlet hole holding a 37mm filter
- ▶ Sampling flow rate is 2.0 liters/min
- ▶ The closed face filter cassette samples total particulate



CFC Filter Cassette

**Typical Total Particulate Sampler
Used in U.S.A.**

2.6.3 Beryllium business of NGK Insulators and topics of beryllium safety issue

K. Nojiri

New Metal Division, NGK Insulators,ltd, Nagoya, Japan

E-mail: nojiri@ngk.co.jp

NGK is one of the worldwide leader companies of in the field of fine ceramic products. The new metal division specialises in metal products specially beryllium and beryllium containing alloys. Beryllium has unique and excellent characteristics like low density, high rigidity, high heat resistance, high sound speed, high X-ray penetration, interesting nuclear properties, etc. The most important property of Beryllium is as the additive to produce copper base alloys. Only few percentage of beryllium addition provides super high mechanical strength, which is equivalent of special steels, in keeping high electrical and thermal conductivity of copper. Beryllium copper alloys are high-end materials for electric and electronic parts that other competitive materials can't follow.

NGK Insulators is producing the beryllium copper alloys and the beryllium metal products with sophisticatedly organised beryllium safety control system. Some topics of beryllium safety issue will be presented in the workshop.

22th September 2017, Narita, Japan

Beryllium business of NGK Insulators and topics of beryllium safety issue

Keigo NOJIRI

NGK Insulators, Ltd

Aichi Japan

Before my presentation,,,



Commented by NOJIRI in 11th IEA International
Workshop on Beryllium Technology, Barcelona, 2013

Beryllium is one of hazardous materials.

Some knowledge and precaution are necessary
to work with beryllium.

ITER will need certain quantity of beryllium very
soon.

We need review and discussion for total safety
& health with beryllium,,,



Today's presentation

- NGK Insulators, Ltd
- NGK's Beryllium Business
- NGK's Beryllium Safety Management System
- Goal
- Topics
 - Beryllium Working Area Control
 - Respiratory Protective Equipment
- Conclusion

NGK Insulators, Ltd



Company Name

NGK INSULATORS, LTD.

Date of Establishment

May 5, 1919

Sales

435.8 Billion Yen

Number of Employees

17,517

Consolidated Subsidiaries

58 companies

As of March 31, 2017

World Network

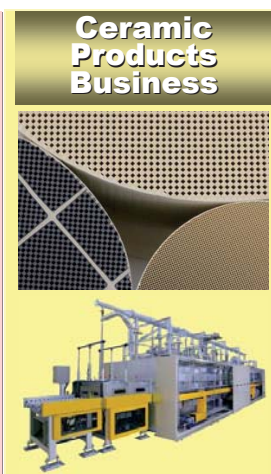


Main Products

Power Business



Ceramic Products Business

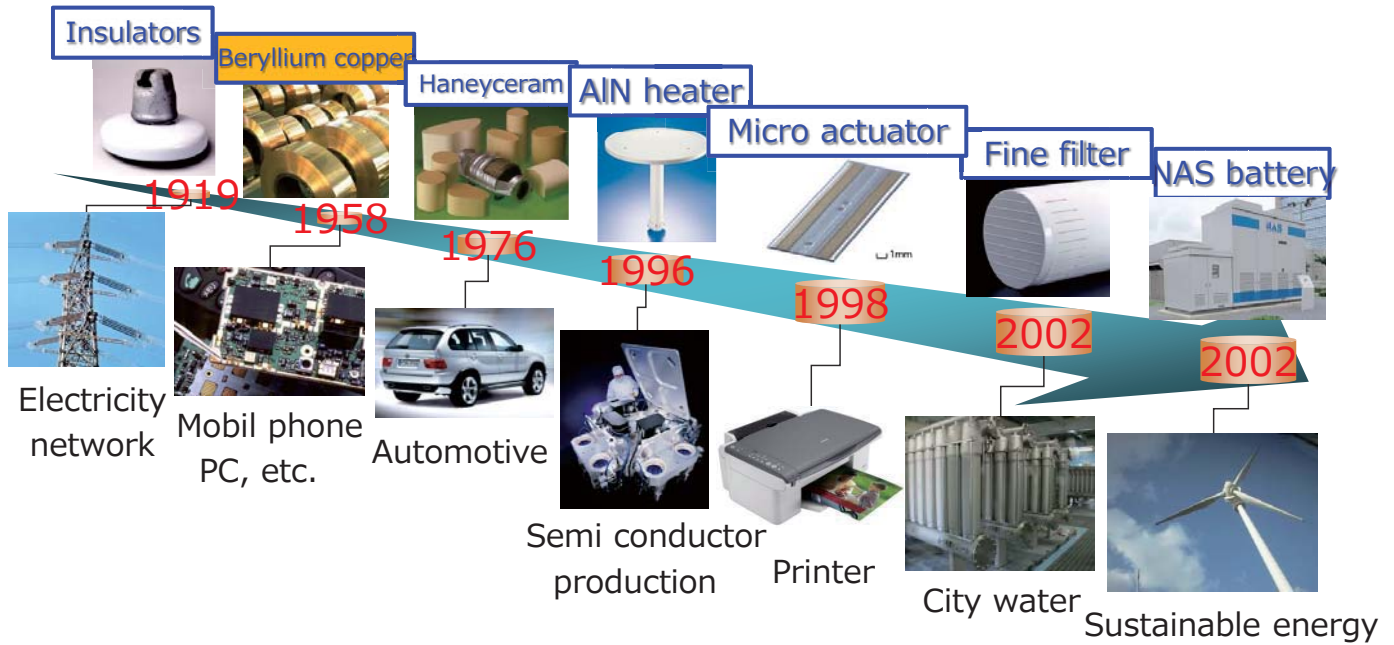


Electronics Business

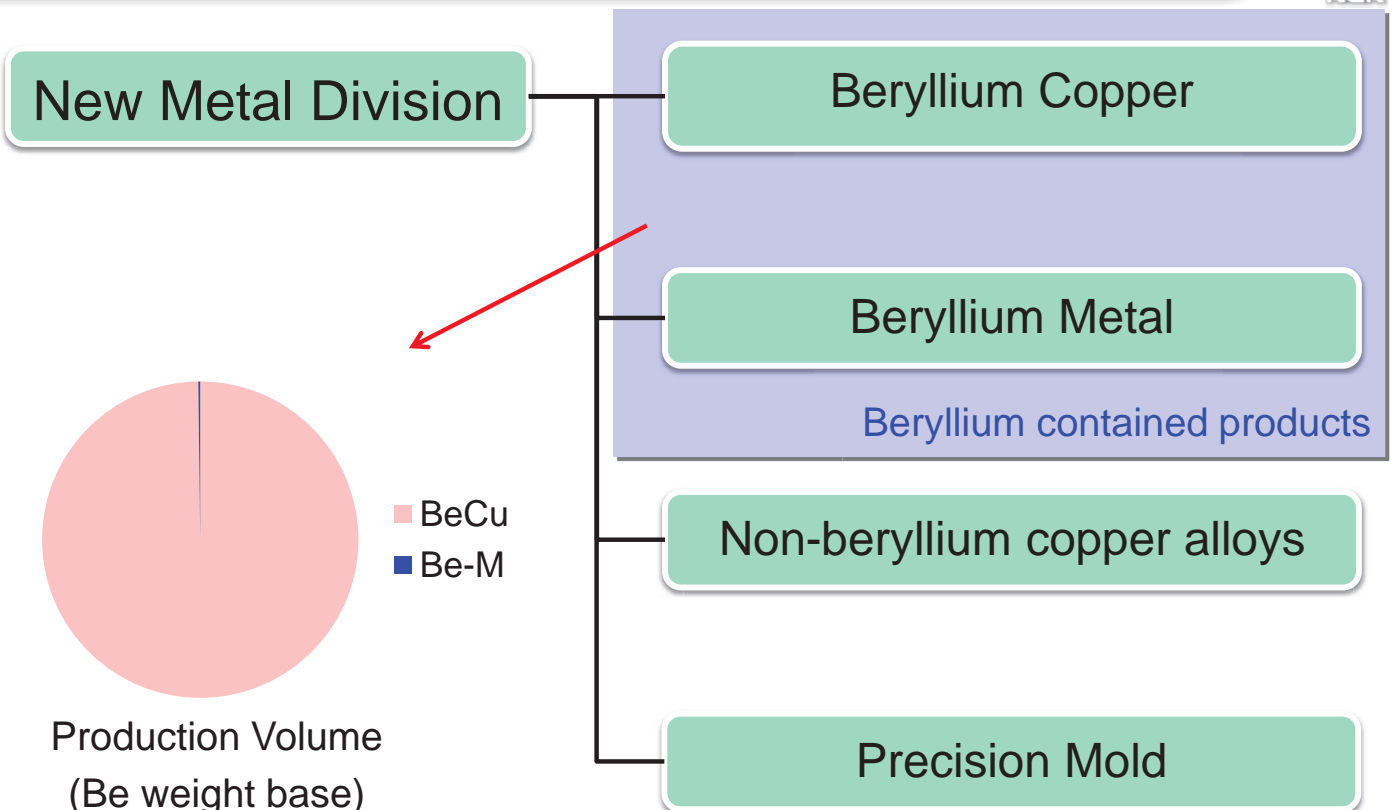




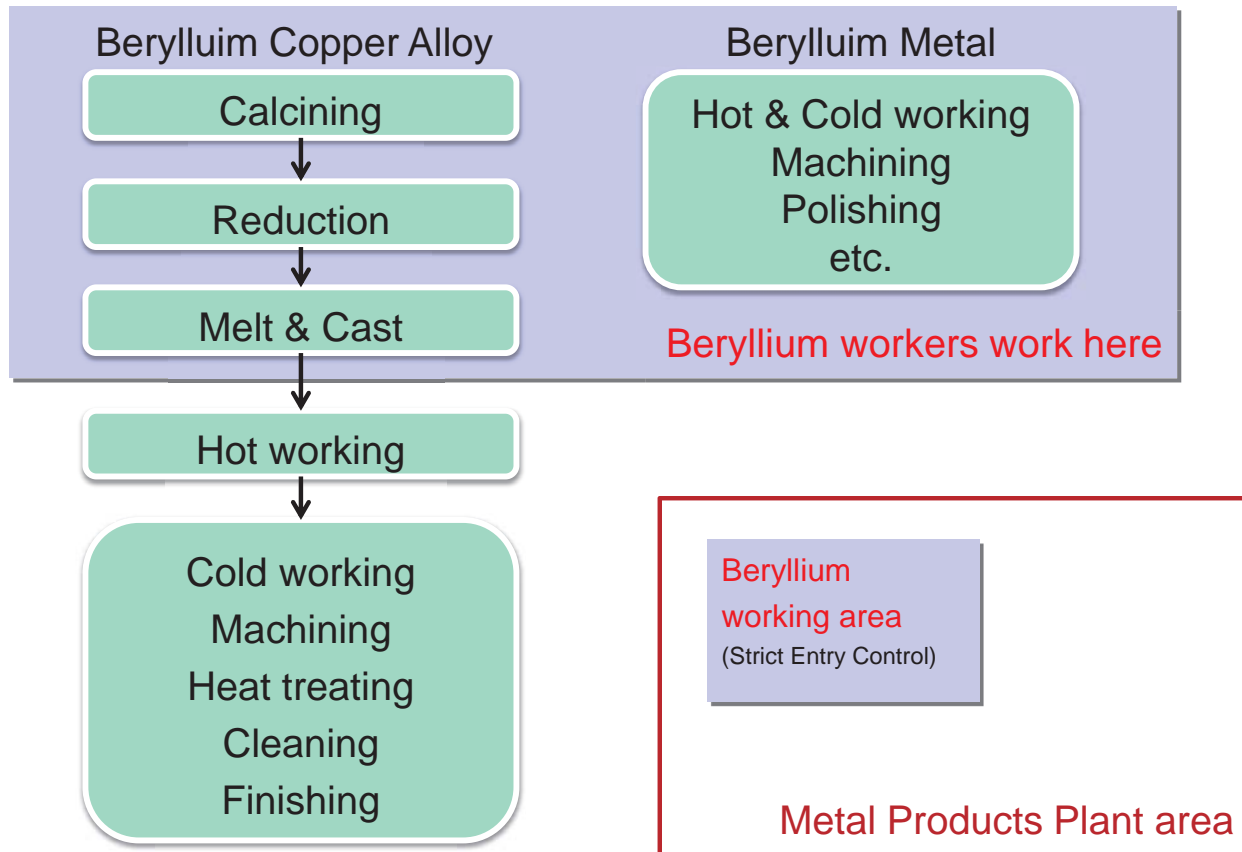
At the beginning of 20th century,,
An engineer visited the United States and impressed so much by higher developed society. He had brought back a small broken piece of Insulator,,



NGK's Beryllium business



NGK's Beryllium business



Beryllium Safety Management in NGK



- NGK's Beryllium Safety Management System
- Goal
- Topics
 - Beryllium Working Area Control
 - Respiratory Protective Equipment

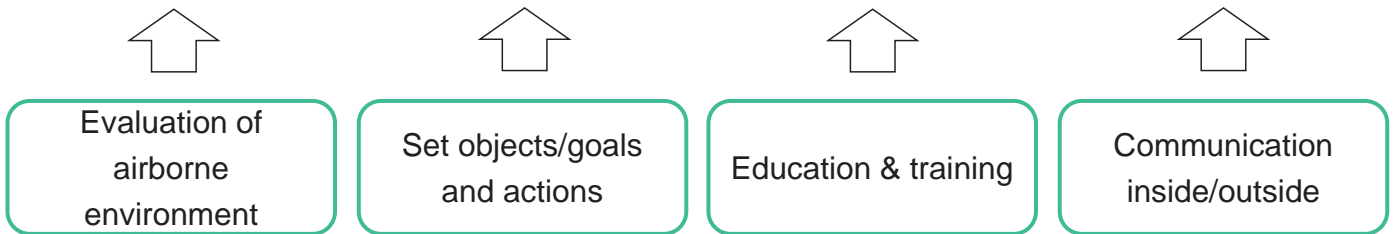
To be audited by top management once a year

Object

- Prevent health disorders of beryllium workers
- Prevent water & air pollution which cause health disorders of local residents

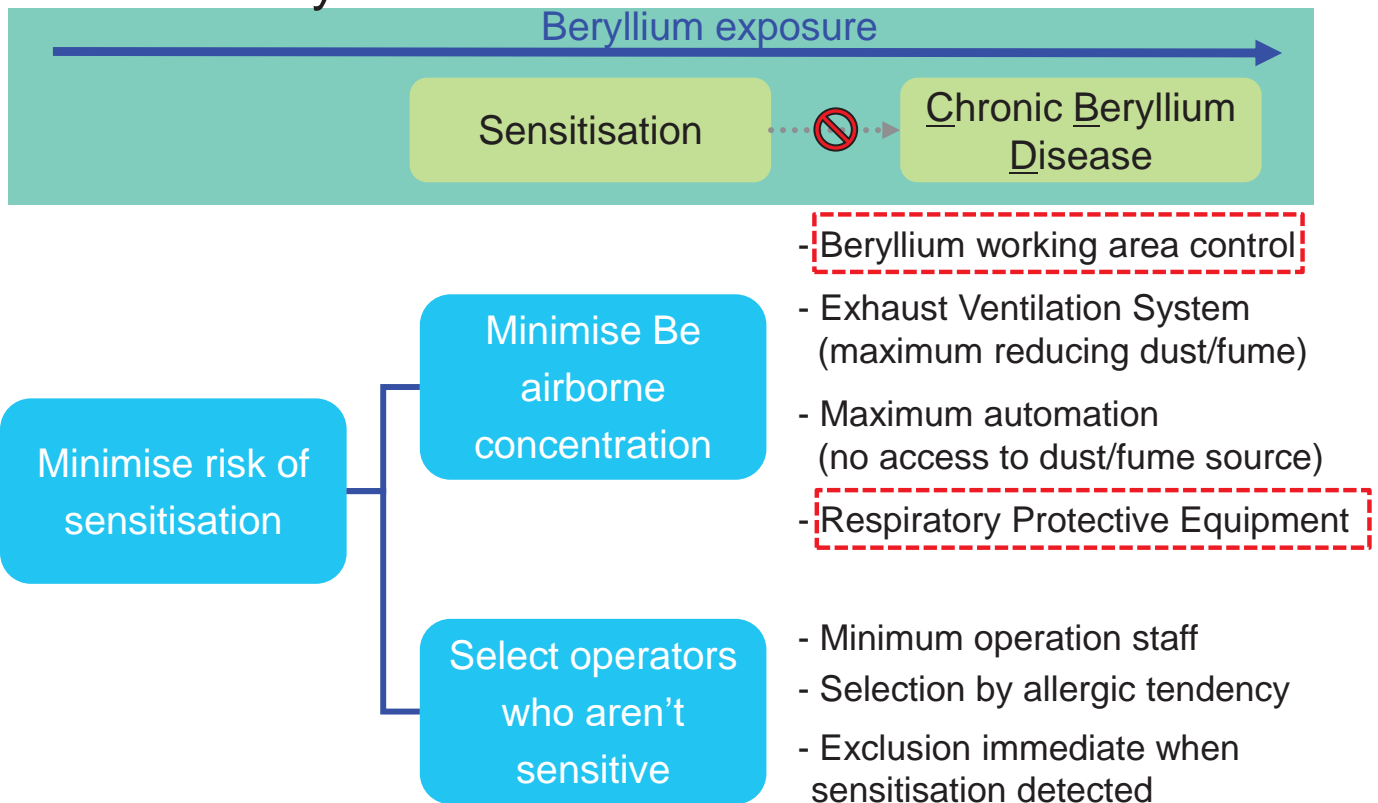
Policy

- First priority is to secure health of people concerned in the NGK's Be operation
- Prevent any pollution and keep strictly related laws and agreements with the authorities
- Promote developments & improvements for reducing airborne concentration
- Push recycling & lifetime extension to reduce beryllium waste
- Raise awareness of employees by education & training
- Continue improving by revising periodically the management system
- Set objects & goals and execute actions and revise them

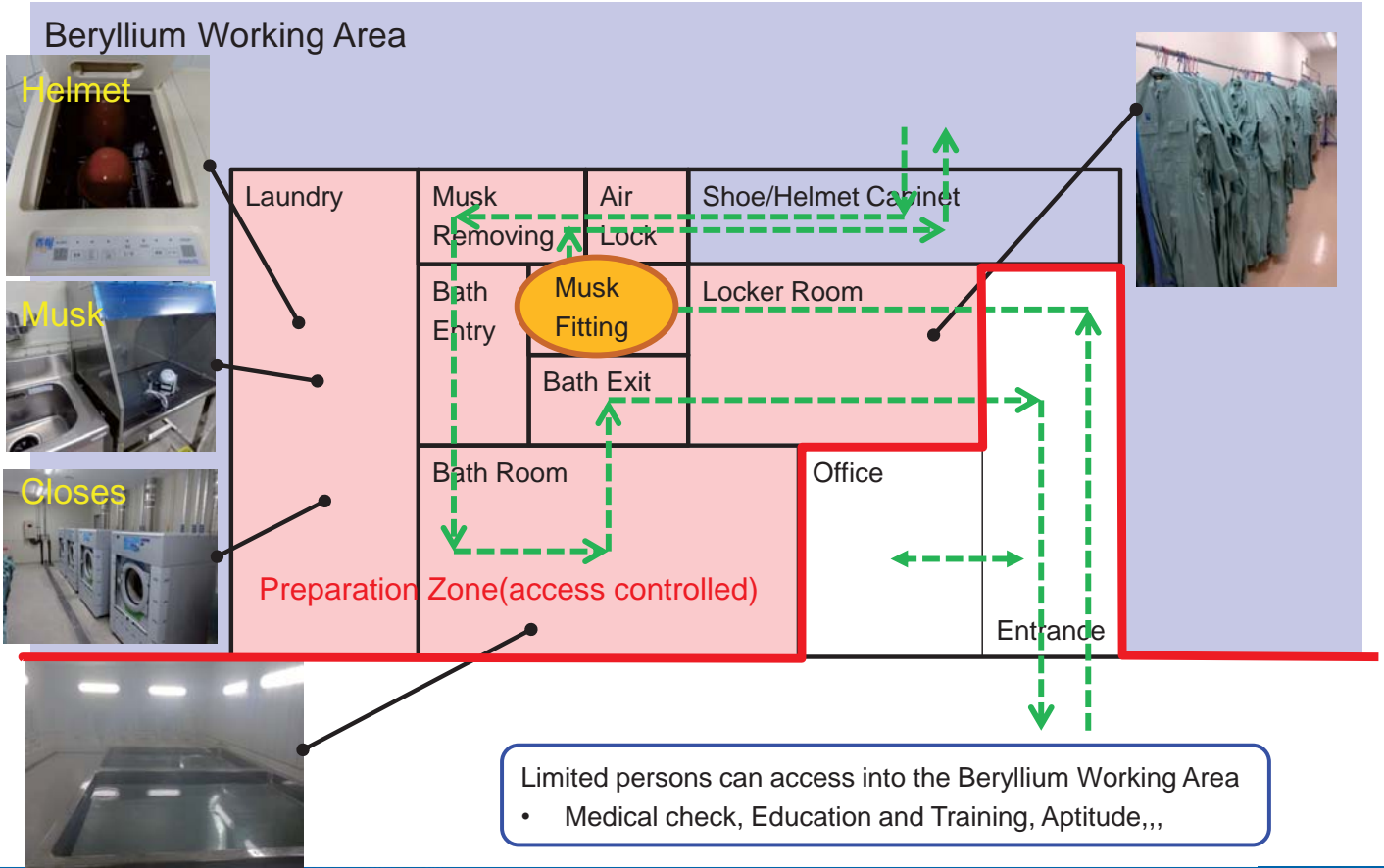


“Goal”

No CBD any more !



Beryllium Working Area Control



Respiratory Protective Equipment



Particle Collection Efficiency

>99.5%



>99.9%

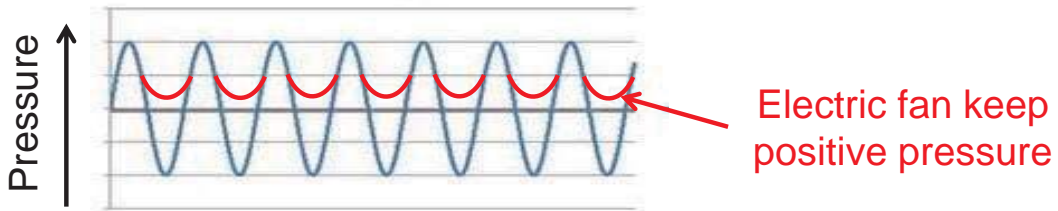


- Speech diaphragm (easy communication)

>99.9%



- Speech diaphragm
- Synchronised Powered Air Purifying respirator



For higher risk zone,,,



Purified air by
compressor

Conclusion

- Beryllium Working Zone control and Respiratory Protective Equipment are very important for Beryllium Safety Management
- NGK will continue improving for Zero CBD



Thank you for your attention

2.6.4 Recent achievements and related safety issues concerning beryllide applications

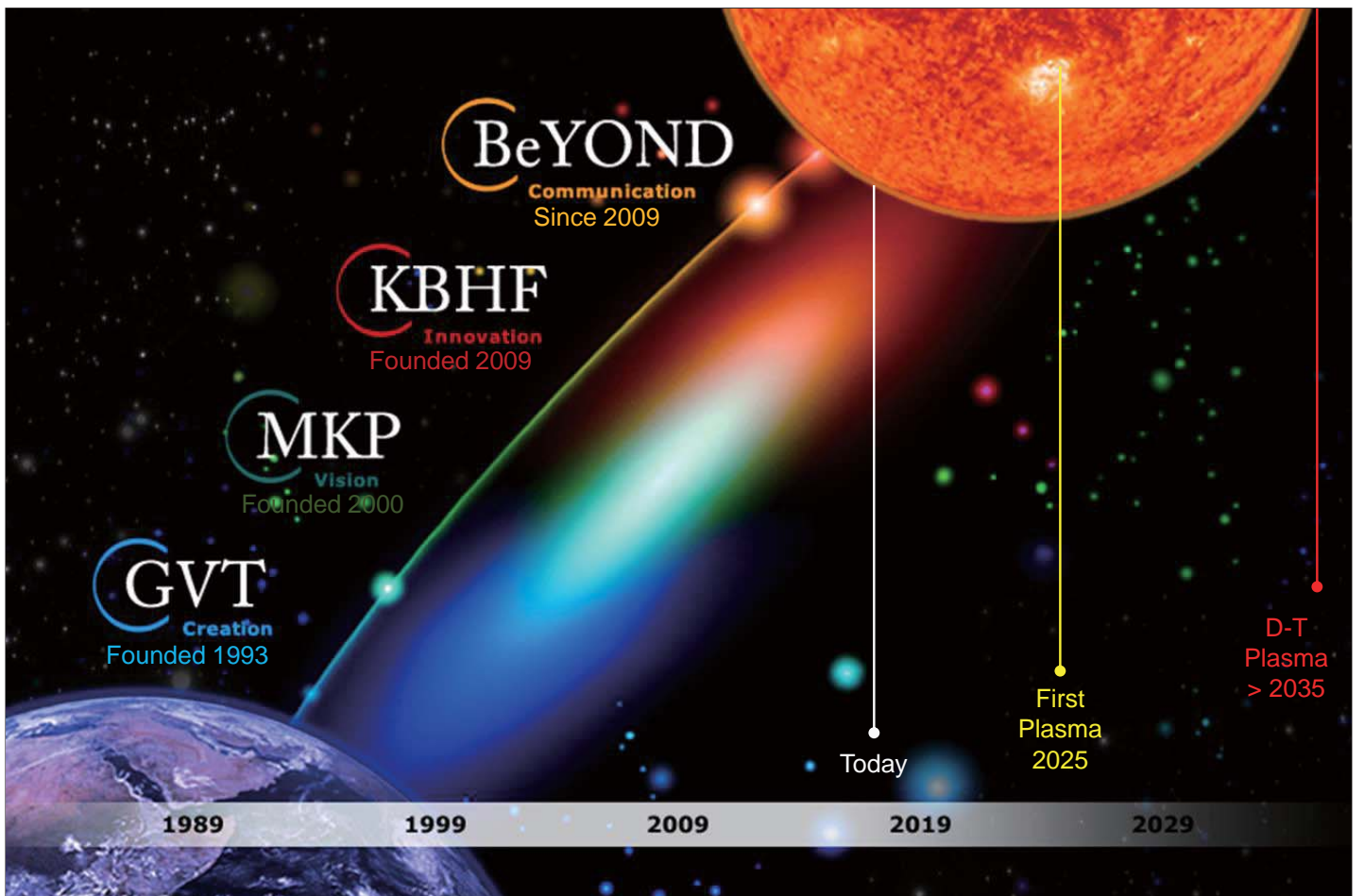
A.Goraieb

KBHF GmbH, Germany

For over 30 years, Karlsruhe Institute of Technology (KIT) has conducted research and development on the fusion blanket, which has several critical functions: along with fuel production and heat removal, the blanket also serves as a radiation shield. To fulfill these tasks in a Solid Breeder Blanket, Lithium is necessary as breeder, while Beryllium serves as a multiplier.

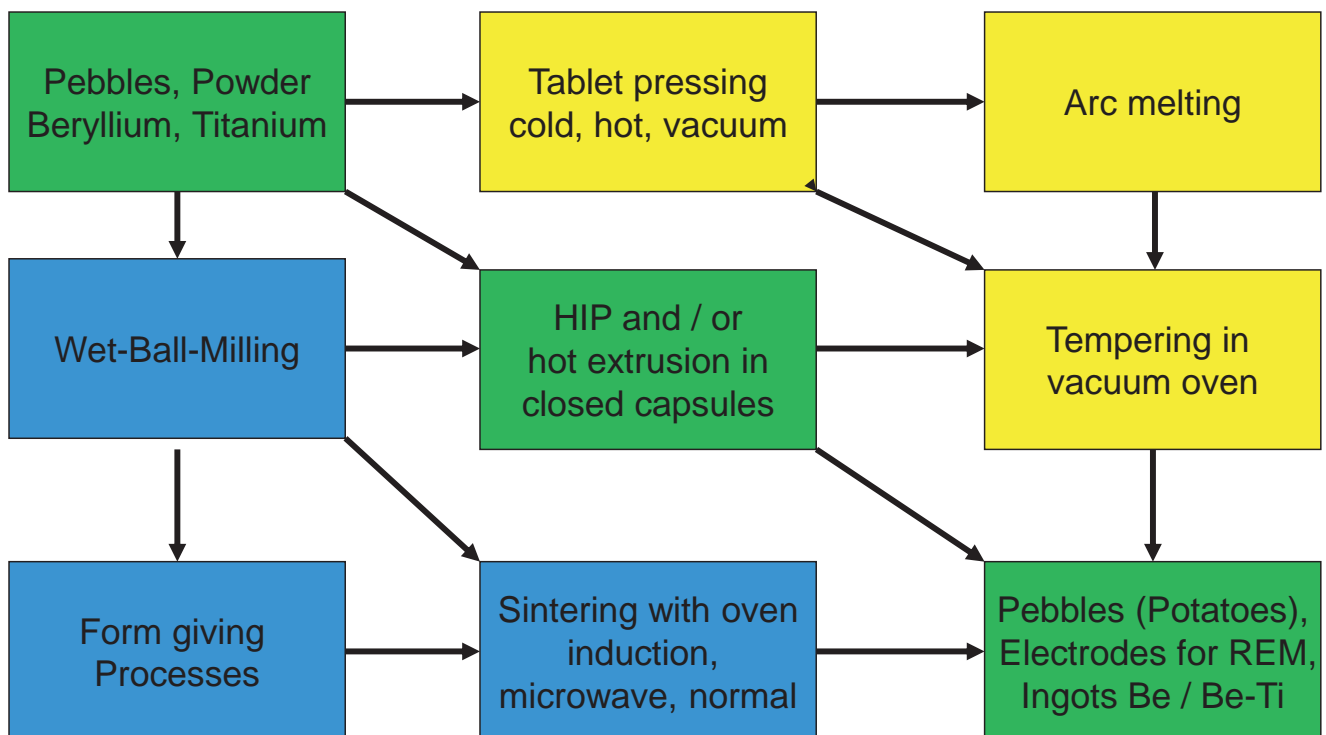
The Karlsruhe Beryllium Handling Facility (KBHF) is a spin-in of KIT and a good example of the “open campus strategy” – a symbiotic partnership based on 25 years of joint R&D projects and extensive experience with beryllium and lithium ceramics. KBHF is tasked with scaling processes and operating pilot facilities for the production of beryllium alloys and lithium ceramics. The lab also serves as a model facility for a future beryllium handling facility as part of ITER. KBHF is located on KIT’s North Campus.

The use of pure beryllium and lithium poses technical challenges and also safety risks. Therefore a special Health & Safety strategy has to be set in place. It involves buildings, equipment, handling as well as training concepts for workers. In this “Safety Talk” several aspects that can be called “best practice” will be shown and can be discussed.



**13th International Workshop on Beryllium Technology (BeWS-13)
21-22 September 2017 Narita, CHIBA, Japan**

Working with Beryllium since 1991



Material Testing on Beryllium Pebble Beds, Material Design (Beryllides), Production Research & Safety



Be-Ti; Be-Zr; Be-V; Be-Cr; Be-W

- Composites are produced by (milling), mixing and canning the powders followed by Hot Extrusion
- The Hot Extruded material is then cut and dismantled (Elektrodes for REM) or capsuled again
- These capsules are evacuated or Electron Beam (EB) welded and Hot Isostatic Pressed (HIP)

Workers' Health Care and Safety

- Medical examination for workers once a year, including the capability to wear respirator masks
- In addition, regular instruction on all aspects of hazard identification and safety regulation
- A safety representative from KIT and I are working out details for the briefing
- In case of new or never done before activities, a risk assessment is foreseen
- Full size respirator masks with P3 Filters are located at every entrance to the safety areas



BERYLLIUM

Topics covered

1. Physical Properties
2. Uses
3. Hazards
4. Medical Treatment
5. Legal Aspects
6. Working Standards



7. Engineering Controls
8. Personal Protective Equipment
9. Monitoring
10. Medical Surveillance
11. Movement of items
12. Waste

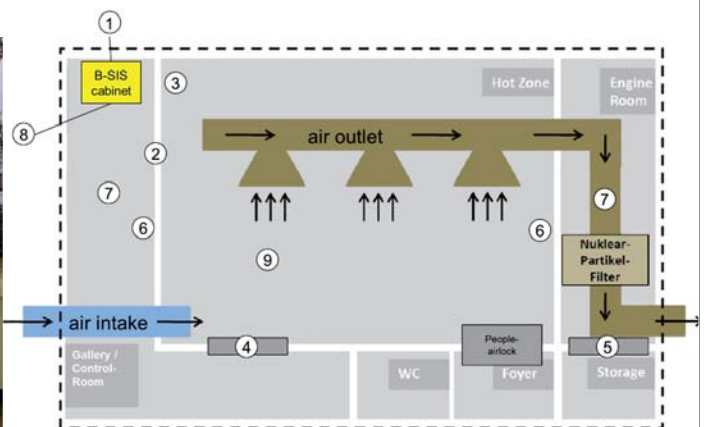


In the event of emergency or for information, contact
 ... based on lessons given at JET, modified for our purpose
 JET Joint Undertaking, Abingdon, Oxfordshire OX14 3EA Tel: 0235 464785

JJ1516C

Usual and ...

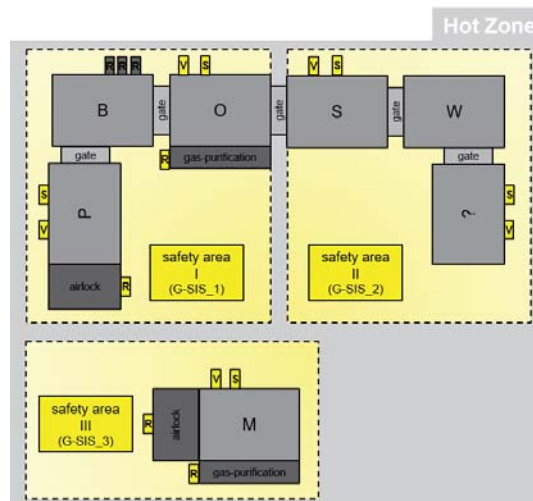
- Building with ventilation, airflow about 10 times an hour
- Lower pressure (- 5 Pa) in the building to save the environment
- Emergency generator
- Particle filtering units
- Inventory that can easily be decontaminated



High Safety Laboratory for the Handling of Beryllium on the KIT Campus

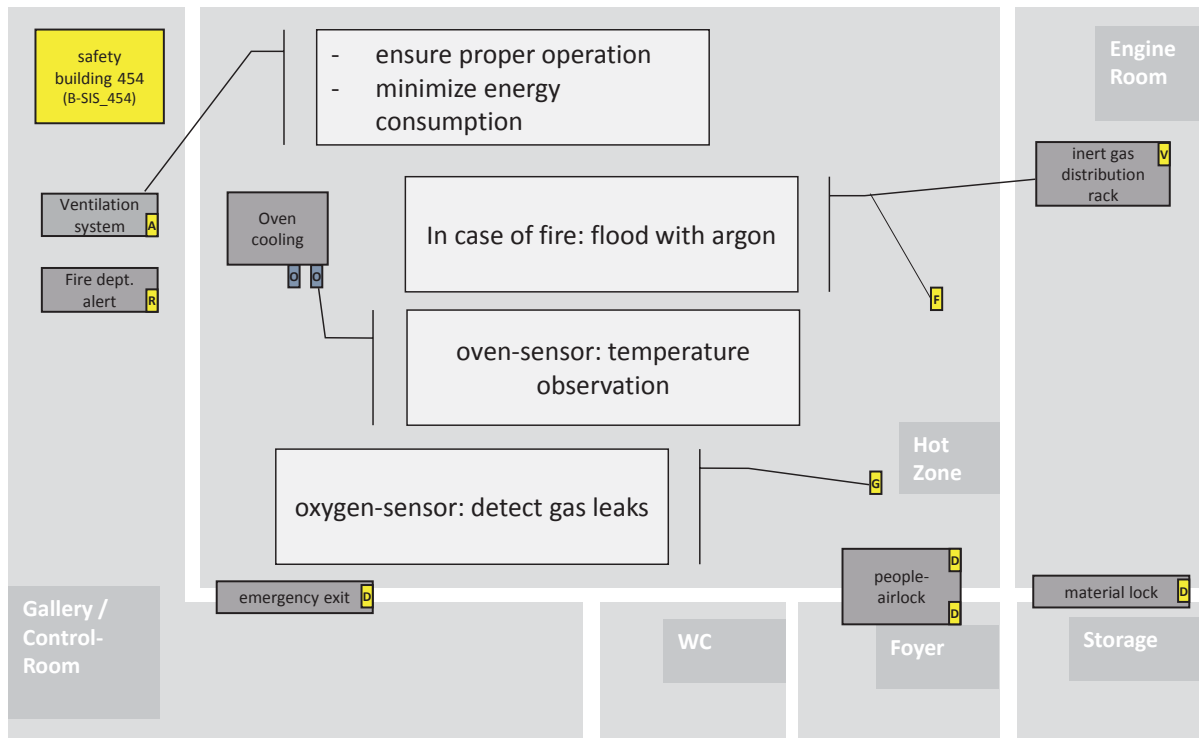
... unusual solutions

- Modular glove boxes for all activities connected to Beryllium
- Controlled lower pressure (- 5 mbar) in the glove boxes
- Inert gas atmosphere to protect materials and allows a leak detection
- Airlock with control panel for all systems
- All systems are connected with the “Central intelligence” of the building



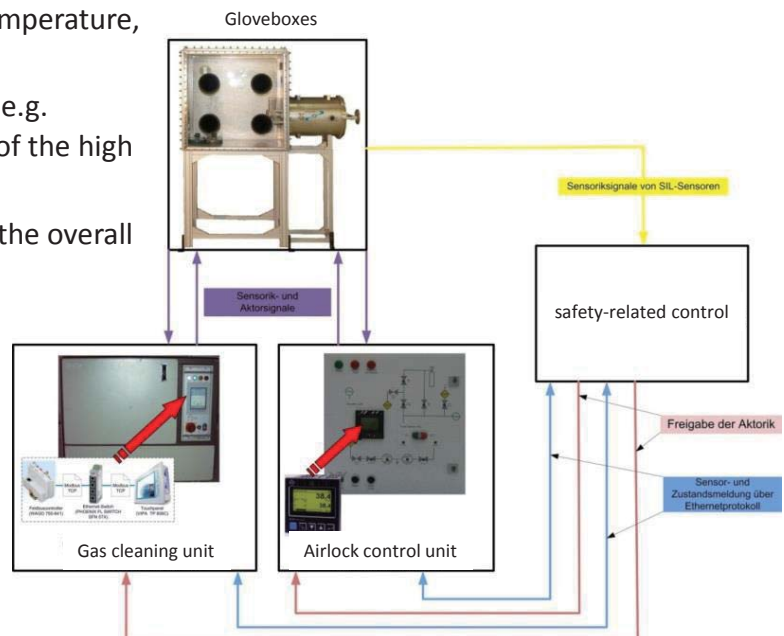
Hazard and risk assessment for developed system Results for the individual hazards

Hazardous event	Building / System	Result	SIL
Defect in the gas line	Building 453, Glove box system	S2, A2, G2, W1	SIL 2
Flammable solids, liquids and Gases can ignite	Building 453, Building 454	S1, A2, G1, W1	No SIL
Undue high-pressure (1) in the glove box (15 mbar > Prel > 0 mbar)	Glove box system	S2, A2, G2, W1	SIL 2
Undue high-pressure (2) in the glove box (Prel > 15 mbar)	Glove box system	S2, A2, G2, W1	SIL 2
Undue low-pressure in the glove box (Prel < -15 mbar)	Glove box system	S2, A2, G2, W1	SIL 2



Safety Requirements

- Central monitoring, fault detection, logging and reporting with top priority across all modules
- Redundancy of the individual sub-systems to bypass in case of failure
- Recording of environmental conditions (e.g. detection of persons, gas warning, temperature, pressure,)
- Minimizing the energy consumption (e.g. situation depends on the ventilation of the high safety laboratory)
- Possibility to use Remote Control for the overall system and individual sub-systems



**Bachelor-/Master-/Studien-/Diplomarbeit
Sicherheitstechnik bei Gefahrstoffverarbeitung**

Rahmen: Das am IFL und Campus Nord stattfindende Projekt „Beryllium-Labor“ im Zusammenhang mit dem Gefahrstoff Beryllium erfordert eine entsprechende Infrastruktur. Aus diesem Grund wurde ein Labor für die Aufnahme einer Pilotanlage für die Produktion von Berylliumlegierungen eingerichtet. Eine Handschuhbox wurde bereits mit neuester Sicherheitstechnik ausgestattet - weitere sollen aufgestellt werden und in ein sicherheitsgerichtetes Gebäudemangementssystem integriert werden.

Problemstellung: Für die Gesamtanlage wurde bereits ein grundlegendes Sicherheitskonzept erstellt. Die vorhandene sicherheits-Hardware soll an die Anlage angepasst werden.

Aufgabe: Die Konzepte sollen überarbeitet, geprüft und implementiert werden. Hierbei müssen Routinen und Verfahren zur sicherheitsgerichteten Programmierung beachtet werden.

Voraussetzung: Ist Interesse an Entwurf, Konstruktion und Testbau der Anlage. Zur Anbindung an die Gebäudesteuerung sind Kenntnisse im Bereich der SPS-Programmierung von Vorteil.

Geboten wird eine spannende Arbeit, die einen Einblick in die Besonderheiten der Programmierung von Sicherheitstechnischen Systemen bietet.

Forschungsbereich: Steuerungs- und Sicherheitstechnik für Kernfusion

Projekt: Beryllium-Labor: Global Facility Safety System (GFSS)

Ausrichtung:

- Experimentell
- Theoretisch
- Praktisch
- Simulation
- Konstruktion (CAD)
- Hardware-Design (CAE)
- Hardwarenahe Programmierung
- SPS-Programmierung
- Anwendungsentwicklung
- Sicherheitstechnik

Studiengang:

- Maschinenbau
- Mechanik
- Elektrotechnik
- Informatik
- Informationswirtschaft
- Wirtschaftsingenieurwesen

Beginn: ab sofort

Bei Interesse einfach kurz melden oder vorher kommen:

Andreas Trenkle
Gottlieb-Frank-Str. 8
Geb. 50.38, Raum 1.12
Telefon: 071 608 48425
trenkle@ifl.kit.edu

**Bachelor-/ Master-/ Studien-/ Diplomarbeit
Konstruktion und Aufbau einer Personenschleuse**

Rahmen: Das am IFL und Campus Nord stattfindende Projekt „Beryllium-Labor“ im Zusammenhang mit dem Gefahrstoff Beryllium erfordert eine entsprechende Infrastruktur. Aus diesem Grund wurde ein Labor für die Aufnahme einer Pilotanlage für die Produktion von Berylliumlegierungen eingerichtet. Eine Handschuhbox wurde bereits mit neuester Sicherheitstechnik ausgestattet - weitere sollen aufgestellt werden und in ein sicherheitsgerichtetes Gebäudemangementssystem integriert werden.

Problemstellung: Der Eingang zum Labor ist durch eine Tür gesichert. Die Gebäudesteuerung hat keine Möglichkeit festzustellen, ob sich eine oder mehrere Personen im Labor befinden. Dies ist insbesondere bei Gasaustritt oder Brand gefährlich.

Aufgabe: Um mittels Gebäudesteuerung zu erfassen, ob und wie viele Personen sich im Labor aufhalten, soll eine Personenschleuse konstruiert und aufgebaut werden. Die Schleuse soll der Identifizierung von Personen (mittels Schmisschlagkarte) und der Personenerkennung dienen. Hierfür sollen Konzepte erstellt, bewertet und eines zur Konstruktion ausgewählt werden.

Voraussetzung: Ist Interesse an Entwurf, Konstruktion und Testbau der Anlage. Zur Anbindung an die Gebäudesteuerung sind Kenntnisse im Bereich der SPS-Programmierung von Vorteil.

Geboten wird eine spannende konstruktive Arbeit, die nach Abschluss direkt eingesetzt werden soll.

Forschungsbereich: Steuerungs- und Sicherheitstechnik für Kernfusion

Projekt: Beryllium-Labor: Global Facility Safety System (GFSS)

Ausrichtung:

- Experimentell
- Theoretisch
- Praktisch
- Simulation
- Konstruktion (CAD)
- Hardware-Design (CAE)
- Hardwarenahe Programmierung
- SPS-Programmierung
- Anwendungsentwicklung
- Sicherheitstechnik

Studiengang:

- Maschinenbau
- Mechanik
- Elektrotechnik
- Informatik
- Informationswirtschaft

Beginn: ab sofort

Bei Interesse einfach kurz melden oder vorher kommen:

Andreas Trenkle
Gottlieb-Frank-Str. 8
Geb. 50.38, Raum 1.12
Telefon: 071 608 48425
trenkle@ifl.kit.edu

**Bachelor-/Master-/Studien-/Diplomarbeit
Sicherheitstechnik bei Gefahrstoffverarbeitung**

Rahmen: Das am IFL und Campus Nord stattfindende Projekt „Beryllium-Labor“ im Zusammenhang mit dem Gefahrstoff Beryllium erfordert eine entsprechende Infrastruktur. Aus diesem Grund wurde ein Labor für die Aufnahme einer Pilotanlage für die Produktion von Berylliumlegierungen eingerichtet. Eine Handschuhbox wurde bereits mit neuester Sicherheitstechnik ausgestattet - weitere sollen aufgestellt werden.

Problemstellung: Bereits genutzte Handschuhboxen sollen mit aktueller Sicherheitstechnik nachgerüstet werden.

Aufgabe: Hauptaufgabe ist die Integration der neuen Sicherheitstechnik in bestehende Systeme. Hierbei müssen - entsprechend der Werkzeuge in den Handschuhboxen (Säge, Schweißzahn, Fräser) - Anpassungen vorgenommen werden.

Voraussetzung: Ist Interesse an Entwurf, Konstruktion und Testbau der Anlage. Zur Anbindung an die Gebäudesteuerung sind Kenntnisse im Bereich der SPS-Programmierung von Vorteil.

Geboten wird eine spannende Arbeit, die einen Einblick in die Besonderheiten der Programmierung von Sicherheitstechnischen Systemen bietet.

Forschungsbereich: Steuerungs- und Sicherheitstechnik für Kernfusion

Projekt: Beryllium-Labor: Global Facility Safety System (GFSS)

Ausrichtung:

- Experimentell
- Theoretisch
- Praktisch
- Simulation
- Konstruktion (CAD)
- Hardware-Design (CAE)
- Hardwarenahe Programmierung
- SPS-Programmierung
- Anwendungsentwicklung
- Sicherheitstechnik

Studiengang:

- Maschinenbau
- Mechanik
- Elektrotechnik
- Informatik
- Informationswirtschaft
- Wirtschaftsingenieurwesen

Beginn: ab sofort

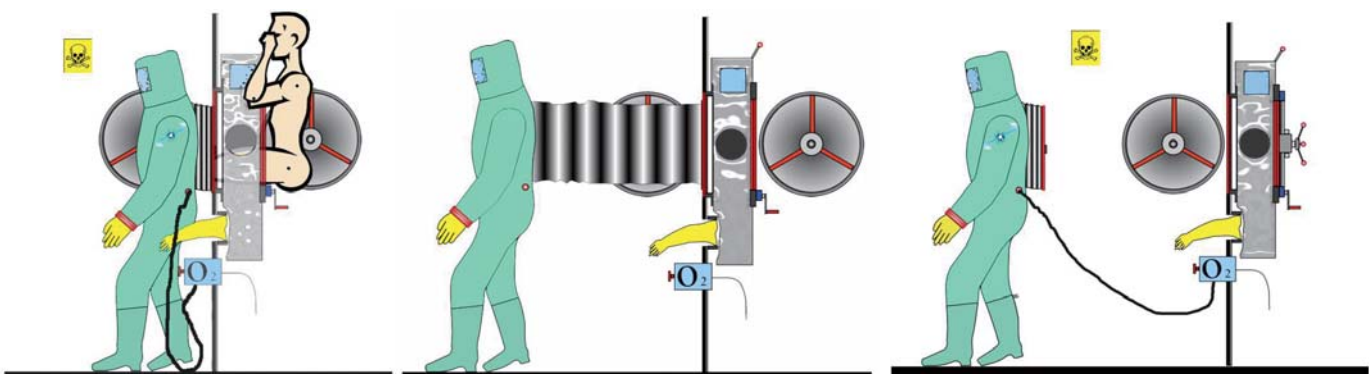
Bei Interesse einfach kurz melden oder vorher kommen:

Andreas Trenkle
Gottlieb-Frank-Str. 8
Geb. 50.38, Raum 1.12
Telefon: 071 608 48425
trenkle@ifl.kit.edu

14 Bachelor- and Master theses were necessary to build up this model facility for the Handling of Beryllium on the KIT Campus

Alternative Health Care and Safety solutions

- The safest solution is not to produce dusts or fumes during the processing of Beryllium
- This can be done by choosing electrical wire- or water-jet cutting as manufacturing method
- The second best solution concerning safety is to encapsulate the process
- Alternatively, a remote control or full automatic manufacturing process (rapid prototyping)
- If all this is not possible a “Frogman-Unit” connected to a Walk-In-Glovebox could be useful
- “Frogman-Units” allow the same safety as Gloveboxes and can contain inert gas atmosphere
- In this case the movement of the flexible connection has to be compensated for or disconnected



BeYOND Nr.-8, 13th and 14th of September 2018

Beryllium Opportunities for New Developments

Based on experience gained thus far with the BeYOND industrial forum, organizers plan to expand the scope of their communications for the period 2018-2025 (First Plasma)

BeYOND will continue to act as a fusion “think tank”, gathering and presenting information on research trends, political developments, business models and transfer ideas on a regular basis (see also article: “From Lab to Practice”, <http://www.atlantic-innovation.org/cases/lab-practice>)

The plan is to expand the scope of the forum to include continuing professional training/development and competency development catering to a diverse range of scientific, economic, national and international interests

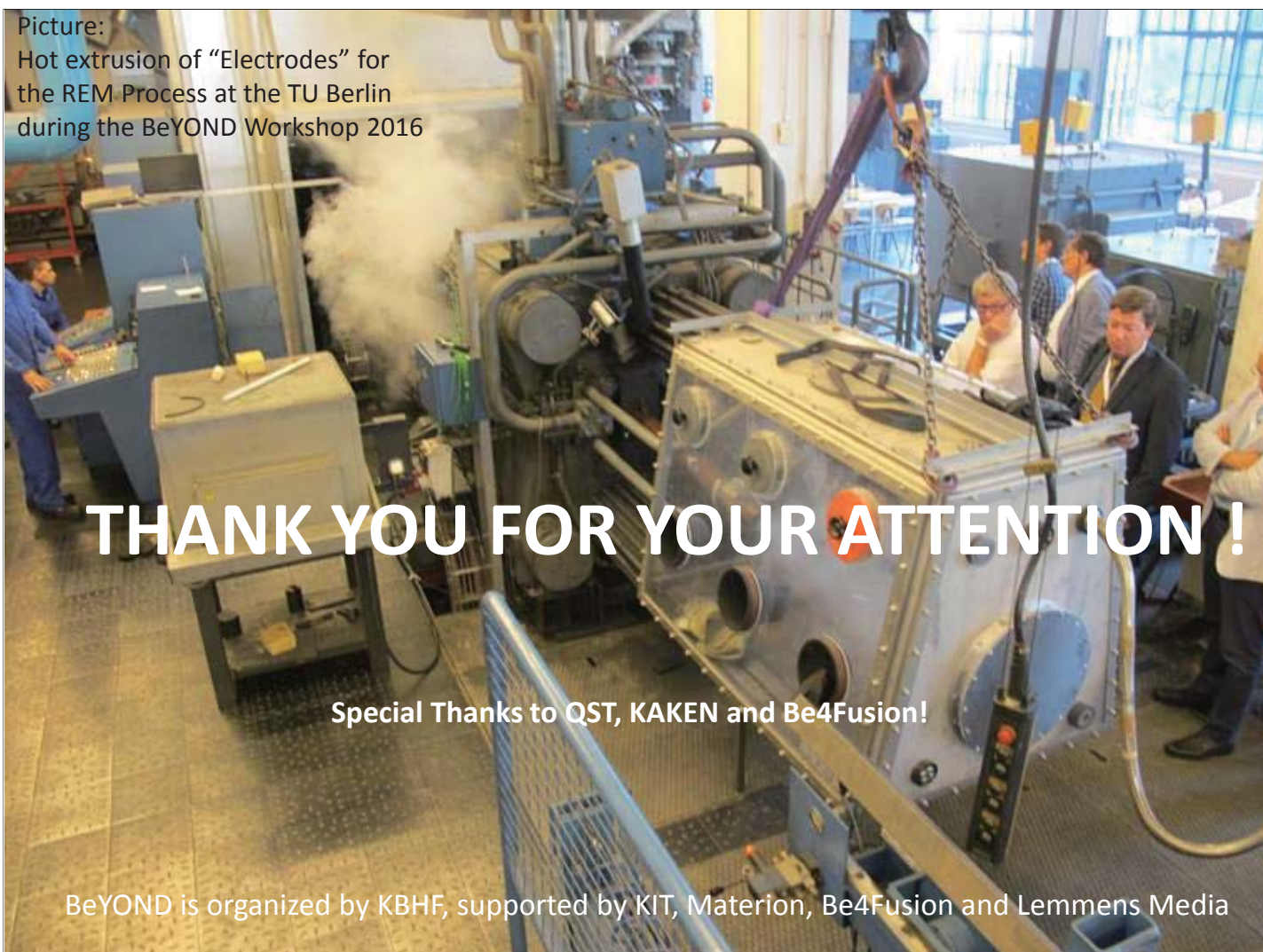
The expanded format will take effect with the BeYOND VIII (fall 2018) forum, which will include various industry workshops on the theme of “Handling Extreme Materials, Fusion and Sustainable Business Models”

Partners from business, research, and the public sector will be invited to attend

You are invited to join us next year in Karlsruhe, as well!

Picture:

Hot extrusion of “Electrodes” for the REM Process at the TU Berlin during the BeYOND Workshop 2016



THANK YOU FOR YOUR ATTENTION !

Special Thanks to OST, KAKEN and Be4Fusion!

BeYOND is organized by KBHF, supported by KIT, Materion, Be4Fusion and Lemmens Media

2.6.5 Facility introduction and safety issues in Rokkasho fusion institute, QST

M. Nakamichi, J-H. Kim, P. Kurinskiy

¹*Fusion Energy Research and Development Directorat, National Institutes for Quantum and Radiological Science and Technology (QST)
2-166, Omotedate, Obuchi, Rokkasho, Kamikita, Aomori, 039-3212, Japan*

E-mail: nakamichi.masaru@qst.go.jp

DEMO reactors require advanced neutron multipliers that have higher stability at high temperature. Beryllium intermetallic compounds (beryllides) are the most promising advanced neutron multipliers. Development of the advanced neutron multipliers has been started between Japan and the EU in the DEMO R&D of the International Fusion Energy Research Centre (IFERC) project as a part of the Broader Approach activities. In Japan, beryllides fabrication R&D has been carried out in the DEMO R&D building at IFERC, Rokkasho. The Beryllium (Be) Handling Room has been installed in the DEMO R&D building. In this facility, synthesis, treatment, machining and characterizations of beryllides and its pebbles are being performed.

In this study, facility introduction and safety issues in Rokkasho fusion institute, QST, will be reported.

Facility introduction and safety issues in Rokkasho Fusion Institute, QST

Masaru NAKAMICHI,
Jae-Hwan KIM, Petr KURINSKIY

National Institutes for Quantum and Radiological Science and Technology, QST



©2017 QST



Japanese Regulation for Beryllium Handling

Beryllium (Be)

3



4
9.012

Material data:

- Atomic Number: 4, •Atomic weight: 9.0,
- Specific weight: 1.85, •Melting point: 1300 °C

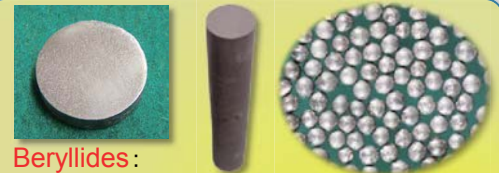
Intended purpose:

- Spring material (Be-Cu alloy),
- Reflector, Radiation window in X-ray equipment, etc.



Beryl (raw material)

Precious forms of beryl are aquamarine and emerald.



Beryllides:

Beryllides are intermetallic compounds of beryllium such as Be_{12}Ti that have higher melting point ($>1600^\circ\text{C}$) and higher stability at high temperature more than Be metal.



Toxicity



Hazardous to health

- Beryllium and this alloys ($>3\text{wt.}\%\text{Be}$).
- Specified chemical substance.
- Respirable beryllium particulate in the form of a dust, fume or mist, of a size less than $10\mu\text{m}$.
- Inhaling particulate may cause a serious, chronic lung disease called Chronic Beryllium Disease (CBD).
- Local exhaust ventilation system or sealed structure are required for beryllium handling.

Regulation System for Beryllium Handling in Japan

4

Beryllium and this alloys ($>3\text{wt}\%\text{Be}$) are defined as **specified chemical substances.**

Establishment of Regulation

Industrial Safety and Health Act

Enforcement Order of the Industrial Safety and Health Act

Ordinance on Industrial Safety and Health

Ordinance on Prevention of Hazards Due to Specified Chemical Substances

Regulation requirement level is different between purpose **for Manufacturing** and that **for Experimentation and Research**.

Administrative government agency:

The Ministry of Health, Labour and Welfare

Major Regulation Requirement comparison with Purposes

5

○ : necessity, —: un-necessity

Items \ Purpose	for Manufacturing	for Experimentation and Research
Manufacturing license	○	—
max. concentration (<0.001mg/m ³)	○	○
local exhaust ventilation system	○	— *
appointment of operations chief	○	—
establishment of work procedure	○	—
periodical voluntary inspection of machines	○	—
medical examination	○	○

*: Sealed structure or local exhaust ventilation system is required.

Notification of ventilation system is necessary to regulation agency without the manufacturing license.

6

Beryllium Handling Facility

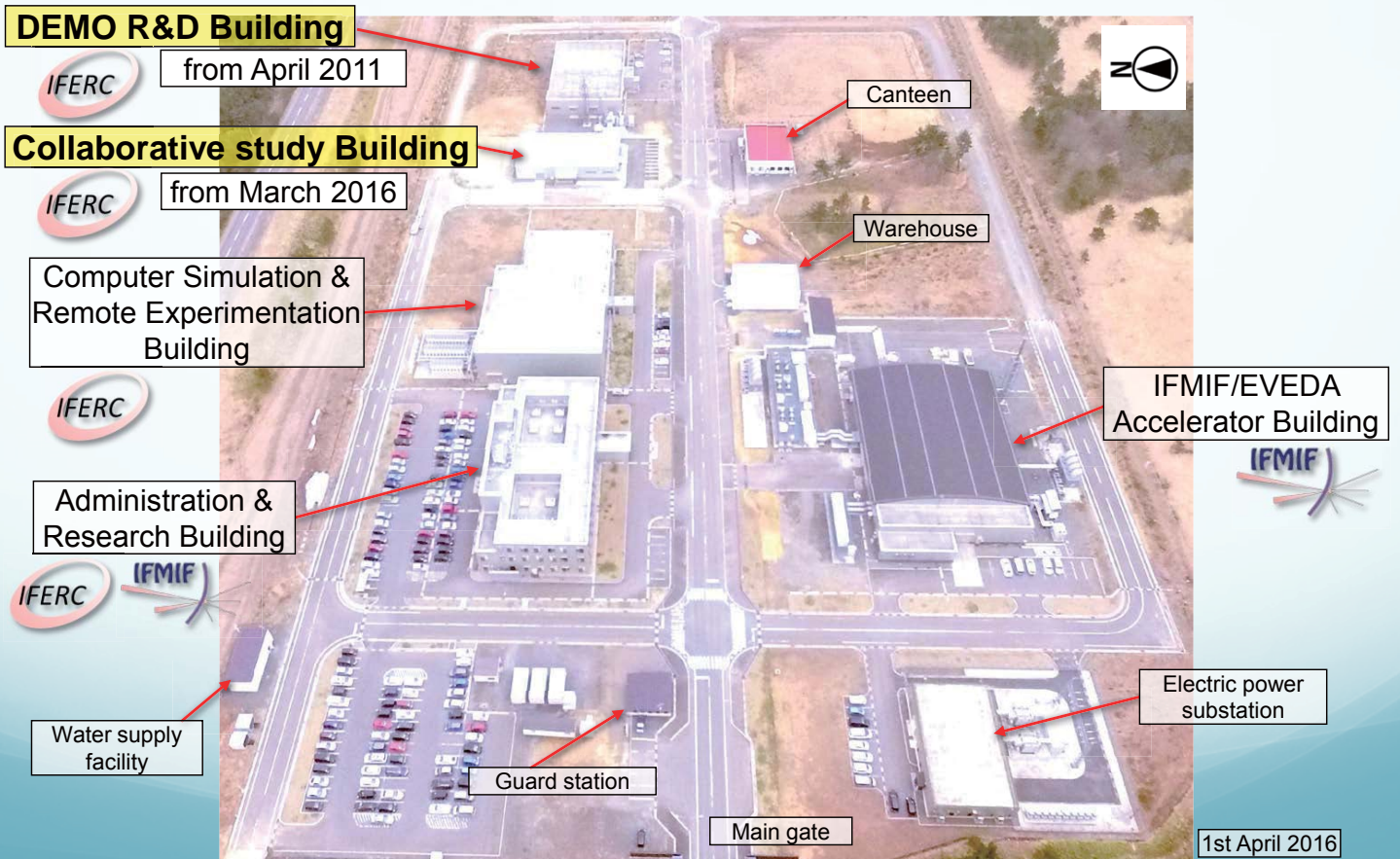
International Fusion Energy Research Centre (IFERC)

7



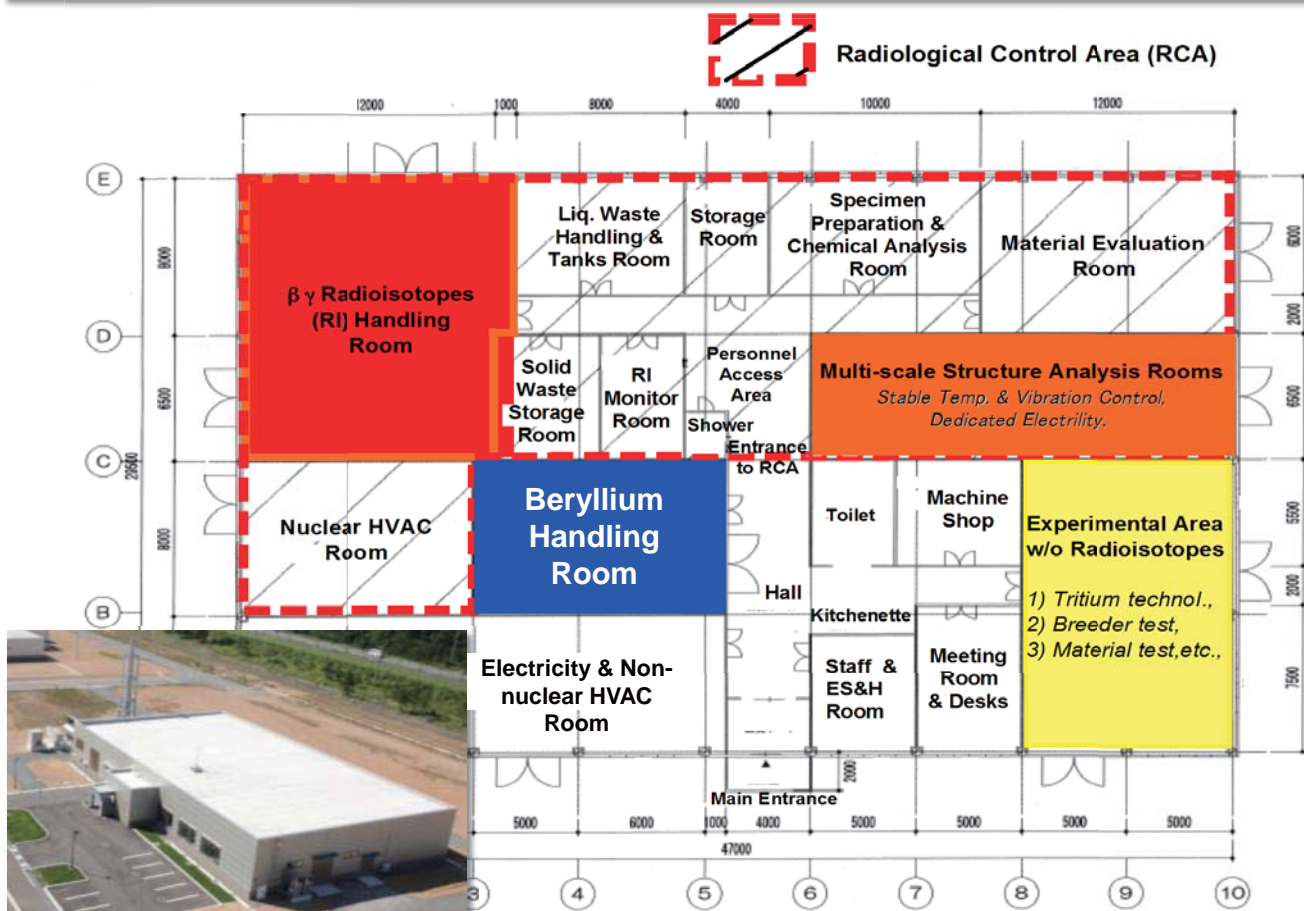
Arrangement in IFERC

8



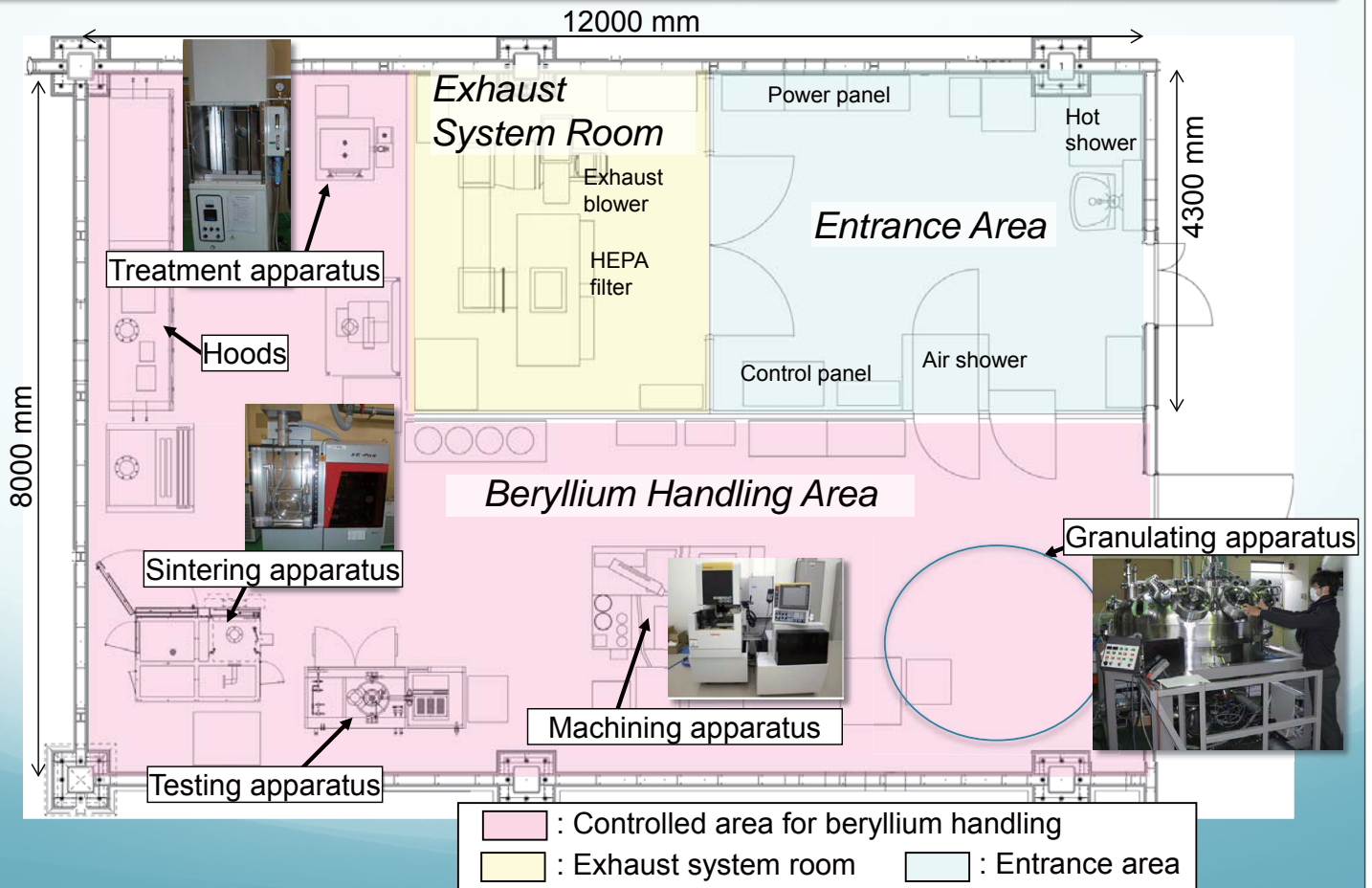
Beryllium Handling Facility in the R&D building

Arrangement in the DEMO R&D Building



Configuration in the Beryllium Handling Room

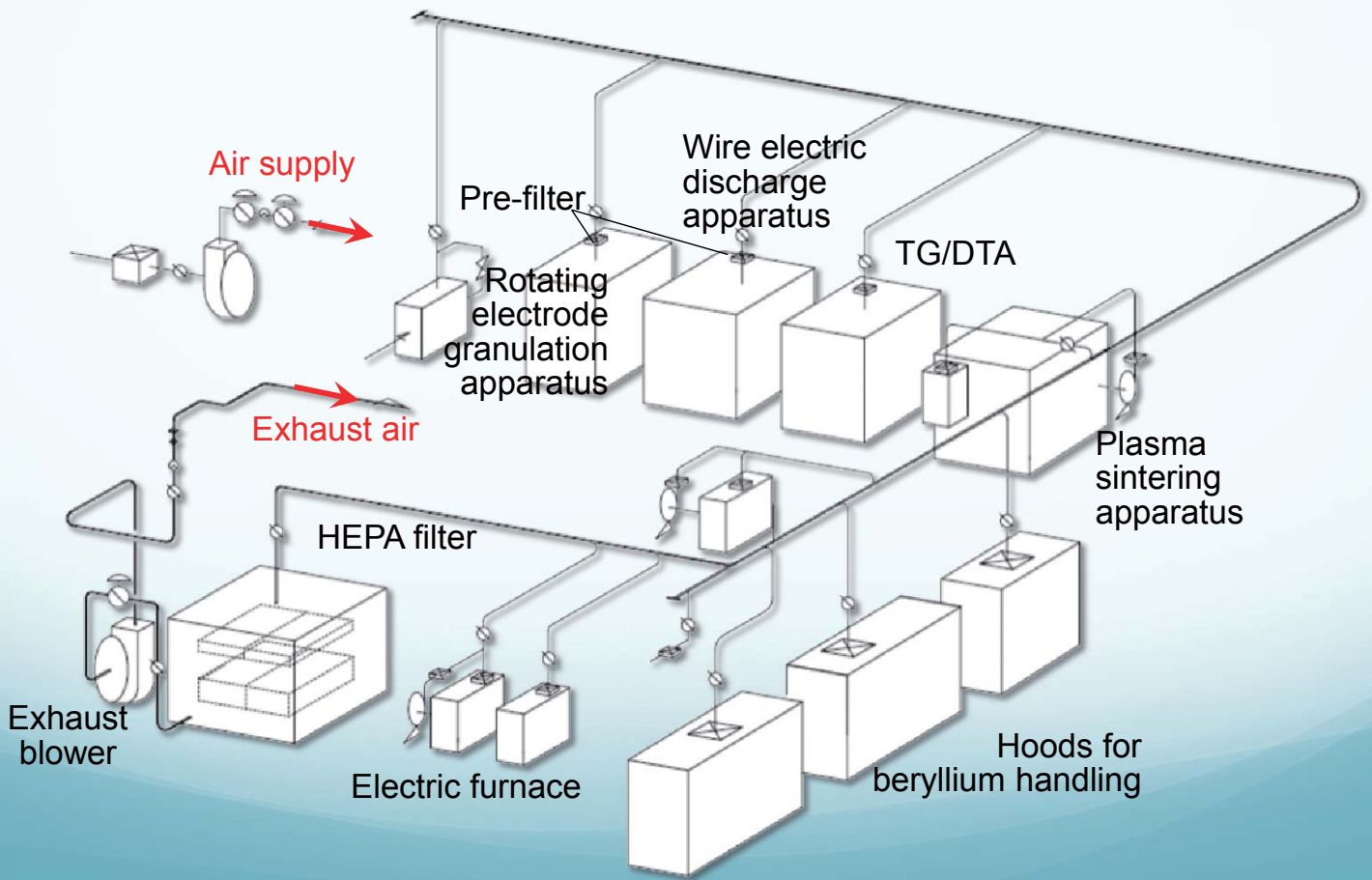
11



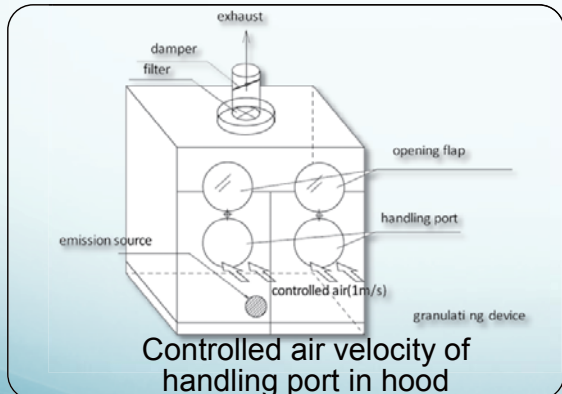
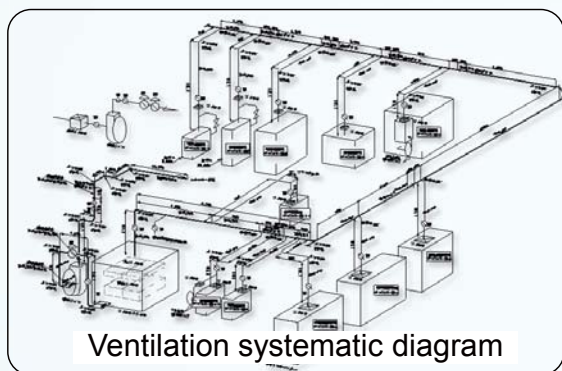
Major design parameters of beryllium handling facility

12

	Item	Condition
1	Area of the Beryllium Handling Facility	96m ² (8 × 12m)
2	Frequency of Ventilation	Controlled area : 16 times/h Exhaust System Room and Entrance Area : 4 times/h
3	Max. Concentration of Beryllium	<0.001mg/m ³ (Area monitor : 2 times per 1 year)
4	Composition of Beryllium in Usage	Beryllium Metal and Beryllium Alloy Beryllium Compounds (BeO, etc.)
5	Quantity of Beryllium	Max. 100g per Experiment (< 2 kg/year)

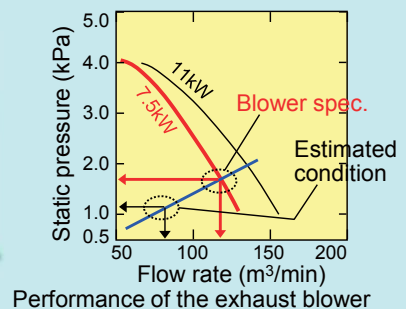


Estimation of ventilation system

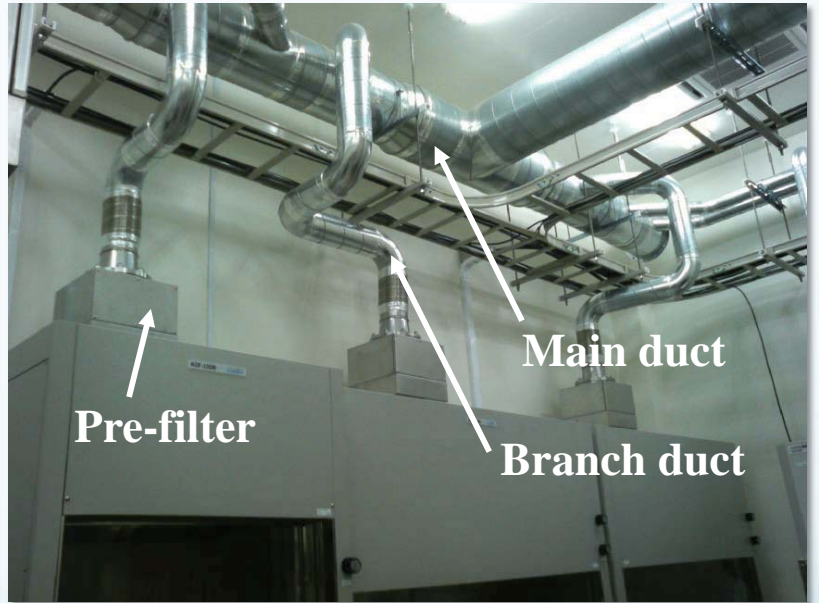


Estimated result of ventilation specification
Total pressure drop : 1205.5 Pa
Exhaust air flow rate: 76.4 m³/min

Specification of the exhaust blower
Type : Turbo Fan T2D5
(SHOWA-ELC INC.)
Output : 7.5 kW
Static pressure : 1720 Pa
Flow rate : 117.2 m³/min



Specification of the exhaust blower was decided by the result of estimation of pressure drop and static pressure based on the ventilation systematic diagram and the controlled air velocity (1 m/s) of handling port in hoods.



**Handling port
(1m/s: ventilation flow)**



**Sintering apparatus
(Plasma sintering)**



**Treatment apparatus
(Infrared melting)**



Beryllium handling worker
with personal protective wear

Beryllium handling workers are wearing the Tyvek suit, the impervious gloves, the dust-protective mask and the protective shoes for beryllium exposure control.

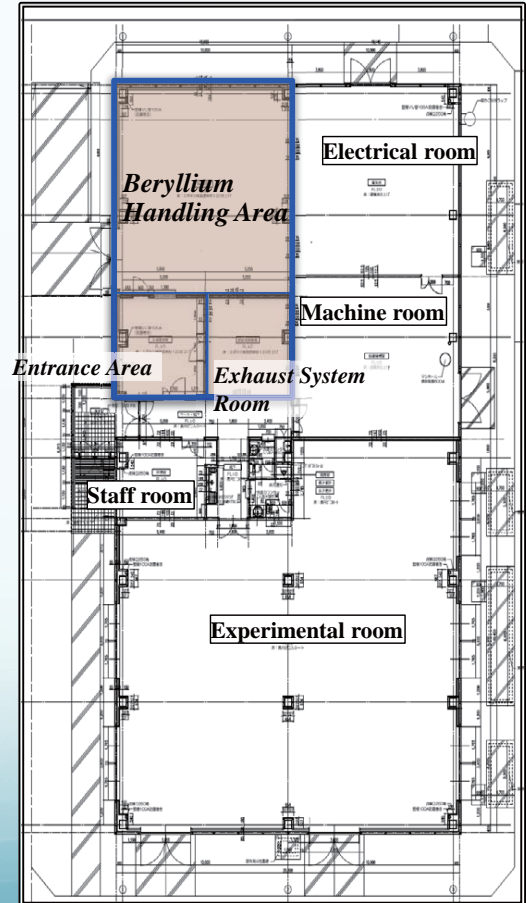


Under examination using the plasma sintering device

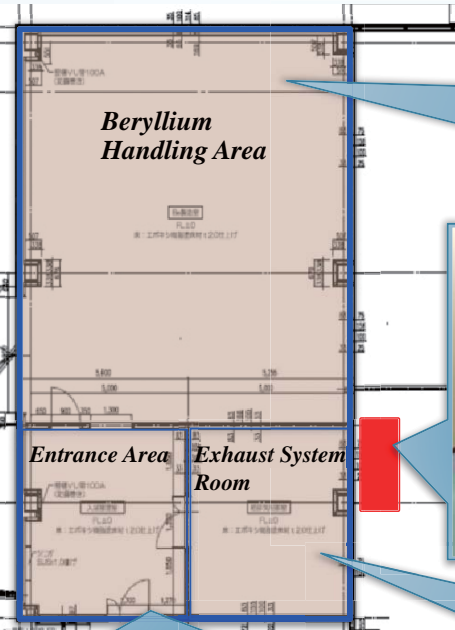
New Beryllium Handling Room in the Collaborative Study Building



Collaborative Study Building



New Beryllium handling Room



Air Supply Unit



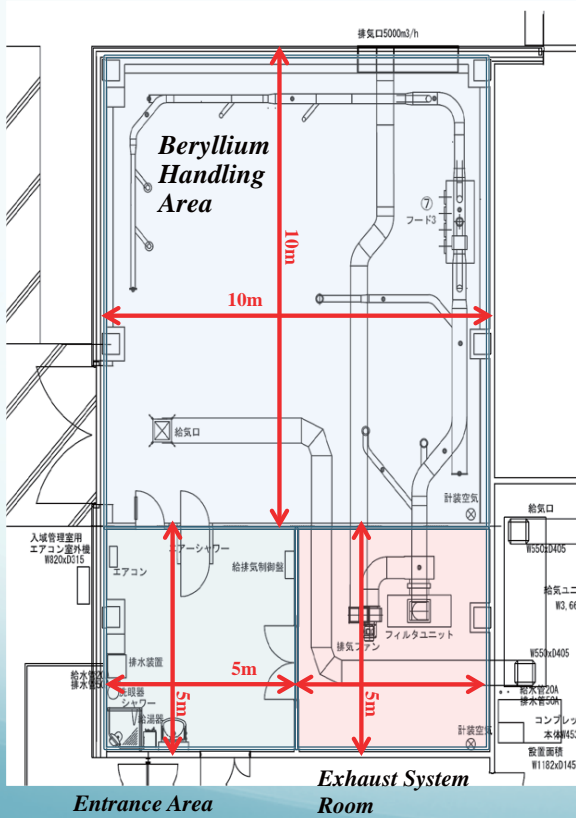
Beryllium Handling Area



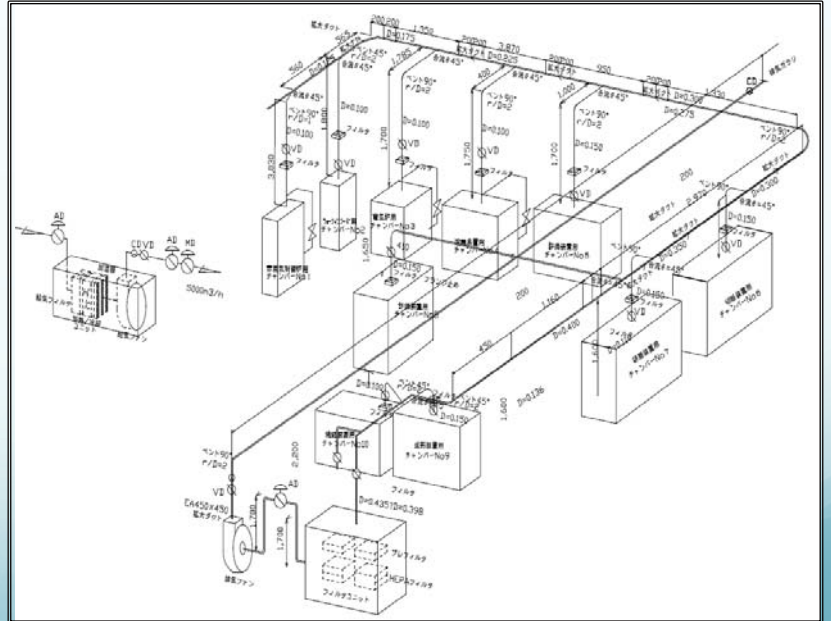
Entrance Area



Exhaust System Room



Ventilation systematic diagram



Arrangement of apparatuses

Beryllium Handling Area

Entrance Area

Exhaust System Room

Thermal conductivity measurement

Thermal expansion measurement

Heat treatment furnace

Dissolved gas measurement (H_2 , N_2 and O_2)

DSC for specific heat measurement

Entrance

Specific surface area measurement

Thank you so much for your attention



One day in winter

2.7 Technical session 4: Modelling

2.7.1 Modeling study of thermal excursion of chemical reactions of beryllium/beryllide pebbles with steam and its implication to fusion DEMO safety

M. Nakamura¹, J.H. Kim¹, M. Nakamichi¹, Y. Someya¹, K. Tobita¹, Y. Sakamoto¹ and Joint Special Design Team for Fusion Demo

¹*Rokkasho Fusion Institute, National Institutes for Quantum and Radiological Science and Technology, Rokkasho, Aomori, 039-3212, Japan*

E-mail: nakamura.makoto@qst.go.jp

While water-cooled pebble-bed blanket is one of blanket concept candidates based on conventional or near-term technologies, its critical safety issue is the chemical reactivity of beryllium/beryllide pebbles, which are the neutron multiplier for tritium breeding, with the coolant water [1]. While numerous experiments were conducted, there is a lack of modeling studies of the beryllium/beryllide chemical reactions. In this presentation, we propose a new phenomenological kinematic model of the beryllium/beryllide pebble reactions with steam toward understanding the reaction dynamics and hydrogen production, and toward obtaining implication to the DEMO safety design against the chemical and hydrogen hazard.

We have studied preliminary the thermal excursion of the chemical reaction of the beryllium (Be) or beryllide (Be_{12}Ti) pebble with steam. The excursion occurs when the reaction heating gets larger than the convective cooling by the steam at the surface. The reactivities of Be_{12}Ti and Be are taken from the experimental data [2] and [3], respectively. We assumed that the pebble is exposed by the steam, the temperature and pressure of which are 325 °C and 10 MPa, respectively. The analysis results of the heating and cooling balances of the Be and Be_{12}Ti pebbles are shown in Fig. 1 in the natural convective cooling mode. In the Be pebble case, the critical pebble temperature, at which the heat source equals to the heat sink, appears. It is 670~680 °C in the pebble diameter range of 1~4 mm. On the other hand, there is no thermal excursion in the Be_{12}Ti case because its reactivity and the resultant heating are several orders of magnitude smaller than those of Be. The finding suggests that the use of Be_{12}Ti , instead of Be, may avoid the ‘clif-edge’ of the hydrogen generation and then significantly enhance the hydrogen safety of the fusion DEMO.

References

- [1] M.S. Tillack, et al., *Fusion Eng. Des.*, **91**, 52 (2015).
- [2] M. Nakamichi, et al., *Nucl. Mat. Ener.*, **9**, 55 (2016).
- [3] L. Topilski, ITER_D_24LSAE (2008).

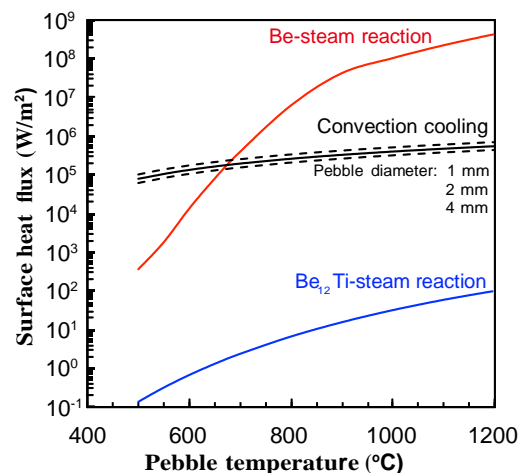


Fig. 1. Heat and cooling fluxes at the surfaces of the Be and Be_{12}Ti pebbles.

Modeling study of thermal excursion of chemical reactions of beryllium/beryllide pebbles with steam and its implication to fusion DEMO safety

Makoto “Mac” Nakamura, J.H. Kim, M. Nakamichi, Y. Someya, K. Tobita, Y. Sakamoto, R. Hiwatari, and Joint Special Design Team for Fusion Demo

Rokkasho Fusion Institute, National Institutes for Quantum and Radiological Science and Technology, Rokkasho, Aomori, Japan

Sep. 22, 2017

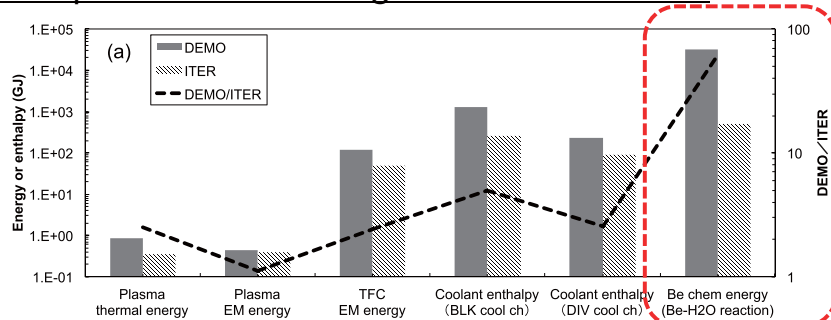
BeWS-13

1

Background

- ◆ Water-cooled pebble-bed (WCPB) blanket is one of blanket concept candidates based on near-term technologies.
- ◆ Fusion DEMO with the WCPB blanket will have several kinds of hazards potentially threatening confinement barriers:
 - ✓ Plasma energy, magnet energy, coolant energy and **chemical energy**.
- ◆ In particular, the energy potentially released by the beryllium/beryllide chemical reaction with steam **in DEMO** will be **1-2 orders of magnitude larger than that expected in ITER**.
- ◆ The **reaction-produced hydrogen** may threaten the confinement barriers.
- ◆ Therefore, **the hydrogen-producing chemical reaction should be avoided or mitigated**.

Comparison of the energies of DEMO & ITER



Sep. 22, 2017

BeWS-13

Nakamura et al., Plasma Fusion Res. (2014);
Nakamura et al., FED (2014)

Motivation

- ◆ There exist **few modeling studies** on behaviors of the reaction and hydrogen generation of the beryllium/ beryllide pebbles with steam.
- ◆ Such a model may **not only explain the experimental results**, but also apply to **safety analyses** of accidents, e.g. in-box LOCA.

Purposes

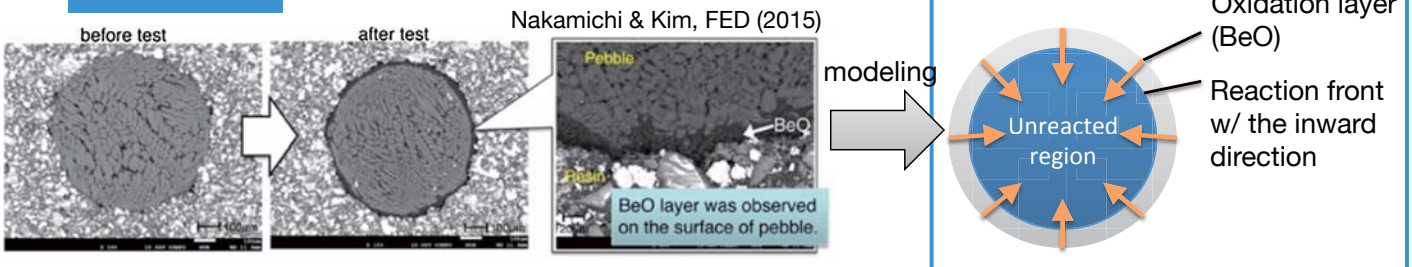
- ◆ To develop a model of the reaction behaviors of a beryllium/ beryllide pebble with steam
- ◆ To demonstrate its application to a safety analysis.
 - The **thermal excursion** phenomenon, in particular.

Contents of the presentation

1. A model we have constructed
2. Comparison of the model calculation with the experimental results
3. Analysis of the thermal excursion by the steam reaction

Model

Basic idea



'0.5-D' model

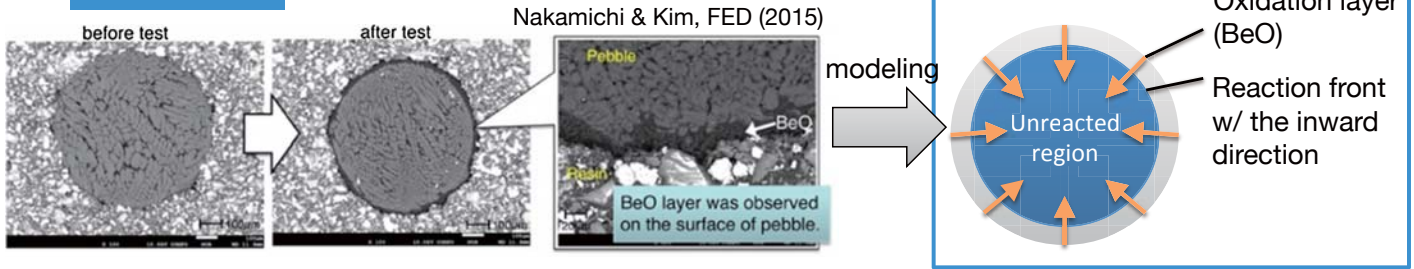
- ◆ Consider
 1. Mass balance
 2. Energy balance
 of the **un-reacted region** of a pebble

$$\frac{d}{dt} \left(\frac{4}{3} \pi r^3 \rho \right) = -4\pi r^2 S_{chem}(T)$$

$$\frac{d}{dt} \left(\frac{4}{3} \pi r^3 \rho c_p T \right) = 4\pi r^2 S_{chem}(T) Q_{chem}(T) - Q_{cool}(T)$$

- ◆ Assumptions
 1. The pebble is **spherically symmetric**.
 2. The energy released by the chemical reaction is '**spontaneously**' transferred to the whole region of a pebble --- **no spatial distribution of the pebble temperature**.
 - Valid for $\Delta T > 70$ s.

Basic idea



'0.5-D' model

◆ Consider

1. Mass balance
2. Energy balance

of the **un-reacted region** of a pebble

$$\frac{d}{dt} \left(\frac{4}{3} \pi r^3 \rho \right) = -4\pi r^2 S_{chem}(T)$$

$$\frac{d}{dt} \left(\frac{4}{3} \pi r^3 \rho c_p T \right) = 4\pi r^2 S_{chem}(T) Q_{chem}(T) - Q_{cool}(T)$$

◆ Taking into account of the experimental facts

1. For the **Be** pebble, the **BeO layer is porous**, so that the reaction velocity is not changed as the reaction proceeds.
2. For the beryllide (**Be₁₂Ti**) pebble, the **BeO layer (1-10 μm) is less porous**, so that the surface region is oxidized by a '**fast reaction**' while the inside region is oxidized by a '**slow reaction**'.

Model and solution method

Model equation

Equations of the time evolution of the un-reacted region of a pebble

For the radius:

$$\frac{dr}{dt} = -\frac{S_{chem}(T)}{\rho}$$

For the temperature:

$$\frac{dT}{dt} = \frac{3}{r\rho c_p} [(Q_{chem} + c_p T) S_{chem}(T)] - \frac{3}{4\pi r^3 \rho c_p} Q_{cool}$$

A **code** of Phenomenological **SY**stems of equations of **CHE**mical reaction kinetics, **PSYCHE**, has been developed.

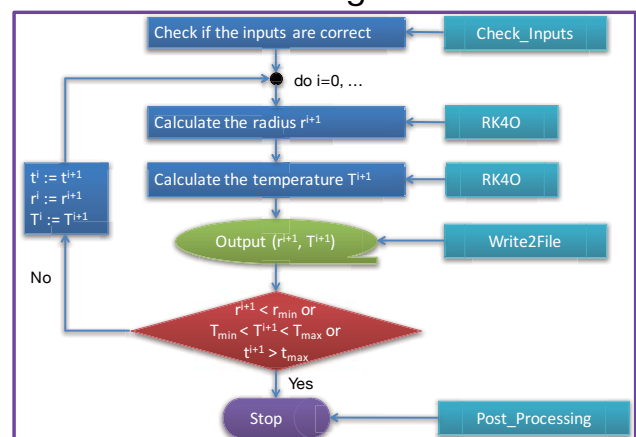
Time integration:

The 4th order Runge-Kutta meth.

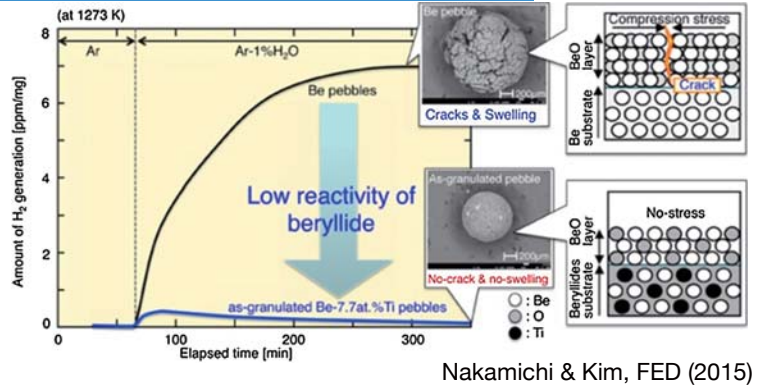
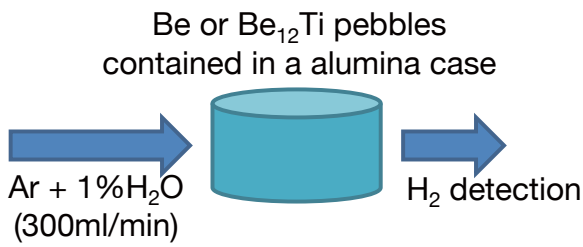
Language:

Fortran95

Solution algorithm



Experimental results used for comparison with the simulation



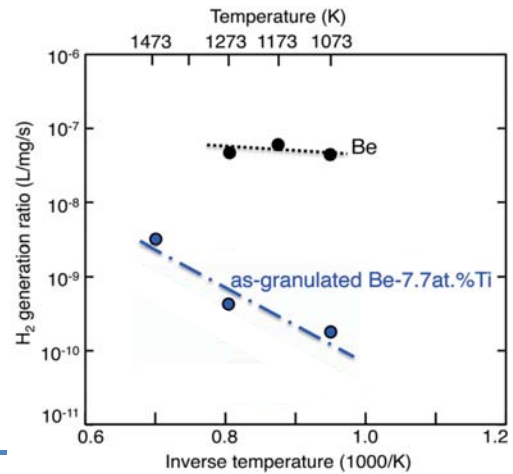
Reaction rates used

For the beryllium pebble, the formula proposed in ITER-SADL

For the beryllide (Be₁₂Ti) pebble, the formula fitted to the experiments^[1]

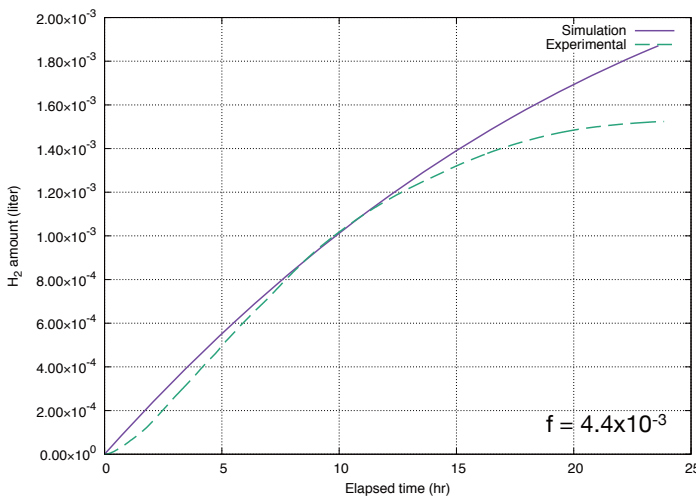
$$S_{chem}^{(Be_{12}Ti)} (\text{liter H}_2/\text{m}^2/\text{s}) = 1.4 \exp(-10741/T)$$

[1] Nakamichi, et al., Nucl. Mat. Ener. (2016)



Amount of H₂ generated by the steam reaction

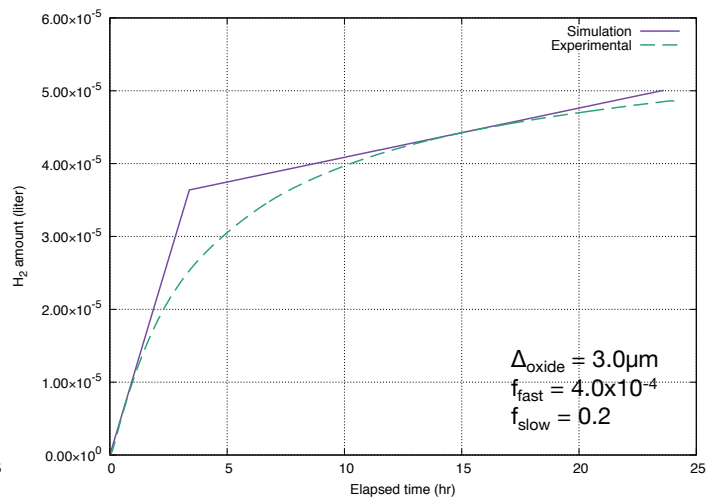
Be-steam reaction



$$S_{model}^{(Be)}(T) = f^{(Be)} S_{chem}^{(Be)}(T)$$

$$f^{(Be)} = f_{shape} f_{BET} f_{H_2O}$$

Be₁₂Ti-steam reaction



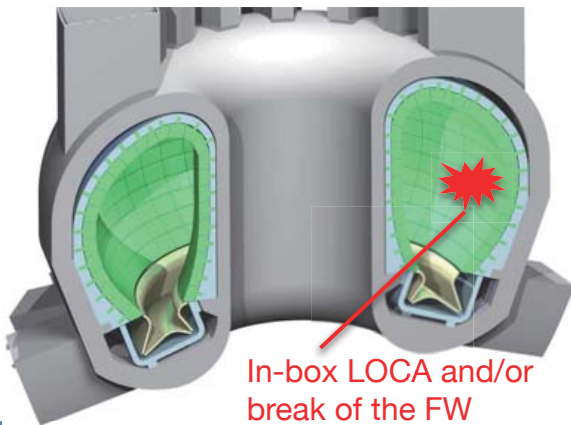
$$S_{model}^{(Be_{12}Ti)}(T) = \begin{cases} f_{fast} S_{chem}^{(Be)}(T) & (r_0 - r < \Delta_{oxide}) \\ f_{slow} S_{chem}^{(Be_{12}Ti)}(T) & (r_0 - r > \Delta_{oxide}) \end{cases}$$

The simulation results agrees with the experiments.

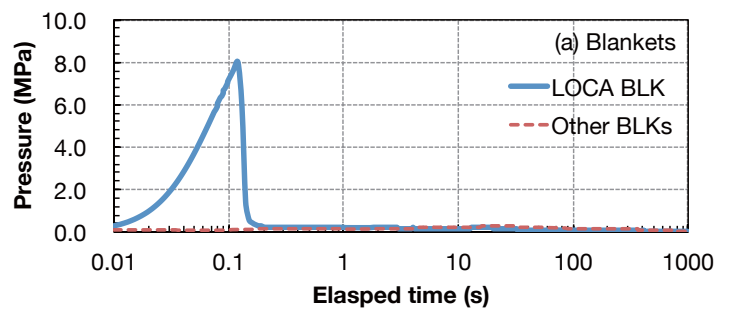
- ◆ However, some quantitative discrepancies are seen.
 - In the experiments, the reaction propagation may stop at the pebble core ?

◆ In-box LOCA in a fusion DEMO with the WCPB blanket

1. Double-ended break of the largest pipe *IN a blanket box*
2. Discharge of the coolant water and pressurization of the blanket
3. Propagation of the discharged water to other blankets via the tritium recovery line.
4. Complete break of the first wall of the LOCA blanket box when overpressurized, $P_{\text{water}} > 8 \text{ MPa}$.
5. Pressurization of the vacuum vessel and depressurization by the pressure suppression system.



Time history of the pressures in the blankets

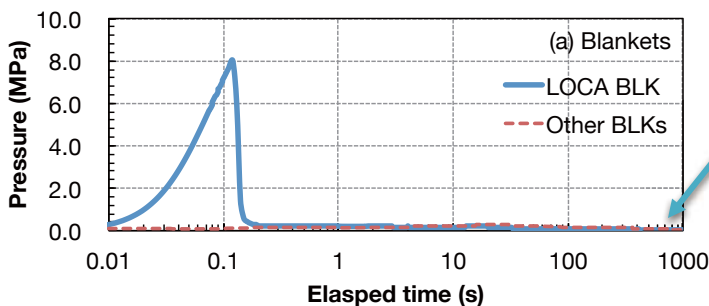


Sep. 22, 2017

BeWS-13

Assumptions in the analysis

Time history of the pressures in the blankets



At the final state,

$$P_{\text{water}} = 0.1 \text{ MPa}$$

$$T_{\text{water}} = 100 \text{ }^\circ\text{C}$$

- ◆ After the onset of the in-box LOCA, the pebble is cooled at the surface by the natural convection of the discharged water.

- The cooling flux is fixed to $q_{\text{cool}} = 80 \text{ W/m}^2/\text{s}$, using the Churchill's formula^[1].

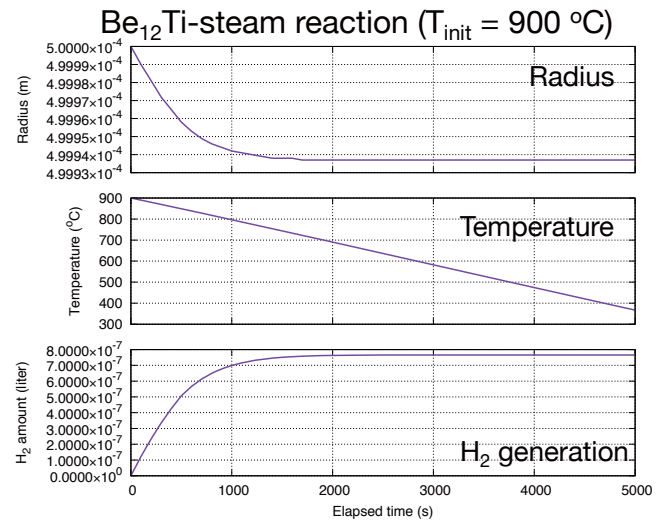
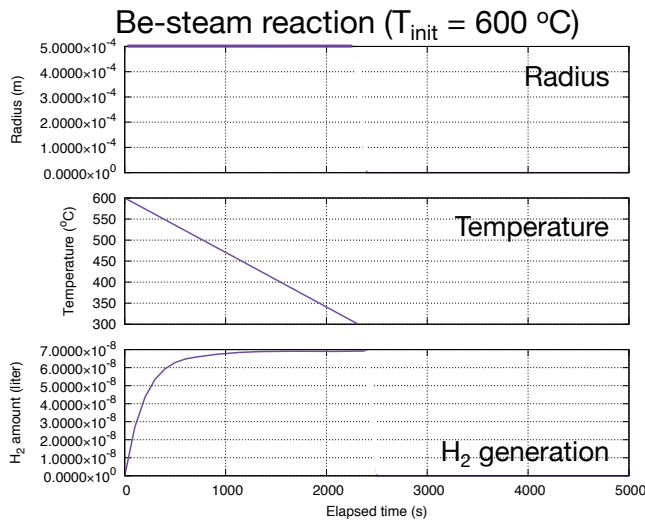
[1] Churchill, 1983, "Free Convection around Immersed Bodies,"

- ◆ The initial radius of the pebble is 0.5 mm.
- ◆ The initial temperature is a scan parameter.

Sep. 22, 2017

BeWS-13

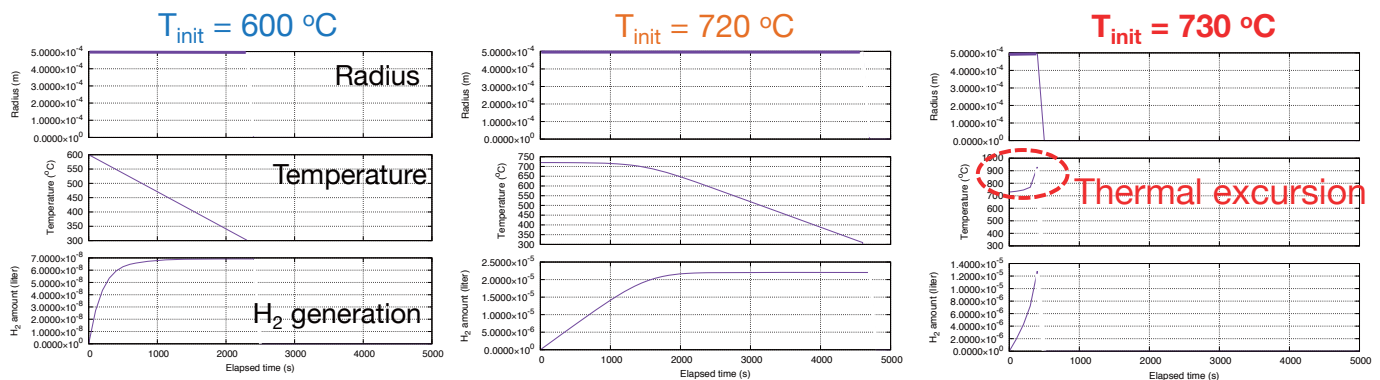
Comparison between the behaviors of the Be & Be₁₂Ti pebbles



- ◆ No thermal excursions by the steam reaction are observed if the initial temperature is at the rated operation condition.
- ◆ The pebble is cooled by the natural convection of the water in a time scale of ~ several 1,000's s.
- ◆ The generation of H₂ is saturated at the time of ~1,000 s.

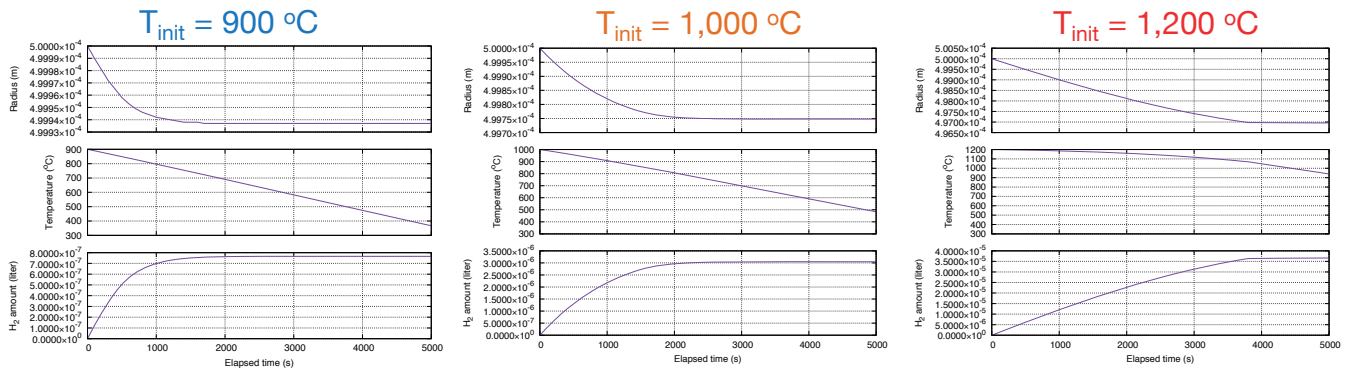
Sensitivity of the initial pebble temperature

Be-steam reaction



- ◆ If the initial temperature is increased (possibly by the loss of heat rejection), the thermal excursion is observed.
- ◆ The thermal excursion proceeds in the time scale of several 100's s.
- ◆ Occurrence of the thermal excursion is very sensitive to the initial temperature.

Be₁₂Ti-steam reaction



- ◆ No thermal excursions are observed even if the initial temperature is increased from the rated temperature.

The good thermal stability of the beryllide Be₁₂Ti has been found by the model simulation.

Summary and future work

- ◆ We have developed a phenomenological model of the chemical reactions of beryllium/beryllide pebbles with steam.
- ◆ We have developed a code PSYCHE to simulate the reaction.
- ◆ The simulation results has been found to agree with the experiments.
- ◆ The code has been applied to the accident analysis: in-box LOCA
 - The thermal stability of the Be₁₂Ti pebble was found against the heating by the steam reaction.

Future work

- ✓ To extend the model to simulate the dynamics in a faster time scale (100 ms – 1 s)
 - The present model is verified in the time scale of (> several 10's s)
- ✓ More thorough validations with experiments
 - Experiments with a variety of the conditions (the H₂O concentration and flow rate of the working fluid) will be conducted.

2.7.2 Beryllium and titanium beryllide Be_{12}Ti as candidates for fusion applications

D.V. Bachurin¹ and P.V. Vladimirov¹

¹*Karlsruhe Institute of Technology, Institute for Applied Materials,
Hermann-von-Helmholtz-Platz 1, 76344 Eggenstein-Leopoldshafen, Germany
E-mail: dmitry.bachurin@kit.edu*

Demonstration fusion reactor DEMO is planned to be operate at more extreme conditions (stronger radiation field and higher temperature) in comparison with the ITER. Under these circumstances it is necessary to improve many physical characteristics of reactor materials. Beryllium is considered as candidate for neutron multiplier for ITER breeder blanket, while intermetallic beryllium compounds is foreseen as advanced material for the DEMO breeder blanket instead of pure beryllium. This choice is dictated by the fact that beryllides manifest higher melting point, higher oxidation resistance, lower tritium retention and lower swelling as opposed to pure beryllium. In the present work we are aimed to find out the origin of the superior properties of titanium beryllide Be_{12}Ti over beryllium by comparison of the corresponding properties of both the materials relevant for fusion applications. All static ab initio calculations were performed using simulation package VASP.

First of all the selected pseudopotentials were evaluated by means of calculation of lattice parameters and elastic constants for beryllium (hexagonal lattice) and Be_{12}Ti (tetragonal lattice) at zero temperature. By now, tetragonal crystal structure of Be_{12}Ti was relatively poor studied and appears to be the only stable structure [1] despite the fact that a few recent publications have used the erroneous hexagonal structure for Be_{12}Ti [2,3].

Tritium solution energy as well as binding energy with a vacancy are important in terms of tritium dissolution, retention and release. In this work we neglect isotope effects and hydrogen was simulated instead of tritium. Hydrogen solution energy in all hydrogen interstitial non-equivalent sites was computed. It was found that the solution energy in Be_{12}Ti is fully determined by the surrounding atoms and is at least circa 0.2 eV lower as compared with the corresponding values in beryllium. This suggests easier dissolution of hydrogen atoms in Be_{12}Ti . Binding energy of hydrogen atoms with a monovacancy at different non-equivalent positions was calculated. Calculations reveal the decrease of the binding energy with the increase of the number of hydrogen atoms in a vacancy. Obtained values are noticeably lower in Be_{12}Ti suggesting the faster and easier tritium release than in beryllium. This study contributes to understanding the origin of the reduced tritium retention and swelling properties of Be_{12}Ti on atomic scale.

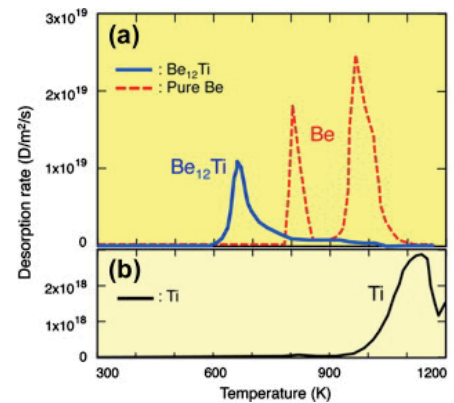
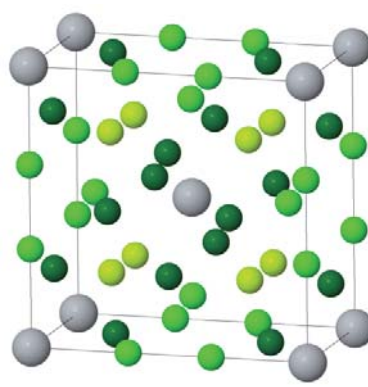
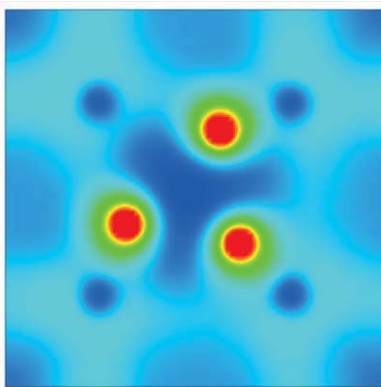
References

- [1] M.L. Jackson, Acta Crystallogr B **72**, 277 (2016)
- [2] X.K. Liu, RSC Adv **5**, 59648 (2015)
- [3] S.M. Peng, J Nucl Mater **464**, 230 (2015)

Beryllium and titanium beryllide Be_{12}Ti as candidates for fusion applications

D. Bachurin, P. Vladimirov

INSTITUTE OF APPLIED MATERIALS (IAM-AWP), Atomistic Modeling and
Validation Group, Department of Metallic Alloys



KIT – University of the State of Baden-Wuerttemberg and
National Research Center of the Helmholtz Association

www.kit.edu

Outline

1. Motivation
2. Computational methodology
3. Structure and lattice parameters
4. Elastic properties
5. Hydrogen in interstitial positions
 - Be
 - Be_{12}Ti
6. Hydrogen in vacancy
 - Be
 - Be_{12}Ti
7. Conclusions

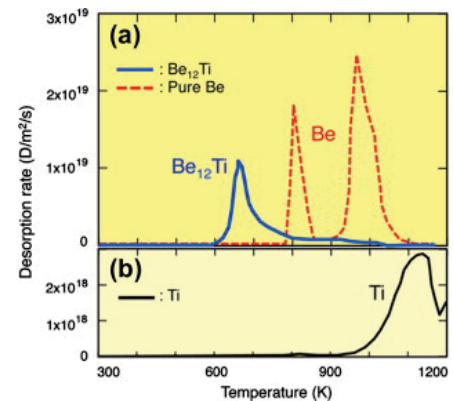
■ **Motivation:** Intermetallic beryllium compounds as Be_{12}Ti , Be_{12}V and Be_{12}Zr are considered as possible candidates for fusion applications, namely as neutron multiplier for the DEMO breeder blanket to be used instead of pure beryllium. Since conceptual design of DEMO supposes an operation at even more extreme conditions in contrast to ITER (stronger radiation field and higher temperatures), therefore increased requirements are on demand to these materials such as

- higher melting point,
- higher oxidation resistance,
- lower tritium retention,
- lower swelling.

Investigation of the origin of the superior properties of beryllium compounds is indispensable for understanding of hydrogen isotope retention and release properties.

■ **Goal:** Elucidation of the origin of the superior properties of Be_{12}Ti by performing comparison of its properties with pure Be.

■ **Approach:** Ab initio methods



M. Nakamichi et al. JNM 442, 1-3, S465-S471 (2013)

Computational methodology

- Static ab-initio calculations (using **VASP**)
- Projector augmented wave potential (PAW)
- Generalized gradient approximation (GGA)

- Fermi broadening: 0.2 eV
- Cut-off energy: 450 eV

- No volume and shape relaxation
- No restrictions on relaxation of atoms

Hydrogen solution energy

$$E_s = E_{total}^{\text{Be+H}} - E_{total}^{\text{Be}} - E_{ref}^{\text{H}}$$

$E_{total}^{\text{Be+H}}$ and E_{total}^{Be} are the total energies of the simulation cells with and without hydrogen
 $E_{ref}^{\text{H}} = -3.3590$ eV is the energy of hydrogen atom in H₂ molecule

Hydrogen binding energy

$$E_b = E(\text{H}_{n-1}\text{V}) - E(\text{H}_n\text{V}) + E(\text{H}_I) - E_{bulk}$$

$E(\text{H}_{n-1}\text{V})$ and $E(\text{H}_n\text{V})$ are the total energies of the simulation cells with (n-1) and n hydrogen atoms in a vacancy

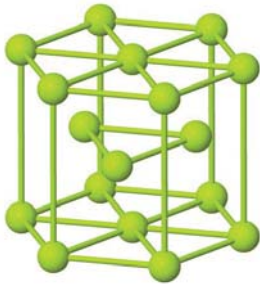
$E(\text{H}_I)$ is the energy of hydrogen atom in interstitial (BT) position

E_{bulk} is the energy of the bulk

Structure and lattice parameters

Be

hexagonal



$a = 2.265 \text{ \AA}$
 $c = 3.562 \text{ \AA}$



Be₁₂Ti

Raeuchle et. el. (1952):
hexagonal

Raeuchle et. el. (1955):
tetragonal

Zalkin et. el. (1961):
tetragonal

Gillam et. el. (1964):
tetragonal

Peng et. el. (2015):
hexagonal

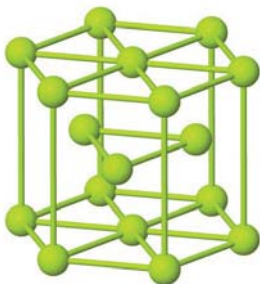
Liu et. el. (2015):
hexagonal

Jackson et. el. (2016):
tetragonal

Structure and lattice parameters

Be

hexagonal



$a = 2.265 \text{ \AA}$
 $c = 3.562 \text{ \AA}$



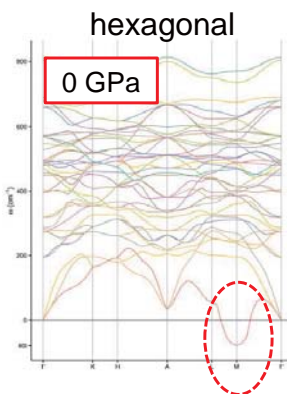
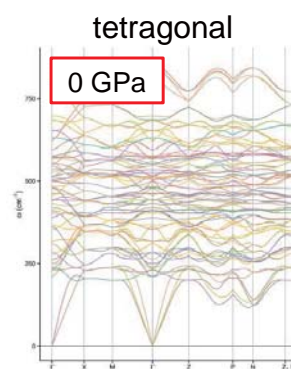
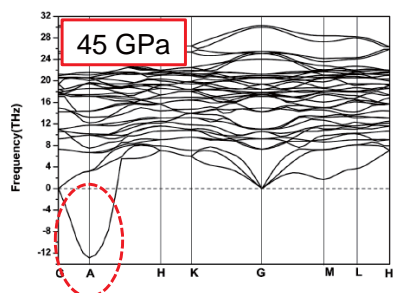
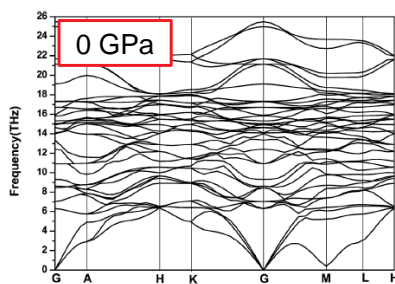
Be₁₂Ti

Liu et. el. (2015):
hexagonal

vs.

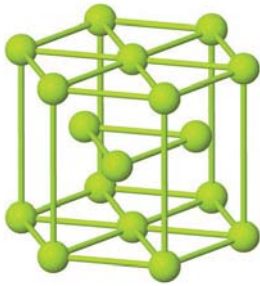
Jackson et. el. (2016):
tetragonal

Phonon dispersion curves

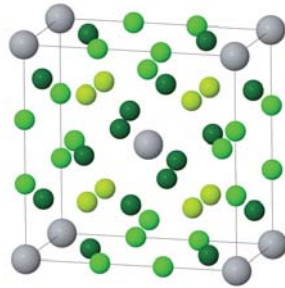


Structure and lattice parameters

Be hexagonal



$a = 2.265 \text{ \AA}$
 $c = 3.562 \text{ \AA}$

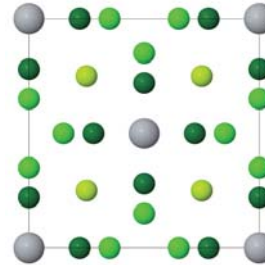


Unit cell: 24 Be atoms, 2 Ti atoms

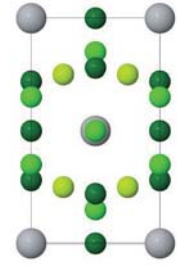
- Be1
- Be2
- Be3
- Ti4

Be₁₂Ti tetragonal

front



left

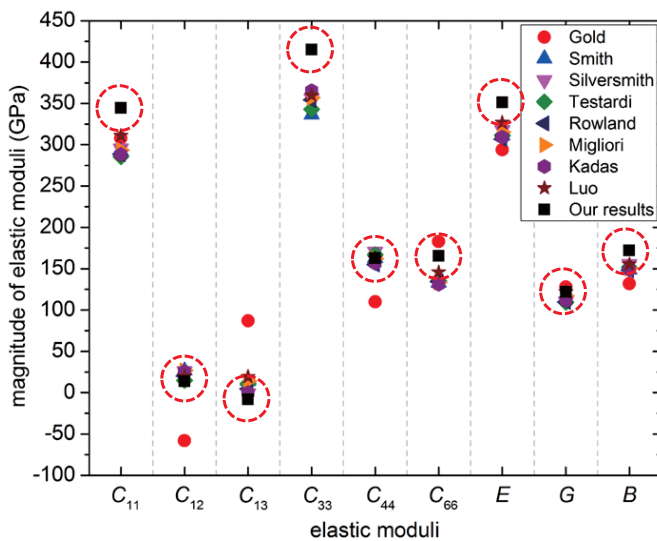


$a = 7.326 \text{ \AA}$
 $c = 4.147 \text{ \AA}$



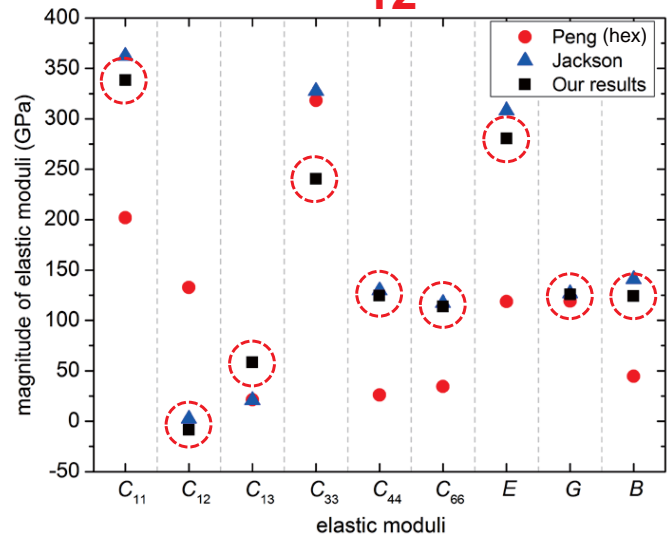
Elastic properties

Be



 - our results

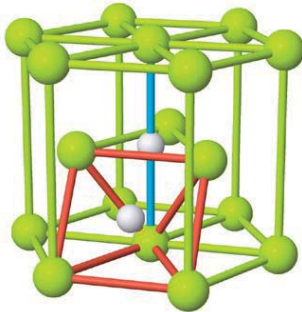
Be₁₂Ti



Results are consistent with the available data

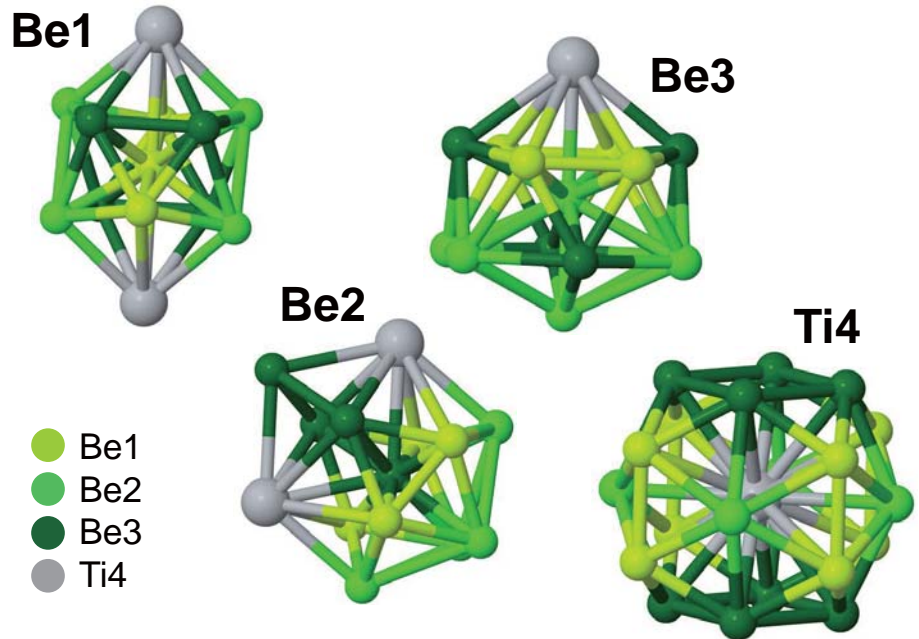
Hydrogen in interstitial positions

Be hexagonal



- Octahedral (O)
- Basal Tetrahedral (BT)

Be₁₂Ti tetragonal



- Be1
- Be2
- Be3
- Ti4

Hydrogen in interstitial positions

Be hexagonal

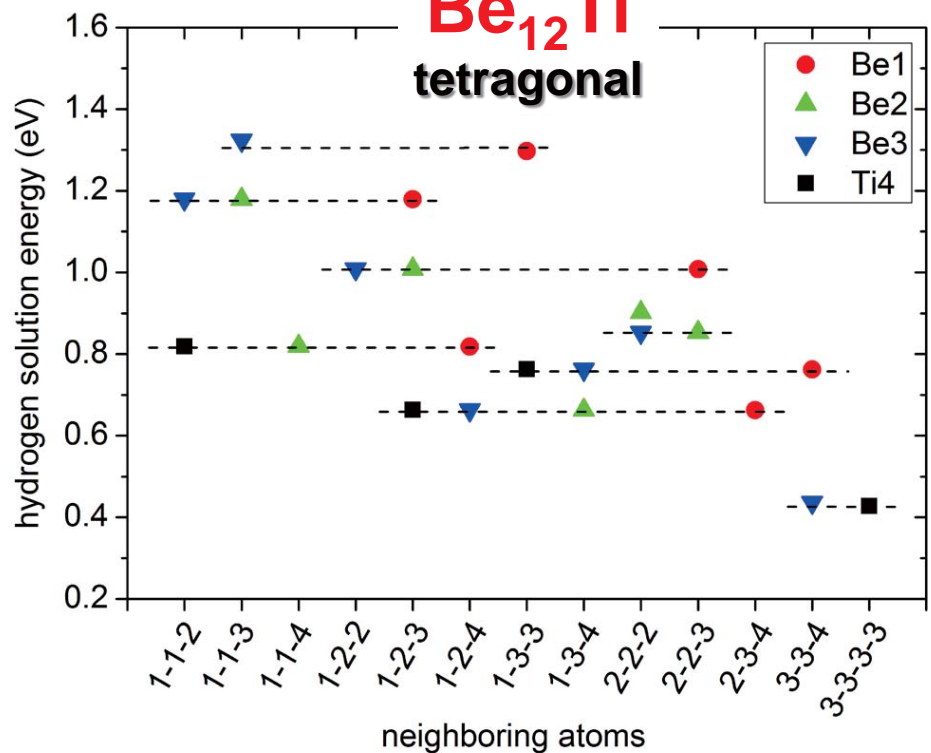
Solution energy:

$$E(\text{H in BT}) = 1.54 \text{ eV}$$

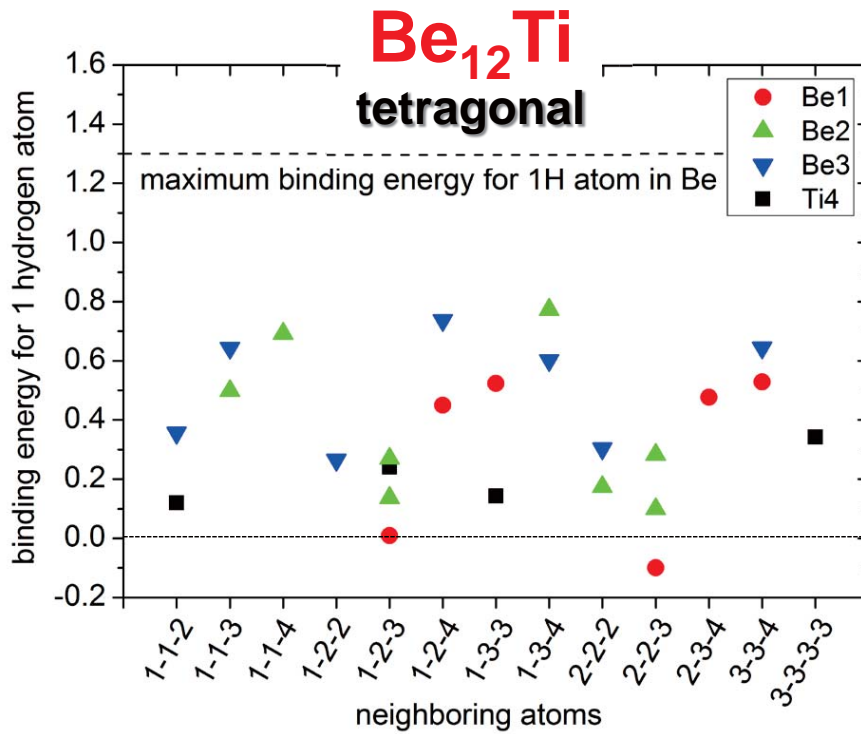
$$E(\text{H in O}) = 1.74 \text{ eV}$$

- Octahedral (O)
- Basal Tetrahedral (BT)

Be₁₂Ti tetragonal

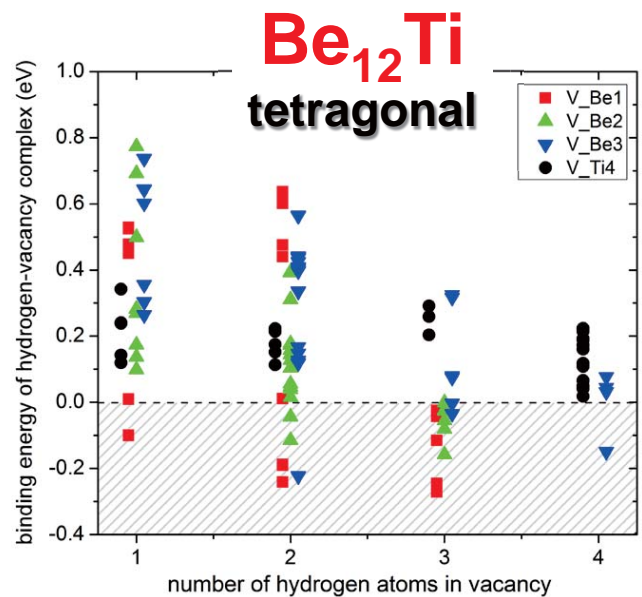
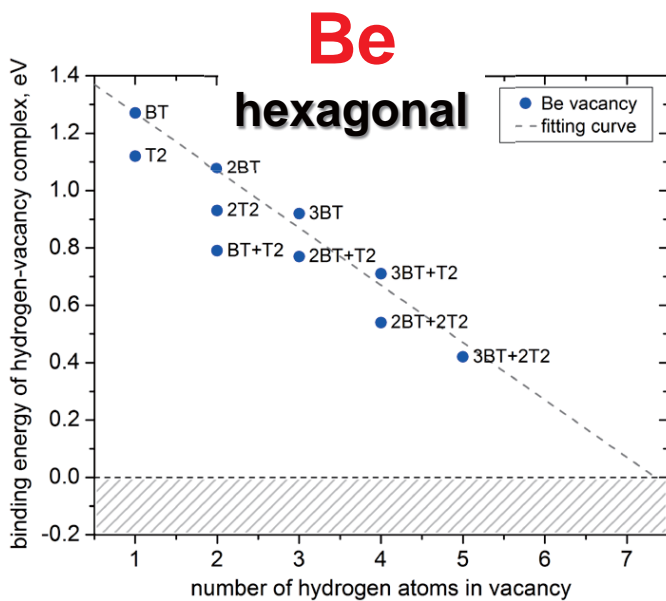


Binding energy of hydrogen atom in vacancy



Binding energy of one hydrogen atom in a vacancy of Be₁₂Ti is at least 0.5 eV lower than that in pure Be

Binding energy of hydrogen atoms in vacancy

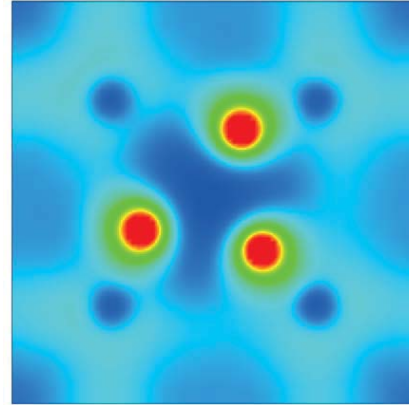
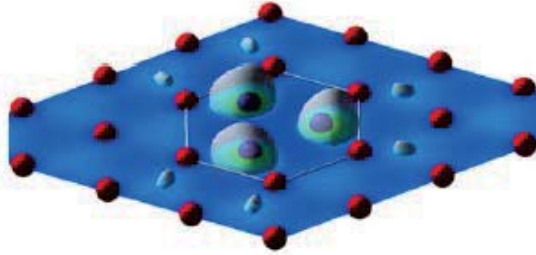


Binding energy of hydrogen with a vacancy decreases with the increase of number of hydrogen atoms

Be
hexagonal

Be₁₂Ti
tetragonal

3 hydrogen atoms in vacancy



M.G. Ganchenkova et al. PRB 79, 134101 (2009)

No chemically bound hydrogen molecule inside a vacancy was found

Conclusions

- Structure and lattice parameters for Be (hexagonal) and Be₁₂Ti (tetragonal) were calculated. Elastic constants for Be and Be₁₂Ti are consistent with the previous experimental and theoretical studies.
- Hydrogen solution energy in interstitial positions of Be₁₂Ti are at least 0.3 eV lower than that for Be suggesting easier dissolution of hydrogen atoms in Be₁₂Ti.
- Maximal binding energy of hydrogen atoms in vacancy linear decreases with the number of hydrogen atoms both in Be and Be₁₂Ti. Hydrogen binding in vacancy is 0.5 eV lower in Be₁₂Ti, suggesting easier release of hydrogen from beryllide with respect to pure beryllium.
- No formation of chemical bounds between hydrogen atoms inside both Be and Be₁₂Ti vacancies were observed.

2.8 Technical session 5: Irradiation properties

2.8.1 Investigation of Neutron Irradiation Behavior of Beryllium using HANARO

Suk Hoon Kang, Young-Bum Chun, Daejong Kim, Tae Kyu Kim

Nuclear Materials Division, Korea Atomic Energy Research Institute, Daejeon 34057

Abstract

The lifetime of the beryllium reflector elements is usually determined by neutron irradiation induced swelling, which results in a bending or mechanical interference of the reflector parts. Therefore, an investigation of the irradiation influence on the dimension stability of beryllium is important. In this research, the neutron irradiation behavior of the beryllium manufactured by vacuum hot pressing (VHP) and hot extrusion (HE) were investigated. Comparing to VHP processed beryllium, a strong fiber texture was developed in the HE processed beryllium; the basal planes in the majority of grains were arranged along the extrusion direction. Therefore, the irradiation growth of HE processed specimen after the irradiation may also show anisotropy. Irradiation growth, hardness changes of the VHP or HE processed beryllium were estimated after neutron irradiation in HANARO, where the neutron fluence was about 10^{21} n/cm² (E>0.1 MeV) at 70 °C.

Email: shkang77@kaeri.re.kr

Tel : +82-42-868-8644, Fax : +82-42-868-8549

Ion and Neutron Irradiation Tests on Beryllium Specimens



Suk Hoon Kang

Korea Atomic Energy Research Institute

Republic of Korea



**Korea Atomic Energy
Research Institute**

Contents

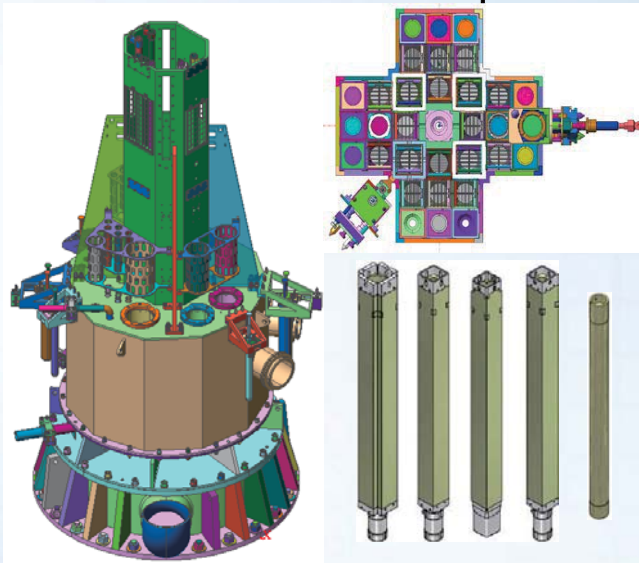
- 1 Beryllium Research in KAERI**
- 2 Proton Irradiation on Beryllium**
- 3 In-pile Tests using HANARO**
- 4 Summary**





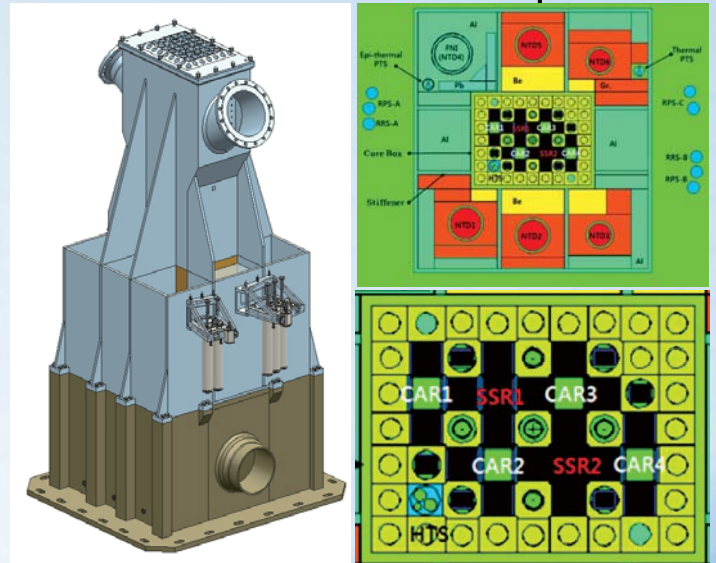
Current Status of JRTR and KJRR

JRTR



- Pre-service inspection (2016. 3.)
- Straightness Measurement
- Ongoing inspection (~present, 1 year)
- Currently no meaningful data (Not the pull power operation)

KJRR

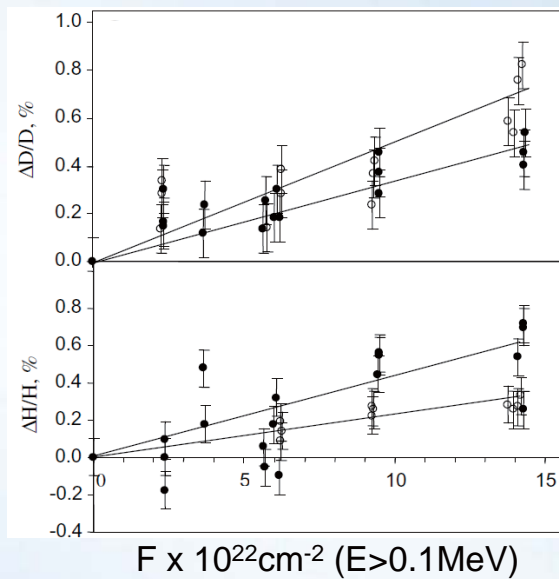


- Delays due to government nuclear policy
- But hopeful movement of resumption
- Internal/external reflectors : ~ 800 Kg

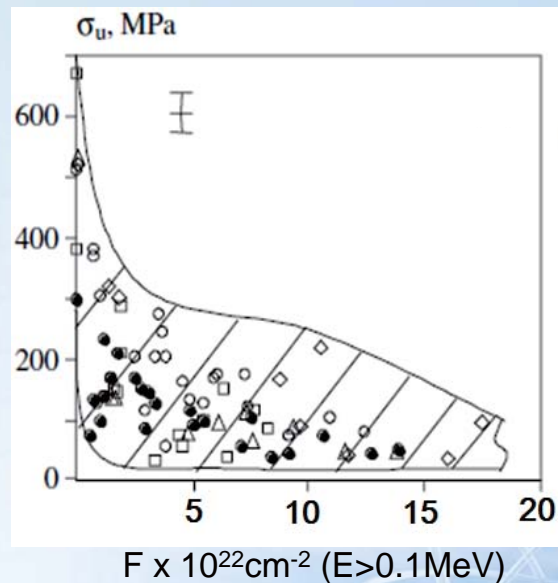


Beryllium Reflector Stability Issues

Dimensional Change



Tensile Property



Dimensional change & Brittleness increase after neutron irradiation
→ Possible mechanical interference, brittle fracture of beryllium

Reference for figures, V. P. Chakin, et al, Atomic Energy, Vol. 101, No. 4, 743-749 (2006)

Beryllium Research in KAERI

Studied Beryllium Grades

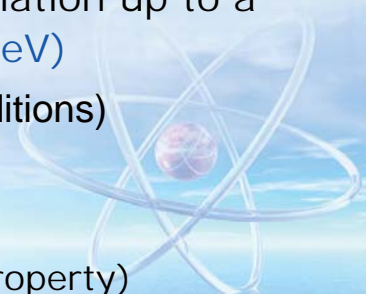
- Materion Brush : S-65 (HIP), S-200-F (Vacuum Hot Pressing)
- Ulba Metallurgical Plant : EHP-56 (Hot Extrusion)

Out-of-pile Test

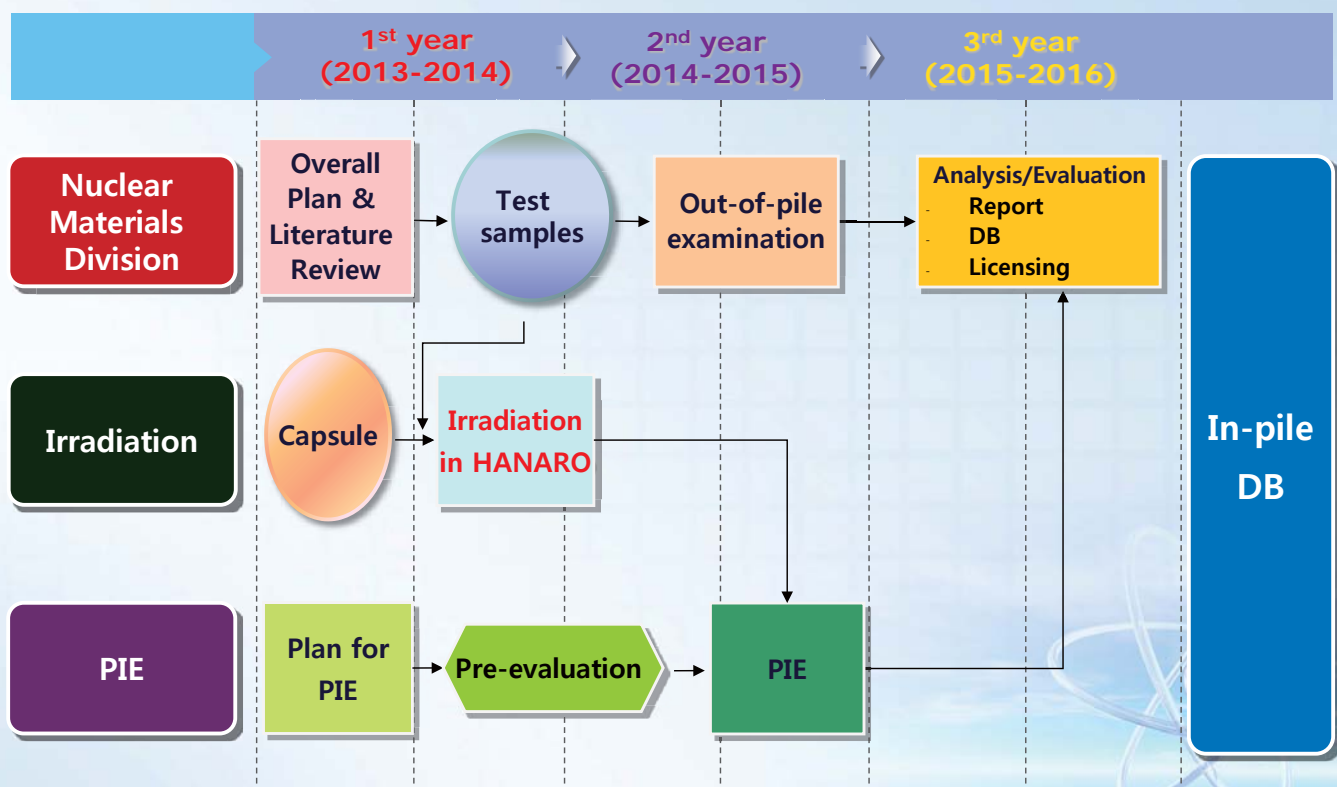
- Microstructure / Mechanical properties
- Proton irradiation

In-pile Test

- PIE (post-irradiation examination) after irradiation up to a neutron fluence of $\sim 2 \times 10^{21}$ n/cm² (E > 0.1 MeV)
- Irradiation temperature: < 70°C (RR operating conditions)
 - Dimensional stability (directional growth)
 - Physical properties (thermal diffusivity)
 - Mechanical properties (Microhardness, tensile property)

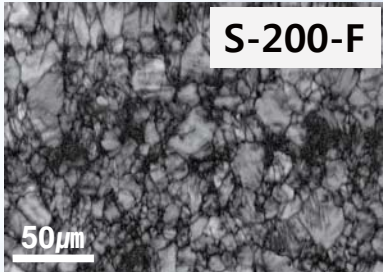


Overall Schedule for In-pile Test

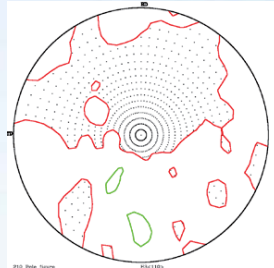


Properties of Beryllium Specimens

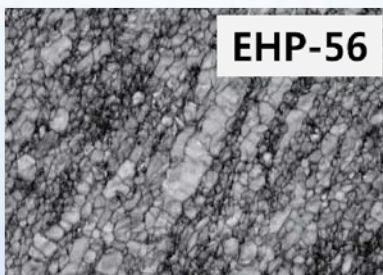
Material	Be	BeO	Fe	C	Al	Si	Etc.
S-200-F, VHP	98.50	1.20	0.10	0.10	0.05	0.03	<0.02
EHP-56, HE	98.30	1.30	0.20	0.12	0.03	0.04	<0.01



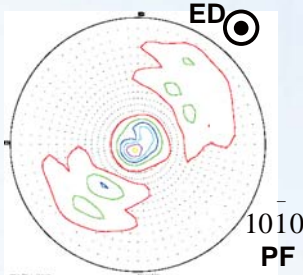
S-200-F



S-200-F (VHP)
Isotropic



EHP-56

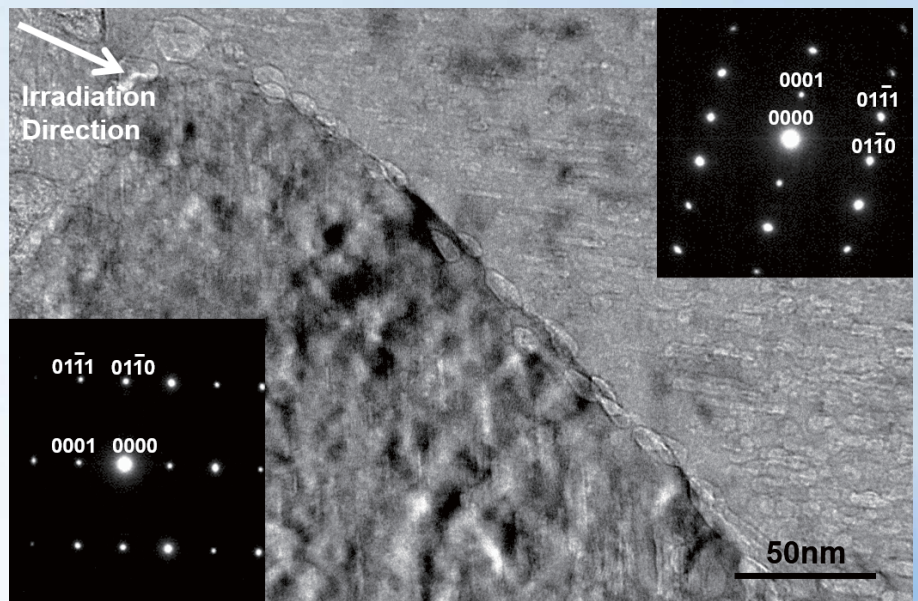


EHP-56 (Hot Extrusion)
Anisotropic
<1010> deformation texture

Proton Irradiation on Beryllium

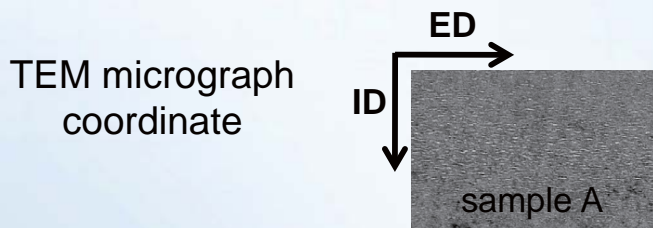
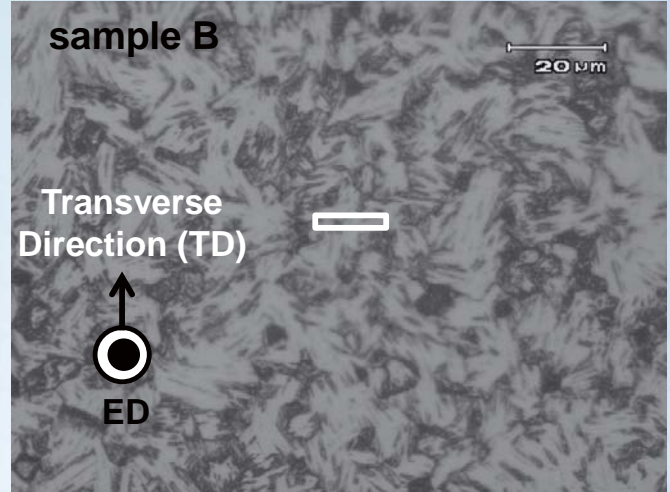
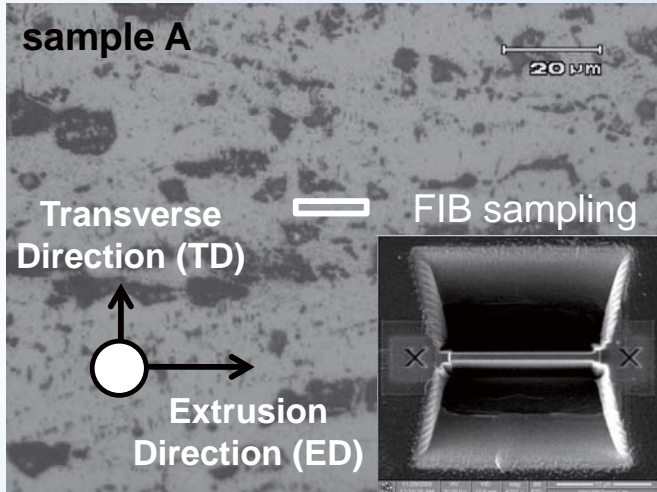


Acceleration Voltage : ~ 120 keV
Beam current : 3 mA
Beam uniformity : ±20%

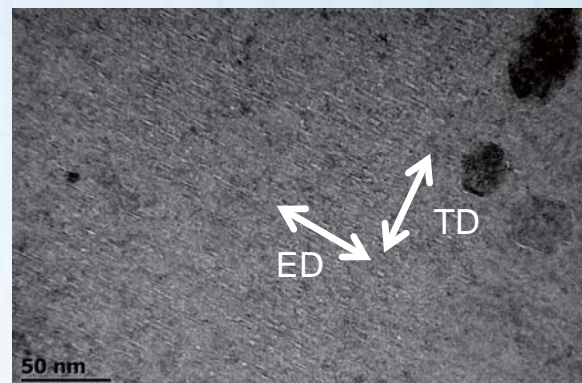
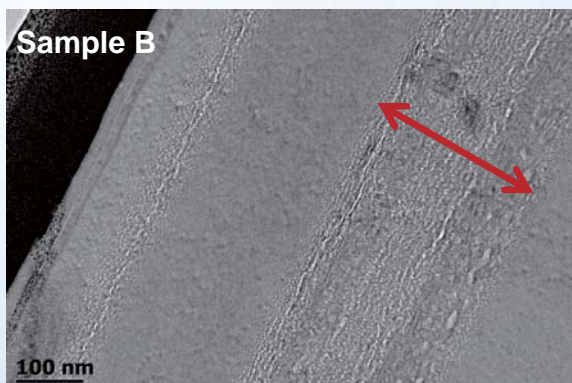
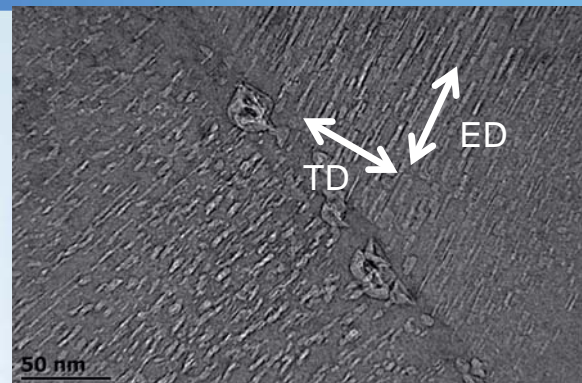
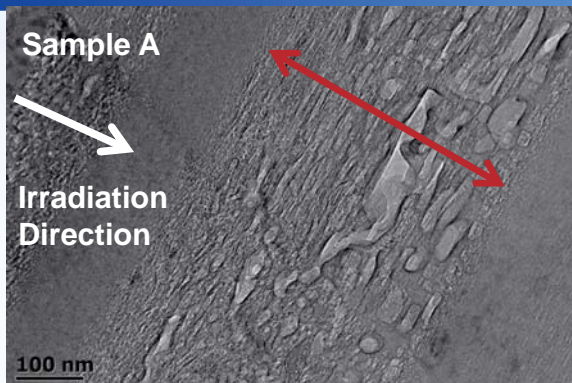


- Cavity distributions : parallel to the basal plane, regardless of irradiation direction
→ More dimensional changes between basal planes

FIB operation on Extruded Specimens



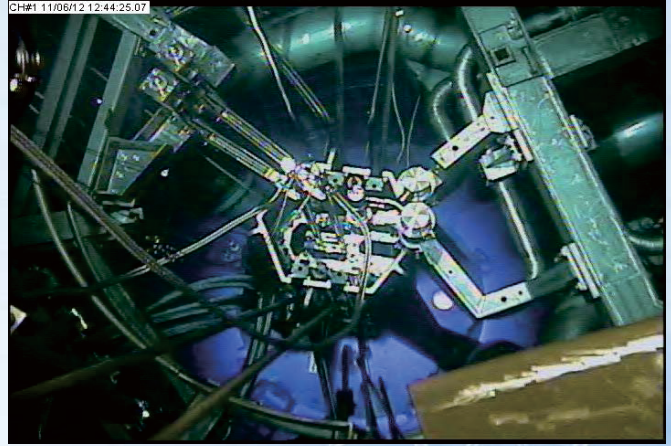
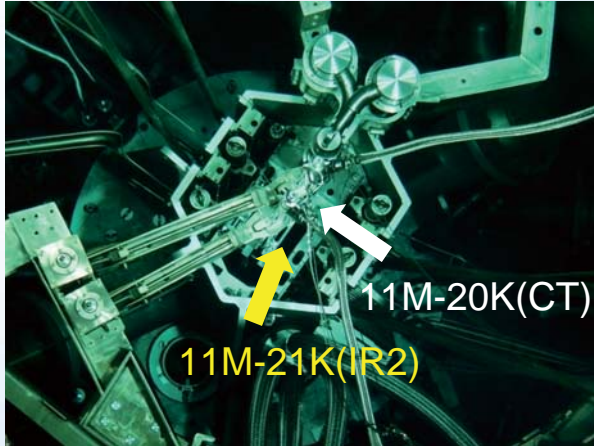
Dimensional Changes in Extruded Specimen



Dimensional change : Extrusion Direction < Transverse Direction

In-pile Test using HANARO

• Schematic of irradiation Capsule



Load capsules at the test holes of HANARO

- Capsule 1 (11M-20K) : CT
- Capsule 2 (11M-20K) : IR2

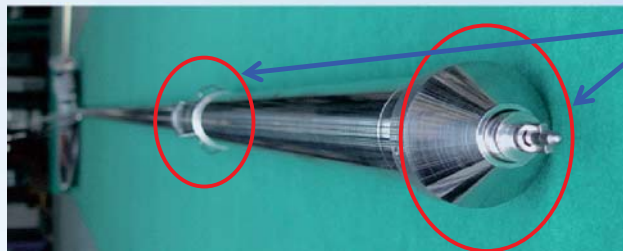
Start irradiation testing at HANARO

- HANARO 1 cycle : Operated for 27 days

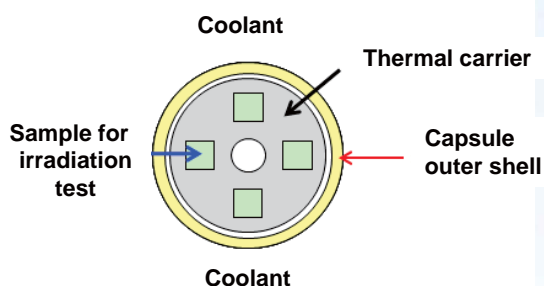
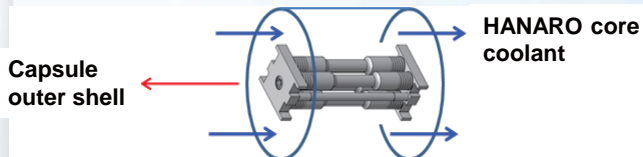
21

Capsule concept for Beryllium irradiation testing

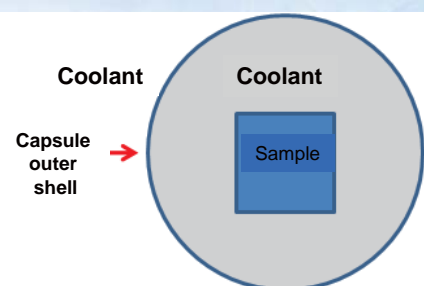
Temp. range : 40~80°C
(RR operating conditions)



Change of previous capsule design
=> Secure available area

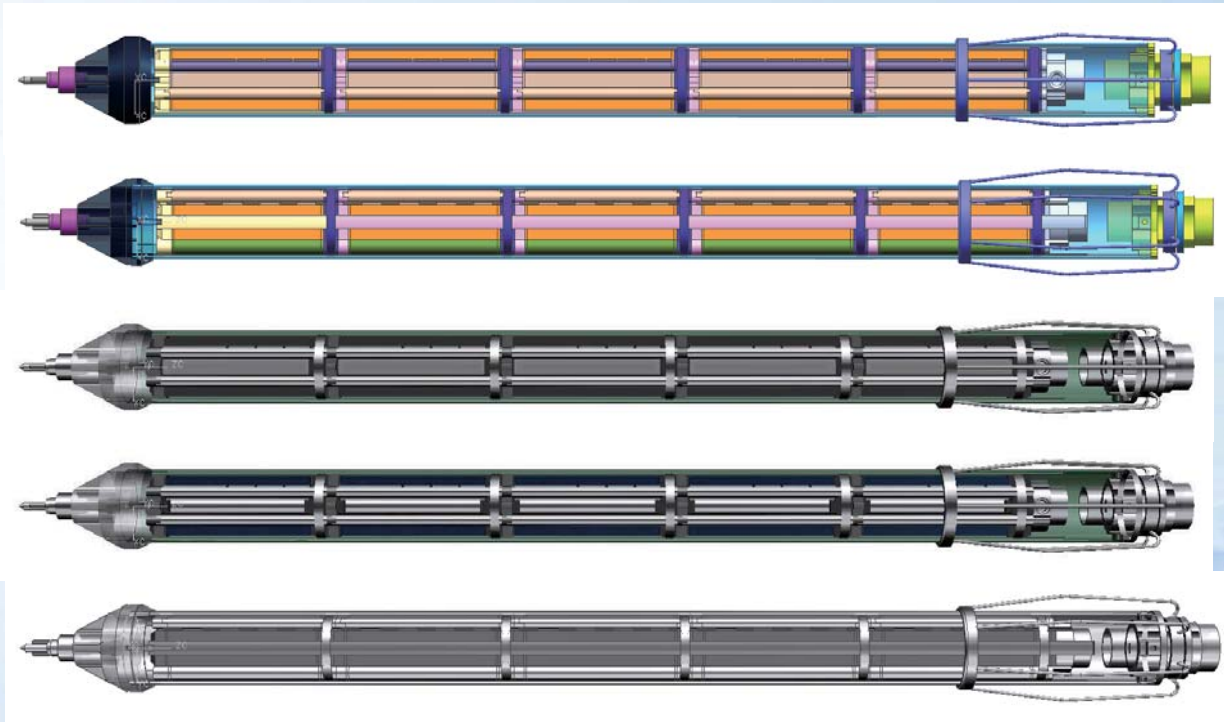


Change of capsule structure



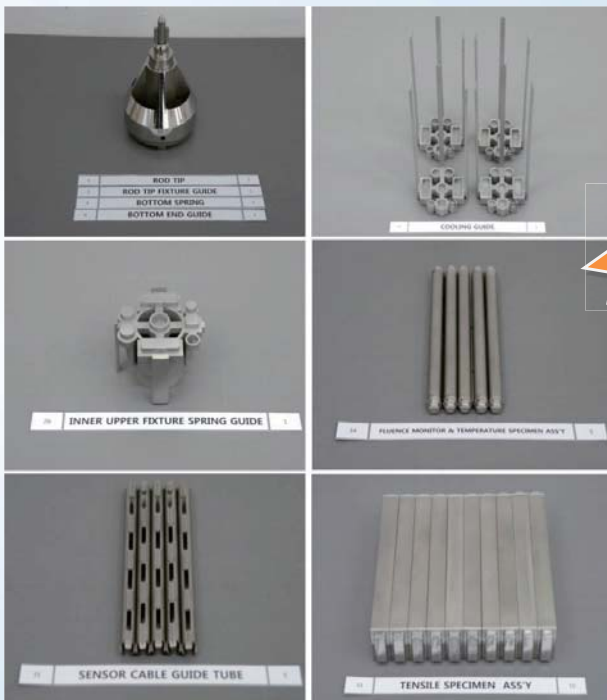
14

Capsule configuration



17

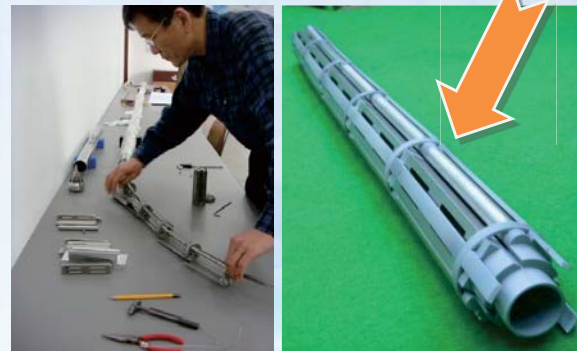
Capsule manufacturing



1. Capsule individual part manufacturing for irradiation testing



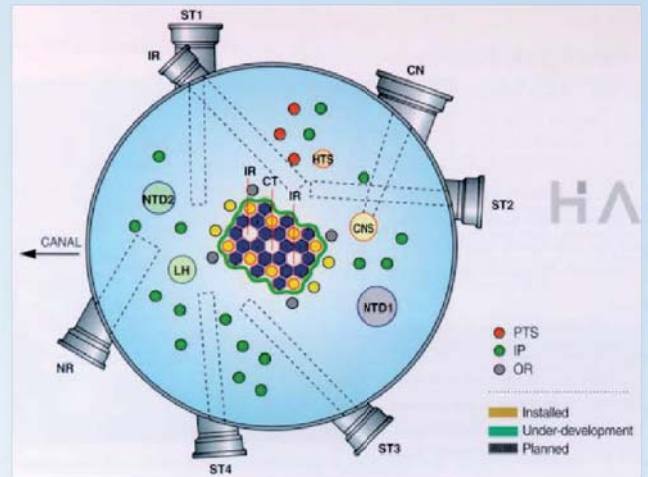
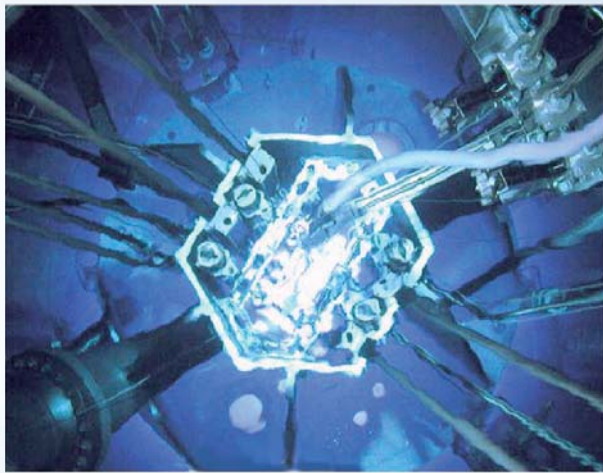
2. Assembly of sample case for each stage



3. Combination of sample cases

18

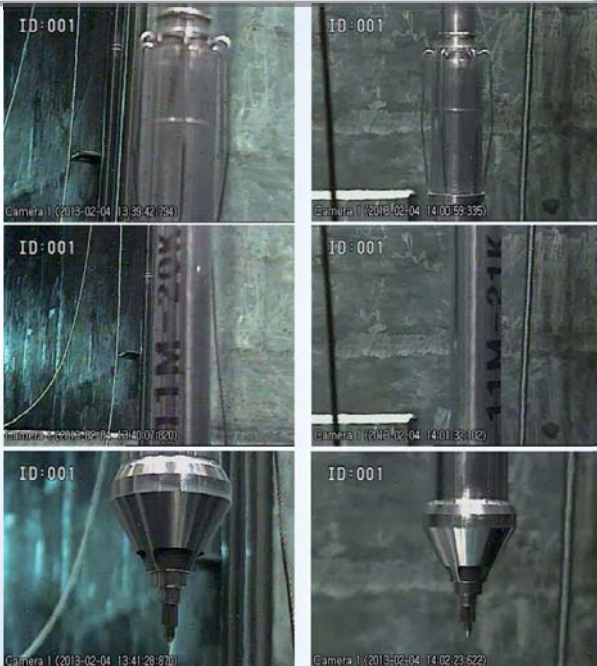
Neutron flux in HANARO



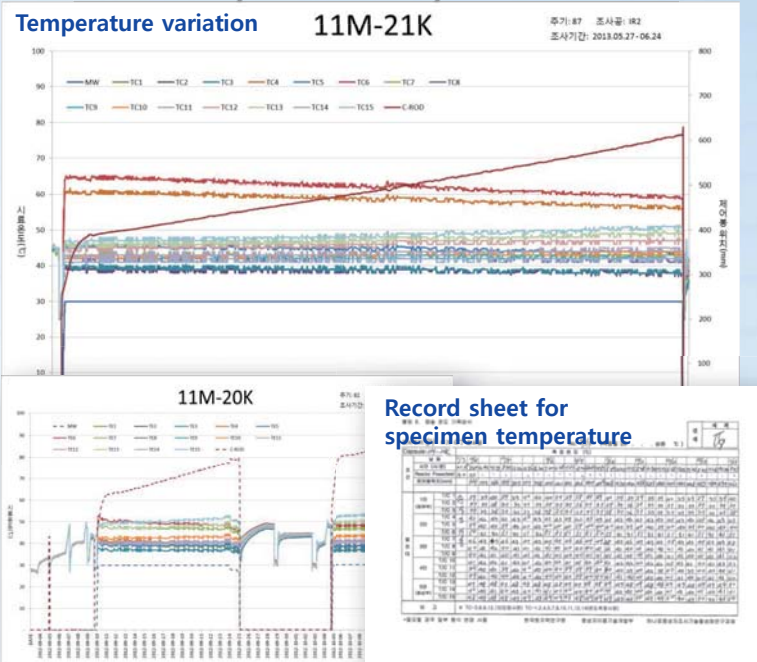
Location	Hole		Inside Dia. (cm)	Neutron Flux (n/cm ² . sec)		Remarks
	Name	No.		Fast Neutron (E>1.0 Mev)	Thermal Neutron (<0.625 eV)	
Core	CT	1	7.44	2.10 x 10 ¹⁴	4.39 x 10 ¹⁴	Fuel/material isotope production
	IR2	2	7.44	1.95 x 10 ¹⁴	3.93 x 10 ¹⁴	
	OR	4	6.00	2.23 x 10 ¹³	3.36 x 10 ¹⁴	
Reflector	LH	1	15.0	6.62 x 10 ¹¹	9.77 x 10 ¹³	Fuel/material Isotope, semi-conductors
	HTS	1	10.0	9.44 x 10 ¹⁰	4.79 x 10 ¹³	
	IP	17	6.0	1.45 x 10 ⁹ ~ 2.10 x 10 ¹²	2.40 x 10 ¹³ ~ 1.95 x 10 ¹⁴	

Irradiation Testing at HANARO

Check capsule integrity every cycle



Measurement of operating variables & specimen temperature



Neutron Irradiation test of Beryllium using the capsules was successfully performed at HANARO !!!

Post-Irradiation Examination (PIE) test

Dimension measurement

• Test Equipment

- Irradiation Deformation Measurement System
- High scope System
- Measured Range: (X:300, Y:300, Z:258 [mm])
- Precision : 1/100 [mm]

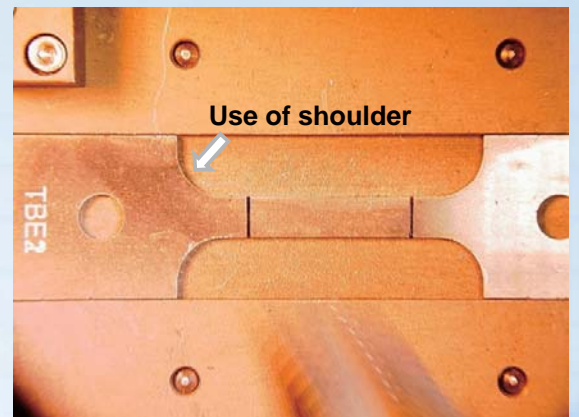
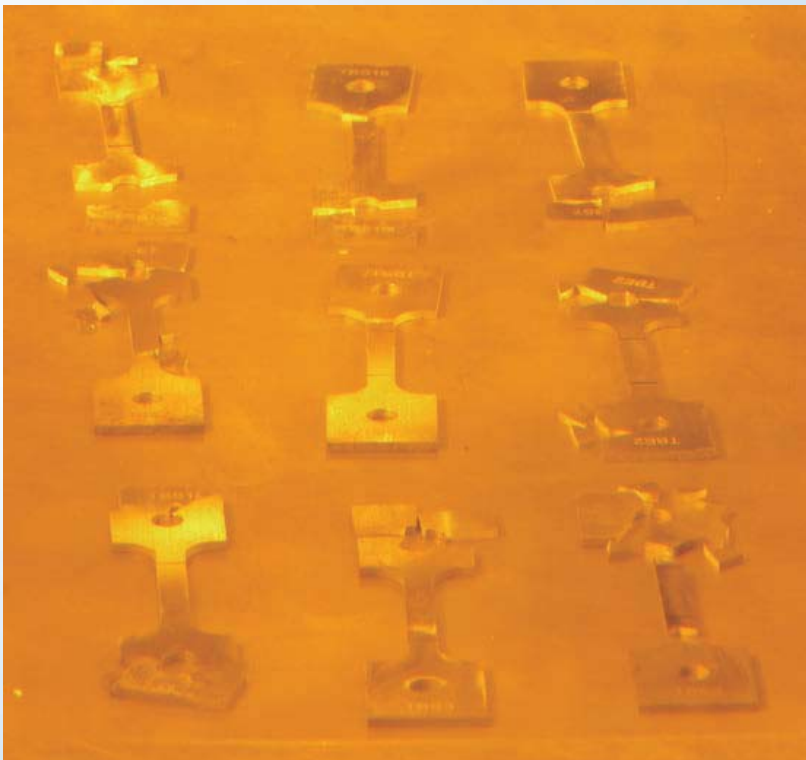


• Test Results

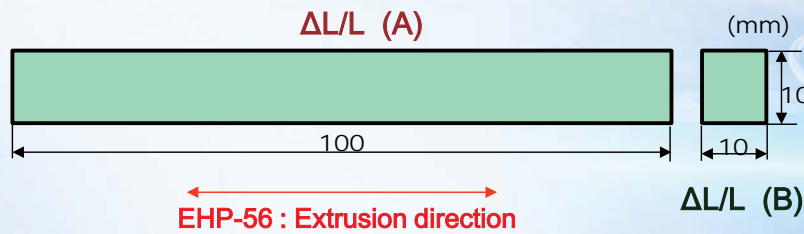
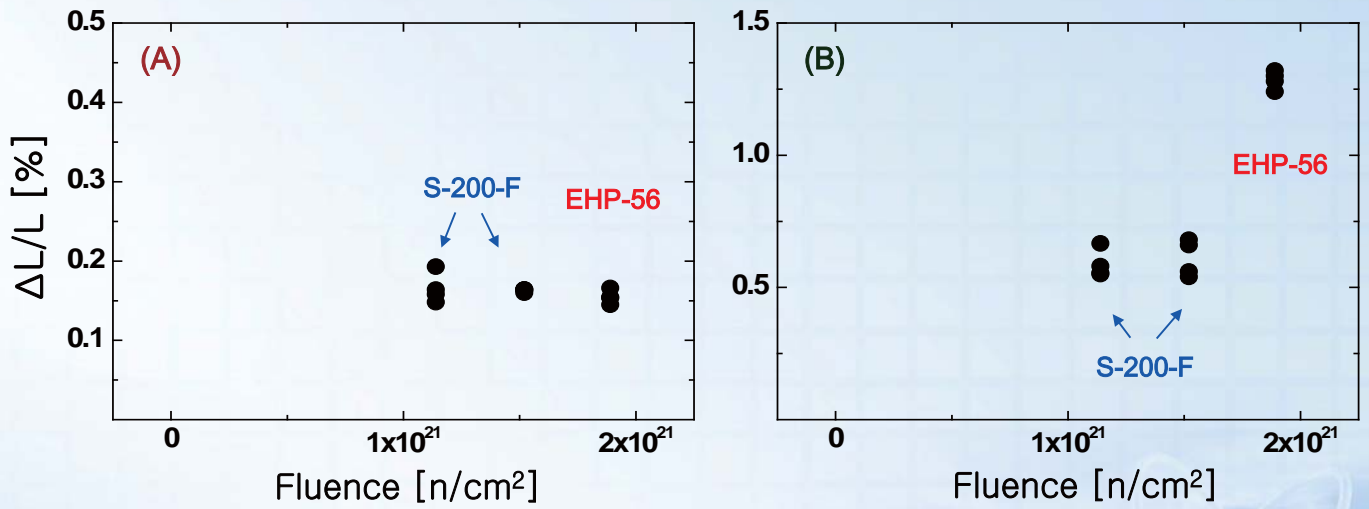
ID	Edge of left side	Edge of right side	Upper width	Lower width	ID	Edge of left side	Edge of right side	Upper width	Lower width
GZW 1					GZA 4				
GZW 2					GZX 1				
GZW 3					GZX 2				
GZW 4					GZX 3				
GZA 1					GZY 1				
GZA 2					GZY 2				
GZA 3					GZY 3				



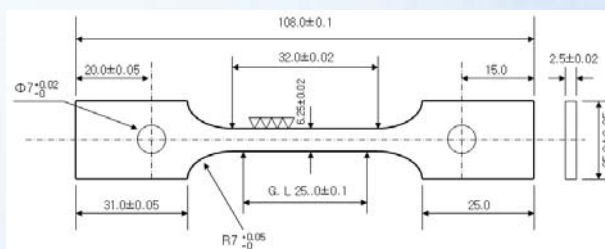
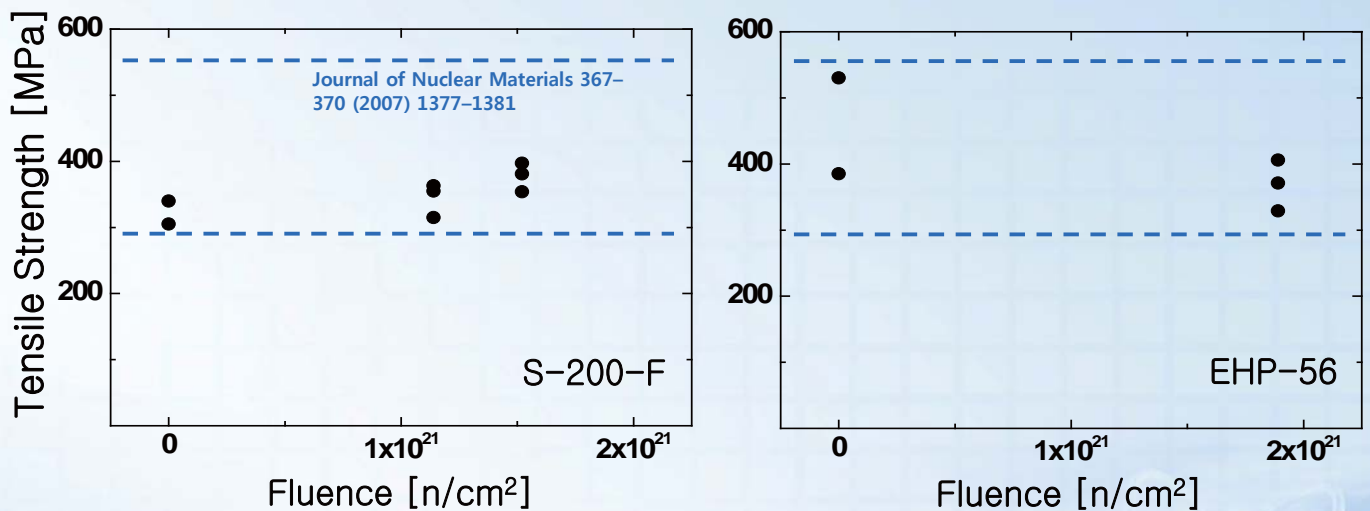
Brittle Fracture of Tensile Specimens



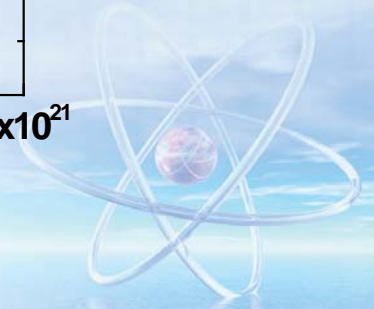
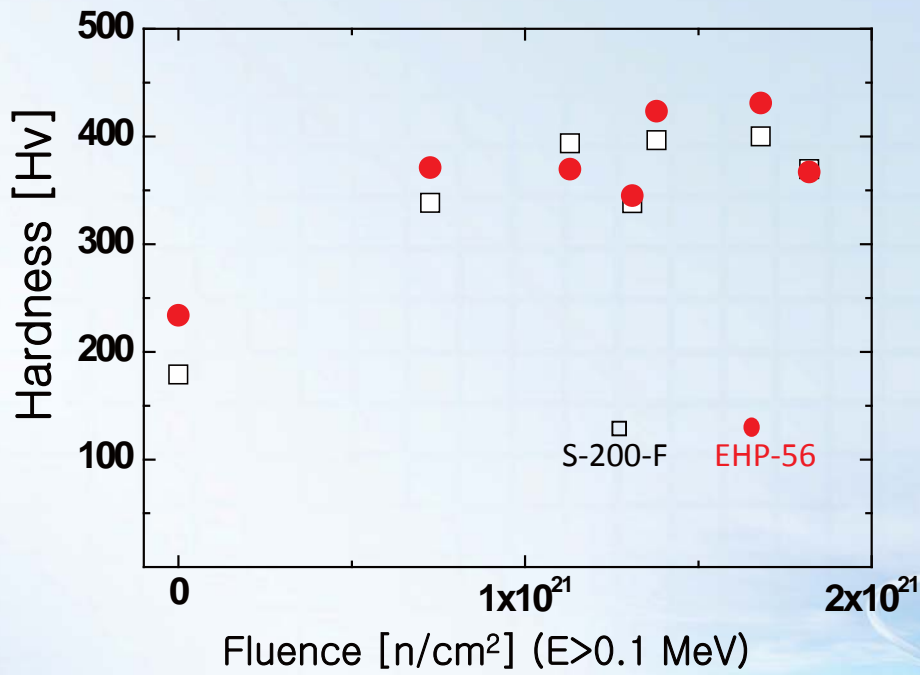
Irradiation Growth



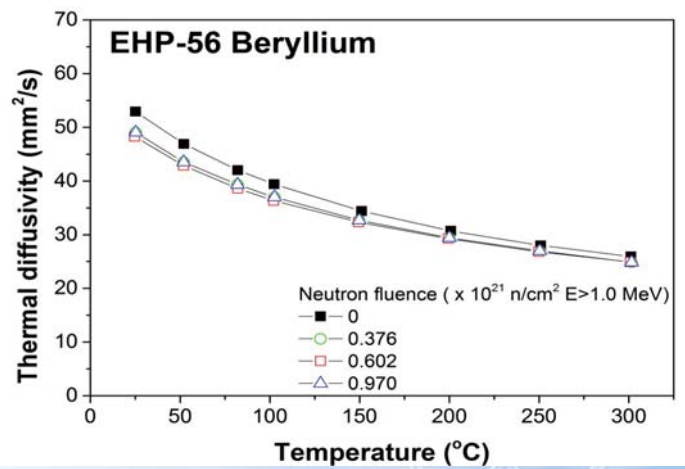
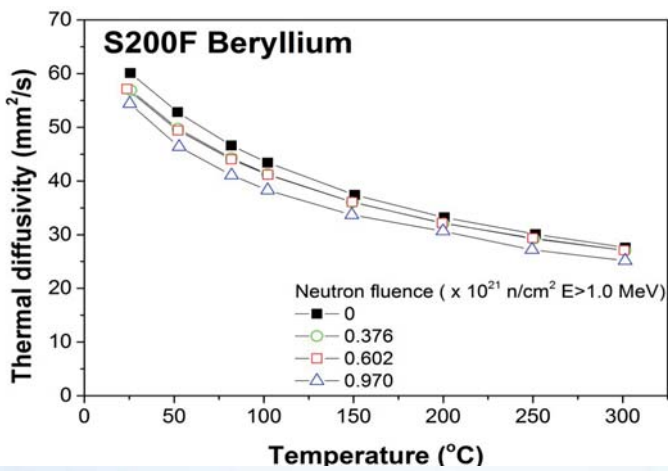
Beryllium – Tensile Strength



Hardness



Thermal diffusivity



Summary

Beryllium Research in KAERI

- Material evaluation research will be launched with upcoming KJRR project

Proton Irradiation on Beryllium

- Anisotropic dimensional change was observed
 - More dimensional changes between basal planes
 - Less dimensional changes along extrusion direction

Establishment of a irradiation behavior DB of Beryllium

- DB up to a neutron fluence of $\sim 2 \times 10^{21}$ n/cm² (E>0.1 MeV)
- Irradiation temperature: < 70°C (RR operating conditions)
 - Dimensional stability, Physical properties, Mechanical properties

Assessment of lifetime and safety of reflector in RRs

28

**Thank you
for your attention!**

Suk Hoon Kang
(shkang77@kaeri.re.kr)

29

2.8.2 Effects of argon and helium ions irradiation on microstructure of beryllium

Pingping Liu*, Wen Hu, Yumei Jia, Wentuo Han, Xiaoou Yi, Qian Zhan, Farong Wan

School of Materials Science and Engineering, University of Science and Technology Beijing, Beijing 100083, China

Beryllium is planned to be used as a neutron multiplier in the Helium-cooled ceramic breeder (HCCB) test blanket module (TBM) which is the primary option of the Chinese TBM. In reactor, the noble gas (such as argon) seeding will be necessary in ITER to reduce heat loads on the divertor target. Helium will be produced in deuterium-tritium and beryllium nuclear reactions. These gases will interact with irradiation damage and result in properties degradation. The character of the microstructural change of beryllium under irradiation is a determining factor in understanding of the processes resulting in the degradation of physical-mechanical properties of the material. Beryllium metal was irradiated with He^+ and Ar^+ ions at room temperature. The microstructural change of beryllium has been investigated using transmission electron microscopy (TEM) and scanning TEM (STEM). After the irradiation, a high density of black-dot-like defects were observed in the sample, some of which were resolved as small dislocation loops with different Burgers vector. Gas-filled bubbles with different size in different samples were observed in the sample. Average size of bubbles in the sample irradiated by Ar^+ ions is about 33.7 nm, which is much larger than that of samples irradiated by He^+ ions. Swelling of beryllium sample induced by gas ions irradiation was discussed.

* *Presenting Author: Pingping Liu*
E-mail: ppliu@ustb.edu.cn



13th International Workshop on Beryllium Technology (BeWS-13)

21-22 September 2017 Narita, CHIBA, Japan

Effects of argon ion irradiation on microstructure of beryllium

Pingping Liu, Wen Hu, Yumei Jia, Qian Zhan, Farong Wan

*School of Material Science and Engineering,
University of Science and Technology Beijing, Beijing 100083, China*



2017-09-22

Acknowledgments

*Thanks to Wen Hu (master student) and Yumei Jia for their work.

*The help and suggestions from Prof. Wan, Prof. Zhan and Prof. Ohnuki were highly appreciated.



Prof. Wan



Prof. Zhan



Prof. Ohnuki



* The authors gratefully acknowledge the Haibao Metal Materials Co., Ltd, China for supplying the material.

Outline

- Background and Objectives
- Microstructure of Be before irradiation
- Microstructure of Be after Ar ion irradiation
- Summary

3

Background

- Plasma facing materials
- Breeder (neutron multiplier)

- *Exposed to high-dose irradiation
- *Implanted by gas e.g. argon, ...

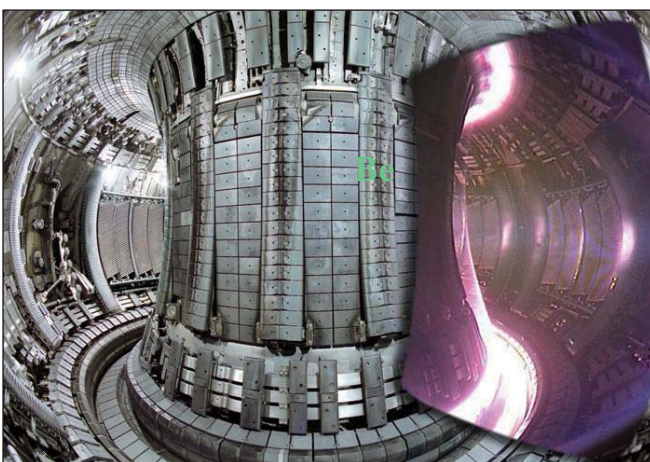


Fig 1. Plasma facing materials-Be ^[1]

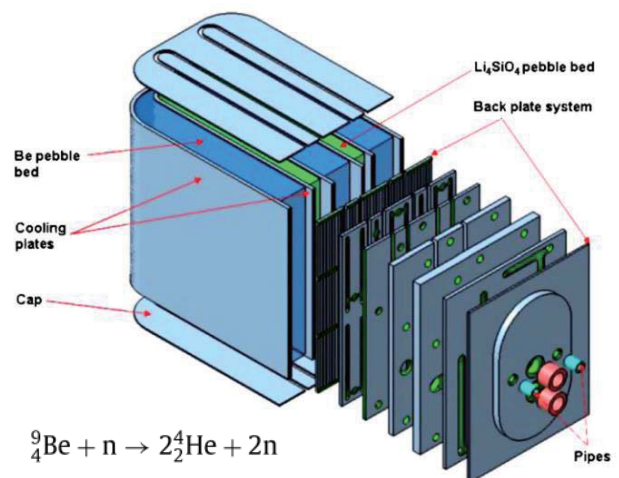


Fig 2. Schematic view of HCCB TBM design ^[2].

[1] K.L. Wilson, et al. Journal of Vacuum Science & Technology A, 8 (1990)1750.
[2] K.M. Feng, et al. Fusion Engineering and Design 87 (2012) 1138-1145.

4

Background and Objectives

Many good work about the microstructure especially gas bubble or voids in irradiated beryllium have been done by using TEM[1-3].

We have interesting in the dislocation loops induced by irradiation in beryllium.

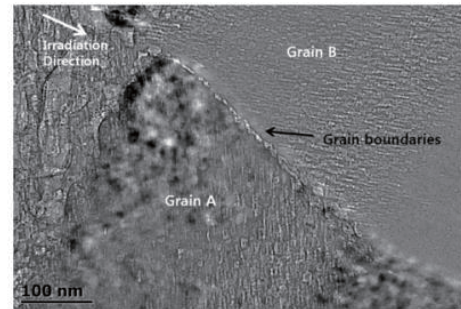
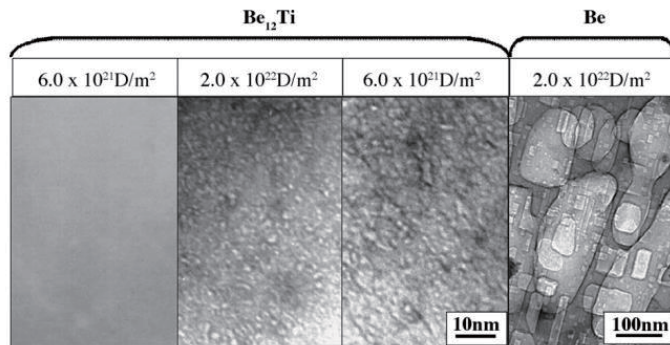


Fig. 3. Cross-sectional image of proton-irradiated (120 keV, 2.0×10^{18} ions/cm²) beryllium, was observed by TEM. Two different grains (Grains A and B) are irradiated simultaneously. The distribution of voids was affected by the crystal orientation and the grain boundaries. [2]

Damage in Be₁₂Ti and Be formed by 8 keV-D₂⁺ ion irradiation at 673K [1].

Objectives:

Dislocation loop induced in the Beryllium by ion irradiation

*Can dislocation loop be induced in Be by ion irradiation?

*What kind of the dislocation loop induced in Be?

[1] Y. Mishima et al., Fusion Engineering and Design, 82 (2007) 91-97.

[2] S.H. Kang, et al., Journal of the Korean Physical Society, 63 (2013) 1414-1417.

[3] M. Klimenkov, et al., Journal of Nuclear Materials, 443 (2013) 409-416.

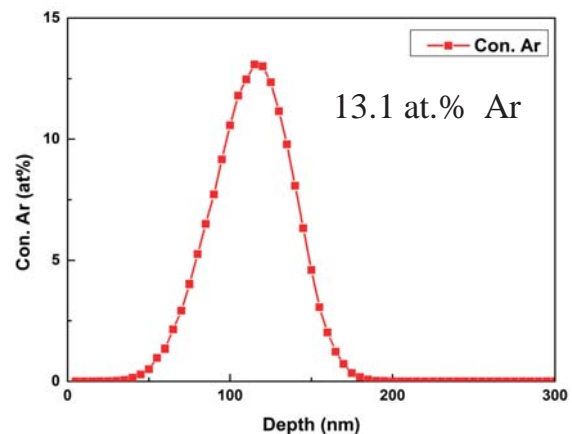
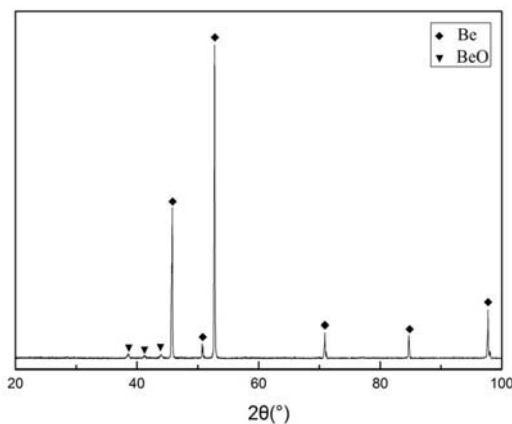
5

Materials and experimental methods

Chemical composition of Beryllium specimen (wt.%).

BeO	C	Ti	Fe	Al	Mg	Si	Mn	Be
~0.1	0.08	<0.01	0.33	0.038	<0.005	0.12	0.021	Balance

Phase composition of Beryllium specimen: Be and BeO



100 keV Ar⁺ ion irradiation: 1×10^{17} ions/cm², RT, 13.1 at.% Ar

Microstructure analysis: TEM and STEM

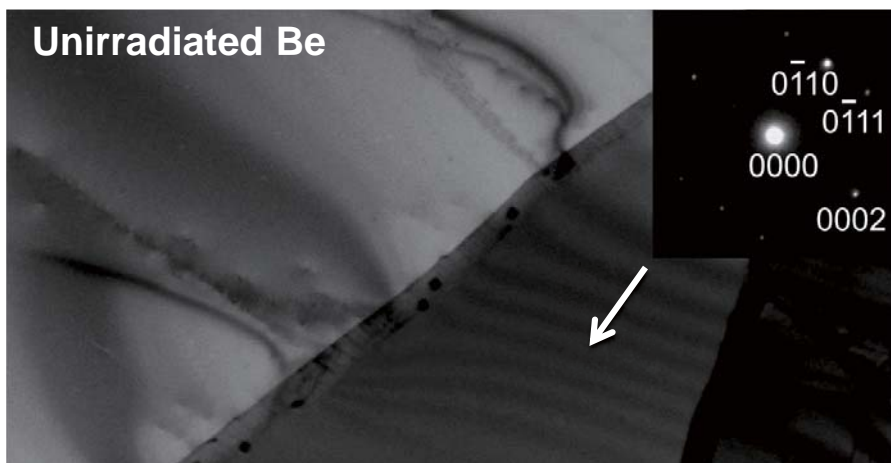
6

Outline

- Background and Objectives
- Microstructure of Be before irradiation
- Microstructure of Be after Ar ion irradiation
- Summary

7

Microstructure of Be before irradiation



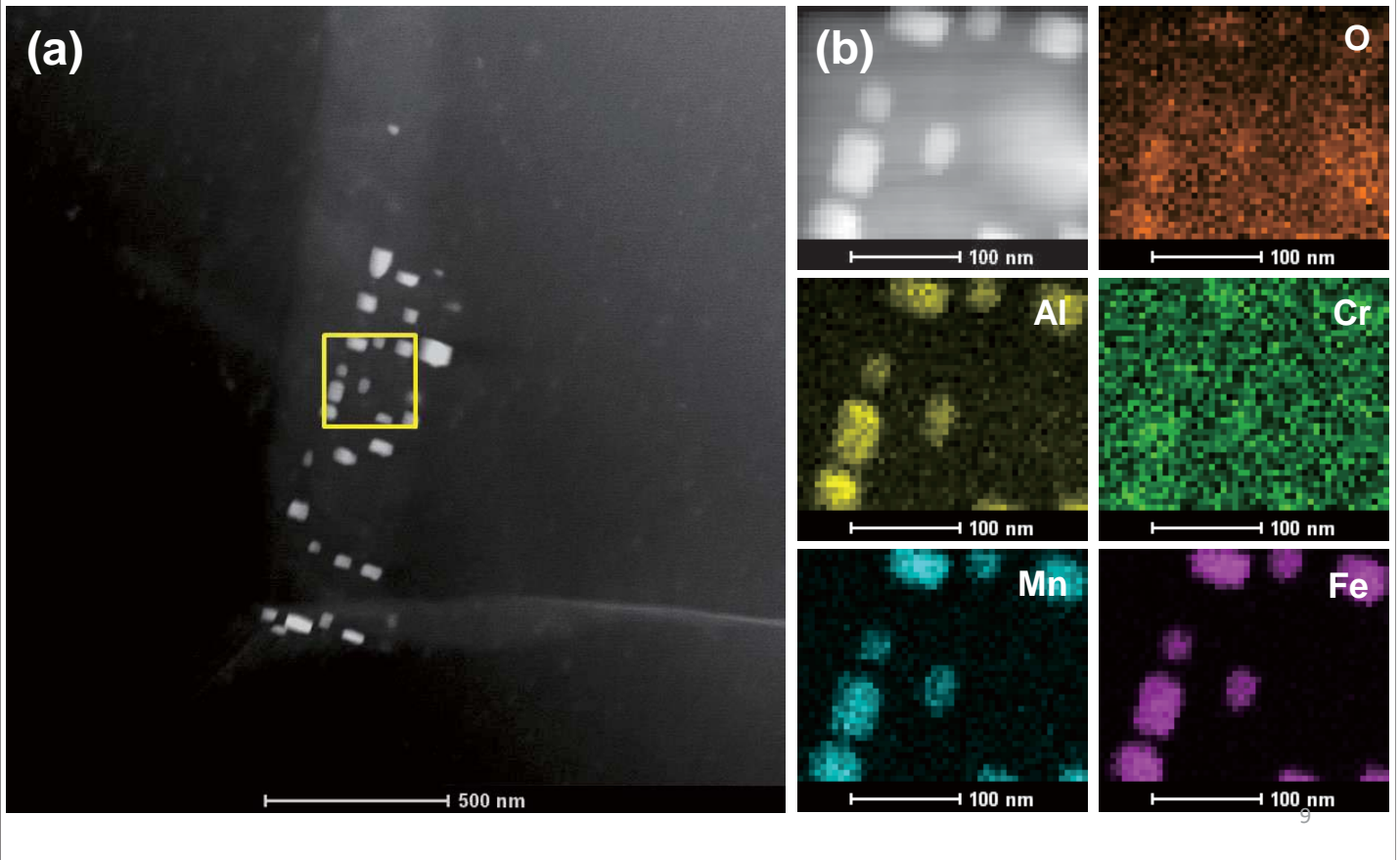
The grain size of the metal fall in the range from several microns to several hundred microns.

Some impurity particles were observed near the grain boundary and Few precipitates in the beryllium matrix.

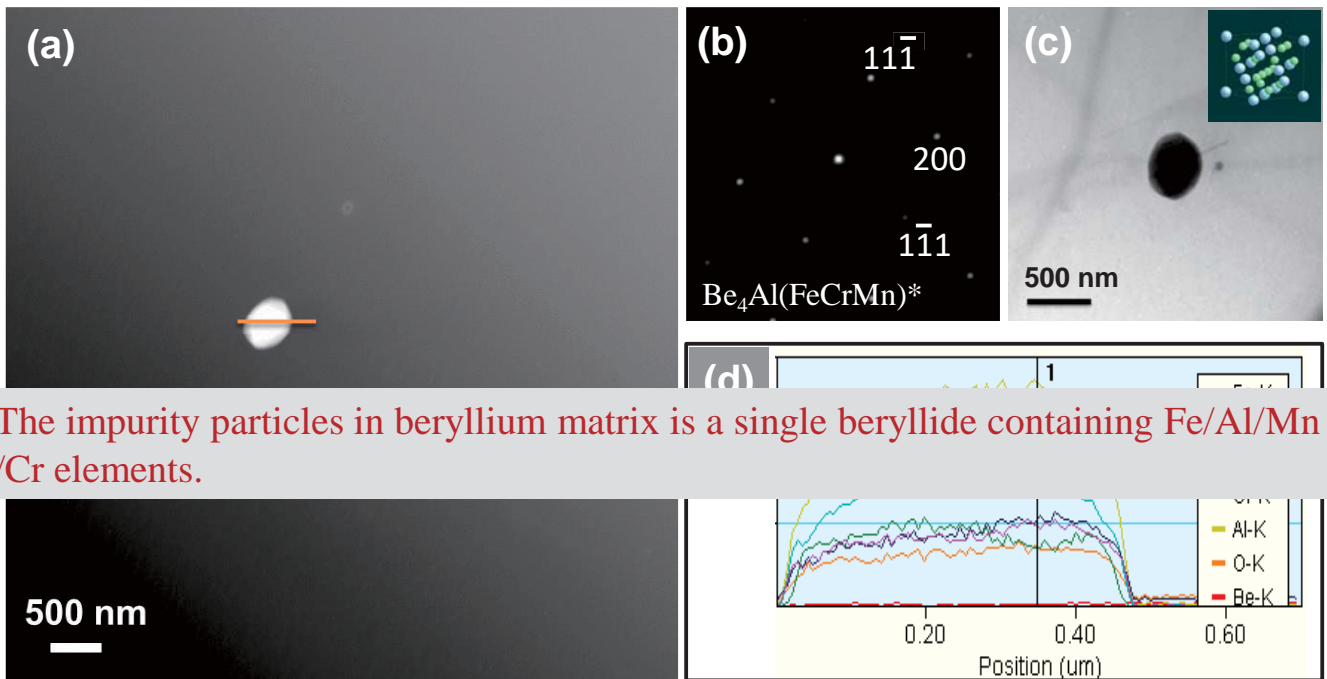


8

HAADF image of impurity particles



Microstructure of Be before irradiation



The impurity particles in beryllium matrix is a single beryllide containing Fe/Al/Mn/Cr elements.

(wt.%).

Al	Cr	Mn	Fe
34.14	12.22	25.77	14.45

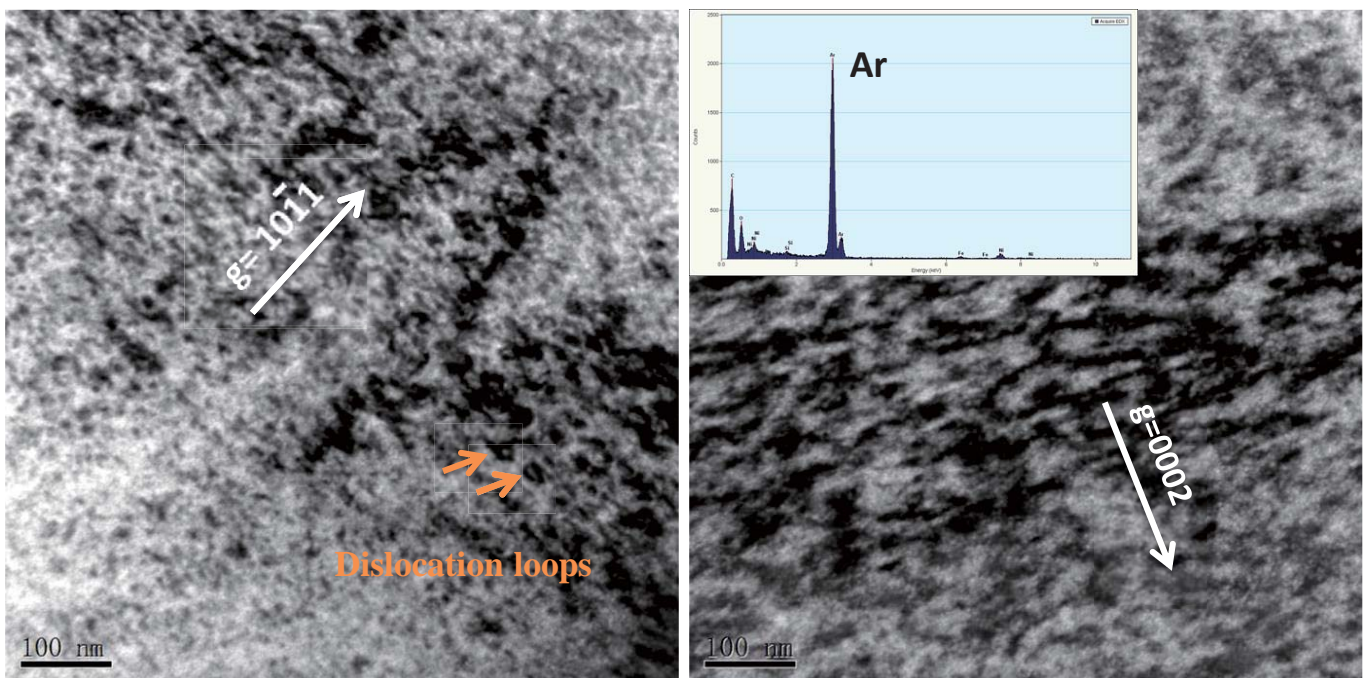
*Carrabine, J.A., J. Nucl. Mater. 8 (1963) 278-280

Outline

- Background and Objectives
- Microstructure of Be before irradiation
- Microstructure of Be after Ar ion irradiation
- Summary

11

Microstructure of Be After irradiation



A large number of dislocation loops were induced in beryllium matrix. The results of EDS shows that the matrix contains lots of argon.

12

Type of dislocation loop in hcp beryllium

Type	\vec{b}	Type	Beam	\vec{g}	$\vec{g} \cdot \vec{b}$	visible
Dislocation loop in hcp Metal	$\frac{1}{3}\langle 11\bar{2}0 \rangle$	a-type	$[11\bar{2}0]$	$10\bar{1}0$	1	$\sqrt{\quad}$
			$[11\bar{2}0]$	0002	0	\times
	$\frac{1}{2}\langle 0001 \rangle$	c-type	$[11\bar{2}0]$	$10\bar{1}0$	0	\times
			$[11\bar{2}0]$	0002	1	$\sqrt{\quad}$
			$[11\bar{2}0]$	$10\bar{1}0$	0	\times
	$\langle 0001 \rangle$	c-type	$[11\bar{2}0]$	0002	2	$\sqrt{\quad}\sqrt{\quad}$
			$[11\bar{2}0]$	$10\bar{1}0$	0	\times
	$\frac{1}{6}\langle 20\bar{2}3 \rangle$	c-complex ($\frac{c}{2} + p$)	$[11\bar{2}0]$	$10\bar{1}0$	$\frac{2}{3}$	$\sqrt{*}$
			$[11\bar{2}0]$	0002	1	$\sqrt{\quad}$
	$\frac{1}{3}\langle 11\bar{2}3 \rangle$	c-complex (c+a)	$[11\bar{2}0]$	$10\bar{1}0$	1	$\sqrt{\quad}$
			$[11\bar{2}0]$	0002	2	$\sqrt{\quad}\sqrt{\quad}$

* In actual practice, if $|\mathbf{g} \cdot \mathbf{b}| > 1/3$, visible. In theory, \mathbf{b} vectors can be further identified according to the contrast of different c-complex loop.

- [1] A. Harte, et al. / Acta Materialia 130 (2017) 69-82.
 [2] 刘文西, 黄孝瑛等 “材料结构电子显微分析”, 1989.
 [3] C.H. Woo, Journal of nuclear materials 276 (2000) 90-103.

13

Type of dislocation loop in hcp beryllium

Type	\vec{b}	Type	Beam	\vec{g}	$\vec{g} \cdot \vec{b}$	visible
Dislocation loop in hcp Metal	$\frac{1}{3}\langle 11\bar{2}0 \rangle$	a-type	$[11\bar{2}0]$	$10\bar{1}0$	1	$\sqrt{\quad}$
			$[11\bar{2}0]$	0002	0	\times
	$\frac{1}{2}\langle 0001 \rangle$	c-type	$[11\bar{2}0]$	$10\bar{1}0$	0	\times
			$[11\bar{2}0]$	0002	1	$\sqrt{\quad}$
			$[11\bar{2}0]$	$10\bar{1}0$	0	\times
	$\langle 0001 \rangle$	c-type	$[11\bar{2}0]$	0002	2	$\sqrt{\quad}\sqrt{\quad}$
			$[11\bar{2}0]$	$10\bar{1}0$	0	\times
	$\frac{1}{6}\langle 20\bar{2}3 \rangle$	c-complex ($\frac{c}{2} + p$)	$[11\bar{2}0]$	$10\bar{1}0$	$\frac{2}{3}$	$\sqrt{*}$
			$[11\bar{2}0]$	0002	1	$\sqrt{\quad}$
	$\frac{1}{3}\langle 11\bar{2}3 \rangle$	c-complex (c+a)	$[11\bar{2}0]$	$10\bar{1}0$	1	$\sqrt{\quad}$
			$[11\bar{2}0]$	0002	2	$\sqrt{\quad}\sqrt{\quad}$

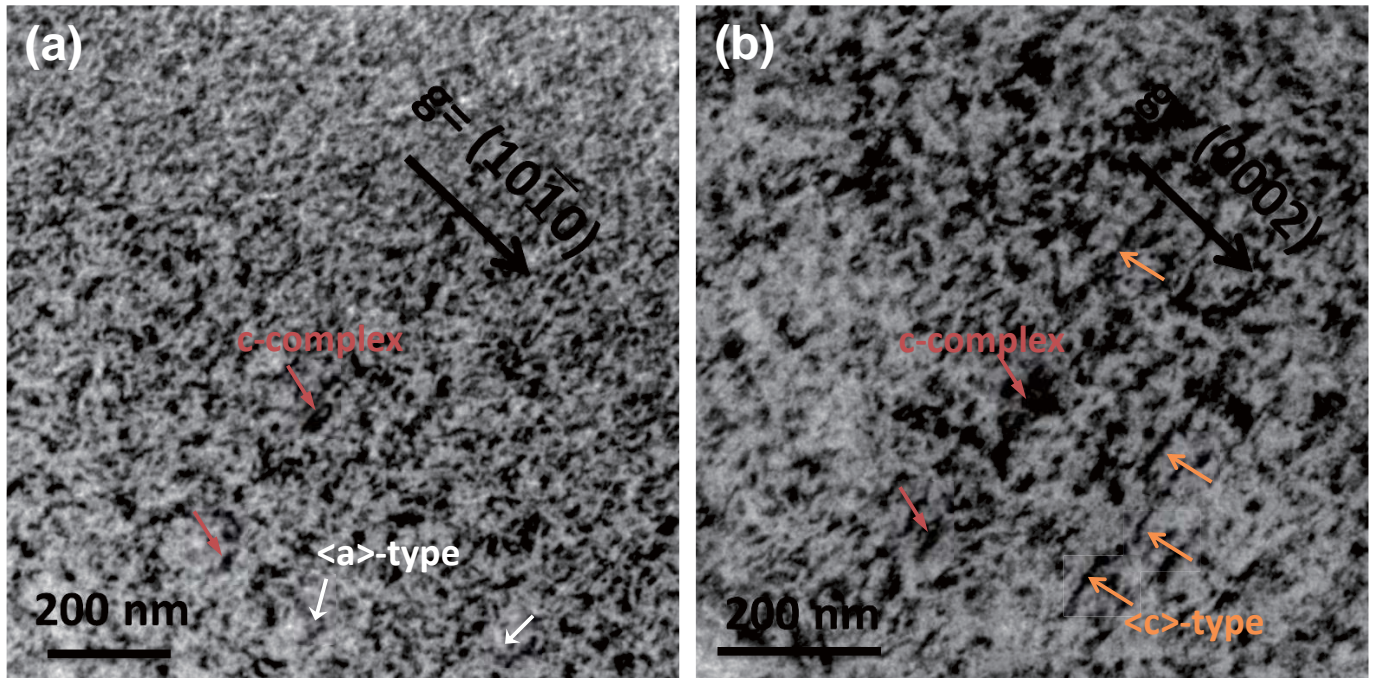
For $\mathbf{g}=10\bar{1}0$, visible; and $\mathbf{g}=0002$, invisible; a-type
 For $\mathbf{g}=10\bar{1}0$, invisible; and $\mathbf{g}=0002$, visible; c-type
 For $\mathbf{g}=10\bar{1}0$, visible; and $\mathbf{g}=0002$, visible; c-complex type

* In actual practice, if $|\mathbf{g} \cdot \mathbf{b}| > 1/3$, visible. In theory, \mathbf{b} vectors can be further identified according to the contrast of different c-complex loop.

- [1] A. Harte, et al. / Acta Materialia 130 (2017) 69-82.
 [2] 刘文西, 黄孝瑛等 “材料结构电子显微分析”, 1989.
 [3] C.H. Woo, Journal of nuclear materials 276 (2000) 90-103.

14

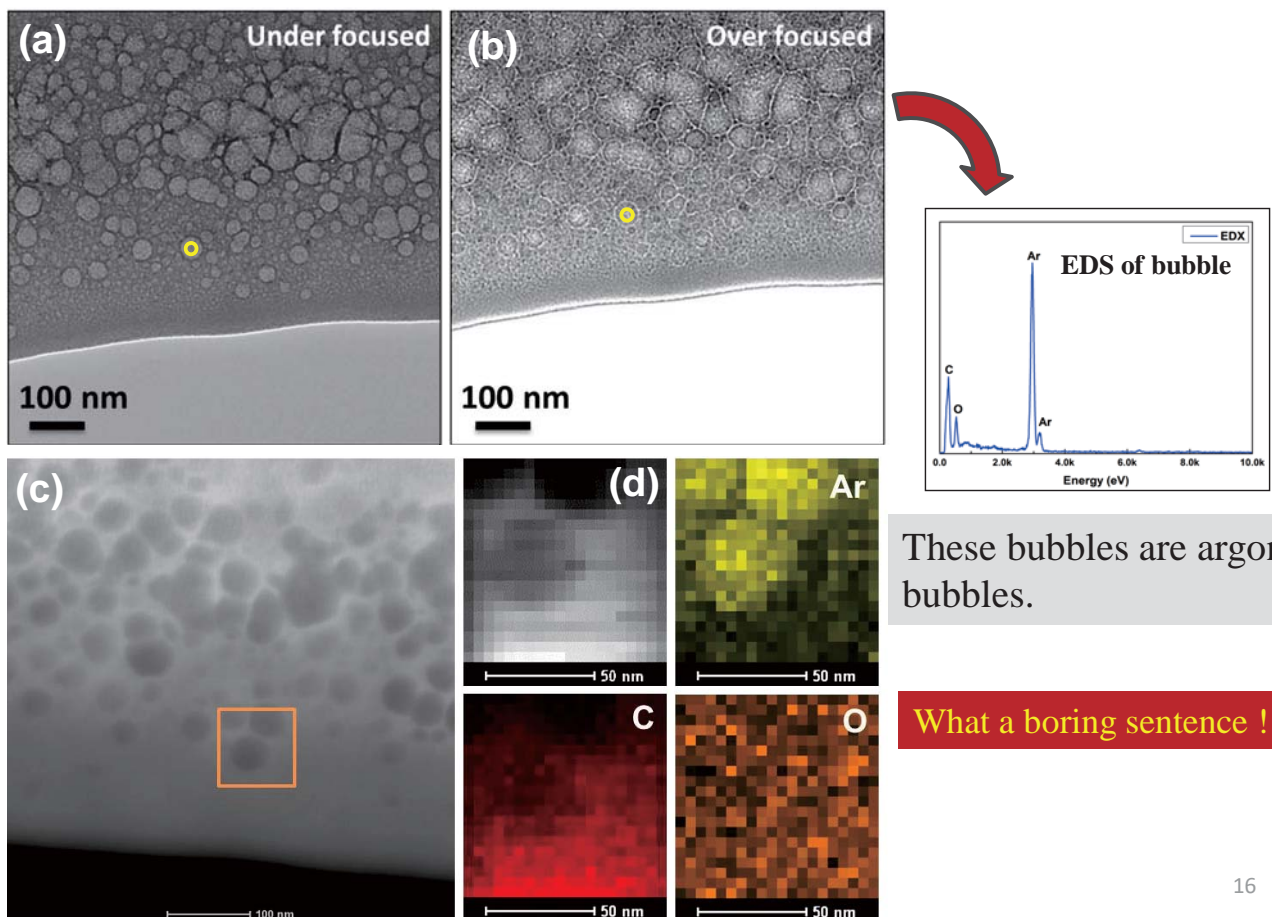
Type of dislocation loop in Be after irradiation



It was shown that $\langle a \rangle$, $\langle c \rangle$ and c-complex type dislocation loops are present in this irradiated beryllium.

15

Bubbles in Be after Ar^+ ion irradiation

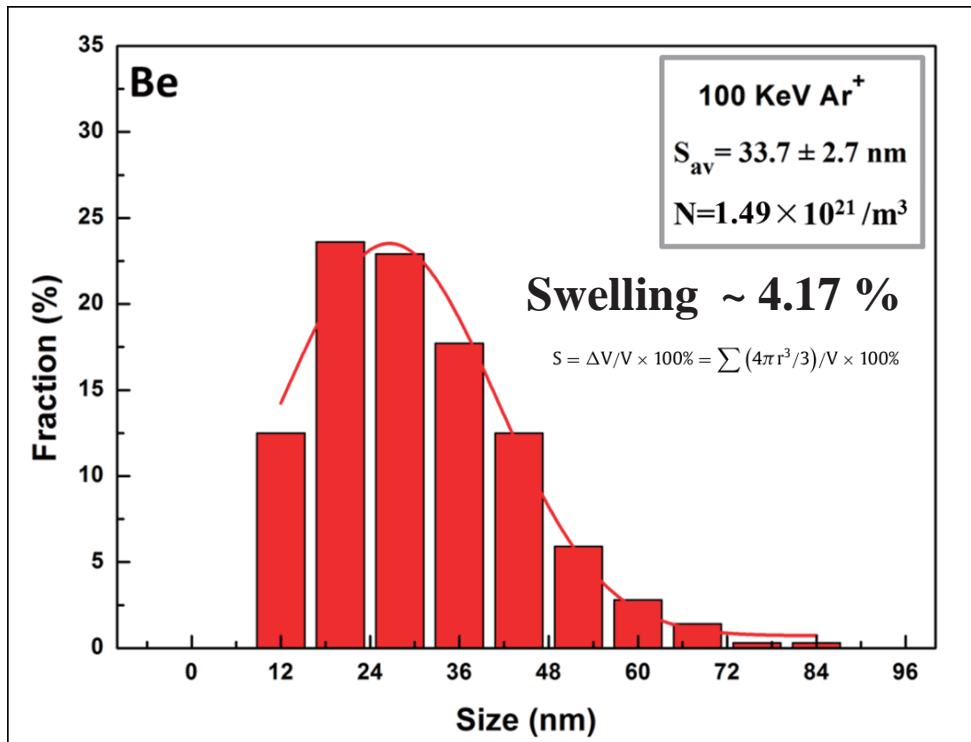


These bubbles are argon bubbles.

What a boring sentence !

16

Swelling of Be after Ar⁺ ion irradiation



The total swelling is about 4.17%. But the average swelling is 0.32% per 10000 appm Ar⁺.

Summary

- Microstructural analysis (TEM and STEM) were performed in beryllium before and after argon ion irradiation at RT.
- the grain size of the beryllium ranged from several microns to several hundred microns.
- Some precipitates were observed. These impurity particles could be beryllide phases containing Fe/Al/Mn/Cr.
- After irradiation, dislocation loops with different Buerger's vector (a-type, c-type, c-complex type) were induced in beryllium.
- A large number of argon bubbles with average size of 33.7 nm were observed and resulted in a swelling (about 4.17%) of the specimen after high fluence argon ion irradiation.
(The average swelling is only 0.32% per 10,000 appm Ar⁺.)



13th International Workshop on Beryllium Technology (BeWS-13)

21-22 September 2017 Narita, CHIBA, Japan

THE END!

Thanks for your attention!

E-mail: ppliu@ustb.edu.cn

19

Why Ar ion irradiation be used?

- *Exposed to high-dose irradiation
- *A large number of helium induced in Be
- *Beryllium will be injected by gas in noble gas, e.g. argon, cooled environment^[*]
- *Argon is a noble gas like helium, and will produce higher damage as it is more massive.
- * Helium ion irradiation also been carried out.

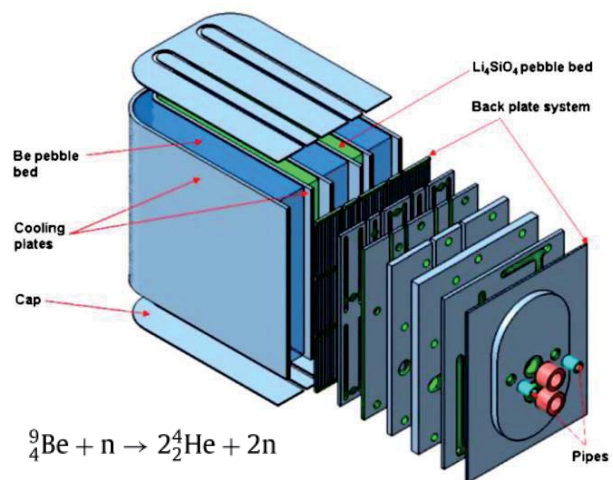


Fig 2. Schematic view of HCCB TBM design.

[*] A. Kreter, D. Nishijima, M.J. Baldwin, et. al., Mitigation of carbon erosion in beryllium seeded deuterium plasma under bombardment by argon and helium ions in PISCES-B, J. Nucl. Mater. 417 (2011) 651-654.

20

2.8.3 Present status of He ion irradiation hardening of Japanese beryllide pebbles by REM

T. Shibayama¹, N. Igarashi² Jae-Hwan Kim³ and M. Nakamichi³

¹*Center for Advanced Research of Energy and Materials, Faculty of Engineering, Hokkaido University, Sapporo, Hokkaido 060-8628, Japan*

²*Graduate student, Graduate school of Engineering, Hokkaido University, Sapporo, Hokkaido 060-8628, Japan*

³*Fusion Energy Research and Development Directorate, National Institute for Quantum and Radiological Science and Technology, 2-166, Omotedate, Obuchi, Rokkasho, Kamikita, Aomori 039-3212, Japan*

E-mail: shiba@qe.eng.hokudai.ac.jp

We investigated He ion irradiation hardening of several kinds of prototype beryllide pebbles (Be_{12}Ti , $\text{Be}_{17}\text{Ti}_2$, and Be_{12}V) made at National Institute for Quantum and Radiological Science and Technology (QST) in Japan. All of beryllide pebbles were fabricated by a combined process with a plasma sintering method for electrode fabrication and a rotary electrode method (REM). Detailed process and their microstructure investigations are described in elsewhere [1-3]. After beryllide pebble were embedded in the resin, the specimen were grinded from one side until appearing the cross section. Then, the surface of the hemisphere of beryllide pebbles were mirror polished for reduction of scattering of experimental results in the beryllium handling laboratory at QST. All of specimens were irradiated up to 10,000 appm/He at R.T. at High Voltage Electron Microscope (HVEM) laboratory in Hokkaido University. He ion irradiation hardening of beryllide pebbles were evaluated by using a nano indenter (Model ENT-1100a, Elionix Inc., Tokyo, Japan). A Berkovich indenter was used and the tip truncation was calibrated using a fused silica disk as a reference specimen. As a result of nano indentation tests, it was confirmed that all of beryllide pebbles showed no brittle fracture behavior and no significant He irradiation hardening up to 10,000 appm/He. Microstructure investigations will be also presented at the work shop.

References

- [1] Masaru Nakamichi and Jae-Hwan Kim, *Fusion Engineering and Design*, **89**, pp.1304-1308 (2014)
- [2] Masaru Nakamichi and Jae-Hwan Kim and Mitsutaka Miyamoto, *Nuclear Materials and Energy*, **9**, pp55-58 (2016)
- [3] Masaru Nakamichi and Jae-Hwan Kim, *Fusion Engineering and Design*, In press (2017), <https://doi.org/10.1016/j.fusengdes.2017.04.039>



Present status of He ion irradiation hardening of Japanese beryllide pebbles by REM

T. Shibayama¹, N. Igarashi² Jae-Hwan Kim³ and M. Nakamichi³

*¹Center for Advanced Research of Energy and Materials, Faculty of Engineering,
Hokkaido University, Sapporo, Hokkaido 060-8628, Japan*

*²Graduate student, Graduate school of Engineering, Hokkaido University, Sapporo,
Hokkaido 060-8628, Japan*

*³Fusion Energy Research and Development Directorate,
National Institute for Quantum and Radiological Science and Technology,
2-166, Omotedate, Obuchi, Rokkasho, Kamikita, Aomori 039-3212, Japan*

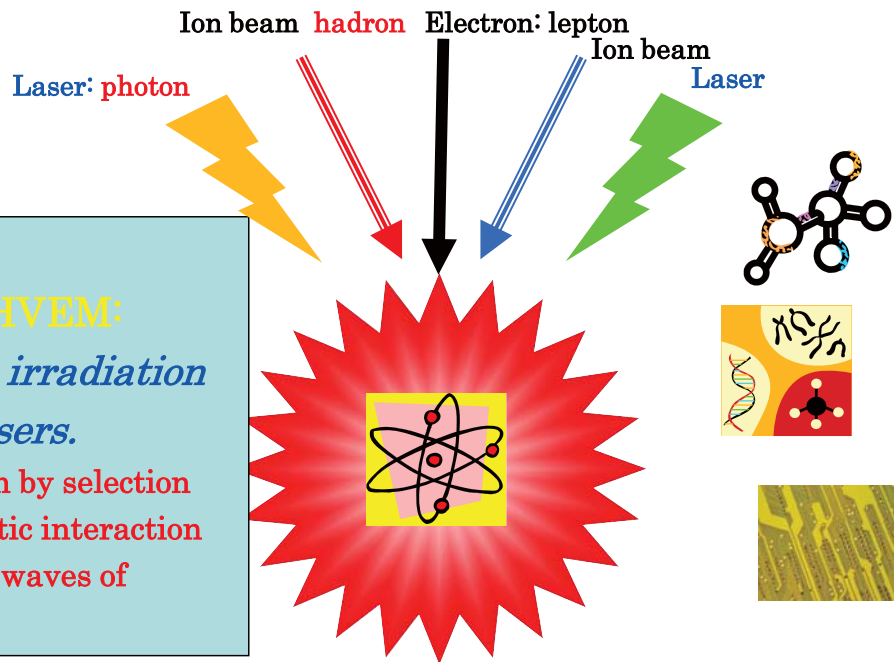
HVEM laboratory in Hokkaido University



An initiative nanodynamic study of matters by MQB-HVEM [Multi-quantum beam HVEM]

Development of
Multi-quantum-beam HVEM:
Capable of multi-beam irradiation
of electron, ions and lasers.

- Inter-atomic bond excitation by selection
- Ultra-short (>130fs) adiabatic interaction
- Interference with quantum waves of electron, ions and lasers

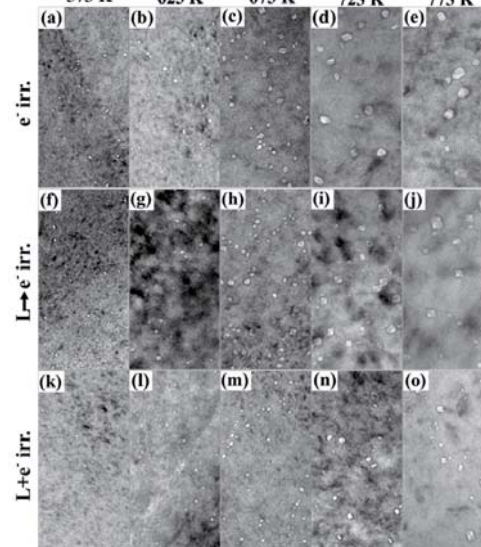
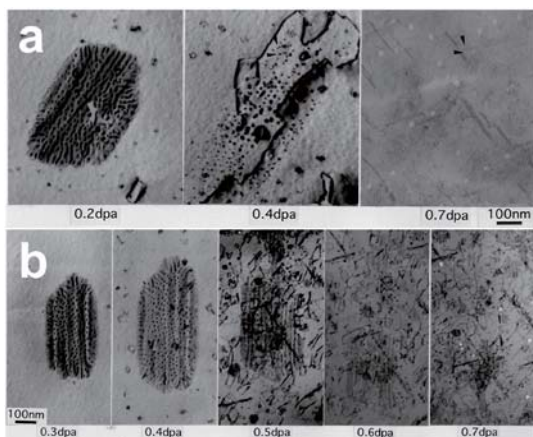
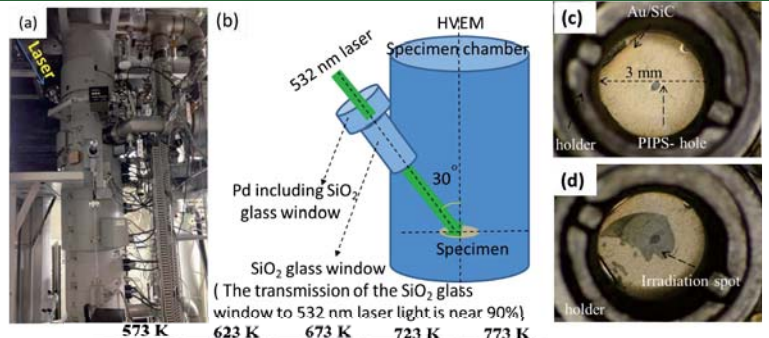


Innovative matter science of nanodynamics at far-from-equilibrium:

*Nonequilibrium matter science and development of new functional materials

*New quantum beam physics and matter study by interference beam effects

In-situ observation of defects formation and growth in SUS316L

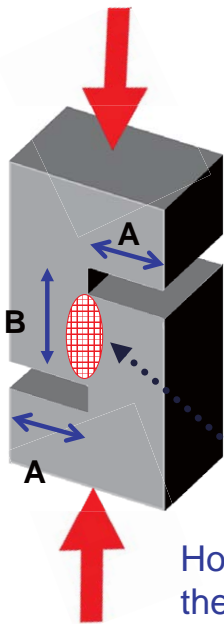


Laser power: nearly
10MJ/cm²·pulse

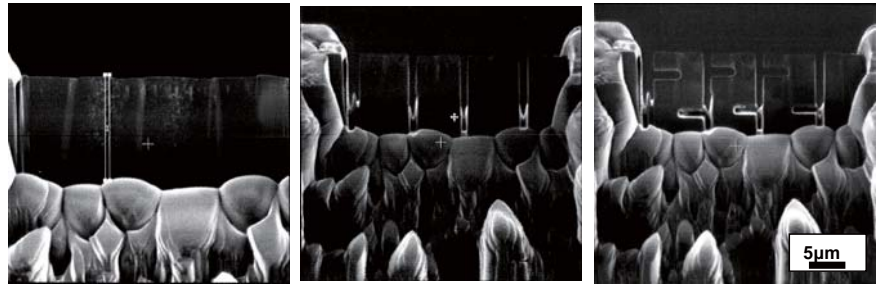
Irradiation effects of SUS316L under (a) electron,
(b) electron/Helium dual irradiation. Helium would behave
nucleus on defects formation. Y. Hidaka, et. al, JNM, (1994)

Irradiation effects of SUS316L under (a) electron,
(b) electron/nanosecond-pulsed laser dual irradiation. CITY
S. Yang, JNM, (2017)

Miniaturized Double Notch Shear(DNS)specimen of SiC/SiC composite



Homogeneous distribute the shear stress



Specimen preparation sequence by FIB

Shibayama, T., Matsuo, G., Hamada, K., Watanabe, S., and Kishimoto, H.
In-situ Observation of Fracture Behavior on Nano Structure in NITE SiC/SiC Composite by HVEM
IOP Conf. Ser.: Mater. Sci. Eng. 18 162013(2011)

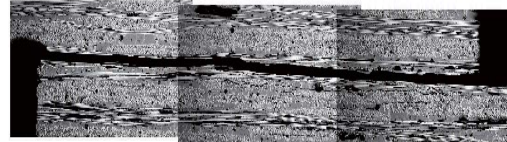


Figure 21. Micrograph of CG-Nicalon™/BN/SiC COFC double-notched specimen after test illustrating the propagation of interlaminar crack between notches (Lora-Curzio & Jenkins, Cocoa Beach 99).

CXXXX-00 Standard Test Method for the **Shear Strength** of Ceramic **Joints**

C1425-99 Standard Test Method for **Interlaminar Shear** Strength of 1-D and 2-D Continuous Fiber-Reinforced Advanced Ceramics at **Elevated Temperature**

C1292-95 Standard Test Method for **Shear Strength** of Continuous Fiber- Reinforced Advanced Ceramics at **Ambient Temperatures**



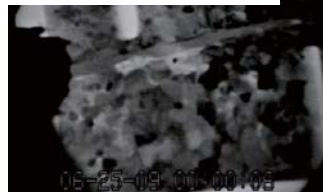
HOKKAIDO UNIVERSITY

In-situ observation of fracture behavior at the interface of SiC/SiC compsite

① Before testing



② Just contacting



③ Prior to crack initiation



④ Crack initiation



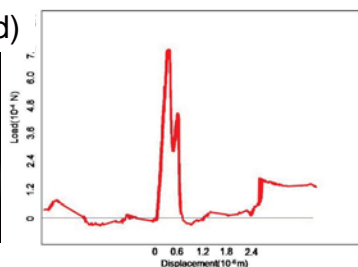
⑤ Crack propagation



⑥ Crack opening



⑦ Fractured (Debonded)



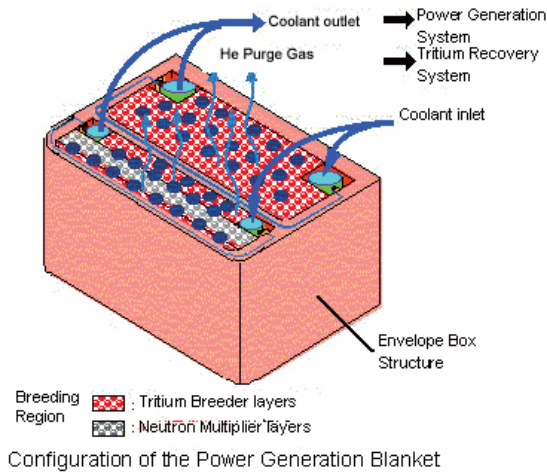
Maximum shear strength: 2.8×10^3 MPa

(Compression strength of nuclear grade pyrolysis carbon: 80MPa)

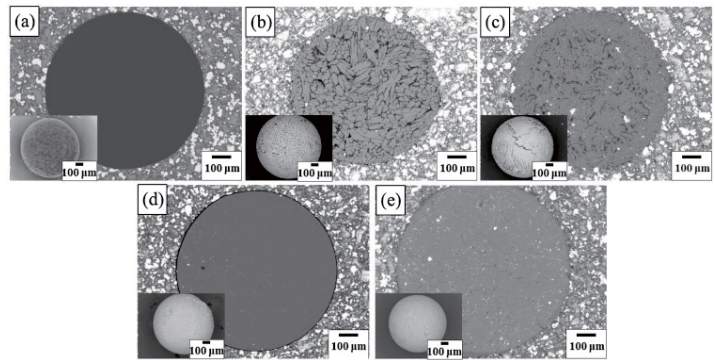


HOKKAIDO UNIVERSITY

Objective



Schematic illustration of a pebble bed type blanket by QST



Surface and cross-section SEM back-scattered electron images of the pebbles: (a) pure beryllium, (b) as-received $Be_{12}Ti$ pebble, (c) as-annealed $Be_{12}Ti$, (d) $Be_{17}Ti_2$ pebble, and (e) $Be_{12}V$ pebble. Jae-Hwan Kim and M. Nakamichi, in press, Fusion Engineering Design (2017)

We investigated He ion irradiation hardening of the above prototype beryllide pebbles ($Be_{12}Ti$, $Be_{17}Ti_2$, and $Be_{12}V$) made at National Institute for Quantum and Radiological Science and Technology (QST) in Japan.

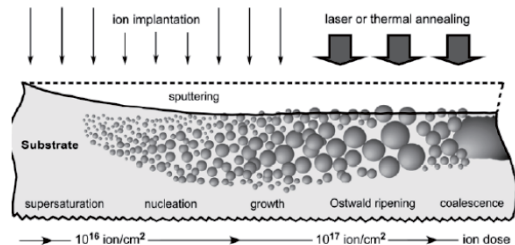


Experimental procedure



Hemisphere of pebbles embedded in the resin.

Notice:
 Surface sputtering would be negligible at this experimental condition. Further investigation is under going by AFM.

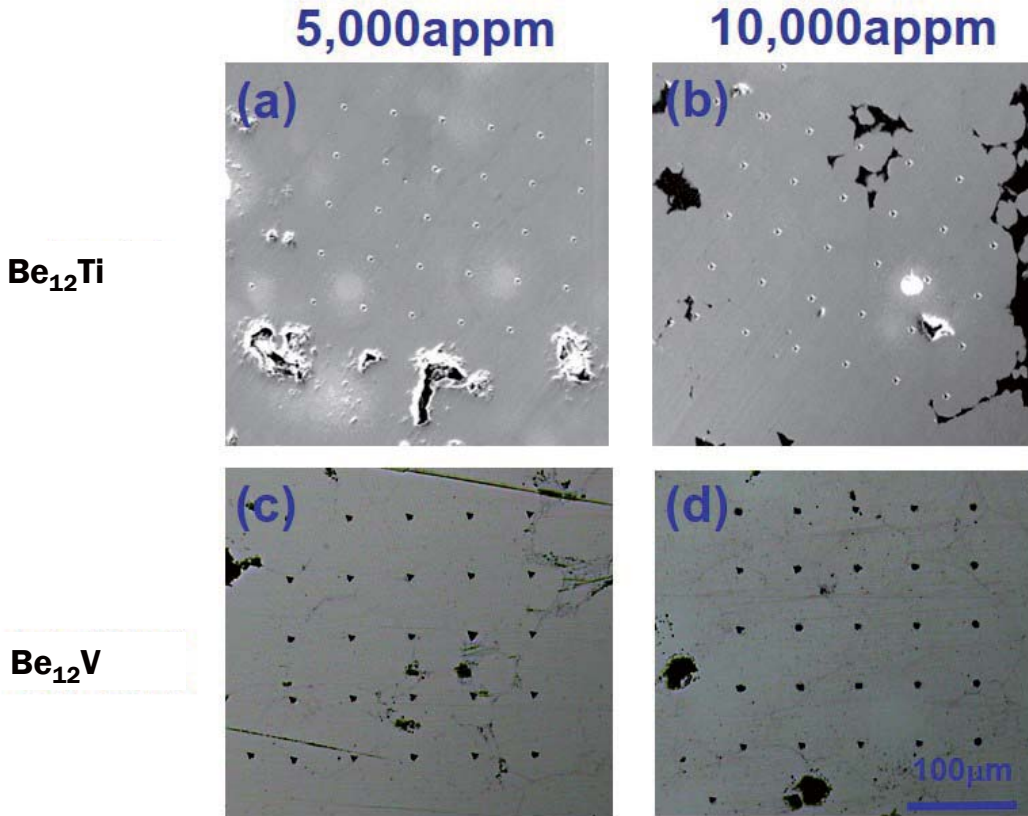


A. L. Stepanov, Rev. Adv. Mater. Sci. 26 (2010) 1-29.

1. This preliminary screening ion irradiation was done at R. T. in vacuum condition.
2. He^+ ion were irradiated to the surface of cross section of beryllium pebbles (the hemisphere) .
3. Nono-indentation testing were done at QST



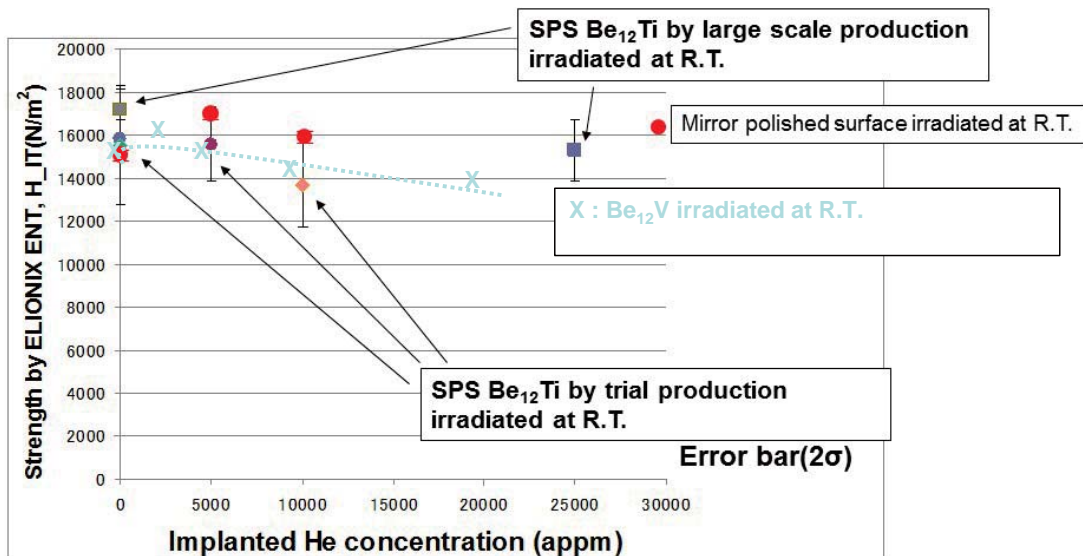
Experimental results (Bulk Be₁₂Ti and Be₁₂V specimens)



No significant surface change after high concentration He implantation.

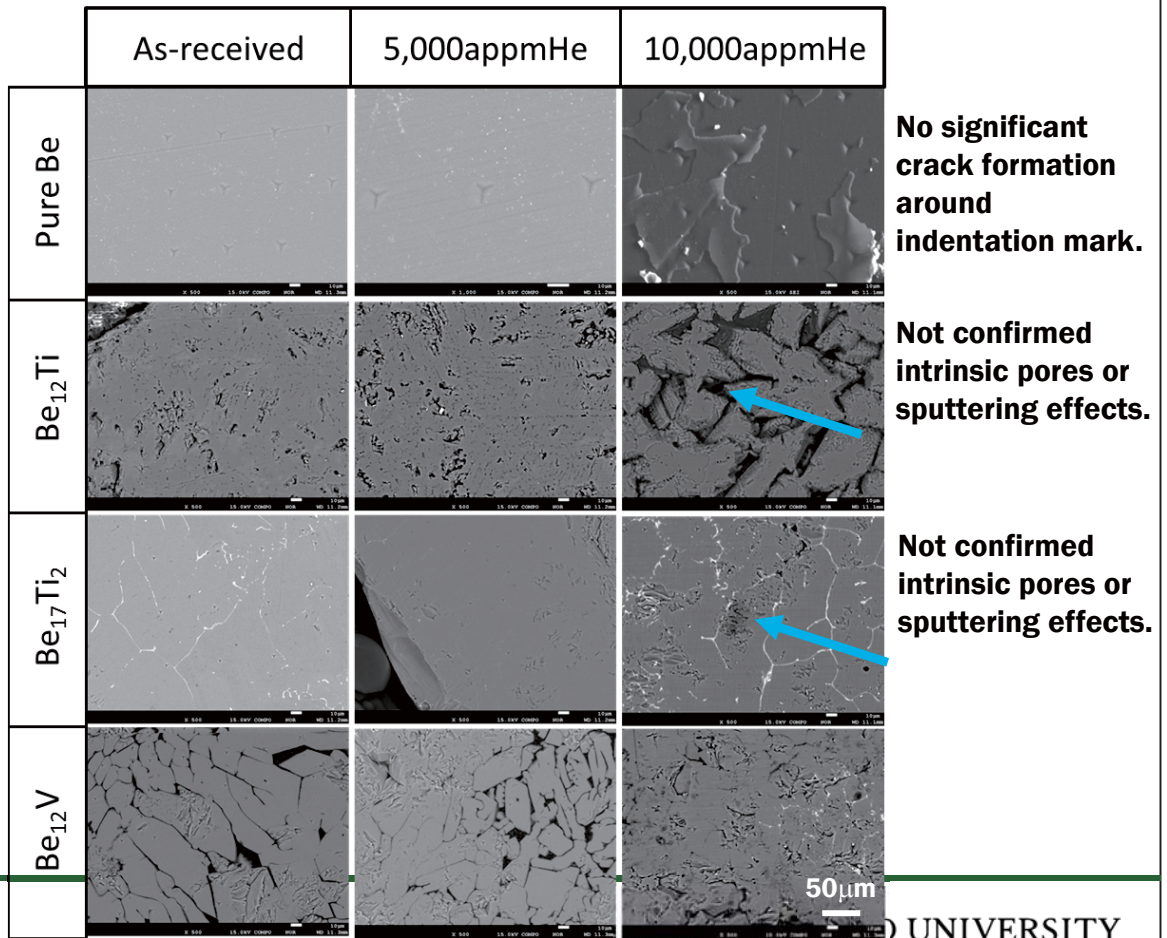
Experimental results (Bulk Be₁₂Ti and Be₁₂V specimens)

- After mirror finish of the surface of beryllides as like F82H and etc., all of error bar of nano-indentation results after irradiation become extremely small compared to the previous experiments.
- Surface finish is quite important to evaluate irradiation hardening with high accuracy.
- Feed back this result to the manufacturing process would be useful to obtain more uniform beryllide phase by optimizing production conditions.



Irradiation hardening of bulk beryllide specimens after He ion irradiation at R.T.

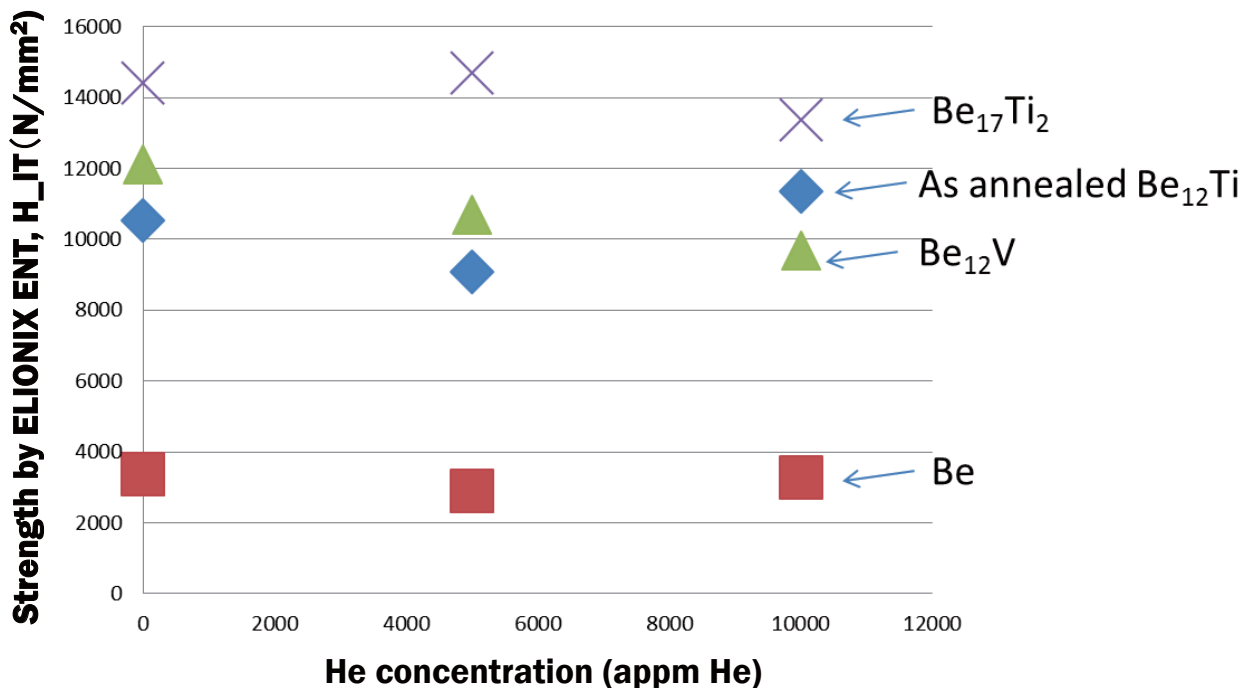
Experimental results (Pebble specimens)



HOKKAIDO UNIVERSITY

Experimental results (Pebble specimens)

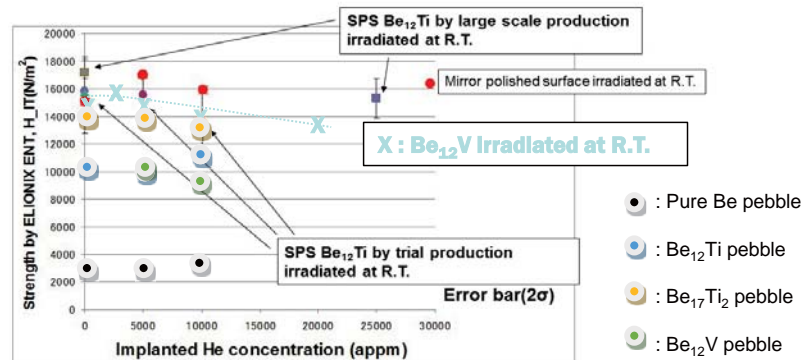
- As increasing He concentration up to 5,000 appm, strength was decreased at once except Be₁₇Ti₂.
- Strength of pure Be and Be₁₂Ti after 10,000 appm was increased again over the as received value.
- Be₁₇Ti₂ shows the opposite tendency. Be₁₂V shows degradation tendency in this experiment.
- Detailed microstructure investigations are under going.



HOKKAIDO UNIVERSITY

Experimental results (Pebble specimens vs Bulk specimens)

- All of pebbles show no significant irradiation hardening up to 10,000 appm He concentration.
- Beryllide pebbles show more than three times higher strength after 10,000 appm He irradiation.
- Further investigations of higher He concentration response should be required to conclude capability of Japanese beryllide pebbles to DEMO and beyond DEMO reactor.



HOKKAIDO UNIVERSITY

Summary

Present status of He ion irradiation hardening of Japanese beryllide pebbles by REM are as follows;

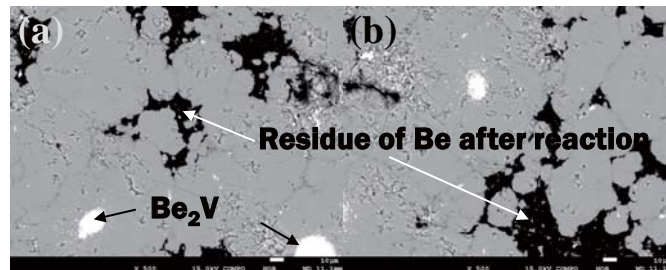
1. We successfully obtained He ion irradiation hardening of the prototype beryllide pebbles (Pure Be, Be₁₂Ti, Be₁₇Ti₂, and Be₁₂V) which made at National Institute for Quantum and Radiological Science and Technology (QST) in Japan up to 10,000 appm at RT.
2. No significant degradation are observed in all of pebbles in this study.
3. Our screening method is easy, but only RT examinations. High temperature testing method should be established soon.
4. Future plan: 20,000 appm He examination, microstructure investigation, surface residual strain analysis by EBSD/cross court method, development of high temperature irradiation examination method.

Thank you for your kind attention. We highly welcome to have your comments and suggestions to present results and furtur plan.



HOKKAIDO UNIVERSITY

Not homogeneous microstructure inside Be_{12}V pebbles.



SEM COMPO images of the surface of Be_{12}V pebble hemisphere after 100keV He ion irradiation at RT (a) 10,000appm, (b) 20,000appm.



HOKKAIDO UNIVERSITY

2.8.4 Deuterium and helium retention properties in beryllium irradiated with low energy ions

Y. Sugimoto¹, M. Miyamoto^{1*}, Jae-Hwan Kim² and M. Nakamichi²

¹*Department of Material Science, Shimane University, 1060, Nishikawatu, Matsue, Shimane 690-8504, Japan*

²*Fusion Energy Research and Development Directorate, National Institutes for Quantum and Radiological Science and Technology, 2-166 Omotedate, Obuchi, Rokkasho, Aomori, 039-3212, Japan*

**Corresponding author's E-mail: miyamoto@riko.shimane-u.ac.jp*

Beryllium was chosen as a plasma facing material (PFM) for the first wall in ITER. In the ITER DT phase, the burning plasma will expose beryllium simultaneously to helium, produced by fusion reactions, besides hydrogen isotopes. The understanding of plasma fuel recycling property on the first wall is one of the most critical issues relating the plasma density controlling. However, available information on surface properties of Be from the view point of microstructures is still limited due to the precautions concerning Be handling. In this study, the deuterium retention behavior in Be and the associated microstructure evolution were investigated while comparing the helium behavior.

Thermal desorption spectroscopy shows large desorption of deuterium or helium from the Be samples irradiated with deuterium or helium ions at room temperature to fluences of $\sim 1 \times 10^{22} \text{ m}^{-2}$, respectively. In-situ TEM observations during annealing after ion irradiation revealed clear difference between the behaviors of deuterium and helium bubbles formed in Be samples due to the ion irradiation. Figure shows the comparison of the dissipation processes of deuterium bubbles (a) and helium bubbles (b) during annealing. While deuterium bubbles gradually shrink and disappear at around 800 K, helium bubbles instantly vanish at the sample surface with bubble migration at relatively high temperature of $\sim 1000 \text{ K}$. In the presentation, we will also discuss the desorption behaviors related to these microstructure evolutions.

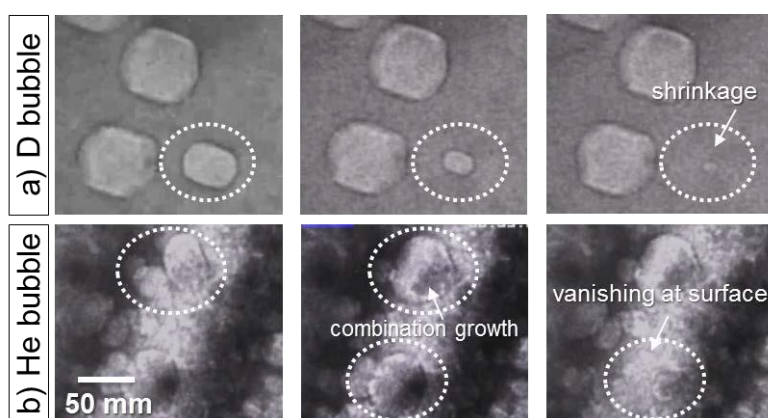


Figure Comparison of the dissipation processes of deuterium bubbles (a) and helium bubbles (b) during annealing for deuterium and helium ions irradiated Be samples.

Deuterium and helium properties in beryllium irradiated with low energy ions

2017/09/21-22

Shimane University in Japan
Department of material science
Miyamoto laboratory

Yutaka Sugimoto

CONTENTS

1. Background of this research

- Environment of the first wall
- Compatibility and issue of Beryllium as a plasma facing material

2. Experimental method

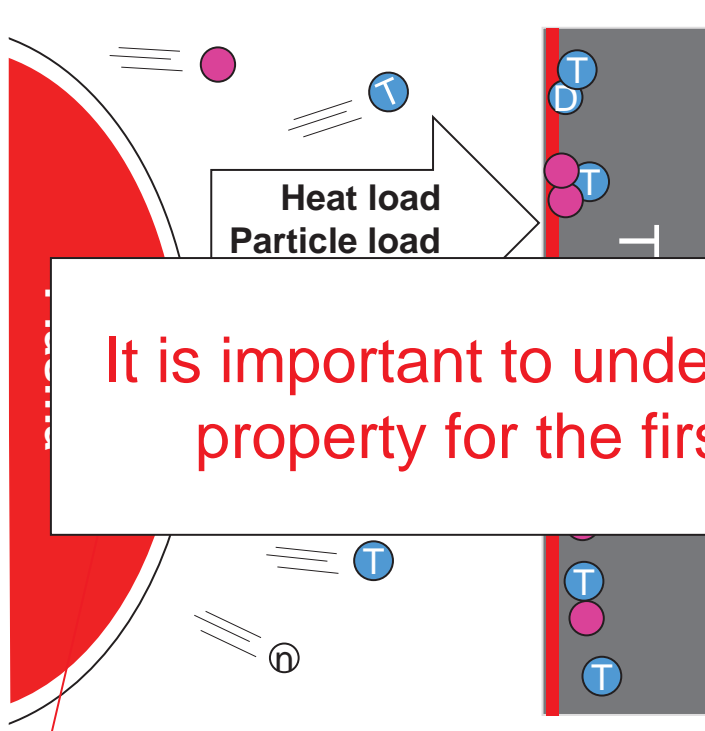
- Experimental condition of ion irradiation
- Analytical method for the gas retention property of Beryllium after irradiation

3. Result and discussion

- What was the cause of the deuterium desorption peak in beryllium ?
- What was the cause of the helium desorption peak in beryllium ?

4. Conclude

Environment of the first wall



In this environment,

By particle damage

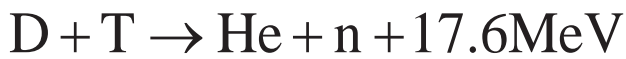
What will happen with the wall ?

It is important to understand the retention property for the first wall material !!

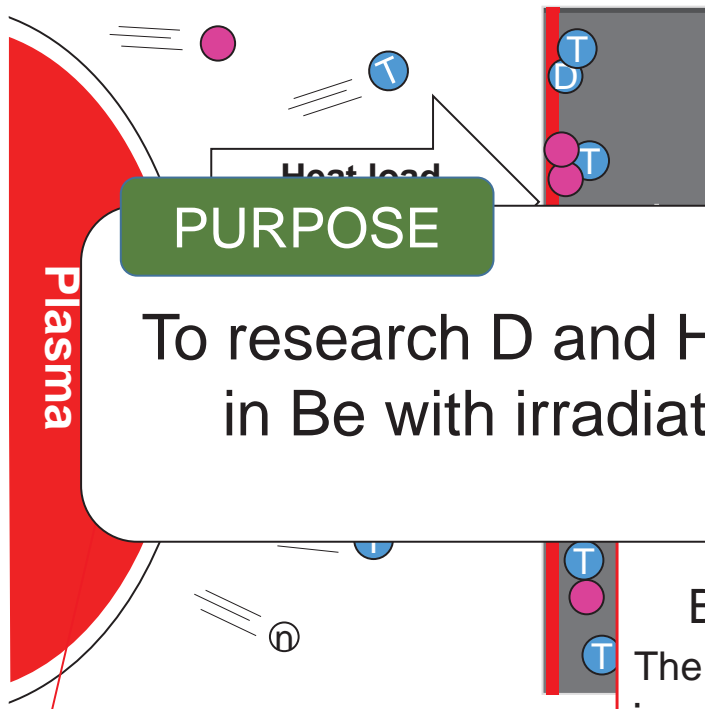
rty

➤ Mechanical problem

➤ Safety problem (tritium)



Why is beryllium subject study?



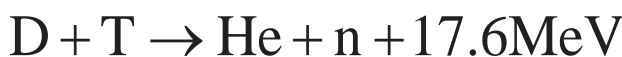
Now, **Beryllium** is chosen as a **PFM for the first wall** in ITER

Because...

PURPOSE

To research D and He retention property in Be with irradiation experimental.

Beryllium is difficult to handle. The study on **retention property in Be** is not enough from the viewpoint of microstructure information.



CONTENTS

1. Background of this research

- Environment of the first wall
- Compatibility and issue of Beryllium as a plasma facing material

2. Experimental method

- Experimental condition of ion irradiation
- Analytical method for the gas retention property of Beryllium after irradiation

3. Result and discussion

- What was the cause of the deuterium desorption peak in beryllium ?
- What was the cause of the helium desorption peak in beryllium ?

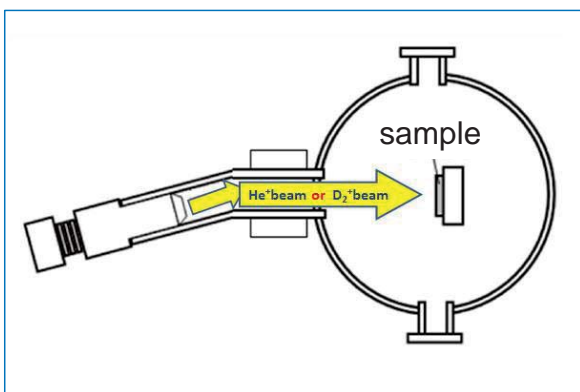
4. Conclude

5

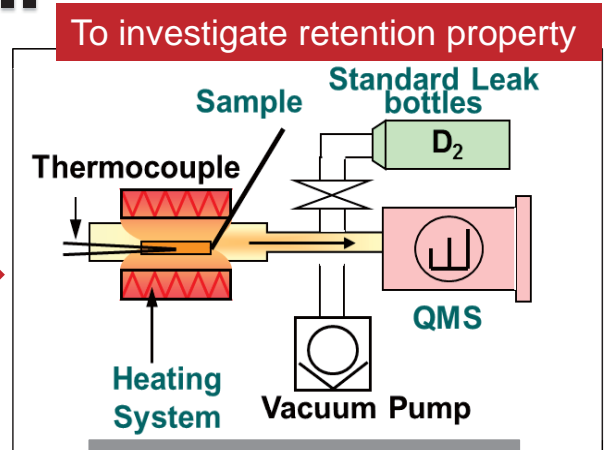
2. Experimental Method

Experimental flow of all

Sample irradiated with D, He



TDS



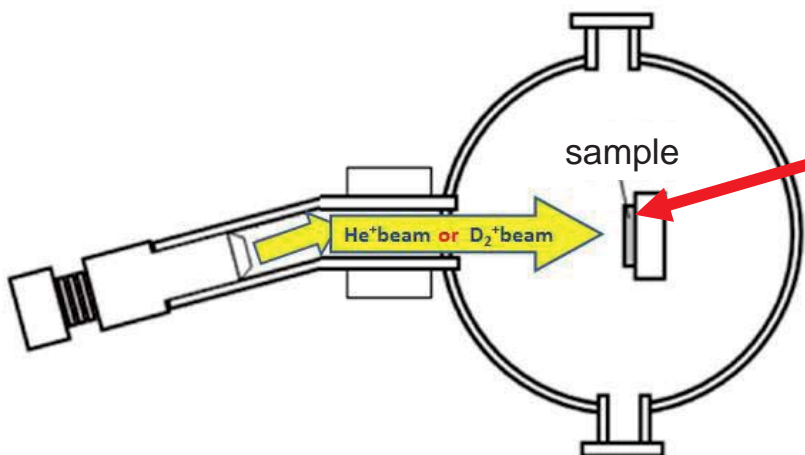
TEM
SEM

Observing microstructure



Next, talk about each
experimental method

Experimental condition on irradiation



$\phi 10 \times t 1.0 \text{ mm}$

Experimental condition: Ion

Sample: Beryllium
 Ion: D / He
 Ion energy : 3 [keV]
 Ion flux : $\sim 10^{18}$ [ions/m²s]
 Ion fluence : $1 \times 10^{21\sim 23}$ [D/m²]
 $1 \times 10^{21\sim 23}$ [He/m²]
 Sample temperature: R.T.

Next, go on to analytical method for the sample

Thermal desorption gas analyzer

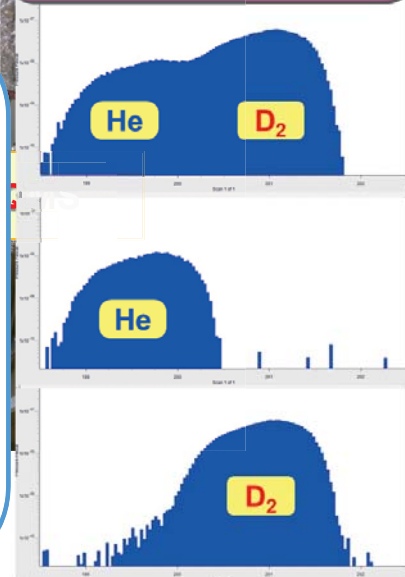
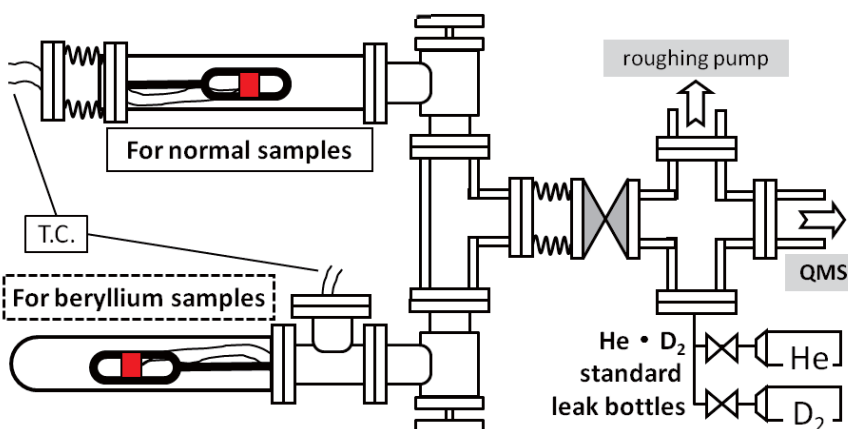


High Res. QMS

Microvision Plus (MKS)

- D₂ :4.02820
- He :4.00260

● Heating chamber



In-situ TEM facility in Shimane Univ.

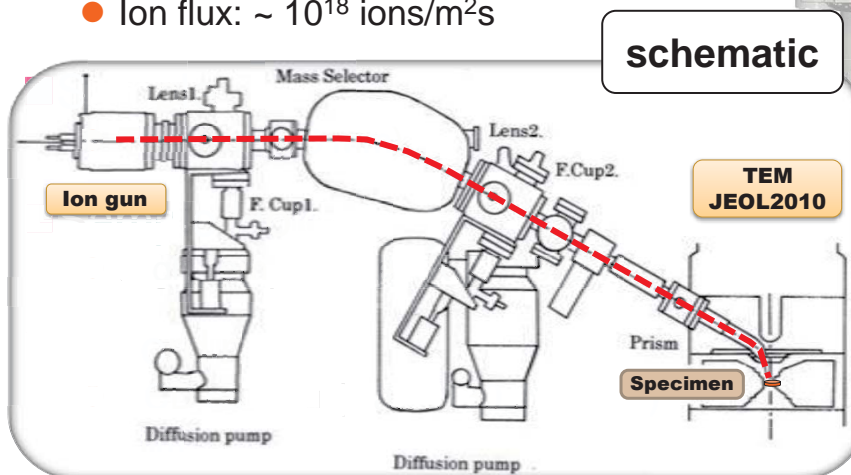
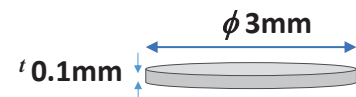
Transmission Electron Microscope

- Model: JEM-2010 (JEOL)
- Electron Accelerating-Voltage: 200kV
- Resolution: ~ 1 nm

Irradiation equipment

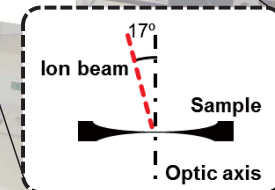
- Ion Species: H-Ar (gas species at R.T.)
- Angle between Electron and Ion Beams: 17°
- Ion Energies: 1-20 keV
- Ion flux: $\sim 10^{18}$ ions/m²s

TEM thin sample



schematic

TEM
JEOL2010



CONTENTS

1. Background of this research

- Environment of the first wall
- Compatibility and issue of Beryllium as a plasma facing material

2. Experimental method

- Experimental condition of and ion irradiation
- Analytical method for the gas retention property of Beryllium after irradiation

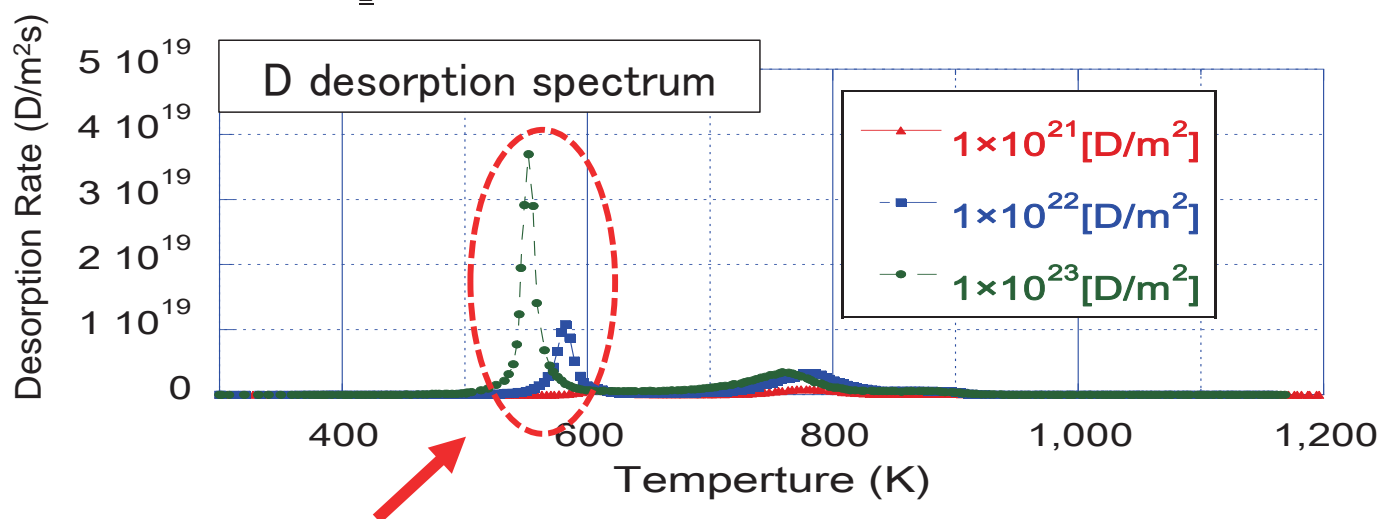
3. Result and discussion

- What was the cause of the deuterium desorption peak in beryllium ?
- What was the cause of the helium desorption peak in beryllium ?

4. Conclude

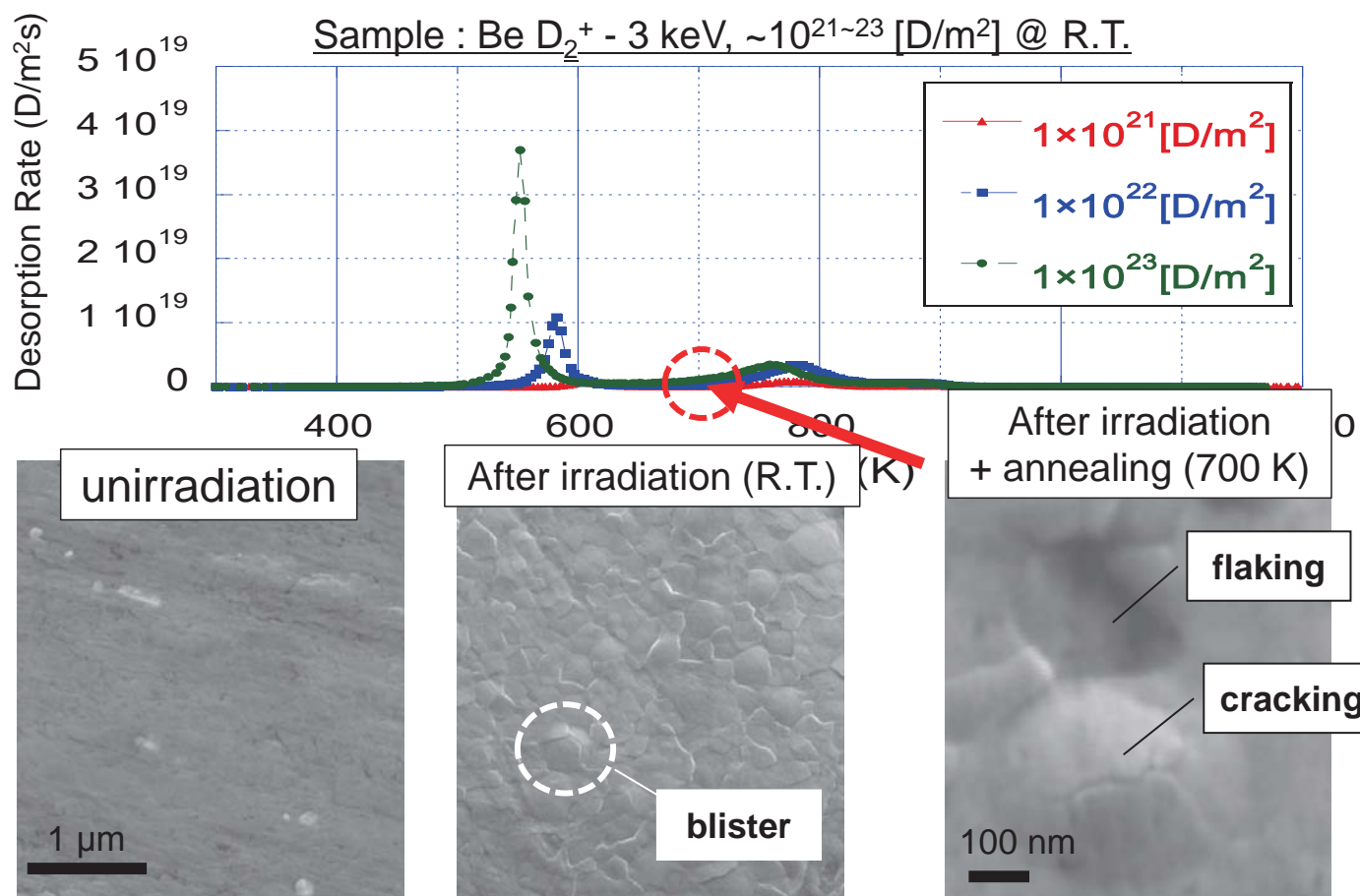
the D peak in lower temperature

Sample : Be D_2^+ - 3 keV, $\sim 10^{21}\sim 23$ [D/m²] @ R.T.

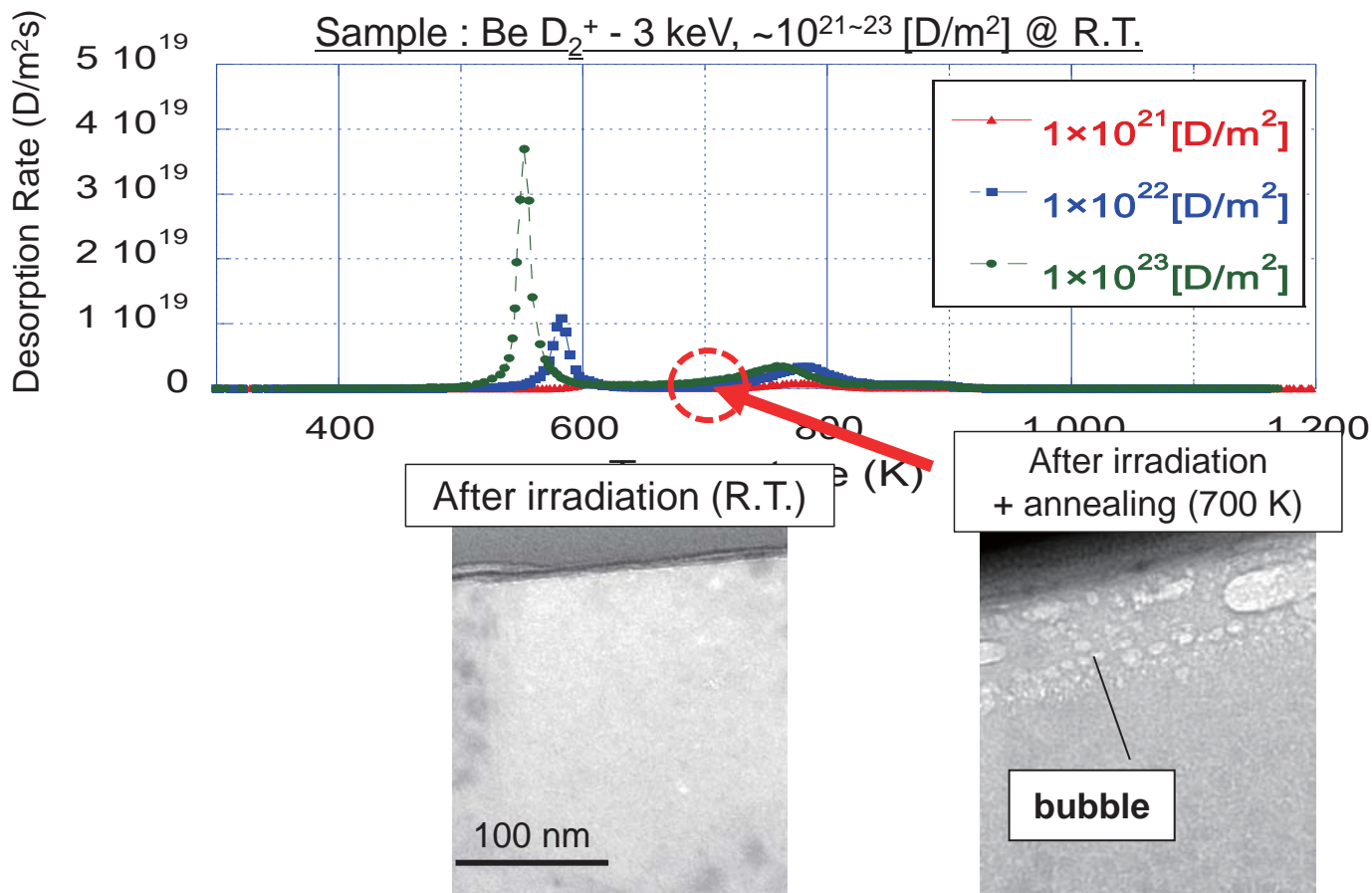


- The peak become high with the fluence increase.
 - The peak is irradiation-induced desorption.
- Observed microstructure of the irradiated Be sample surface or inside.
 - To understand the cause of the peak.

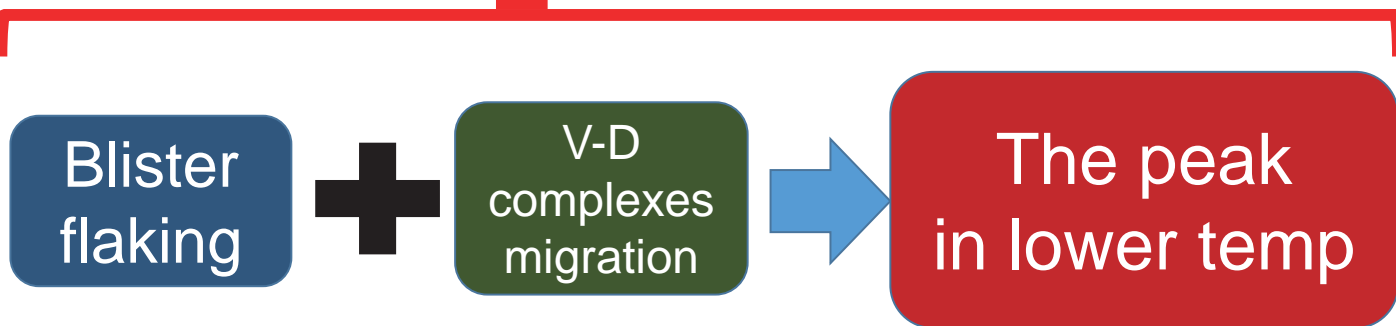
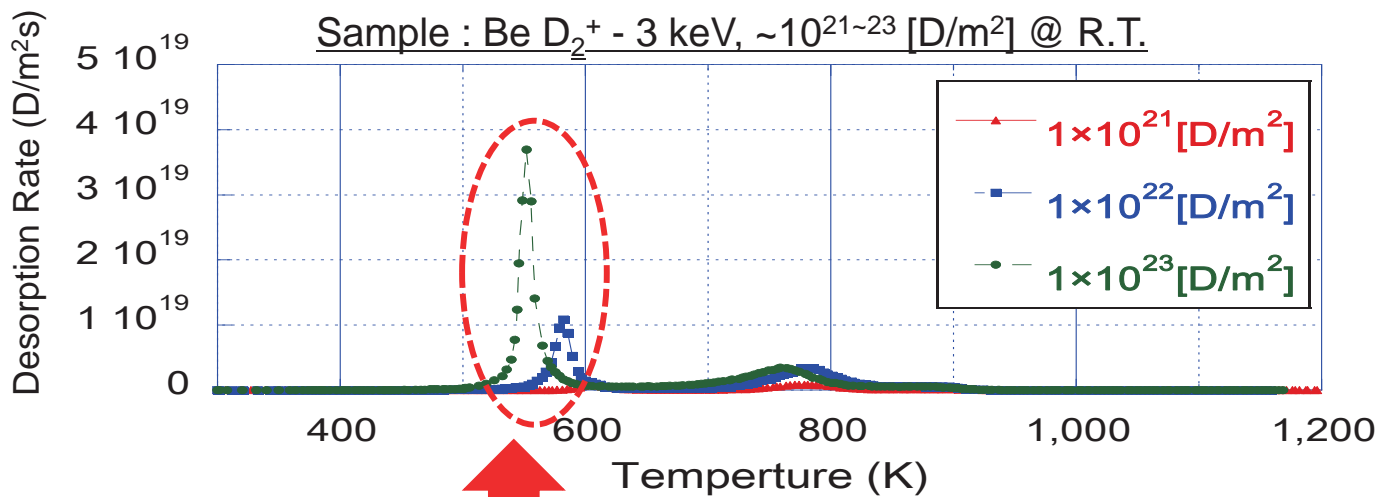
First is the gas release from blister



Migration of V-D complexes

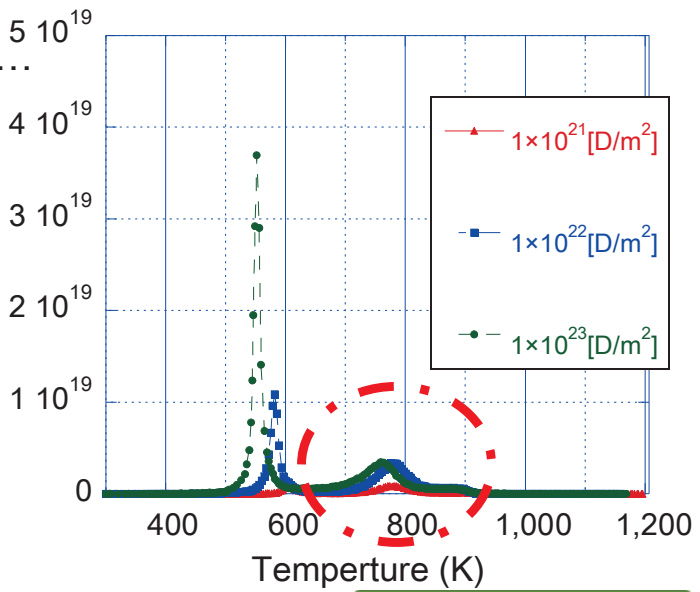
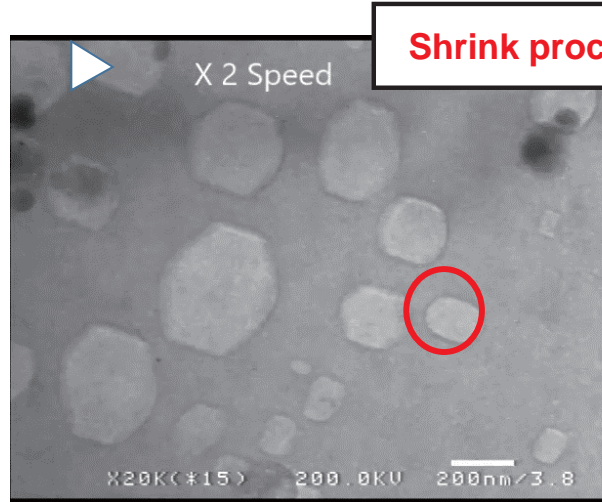


What cause the D peak in lower temperature?



Desorption from D trap site

In-situ TEM observations revealed...

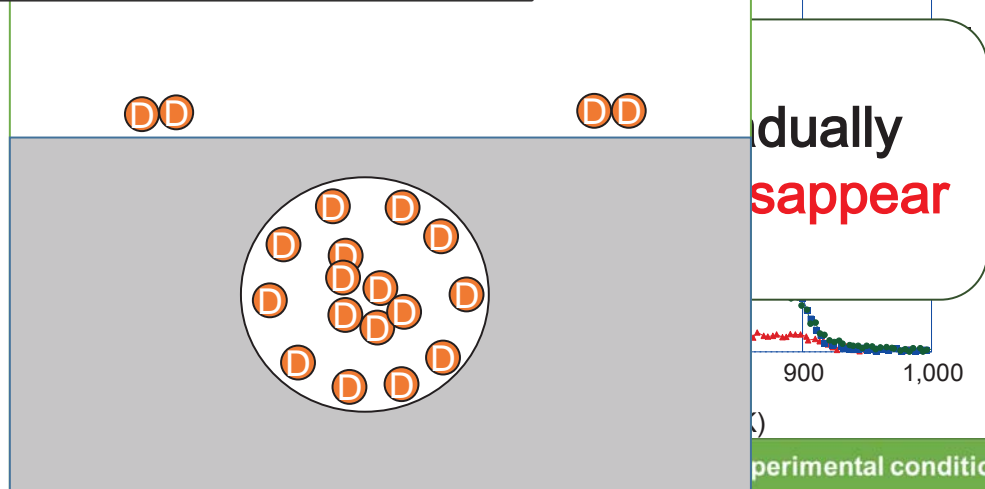


Experimental condition

Sample: Beryllium
 Ion energy : 3 keV – D₂⁺
 Ion flux : ~10¹⁸ [ions/m²s]
 Ion fluence : 1 × 10²¹⁻²³ [D/m²]
 1 × 10²¹⁻²³ [He/m²]
 Sample temperature: R.T.

Desorption from D trap site

The process of D dissociating



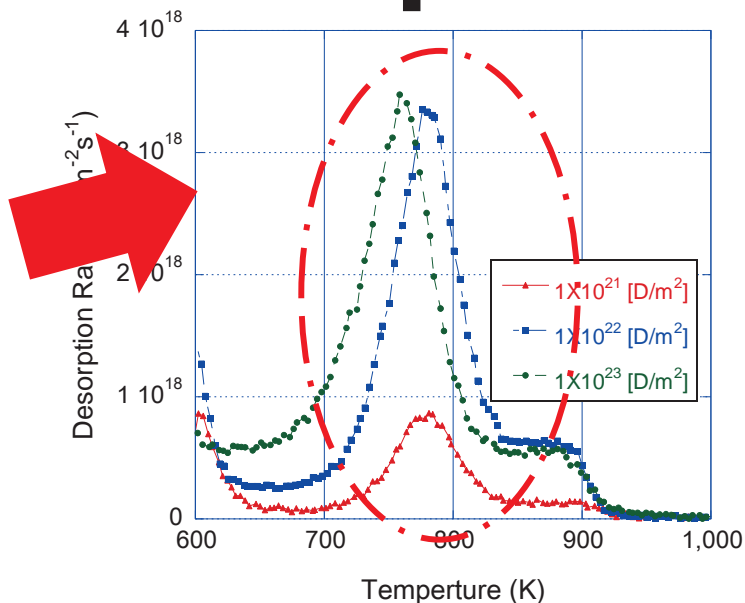
Experimental condition

Sample: Beryllium
 Ion energy : 3 keV – D₂⁺
 Ion flux : ~10¹⁸ [ions/m²s]
 Ion fluence : 1 × 10²¹⁻²³ [D/m²]
 1 × 10²¹⁻²³ [He/m²]
 Sample temperature: R.T.

Desorption from D trap site

D desorption

Deuterium *dissociate* from bubble

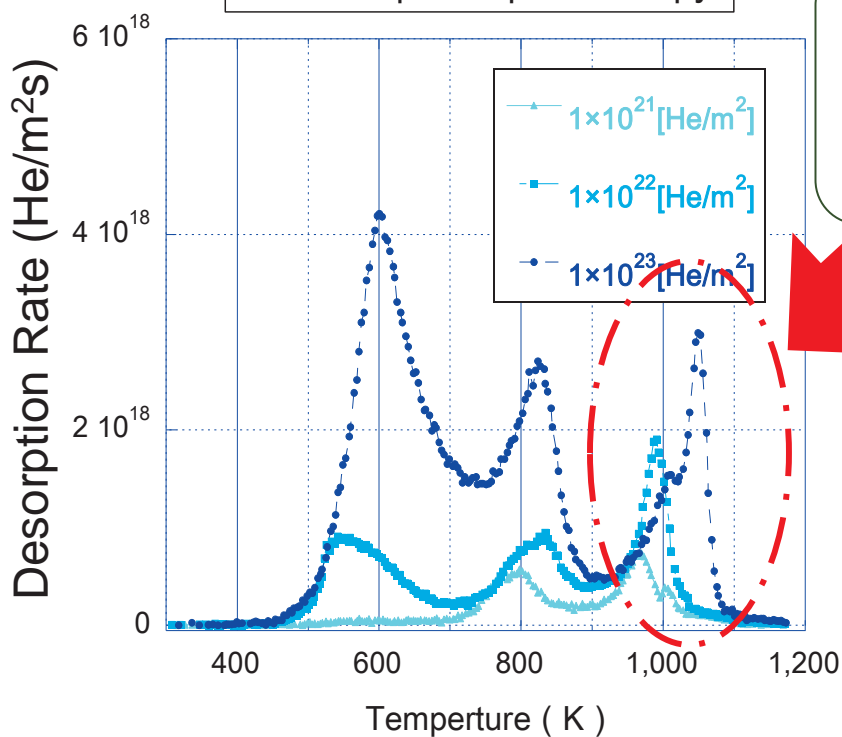


Experimental condition

Sample: Beryllium
 Ion energy : 3 keV – D₂⁺
 Ion flux : ~10¹⁸ [ions/m²s]
 Ion fluence : 1 × 10²¹⁻²³ [D/m²]
 1 × 10²¹⁻²³ [He/m²]
 Sample temperature: R.T.

the He peak in high temperature range

He desorption spectroscopy



He bubble

He bubble disappear process is difference in compare with D case .

Experimental condition: Ion

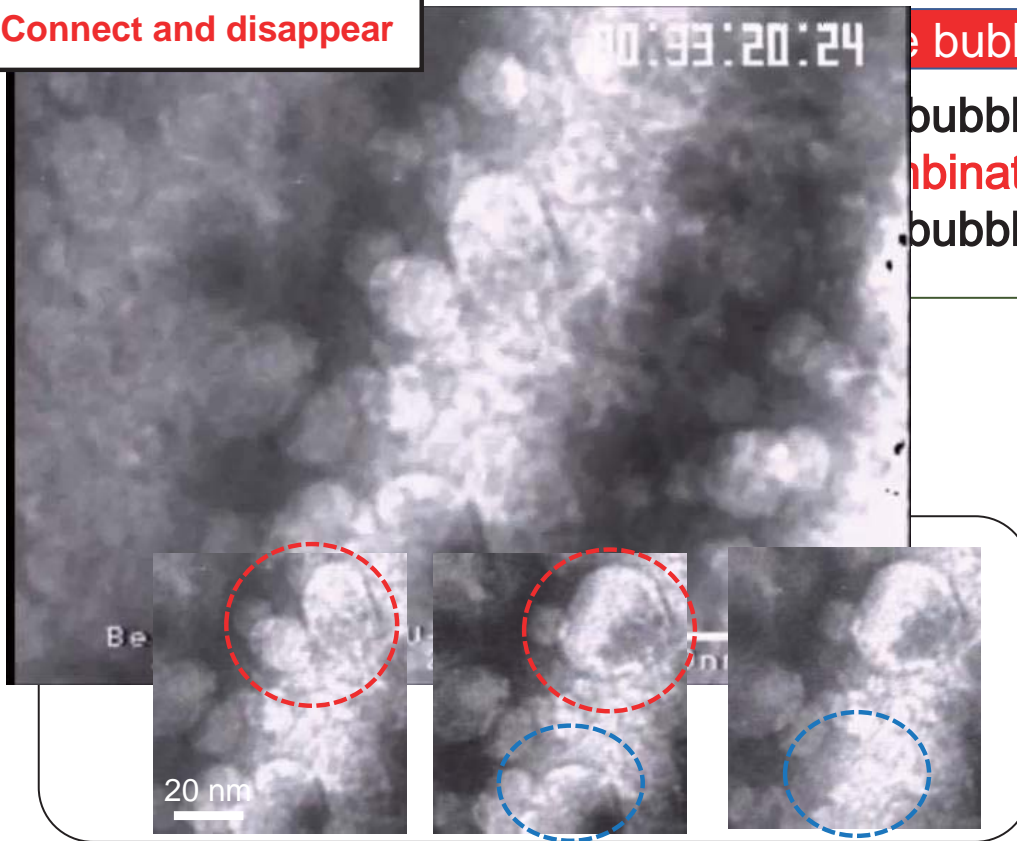
Sample: Beryllium
 Ion: He
 Ion energy : 3 [keV]
 Ion flux : 1 × 10¹⁸ [ions/m²s]
 Ion fluence : 1 × 10²¹⁻²³ [He/m²]
 Sample temperature: R.T.

Desorption from He trap site

Connect and disappear

He bubble

Bubbles are
combination growth.
Bubble is vanishing.



Desorption from He trap site

He desorption

The He bubble migration process

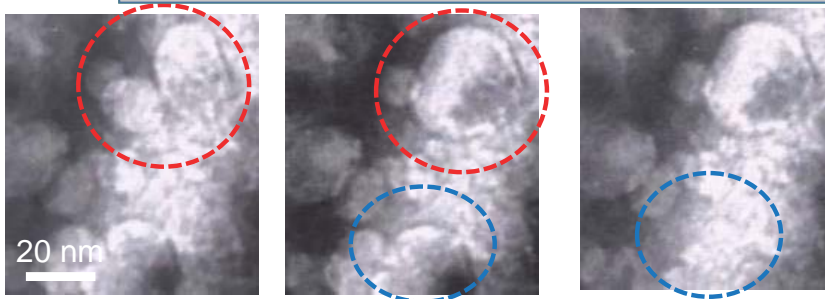
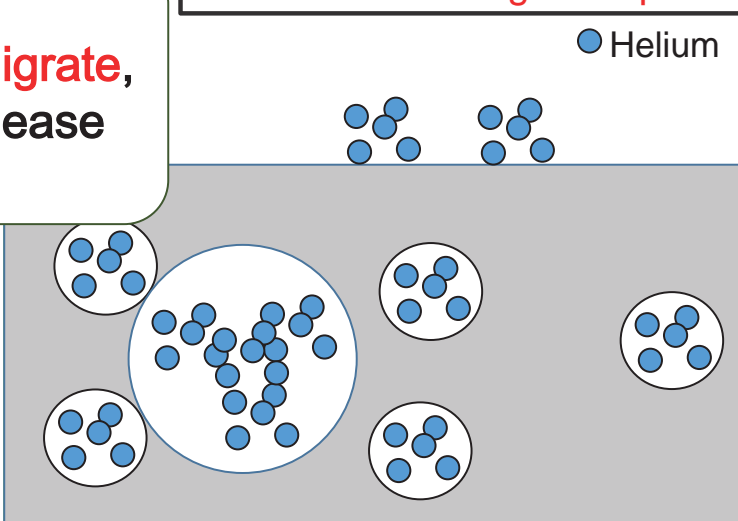
He bubble

He bubble migrate,
hence He release

Bubbles are
combination growth.
Bubble is vanishing.

Desorption Rate

● Helium



CONTENTS

1. Background of this research

- Environment of the first wall
- Compatibility and issue of Beryllium as a plasma facing material

2. Experimental method

- Experimental condition of and ion irradiation
- Analytical method for the gas retention property of Beryllium after irradiation

3. Result and discussion

- What was the cause of the deuterium desorption peak in beryllium ?
- What was the cause of the helium desorption peak in beryllium ?

4. Conclude

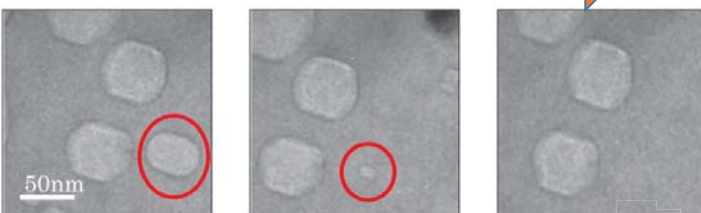
21

4. Conclude

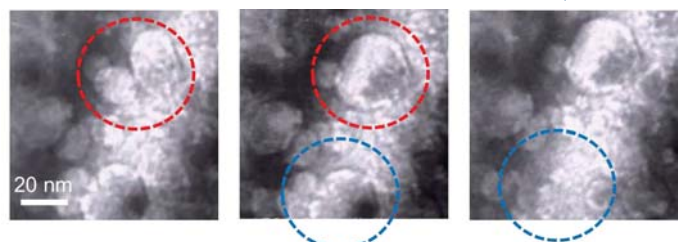
The gas retention properties and microstructure in Be irradiated with D and He ions were investigated.

- D release at low temperature range seems to attribute to flaking of blisters and migration of small D-V complexes.
- Bubble behaviors of D and He at high temperature were significantly different.
 - deuterium bubbles gradually shrink and disappear at around 800 K
 - helium bubbles instantly vanish at the sample surface with bubble migration at relatively high temperature of ~1000 K

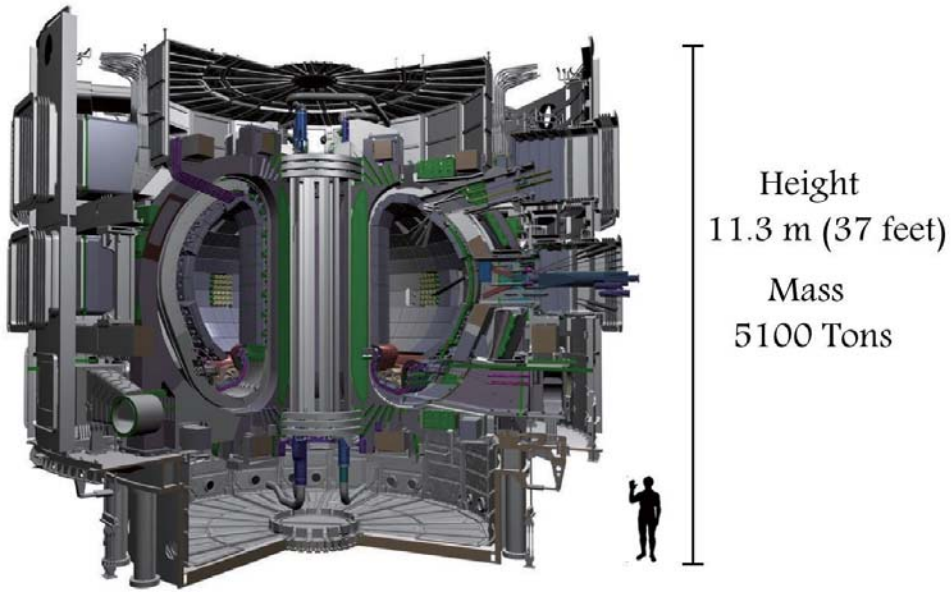
Deuterium dissociation



He bubble migration



ITER Tokamak Fusion Reactor



Thank you for watching !!

2.8.5 Surface property of tungsten exposed to beryllium containing high density plasma in PISCES

M. Miyamoto¹, D. Nishijima², M.J. Baldwin² and R.P. Doerner²

¹*Department of Material Science, Shimane University, Matsue, Shimane 690-8504, Japan*

²*Center for Energy Research, University of California at San Diego, La Jolla, CA 92093-0417, USA*

E-mail: miyamoto@riko.shimane-u.ac.jp

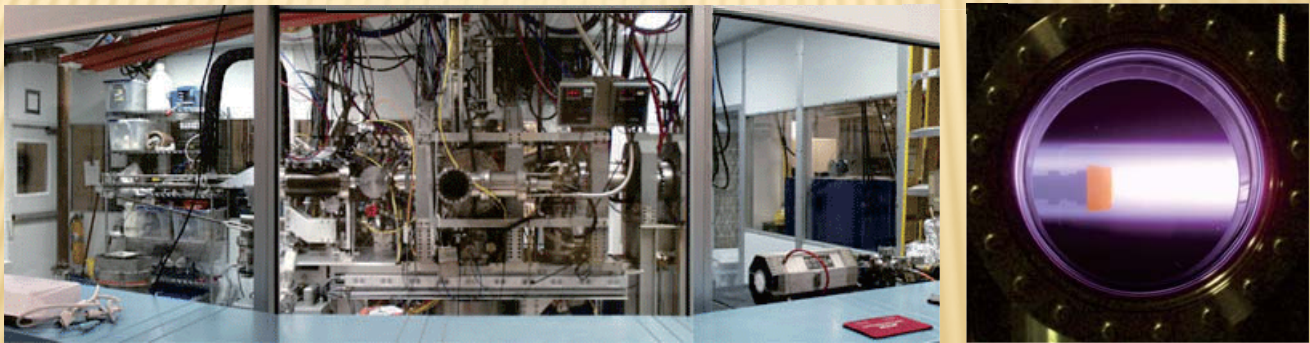
Co-deposition of beryllium with tritium is expected to be the main source of tritium accumulation in the ITER vessel, since beryllium will be used as the main plasma facing material for the first wall. To investigate the hydrogen isotope retention and surface damage for W in the burning plasma condition, the influence of Be seeding on microstructures and D retention in W exposed to high density D+He+Be mixed plasmas was systematically examined.

Tungsten samples were exposed to D+Be(~0.1%) and D+He(~5%)+Be(~0.1%) mixture plasmas in the linear divertor plasma simulator PISCES-B under low energy (~10 and ~60 eV), high flux (~ 10^{22} m⁻²s⁻¹), high fluence (~ 5×10^{25} m⁻²) ion bombardment, and several temperatures (373-973 K) conditions. Two types of the ion incident energy correspond to deposition (10 eV) and erosion (60 eV) conditions for Be deposition layer. Cross-sectional microstructures of the deposition layers were observed by means of transmission electron microscopy after focused ion beam fabrication. Deuterium retention was evaluated with thermal desorption spectroscopy.

The seeding of He into D plasma caused a significant reduction in D retention and the formation of nanometer-sized He bubbles in W without Be [1]. However, these remarkable He effects are suppressed by Be seeding under both conditions of deposition and erosion. At the Be deposition condition, the layer consisting of small grains of ~10 nm with original hexagonal close-packed structure of beryllium was formed on a sample exposed to D+Be mixture plasmas at low temperature of 373 K. He seeding to the D+Be mixture plasmas was found to cause amorphization of the layer. In contrast, columnar structure consisting of Be₂C due to crystal growth appeared at high temperature exposure cases of >773 K both with and without He seeding. The formation of these deposition layers brought about a significant D retention, and the D/Be ratios were estimated to be about 0.05 for the low temperature exposure case of 573 K, and to be about 0.01 even for the high temperature at 773 K.

[1] M. Miyamoto et al., Nucl. Fusion 49 (2009) 065035.

Surface property of tungsten exposed to beryllium containing high density plasma in PISCES



Mitsutaka Miyamoto, D. Nishijima*, M.J. Baldwin*, R.P. Doerner*
Department of Material Science, Shimane University
*University of California, San Diego
E-mail: miyamoto@riko.shimane-u.ac.jp

Table of Contents

◆ Introduction & Experimental

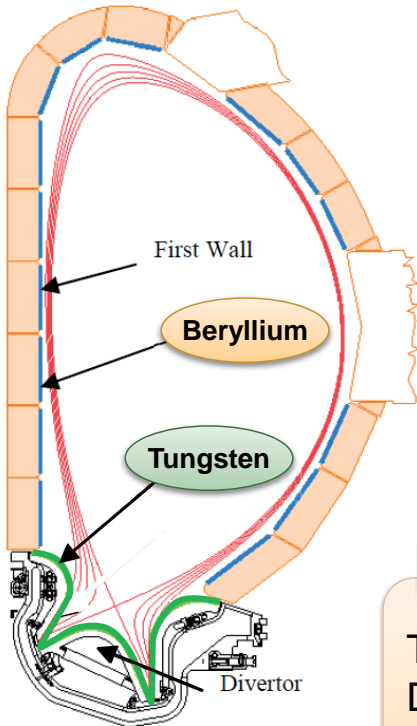
- PSI under mixed ions irradiation
- Experiment in PISCES-B at UCSD

◆ Results

- *Previous results*
 - D-He-Be mixed plasma exposures
- *Highlight Data*
 - Microstructure of Be/D co-deposition layer
 - Deuterium desorption from Be/D co-deposition layer
- *Recent results (Preliminary)*
 - Microstructure and D retention of Be bulk

◆ Summary

PSI under Mixed Ions irradiation



J. Roth, J. Physics, 100(2008)062003

- ◆ W and Be will be used as armor materials for ITER PFCs.
- ◆ In future DT phase, the burning plasma will expose W simultaneously to He and other trace impurities such as C and Be besides H isotopes.

Concerning H isotope retention,

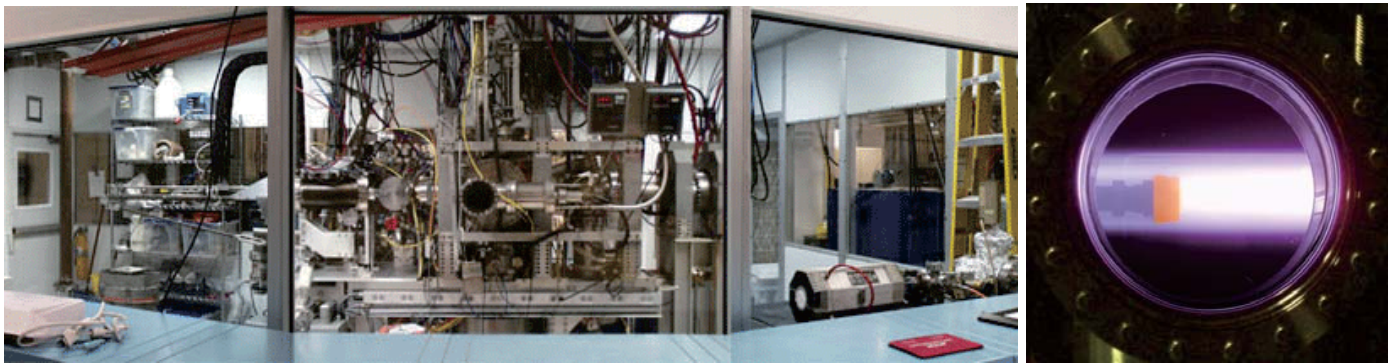
- Effects of He and C have been actively examined.
- However, effects of Be remain obscure due to its toxicity. Especially, available information from the view point of microstructure is limited.

Objective in Present Study

The influence of Be seeding on microstructures and D retention in W exposed to D-He-Be mixture plasmas were examined with SEM, TEM and TDS.

PISCES-B ~divertor plasma simulator ~

■ Investigation of ITER mixed materials PSI



PISCES-B allows exposure of samples to Be seeded plasma

PISCES-B is contained within an isolated safety enclosure to prevent the release of Be dust.

	PISCES	ITER (edge)
Ion flux (m^2s^{-1})	$10^{21}\text{--}10^{23}$	$\sim 10^{23} - 10^{24}$
Ion energy (eV)	20–300 (bias)	10–300 (thermal)
T_e (eV)	4–40	1–100
n_e (m^{-3})	$10^{18}\text{--}10^{19}$	$\sim 10^{19}$
Be Imp. fraction (%)	Up to a few %	1–10 (ITER)
Pulse length (s)	Steady state	1000
PSI materials	C, W, Be	C, W, Be ..
Plasma species	H, D, He	H, D, T, He

Table of Contents

◆ Introduction & Experimental

- PSI under mixed ions irradiation
- Experiment in PISCES-B at UCSD

◆ Results

□ Previous results

- D-He-Be mixed plasma exposures

□ Highlight Data

- Microstructure of Be/D co-deposition layer
- Deuterium desorption from Be/D co-deposition layer

□ Preliminary

- Microstructure and D retention of Be bulk

◆ Summary

Summary of previous results

Microstructure and D retention of W exposed to Mixture Plasma

M. Miyamoto et al., Nucl. Fusion 49(2009)065035, JNM 415(2011)S657, JNM 438(2013)S216

- He seeding to D plasma causes suppression of blister formation and significant reduction in D retention.
- The co-deposits with high ratio of D/Be (~0.03) is obtained at the Be deposition condition.
- D retention is suppressed again at Be erosion condition, regardless of He seeding.

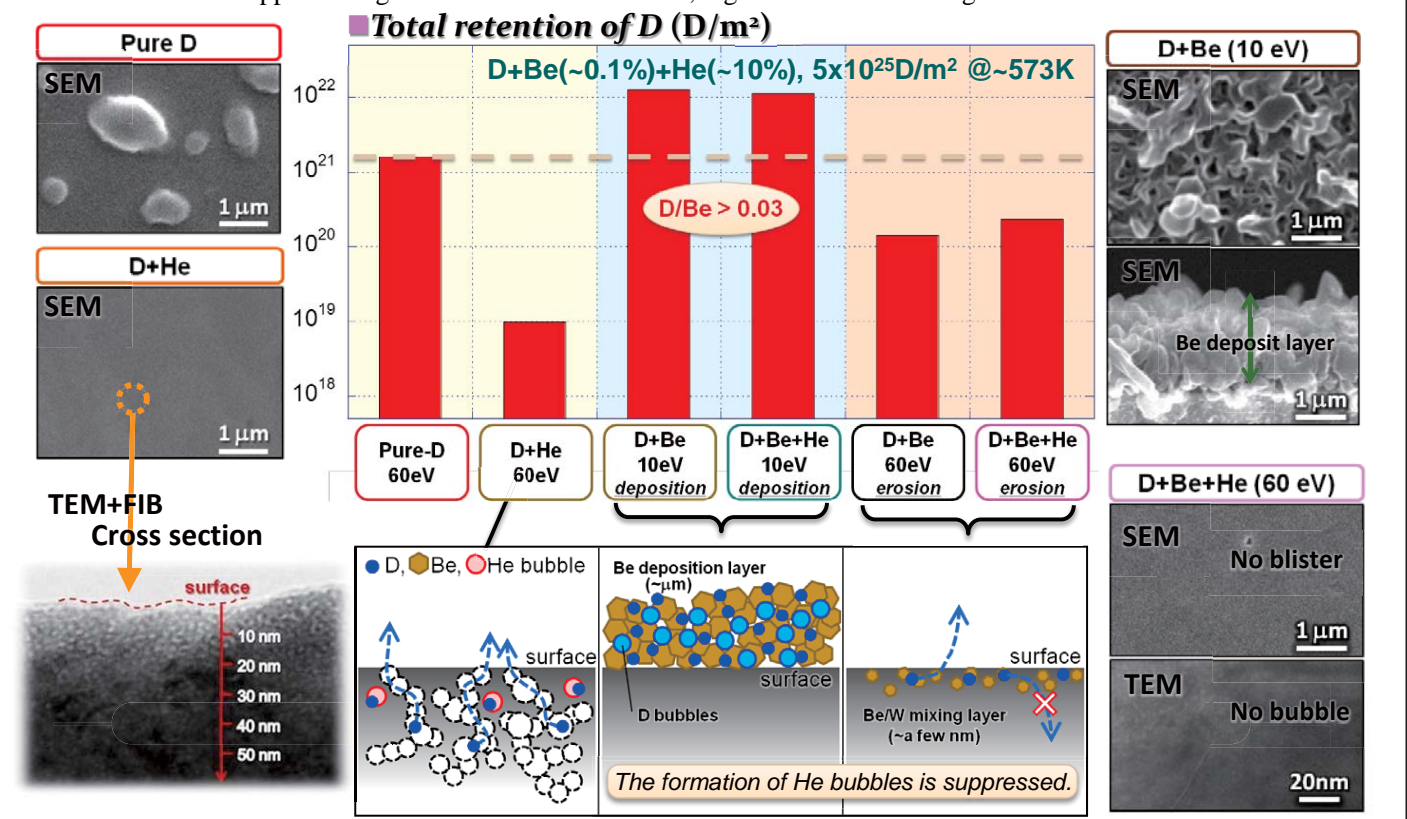


Table of Contents

◆ Introduction & Experimental

- PSI under mixed ions irradiation
- Experiment in PISCES-B at UCSD

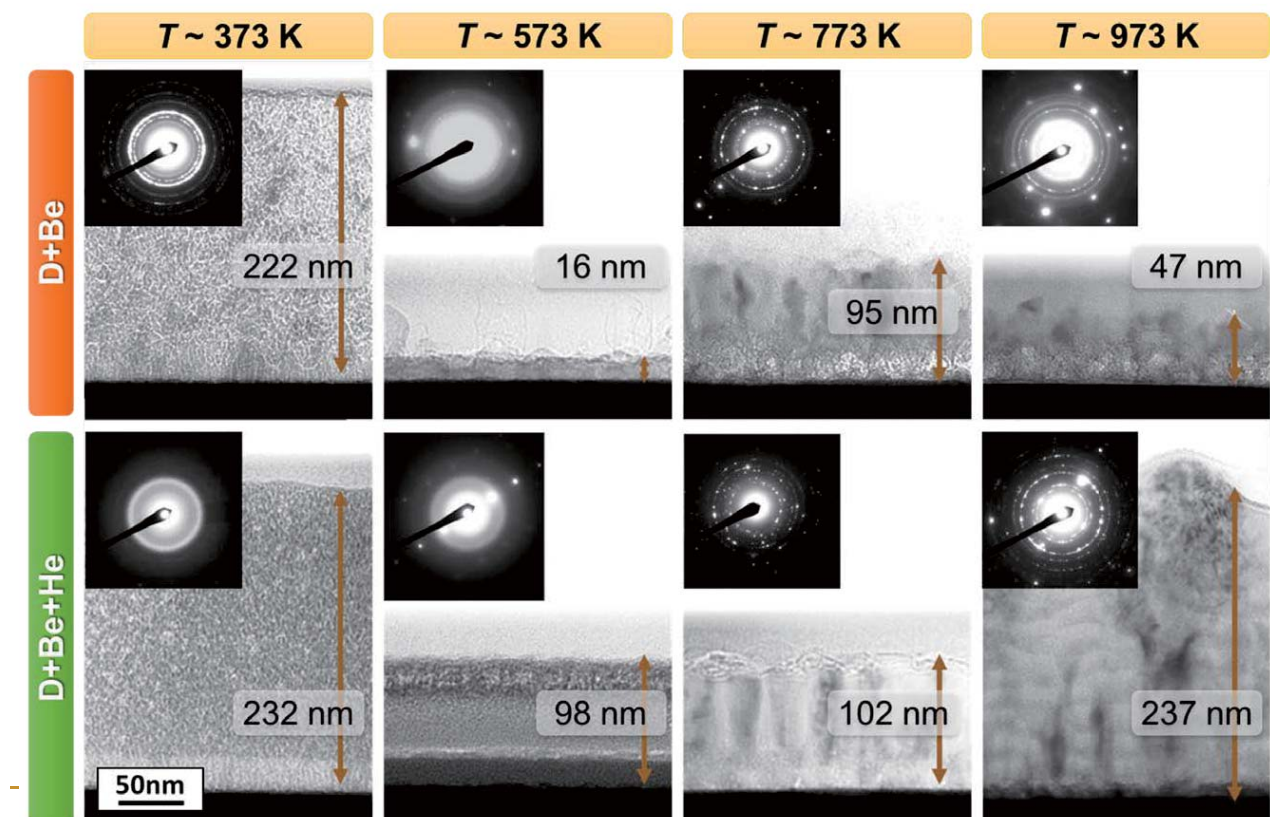
◆ Results

- *Previous results*
 - D-He-Be mixed plasma exposures
- *Highlight Data*
 - Microstructure of Be/D co-deposition layer
 - Deuterium desorption from Be/D co-deposition layer
- *Preliminary*
 - Microstructure and D retention of Be bulk

◆ Summary

Microstructure of Be deposition layers

■ TEM ($E_i \sim 10$ eV, $\Gamma_i \sim 10^{22}$ ions/m²s, $\Phi_i \sim 5 \times 10^{25}$ D⁺/m²)

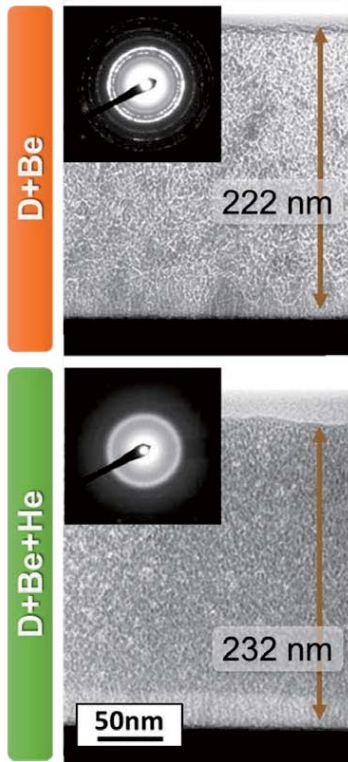


Microstructure – at low T_s

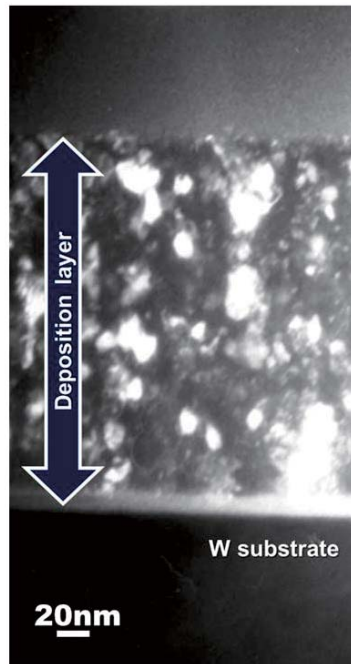
■ TEM ($E_i \sim 10$ eV, $\Gamma_i \sim 10^{22}$ ions/m²s, $\Phi_i \sim 5 \times 10^{25}$ D⁺/m²)

$T \sim 373$ K

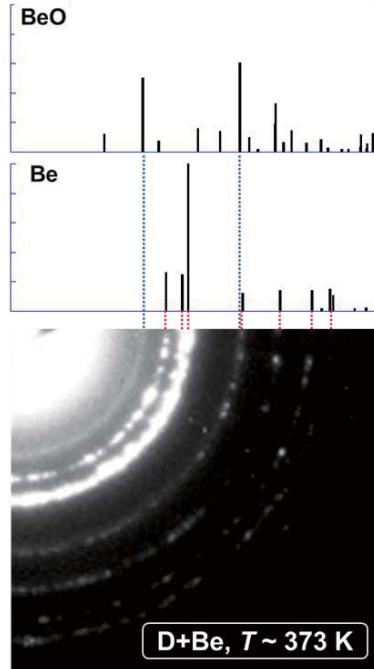
● Low $T_s \sim 373$ K



TEM image (dark field)



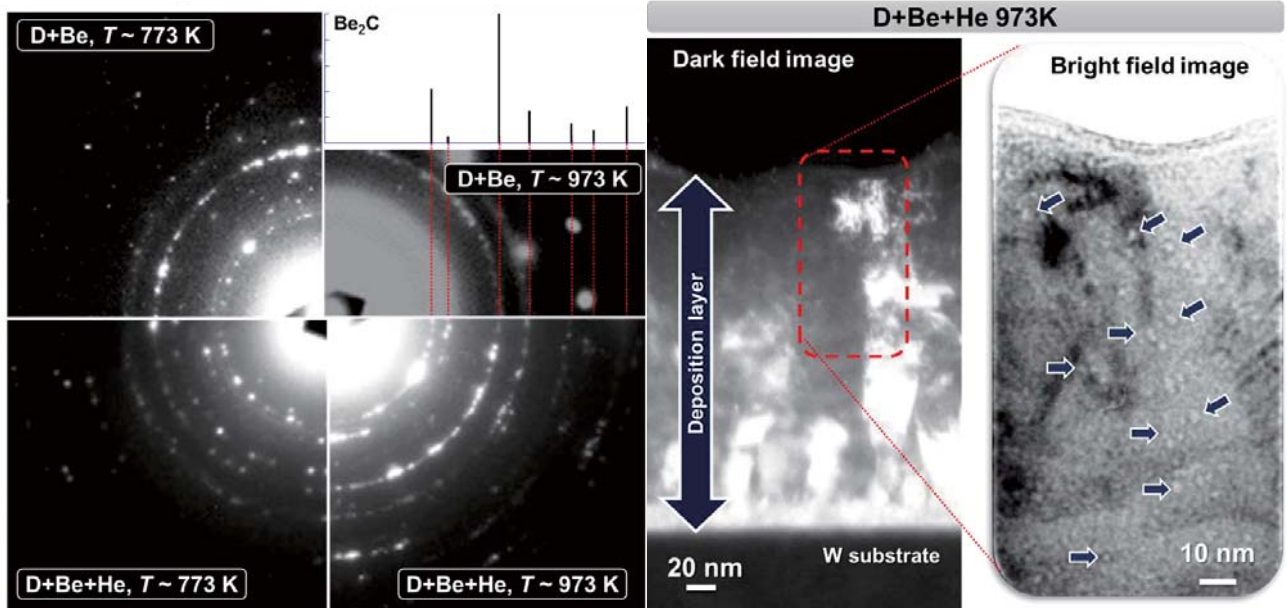
Electron Diffraction



Microstructure – at high T_s

■ TEM ($E_i \sim 10$ eV, $\Gamma_i \sim 10^{22}$ ions/m²s, $\Phi_i \sim 5 \times 10^{25}$ D⁺/m²)

● High $T_s \geq 773$ K



➤ The formation of Beryllium carbide with a fluorite structure were observed regardless of He seeding.

➤ The deposition layer are found to include grains growing into the columnar structures.

➤ He bubbles with white contrasts in the bright field image are observed in the deposition layer.

TDS from Be depo.

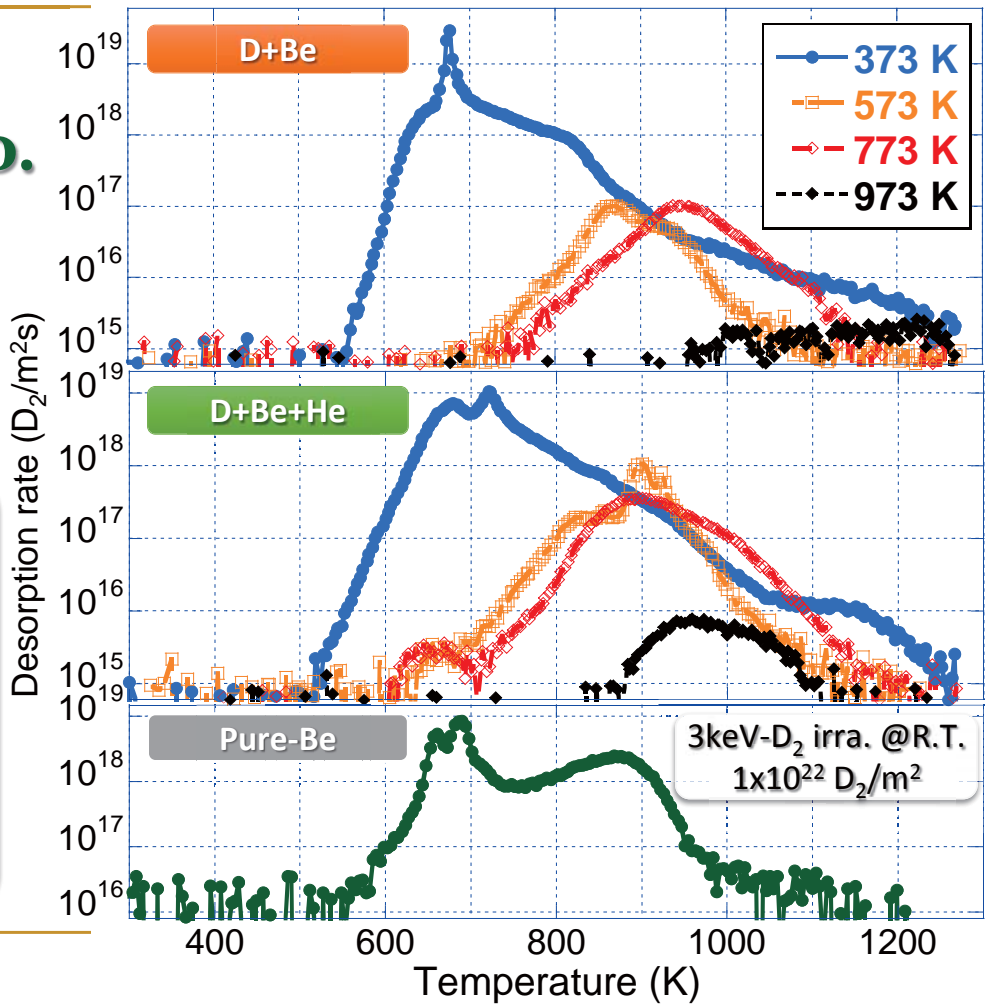
- $E_i \sim 10$ eV
- $\Gamma_i \sim 10^{22}$ ions/m²s
- $\Phi_i \sim 5 \times 10^{25}$ D⁺/m²

D+Be (~0.1%)

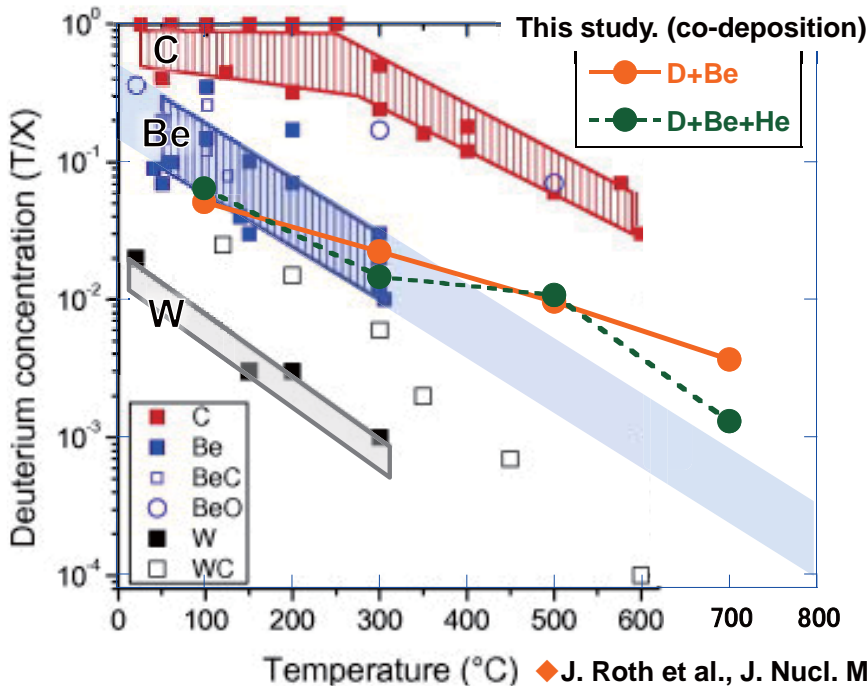
D+Be (~0.1%) + He (~5%)

Sharp large desorption peak occurs for the sample exposed to the plasma at 373 K and Be bulk at the similar temp. range of ~700 K .

Desorption is detectable for the sample exposed to the plasma even at high temp of ~ 973 K.



Deuterium concentration in depo. layers



D/Be

> 373 K

0.05-0.06

> 573 K

0.01-0.02

> 773 K

0.009-0.01

> 973 K

0.001-0.004

The deuterium concentration in Be deposition layer obtained from this experiment is consistent with the data in the literature, and the trend is extended up to 973 K.

Table of Contents

◆ Introduction & Experimental

- PSI under mixed ions irradiation
- Experiment in PISCES-B at UCSD

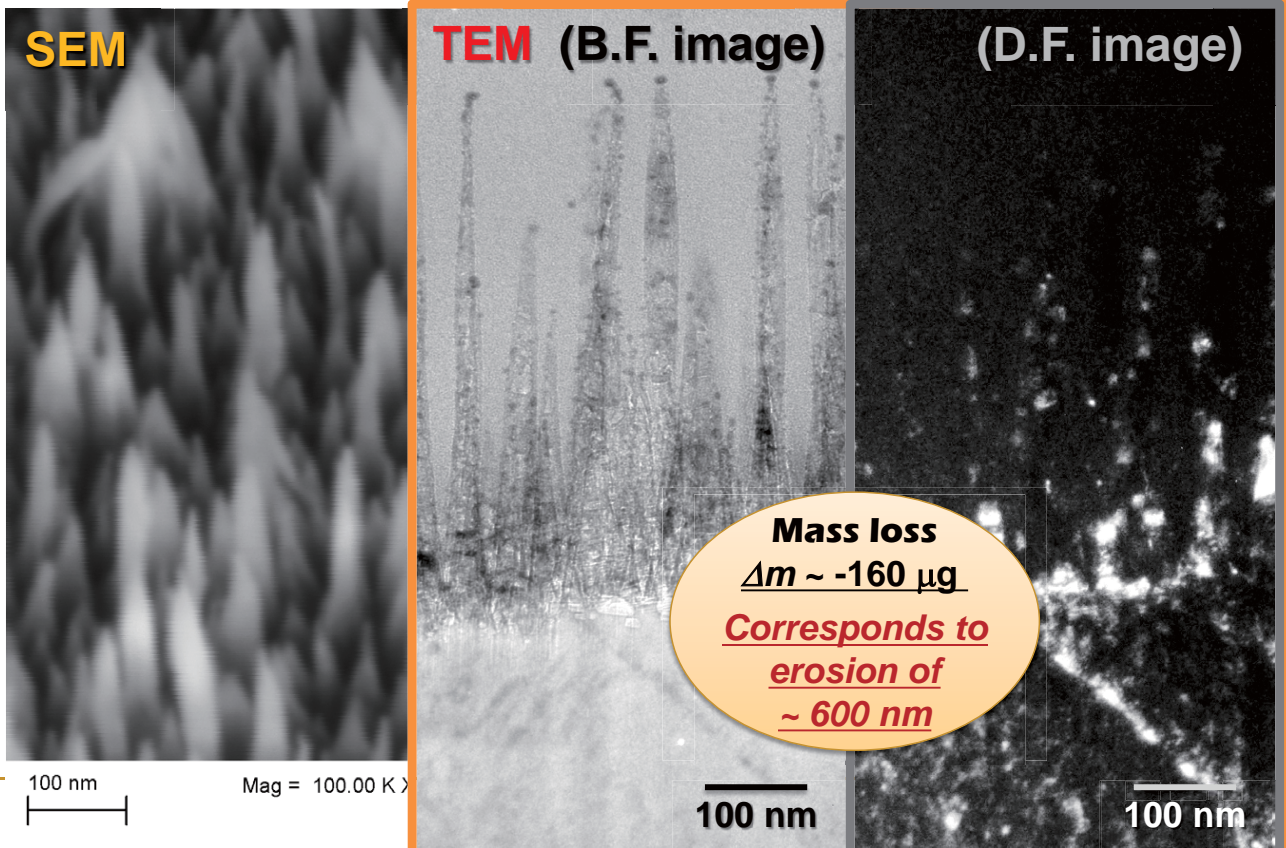
◆ Results

- *Previous results*
 - D-He-Be mixed plasma exposures
- *Highlight Data*
 - Microstructure of Be/D co-deposition layer
 - Deuterium desorption from Be/D co-deposition layer
- *Recent results (Preliminary)*
 - Microstructure and D retention of Be bulk

◆ Summary

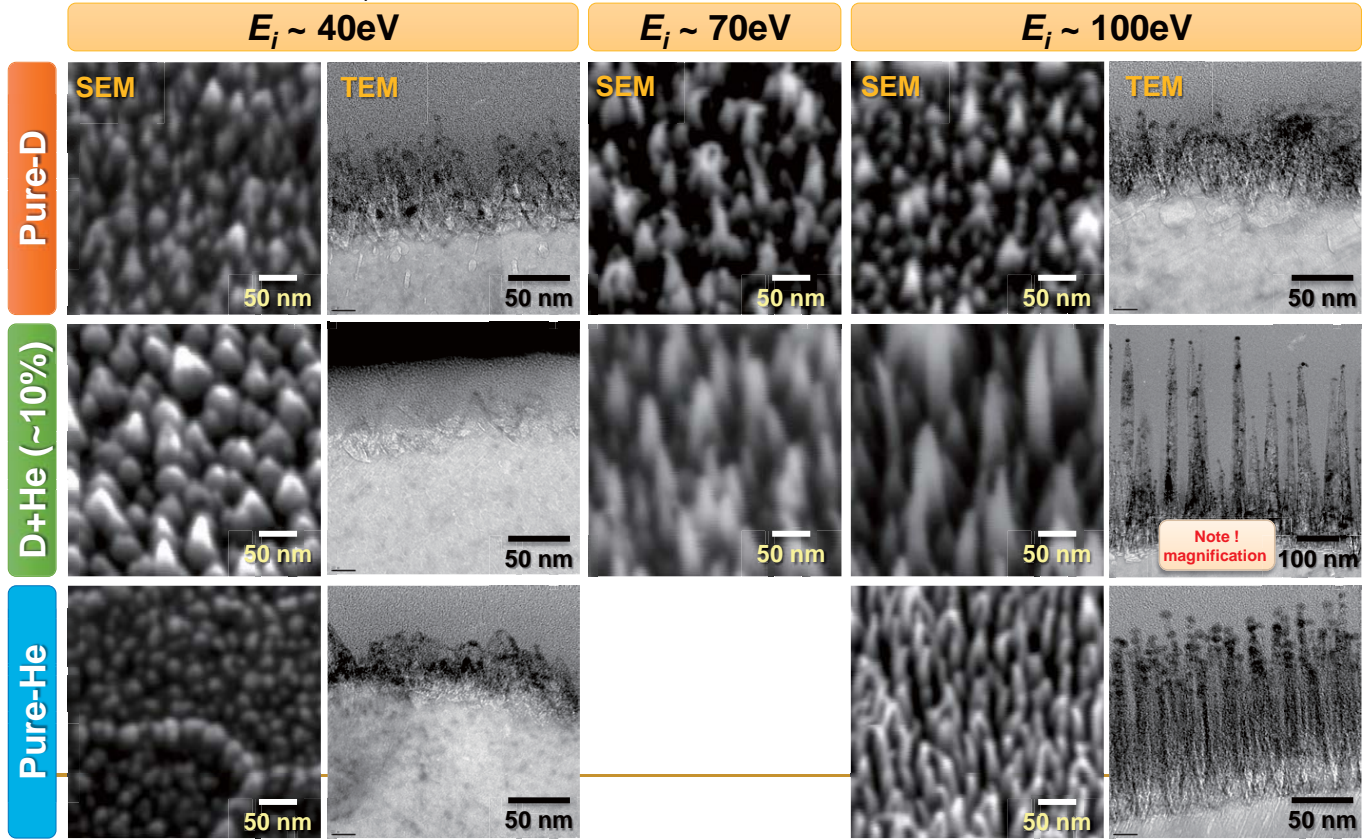
Microstructure of Be bulk exposed to Mixture Plasma

■ SEM & TEM (D+He(~10%), $E_i \sim 100$ eV, $\Phi_i \sim 1 \times 10^{26}$ D⁺/m², $T_{\text{sample}} \sim 573$ K,)



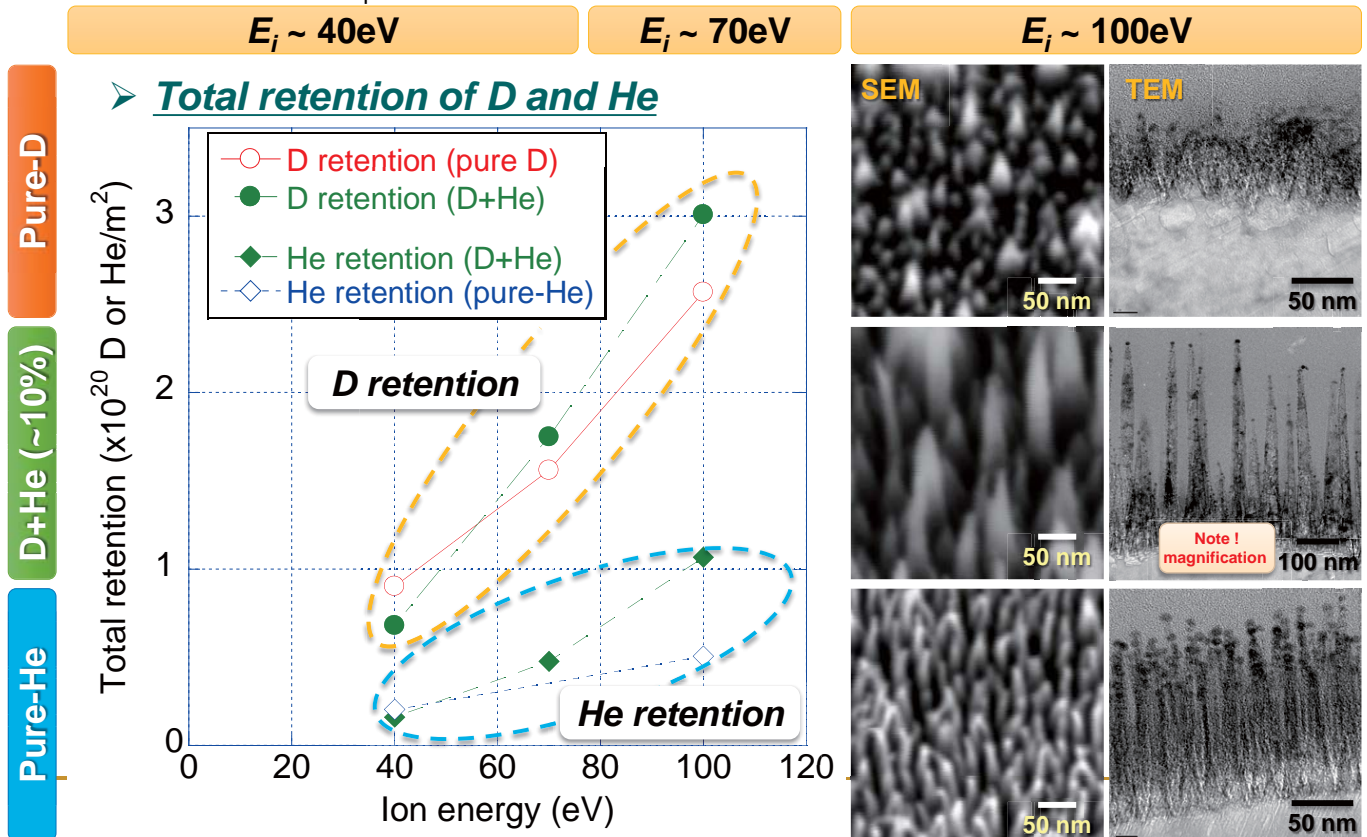
Microstructure of Be bulk exposed to Mixture Plasma

SEM & TEM ($T_{\text{sample}} \sim 573 \text{ K}$, $\Phi_i \sim 1 \times 10^{26} \text{ D}^+/\text{m}^2$)



D retention in Be bulk exposed to Mixture Plasma

SEM & TEM ($T_{\text{sample}} \sim 573 \text{ K}$, $\Phi_i \sim 1 \times 10^{26} \text{ D}^+/\text{m}^2$)

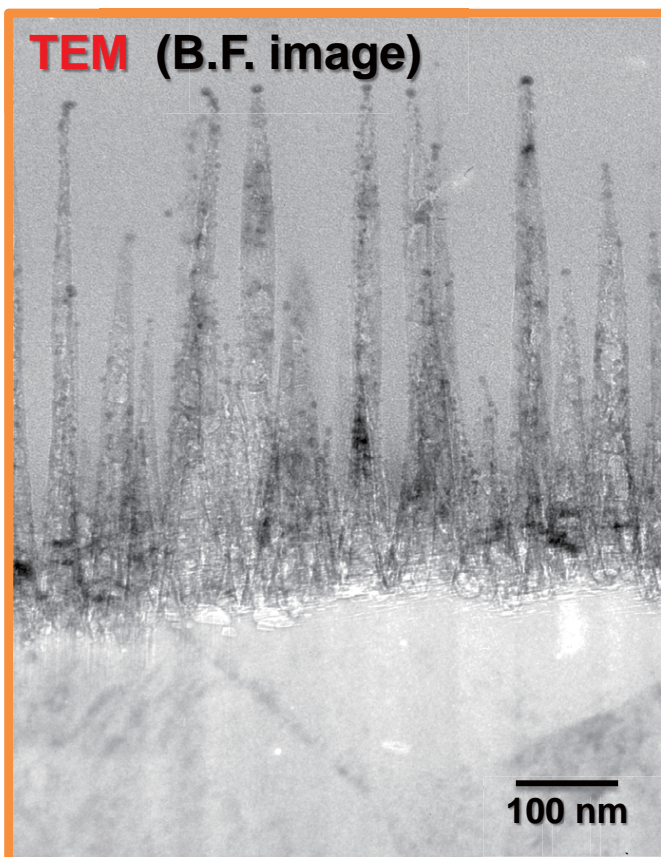


Summary

A systematic study of the temperature effect on the microstructure and the deuterium retention property in beryllium co-deposition layers has been carried out using W samples exposed to mixture plasmas in PISCES-B.

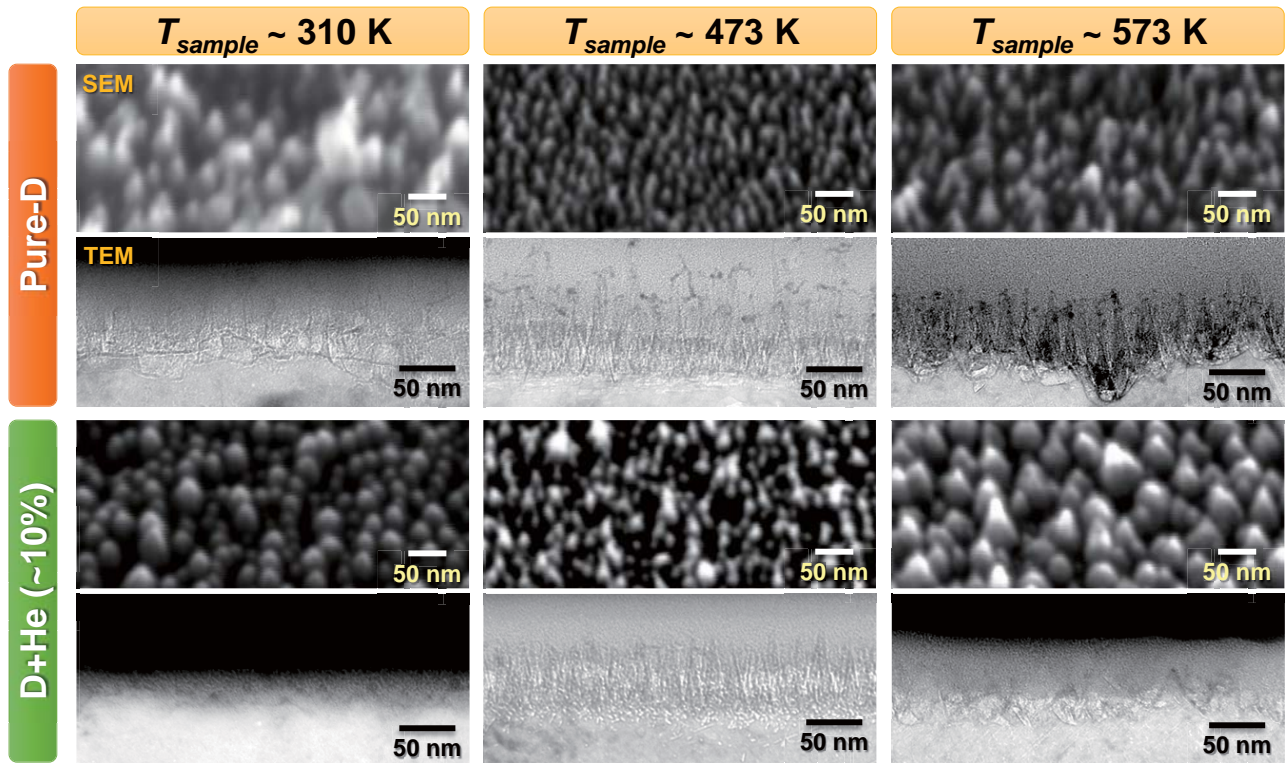
- The deposition layer formed on the sample exposed to D+Be plasma at 373 K mainly consists of polycrystalline hcp metallic Be with a grain size of about 10-20 nm, and He seeding to the mixture plasmas causes amorphization of the layer.
- The columnar structure consisting of Be_2C due to crystal growth appeared at high temperature exposure cases of $>773\text{ K}$ both with and without He seeding.
- The formation of these deposition layers brought about a significant D retention. $D/\text{Be} \sim 0.05$ (373K), ~ 0.001 (973K)
- Peculiar cone structure was observed on the Be bulk samples exposed to D+Be mixture plasma, and their D retentions were reported.

Microstructure of Be bulk exposed to Mixture Plasma



Beバルク試料への高密度プラズマ照射

SEM & TEM観察 ($E_i \sim 40$ eV)



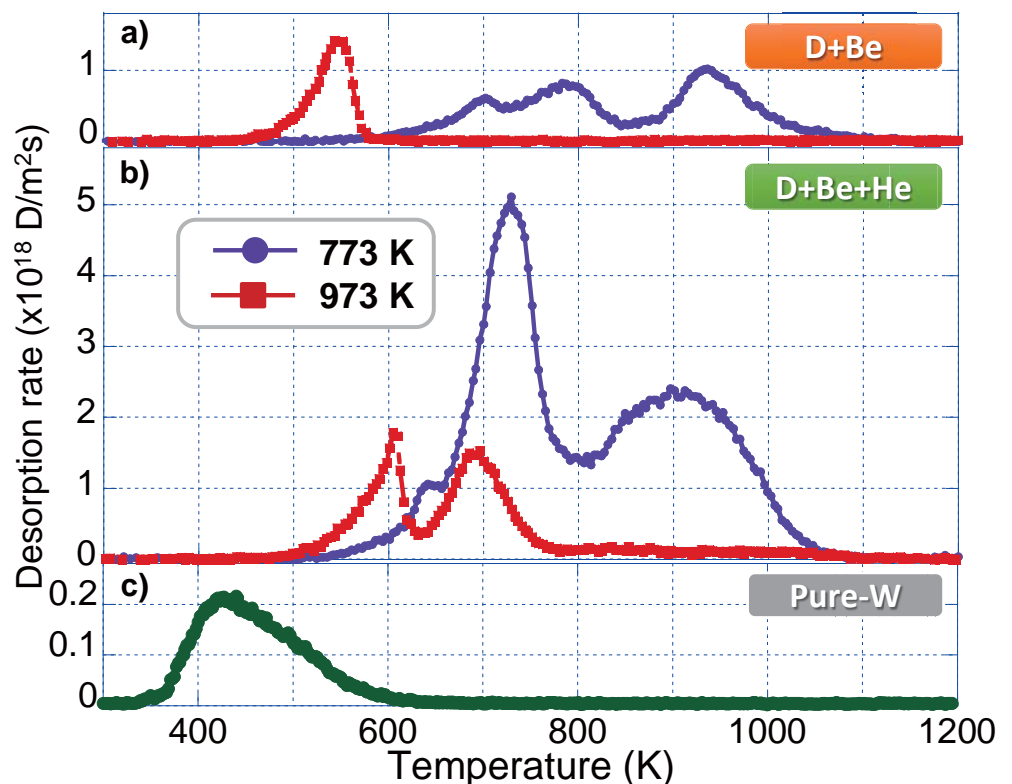
D high trapping efficiency of Be deposition layer

Post irradiation:

- $E_i \sim 3$ keV- D_2^+
- $\Gamma_i \sim 10^{18}$ ions/ m^2s
- $\Phi_i \sim 1 \times 10^{21}$ D^+/m^2
- $T \sim$ R.T.

□ **D retention**

- $D+Be+He$ @773K:
 8.7×10^{20} D/m^2
 $D/Be \sim 0.069$



The hydrogen isotope behavior can be modified drastically, once the Be deposition layer is formed.

2.8.6 Beryllium as plasma facing material: Erosion and surface damage behavior under intense transient plasma heat loads

I. Kupriyanov¹, G. Nikolaev¹, L. Kurbatova¹, N. Porezanov¹, V. Podkovyrov², A. Muzichenko², A. Zhitlukhin² and V. Safronov³

¹ A.A. Bochvar High Technology Research Institute of Inorganic Materials, Moscow, Russia

² SRC RF TRINITI, Troitsk, Moscow reg., Russia

³ Project Center of ITER, Moscow, Russia

E-mail: igkupr@gmail.ru

The first wall panels of the ITER main chamber will be completely armored with beryllium. The primary reasons for the selection of beryllium as an armor material for the ITER first wall are its low Z, high oxygen gettering characteristics and also high thermal conductivity. During plasma operation in the ITER, beryllium besides low cyclic heat loads (normal events) will be suffered by high transient heat loads, such as ELMs, disruptions, VDE, etc. (off normal events). These transient loads cause rapid heating of beryllium surface and can result in significant changes in surface and near-surface regions, such as material loss, melting, cracking, evaporation and formation of beryllium dust as well as hydrogen isotopes retention both in the armour and in the dust. It is expected that the erosion of beryllium under transient plasma loads such as ELMs and disruptions will have significant impact on lifetime of ITER first wall.

It is known that plasma heat loads expected during ITER ELMs and disruptions could not be achieved in the existing tokamak machines. Therefore, other devices (plasma guns, electron beam facilities, ion sources etc.) are used for the testing of candidate PFCs materials.

This paper presents the main results of numerous experiments carried out over the past 5 years at QSPA-Be facility in Bochvar Institute. QSPA-Be facility represents a single-stage coaxial quasi-stationary plasma accelerator with its own magnetic field and it is capable to provide plasma (hydrogen or deuterium) and radiation heat loads on target surface relevant to ITER ELMs and mitigated disruptions. Special Be and Be/CuCrZr mock-ups were tested by hydrogen/deuterium plasma streams (5 cm in diameter) with pulse duration of 0.5 ms in wide heat loads range of 0.2-2.2 MJ/m² and maximum quantities of plasma pulses up to 100-250 shots. The angle between plasma stream direction and mock-up surfaces was 30°. During the experiments, the mock-ups temperature has been maintained in the range of RT-500°C. Two beryllium grades: TGP-56FW (RF, Bochvar Institute) and S-65C (USA, Materion Brush) were studied in these experiments. Influences of plasma heat loads, surface temperature and quantities of plasma pulses on the Be erosion and surface damage are presented.

The experimental data obtained are used for validation of appropriate numerical models and for the estimation of lifetime of the Be armor.



Beryllium as plasma facing material: Erosion and surface damage behavior under intense transient plasma heat loads

I. Kupriyanov, N. Porezanov¹, G. Nikolaev, L. Kurbatova,
V. Podkovyrov¹, A. Muzichenko¹, A. Zhitlukhin¹,
V.M. Safronov²

A.A. Bochvar Research Institute of Inorganic Materials, Moscow, Russia

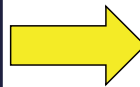
¹ TRINITI, Troitsk, Moscow reg., Russia

² Project Centre of ITER, Moscow, Russia



Introduction

Plasma heat fluxes expected during ITER ELMs and disruptions are difficult to achieve in the existing tokamak machines.



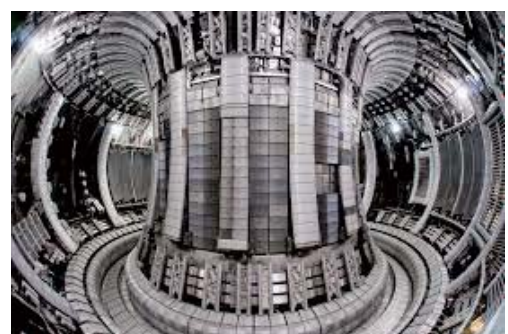
Behavior of FW materials is studied by use of various facilities like powerful plasma guns, electron beam facilities and so on.

The work presents the main results of numerous experiments carried out over the past 5 years in Bochvar Institute at QSPA-Be plasma gun facility.

Motivation:

- to evaluate of the beryllium armor behavior and to determine the main erosion mechanisms of Be under ITER ELMs and disruptions plasma heat loads
- to study properties of the erosion products formed as a result of pulsed plasma action

The obtained experimental data are used for validation of appropriate numerical models, estimation of the tolerable size of ITER ELMs and lifetime of the armour.





Outline

- QSPA facility and experimental schemes
- Plasma testing
- Tested materials
- Experimental results
- Conclusion

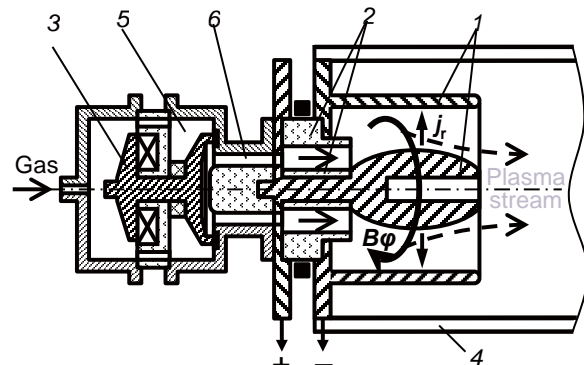


Experimental facility

Quasistationary plasma accelerator (QSPA-Be)



QSPA-Be (Bochvar Institute)



1 - electrodes, 2 - insulator, 3 - pulse electromagnetic gas valve, 4 - vacuum chamber, 5 - volume of valve, 6 - throttling channel

QSPA parameters

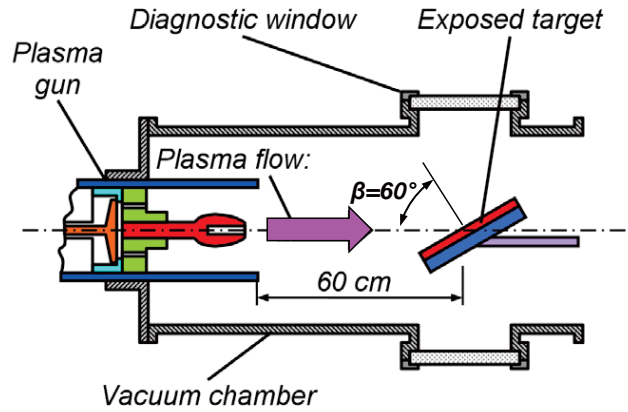
- | | |
|---------------------------------------|---|
| • Heat load | 0.1 ÷ 5 MJm ⁻² |
| • Pulse duration | 0.1 ÷ 0.6 ms |
| • Heat flux factor | 5 ÷ 500 MJm ⁻² s ^{-0.5} |
| • Magnetic field | 0 T |
| • Ion impact energy (H ₂) | <1 keV |
| • Plasma stream pressure | 1 ÷ 10 bar |
| • Diameter | 5 ÷ 10 cm |
| • Electron temperature | < 10 eV |
| • Plasma density | 10 ²² ÷ 10 ²³ m ⁻³ |



Experimental facilities

Experimental schemes

Simulation of ELMs and disruptions *plasma* heat loads



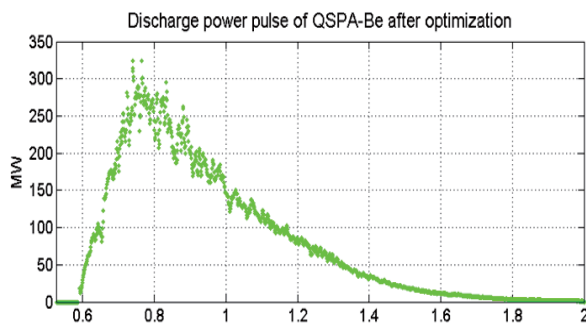
Targets: Beryllium



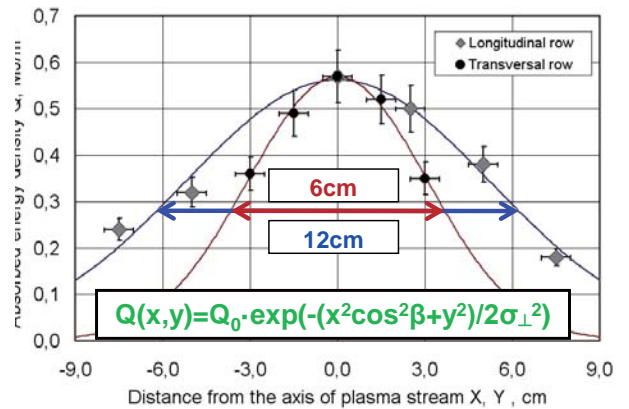
Plasma testing

Experimental conditions: key features

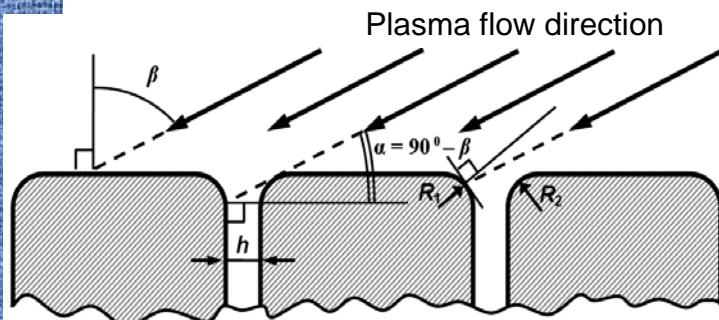
Pulse duration and waveform



Absorbed energy density distribution



Inclined plasma impact



Due to inclined plasma impact the maximum value of the energy density Q is achieved on the edges.

$$Q_{\text{edge max}} = Q_{\text{surface}} / \cos(\beta)$$



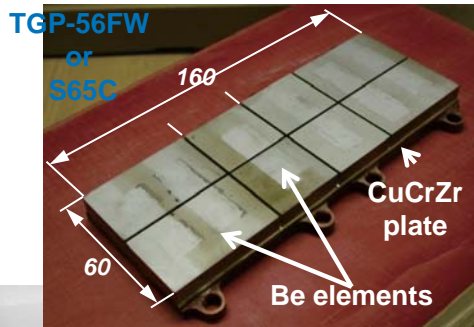
Testing of beryllium materials/target design

Two ITER beryllium grades were used for testing:

TGP - 56FW grade, Russia
(produced by A.A. Bochvar Institute):
Composition : 99.0% Be, <1,0 % BeO
Density: >1.84 g/cm³
Average grain size: <20 micron

S – 65C grade, USA (produced by
Materion Beryllium & Composites)
Composition : 99.0% Be, <1,0 % BeO
Density: >1.84 g/cm³
Average grain size: <20 micron

Typical target design



Be plates - 80x80x10 mm



Mock up assembly



Testing conditions

Absorbed heat loads (central area of spot)-0.5, 1.0, 1.7 and 2.1 MJ/ m²

Initial temperature of Be targets – RT, 250 and 500°C

Pulse (shot) duration - 0.5 ms

Diameter of hydrogen/deuterium plasma stream - 6 cm

Angle between plasma stream and mockup surface - 30°

Area exposed to plasma irradiation - 160 × 60 mm²

Number of shots: up to 250 (0.5 and 1 MJ/ m²), RT

up to 100 (1.7 and 2.1 MJ/ m²), RT

up to 100 (0.5 and 1 MJ/ m²), 250 and 500°C

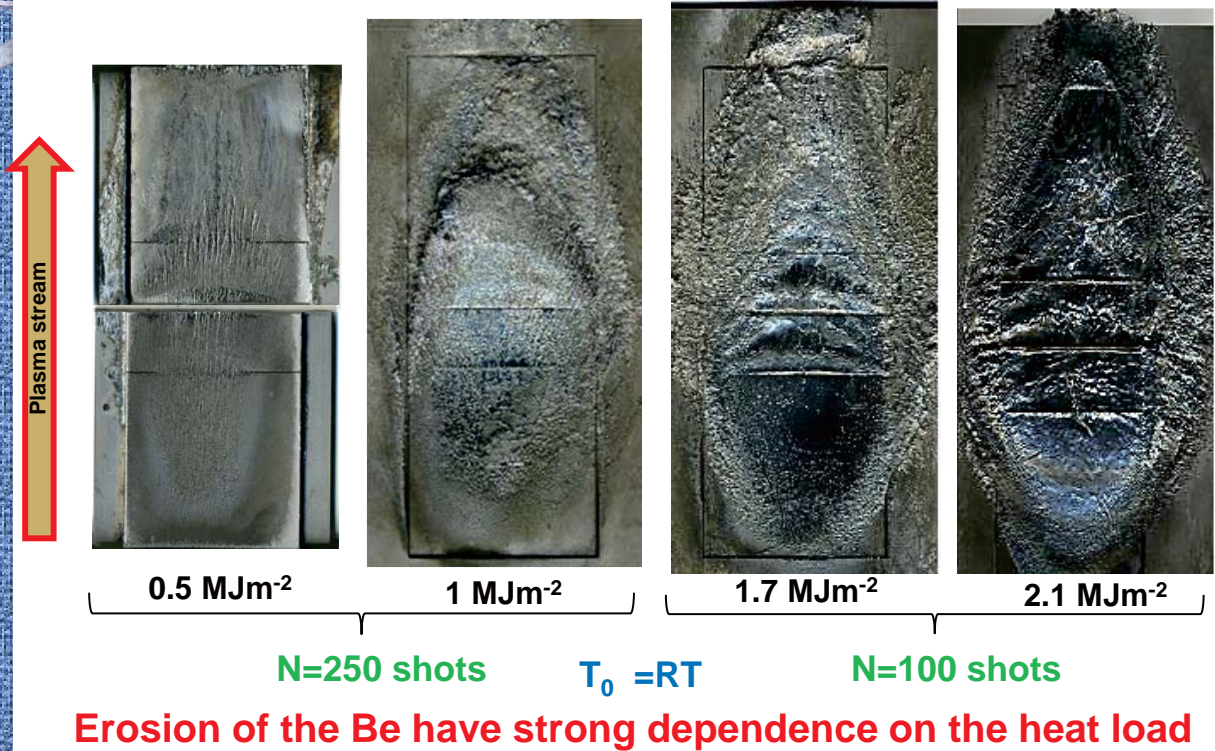


Experimental results

Erosion - Surface evolution vs plasma heat load

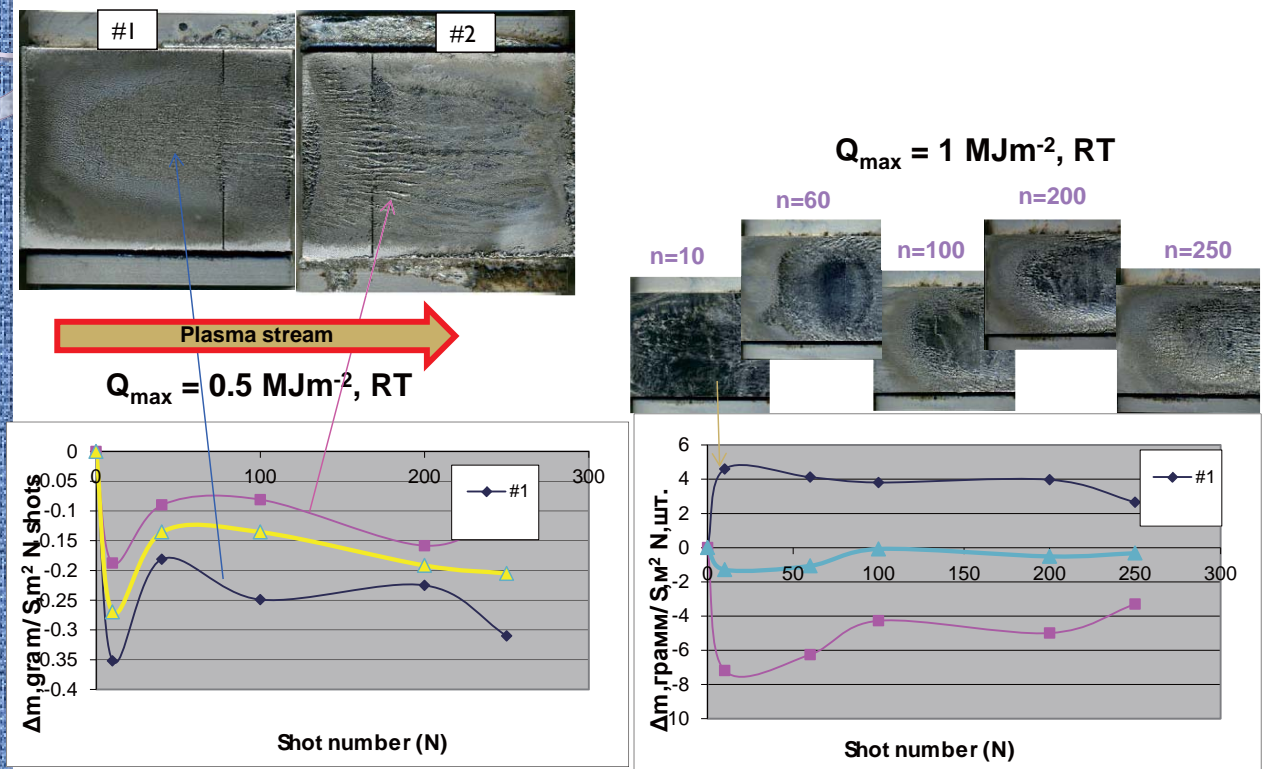
Exposed targets: TGP-56FW

Heat loads: 0.5, 1.0, 1.7 and 2.1 MJ/m²



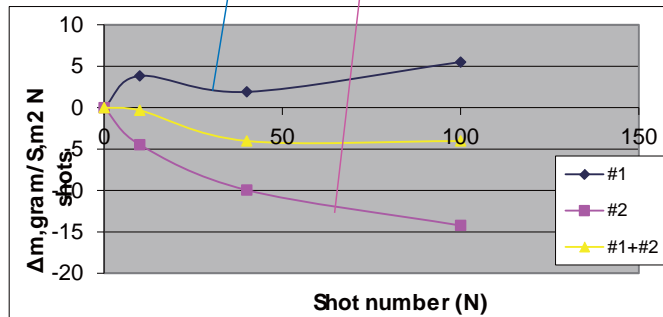
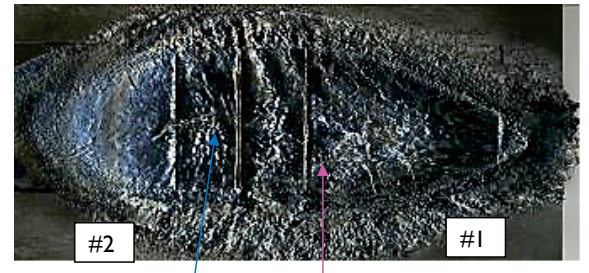
Experimental results

Mass loss/gain dependencies and surface evolution vs number of shots

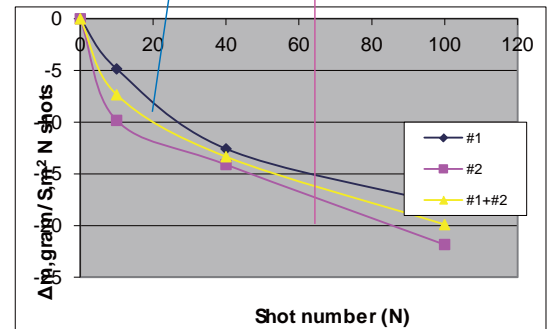




Mass loss/gain dependencies and surface evolution vs number of shots



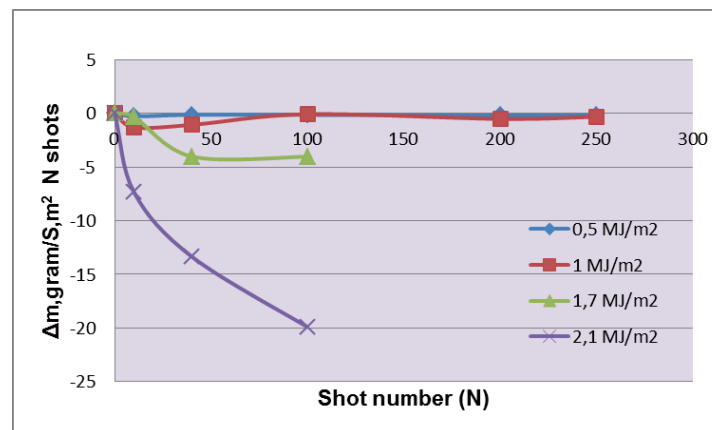
$Q_{\max} = 1.7 \text{ MJm}^{-2}$



$Q_{\max} = 2.1 \text{ MJm}^{-2}$



Erosion/Mass loss dependencies vs absorbed heat load



Load energy, MJ/m ²	Mass loss, Δm, g/m ²	Rate of erosion, Δh, μm/shot
0.5	~ 0.44	~ 0.24
1.0	~ 1.4	~ 0.75
1.7	~3.7	~2.0
2.1	~19.9	~10.8

The erosion of beryllium in plasma spot nonlinearly increase with trasients energy load

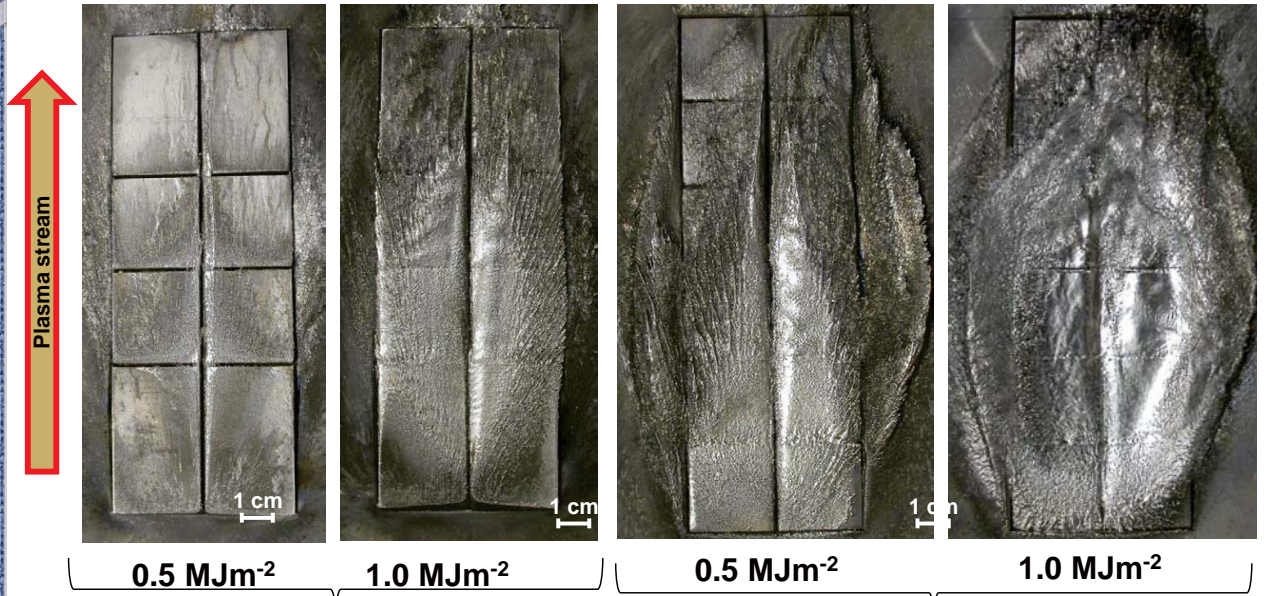


Experimental results

Erosion - Surface evolution vs heat load and initial surface temperature

Exposed targets: TGP-56FW

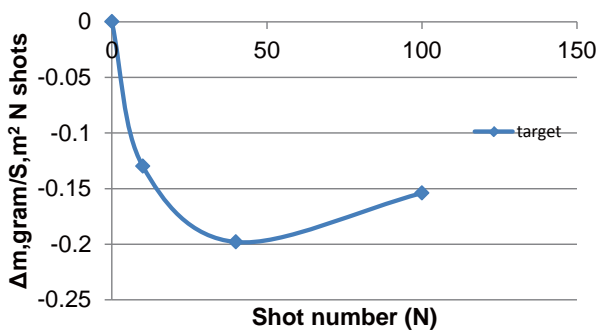
Heat loads: 0.5 and 1.0 MJ/m²; N=100 shots



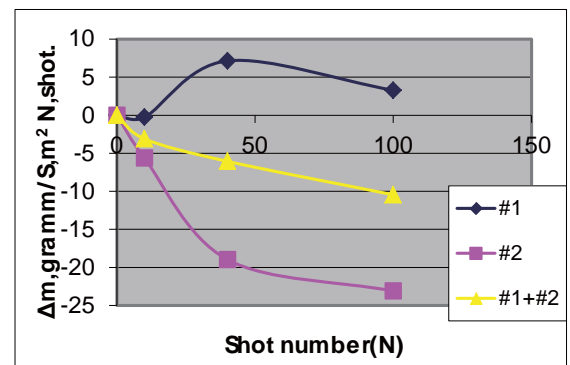
T₀=250°C **T₀=500°C**
Erosion of the Be have strong dependence on the heat load and initial surface temperature



Erosion/Mass loss dependencies vs absorbed heat load and surface temperature



0,5 MJ/m², 250°C

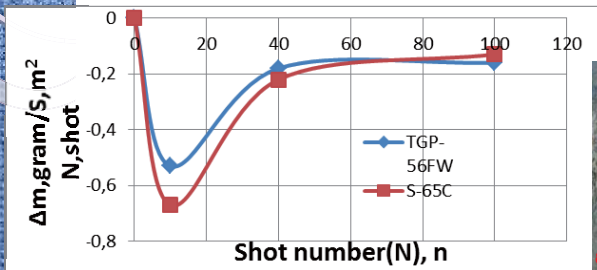


1 MJ/m², 500°C

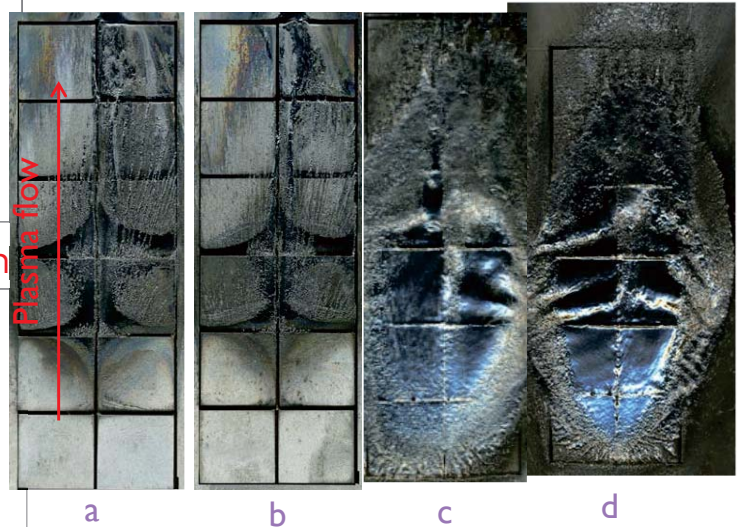
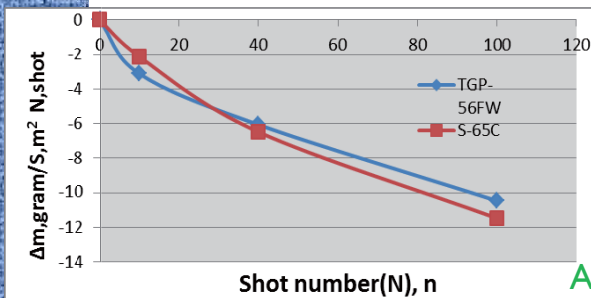
Erosion of the Be have strong dependence on the heat load and initial surface temperature



$E=0.5 \text{ MJ/m}^2$, $T=250^\circ\text{C}$, 100 shots



$E=1 \text{ MJ/m}^2$, $T=500^\circ\text{C}$, 100 shots



A view of mockups surface made of TGP-56FW (a,c) and S-65C (b,d) grades after 100 shots, where a-b: $E=0.55 \text{ MJ/m}^2$ at 250°C , c-d: $E=1 \text{ MJ/m}^2$ at 500°C

Macroscopic erosion of Be caused by melting is identical for TGP-56FW and S65C grades

Conclusion

- It was found that the main erosion mechanism of Be are: melting of beryllium, the movement of the melt layer along the plasma flow direction, resolidification the melt layer and the ejection of droplets and the cracks formation
- Macroscopic erosion of Be strongly depends on the absorbed heat load and initial surface temperature. There is no significant difference of macroscopic erosion of TGP-56FW and S65C Be grades.



A.A. Bochvar Institute
of Inorganic Materials

Thanks for your
attention



A.A. Bochvar Institute
of Inorganic Materials

Appendix-Group photo (付録、集合写真)



The 13th International Workshop on Beryllium Technology (BeWS-13), 21-22 Sep. 2017, Hilton Tokyo Narita Airport Hotel, Chiba, Japan

第13回ベリリウム技術に関する国際会議、平成29年9月21日～22日、ヒルトン東京成田空港ホテル、千葉、日本



Photo of the Venue (会議場)



Photo of the Venue (会議場)



Group photo of banquet



Winner of MDDMA (Dr. Joerg Reimann, KIT)
MDDMA 受賞者 (Dr. Joerg Reimann, KIT)



QST-P-3

ISBN 978-4-907894-09-2

<http://www.qst.go.jp/>